Ecological Studies 236

Takeshi Ohta
Tetsuya Hiyama
Yoshihiro Iijima
Ayumi Kotani
Trofim C. Maximov *Editors*

Water-Carbon Dynamics in Eastern Siberia

Springer

Ecological Studies

Analysis and Synthesis

Volume 236

Ecological Studies is Springer's premier book series treating all aspects of ecology. These volumes, either authored or edited collections, appear several times each year. They are intended to analyze and synthesize our understanding of natural and managed ecosystems and their constituent organisms and resources at different scales from the biosphere to communities, populations, individual organisms and molecular interactions. Many volumes constitute case studies illustrating and synthesizing ecological principles for an intended audience of scientists, students, environmental managers and policy experts. Recent volumes address biodiversity, global change, landscape ecology, air pollution, ecosystem analysis, microbial ecology, ecophysiology and molecular ecology.

More information about this series at http://www.springer.com/series/86

Takeshi Ohta • Tetsuya Hiyama
Yoshihiro Iijima • Ayumi Kotani
Trofim C. Maximov
Editors

Water-Carbon Dynamics in Eastern Siberia

Springer

Editors
Takeshi Ohta
Graduate School of Bioagricultural Sciences
Nagoya University
Nagoya, Aichi, Japan

Tetsuya Hiyama
Institute for Space-Earth Environmental Research
Nagoya University
Nagoya, Aichi, Japan

Yoshihiro Iijima
Graduate School of Bioresources
Mie University
Tsu, Mie, Japan

Ayumi Kotani
Graduate School of Bioagricultural Sciences
Nagoya University
Nagoya, Aichi, Japan

Trofim C. Maximov
Institute for Biological Problems of Cryolithozone
Russian Academy of Sciences
Yakutsk, Yakutiya-Saha Republic, Russia

ISSN 0070-8356 ISSN 2196-971X (electronic)
Ecological Studies
ISBN 978-981-13-6316-0 ISBN 978-981-13-6317-7 (eBook)
https://doi.org/10.1007/978-981-13-6317-7

This Springer imprint is published by the registered company Springer Nature Singapore Pte Ltd.
The registered company address is: 152 Beach Road, #21-01/04 Gateway East, Singapore 189721, Singapore

Preface

This publication is the first to describe the processes of ecohydrology, permafrost hydrology, meteorology, and climatology in the context of water, energy, and carbon exchanges in the Arctic circumpolar region of eastern Siberia. The material presented in this work represents the culmination of our extensive research in this region. In this preface, we will describe the objectives and outcomes of some of these research projects and provide a short history of our main observational site.

In the 1990s, an international and multidisciplinary research collaboration was initiated in Yakutsk, Sakha Republic (Yakutia), Russia, to study environmental and climate changes in eastern Siberia. This initiative was part of the Global Energy and Water Exchanges (GEWEX) Asian Monsoon Experiment (GAME) project, which was planned within the framework of the World Climate Research Programme (WCRP). The GAME project comprised several regional projects focusing on Southeast Asia, East Asia, the Tibetan Plateau, and north-eastern Eurasia and was conducted mainly by the Japanese research community in collaboration with researchers from other Asian countries. GAME–Siberia focused on the Lena River Basin in eastern Siberia, where the Asian winter monsoon originates. The GAME–Siberia project was the first international and experimental campaign in this region, and its purpose was to improve our understanding of land surface processes, including ecohydrology and river hydrology, under changing climate conditions. To achieve this objective, a ground-based observation network was established, and atmospheric observations, satellite remote sensing data analysis, and land surface and hydrological (river discharge) modelling studies were conducted. The project has greatly contributed to our knowledge of these systems and has become a focus for research on the land surface processes of cold regions.

The main GAME–Siberia experimental site was the Spasskaya Pad (SPA) station located near Yakutsk, where we established a flux tower through Russian and

Japanese collaboration in 1996. The SPA station was subsequently used to collect data for several Japanese-funded research projects: Core Research for Evolutionary Science and Technology/Water, Energy and Carbon Cycles in Northern Forests (CREST/WECNoF), Research Institute for Humanity and Nature (RIHN)–Siberia, and Green Network of Excellence (GRENE) Arctic Climate Change Research Project–Terrestrial Ecosystem in the Arctic (TEA). Through these projects, the SPA station became the central base in eastern Siberia for taiga forest meteorological and hydrological observations. Many significant findings have been obtained through observations of the permafrost–vegetation hydrological cycle. The SPA station was thus recognised globally as the most important location for development and verification of land surface models of the cryolithozone, especially over a continuous permafrost region. In recent years, the site has been recognised as an international collaboration site for the Arctic Challenge for Sustainability (ArCS) project, and it continues to provide meteorological and hydrological datasets under the changing climate of the Arctic circumpolar region. Furthermore, the station is a member of international research networks including the International Network for Terrestrial Research and Monitoring in the Arctic (INTERACT) and Changing Permafrost in the Arctic and its Global Effects in the 21st Century (PAGE21). Observation data obtained at the SPA station are freely distributed through FLUXNET and the Phenological Eyes Network (PEN).

The unique and long-term consecutive datasets obtained at the SPA station in eastern Siberia have therefore been widely used by international researchers. Especially in the 2000s, it was recognised that changes in meteorological and hydrological variables represented large-scale humidification in conjunction with climate change in the Arctic circumpolar region. The large amount of data accumulated at the SPA station describes the effects of declining processes in boreal forests, as well as recent and ongoing climate changes. This book is therefore intended as a milestone of our achievements.

In preparation for the publication of this work, a kick-off editing workshop (the ISEE/CICR International Workshop) was conducted from 19 to 21 January, 2017, with the support of the Joint Research Program of the Center for International Collaborative Research (CICR) of the Institute for Space–Earth Environmental Research (ISEE) at Nagoya University. The editors thank the ISEE, Nagoya University, as well as all research agencies and institutes that supported the research activities described above. Finally, we thank Dr. Tetsuzo Yasunari, Director General of the Research Institute for Humanity and Nature; Dr. Yoshihiro Fukushima, Emeritus Professor of the Research Institute for Humanity and Nature; Professor Tetsuo Ohata of the National Institute of Polar Research; Professor Boris Ivanov, Director of the Institute for Biological Problems of Cryolithozone of Siberian Branch of Russian Academy of Sciences; and Professor Rostislav Kamensky, Director of the Permafrost Institute of Siberian Branch of Russian Academy of Sciences for their extraordinary leadership in establishing the research partnership

between Russia and Japan, as well as for funding our research projects. In addition, we thank the many international researchers who engaged in our projects described above.

Nagoya, Japan — Takeshi Ohta
Nagoya, Japan — Tetsuya Hiyama
Tsu, Japan — Yoshihiro Iijima
Nagoya, Japan — Ayumi Kotani
Yakutsk, Russia — Trofim C. Maximov

Contents

Chapter 1
Water and Carbon Dynamics in Eastern Siberia: Introduction

Takeshi Ohta, Trofim C. Maximov, Alexander N. Fedorov, and Alexey R. Desyatkin

All land creatures influence terrestrial water and carbon fluxes and influenced by them. Thus it is important to understand the water, energy, and carbon cycles to solve problems in the fields of hydrology, meteorology, and ecology. The area of global forest cover including tropical, temperate, and boreal forest accounts for 30% of all land cover (Dixon et al. 1994; Liu and Yin 2013), with distinct contributions from each of the different forest types (Malhi et al. 1999; Baldocchi et al. 2000). The annual evapotranspiration from a forest decreases with the decrease in temperature during the growing season (Huntington 2006), and changes in forest carbon budgets depend on the climatic zone (Malhi et al. 1999; Luyssaert et al. 2007).

Bonan et al. (1992) and Bonan (1995) conducted studies on boreal forests based on numerical experiments; they used general circulation models (GCMs) in their investigations. Broader experimental studies of land surfaces include the Boreal Ecosystem-Atmosphere Study (BOREAS; Sellers et al. 1995) in North America and the Northern Hemisphere Climate Process Land Surface Experiment (NOPEX; Halldin et al. 1999) in the Scandinavian Peninsula. An important object of these projects is collect the data needed to computer simulation models, and in BOREAS analysis of the data indicated that area-averaged photosynthetic capacity of the boreal forest is much less than that of the temperate forest (Sellers et al. 1995). In NOPEX project, simple land-use-weighted averaging of fluxes from grasslands, forests, and lakes agreed well with regional fluxes (Halldin et al. 1999).

Eastern Siberia occupies the eastern half of the Eurasian continent, and the exact details of the region's water, energy, and carbon cycles and ecosystems remain

T. Ohta (✉)
Graduate School of Bioagricultural Sciences, Nagoya University, Nagoya, Japan
e-mail: takeshi_1956@grace.ocn.ne.jp

T. C. Maximov · A. R. Desyatkin
Institute for Biological Problems of Cryolithozone, RAS, Yakutsk, Russia

A. N. Fedorov
Melnikov Permafrost Institute, RAS, Yakutsk, Russia

T. Ohta et al. (eds.), *Water-Carbon Dynamics in Eastern Siberia*,
Ecological Studies 236, https://doi.org/10.1007/978-981-13-6317-7_1

unknown. Schulze et al. (2002) investigated the water, energy, and carbon cycles from western Siberia to central Siberia (TCOS-Siberia). The objects of TCOS-Siberia were the water, energy, and carbon cycles in western and central Siberia and the important results obtained from the seasonal variations of energy and water fluxes above a forest ecosystem (Tchebakave et al. 2002) to the remote sensing of a Siberian boreal forest (Nichol et al. 2002). In contrast, in eastern Siberia, widespread ecological investigations have been conducted, and many results of these studies have been reported (Osawa et al. 2010). The results describing water, energy, and carbon dioxide fluxes build on the work of Kelliher et al. (1997), who studied the circulation of water, energy, and carbon in the region. For such an early study, their observations were successfully carried out, and the characteristics of the water, energy, and carbon cycles in a larch (*Larix cajanderi*) forest were measured effectively despite the research occurring over only a short period in the summer of one season.

Researchers from Japan, Russia, and the Netherlands have played a key role in investigations of water, energy, and carbon cycles in eastern Siberia, and their results have helped to inform many subsequent studies, including the GEWEX/GAME-Siberia (Lawford et al. 2004; Yasunari 2007), PIN-Matra (Moors et al. 2004), CREST/WECNoF (Ohta 2010), PAGE21 (van Huissteden and Dolman 2012), and RIHN/Siberia (Hiyama et al. 2013) projects. Additionally, methane (CH_4) and biogenic volatile organic compound (BVOC) emissions (van Huissteden et al. 2005; Arneth et al. 2016) and the physical evaluation of permafrost processes (Iijima et al. 2010) have been incorporated into analyses of the water, energy, and carbon cycles in the soil-vegetation-atmosphere systems of the region. Remote sensing technology (Suzuki et al. 2006) has also been applied after a second half of 2000s.

Despite all of the research on this topic published in scientific journals, no textbooks have been published on the water, energy, and carbon cycles in eastern Siberia. This book fills this gap. It begins by considering the water, energy, and carbon dynamics of eastern Siberia and then discusses CH_4 and BVOC emissions, the physics of permafrost processes, the use of remote sensing technology, and finally the water and carbon cycles in the watersheds of eastern Siberia.

1.1 Climate, Permafrost, and Vegetation

Eastern Siberia, located in the eastern part of the Eurasian continent, spans from 55° to 77°N and from 110° to 180°E. Figure 1.1 shows the topographical map of eastern Siberia indicating the major river basins, mountains, and main observational points. The region experiences very little precipitation and severely cold temperatures in winter. The average annual precipitation was 236.9 mm $year^{-1}$ on average from 1961 to 1990, which ranges from a minimum of 8.1 mm in January to a maximum of 39.1 mm in July in Yakutsk on the left bank of the middle reaches of the Lena River,

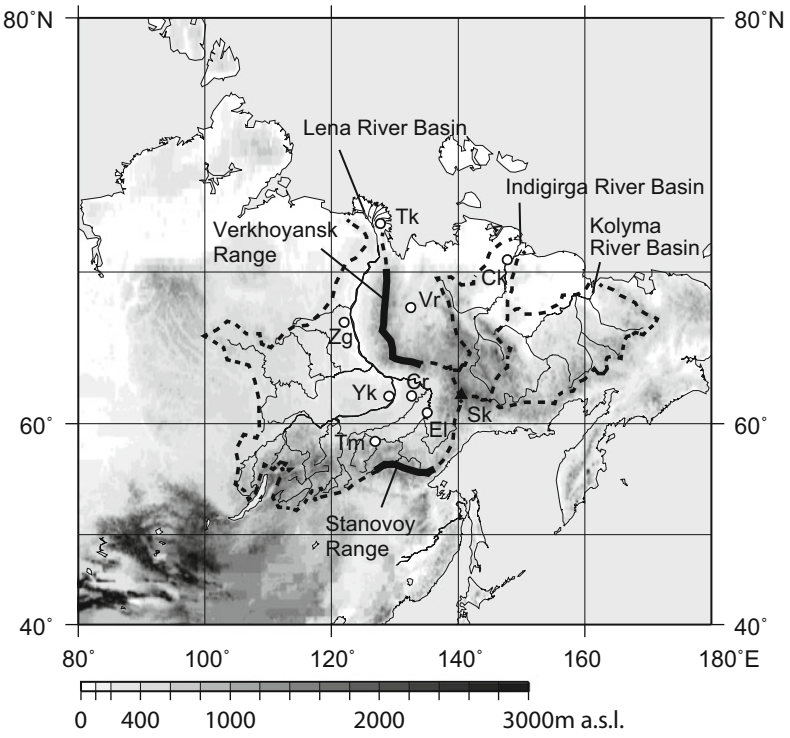

Fig. 1.1 Topographical map in eastern Siberia with major river basins and main observational points
Tk Tiksi, *Ck* Chokurdakh, *Vr* Verkhoyansk, *Zg* Zhigansk, *Yk* Yakutsk, *Cr* Churapcha, *El* Elgeeii, *Tm* Tommot, *Sk* Suntar-Khayata (Mt. Mus-Khaya: 2959 m)

62° 15′N, 129° 14′E. (Ohta et al. 2001). The winter temperature is extremely cold. The average annual temperature was −10.0 °C in the same averaging period, ranging from a minimum of −41.2 °C in January to a maximum of 18.7 °C in July (Ohta et al. 2001). Figure 1.2 shows the locations of the main cities of the world's northern countries and their average monthly precipitation and temperatures. Clearly, Yakutsk has less precipitation and much colder temperatures in winter than the other cities.

What causes this phenomenon of little precipitation and very cold temperatures? Figure 1.3 shows the distribution of permafrost around the globe. Much of the frozen ground is distributed in the northern hemisphere, and continuous and discontinuous permafrost is widely distributed throughout eastern Siberia. The depth of continuous permafrost is estimated to be on average about 200 m and maximally about 500–600 m in the area of the Lena watershed, whereas it has been reported to be maximally about 200–300 m in Alaska (McGuire et al. 2002). What is the reason for

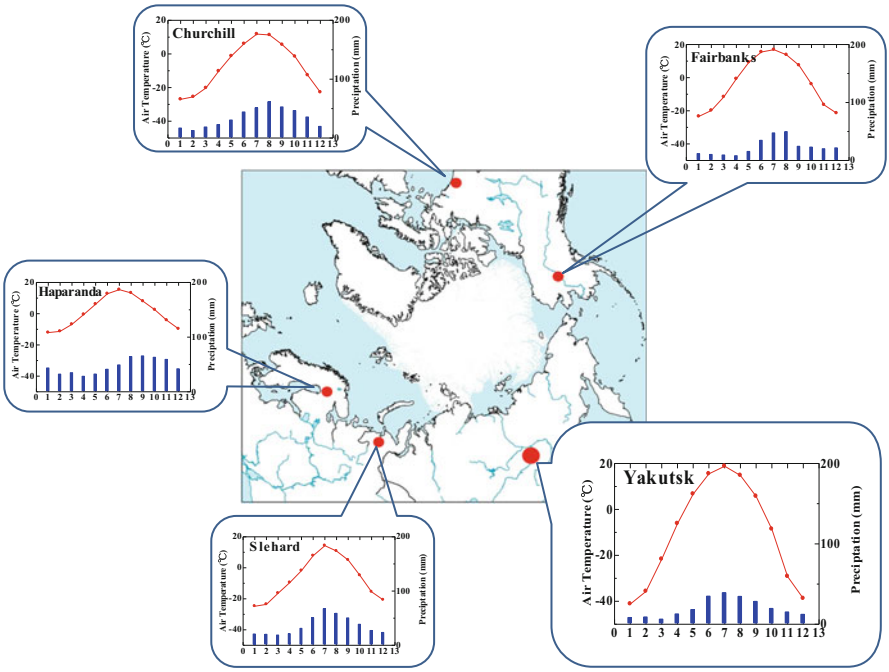

Fig. 1.2 Monthly temperature and precipitation in Yakutsk and the other cities. Temperature and precipitation is much lower in Yakutsk than in the other cities on the boreal zone in the globe

the differences in permafrost depth between Alaska and eastern Siberia? The last glacial stage began approximately 70,000 years ago, with glaciers reaching their greatest extent approximately 20,000 years ago (Carlson and Winsor 2012). At this time, the Laurentide Ice Sheet and Cordilleran Ice Sheet covered the surface of the Earth in North America, and the Scandinavian Ice Sheet extended extensively from northern Europe to western and central Siberia. Due to the thermal conductivity of the thick ice sheets from northern America and northern Europe and western and central Siberia, the ground surface of the Earth was likely very rarely exposed. In contrast, small glaciers were located across eastern Siberia, but the impenetrable ice sheet did not cover the entire surface of the land. Thermal conductivity remained high because there were no ice sheets, and the heat of the winter atmosphere reached the surface soil directly through heat conductivity. Thick layers of permanently frozen ground, i.e. permafrost, occur in eastern Siberia, which has not been covered by thick ice for approximately 20,000 years to the present day. This permafrost produces a 'vegetation-permafrost' symbiotic system, with characteristic vegetation that is described in the next section.

1.2 Climate of the Boreal Forest and Tundra

1.2.1 Formation of the Boreal Forest

After tropical forest, boreal forest accounts for the largest extent of forest on Earth, with an area extending for 12.7–14.0 million km^2 (Malhi et al. 1999; Baldocchi et al. 2000). Figure 1.4 presents a vegetation distribution map, which shows the extent of boreal forest near the North Pole. Surface soil in most of Greenland and the islands north of 75°N is covered by snow and ice, and the humid-wetland referred to as Arctic tundra spreads out in a zone in the southern direction. A forest belt called taiga extends along the southern side of this zone. The boreal forest in eastern Siberia consists of larch trees and is classified as a deciduous conifer forest (Ermakov et al. 2002; Osawa et al. 2010), whereas the boreal forests in northern America, northern Europe, and western and central Siberia consist of spruce (*Picea ariana*), pine (*Pinus morrisonicola*), and fir (*Pseudotsuga menziesii*) trees and are classified as evergreen conifer forests (Bonan and Shugart 1989; Greene et al. 1999; Gower et al. 2001). Evergreen conifer forests called 'dark taiga' flourish in western Siberia and extend along the left bank of the Yenisei River in central Siberia, whereas deciduous conifer forests grow in eastern Siberia and are referred as 'light taiga'. The distribution of the larch forest zone in eastern Siberia is almost coincident with the distribution of permafrost, as shown in Fig. 1.3. The larch forest ecosystem situated mainly in eastern Siberia could be considered a permafrost ecosystem (Osawa et al. 2010).

We have a general understanding of how the larch forest area of eastern Siberia was formed. Velichko and Spasskaya (2002) explained the relationships between climate and vegetation in eastern Siberia from the Tertiary period (from 66 million to 2.58 million years ago) to the present day. Until the end of the Tertiary period, the global climate was generally warm, with temperate and/or subtropical vegetation flourishing in eastern Siberia on a large scale. Rapid cooling and sudden aridification advanced globally from the end of the Tertiary period and/or the beginning of the Quaternary period (from 2.58 million years ago to the present day), and the formation of permafrost began in eastern Siberia during this period. The Quaternary period had alternating glacial and interglacial periods, and it is estimated that larch forest occurred in locations where Scotch pine (*Pinus sylvestris*) and birch (*Betula pendula*) grow in present-day eastern Siberia. During the cold period of the last glacial period, permafrost extended across the whole land surface of Russia, except for the southwestern area. It is thought that the southern limit of the continuous permafrost zone retreated back north in the warmer period of the Holocene epoch. The climatic conditions are thought to have then turned cold again, setting the southern limit of the continuous permafrost at the present location.

The details of why the distribution of the larch forests has become established in its present location are unknown, but it is thought that they formed due to phases of warming and cooling of the climate at the southern limit of the continuous

Fig. 1.3 Map in the distribution of permafrost on the globe. The continuous permafrost zone is widely extended in the eastern Eurasia than in the other parts of the globe. (Web site: http://ipa.arcticportal.org/images/stories/permafrost%20map.jpg)

permafrost during the Pleistocene age (2.58 million years ago to 11.7 thousand years ago) in the Quaternary period. The forest areas of the 'vegetation-permafrost' symbiotic system were gradually developed from larch forests and permafrost in eastern Siberia.

1.2.2 Formation of Forest/Tundra Vegetation

In eastern Siberia, in addition to the Lena River, which is a key focus of this book, the Yana, Indigirka, and Kolyma rivers also flow into the Arctic Ocean. The

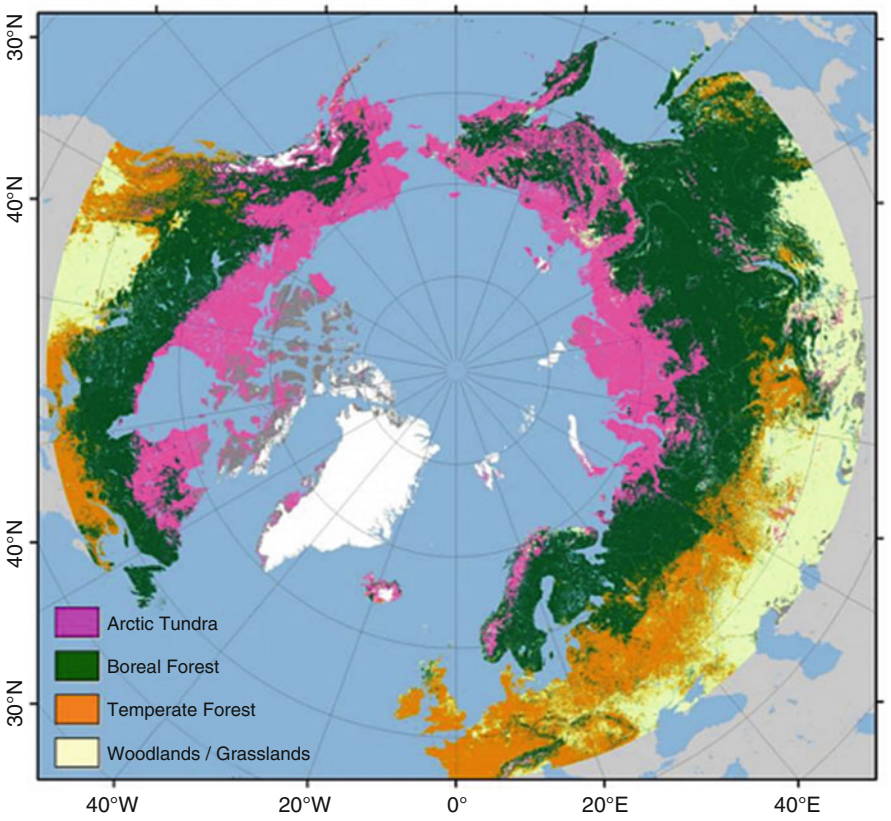

Fig. 1.4 Distribution of the polar vegetation map from the location of the high latitude. (Web site: http://www.lter.uaf.edu/boreal-forest/about)

mountain areas extend to the middle and lower watersheds of the rivers, and the larch forests grow along the rivers in the Lena and Yana river watersheds. These reaches in the Indigirka and Kolyma river watersheds consist of broad wetlands where forest-tundra vegetation grows extensively (Huh et al. 1998). There is an area where sparse groves of larch trees are mixed with damp ground, and it is not easy to determine the northern limits of 'light taiga' forests in eastern Siberia.

We need to understand how the northern timberline of larch forest is determined because the environmental factors will hinder the growth of larch forest. It is thought that low temperatures determine the growth limit of plants, but this hypothesis is not necessarily correct. For larch and birch trees, the low temperatures in winter are not important, as shown in Fig. 1.2. Larch and birch trees growing around Yakutsk can survive at temperatures as low as −70 °C (Sakai 1983) if sufficient preparations for the low temperature are made. Photosynthesis in vegetation begins at temperatures of almost 0 °C (Ch and Diemer 1987; Ensminger et al. 2004), but photosynthetic activity decreases at temperatures exceeding 25 °C (Ch and Diemer 1987; Xu and

Baldocchi 2003). The temperature difference between tundra vegetation, where larch trees do not grow, and forest-tundra vegetation is not an important factor for plant growth, with the presence of oxidative soil soaking in water being a more significant factor for the growth of plants. Additionally, the root channels of larch trees must stretch out horizontally to acquire the nutrient salts necessary for survival, because the tundra area is an oligotrophic permafrost zone. The dry soil requires auxesis of the roots of larch trees because the soil soaked in water decays the roots and the nutrient salts are not positively absorbed (Liang et al. 2014).

Methane, a powerful greenhouse gas, can be generated in the soil in tundra areas because the soil layers in tundra are in a relatively reduced state compared to the forest-tundra soil (van Huissteden et al. 2005; Sachs et al. 2008). Therefore, land use changes that result in a conversion from the forest to tundra increases the quantity of methane generated and may accelerate global warming.

The relationships between vegetation and geology, and the permafrost characteristics in the 'light taiga' belt and the tundra zone in eastern Siberia, differ greatly. This book clarifies (1) water and carbon dynamics in eastern Siberia by determining water and carbon circulation at the plot scale using several methods, (2) the water cycle at the watershed scale by applying remote sensing technology, and (3) analyses of the water and carbon dynamics by numerical modelling.

Before 1991, eastern Siberia was controlled as part of the former Soviet Union, and researchers in Western countries had no information regarding the water, energy, and carbon cycles in the region. We therefore begin by describing research regarding water and carbon circulation in eastern Siberia from the 1950s to 1990s before the GEWEX-GAME/Siberia project.

1.3 Water and Carbon Dynamics in Eastern Siberia During the Former Soviet Union Period

Permafrost leads to a certain soil thermal regime and also to specific water and carbon regimes. We introduce researches of the hydrological processes, carbon dioxide cycles, permafrost, and soils in eastern Siberia while it was a part of the former Soviet Union, before presenting detailed explanations.

1.3.1 Hydrological Processes Studies in the Soviet Union

1.3.1.1 Outline of Hydrological Cycles

Following the end of World War II, researchers in the former Soviet Union focused on the soil hydrothermal regime in the larch forests of eastern Siberia (Zolnikov 1954a, b, 1957; Zolnikov et al. 1962; Shashko 1961). Long-term studies on the hydrothermal regimes of permafrost soils in forests, including larch forests, were

carried out in the Yana River basin (Pozdnyakov 1961), in Central Yakutia (Pozdnyakov 1963; Gavrilova 1967), in Zhigansky District, and in the Centre and South-West regions of Yakutia (Savvinov 1971). The most long-term hydrological observations were conducted at the Spasskaya Pad Scientific Forest Station of the Institute of Forest and Wood (transferred to the Institute for Biological Problems of Cryolithozone in 1992) in Central Yakutia, and the results of these studies were published by Pozdnyakov (1963).

1.3.1.2 Depth of Active Layer

No comprehensive data are available regarding the maximum depth of the seasonal thawing of permafrost for forest area hydrothermal regimes. According to temperature observations between rivers in Lena-Amga, seasonal thawing of permafrost soil reached 150–160 cm depths in a cowberry (*Vaccinium vitis-idaea*)–larch forest (Gavrilova 1967), and 170–180 cm depths in the same forest type around Yakutsk (Savvinov 1971), which was similar to long-term average data obtained at Spasskaya Pad in Central Yakutia (Pozdnyakov 1975). Savvinov (1971) studied soil temperatures in the area surrounding Zhigansk (66°N, 123°E); in a blueberry (*Vaccinium corymbosum*)–moss–larch forest, the depth of soil thawing in permafrost was approximately 60 cm, but about 80 cm in a clear-cut plot of the same forest type.

1.3.1.3 Evaporation and Transpiration

The woody canopy, understory, ground cover, and forest litter intercept a portion of rainfall and transpire water into the atmosphere. In an annual cycle, interception in most types of pure larch forest contains approximately 20–25% of the liquid and solid precipitation that did not reach the soil surface but evaporated into the atmosphere. Retained by the ground surface cover, this part of liquid precipitation could be taken up by plants (lichens), reducing summary evaporation from the soil surface in permafrost (Savvinov 1971).

According to observations in Central Yakutia (Pozdnyakov 1963), the maximum transpiration intensity was 420–440 mg g^{-1} hr^{-1} in a middle-aged larch forest in July; 300–340 mg g^{-1} hr^{-1} in a reforested larch forest; and 110–150 mg g^{-1} hr^{-1} in pine forest. Cowberries and wintergreen grasses in individual blade used much less soil moisture (approximately 300 mg g^{-1} h^{-1}), whereas the transpiration intensity of Arctus, beans, and cereals ranged from 600 to 700 mg g^{-1} h^{-1}. In reforested larch forests, transpiration flux is comparable to forest stand flow, because the leaf biomass of the herb–dwarf shrub layer can reach one-half of the volume of the needle biomass of a larch tree.

Based on observations of the thawing soil layer in permafrost (Pozdnyakov 1975), vertical movement of soil moisture, rather than horizontal, is clearly the dominant. This is influenced more greatly by the short residence time of water in its liquid form than by the infiltration properties of subsoils; there is a small amount of precipitation and inhomogeneity in the relief of the frozen confining layer. The

water cycles of soils under these conditions are determined mainly by the effects of atmospheric precipitation and moisture flow on transpiration and evaporation.

During the growing season, soil moisture in the root layers of permafrost–taiga soils under the most common types of larch forests generally does not exceed the smallest water capacity volume. The moisture capacity of the lowest soil layer above the permafrost is often above that index. The middle soil layers become drier than lower and upper active layers in the permafrost region (Savvinov 2013).

1.3.1.4 Water Balance

The forest water balance can be determined to examine the total flow of moisture in transpiration and evaporation. According to Zolnikov (1954b), 80 km south from Yakutsk (Porrovsk), the annual soil water evaporation in a cowberry–larch forest was 163 mm, and in a fallow land 141 mm. From 1955 to 1956 in a 50-year-old larch forest in Central Yakutia, the annual total flow was 213 mm; in a 100-year-old forest, it was 169 mm; and in two plots of a 90-year-old larch forest, it was 184 and 174 mm (Utkin 1960). The annual water evaporation was 155 and 188 mm during 1967 and 1968, respectively (Savvinov 1971). In 1961, the evaporation observations at Spasskaya Pad were 177 mm in a 50-year-old larch forest, 210 mm in a 130-year-old forest, and 158 mm in the deforested plots of a larch forest. Since the period 1952–1961, evaporation from the afforested basin of the small Shestakovka River, near Yakutsk, was calculated by the difference between precipitation and runoff and averaged 195 mm. In southwestern Yakutia, the discharge of the soil layer in a cowberry–larch forest was measured in 1966: the discharge was 190 mm in an alder tree stand; 236 mm in a deforested plot in the same forest type; 186 mm in a larch forest with pine–cowberry–moss; 240 mm in a grass sward. In 1967, discharges of soil moisture of these areas were 139, 218, 145, and 206 mm, respectively, for the above four forest types (Savvinov 1971). Thus, in a warm season, reforested larch forests in southwestern Yakutia discharged 140–190 mm of moisture; in Central Yakutia, 180–200 mm for the hydrological year; and in the northern part of the Sakha Republic, 130–150 mm during summer (June, July and August). A portion of the rainfall, up to 20–25%, was intercepted by forest canopy and evaporated into the atmosphere. The supply of moisture to the soil decreased by this amount, and these phenomena reduced the overall level of productive flow of soil moisture on transpiration in trees.

1.3.2 Carbon Dioxide Cycles in the Soviet Union

1.3.2.1 Outline of Carbon Dioxide Cycles

During the Soviet period, few researchers in few publications examined the carbon dioxide cycle in forest ecosystems in Yakutia, and these studies were mainly concerned with permafrost soil.

1.3.2.2 Microbiology in Permafrost

During 1952–1953, soil and microbiological studies were conducted in Olyokminsky District in Yakutia (Mazilkin 1956). In particular, the rate of humus decomposition was determined through the study of biological activity of permafrost soil by common chemical-based method (Shtatov 1952). Research revealed that in sod–forest pale soils (similar to the soils of Central Yakutia), carbon dioxide emissions were considerably accelerated in July, at a rate of 0.99 gC m^{-2} day^{-1}; in August, 0.95 gC m^{-2} day^{-1}; the monthly equivalent was 29.45 gC m^{-2} per month or 28.90 gC m^{-2} per season (JJA). In permafrost, cold soils greatly slowed the processes of organic matter mineralisation. The principal role in this process belonged to numerous basidiomycetes and microfungi, which completed the first stage of decomposition of plant remains. Cellulose-fermenting and nitrifying bacteria were insufficient for these processes, and fulvic acids and insoluble precipitate dominated in the humus composition of permafrost pale soils. A sufficient amount of spore bacteria was related to the intensity of the soil absorption in basement complexes (in particular, calcium). A few *Azotobacter* are the subject of unanswered questions; the relatively high content of nitrogen observed in permafrost soils remains unexplained (Mazilkin 1956). Probably, these values could be underestimated due to not relevant or inaccurate chemical method.

At Spasskaya Pad in Central Yakutia, studies were conducted on soil biological activity expressed by the amount of carbon dioxide released from forest ecosystems (Pozdnyakov 1975). This process was studied in different forest types at the Spasskaya Pad station from April to September in 1962. In a 130-year-old larch forest, daily average carbon dioxide emissions amounted to 1.75 gC m^{-2}. The emission of carbon dioxide flux amounted to 38.18 gC m^{-2} during 3 months, which corresponded to approximately 2.5 t ha^{-1} of decomposed organic matter, i.e. approximately 3 tons for the entire warm period (May–September). The organic matter decomposition occurs mainly due to the decay of needles, and their proportion in the leaf fall (88%) was higher than in the forest litter (76%).

During 1977–1980, research on soil biological activity in permafrost was conducted in South Yakutia (Konorovskiy 1984). Measurements of the carbon dioxide release intensity revealed that uprooting trees on podzolic soil enhanced the decomposition of soil organic matter. The annual average intensity of soil carbon dioxide emissions was estimated: for 1977, 1.57 gC m^{-2} day^{-1} (maximum: 2.29 gC m^{-2} day^{-1}); for 1978, 1.83 gC m^{-2} day^{-1} (maximum: 2.49 gC m^{-2} day^{-1}); for 1979, 2.29 gC m^{-2} day^{-1} (maximum: 3.27 gC m^{-2} day^{-1}); and for 1980, 3.53 gC m^{-2} day^{-1} (maximum: 4.45 gC m^{-2} day^{-1}). It was very dry in 1977, 1978, and the first half of 1979, and the dry atmospheric conditions resulted in low CO_2 emissions. In the second half of 1979 and 1980, optimal soil moisture conditions were recorded. During these years, soil respiration rates consistently increased, and this condition was also associated with high temperatures in the soil surface layers. Soil microflora activity was very high (1.5–3 kg CO_2 ha^{-1} h^{-1}), even at low

soil temperatures (5–10 °C), due to the adaptability of soil and rhizosphere microflora to intensive activity at low positive temperatures in permafrost.

In 1984, a study on biological activity in a chernozem permafrost meadow was conducted at the Amga River (Volotovskaya and Savvinov 1988). It revealed that carbon dioxide emission values were higher in virgin land under well-developed meadow steppe vegetation (6.5–4.0 kg CO_2 ha^{-1} h^{-1}) than on farmland (4.0–-3.0 kg CO_2 ha^{-1} h^{-1}). All carbon dioxide released was the result of the mineralization and humification of organic matter, whereas half of the volume of carbon dioxide was emitted by roots in soil containing plants in the permafrost during the respiration process. The maximum carbon dioxide emissions occurred during the day (10–19 h), while soil carbon dioxide emissions were reduced at night (1–7 h) during growing season.

In 1985, near Pokrovsk, 70 km south of Yakutsk, Savvinov and Sleptsov (1987) performed a comprehensive study of pale solodic soil in permafrost. They found that biological activity was insufficiently intense in permafrost and that the total carbon dioxide production in permafrost soils was higher than the level of enzymatic activity of soil; they were unable to explain this phenomenon. Research on the potential activity of hydrolytic enzymes in these soils revealed that enzymatic activity was poor in forest soils in the permafrost area and increased with agricultural use.

In our opinion, the relatively high rates of carbon dioxide emission from virgin land are probably associated with the activities of herbaceous and woody plants, and the lower rates are associated with a reduction in temperature under the influence of artificial irrigation.

The carbon dioxide flux in forest ecosystems in eastern Siberia was not rigorously investigated during the Soviet period, and the carbon dioxide flux due to biophysical and biochemical activities by forest vegetation is an important issue that remains to be thoroughly studied in permafrost regions.

1.3.3 Permafrost Dynamics Studies During the Soviet Period

1.3.3.1 Outline of Permafrost Dynamics

The first scientific observations of permafrost temperature dynamics were made by A.F. Middendorf in 1844, in the ‘Shergin Shaft’ to a depth of 116 m; this work provided a basis for estimates of permafrost thickness in the Yakutsk area (Middendorf 1862). However, by the late nineteenth–early twentieth century, scientists from other disciplines began to conduct research from the perspective of permafrost dynamics. Zubrilov (1891), for example, related lake development in central Yakutia to the melting of ground ice, and Abolin (1929) studied vegetation and soils in the Lena–Viluy interfluve in connection to thaw depths.

1.3.3.2 Observational Studies of Permafrost

In the late 1920s and early 1930s, active development of natural resources began in eastern Siberia, which necessitated the study of permafrost conditions in mining and construction areas. Under the chairmanship of V.A. Obruchev, the USSR Academy of Sciences established a commission for the study of permafrost in 1930, which was later reorganised into a Committee for permafrost studies in 1936. In 1938, a Yakutian expedition was organised by the Academy's Council for Investigation of Productive Resources, which conducted comprehensive studies of permafrost in central Yakutia. This expedition led to the establishment of a permafrost station of the Obruchev Permafrost Institute at Yakutsk in 1941. Since then, permafrost research in eastern Siberia has been carried out in a regular and systematic manner.

The first permafrost studies at the Yakutsk Permafrost Station focused on groundwater exploration for a municipal water supply in central Yakutia. In 1940, a Yakutsk artesian basin was discovered. Research at the station also included fundamental studies of different aspects of permafrost, such as hydrogeology (Melnikov and Efimov 1953), formation of the ice complex (Shumsky 1952), cryofacies analysis (Katasonov 1954), origin of alasses (Soloviev 1959), and physical and mechanical properties of frozen soils (Votyakov 1961). Investigations during this period specified the science of geocryology as the subject matter and laid the groundwork for studies of permafrost dynamics.

Geocryological studies were expanded with the establishment of the North-Eastern Department of the Obruchev Permafrost Institute of the USSR Academy of Sciences in 1956 and its reorganisation to the Permafrost Institute subordinate to the Siberian Branch of the Academy in 1960. This stage was a period of extensive regional studies and data collection for subsequent studies of permafrost dynamics. During this period, the general observation areas were southern Yakutia (Fotiev 1965), the coastal lowlands of Yakutia (Grigoriev 1966), the Verkhoyansk Mountains (Shvetsov 1968), and the mountainous regions of eastern Siberia (Lugovoi 1970). These expeditions were comprehensive, covering almost all aspects of permafrost. Expeditions in the Upper Viluy River in western Yakutia (Balobaev 1963) and in the Suntar-Hayata Range as part of the First Geophysical Year programme (Grave et al. 1964) included monitoring observations, which made it possible to identify seasonal and interannual patterns in the distribution of heat transfer components within the atmosphere–permafrost system.

In the 1970s and 1980s, a number of fundamental generalisations about permafrost conditions were published regarding the climate of central Yakutia (Gavrilova 1973), the glaciation and permafrost of the southern Verkhoyansk Mountains (Nekrasov et al. 1973), the permafrost systems of the Yana River basin (Nekrasov and Deviatkin 1974), and icings and groundwater in permafrost of the north-eastern USSR (Tolstikhin 1974). An expedition of the Moscow State University in southern Yakutia yielded major generalizable results, which revealed the main regularities of the distribution and development of permafrost in mountainous areas of southern Siberia (Trush et al. 1975). Nekrasov (1976) summarized the results of long-term

permafrost investigations focusing on permafrost thickness and temperature in north-eastern and southern Siberia. These investigations helped clarify the latitudinal and altitudinal relationships of permafrost distribution, which are all widely used today by researchers engaged in current studies of permafrost dynamics in the region. Temperature measurements conducted during those decades provide baseline data for studies of current climate warming effects.

E.M. Katasonov and his followers on cryofacies analysis described the development of the cryogenic processes that lead to negative consequences and the degradation of permafrost (Katasonov et al. 1979; Ivanov 1984). The cryogenic structure, age, mineralogical composition, and depositional sequence of permafrost sediments, as well as the type and amount of ground ice contained in permafrost, play an important role in the transformation and dynamics of permafrost landscapes. In the USSR, first studies in the USSR on permafrost stability to anthropogenic impacts were conducted in the 1980s. Grave (1979) and Brown and Grave (1981) were the pioneer of these types of research. Further studies assessed permafrost sensitivity in the coastal lowlands (Kuznetsova 1980), in the Leno–Aldan interfluve (Bosikov et al. 1985), and in the middle reaches of the Lena River (Stashenko 1987a). Permafrost dynamics and stability are directly related to climate change, and these investigations in eastern Siberia provided important information (Gavrilova 1978, 1981, 1987). The results ranged from the identification of permafrost materials that were stable or unstable to external effects on permafrost.

In the 1980s, landscape geography methods were introduced to permafrost dynamics studies. Landscape maps began to display spatial and temporal models of permafrost development. By identifying the patterns of vegetation succession, researchers began to study permafrost recovery following disturbance (Fedorov 1985; Stashenko 1987b). Under these conditions, studies of permafrost landscapes were in high demand (Vasiliev 1982; Bosikov et al. 1985). The findings revealed the high diversity of permafrost landscapes and variations in response to climate change and anthropogenic effects.

1.3.3.3 Modelling Investigations of Permafrost

Modelling the heat transfer from the atmosphere to the lithosphere is one of the main methods of permafrost dynamics studies. In eastern Siberia, this area of research was developed by Feldman (1984), Feldman et al. (1988), and Shur (1988) to predict thermokarst development and ground temperature changes. Balobaev (1991) studied the dynamics of permafrost thickness in eastern Siberia by modelling heat fluxes in permafrost. His studies were accompanied by the collection of large amounts of field data, which were then compiled into a geothermal database at the Melnikov Permafrost Institute.

1.3.3.4 Monitoring Observations in Permafrost

Monitoring observations were an important part of Soviet permafrost research in eastern Siberia. The first year-round observations of permafrost dynamics in eastern Siberia were conducted by the Northern Expedition of the Yakutsk Permafrost Station of the Obruchev Permafrost Institute at Kazachye in the Yana River estuary from 1952 to 1953 and at Chokurdakh in the Lower Indigirka River from 1952 to 1954. Further, long-term monitoring studies were conducted in the Irelyakh River area in western Yakutia from 1956 to 1959, at Tyungyulyu in central Yakutia from 1961 to 1963, on Muostakh Island in the Laptev Sea from 1962 to 1966, at Yakutsk from 1964 to 1984, etc. The findings from these studies have been reported in voluminous published and unpublished papers, available at the Melnikov Permafrost Institute in Yakutsk.

A considerable amount of literature was published during the Soviet period by the Industrial and Scientific Research Institute for Engineering Survey in Construction and All-Russian Scientific Research Institute of Hydrogeology and Engineering Geology, Moscow State University, and other organisations that described geotechnical and permafrost conditions in Siberian regions (Fotiev et al. 1974: Trush et al. 1975: Ospennikov et al. 1980: Shur 1988). Field research results with specific, factual data were published in these scientific articles. An important event for geocryological science in the Soviet period was the release of five volumes of the book *Geocryology of the USSR*, two volumes of which were devoted to eastern Siberia: Middle Siberia (Kondratieva et al. 1989) and Eastern Siberia and the Far East (Romanovskii et al. 1989). This monograph contained all of the data collected on permafrost during this period. A cartographic generalisation of this work was published much later (Kondratieva et al. 1996).

In conclusion, during the Soviet period of study, the foundations were laid in eastern Siberia to study the dynamics of permafrost. Patterns of permafrost distribution were determined, and methods were developed for stationary studies, landscape differentiation, and mathematical modelling. All these processes of permafrost research allowed us to continue studying the dynamics of permafrost in the period of global warming, to create cartographic models of permafrost in the regions and in Russia as a whole, thereby ensuring the successful development of geocryology in the post-Soviet period.

1.3.4 Soil Investigation for the Soviet Union

The first physical and chemical studies of soil in boreal areas were carried out by the members of the Resettlement Department expedition of tsarist Russia during 1909–1914 in Yakutia. At that time, soil–geobotanical studies covered some parts of the Lena–Vilyui watershed, the Lena–Aldan plateau, the valley of the Lena and Vilyui Rivers, the area near the coast of the Okhotsk Sea, and the Ayan–Nelkan area.

These expeditions established boundaries in the research field of soil layer zones and provided rich material for the preparation of Russian soil maps. They yielded practical conclusions on the suitability of land for different crops, and agronomic experiments were conducted in permafrost field research (Dolenko 1913, 1916; Drobov 1914). Soils developed under taiga forest were attributed to the podzolic type, and the first of these were the widespread saline soils in the Lena and Vilyui Rivers. This field investigation revealed that the soil frost table was extremely widespread in Far East of Siberia and that permafrost involved a number of peculiar phenomena observed in relation to changes in the forms of relief and to the processes of soil formation (Glinka 1923). At that time, it was already known that the presence of permafrost has a significant effect on natural components.

Since 1925, the soil cover of Central Yakutia has been studied in a comprehensive expedition of the USSR Academy of Science. Research teams in the Verkhoyansk mountain range investigated in three comprehensive expedition groups: the soil group, the geomorphological group, and the botanical group. These studies were the basis of a scientific monograph on the soils of Yakutia (Krasyuk and Ognev 1927). In 1926, research on soil study had covered the lower reaches of the Vilyui and Tyung Rivers, and the results of this field campaign were published in a monograph, which established the absence of sharply expressed podzolic soils and the presence of solodised soils under taiga vegetation (Blagovidov 1935). These results were expressed in widespread soil complexes inherent in steppe areas within the forest zone (Glinka 1927). Abolin (1929) reported that permafrost in the arid conditions of Central Yakutia was an accumulator of autumn surplus and a water supply for vegetation, particularly during the first half of the next summer's growing season. The first data on carbon and nitrogen content in soils were collected from permafrost areas: the largest concentrations of carbon stocks were found in the upper layers of alas soil, which reached 10–11%, followed by alluvial soils in river valleys at 5.6–8%. The lowest carbon content was recorded in the humus horizons of forest soils: 0.8–2.5%. The total nitrogen content in the same horizons was 0.5–0.7%, 0.8%, and 0.2%, respectively. The results of this field observation were presented in the first soil survey maps of the studied areas, along with recommendations for the priority development of 60,000 ha of land under cultivation with dark-coloured soils in the valleys of the Lena and Amga Rivers in eastern Siberia (Abolin 1929).

During the period 1938–1940, Soviet Union expeditions were conducted by the Agronomic Institute of Fertilizers and Agricultural Chemistry. For the first time, researchers explored permafrost soil layers, focusing on nutrients, heat and water regimes, agro-physical and physical properties, and the microflora compositions of the most typical soils. The weak mobility of nitrogen in permafrost soils was revealed, which is sharply reduced in soil (from 11–12 mg to 3–4 mg N per 100 g of soil) from the beginning of the growing season to the autumn. Microbiological studies revealed that bacterial flora were generally concentrated in a thin upper layer (15–20 cm), and the underlying soil horizons were very poor in terms of microorganisms (Tsyplenkin 1946).

The systematic study of soil science was continued by the Institute of Biology of the Yakut Branch of the USSR (now IBPC SB RAS). Soil investigations were led by

Dr. Zolnikov from 1947 to 1960, by Prof. Elovskaya from 1960 to 1992, by Dr. Konorovsky from 1992 to 1993, and since 1994 by Dr. Desyatkin. Under their leadership, soil science was studied as a facet of geography, and the genesis of permafrost soils regarding morphological and physiochemical characteristics, classification and taxonomy of soil differences and soil inventories, and the registration of land resources, measures for rational use, and protection of soils emerged in eastern Siberia (Desyatkin 2008). From the second half of the 1950s, the soils of circumpolar and mountainous areas and islands of the Arctic Ocean were investigated by soil scientists at the Soil Institute and the Institute of Geography of the USSR. Their findings were published in academic journals (Ivanova 1965, 1971; Gerasimov 1952, 1985; Karavaeva 1969; Targulian 1971; Naumov and Gradusov 1974). In a vast territory, exceeding 3 million km^2, a wide variety of geological and geomorphological structure and relief (42% plains and 58% mountains), the presence of three latitudinal climatic zones on the flat part and a number of vertical belts in the mountains, and an abundance of water bodies in conditions of widespread permafrost has led to a wide variety of soil cover in permafrost regions. Based on the methods described above, the soil types were classified into 44 types and 67 subtypes of soils (Elovskaya 1987).

On the basis of soil cover geographical research conducted in Yakutia, a series of soil maps in the region were compiled and published in different scales, including 30 sheets of soil maps at a scale of 1:1,000,000 (State Soil Map, 1980–1989). From the early 1950s, research on soil processes was conducted in different natural areas of the Sakha republic. Soil processes were studied at research stations, revealing the specific nutrient, water, heat, and salt regimes of permafrost soils and their biological activities. These studies established the exclusive influence of cryogenic processes in soil formation and functioning. The environmental conditions in forests and tundra allow vegetation to grow in the harsh and arid conditions of the boreal regions.

1.4 Concluding Remarks

In this section, we described the background for the studies of water and carbon dynamics of eastern Siberia. The regional characteristics of hydrological and climate systems include cool temperatures, especially in winter, and small amounts of precipitation. We provided measurements regarding water and carbon dynamics and the permafrost and soil layers in eastern Siberia during the regime of the former Soviet Union.

Among outside of Russia, the scientific history of research on water and carbon dioxide cycles in eastern Siberia is relatively new, and research contributions in this region began in the second half of the 1990s. Here, we described the particular environmental conditions for the climate and the permafrost systems in eastern Siberia. The permafrost systems constituted strong, cold air percolation from a ground surface that had been free of glaciers for 70,000 years. The vegetation of larch forests persists in cold temperatures, and the reasons for the current global

distribution of larch forests are established. The type of larch forest in eastern Siberia is called the 'light taiga'. In the tundra, where the vegetation systems were located in the northern part of the 'light taiga', the limiting factors for vegetation are ground and surface water quality, not cold temperatures. The climate, permafrost, and vegetation form the complex characteristics of this symbiotic system of eastern Siberia.

This chapter has provided a more comprehensive understanding of the work completed by researchers in Russia, Japan, and other countries about water and carbon dioxide dynamics in eastern Siberia.

References

Abolin RI (1929) Geobotanical and soil description Leno-Vilyui plains. USSR Academy of Science, Leningrad, p 378. (in Russian)

Arneth A, Makkonen R, Olin S, Paasonen P, Holst T, Kajos MK, Kulmala M, Maximov TC, Miller PA, Schurgers G (2016) Future vegetation-climate interactions in Eastern Siberia: an assessment of the competing effects of CO_2 and secondary organic aerosols. Atmos Chem Phys 16:5243–5262. https://doi.org/10.5194/acp-16-5243-2016

Baldocchi D, Kelliher FM, Black TA, Jarvis P (2000) Climate and vegetation controls on boreal zone energy exchange. Glob Chang Biol 6:69–83. https://doi.org/10.1046/j.1365-2486.2000.06014.x

Balobaev VT (1963) Thawing of frozen ground in interaction with the atmosphere. In: Heat and mass exchange in frozen soils and rocks. USSR Academy of Sciences, Moscow, pp 105–123. (in Russian)

Balobaev VT (1991) Geothermal of frozen zone of lithosphere in Northern Asia. Nauka, Novosibirsk, p 194. (in Russian)

Blagovidov NL (1935) Quaternary deposits, climate and soils of Tyung river basin. Works of Natural Resources Study Council. Yakutia series, vol 18, p 128. (in Russian)

Bonan GB (1995) Land-atmosphere CO_2 exchange simulated by a land surface process model coupled to an atmospheric general circulation model. J Geophys Res 100:2817–2831

Bonan GB, Shugart HH (1989) Environmental factors and ecological processes in boreal forests. Annu Rev Ecol Syst 20:1–28

Bonan GB, Pollard D, Thompson SL (1992) Effects of boreal forest vegetation on global climate. Nature 359:716–718. https://doi.org/10.1038/359716a0

Bosikov NP, Vasiliev IS, Fedorov AN (1985) Permafrost landscapes of reclaimed zone of Leno-Aldan interfluve. Permafrost Institute, Yakutsk, p 124. (in Russian)

Brown J, Grave NA (1981) The surface disturbance and its protection during economic development of northern areas. Nauka, Novosibirsk, p 88. (in Russian)

Carlson AE, Winsor K (2012) Northern Hemisphere ice-sheet responses to pat climate warming. Nat Geosci 5:607–613. https://doi.org/10.1038/ngeo1528

Ch K, Diemer M (1987) In situ photosynthetic responses to light, temperature and carbon dioxide in herbaceous plants from low and high altitude. Funct Ecol 1:179–194

Desyatkin RV (2008) Soil formation in thermokarst depressions – alases of cryolithozone. Nauka, Novosibirsk, p 324. (in Russian)

Dixon RK, Brown S, Houghton RA, Solomon AM, Trexler MC, Wisniewski J (1994) Carbon pools and flux if global forest ecosystems. Science 263:185–190. https://doi.org/10.1126/science.263.5144.185

Dolenko GI (1913) The Lena River valley near Yakutsk. In: Glinka KD (ed) Preliminary report of Russian Asia soil investigation organization and fulfillment in 1912. Publishing house of Erlikh Yu. N, St. Petersburg, pp 221–224. (in Russian)
Dolenko GI (1916) The parts of the Lena-Vilyui basin of Yakutskaya oblast. In: Glinka KD (ed) Preliminary report ofRussian Asia soil investigation organization and fulfillment in 1914. Publishing house of Kollins A.E, St. Petersburg, pp 251–262. (in Russian)
Drobov VP (1914) Vegetation of Yakutsk-Ust Maya road region of Yakutskaya oblast. Publishing house of Kollins A.E, St. Petersburg, p 251. (in Russian)
Elovskaya LG (1987) Classification and diagnostics of permafrost soils of Yakutia. Yakut branch of the Siberian Branch of the USSR Academy of Sciences, Yakutsk, 172p. (in Russian)
Ensminger I, Sveshnikov D, Campbell DA, Funk C, Jansson S, Lloyd J, Shibistova O, Oquist G (2004) Intermittent low temperatures constrain spring recovery of photosynthesis in boreal Scots pine forests. Glob Chang Biol 10:995–1008. https://doi.org/10.1111/j.1365-2486.2004.00781.x
Ermakov N, Cherosov M, Gogoleva R (2002) Classification of ultracontinental boreal forests in central Yakutia. Folia Geobot 37:419–440. https://doi.org/10.1007/BF02803256
Fedorov AN (1985) The role of logging in the permafrost landscapes development in Central Yakutia. Permafrost Institute, Yakutsk, pp 111–117. (in Russian)
Feldman GM (1984) Thermokarst and permafrost. Nauka, Novosibirsk, p 261. (in Russian)
Feldman GM, Tetelbaum AS, Shender NI, Gavriliev RI (1988) Handbook of temperature forecast of the soils in Yakutia. Permafrost Institute, Yakutsk, p 240. (in Russian)
Fotiev SM (1965) Groundwater and permafrost of the South Yakutian coal-bearing basin. Nauka, Moscow, p 230. (in Russian)
Fotiev SM, Danilova NS, Sheveleva NS (1974) Geocryological conditions of the Middle Siberia. Nauka, Moscow, p 148. (in Russian)
Gavrilova MK (1967) Thermal balance of larch forests in Leno-Amga interfluve area. Hydroclimatic research in the forests of Siberia. Nauka, Moscow, pp 28–52. (in Russian).
Gavrilova MK (1973) Climate of Central Yakutia. 2nd edn. Book Publishing House, Yakutsk, p 120. (in Russian).
Gavrilova MK (1978) Climate and long-term freezing of rocks. Nauka, Novosibirsk, p 214. (in Russian)
Gavrilova MK (1981) Recent climate and permafrost on the continents. Nauka, Novosibirsk, p 112. (in Russian)
Gavrilova MK (1987) Analysis of climatic conditions in Yakutia to the beginning of the next century. In: Natural conditions in the reclaimed regions of Siberia. Permafrost Institute, Yakutsk, pp 146–159. (in Russian)
Gerasimov IP (1952) Modern remnants of late glaciations phenomena near the coldest region of the world. News of Academy of Science of USSR. Geography series, vol 5, pp 16–22. (in Russian).
Gerasimov IP (1985) Ecological problems of past, present and future geography of the world. Наука, Moscow. p 247. (in Russian)
Glinka KD (1923) Soils of Russia and surrounding countries. Moscow. p 348
Glinka KD (1927) Essay of Yakutia soils. Yakutia, pp 131–164. (in Russian)
Gower ST, Krankina O, Olson RJ, Apps M, Kinder S, Wang C (2001) Net promary production and carbon allocation patterns if boreal forest ecosystwm. Ecol Appl 11:1395–1411
Grave NA (1979) Principles of surface sensitivity evaluation on anthropogenic impacts. In: Nature protection of Yakutia. Yakutsk branch of USSR Academy of Sciences, pp 91–94. (in Russian)
Grave NA, Gavrilova MK, Gravis GF (1964) Freezing of Earth surface and glaciation of Syntar-Hayata (Eastern Yakutia). Nauka, Moscow, p 143. (in Russian)
Greene DF, Zasada JC, Sirois L, Kneeshaw D, Morin H, Charron I, Simard M-J (1999) A review of the regeneration dynamics of Northern American boreal tree species. Can J For Res 29:824–839. https://doi.org/10.1139/cjfr-2015-0439
Grigoriev NF (1966) Permafrost in littoral zone of Yakutia. Nauka, Moscow, p 180. (in Russian)

Halldin S, Gryning S-E, Gottschalk L, Jochom A, Lundin L-C, van de Griend AA (1999) Energy, water and carbon exchange in a boreal forest landscape – NOPEX experiences. Agric For Meteorol 98–99:5–29. https://doi.org/10.1016/S0168-1923(99)00148-3

Hiyama T, Ohta T, Sugimoto A, Yamazaki T, Oshima K, Yonenobu H, Yamamoto K, Kotani A, Park H, Kodama Y, Hatta S, Fedorov AN, Maximov TC (2013) Changes in eco-hydrological systems under recent climate change in eastern Siberia. IAHS Publ 360:155–160. https://iahs.info/uploads/dms/15562.29-155-160-360-09-Hiyama_et_al.pdf

Huh Y, Panteleyev G, Babich D, Zaitsev A, Edmond JM (1998) The fluvial geochemistry of rivers of Eastern Siberia: II. Tributaries of the Lena, Omoloy, Yana, Indigirka, Kolyma, and Anadyr draining the collisional/accretionary zone of the Verkhoyansk and Cherskiy ranges. Geochim Cosmochim Acta 62:2053–2075. https://doi.org/10.1016/S0016-7073(98)00127-6

Huntington TG (2006) Evidence for intensification of the global water cycle: review and synthesis. J Hydrol 319:83–95. https://doi.org/10.1016/jhydrol.2005.07.003

Iijima Y, Fedorov AN, Park H, Suzuki K, Yabuki H, Maximov TC, Ohata T (2010) Abrupt increases in soil temperature following increased precipitation in a permafrost region, central Lena River basin, Russia. Permafr Periglac Process 21:30–41. https://doi.org/10.1002/ppp.662

Ivanov MS (1984) The cryogenic structure of Quaternary deposits of the Leno-Aldan depression. Nauka, Novosibirsk, p 125. (in Russian)

Ivanova EI (1965) Permafrost-taiga soils of Northern Yakutia. Pochvovedenie 7:1–14. (in Russian)

Ivanova EI (1971) Soils of Central Yakutia. Pochvovedenie 9:3–17. (in Russian)

Karavaeva NA (1969) Tundra soils of Northern Yakutia. PhD thesis, Moscow, p 205. (in Russian)

Katasonov EM (1954) Lithology of frozen Quaternary deposits of the Yana coastal lowland. Thesis of Candidate of geology-mineralogical science, Moscow, p 26. (in Russian)

Katasonov EM, Ivanov MS, Pudov GG. 1979 In: Katasonov (ed) The structure and absolute geochronology of alas deposits in Central Yakutia. Nauka, Novosibirsk, p 95. (in Russian)

Kelliher FM, Hollinger DY, Schulze E-D, Vygodskaya NN, Byers JN, Hunt JE, McSeveny TM, Milukova I, Sogatchev A, Varlargon A, Ziegler W, Arneth A, Bauer G (1997) Evaporation from an eastern Siberian larch forest. Agric For Meteorol 85:135–147. https://doi.org/10.1016/S0168-1923(96)02424-0

Kondratieva KA, Fotiev SM, Danilova NS (1989) Geocryology USSR. In: Ershov (ed) Middle Siberia. Nedra, Moscow, p 413. (in Russian)

Kondratieva KA, Afanasenko VE, Gavrilov AV (1996) Geocryological map of the USSR. Scale 1:2 500 000. Edited by Ershov.Central Department of Geodesy and Cartography, Vinnitca, 16p. (in Russian)

Konorovskiy AK (1984) Soils of the northern zone of Small Baikal-Amur Mainline. Nauka, Novosibirsk, p 121. (in Russian).

Krasyuk AA, Ognev GN (1927) The soils of the Lena-Aldan watershed. Materials of the Commission to explore Yakutian Autonomous Soviet Socialist Republic. Publishing House of the Academy of Sciences of the USSR, Moscow, p 176. (in Russian)

Kuznetsova IL (1980) Engineering and permafrost conditions and the stability of the permafrost in coastal lowlands of Yakutia to disturbances of the natural environment. In: Stability of the surface to anthropogenic influences in the permafrost. Permafrost Institute, Yakutsk, pp 75–107. (in Russian)

Lawford RG, Stewart R, Roads J, Isemer H-J, Manton M, Marengo J, Yasunari T, Benedict S, Koike T, Williams S (2004) Advancing global- and continental-scale hydrometeorology: contributions of GEWEX hydrometeorology panel. Bull Am Meteorol Soc 85:1917–1930. https://doi.org/10.1175/BAMS-85-12-1917

Liang M, Sugimoto A, Tei A, Bragin IV, Takano S, Morozumi T, Shingubara R, Maximov TC, Kiyashko SI, Velivetskaya TA, Ignatiev AV (2014) Importance of soil moisture and N availability to larch growth and distribution in Arctic taiga-tundra boundary ecosystem, northeastern Siberia. Pol Sci 8:327–341. https://doi.org/10.1016/j.polar.2014.07.008

Liu HY, Yin Y (2013) Response of forest distribution to past climate change: an insight into future predictions. Chin Sci Bull 58:4426–4436. https://doi.org/10.1007/s1143-013-6032-7

Lugovoi PN (1970) Features of the mountain permafrost regions condition. Nauka, Moscow, p 135. (in Russian)

Luyssaert S, Inglima I, Jung M, Richardson D, Reichstein M, Papale D, Piao SL, Schulze E-D, Wingate L, Matteucci G, Aragao L, Aubinet M, Beer C, Bernhofer C, Black KG, Bonal D, Bonnefond J-M, Chamber J, Ciais P, Cook B, Davis KJ, Dolman AJ, Gielen B, Goulden M, Grace J, Granier A, Grelle A, Griffis T, Grunwald T, Guidolotti G, Hanson PJ, Harding R, Hollonger DY, Hutyra LR, Kolar P, Kruijt B, Lagergren F, Laurila T, Law BE, Lemaire G, Lindroth A, Loustau D, Malhi Y, Mateus J, Migliavacca M, Misson L, Montagnani L, Moncrieff J, Moors E, Munger JW, Nikinmaa E, Ollinger SV, Pita G, Rebmann C, Roupsard O, Saigusa N, Sanz MJ, Seufert G, Sierra C, Smith M-L, Tang J, Valentini R, Vesala T, Janssens IA (2007) CO_2 balance of boreal, temperate, and tropical forests derived from global dataset. Glob Chang Biol 13:2509–2537. https://doi.org/10.1111/j.1365-2486.2007.01439.x

Malhi Y, Baldocchi DD, Jarvis PG (1999) The carbon balance of tropical, temperate and boreal forests. Plant Cell Environ 22:715–740. https://doi.org/10.1046/j.1365-3040.1999.00453.x

Mazilkin IA (1956) Microbiological characteristics of sod-forest and humus-carbonate soils of Olyokminsky district in Yakut ASSR. Materials on the environmental conditions and agriculture of south-western Yakutia. AS USSR, Moscow, pp 134–175. (in Russian)

McGuire AD, Wirth C, Apps M, Beringer J, Clein J, Epstein H, Kicklighter DW, Bhatti J, Chapin FS III, de Groot B, Efremov D, Eugster W, Fukuda M, Gower T, Hinzman L, Huntley B, Jia GJ, Kasischke E, Melillo J, Romanovsky V, Shvidenko A, Vaganov E, Walker D (2002) Environmental variation, vegetation distribution, carbon dynamics and water/energy exchange at high latitudes. J Veg Sci 13:301–314. https://doi.org/10.1111/j.1654-1103.2002.tb02055.x

Melnikov PI, Efimov AI (1953) Experience of exploitation of groundwater in the permafrost area in Central Yakutia. USSP Academy of Science, Moscow, p 33. (in Russian)

Middendorf AF (1862) Journey to the North and East of Siberia: North and East of Siberia in a natural historical sense. St. Petersburg. Imperial Acad Sci 1(3):489. (in Russian)

Moors E, Dolman AJ, Maximov TC (2004) Overview of joint research at Spasskaya Pad as part of the PINMATRA and TCOS-Siberia programmes. In: Proceeding of the international semi-open workshop "C/H2O/Energy balance and climate over boreal regions with special emphasis on eastern Eurasia", pp 15–18

Naumov EM, Gradusov BV (1974) Features of taiga soil formation on the Far North-East of Eurasia. Kolos, Moscow, p 147. (in Russian)

Nekrasov IA (1976) Permafrost of the North-East and the South of Siberia and the regularities of its development. Book Publishing House, Yakutsk, p 246. (in Russian)

Nekrasov IA, Deviatkin VN (1974) Morphology of the Yana River basin Cryolithozone and adjacent areas. Nauka, Novosibirsk, p 72. (in Russian)

Nekrasov IA, Maksimov EV, Klimovskii IV (1973). The last glaciation and permafrost of south of Verkhoyansk region. Book Publishing House, Yakutsk, p 151. (in Russian)

Nichol CJ, Lloyd J, Olgahibistova O, Arneth A, Roser C, Knohl A, Matsubara S, Grace J (2002) Remote sensing of photosynthetic-light-use efficiency of a Siberian boreal forest. Tellus 54B:677–687

Ohta T (2010) Hydrological aspects in a Siberian larch forest. In: Osawa A (ed) Permafrost ecosystems. Springer, London, pp 245–269

Ohta T, Hiyama T, Tanaka H, Kuwada T, Maximov TC, Ohata T, Fukushima Y (2001) Seasonal variation in the energy and water exchanges above and below a larch forest in eastern Siberia. Hydrol Process 15:1459–1476. https://doi.org/10.1002/hyp.219

Osawa A, Zyryanova OA, Matsuura Y, Kajimoto T, Wein RW (2010) Permafrost ecosystems – Siberian larch forests, Ecological studies, vol 209. Springer, London, p 502. https://doi.org/10.1007/978-1-4020-9693-8.

Ospennikov EN, Trush NI, Chizhov AB, Chizhova NI (1980) Exogenous geological processes and phenomena (South Yakutia). Moscow State University, Moscow, p 226. (in Russian)

Pozdnyakov LK (1961) Forests in the up-stream flow of Yana river, vol 7. AS USSR, Moscow, pp 142–162. (in Russian)
Pozdnyakov LK (1963) Hydroclimatic regime of larch forests of Central Yakutia. AS USSR, Moscow, p 146. (in Russian)
Pozdnyakov LK (1975) Daurian larch. Nauka, Moscow, p 310. (in Russian)
Romanovskii NN, Gavrilov AV, Zaitsev VN (1989) Geocryology USSR. In: Ershov (ed) Eastern Siberia and the Far East. Nedra, Moscow, p 516. (in Russian)
Sachs T, Wille C, Boike J, Kutzbach L (2008) Environmental controls on ecosystem-scale CH_4 emission from polygonal tundra in the Lena River Delta. Sib J Geophys Res 113:G00A03. https://doi.org/10.1029/2007JG000505
Sakai A (1983) Comparatively study on freezing resistance of conifers with special reference to cold adaptation and its evolutive aspects. Can J Bot 63:156–160
Savvinov DD (1971) Thermal and water regimes of forest soils of Yakutia. Studies on vegetation and soils in the forests of north-eastern USSR. Yakutsk, pp 118–175. (in Russian)
Savvinov DD (2013) Physics of permafrost soils. Nauka, Novosibirsk. p 504. (in Russian)
Savvinov DD, Sleptsov VI (1987) Characteristics and modes of permafrost pale soils. YF SB AS USSR, Yakutsk, p 128. (in Russian)
Schulze E-D, Vygodskaya NN, Tchebakova NM, Czimczik CI, Kozlov DN, Lloyd J, Mollicone D, Parfenova E, Sidorov KN, Varlagin AV, Wirth C (2002) The Eurosiberian transect: an introduction to the experimental region. Tellus 54B:421–428. https://doi.org/10.1034/j.1600-0889.2002.01342.x.
Sellers P, Hall F, Margolis H, Kelly B, Baldocchi D, den Hartog G, Cihlar J, Ryan MG, Godison B, Crill P, Ranson KJ, Lettenmair D, Wickland DE (1995) The boreal ecosystem-atmosphere study (BOREAS): an overview and early results from the 1994 field year. Bull Am Meteorol Soc 76:1549–1577. https://doi.org/10.1175/1520-0477(1995)076<1549:TBESAO>2.0.CO;2
Shashko DI (1961) Climatic conditions of agriculture in Central Yakutia. AS USSR, Moscow, p 264. (in Russian)
Shtatov VI (1952) Methods for determining the biological activity of soil. VASKHNIL report 6, p 27. (in Russian)
Shumsky PA (1952) The study of fossil ice in Central Yakutia. In: Investigation of permafrost in the Yakutskaya ASSR, vol 3. USSR Academy of Sciences, Moscow, pp 142–161. (in Russian)
Shur YL (1988) The upper horizon of permafrost and thermokarst. Nauka, Novosibirsk, p 213. (in Russian)
Shvetsov PF (1968) The regularities of hydrogeological processes in the Far North and North-East of the USSR. Nauka, Moscow, p 111. (in Russian)
Soloviev PA (1959) Permafrost of northern part of the Lena-Amga interfluve. USSR Academy of Sciences, Moscow, p 144. (in Russian)
Stashenko AI (1987a) Evaluation of environmental stability of permafrost areas to anthropogenic influences. Lett USSR Geograph Soc 119(4):301–306. (in Russian).
Stashenko AI (1987b) Study of transformation of permafrost conditions during of reclamation of forest natural complexes in the south of the Central Yakutia. In: Grechishev (ed) Cryogenic physio-geological processes and methods for the study their development. USSR's Scientific Institute of Hydrogeology and Engineering Geology, Moscow, pp 93–100 (in Russian)
Suzuki R, Xu J, Motoya K (2006) Global analyses of satellite-derived vegetation index related to climatological wetness and warmth. Int J Climatol 26:425–438. https://doi.org/10.1002/joc.1256
Targulian VO (1971) Soil formation and weathering in cold humid areas. Nauka, Moscow, p 268. (in Russian)
Tchebakave NM, Kolle O, Zolotoukhine D, Arneth A, Styles JM, Vygodskaya NN, Schulze E-D, Shibistova O, Lloyd J (2002) Inter-annual and seasonal variations of energy and water vapour fluxes above a pine sylvestris forest in the Siberian middle taiga. Tellus 54B:537–551
Tolstikhin ON (1974) Icing and underground waters of the USSR's North-East. Nauka, Novosibirsk, p 164. (in Russian)

Trush NI, Chizhov AB, Chizhova NI (1975) South Yakutia. Edited by. Kudryavtsev.Moscow State University, Moscow, p 444. (in Russian)
Tsyplenkin EI (1946) Agrotechnics of crops in the Yakut Autonomous Soviet Socialist Republic. Yakutsk Publishing House, p 91. (in Russian)
Utkin AI (1960) About natural regeneration of Larch duarica in Central Yakutia. Forestry 12:64–68. (in Russian)
van Huissteden J, Dolman AJ (2012) Soil carbon in the Arctic and permafrost carbon feedback. Curr Opin Environ Sustain 4:545–551. https://doi.org/10.1016/j.cosust.2012.09.008
van Huissteden J, Maximov TC, Dolman AJ (2005) High methane flux from an arctic floodplain (Indigirka lowland, eastern Siberia). J Geophys Res 110:G02002. https://doi.org/10.1029/2005JG00010
Vasiliev IS (1982) The regularities seasonal thawing in Eastern. Nauka, Novosibirsk, p 133. (in Russian)
Velichko A, Spasskaya I (2002) Climatic change and the development of landscape. In: Shahgedanova M (ed) The physical geography of northern Eurasia. Oxford University Press, Oxford, pp 36–69
Volotovskaya TN, Savvinov GN (1988) Biological activity of permafrost-affected meadow-chernozemic soils of Amga river valley. In: Hydrothermic problems of permafrost soils. Nauka, Novosibirsk, p 128. (in Russian)
Votyakov IN (1961) Physical and mechanical properties of permafrost grounds of Central Yakutia. USSR Academy of Science, Moscow, p 63. (in Russian)
Xu L, Baldocchi DD (2003) Seasonal trends in photosynthetic parameters and stomatal conductance of blue oak (Quercus douglasii) under prolonged summer drought and high temperature. Tree Physiol 23:865–877. https://doi.org/10.1093/treephys/23.13.865
Yasunari T (2007) Role of land-atmosphere interaction on Asian monsoon climate. J Meteorol Soc Jpn 85B:55–75. https://doi.org/10.2151/jmsj85B.55
Zolnikov VG (1954a) Topography and soil forming rocks in the eastern part of Central Yakutia. In: Materials on environmental conditions and agriculture in Central Yakutia. AS USSR, Moscow, pp 7–54. (in Russian)
Zolnikov VG (1954b) Soils in the eastern part of Central Yakutia and their applying. In: Materials on environmental conditions and agriculture in Central Yakutia. AS USSR, Moscow, pp 7–54. (in Russian)
Zolnikov VG (1957) Soils in Lensky and Olyokminsky regions of Yakutia and perspectives of their agricultural use. In: Materials on environmental conditions and agriculture in the South-West of Yakut ASSR, vol 2, AS USSR, Moscow, p 113. (in Russian)
Zolnikov VG, Elovskaya LG, Teterina LV, Chernyak EI (1962) Soils of Vilyui basin and its applying. AS USSR, Moscow, p 204. (in Russian)
Zubrilov V (1891) About mineral in Yakutsk region. The memorial book of the Yakutsk region for 1891. Yakutsk Printing-Office, Yakutsk, pp 129–148. (in Russian)

Chapter 2
Atmospheric Water Cycle

Kazuhiro Oshima and Koji Yamazaki

2.1 Introduction

River discharge from the Eurasian continent supplies a large amount of freshwater to the Arctic Ocean and plays an important role in the Arctic climate system, i.e., formations of sea ice and the North Atlantic Deep Water, and in turn the ocean thermohaline circulation which affects climate in Europe and other regions (e.g., Aagaard and Carmack 1989, 1994; Carmack 2000). There are three sources of freshwater inflow into the Arctic Ocean: ocean currents from the Atlantic and Pacific Oceans, river discharge (R) from the surrounding land, and net precipitation (P–ET) from the atmosphere which is the difference between precipitation (P) and evapotranspiration (ET). Among them, the river discharge from the three great Siberian rivers, the Lena, Yenisei, and Ob (Fig. 2.1), accounts for about 20% of the total freshwater inflow, with the Lena River alone accounting for about 7% (based on Serreze et al. 2006; Dickson et al. 2007).

The Lena River, which is the second largest river in the Arctic in terms of discharge, flows in eastern Siberia originating from the Baikal mountains near Lake Baikal (Fig. 2.1) where the climate is characterized by cold temperature and little precipitation. The cold climate induces the formation of river ice during the winter season. The local residents use the freezing river as an ice road for transportation. However, the breaking up of the river ice due to spring warming sometimes causes ice jams and floods (Fujiwara 2011; Sakai et al. 2015). Thus, the condition of the river strongly impacts the residents' lives. Changes in the river condition are mainly governed by the weather; P over the basin affects the R, and regional

K. Oshima (✉)
Japan Agency for Marine-Earth Science and Technology, Yokosuka, Japan

Institute for Environmental Sciences, Rokkasho, Japan
e-mail: oshima@ies.or.jp

K. Yamazaki
Hokkaido University, Sapporo, Japan

T. Ohta et al. (eds.), *Water-Carbon Dynamics in Eastern Siberia*,
Ecological Studies 236, https://doi.org/10.1007/978-981-13-6317-7_2

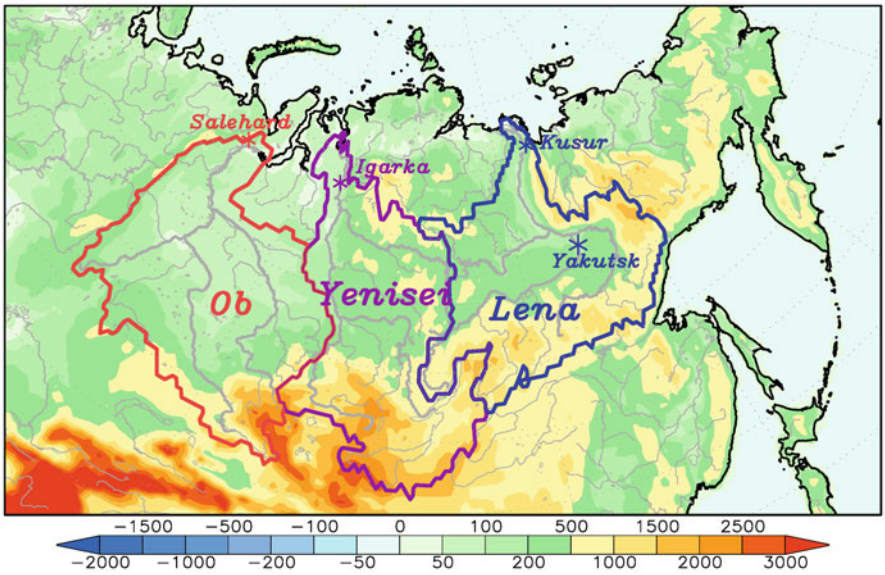

Fig. 2.1 Map of the three great Siberian rivers. Colored contours show the boundaries of each river basin (Lena, blue; Yenisei, purple; Ob, red). Asterisks denote the locations of Kusur, Igarka, and Salekhard, the observation stations nearest the river mouths. Color shades and gray lines show elevation (m) and river channels, respectively

temperatures affect the river ice. The *P* is supplied by moisture transport in the atmosphere, and the temperature is related to large-scale atmospheric circulation over the region.

Features of the atmospheric water cycle reflect the regional differences in the Siberian climate: low surface air temperature (SAT), low humidity, and low *P*, especially in the east. The SAT over the Siberia is relatively warm in the west and cold in the east (e.g., Serreze and Barry 2005; Yamazaki 2010), the result being relatively high humidity in the west and low humidity in the east. The east-west humidity gradient results in relatively high *P* in the west and low *P* in the east (e.g., Takashima et al. 2009). The long distance from the ocean also impacts the lower *P* in the east. The *P* over each Siberian river basin is the source of *R* at each of the river mouths.

While numerous studies have investigated the *R* of Siberian rivers (e.g., Berezovskaya et al. 2004; Ye et al. 2004; McClelland et al. 2004, 2006; Rawlins et al. 2006; Su et al. 2006; MacDonald et al. 2007; Shiklomanov and Lammers 2009; Troy et al. 2011), only a few studies have looked at the linkages among atmospheric circulation, moisture transport, *P*, *P–ET*, and *R* of the Siberian rivers using meteorological data such as atmospheric reanalysis combined with the *R* dataset (Fukutomi et al. 2003; Serreze et al. 2003; Zhang et al. 2012; Oshima et al. 2015). In order to

understand such linkages, it is necessary to examine the Siberian water cycle from an atmospheric perspective.

In this chapter, we review the atmospheric water cycle, in terms of moisture transport, *P–ET*, and *R* in eastern Siberia. While comparisons are made between features across the three great Siberian rivers (Fig. 2.1) in our previous studies (Oshima 2014; Oshima et al. 2015), here we focus on the Lena River in eastern Siberia.

2.2 Climatological Water Budget

On the terrestrial water budget $\partial TWS/\partial t = P - ET - R$, when calculated as a long-term average, the left-hand side of time change in terrestrial water storage (*TWS*) is expected to be negligible. Then *P–ET* as the net input of water to the basin balances with *R* output at the river mouth, i.e., $P - ET \approx R$. The *P–ET* can be estimated from meteorological data based on the atmospheric water budget $P - ET = -\partial PW/\partial t - \nabla \langle q\mathbf{v} \rangle$, where the first and second terms of the right-hand side denote time change in precipitable water (*PW*) which is the amount of water vapor in the atmosphere column and divergence of vertically integrated moisture flux, respectively (e.g., Peixoto and Oort 1983, 1992). As expected, the *P–ET* over the Lena River basin estimated from the Japanese 25-year reanalysis data (JRA-25, Onogi et al. 2007) are almost comparable in magnitude to the observed *R* at Kusur nearest the river mouth (Table 2.1). The (*P–ET*)s over the Yenisei and Ob rivers are also comparable to each of the *R*s. In addition to the results from the JRA-25, the estimates of *P–ET* from the other reanalyses correspond more or less to the observed *R*s in each Siberian river, the discrepancies being about 10–20% (Fukutomi et al. 2003; Serreze et al. 2003; Zhang et al. 2012; Oshima et al. 2015). The discrepancies may be due to differences in the study period, the definition of the basin boundary, the method of calculation, and the dataset. Another possibility is a bias in the

Table 2.1 Climatological means of *R* and *P–ET* for the Lena, Yenisei, and Ob Rivers

River name (area, km^2)	*R* (mm/year) (m^3/s)	*P–ET* (mm/year)	Total MFC	Stationary component of MFC	Transient component of MFC
Lena (2.43×10^6)	228 (1.76×10^4)	204	204	59	145
Yenisei (2.44×10^6)	247 (1.91×10^4)	199	199	112	87
Ob (2.95×10^6)	136 (1.27×10^4)	133	133	127	6

The total, stationary, and transient components of the moisture flux convergences (MFCs) averaged over the individual river basins are also shown. The values are averages from 1980 to 2008. The *R* is from the ArcticRIMS. The *P–ET* and MFCs are estimated from the JRA-25. River basin size is indicated in the first column. Adapted from Oshima and Hiyama (2012)

observations that were assimilated in the reanalysis. If the observations have a dry bias, then *P–ET* will be underestimated. Such a bias is, however, difficult to identify.

The results in Table 2.1 further represent regional differences among the Siberian rivers regarding the relationships between *P–ET* and *R*. The magnitudes of *P–ET* and *R* of the Lena and Yenisei rivers are almost the same, whereas those of the Ob River are smaller. The relatively high *P* over the Ob basin would be expected to result in the largest *P–ET* and *R* among the three rivers, but that is not the case. The large spatial coverage of wetlands and lakes in the Ob basin induces the larger *ET* than those over the other two river basins. Therefore, the regional difference in *ET* over Siberia influences the *P–ET* over the individual river basins. These regional features are also seen in the seasonal cycle and in moisture transport as is discussed in later sections (Sect. 2.3 and 2.4).

The *P–ET* over each river is almost equivalent to the moisture flux convergence (MFC) over the basin. The moisture flux can be decomposed into stationary and transient components, which are interpreted as moisture transport accompanied by seasonal mean wind and cyclone activity, respectively (e.g., Oshima et al. 2015). Over the Lena, the transient component contributes to most of the MFC, whereas the stationary component is the primary contributor over the Ob. Both the components contribute to the MFC over the Yenisei (Table 2.1). This indicates that the *P–ET* over the Lena River is supplied mainly by moisture transport associated with cyclone activity and that over the Ob River is supplied by moisture transport associated with seasonal mean wind. Whereas, the *P–ET* over the Yenisei River depends on both cyclone activity and seasonal mean wind. Thus, the moisture transport process associated with *P–ET* differs among the Siberian rivers.

2.3 Seasonal Cycle

As mentioned in the Introduction (Sect. 2.1), the Lena River basin experiences low SAT and low *P*. Climatological seasonal cycles of SAT averaged over the Lena River basin show a minimum in January (−31.7 °C) and a maximum in July (15.7 °C) with a resulting large annual amplitude (47.4 °C, black line in Fig. 2.2a). The fact that the SAT becomes negative in October and positive in May suggests that the snow season begins in October and ends in May. Indeed, areal snow cover rapidly increases from September to November, decreases from April to June, and is almost at 100% from December to March (gray bars in Fig. 2.2a). Associated with the increase in SAT and decrease in snow cover in spring, *R* shows a maximum in June (red line in Fig. 2.2d), reflecting the rapid increase of *R* due to the snow and river ice melt. This is explained by a temporal change in *TWS* ($\partial TWS/\partial t$) in the river basin, including soil moisture and snow accumulation. The increase in *R* corresponds to large negative value of $\partial TWS/\partial t$ in June, while the positive values of $\partial TWS/\partial t$ during winter reflect *P* accumulation as snow (dashed gray line in Fig. 2.2d). The fact that the *R* is low from November to April reflects frozen river conditions, the duration of which is consistent with the negative SAT.

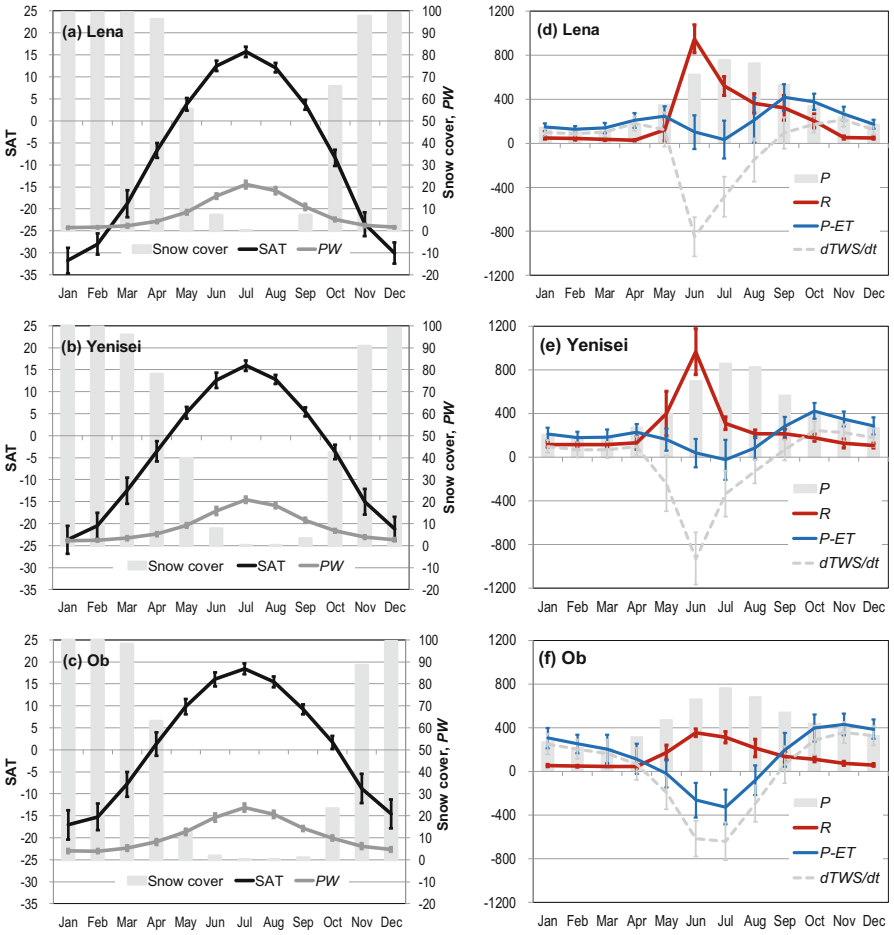

Fig. 2.2 Climatological seasonal cycles of SAT (black line), *PW* (gray line), and snow cover (gray bars) averaged over (**a**) the Lena, (**b**) Yenisei, and (**c**) Ob River basins. (**d**–**f**) Same as in (**a**–**c**), but for *R* (red line), *P*–*ET* (blue line), $\partial TWS/\partial t$ (gray dashed line), and *P* (gray bars) for (**d**) the Lena, (**e**) Yenisei, and (**f**) Ob. The variables are the monthly averages over the period of 1980–2008. Error bars denote the standard deviation during the period. The $\partial TWS/\partial t$ is calculated by subtracting *R* from *P*–*ET*. Note that the axis of the SAT (*PW*, snow cover) is shown on the left (right) side of (**a**–**c**). The SAT, *PW*, and *P*–*ET* are obtained from JRA-25. The *R*, *P*, and snow cover are based on the ArcticRIMS, NOAA PREC/L (Chen et al. 2002), and NOAA NESDIS-CPC (Robinson et al. 1993), respectively. Units of the SAT, *PW*, and snow cover are °C, mm, and %, respectively, and those of the *R*, *P*–*ET*, *P*, and $\partial TWS/\partial t$ are mm year^{-1}. (Adapted from Oshima et al. 2015)

The seasonal cycle of SAT over the Lena is similar to those of *PW* (gray line in Fig. 2.2a) and *P* (gray bar in Fig. 2.2d), which show single peaks in summer. Whereas the *P* reaches maxima in July, the *P*–*ET* shows a minimum value (nearly zero) in that same month (blue line in Fig. 2.2d). This indicates that the *ET* over the Lena basin is as large as the *P* in summer. In addition, the *P*–*ET* shows local maxima

in May and September, and the *ET* affects this seasonal cycle in *P–ET*. While it is hard, if not impossible, to estimate *ET* over a large area based on direct observations, the *ET* simulated by the land surface models (LSMs) shows a maximum peak in summer and is relatively low over the Lena and relatively high over the Ob (Su et al. 2006; Troy et al. 2011; *Handoh* of RIHN, personal communication, 2013). The above features of the seasonal cycles are the same as in the Yenisei and Ob rivers (Figs. 2.2b–c, e–f), but the *P–ET* over the Ob shows negative values in June and July (Fig. 2.2f) due to the large *ET*.

The seasonal cycle and spatial distribution of *ET* may be affected by the seasonal cycle of SAT and the phenology of the boreal forest. A simulation using a LSM with dynamic vegetation indicated that transpiration accounts for about half of the *ET* over the Lena basin (Park et al. 2008). Other simulation using other LSM (Quegan et al. 2011) indicated that transpiration accounts for more than 50% of the *ET* over the three Siberian river basins (*Handoh* of RIHN, personal communication, 2013). These simulated results suggest that transpiration from the boreal forest, which covers vast areas of Siberia, is an important driver in the distribution of *ET* over the region. As pointed out by Serreze et al. (2003), evaporation from lakes, ponds, and bogs is another factor that influences *ET*, especially over western Siberia.

The seasonal cycles of *P–ET* and MFC over the Siberian river basins are roughly equal (see Fig. 3 in Oshima et al. 2015). However, there are some differences between the *P–ET* and MFC in spring and autumn because of non-negligible changes in *PW* in those seasons. Similar to the water budget (Table 2.1), contributions of the stationary and transient components to the total MFC are different in each river basin and also in each season. Over the Lena River basin, the transient component contributes a large part of the total MFC throughout most of the year, although the stationary component dominates in June and July. In contrast, over the Ob River basin, the stationary component dominates throughout most of the year, although both components contribute during the summer. Over the Yenisei River basin, the transient component dominates from May to September, and both components contribute during the other seasons. While cyclone activity over Siberia also has influence on the summer and winter *P* events on daily timescales (Serreze and Etringer 2003), the above results of both the climatological water budgets and the seasonal cycles indicate that the moisture transport process differs in each of the three great Siberian rivers.

2.4 Moisture Transport

The (*P–ET*)s over the Siberian river basins are associated with MFC, that is, moisture transport from the surrounding region. The total moisture flux over Siberia is mostly eastward throughout the year (Figs. 2.3a–d) because of the prevailing westerly winds over the region, indicating that moisture is transported from the Atlantic Ocean side (Fukutomi et al. 2003; Serreze et al. 2003; Kurita et al. 2004; Oshima et al. 2015). As explained in the Introduction, the humidity over Siberia has regional difference; thus, the magnitudes of moisture flux are relatively large in the

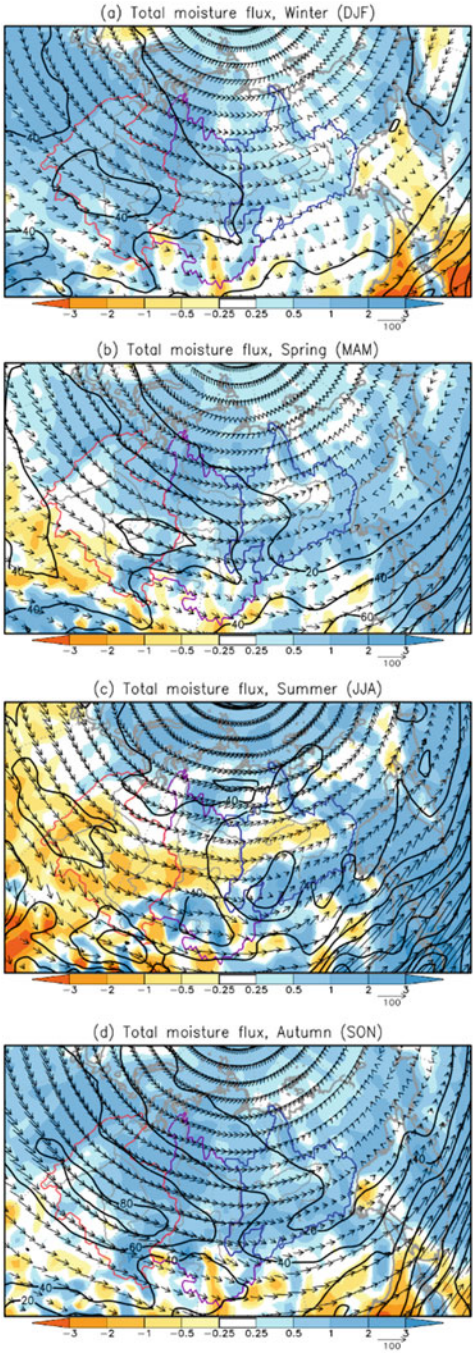

Fig. 2.3 Spatial distributions of vertical integrated moisture flux (vector), its magnitude (contour), and convergence (color) over Siberia in (**a**) winter (December, January, and February), (**b**) spring (March, April, and May), (**c**) summer (June, July, and August), and (**d**) autumn (September, October, and November). Contour interval of the magnitude is 20 kg m^{-1} s^{-1}. These are based on JRA-25. The color and vector scales are indicated at the bottom of each panel. Units of the moisture flux and convergence are kg m^{-1} s^{-1} and mm day^{-1}, respectively. (Adapted from Oshima et al. 2015)

west and small in the east. As a result, the MFC is positive over almost all areas of Siberia in the winter, spring, and autumn (Figs. 2.3a, b, d). The spatial distributions of MFC are similar to those of *P* in each season. On the other hand, moisture flux divergences emerge in summer from the Ob basin through the middle reaches of the Yenisei and Lena rivers (Fig. 2.3c). This indicates that the large *ET* in summer exceeds *P* over these regions. The divergences should activate precipitation recycling in this season (see Sect. 2.5). The spatial distributions of total moisture flux and MFC over the Siberian rivers (Figs. 2.3a–d) seem to be broadly similar to those of the stationary components (Figs. 2.4a–d). This similarity suggests that the seasonal mean wind dominates the total moisture flux over the regions. But the transient components associated with the cyclone activity mainly transport moisture northward (Figs. 2.4e–h). Indeed, the transient moisture fluxes are large over the lower reaches of Ob basin in spring, summer, and autumn and also over the Yenisei and Lena basins in summer.

The upper reaches and eastern side of the Lena River basin, located in the mountainous areas (Fig. 2.1), are MFC areas associated with northward moisture fluxes throughout the year (Figs. 2.3a–e). The transient fluxes contribute a large part of these MFCs (Figs. 2.4e–h); however, the stationary fluxes also contribute to some areas of the basin. The stationary fluxes affect the MFCs over the western side in winter, spring, and autumn (Figs. 2.4a, b, d), over the upper reaches in spring and summer (Figs. 2.4b, c), and over the eastern side of the lower reaches in winter, spring, and autumn (Figs. 2.4a, b, d). In addition, the stationary flux largely contributes to moisture flux divergence over the lower and middle reaches of the basin in summer (Fig. 2.4c). The large contribution of the stationary component in summer is consistent with the results of the seasonal cycle of MFC (Fig. 3f in Oshima et al. 2015). The northward transient flux over eastern Siberia is enhanced especially in summer (Fig. 2.4g), as well as in spring and autumn (Fig. 2.4f, h). This indicates that large amount of water vapor is transported from the southern region of the Pacific Ocean, through the Lena basin and further north to the Arctic Ocean, resulting in a very weak MFC over the basin. The results imply that there is cyclonic activity over all areas of eastern Siberia, including the Lena. Overall, transient fluxes are weak in winter (Fig. 2.4e) because humidity is low and cyclones are inactive over eastern Siberia due to the enhanced Siberian High. Nonetheless, it is expected that a few cyclones affect a large part of snow accumulation during the winter. The MFCs associated with transient fluxes are related to cyclone activities, whose differences in intensity and path in each season have been shown in previous studies (Zhang et al. 2004; Sorteberg and Walsh 2008). These must play a crucial role in the transient moisture transport and associated *P–ET*, especially over the Lena River.

2.5 Origin of Precipitating Water and Recycling

An interesting feature of the Siberian atmospheric water cycle is precipitation recycling (e.g., Numaguti 1999; Trenberth 1999). Some of the water precipitated onto the land surface evaporates into the atmosphere and then contributes to another

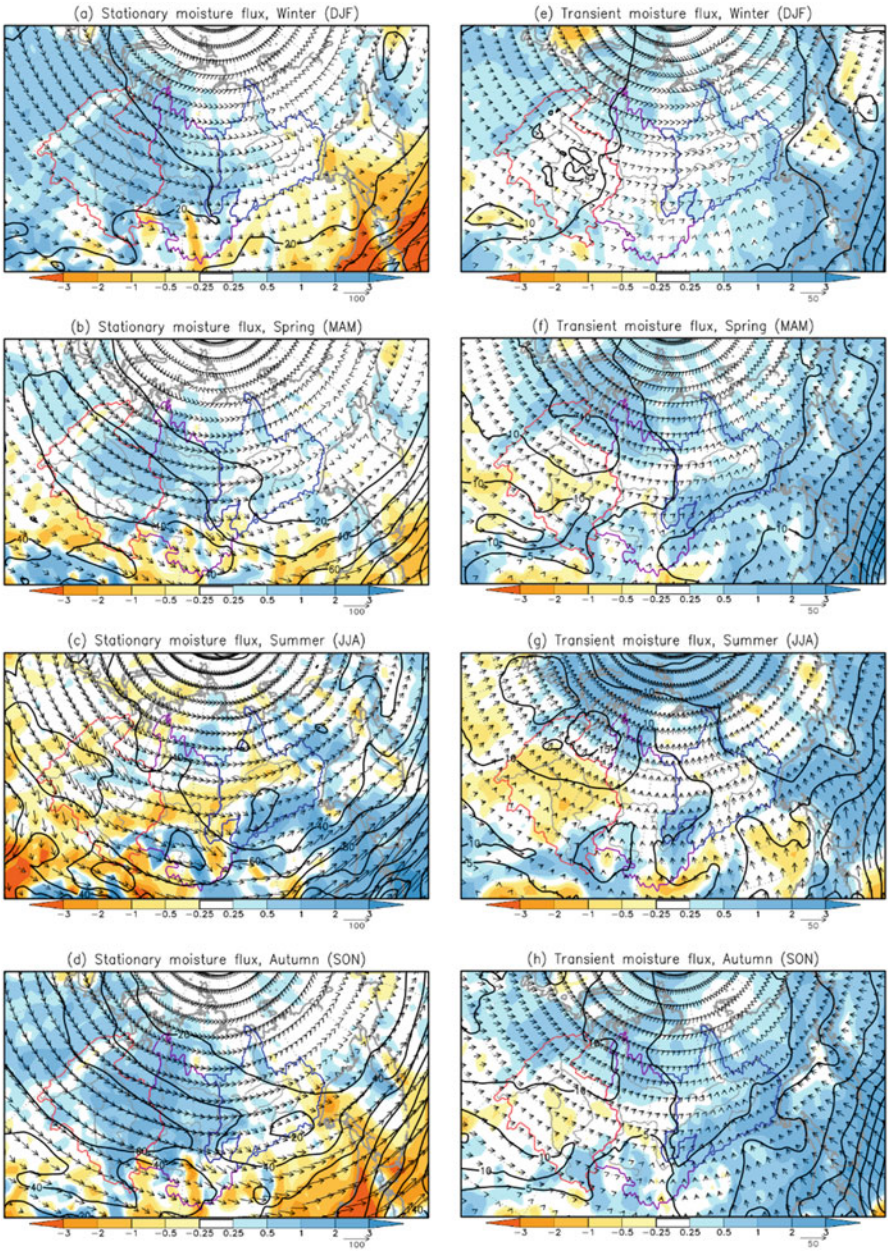

Fig. 2.4 Same as in Fig. 2.3, but for stationary (**a**–**d**) and transient (**e**–**h**) components of moisture flux (vector), those magnitude (contour) and convergence (color) in (**a**, **e**) winter (December, January, and February), (**b**, **f**) spring (March, April, and May), (**c**, **g**) summer (June, July, and August), and (**d**, **h**) autumn (September, October, and November). Note that the vector length of the transient flux is twice as long as the stationary flux as shown at the bottom right of each panel. The color scales of the two components are the same as indicated at the bottom of each panel. Contour intervals of the magnitude are 20 kg m^{-1} s^{-1} for the stationary component in (**a**–**d**) and 5 kg m^{-1} s^{-1} for the transient component in (**e**–**h**). (Adapted from Oshima et al. 2015)

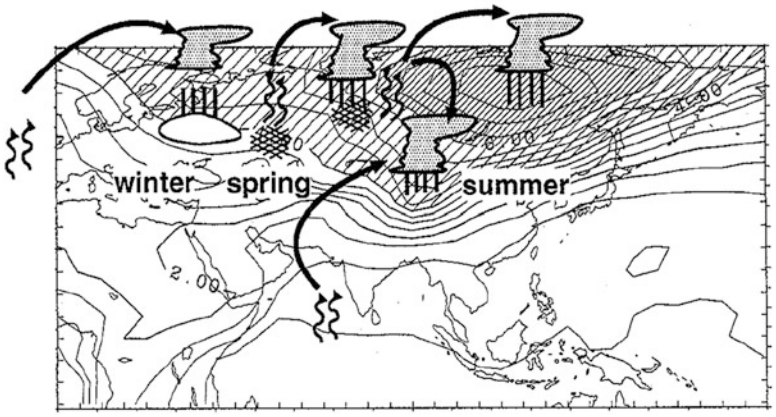

Fig. 2.5 Schematic diagram of precipitation recycling over the Eurasian continent. Contours denote the age of precipitating water during June to August. The "Age" of water means how much time it takes from when it evaporates from the ocean to when it precipitates. Units are months. Light and dense shadings indicate greater than 4 months and 6 months, respectively. See Fig. 8 in Numaguti (1999). (Reprinted with permission from Numaguti 2000, copyright 2000 Meteorological Society of Japan)

event of precipitation over the same or surrounding region. Figure 2.5 shows a schematic diagram of precipitation recycling. Eastern Siberia is one of the regions of active recycling, which accounts for about 20% of the summer P over the region (Trenberth 1999; Serreze et al. 2003). Moreover, tagged water experiments with an atmospheric general circulation model (AGCM) tracked water from the source to the sink like a forward trajectory and indicated that evaporation from the land surface accounts for more than 80% of the summer P and over 50% of the annual P in eastern Siberia (Numaguti 1999).

The source of P over eastern Siberia is mainly from the west. The water evaporated from the Atlantic Ocean is transported by westerly winds over Siberia and is precipitated and accumulates as snow during winter. In spring, some of the snowmelt water flows into the river, while some evaporates again to the atmosphere and provides another precipitation event over that region or slightly to the east side. Such precipitation recycling between the ET and P via land-atmosphere interactions occurs several times during the summer. The AGCM experiments demonstrated that the summer P over eastern Siberia experiences about two times of precipitation recycling, and the precipitating water in this region takes over 6 months from the time of evaporation from the Atlantic Ocean to when it is precipitated (Numaguti 1999). As shown in Fig. 2.5, the evaporated water from the Atlantic Ocean once precipitates over western Siberia in winter, the water evaporates in spring and precipitates again over central Siberia during spring and summer (first recycling), and then that water evaporates and precipitates once more over eastern Siberia in summer (second recycling). For the winter P, on the other hand, the recycling over eastern Siberia is less than one, and the water from the Atlantic Ocean tends to reach eastern Siberia directly, while the wintertime P is low in this region (Fig. 2.2d).

Alternative evidence is based on analysis of stable isotopes in P (snow/rain) over Siberia (Kurita et al. 2004, 2005). The stable isotope results also indicated that the evaporated water from the Atlantic is transported from west to east over Siberia and that water experiences several precipitation recycling events during the transportation.

Precipitation recycling affects the spatial distribution of P over Siberia. The P in winter clearly shows the east-west gradient over Siberia, whereas the distribution of P in summer is more zonally uniform (e.g., Fig. 3 in Takashima et al. 2009). The active recycling in summer promotes eastward moisture transport to eastern Siberia, although the recycling is inactive in winter. These east-west gradients of climate should affect regional features of the water cycle that characterize the individual Siberian rivers.

2.6 Seasonal Time Lag Between *P–ET* and *R*

It is expected that there are some seasonal time lags between the $P–ET$ and R for Siberian rivers. Because of the large spatial extent of the river basins, it takes considerable time for the water input as $P–ET$ to reach the river mouth as R. In winter, the rivers are frozen over and P accumulates as snow. As such, the winter $P–ET$ begins to reach the Arctic Ocean the following spring. Most previous studies have used a simple water year for the comparison between the R and $P–ET$ of the Siberian rivers. Those water years are averages from autumn (October or September) of the previous year to summer (September or August) of the current year (Serreze et al. 2003; Zhang et al. 2012). The definition of the conventional water year is the same annual averaging period both for $P–ET$ and R, and does not take explicit account of actual time lags. However, the time lag likely differs in each region because of the regional differences in climate, seasonality, terrestrial process, vegetation, and so on (see in detail in Oshima et al. 2015).

To objectively detect seasonal time lags for the Lena River, Oshima and Hiyama (2012) compared various combinations of seasonal averaging periods of $P–ET$ and R based on the same method used by Tachibana et al. (2008). As a result, we defined the winter (summer) averaging period for the $P–ET$ to be from October of the previous year to May of the current year (from June to September of the current year) and the spring (autumn) averaging period for the R to be from November of the previous year to July of the current year (from August to October of the current year). The seasonal combinations show strong positive correlations during the period between 1980 and 2011 (Fig. 2.6). The correlation between the summer $P–ET$ and autumn R was 0.87, and that between the winter $P–ET$ and spring R was 0.72. In addition, the annual $P–ET$ averaged from October of the previous year to September of the current year and the annual R averaged from November of the previous year to October of the current year were positively correlated with a coefficient of 0.85. Rightly, magnitudes of the seasonal mean $P–ET$ and R are equivalent to each other (winter $P–ET$, 141 mm/8 months; spring R, 154 mm/9 months; summer $P–ET$, 64 mm/4 months; autumn R, 74 mm/3 months). Therefore, in the Lena River, the

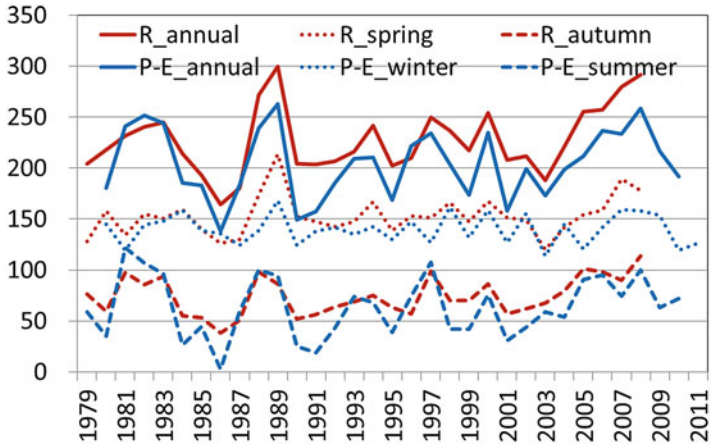

Fig. 2.6 Time series of interannual variations of *R* (red lines) and *P–ET* (blue lines) for the Lena River during the past three decades (1979–2011). The *R* in annual mean (red solid) and spring (red dot) and autumn (red dashed) means and *P–ET* in annual mean (blue solid) and winter (blue dot) and summer (blue dashed) means are shown. The *R* and *P–ET* are from the ArcticRIMS and JRA-25. Units are mm year^{-1}. (Reprinted from Oshima and Hiyama 2012)

summer *P–ET* quantitatively corresponds to autumn *R*, and winter *P–ET* corresponds to spring *R* (Fig. 2.6). The important point is that magnitudes in winter *P–ET* and spring *R* are larger than other seasonal combination of summer *P–ET* and autumn *R* because of longer period of the former seasonal combination, but amplitudes of the variations are greater in the summer *P–ET* and autumn *R*. Therefore, the summer *P–ET* and autumn *R* dominate the interannual variations of the annual means of each variable (Fig. 2.6).

The seasonal combination and time lag mentioned above are interpreted as follows. It is inarguable that, in winter, snow accumulation and frozen rivers need to be taken into account in the seasonal time lag. This means that the winter *P–ET* corresponds to the spring *R*. The averaging period of winter *P–ET* is almost equivalent to the periods of negative SAT, high snow cover (Fig. 2.2a), and also positive $\partial TWS/\partial t$ (Fig. 2.2d), indicative of snow accumulation. On the other hand, several terrestrial processes occurring throughout spring to summer relate to the summer *P–ET* and autumn *R*. The time lag between the summer *P–ET* and autumn *R* is affected by $\partial TWS/\partial t$ and associated with the deepening of seasonal thawing (active layer) in permafrost region during spring to summer transition. The active layer deepens from May to August, and the soil moisture (*TWS*) decreases during this season as shown in Fig. 2.2d. In addition, the large *ET* in summer indicates that a large part of precipitating water goes back to the atmosphere. These processes result in a few months of time lag between the summer *P–ET* and autumn *R*.

2.7 Interannual Variation

With respect to the interannual variation of the Siberian water cycle, Fukutomi et al. (2003) have shown an interesting result. They revealed that the summer *P* over the Lena was negatively correlated with that over the Ob during the 1980s to mid-1990s. The summer *P–ET* and autumn *R* of the Lena and Ob Rivers were also negatively correlated during the same period. The negative correlations were affected by an east-west seesaw pattern of large-scale atmospheric circulation and associated moisture transport over Siberia (Fig. 2.7). When the *P* is large over the Lena, the cyclonic anomaly of atmospheric circulation emerges over the Lena basin. At that time, over the Ob, the *P* is small, and the anticyclonic anomaly emerges. These anomalies result in a convergence and divergence of moisture flux over the basins, and the coinciding changes in *P* then produce the negative correlation of *R* between the two rivers. In addition, our recent study (Oshima et al. 2018) further elucidated that the out of phase of the Lena and Ob *R*s was also observed during the past two centuries using

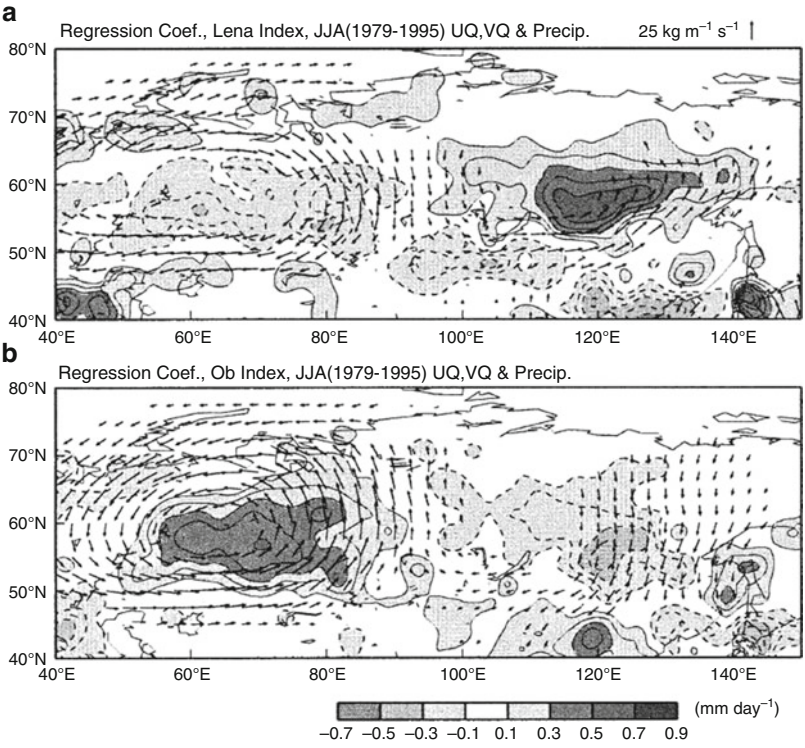

Fig. 2.7 East-west seesaw pattern of summertime moisture flux (vector) associated with *P* over (**a**) the Lena and (**b**) the Ob. Anomalies of *P* (shade) are also shown. (Reprinted with permission from Fukutomi et al. 2003, copyright 2003 American Meteorological Society)

the tree-ring reconstruction (MacDonald et al. 2007). An AGCM control simulation further demonstrated that the east-west seesaw pattern of atmospheric circulation frequently emerges as a summertime natural internal variability over Siberia.

Other factor influencing the change in *P* over eastern Siberia is a dipole pattern over the Arctic Ocean (Iijima et al. 2016), which shows an anticyclonic anomaly over the North American side and a cyclonic anomaly over the Siberian side. While the Arctic dipole anomaly is known to cause the Arctic sea ice reduction (Inoue and Kikuchi 2007; Ogi and Wallace 2007; Wang et al. 2009), it is unclear why the dipole pattern emerges. Other studies have also indicated the effect of the Arctic dipole anomaly on the *P* over eastern Siberia (Fujinami et al. 2016; Hiyama et al. 2016). In addition to the above, it has been reported that the Rossby wave propagated from the North Atlantic Ocean affects the summertime *P* seesaw mode between northeast Asia and eastern Siberia (Iwao and Takahashi 2006, 2008), and the Atlantic multidecadal variability influences the summer *P* over Siberia (Sun et al. 2015).

2.8 Concluding Remarks

The Siberian atmospheric water cycle has regional differences (Fig. 2.8), which are characterized by geographical and terrestrial environments such as topography, distance from the ocean, vegetation type, and permafrost, in addition to the regional climate. It is obvious that *P* is a key player in the water cycle of the Siberian rivers, but the regional difference in *ET* also affects the climatological mean and seasonal cycle of *P*–*ET* (Table 2.1, Fig. 2.2, e.g., Serreze et al. 2003). As a result, the *ET* over each river affects the magnitude of *R*. The *P*–*ET* is greatly affected by moisture transport over the region, and the moisture transport processes differ among the Siberian rivers (Table 2.1, Figs. 2.3 and 2.4, Oshima et al. 2015). The *P*–*ET* over the

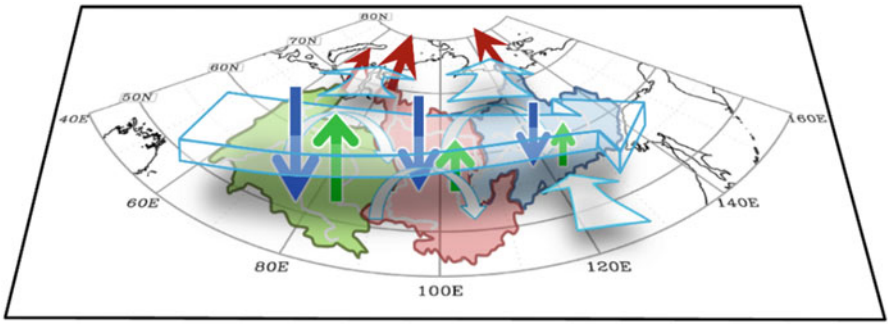

Fig. 2.8 Schematic diagram of regional features of the atmospheric and terrestrial water cycles in the Siberian rivers. Blue, green, red, and white arrows show *P*, *ET*, *R*, and atmospheric moisture transport including precipitation recycling, respectively. Differences in the arrow lengths and widths roughly denote differences in the magnitude of the fluxes. (Reprinted with permission from Oshima et al. 2015, copyright 2015 American Geophysical Union)

Lena River basin is affected mainly by the transient component of the moisture flux associated with cyclone activity.

The Lena River is frozen over during the winter months from October to May (Fig. 2.2a). The snow and river ice melt in spring, and then *R* abruptly increases with a maximum in June (Fig. 2.2d). Both *P* and *ET* over the basin show a maximum in summer, with transpiration accounting for about half of *ET*, resulting in a near-zero *P–ET* in summer and almost no water input to the basin. However, the frozen soil and snow start to melt in spring, and the melting water flows into the river (Fig. 2.2d). Some of the melting water also evaporates to the atmosphere. The evaporated water is transported by the westerly wind, which then precipitates again over Siberia (Numaguti 1999; Kurita et al. 2004, 2005). Such precipitation recycling occurs several times over Siberia. The summertime precipitating water over eastern Siberia experiences about two times of recycling, and it takes about 6 months from the date of evaporation from the Atlantic Ocean to reach eastern Siberia (Numaguti 1999, Fig. 2.5). In winter, on the other hand, the recycling over eastern Siberia is less than one, and the evaporated water from the Atlantic Ocean tends to reach eastern Siberia directly, while the *P* is low during winter (Fig. 2.2d). Up to 80% of the water precipitating in summer over the Lena in eastern Siberia originates from evapotranspiration from the Siberian land surface (Numaguti 1999). In addition to the westerly winds associated with the seasonal mean wind (Figs. 2.4a–d), the moisture transport associated with cyclone activity, i.e., transient moisture flux (Figs. 2.4e–h), also contributes to the northward transport. In summer, the water vapor evaporated from the Pacific Ocean, and possibly also from the Sea of Okhotsk, is transported by cyclone activity from the southern region, through the Lena basin, and further north into the Arctic Ocean.

In order to understand the interannual variation of *P–ET* and *R* of the Lena River, the seasonal time lags need to be taken into consideration (Fig. 2.6, Oshima 2014; Oshima et al. 2015). The winter *P–ET* corresponds to the spring *R*, reflecting the *P* accumulated as snow in winter that then turns into spring flow. On the other hand, summer *P–ET* corresponds to autumn *R*. It is worth noting that although the magnitudes of winter *P–ET* and spring *R* are larger than those of summer *P–ET* and the autumn *R*, the amplitudes of variations of summer *P–ET* and autumn *R* are larger (Fig. 2.6). This is due to the large variability in summer *P* over this region. There were several causes for the *P* variation over the Lena basin and eastern Siberia. During the 1980s–1990s, the variation in *P* and *P–ET* in summer is affected by the east-west seesaw pattern of large-scale circulation (Fukutomi et al. 2003), which originates from the summertime natural internal variability over Siberia (Oshima et al. 2018). As a result, the *P*, *P–ET*, and *R* of the Lena were negatively correlated with those of the Ob. During the mid-2000s, a large *P* and wet conditions were observed in and around Yakutsk located in the middle reach of the Lena River (Ohta et al. 2014; Iijima et al. 2016). The wet conditions in the mid-2000s were influenced by cyclone activity associated with the Arctic dipole anomaly (Fujinami et al. 2016; Hiyama et al. 2016; Iijima et al. 2016). The historical *P* variability over eastern Siberia reflects the combination of these contributing factors.

It is expected that *P* over Siberia will increase with an increase in water vapor due to a rise in Siberian SAT under global warming (IPCC AR5 2013). To elucidate the

Siberian water cycle in future climate, we need to further understand the current state of hydrological climate under long-term climate change and predicted changes in hydrological processes under global warming in consideration with interaction, feedback, natural variability, uncertainty, and regional difference. Those findings inform future research challenges regarding the water cycle in eastern Siberia.

References

Aagaard K, Carmack EC (1989) The role of sea ice and other fresh water in the Arctic circulation. J Geophys Res: Oceans 94(C10):14485–14498. https://doi.org/10.1029/JC094iC10p14485

Aagaard K, Carmack EC (1994) The Arctic Ocean and climate: a perspective. In: Johannessen OM, Muench RD, Overland JE (eds) The polar oceans and their role in shaping the global environment. AGU, Washington, DC, pp 5–20. https://doi.org/10.1029/GM085p0005

Berezovskaya S, Yang D, Kane DL (2004) Compatibility analysis of precipitation and runoff trends over the large Siberian watersheds. Geophys Res Lett 31:L21502. https://doi.org/10.1029/2004GL021277

Carmack EC (2000) The Arctic Ocean's freshwater budget: sources, storage and export. In: Lewis E, Jones EP, Lemke P et al (eds) The fresh water budget of the Arctic Ocean. Kluwer, Dordrecht, pp 91–126

Chen M, Xie P, Janowiak JE et al (2002) Global land precipitation: a 50-yr monthly analysis based on gauge observations. J Hydrometeorol 3:249–266

Dickson R, Rudels B, Dye S et al (2007) Current estimates of freshwater flux through Arctic and subarctic seas. Prog Oceanogr 73(3–4):210–230. https://doi.org/10.1016/j.pocean.2006.12.003

Fujinami H, Yasunari T, Watanabe T (2016) Trend and interannual variation in summer precipitation in eastern Siberia in recent decades. Int J Climatol 36:355–368. https://doi.org/10.1002/joc.4352

Fujiwara J (2011) Climate change and migration policy in the Republic of Sakha. In: Hiyama T (ed) FY2010 FR22 research project report "Global warming and the human-nature dimension in Siberia: social adaptation to the changes of the terrestrial ecosystem, with an emphasis on water environments" (RIHN Project C-07), Research Institute for Humanity and Nature, p 192–196 (in Japanese)

Fukutomi Y, Igarashi H, Masuda K et al (2003) Interannual variability of summer water balance components in three major river basins of Northern Eurasia. J Hydrometeorol 4(2):283–296. https://doi.org/10.1175/1525-7541(2003)4<283:IVOSWB>2.0.CO;2

Hiyama T, Fujinami H, Kanamori H et al (2016) Interdecadal modulation of the interannual variability in precipitation and atmospheric circulation pattern over northern Eurasia. Env Res Lett 11:065001. https://doi.org/10.1088/1748-9326/11/6/065001

Iijima Y, Nakamura T, Park H et al (2016) Enhancement of Arctic storm activity in relation to permafrost degradation in eastern Siberia. Int J Climatol 36:4265–4275. https://doi.org/10.1002/joc.4629

Inoue J, Kikuchi T (2007) Outflow of summertime arctic sea ice observed by ice drifting buoys and its linkage with ice reduction and atmospheric circulation patterns. J Meteor Soc Japan 85:881–887. https://doi.org/10.2151/jmsj.85.881

IPCC (2013) Climate change 2013: the physical science basis. Contribution of working group I to the fifth assessment report (AR5) of the intergovernmental panel on climate change. In: Stocker TF, Qin D, Plattner GK et al (eds). Cambridge University Press, p 1535

Iwao K, Takahashi M (2006) Interannual change in summertime precipitation over northeast Asia. Geophys Res Lett 33:L16703. https://doi.org/10.1029/2006GL027119

Iwao K, Takahashi M (2008) A precipitation seesaw mode between northeast Asia and Siberia in summer caused by Rossby waves over the Eurasian Continent. J Clim 21:2401–2419. https://doi.org/10.1175/2007JCLI1949.1

Kurita N, Yoshida N, Inoue G et al (2004) Modern isotope climatology of Russia: a first assessment. J Geophys Res 109:D03102. https://doi.org/10.1029/2003JD003404
Kurita N, Sugimoto A, Fujii Y et al (2005) Isotopic composition and origin of snow over Siberia. J Geophys Res 110:D13102. https://doi.org/10.1029/2004JD005053
MacDonald GM, Kremenetski KV, Smith LC et al (2007) Recent Eurasian river discharge to the Arctic Ocean in the context of longer-term dendrohydrological records. J Geophys Res 112: G04S50. https://doi.org/10.1029/2006JG000333
McClelland JW, Holmes RM, Peterson BJ et al (2004) Increasing river discharge in the Eurasian Arctic: consideration of dams, permafrost thaw, and fires as potential agents of change. J Geophys Res 109:D18102. https://doi.org/10.1029/2004JD004583
McClelland JW, Déry SJ, Peterson BJ et al (2006) A pan-Arctic evaluation of changes in river discharge during the latter half of the 20th century. Geophys Res Lett 33:L06715. https://doi.org/10.1029/2006GL025753
Numaguti A (1999) Origin and recycling processes of precipitating water over the Eurasian continent: experiments using an atmospheric general circulation model. J Geophys Res 104 (D2):1957–1972. https://doi.org/10.1029/1998JD200026
Numaguti A (2000) Continental-scale water cycle and application of stable isotopes. TENKI 47 (11):802–803. in Japanese
Ogi M, Wallace JM (2007) Summer minimum Arctic sea ice extent and the associated summer atmospheric circulation. Geophys Res Lett 34:L12705. https://doi.org/10.1029/2007GL029897
Ohta T, Kotani A, Iijima Y et al (2014) Effects of waterlogging on water and carbon dioxide fluxes and environmental variables in a Siberian larch forest, 1998–2011. Agric For Meteorol 188:64–75. https://doi.org/10.1016/j.agrformet.2013.12.012
Onogi K, Tsutsui J, Koide H et al (2007) The JRA-25 reanalysis. J Meteor Soc Japan 85:369–432. https://doi.org/10.2151/jmsj.85.369
Oshima K (2014) Atmospheric and terrestrial water cycle over Siberia. In: Iijima Y, Sato T (eds) Terrestrial climate and environmental changes in Northern Hemisphere cold regions, Kisho-Kenkyu Note (Meteorological research note) 230:12–26, Meteorological Society of Japan (in Japanese)
Oshima K, Hiyama T (2012) Seasonal and interannual variations of the Lena river discharge and those relationships with atmospheric water cycle. In: Proceedings of 1st international conference on global warming and the human-nature dimension in Siberia: social adaptation to the changes of the terrestrial ecosystem, with an emphasis on water environments. Research Institute for Humanity and Nature, p 28–31
Oshima K, Tachibana Y, Hiyama T (2015) Climate and year-to-year variability of atmospheric and terrestrial water cycles in the three great Siberian rivers. J Geophys Res Atmos 120:3043–3062. https://doi.org/10.1002/2014JD022489
Oshima K, Ogata K, Park H, Tachibana Y (2018) Influence of atmospheric internal variability on the long-term Siberian water cycle during the past 2 centuries. Earth Syst Dynam 9:497–506. https://doi.org/10.5194/esd-9-497-2018
Park H, Yamazaki T, Yamamoto K, Ohta T (2008) Tempo-spatial characteristics of energy budget and evapotranspiration in the eastern Siberia. Agric For Meteorol 148:1990–2005. https://doi.org/10.1016/j.agrformet.2008.06.018
Peixoto JP, Oort AH (1983) The atmospheric branch of the hydrological cycle and climate. In: Street-Perrott A, Beran M, Ratcliffe R (eds) Variations in the global water budget. Reidel, Dordrecht, pp 5–65
Peixoto JP, Oort AH (1992) Physics of climate. AIP, New York, p 520
Quegan S, Beer C, Shvidenko A et al (2011) Estimating the carbon balance of central Siberia using a landscape-ecosystem approach, atmospheric inversion and dynamic global vegetation models. Glob Chang Biol 17:351–365. https://doi.org/10.1111/j.1365-2486.2010.02275.x
Rawlins MA, Willmott CJ, Shiklomanov A et al (2006) Evaluation of trends in derived snowfall and rainfall across Eurasia and linkages with discharge to the Arctic Ocean. Geophys Res Lett 33:L07403. https://doi.org/10.1029/2005GL025231

Robinson DA, Dewey KF, Heim RR Jr (1993) Global snow cover monitoring: an update. Bull Am Meteor Soc 74:1689–1696. https://doi.org/10.1175/1520-0477(1993)074<1689:GSCMAU>2.0.CO;2

Sakai T, Hatta S, Okumura M et al (2015) Use of landsat TM/ETM + to monitor the spatial and temporal extent of spring breakup floods in the Lena River, Siberia. Int J Remote Sens 36 (3):719–733. https://doi.org/10.1080/01431161.2014.995271

Serreze M, Barry R (2005) The Arctic climate system, Cambridge atmospheric and space science series. Cambridge University Press, Cambridge, UK. https://doi.org/10.1017/CBO9780511535888

Serreze MC, Etringer AJ (2003) Precipitation characteristics of the Eurasian Arctic drainage system. Int J Climatol 23:1267–1291. https://doi.org/10.1002/joc.941

Serreze MC, Bromwich DH, Clark MP et al (2003) The large-scale hydro-climatology of the terrestrial Arctic drainage system. J Geophys Res 108(D2):8160. https://doi.org/10.1029/2001JD000919

Serreze MC, Barrett AP, Slater AG et al (2006) The large-scale freshwater cycle of the Arctic. J Geophys Res 111:C11010. https://doi.org/10.1029/2005JC003424

Shiklomanov AI, Lammers RB (2009) Record Russian river discharge in 2007 and the limits of analysis. Env Res Lett 4:045015. https://doi.org/10.1088/1748-9326/4/4/045015

Sorteberg A, Walsh JE (2008) Seasonal cyclone variability at 70°N and its impact on moisture transport into the Arctic. Tellus A 60:570–586. https://doi.org/10.1111/j.1600-0870.2008.00314.x

Su F, Adam JC, Trenberth KE, Lettenmaier DP (2006) Evaluation of surface water fluxes of the pan-Arctic land region with a land surface model and ERA-40 reanalysis. J Geophys Res 113: D05110. https://doi.org/10.1029/2005JD006387

Sun C, Li J, Zhao S (2015) Remote influence of Atlantic multidecadal variability on Siberian warm season precipitation. Sci Rep 5:16853. https://doi.org/10.1038/srep16853

Tachibana Y, Oshima K, Ogi M (2008) Seasonal and interannual variations of Amur River discharge and their relationships to large-scale atmospheric patterns and moisture fluxes. J Geophys Res 113:D16102. https://doi.org/10.1029/2007JD009555

Takashima H, Yatagai A, Kawamoto H et al (2009) Hydrological balance over northern Eurasia from gauge-based high-resolution daily precipitation data. In: Taniguchi M, Burnett WC, Fukushima Y et al (eds) From headwaters to the Ocean: hydrological change and watershed management. Taylor & Francis Group, Oxford, pp 37–41

Trenberth KE (1999) Atmospheric moisture recycling: Role of advection and local evaporation. J Clim 12:1368–1381. https://doi.org/10.1175/1520-0442(1999)012<1368:AMRROA>2.0.CO;2

Troy TJ, Sheffield J, Wood EF (2011) Estimation of the terrestrial water budget over Northern Eurasia through the use of multiple data sources. J Clim 24:3272–3293. https://doi.org/10.1175/2011JCLI3936.1

Wang J, Zhang J, Watanabe E et al (2009) Is the dipole anomaly a major driver to record lows in Arctic summer sea ice extent? Geophys Res Lett 36:L05706. https://doi.org/10.1029/2008GL036706

Yamazaki K (2010) Arctic oscillation and climate change in Eurasia. In: Endo K, Yamakawa S, Waragai T (eds) The polar circles, cryosphere and Global environment. Ninomiya-Shoten, Tokyo, pp 199–215. (in Japanese)

Ye H, Ladochy S, Yang D et al (2004) The impact of climatic conditions on seasonal river discharges in Siberia. J Hydrometeorol 5:286–295. https://doi.org/10.1175/1525-7541(2004)005<0286:TIOCCO>2.0.CO;2

Zhang X, Walsh JE, Zhang J et al (2004) Climatology and interannual variability of arctic cyclone activity: 1948–2002. J Clim 17:2300–2317. https://doi.org/10.1175/1520-0442(2004)017<2300:CAIVOA>2.0.CO;2

Zhang X, He JZJ et al (2012) Enhanced poleward moisture transport and amplified northern high-latitude wetting trend. Nat Clim Chang 3:47–51. https://doi.org/10.1038/nclimate1631

Chapter 3
Water Cycles in Forests

Ayumi Kotani and Takeshi Ohta

3.1 Introduction

Forests play an important role in the terrestrial water cycle. The rainfall brought to forest ecosystems is drained via surface and ground flow and partially transported into the atmosphere via evapotranspiration. These water balances are expressed in Eq. (3.1), in which precipitation (P) is distributed between evapotranspiration (ET), which includes transpiration by plants and evaporation from wet surfaces (e.g., soil and wet plant surfaces), change of storage (ΔQ), and runoff (outflow/inflow calculated as the residual component of the water balance, R):

$$P = ET + \Delta Q + R. \tag{3.1}$$

This water balance is linked to the heat balance via the evapotranspiration in the same domain:

$$R_n = H + LE + G, \tag{3.2}$$

where R_n is the net radiation as a budget of the shortwave and longwave radiation, H is the sensible heat flux, LE is the latent heat flux, which is ET multiplied by the latent heat of evaporation, and G is the heat flux into the ground. Evapotranspiration ET, which appears in Eqs. (3.1) and (3.2), plays a role in both the forest water cycle and the climate via the surface energy balance.

In boreal regions, the ecosystem has adapted to the environment, which is formed by the high latitude climate, snow, and frozen ground processes. Particularly, in eastern Siberia, the characteristics of the continental climate appear more strongly in comparison to other boreal regions (Schulze et al. 2002). The climate has strong

A. Kotani (✉) · T. Ohta
Graduate School of Bioagricultural Sciences, Nagoya University, Nagoya, Japan
e-mail: kotani@agr.nagoya-u.ac.jp; takeshi_1956@grace.ocn.ne.jp

T. Ohta et al. (eds.), *Water-Carbon Dynamics in Eastern Siberia*,
Ecological Studies 236, https://doi.org/10.1007/978-981-13-6317-7_3

continental characteristics, with a low precipitation of approximately 200–300 mm y^{-1} and an annual range of daily mean air temperature of more than 60 °C. The growth period of the plants is approximately the three summer months. The establishment of the forest is primarily composed of deciduous conifer, larch, which is enabled in spite of the small amounts of precipitation because permafrost is distributed continually over the area and the seasonally thawing ground supplies water for plant use (Chap. 1). The plant cover prevents rapid thawing of the frozen ground, while plants gain benefits from the water in the thawed ground. The forest ecosystem adapted to the environment of eastern Siberia in this way via frozen ground processes and plays a role that is important to the formation of the local water cycle.

In recent years, the ecosystem has faced an intensification and an increased frequency of occurrences of extreme precipitation and temperature phenomena (Groisman and Soja 2009; Groisman and Gutman 2013). In the last decade, environmental changes on various scales have been observed in Eurasia at high latitudes, for example, increases in river discharge into the Arctic Sea (e.g., Shiklomanov and Lammers 2009), increases in atmospheric water vapor transport to high latitudes (Zhang et al. 2012), increases in snowfall over Siberia (Bulygina et al. 2011), increases in subsurface water storage over the Lena watershed (Chap. 11, Muskett and Romanovsky 2009; Velicogna et al. 2012), and increases in the area of surface water (Chap. 8, Fedrov et al. 2014; Boike et al. 2016). It is important to examine how the responses of the forest ecosystems of eastern Siberia to the changes in the water environment and sequentially the water cycles will change.

This chapter introduces observational studies of the water and energy balance primarily of forest ecosystems during the plant-growing season. Evapotranspiration over the larch forest and its biophysical responses are focused on and the recently observed wet climate environment is presented.

3.2 Study Area

The Spasskaya Pad Scientific Forest Station (62°15′N, 129°37′E, 214 m a.s.l.) is located on a terrace of the Lena River in the Central Yakutia region of the Republic of Sakha, Russia. The observation site is operated by the Institute of Biological Problems in the Cryolithozone (Siberian Branch of the Russian Academy of Sciences – IBPC SB RAS). The mean annual precipitation in this area is 234 mm, and the mean annual air temperature is −8.4 °C, and the minimum monthly temperature is −38.1 °C in January and the maximum 19.8 °C in July (1986–2015).

The dominant species in the local forest is larch (*Larix cajanderi*), mixed with birch (*Betula pendula*) and willow (*Salix bebbiana*), with floor vegetation primarily composed of evergreen cowberry (*Vaccinium vitis-idaea*) mixed with several herbs (e.g., *Actaea erythrocarpa* and *Pyrola asarifolia*). The composition rate and height distribution of these species changed over the studied decade (from 1998 to 2014; Figs. 3.1 and 3.2). In 1998, the stand density of the larch trees was 848 trees ha^{-1}, the mean height was 18 m, and the wood volume was 221 m^3 ha^{-1} (based on allometric

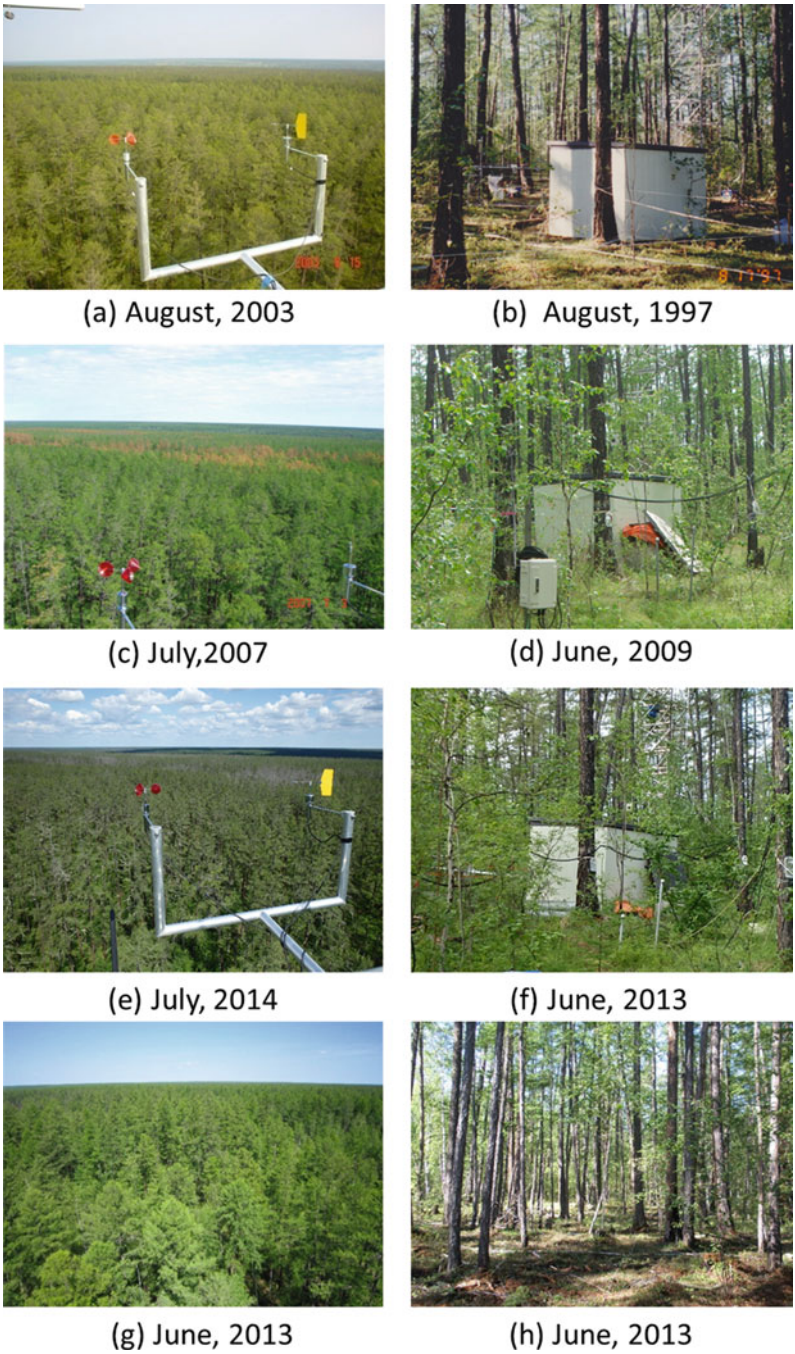

Fig. 3.1 Photograph of larch forest of SPA (**a**–**f**) and ELG (**g**–**h**)

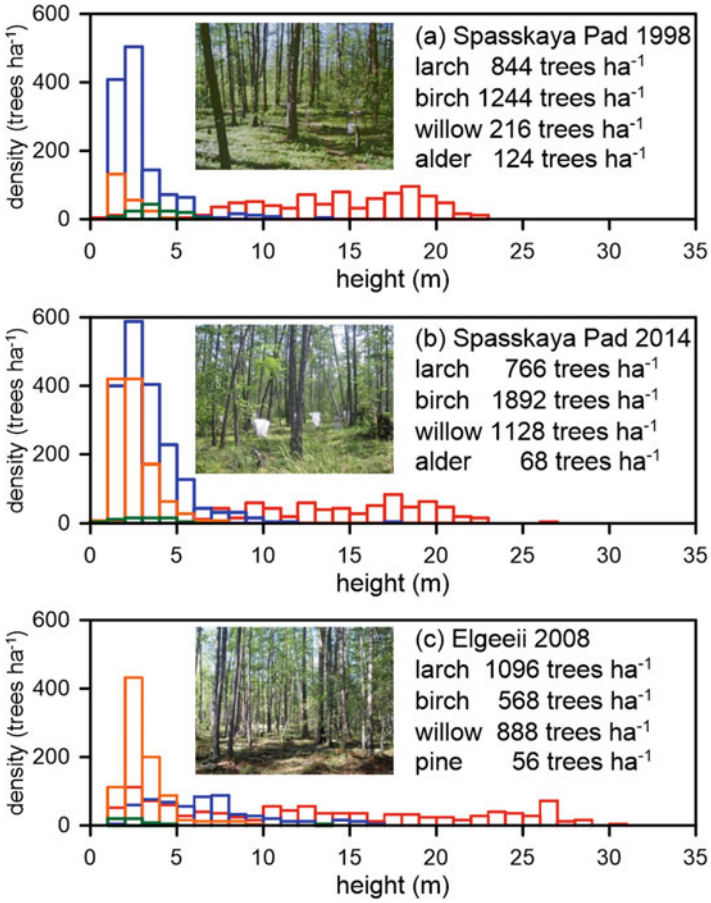

Fig. 3.2 Height class distribution and tree density for main tree species at Spasskaya Pad in 1998 (**a**), 2014 (**b**), and Elgeeii in 2008 (**c**). Red, blue, orange, and green colors indicate larch, birch, willow, and alder, respectively. Reduction of larch trees in Spasskaya Pad is due to fallen/felled dead trees

relationship of Schulze et al. (1995)). During the wet climate period of 2005–2008 (described below), the birch developed from 1244 trees ha^{-1} to 1892 trees ha^{-1}, and the willow trees developed from 216 trees ha^{-1} to 1128 trees ha^{-1} (Fig. 3.2). Other species, such as birch and pine (*Pinus sylvestris*), are clustered in 10–100 m scale patches around the larch forest observation site. Soils in the larch forest consist of an alluvial sandy loam classified as sod-pale solodic (Kononov et al. 2012) with a sandy loam texture. The upper layer has previously been reported to be sandy loam and the deeper layer to be silt loam (Lopez et al. 2007a) with vertical inversions in some places. The geographical features of an alluvial plain and the effect of cryoturbation (Sawada 2006) can produce these heterogeneous structures.

As a comparison to Spasskaya Pad, field observations were conducted at the Elgeeii Forest Station (60°01′ N 133°49′ E, 202 m a.s.l.) located on a terrace of the Aldan River (a tributary of the Lena River). Ust-Maya (60 km east of Elgeeii) has a mean annual precipitation of 302 mm and a mean annual air temperature of −8.5 °C (−39.4 °C in January and 18.8 °C in July, 1986–2015). The air temperature is similar to that in Yakutsk; however, the precipitation is 30% greater than that in Yakutsk. The species composition is similar to that of the Spasskaya Pad larch forest but with a more remarkably dominant development of larch trees. The stand densities of larch, birch, and willow are 1096, 568, and 888 trees ha^{-1}, respectively. The floor vegetation is primarily evergreen cowberry with shrubs such as dog rose and honeysuckle. Sod-pale soils with silt loam texture are found at Elgeeii. Traces of a former wildfire were detected in some locations within the forest.

Continuous observations have been conducted at these stations to obtain the energy balance, relating meteorological components such as air temperature, humidity, radiation, and wind and, inside the forest canopy, soil environmental components such as ground temperature and water content since 1998 at Spasskaya Pad and since 2009 at Elgeeii (Ohta et al. 2008; Iijima et al. 2014). Evapotranspiration has been observed at 32 m since 1998, at 3 m (inside the forest) since 2004 at Spasskaya Pad (Dolman et al. 2004; Ohta et al. 2008; Iida et al. 2009), and at 35 m since 2009 at Elgeeii (Kotani et al. 2014).

3.3 Evapotranspiration of the Larch Forest in Eastern Siberia

Figure 3.3 shows the climate and soil environment conditions in Spasskaya Pad since 1998, in which various climate conditions including dry and wet years were reported. In this chapter, characteristics of the forest evapotranspiration on primarily the Spasskaya Pad larch forest based on field observations over two decades are presented.

3.3.1 Seasonal Variation of the Forest Evapotranspiration

The energy balance of the larch forest showed seasonal variation reflecting the physical environment, such as solar radiation, air and ground temperature, soil water, and the plant phenology at Spasskaya Pad (Fig. 3.4; Ohta et al. 2001). Before snowmelt and the thaw of the frozen soils in spring, most of the net radiation is divided into the sensible heat flux, which increases following the net radiation. As snowmelt and the thaw of frozen soils commence, latent heat flux, which is evaporation from the ground surface because the trees do not have open leaves, gradually increases (Iida et al. 2009). The sensible heat flux is remarkably dominant compared

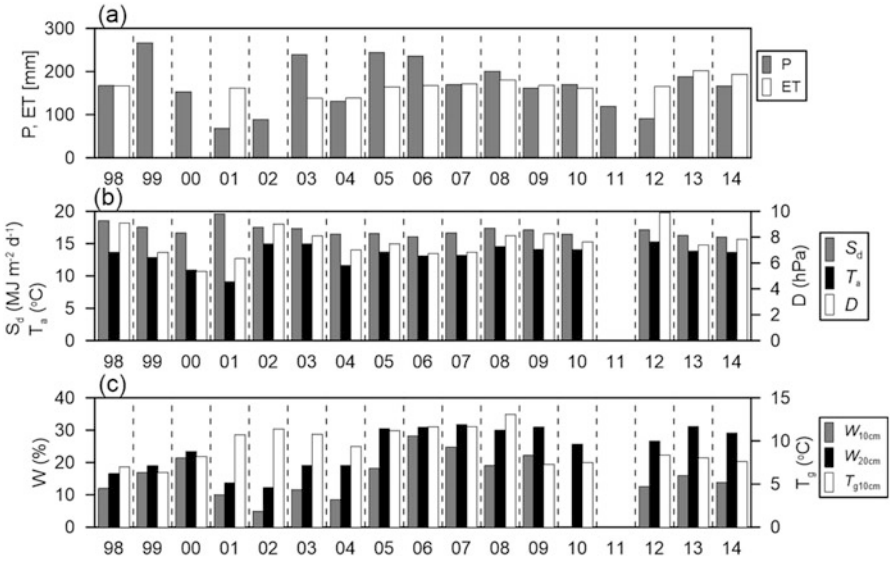

Fig. 3.3 Variability of meteorology and soil conditions in warm season (May–September) from 1998 to 2014 at SPA larch forest. (**a**) Sum of precipitation *P* and evapotranspiration *ET*, (**b**) average of daily solar radiation S_d, air temperature T_a, and vapor pressure deficit *D*, and (**c**) average of soil water contents *W* at 10 and 20 cm depth, and soil temperature T_g at 10 cm depth

to the latent heat flux during this period, and the Bowen ratio, which is ratio of sensible heat flux to latent heat flux (H/LE), is approximately 5–20. When the larch trees and the other deciduous plants come into emergence and expand their leaves, the latent heat rapidly increases due to plant transpiration (Ohta et al. 2001; Dolman et al. 2004). The seasonal maximum of the latent heat flux appears in June–July, while the sensible heat flux decreases. During this period, the latent and sensible heat fluxes are nearly equal, or the sensible heat is slightly larger (the Bowen ratio is close to 1). In the latter half of the foliation period (August–September), the latent heat flux gradually decreases due to the browning and shedding of leaves and again the Bowen ratio increases beyond 1 (Ohta et al. 2001; Dolman et al. 2004). The rate of the latent heat decrease depends on the soil moisture at the time, which depends on the summer precipitation; after a summer with higher precipitation, the latent heat flux does not decrease rapidly and is maintained in the late summer. In a young larch forest in the same region, seasonal variations similar to the Spasskaya Pad larch forest were found; the seasonal maximum of the sensible heat flux preceded that of the latent heat flux and the Bowen ratio was close to 1 during the summer (Tanaka et al. 2008). Tanaka et al. (2008) also found that, during the summertime, the daily sensible heat flux responded to variations in the daily net radiation, while the latent heat flux (evapotranspiration) was relatively stable.

Seasonal variations in the energy balance over forests, particularly deciduous forests, strongly reflect plant phenologies, such as leaf emergence, expansion, and dormancy, as shown above. Therefore, interannual variations in the length of the

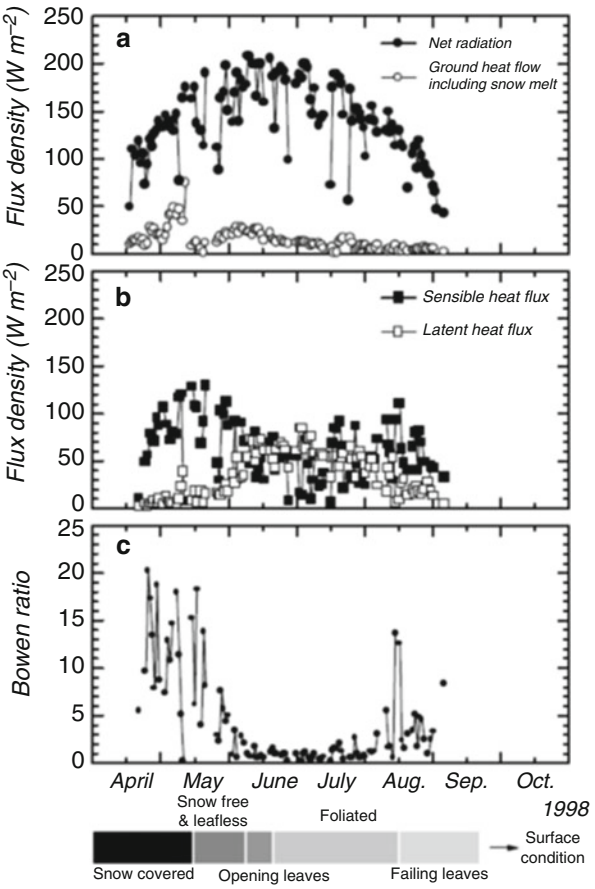

Fig. 3.4 Seasonal variation of (**a**) net radiation and ground heat flux including snowmelt, (**b**) sensible and latent heat flux, and (**c**) Bowen ratio at SPA larch forest. (Ohta et al 2001)

foliation period should affect the annual evapotranspiration. However, even though the date of the leaf emergence at the Spasskaya Pad larch forest varied by a maximum of 30 days, the evapotranspiration summed over the warm season (May–September) did not correlate to the length of the foliation period (Xue et al. 2012). The seasonal sum of the evapotranspiration depended on the evapotranspiration during the maximum leaf area period (middle of June–end of August), and the evapotranspiration during leaf expansion and shedding had little influence (Xue et al. 2012). The non-negligible contribution of the understory vegetation to the forest evapotranspiration, as described below (Sect. 3.3.2), makes it difficult to explain the whole-forest dynamics with only larch phenology.

As shown above, periods of the snow cover and plant phenology at the larch forest were major drivers of the seasonal variation in the energy balance. Phenological observation from 2013 to 2015 found that onset of snowmelt and leaf emergence was earlier, and leaf senescence at autumn was later (Sect. 10.4.3) compared to the late 1990s to early 2000s (Ohta et al. 2001). Typical seasonal sequence of the Bowen

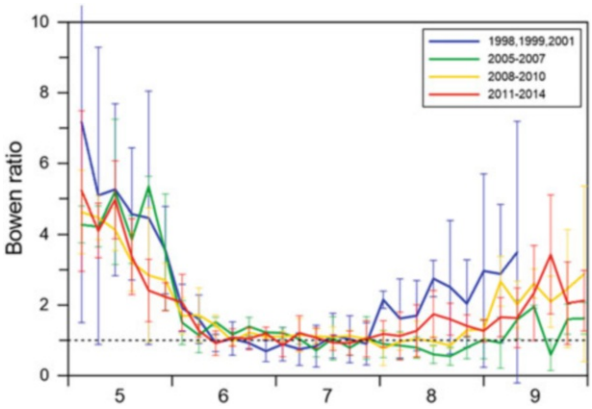

Fig. 3.5 Seasonal variation of 5 days average of the Bowen ratio at SPA larch forest. Only days without rainfall was averaged in 1998–2001 (excluding 2000), 2005–2007, 2008–2010, and 2011–2014. Error bars show standard deviations between years

ratio as described above (Ohta et al. 2001; Dolman et al. 2004) was modified following these changes (Fig. 3.5). Decrease of the Bowen ratio in spring started half month early. In contrast, the summer lowest values around 1 were kept until late August. This is particularly remarkable around 2005 through 2007 because of much soil water near the ground surface (see Sect. 3.6), which could support soil evaporation and transpiration of plants, and this effect was prolonged even after surface water disappeared probably because deeper soils were still wet (Fig. 3.3).

3.3.2 Evapotranspiration from the Understory Vegetation

In general, in boreal forests with sparse crown structures compared to temperate and tropical forests, the contribution to transpiration of the understory vegetation and the soil evaporation is large (Baldocchi et al. 2000). At Spasskaya Pad, the contribution of the understory vegetation to the forest evapotranspiration is approximately 50% during the foliation period, as revealed by several independent means. The transpiration of the larch trees, which was evaluated via sap flow measurements, was approximately 35% (Ohta et al. 2001) to 50–60% (Lopez et al. 2007a). Measurements of the water vapor flux based on the eddy covariance method at 3-m height inside the forest indicated that evapotranspiration from the underground vegetation including evaporation from the soil was equal to approximately 50% of the forest evapotranspiration (Iida et al. 2009, Fig. 3.6). Isotopic analyses of the water vapor sampled above the forest indicated that 80% of the forest evapotranspiration originated in plant transpiration under plant active conditions in the summer daytime (Ueta et al. 2014). The transpiration from evergreen cowberry on the floor, based on leaf chamber measurements, corresponded to 35–60% of the forest evapotranspiration (Miyahara et al. 2004); this is 40–65% of the sum contribution of transpiration by tree and soil evaporation. During the summer, the transpiration of the cowberry decreased just after emergence of the larch needles that means increased

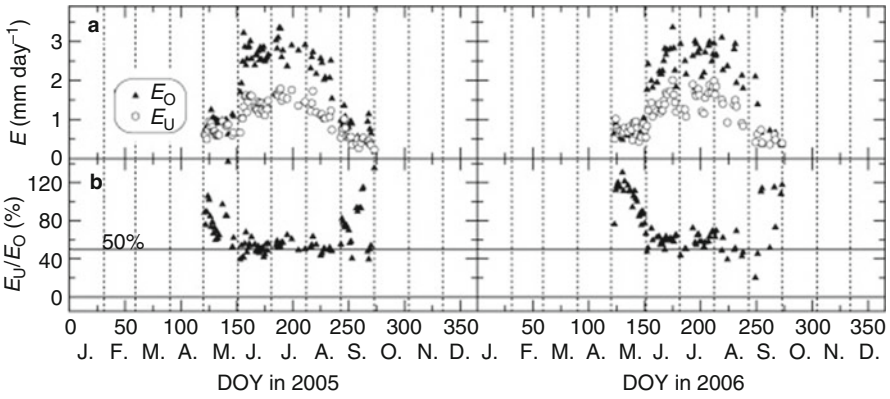

Fig. 3.6 Seasonal variation of daily evapotranspiration at SPA larch forest. (**a**) Total evapotranspiration of forest E_o and understory evapotranspiration E_u, and (**b**) ratio of E_u to E_o. (Iida et al. 2009)

transpiration by larch, likely indicating competition for the use of the soil water close to the ground surface (Miyahara et al. 2004), as well as reduced solar radiation reached into the forest floor (Iida et al. 2009).

The contribution of the understory vegetation including soil evaporation in the boreal forests in various regions ranges from 10% to 60% during the summer (lists are provided in Lindroth and Crill 2011; Iida et al. 2009). A relatively large contribution was found in the larch forests in eastern Siberia compared to the boreal forests in Canada and Scandinavia. The effective penetration of solar radiation through the sparse canopy and the larger atmospheric humidity deficit inside the forests due to the arid climate are likely the main reasons for this phenomenon (Iida et al. 2009).

3.3.3 Interception Evaporation

Interception evaporation during rainfall and just after rainfall is also affected by characteristics of the forest environment such as an arid climate with large atmospheric humidity deficits and a large contribution by understory vegetation. The interception evaporation of the Spasskaya Pad larch forest was estimated to be 15% of the gross rainfall (Ohta et al. 2001). This value seems rather small compared to other boreal forests such as spruce forests in Sweden (26.6%, Bergkvist and Folkeson 1995), mixed forests of spruce and pine in Sweden (30%, Grelle et al. 1997), and spruce forests in Canada (23%, Price et al. 1997), likely due to the small interception storage capacity of the sparse canopy crown (Lindroth and Crill 2011). The energy source for interception evaporation during rainfall is the net radiation at the Spasskaya Pad larch forest in contrast to those at temperate and tropical forests, in which the sensible heat flux from the atmosphere is typically the main energy source (Toba and Ohta 2005).

3.3.4 *Forest Water Balance*

The daily evapotranspiration in the Spasskaya Pad larch forest was 2–3 mm day^{-1} at the seasonal maximum, which is comparable to other larch forests in eastern Siberia (Kelliher et al. 1997; Lopez et al. 2008; Kotani et al. 2014) and in northern Mongolia (Miyazaki et al. 2014). It is also similar to the evapotranspiration of the other boreal forests summarized in Eugester et al. (2000), Lindroth and Crill (2011), and Miyazaki et al. (2014). Evapotranspiration in the warm season (May–September) ranged between 138 mm and 180 mm during the period of 1998–2011 (Ohta et al. 2014), and this interannual variation was smaller than the variation in the annual precipitation (111–347 mm). The interannual variation of the one-dimensional water balance based on Eq. (3.1) from 1998 to 2006 is shown in Fig. 3.7 (Ohta et al. 2008). Despite the interannual difference in precipitation, that in evapotranspiration is rather stable, as stated above, and the change in the soil water storage and residual flux (runoff) responded to the precipitation. The remarkable increase in the soil water storage since 2005 was caused by both the precipitation and water inflow from outside the system (negative runoff), which indicates an expanding seasonal thaw depth of the permafrost (Ohta et al. 2008).

One possible reason for the relatively stable evapotranspiration in spite of the small amount of precipitation and its large interannual variability is the supply of water from thawed frozen ground and snowmelt. The frozen ground layer extends to the ground surface in the winter season, and thawing commences from the ground

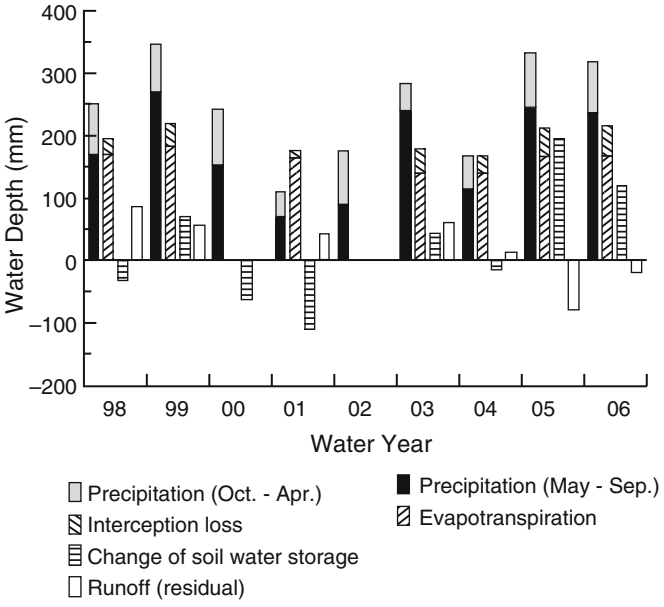

Fig. 3.7 Annual water balance in SPA larch forest. (Ohta et al. 2008)

surface just after the snow melts; the thaw water is stored in the active layer (the layer of the soil above the permafrost that thaws and freezes seasonally). Plants consume rainwater during wet summers and soil water from the deeper layers during dry summers (Chap. 6, Sugimoto et al. 2002). Furthermore, soil water in the active layer correlates better with the precipitation of the previous year rather than that of the current year indicating that soil water storage before freezing is carried over to the next year (Ohta et al. 2008). Soil water in the active layer increases in summers with more precipitation, and that water decreases gradually until frozen due to the stable evapotranspiration. Conversely, during summers with less precipitation, the shortage of soil water close to the ground surface results in reduced heat conductivity, suppressed thawing speed, and soil water being stored in shallower layers where the root depth is concentrated, resulting in maintaining the transpiration (Lopez et al. 2007a).

Snowmelt water is also essential to the soil water dynamics in the active layer. When little soil water was stored before soil freezing, there is little water supplied by the thawing frozen soil in the next summer; however, in such years, infiltration of the snowmelt water into the non-water/ice-saturated ground is effectively accelerated and supports plants taking water, particularly in periods of leaf emergence (Lopez et al. 2015). Conversely, ice-rich frozen soil prevents the infiltration of snowmelt water, and excess water can be discharged to the surrounding lower grassland depression, called an Alas (Sect. 3.5 and Chap. 8), and recharge thermokarst lake water (Lopez et al. 2015). The discharge water also transports salts from the forest to the Alas and plays a role in reducing salt accumulation in the forest soil (Lopez et al. 2007b; Herzschuh et al. 2013).

Interactions between the permafrost and forest ecosystem, in which the soil freezing–thawing process and the plant water use are connected, are an essential feature in addition to the interaction between the forest and atmosphere in terrestrial processes in eastern Siberia. With changing permafrost and forest conditions in the future, it is unknown whether the stable water cycle, particularly the evapotranspiration, which has considered to be a peculiarity of this region, will be maintained. Climate warming sensitivity experiments based on vegetation dynamic modeling indicate that a two-degree warming would result in the collapse of the interaction system between the permafrost–forest–atmosphere and a transition from a deciduous conifer (larch) forest to an evergreen conifer forest (Zhang et al. 2011). Other experiments indicate an increase in the larch productivity due to an increase in the precipitation and soil water (Sato et al. 2016). Furthermore, more local damage to forests and permafrost by ether forest fires or waterlogging (Sect. 3.6) could cause local modifications in the surface water and energy balance. Sensitivity experiments using nonhydrostatic atmospheric modeling to detect the influence of land cover changes in the Lena Basin on the regional water cycle revealed that changes in the evapotranspiration due to transitions from forests to grasslands or water areas are sensitive to the size of the water area (Yoshida et al. 2013). They also indicated an increase in the precipitation consistent with the evapotranspiration indicating a strong interaction between the forest and atmosphere (Yoshida et al. 2013).

3.4 Response of the Forest to Environmental Conditions

3.4.1 Evapotranspiration

Causes of variations in the forest evapotranspiration can be divided into plant physiological responses (stomata control) to control transpiration and the physical environment (atmosphere and radiation) deciding the atmospheric evaporation demand. Under a cool or cold climate with modest precipitation, boreal forests have restricted growth and photosynthesis capacities but survive by using water effectively via the regulation of stomatal closure (e.g., Baldocchi et al. 2000).

In the Central Yakutia middle taiga, stomatal control on larch transpiration is remarkable because the atmospheric humidity deficit is high during the hot and dry summers (Vygodskaya et al. 1997). Stand transpiration based on sap flow measurements of larch trees at the Spasskaya Pad station revealed a strong regulation due to the atmospheric humidity deficit (Kuwada et al. 2002, Lopez et al. 2007a). Even though the nitrogen density in the larch needle is small because there is less soil nitrogen available for the plant, larch trees adapt to the dry climate by increasing the leaf weight per unit area (Schulz et al. 1995; Popova et al. 2013). As another adaptation to the dry climate, the reduced sensitivity of the stomatal conductance to the atmospheric humidity deficit under high humidity deficits results in avoiding a drop in the conductance in the afternoons when the humidity deficit increases (Arneth et al. 1996). These physiological responses of individual larch trees to adapt to the dry climate support assimilating CO_2 efficiently during the short foliation period in this region (see also the photosynthesis of larch in Sect. 4.1).

Forest evapotranspiration is less sensitive to increases in the atmospheric humidity deficit compared to the CO_2 uptake of the forest ecosystem (Tanaka et al. 2000; Dolman et al. 2004). Reduced CO_2 uptake indicates closed stomata; therefore, at the same time, larch transpiration would be reduced. In actuality, decreased transpiration was observed during dry summers with reduced soil water (Lopez et al. 2007a). However, forest evapotranspiration includes both plant transpiration and soil evaporation and the enhanced evaporation owing to a high atmospheric humidity deficit compensates for the reduced transpiration (Schulze et al. 1999). In addition, the water supply from the active layer supports plant water uptake during dry summers, as noted above, and avoids fatal stress on water uptake by plants, while floor vegetation without deeper roots could be affected by water deficits in the surface soil. Such an efficient mechanism, supported by a stable water supply from thawing soil water as noted above, enables a relatively stable level of ET compared to the highly variable annual precipitation in this region (Ohta et al. 2008).

By contrast, the influence of soil water in the active layer on forest evapotranspiration at Spasskaya Pad was unclear compared to those of the atmospheric condition, such as the atmospheric humidity deficit and solar radiation in diurnal and seasonal scale variations (Yoshida et al. 2010). The relatively stable supply of thaw water is one of the main reasons for this. Correlations between the forest evapotranspiration and the soil water content (0–50 cm) appeared on time scales

longer than 2 months, and stronger correlations were found on longer time scales, such as interannual scales (Yoshida et al. 2010). Evapotranspiration at larch forests with deeper active layers (3 m maximum) in northern Mongolia also depends on summer soil water and precipitation (Miyazaki et al. 2014). The influence of soil water on evapotranspiration was not found in black spruce forests in shallower active layers, in which volumetric soil water content was maintained at as high as 40–80%, in Interior Alaska (Iwata et al. 2012).

Environmental control factors including the atmospheric humidity deficit and the soil water content on the forest evapotranspiration at Spasskaya Pad were also variables that could explain the differences in forest evapotranspiration compared to other regions. Comparing the characteristics of the water and energy exchanges at five sites of evergreen, deciduous, and mixed forests, including the Spasskaya Pad larch forest, in three different climate zones, Matsumoto et al. (2008a) revealed that the spatial difference was not due to the atmospheric demand and that the land surface regulation makes a difference in evapotranspiration. The primary reasons for the low levels of evapotranspiration at the Spasskaya Pad forest were the reduced transpiration due to the high atmospheric humidity deficit and the small leaf area of the conifer needles (Matsumoto et al. 2008a).

3.4.2 Conductance

Forest evapotranspiration is driven by atmospheric conditions and controlled by plant and soil conditions. Surface conductance, which indicates efficiency in canopy-scale evapotranspiration with regard to physical environmental variability, is generally smaller in boreal forests than in temperate and tropical forests (Baldocchi et al. 2000; Hall et al. 2004). The surface conductance of larch and pine forests in eastern Siberia is smaller than that of other climate forests, and this difference can be explained by the leaf area index (LAI) difference (Matsumoto et al. 2008b; Khatun et al. 2011). The decoupling factor, which is derived from the Penman–Monteith formula and presents the contribution of radiation and aerodynamic drivers on the evapotranspiration (McNaughton and Jarvis 1983), represents the importance of surface conductance on forest evapotranspiration in Spasskaya Pad larch forests (Iida et al. 2009). This feature indicates that the atmospheric demand of evaporation strongly covariates with evapotranspiration and is common in boreal forests, which generally have large roughness (Khatun et al. 2011).

The daily mean surface conductance of the larch forest at Spasskaya Pad decreased when the atmospheric humidity deficit increased (Ohta et al. 2001; Dolman et al. 2004). Otherwise, the yearly mean surface conductance was well correlated with the soil water content (Yoshida et al. 2010; Xue et al. 2012). The interannual variation in the evapotranspiration normalized by the potential evaporation, which, similar to the surface conductance, represents the land surface control of the evapotranspiration, was also explained by the soil water content (Ohta et al. 2008). A strong correlation between the soil water and the surface conductance was

found on a yearly scale, and this correlation decreased in the daily or seasonal scale variations (Yoshida et al. 2010). To focus on the contribution to transpiration by the upper canopy primarily consisting of larch leaves, the difference between the forest evapotranspiration and the floor evapotranspiration was considered to be the larch layer, and the surface conductance (canopy conductance) of this larch layer was then calculated (Xue et al. 2014). The conductance under the standard condition (an assumed vapor pressure deficit of 1 kPa and saturated solar radiation) at the Spasskaya Pad larch forest was larger than that at other boreal forests (Xue et al. 2014). This is evidence of the reduced surface conductance due to the increase in the atmospheric humidity deficit, similar to the response of the stomatal conductance at the leaf scale discussed above.

Observations of the Spasskaya Pad larch forest with datasets of other climate and forest types were used for parameterization for biogeochemical models. Matsumoto et al. (2008b) compared the responses of the surface conductance to environmental factors in five forest sites in Siberia and Japan. They presented a function of the LAI to explain the inter-site differences in the maximum surface conductance and applied this function to a Jarvis-type conductance model (Fig. 3.8, Matsumoto et al. 2008b). They also showed that their model was optimized for each site and that the bundle of all sites did not differ in precision when estimating the surface conductance (Matsumoto et al. 2008b). These results suggest that the surface conductance of the various mature forests had the same maximum value and response properties, that is, the spatial differences of the environmental responses of forest evapotranspiration depend on the ambient environment rather than the type of forest.

Forest structures such as canopy roughness and tree density also influence the heat and water vapor transport. Such aerodynamic parameters, e.g., surface roughness length and zero plane displacement, which are usually normalized by the canopy height, can be parameterized with the LAI or be assumed constant (Dolman et al. 2003). Boreal forests with large ratios of height to diameter for trees and small ratios of leaf area to stem area, however, are not always applicable to the functions used to evaluate temperate and tropical forests. Nakai et al. (2008) compared these aerodynamic parameters for five forests with various tree densities and height distributions from Siberia and Japan and explained the differences between them using the tree density. They showed a seasonal variation in the aerodynamic parameters following the LAI and found that larch forests with small leaf area varied less compared to other forests. However, an evaluation of these parameters is important for energy and water vapor transport in the larch forest, in which the aerodynamic driver dominates the evapotranspiration.

3.5 Spatial Variability in Eastern Siberia

In the Central Yakutia, precipitation increases toward the south owing to the influence of the surrounding mountains (Yoshida et al. 2012), and forests with high productivity are distributed in the south (Troeva et al. 2010). In the southern

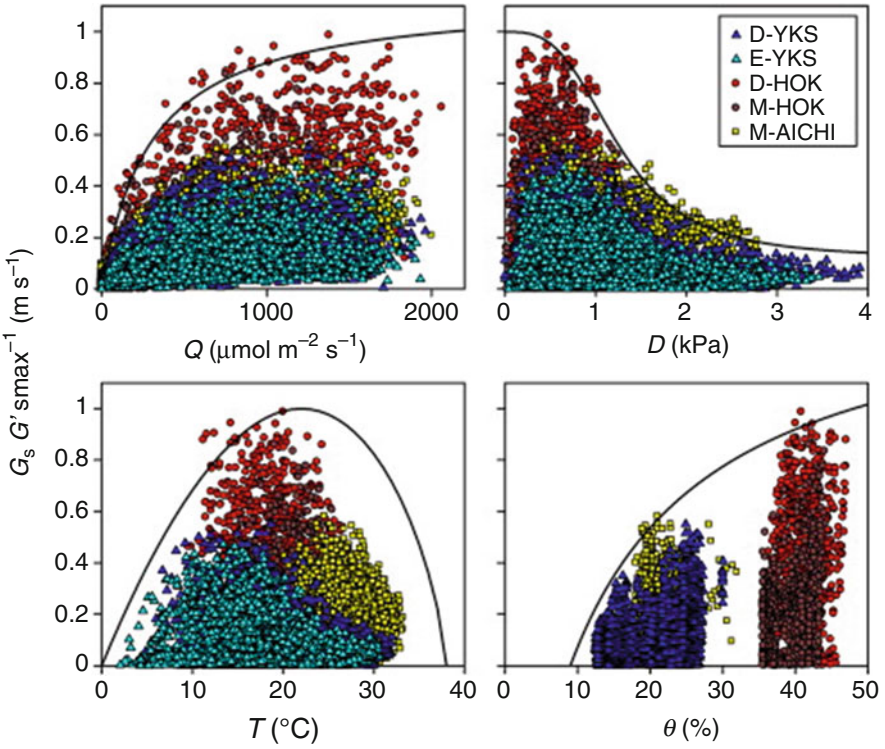

Fig. 3.8 Relation between surface conductance normalized by maximum surface conductance and environmental variables (photosynthesis active radiation Q, atmospheric water vapor deficit D, air temperature T, and volumetric soil water content θ). D-YKS is deciduous (larch) forest in SPA; E-YKA is evergreen (pine) forest in SPA; D-HOK and M-HOK are deciduous and deciduous-evergreen mixed forests in Hokkaido, Japan; and M-AICHI is deciduous-evergreen mixed forest in Aichi, Japan. (Matsumoto et al 2008b)

forest, Elgeeii, more precipitation, soil water, and larger carbon assimilation are found compared to the larch forest in Spasskaya Pad (Chap. 4); however, the difference in the forest evapotranspiration is surprisingly small (Kotani et al. 2014). One possible reason could be the underestimation of the interception evaporation at Elgeeii, where the leaf area is larger than Spasskaya Pad. Soils at Elgeeii consist of finer grain sizes than those at Spasskaya Pad and had higher water retention but lower permeability, which restricted water movement and plant water uptake. At Spasskaya Pad, soil water close to the ground surface decreased without precipitation inputs due to active evapotranspiration from the floor vegetation and soil, whereas soil water in the 20-cm layer was relatively stable likely due to rapid percolation from the upper layers and supply from the deeper layer owing to the vertical gradient of the water potential (Sugimoto et al. 2003). Furthermore, large contributions of soil evaporation and floor plant transpiration could achieve total evapotranspiration comparable to the Elgeeii forest. Different ways of control due to

different soil and forest structures work on forest evapotranspiration. Under the evaporation demand determined by the atmosphere, which is similar at both sites, forest evapotranspiration is usually optimized to the meteorological conditions in the region. This effect could be one of the reasons for the small variability in the annual evapotranspiration (e.g., Ohta et al. 2008).

Larch forests in the southern mountain area with discontinuous permafrost also showed similar seasonal variations in the energy balance, in which the Bowen rate consistently decreased with the emergence of larch needles and increased following larch shedding (Kubota et al. 2004). The latent heat flux before leaf emergence was larger than that in the Spasskaya Pad larch forest because the net radiation on the floor did not conduct into the ground due to the insulating effect of the moss layer, and the majority of the net radiation on the floor was distributed as sensible and latent heat fluxes (Kubota et al. 2004; Suzuki et al. 2007). Evaporation before leaf emergence was equal to 22% of the total forest evapotranspiration from April to October and made a large contribution to the annual water and energy balance of the forest (Suzuki et al. 2007).

The pine forest at the Spasskaya Pad station (2 km from the larch site) presented a small difference in its seasonal variation due to its evergreen species. The onset of evapotranspiration in the pine forest was earlier than that in the larch forest because the pine trees started transpiration just after snowmelt (Hamada et al. 2004). Gradual increases in the evapotranspiration and remarkable reductions in the sensible heat flux in midsummer were not observed. Therefore, distinct seasonal variations in the Bowen ratio similar to those in the larch forest were not found (Hamada et al. 2004). Seasonal variations similar to those of the Spasskaya Pad pine forest were observed in the same species of pine forest in Central Siberia (Yenisei River), where both the sensible heat flux and the latent heat flux followed the net radiation (Tchebakova et al. 2002). In the Central Siberia pine forest, however, the latent heat flux did not decrease with the net radiation and sensible heat flux during the late summer; therefore, the seasonal minimum of the Bowen ratio appeared in the late summer (Tchebakova et al. 2002).

In the Central Yakutia Taiga region, grasslands and lakes formed in the thermokarst depression were found sporadically in the forest (Chap. 8). There are lakes in center of the grasslands, which are lowlands relative to the surrounding forests, and soil water decreases from the vicinity of the lake to the surrounding forest. Such Alas landscapes cover approximately 20% of the Lena lowland (Lopez et al. 2008), and the surface energy and water balance in these grasslands should be considered when evaluating the regional energy and water balance. Seasonal variations in the surface heat balance of the grassland and adjacent forests are contrasting. The grasslands are flooded or nearly saturated by water after the snowmelt at the end of April, and then gradually the water area diminishes and grasses begin to grow by the beginning of June (Yabuki et al. 2004). Following grass expansion, there is a rapid increase in the latent heat flux that exceeds the sensible heat flux, and the Bowen ratio is close to 0.1 until the grass is cut. Even though the net radiation of the grassland is smaller than that of the forest, its remarkably small Bowen ratio results in the latent heat flux at the grassland being similar or at least half

of that in the forest. At the same time, the sensible heat flux in the grassland is 1/2–1/3 of that in the forest, which means the atmosphere is heated less by the grassland than by the forest (Yabuki et al. 2004). At other Alas grasslands, evapotranspiration from the grassland is 10% smaller than that of adjacent forests, and its variability depends on the lake area (Lopez et al. 2008). Larger yearly variation was found in the grassland evapotranspiration due to the larger yearly variation in the depth of the active layer and the associated soil water and plant biomass (Lopez et al. 2008). Lastly, the evaporation from lakes located at the centers of the grasslands reached twice the grassland evapotranspiration (Ishii et al. 2001). Lake area varies each year and therefore could have a large influence on the energy and water balances in Alas ecosystems.

3.6 Response of Larch Forests to Wetting Climates

Over the two decades of observations, knowledge of forest evapotranspiration without remarkable disturbance in the Central Yakutia middle taiga region has been collected. Long-term observations also provide unexpected environmental variations on longer time scales. Large precipitation before winter and snow accumulation during the period of 2004–2008 caused an increase in the soil water coincident with an increase in the ground temperature and active layer thickness around Yakutsk (Iijima et al. 2010). In particular, unusually high soil water during the period of 2006–2007 in comparison to the past 100 years was detected using tree-ring stable isotope chronology (Tei et al. 2013, Chap. 7). In the following summer of 2007, damage to larch trees in areas with elevated soil water, where the degree of saturation increased and the gas diffusivity decreased, was apparent in the form of yellowing and browning leaves (Iwasaki et al. 2010). A decline in tree transpiration as estimated from sap flow measurements was also detected for trees located over a locally moistened and deepened active layer due to micro-topography (Fig. 3.9, Iijima et al. 2014, Chap. 8).

During this period, forest evapotranspiration increased in 2005 and 2006 in response to the high soil water but decreased in 2007 in spite of plentiful soil water (Ohta et al. 2014). By contrast, evapotranspiration from the understory vegetation increased. During the years of continuous wet soil conditions, some of the larch trees and other plants in this forest ecosystem changed; there was an invasion of water-tolerant grass species and growth of young trees (Fig. 3.2). However, yearly mean surface conductance, which had a strong positive correlation to the soil water before the larch damage (Sect. 3.4.2), decreased as expected from the previous correlation (Fig. 3.10, Ohta et al. 2014). By contrast, the surface conductance of the understory vegetation was relatively stable. The aerodynamic conductance of the understory evapotranspiration increased likely due to sufficient soil water leading to the growth of understory vegetation and the simultaneous partial decline in the larch crown altering the environment inside the forest by increasing the light and enhancing the turbulent mixing. The decline in the larch

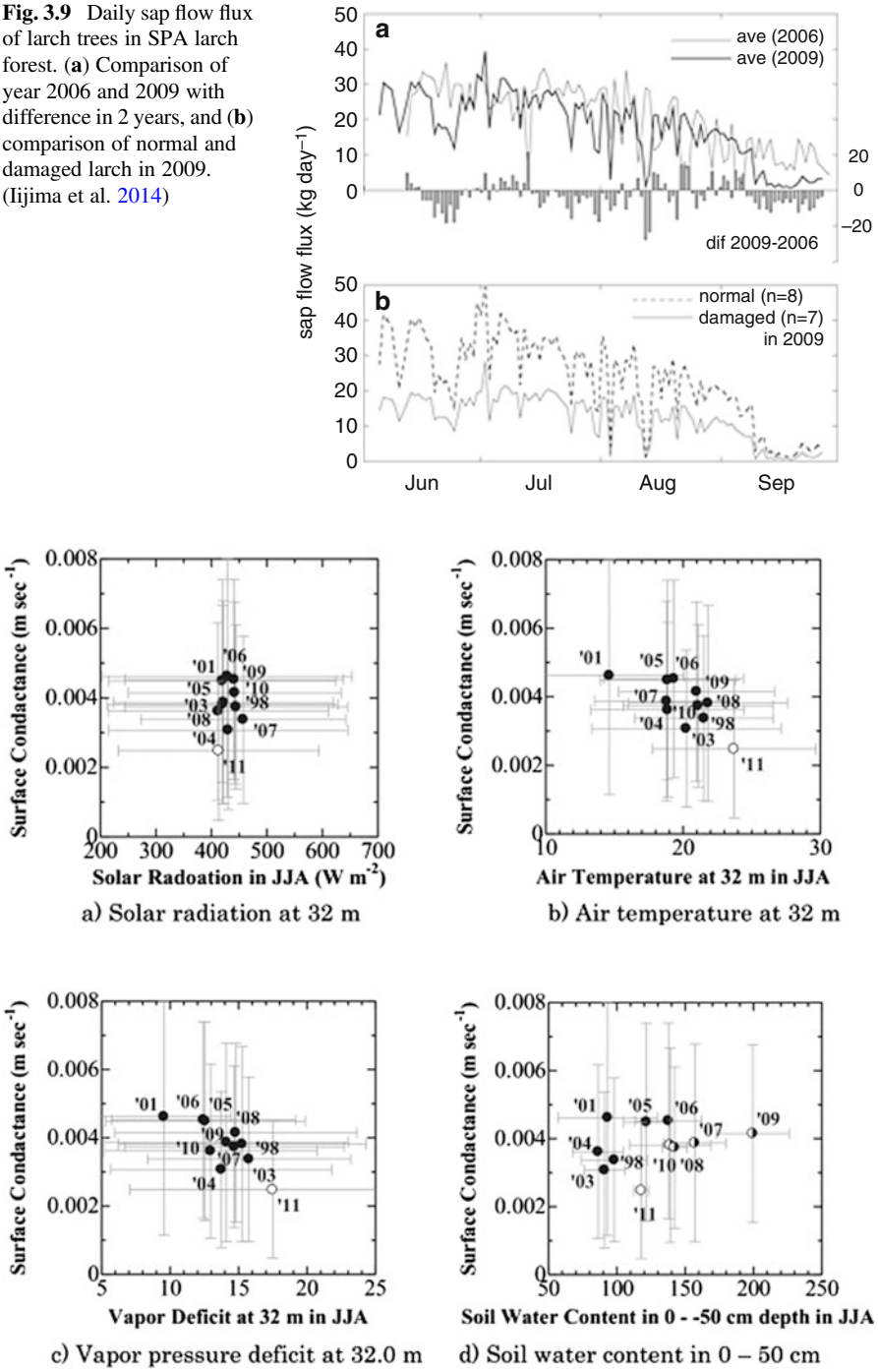

Fig. 3.9 Daily sap flow flux of larch trees in SPA larch forest. (**a**) Comparison of year 2006 and 2009 with difference in 2 years, and (**b**) comparison of normal and damaged larch in 2009. (Iijima et al. 2014)

Fig. 3.10 Relation between surface conductance and (**a**) solar radiation, (**b**) air temperature, (**c**) vapor pressure deficit, and (**d**) soil water content in SPA larch forest. Each plot indicates average in summertime (June–August) from 1998 to 2011 (Ohta et al. 2014)

contribution was compensated for by the understory growth, resulting in a relatively stable whole-forest exchange rate, at least during this study period. Interactions between larches and understory vegetation could support the resilience of this forest ecosystem and the water cycle under environmental variability.

Waterlogging in the soil affects various plant physiological responses such as metabolism, carbon assimilation, transpiration, and nitrogen cycles via the lowered oxygen concentration around the roots (Drew 1997; Bacon 2004). In particular, coniferous species have difficulty managing under insufficient oxygen conditions due to their limited ability to transport oxygen (Kozlowski 1984). Several experimental studies have been conducted to reveal the effects of excessive soil water in various parts of the forest ecosystem at the Spasskaya Pad station. Irrigation experiments, in which twice the natural precipitation was supplied resulting in excess water, did not change the larch transpiration and water storage at root depth indicating infiltration into deeper layers or horizontal drainage (Lopez et al. 2010). Under a water controling experiment, the response of larch seedlings to excess water did not appear in the current year, while root development and the gas exchange rate of needles were reduced in the following year (Takenaka et al. 2016a). A more remarkable reduction appeared in the case of exposure to drought conditions in the year prior to the excess water experiment (Takenaka et al. 2016a). Mature larch trees that experienced drought soil in the previous year suppressed root development and vice versa (Takenaka et al. 2016b). These results indicate the longer than yearly scale memory of previous environmental stresses experienced by individual trees.

While knowledge concerning various responses of individual trees to wet conditions (e.g., Kozlowski 1997; Kreuzwieser and Gessler 2010) has been accumulated, studies on the forest ecosystem scale are relatively rare. Most such studies have investigated riparian forests or maritime forests (e.g., Crawfold et al. 2003). Even though studies on boreal forests are limited, it is noteworthy that the wetting situation of forests in permafrost regions, e.g., the vegetation transition from forest to wetland progressing with permafrost degradation, was reported in sporadic and discontinuous permafrost regions of Canada and Alaska. Forest fragmentation due to thawing permafrost and expanding wetlands was observed, as well as the reduced water uptake and leaf area of black spruce trees located on forest edges in boreal peatland in the Northern Territories in Canada (Baltzler et al. 2014). The transition from birch to spruce occurred with thermokarst succession in boreal wetlands in Interior Alaska (Lara et al. 2016). These vegetation transitions could likely change the forest evapotranspiration and water cycles. Because forests located on wetlands are a common ecosystem in Scandinavia and West Siberia, the variability of rain and snowfall as well as the air temperature has caused prolonged flooding periods (Wang et al. 2013) and root pathogens (Pavlov 2015).

The processes of changes in forest components caused by excess soil water differ from those resulting from disturbances such as forest fires or lodgings, which have been intensively investigated. While there have been many studies focusing on drought stress, the response of forest evapotranspiration to too wet conditions is yet not sufficiently understood. Knowledge of energy and water cycles in grassland–forest ecosystems, as shown above, will help predict water cycle changes in the case

of a transition from forest to grassland in this region. At the same time, grasslands act as buffer for excess water from surrounding forests (Lopez et al. 2010) and, therefore, considering energy and water cycles at a landscape scale will be beneficial to our understanding of regional water cycles.

3.7 Concluding Remarks

Two decades of field observations and a comparison to other climate regions has resulted in various knowledge concerning the forest water cycle, where the forest ecosystem is adapted to a continental climate with low precipitation and a hot and dry summer and foliation periods as short as a few months. Concerning larch forest evapotranspiration, which is the primary focus of this chapter, there are many important features including stomata regulation against atmospheric humidity deficits, the contribution of evapotranspiration from floor and understory vegetation, and the relatively stable evapotranspiration compared to soil water and precipitation. These features occur due to the underlying permafrost and in part the complementary support of the thermokarst grassland and forest via water flow.

Climate change in eastern Siberia in the future will likely bring both drying and wetting terrestrial conditions. Either way, changes in the forest energy and water cycles are possible via the responses of the forest and will feedback into the atmospheric processes. Changes in the water cycle also will affect the forest ecosystem via material transport including salt accumulation. Continuous monitoring of water and biogeochemical cycles (Chaps. 4 and 5) combined with the water and energy cycles is necessary to understand the terrestrial processes and predict the fate of the forests in this region.

References

Arneth A, Kelliher FM, Bauer G, Hollinger DY, Byers JN, Hunt JE, Mcseveny TM, Ziegler W, Vygodskaya NN, Milukova I, Sogachov A, Varlagin A, Schulze ED (1996) Environmental regulation of xylem sap flow and total conductance of Larix gmelinii trees in eastern Siberia. Tree Physiol 16:247–255. https://doi.org/10.1093/treephys/16.1-2.247

Bacon MA (2004) Water use efficiency in plant biology. Blackwell, London

Baldocchi D, Kelliher FM, Black TA, Jarvis P (2000) Climate and vegetation controls on boreal zone energy exchange. Glob Chang Biol 6:69–83. https://doi.org/10.1046/j.1365-2486.2000.06014.x

Baltzler J, Veness T, Chasmer LE, Sniderhan AE, Quinton WL (2014) Forests on thawing permafrost: fragmentation, edge effects, and net forest loss. Glob Chang Biol 20:824–834. https://doi.org/10.1111/gcb.12349

Bergkvit and Folkeson (1995) The influence of tree species on acid deposition, proton budgets and element fluxes in South Swedish forest ecosystems. Ecol Bull 44:90–99

Boike J, Grau T, Heim B, Günther F, Langer M, Muster S, Gouttevin I, Lange S (2016) Satellite-derived changes in the permafrost landscape of central Yakutia, 2000–2011: wetting, drying, and fires. Glob Planet Chang 139:116–127. https://doi.org/10.1016/j.gloplacha.2016.01.001

Bulygina ON, Groisman PY, Razuvaev VN, Korshunova NN (2011) Changes in snow cover characteristics over Northern Eurasia since 1966. Environ Res Lett 6:045204. https://doi.org/10.1088/1748-9326/6/4/045204

Crawford RMM, Jeffree CE, Rees WG (2003) Paludification and forest retreat in Northern Oceanic environments. Ann Bot 91:213–226. https://doi.org/10.1093/aob/mcf185

Dolman AJ, Moors EJ, Grunwald T, Berbigier P, Bernhofer C (2003) Factors controlling forest atmosphere exchange of water, energy, and carbon. In: Valentini R (ed) Fluxes of carbon, water, and energy of European forests, Ecological Studies, vol 63. Springer, Berlin, pp 207–223

Dolman AJ, Maximov TC, Moors J, Maximov AP, Elbers JA, Kononov AV, Waterloo MJ, van der Molen MK (2004) Net ecosystem exchange of carbon dioxide and water of far eastern Siberian Larch (Larix cajanderii) on permafrost. Biogeosciences 1:133–146. https://doi.org/10.5194/bg-1-133-2004

Drew MC (1997) Oxygen deficiency and root metabolism: injury and acclimation under hypoxia and anoxia. Annu Rev Plant Physiol Plant Mol Biol 4:223–250. https://doi.org/10.1146/annurev.arplant.48.1.223

Eugster W, Rouse WR, Pielke SA Sr, McFadden JP, Baldocchi DD, Kittel TGF, Vaganov E, Chambers S (2000) Land-atmosphere energy exchange in Arctic tundra and boreal forest: available data and feedbacks to climate. Glob Chang Biol 6:84–115. https://doi.org/10.1046/j.1365-2486.2000.06015.x

Fedrov AN, Gavrilief PP, Konstantinov PY, Hiyama T, Iijiima Y, Iwahana G (2014) Estimating the water balance of a thermokarst lake in the middle of the Lena River basin, eastern Siberia. Ecohydrology 7:188–196. https://doi.org/10.1002/eco.1378

Grelle A, Lundberg A, Lindroth A, Morén S, Cienciala E (1997) Evaporation components of a boreal forest: variations during the growing season. J Hydrol 197:70–87. https://doi.org/10.1016/S0022-1694(96)03267-2

Groisman PY, Gutman G (2013) Regional environmental changes in Siberia and their global consequences. Springer, Berlin

Groisman PY, Soja AJ (2009) Ongoing climatic change in Northern Eurasia: justification for expedient research. Environ Res Lett 4:045002. https://doi.org/10.1088/1748-9326/4/4/045002

Hall FG, Betts AK, Frolking S, Brown R, Chen JM, Chen W, Halldin S, Lettenmaier DP, Schafer J (2004) The boreal climate. In: Kabat P (ed) Vegetation, water, humans and the climate: a new perspective on an interactive system. Springer, Berlin, pp 93–114

Hamada S, Ohta T, Hiyama T, Kuwada T, Takahashi A, Maximov TC (2004) Hydrometeorological behaviour of pine and larch forests in eastern Siberia. Hydrol Process 18:23–39. https://doi.org/10.1002/hyp.1308

Herzschuh U, Pestryakova LA, Savelieva LA, Heinecke L, Böhmer T, Biskaborn BK, Andreev A, Ramisch A, Shinneman ALC, Birks HJB (2013) Siberian larch forests and the ion content of thaw lakes form a geochemically functional entity. Nat Commun 4:2408. https://doi.org/10.1038/ncomms3408

Iida S, Ohta T, Matsumoto K, Nakai T, Kuwada T, Kononov AV, Maximov TC, van der Molen MK, Dolman AJ, Tanaka H, Yabuki H (2009) Evapotranspiration from understory vegetation in an eastern Siberian boreal larch forest. Agric For Meteorol 149:1129–1139. https://doi.org/10.1016/j.agrformet.2009.02.003

Iijima Y, Fedorov AN, Park H, Suzuki K, Yabuki H, Maximov TC, Ohata T (2010) Abrupt increase in soil temperature following increased precipitation in a permafrost region, central Lena river basin, Russia. Permafr Periglac Process 21(1):30–41. https://doi.org/10.1002/ppp.662

Iijima Y, Ohta T, Kotani A, Fedrov AN, Kodama Y, Maximov TC (2014) Sap flow changes in relation to permafrost degradation under increasing precipitation in an eastern Siberian larch forest. Ecohydrology 7:177–187. https://doi.org/10.1002/eco.1366

Ishii Y, Yabuki H, Nomura M, Kobayashi N, Tanaka H, Tanaka H, Desyatkin RV (2001) Water and energy flux observation an alas lake in central Yakutia, eastern Siberia. In: Proceedings 5th International study conference on GEWEX in Asia and GAME (GAME Publ. 31), pp 117–120

Iwasaki H, Saito H, Kuwao K, Maximov TC, Hasegawa S (2010) Forest decline caused by high soil water conditions in a permafrost region. Hydrol Earth Syst Sci 14:301–307. https://doi.org/10.5194/hess-14-301-2010

Iwata H, Harazono Y, Ueyama M (2012) The role of permafrost in water exchange of a black spruce forest in Interior Alaska. Agric For Meteorol 161:107–115. https://doi.org/10.1016/j.agrformet.2012.03.017

Kelliher FM, Hollinger DY, Schulze ED, Vygodskaya NN, Byers JN, Hunt JE, McSeveny TM, Milukova I, Sogatchev A, Varlargin A, Ziegler W, Arneth A, Bauer G (1997) Evaporation from an eastern Siberian larch forest. Agric For Meteorol 85:135–147. https://doi.org/10.1016/S0168-1923(96)02424-0

Khatun R, Ohta T, Kotani A, Asanuma J, Gamo M, Han S, Hirano T, Nakai Y, Saigusa N, Takagi K, Wang H, Yoshifuji N (2011) Spatial variations in evapotranspiration over East Asian forest sites. I. Evapotraspiration and decoupling coefficient. Hydrol Res Lett 5:83–87. https://doi.org/10.3178/hrl.5.83

Kononov AV, Maximov TC, Maximov AP, Petrov RE (2012) Annual soil carbon dioxide fluxes in larch forests of central and south-east Yakutia. In: Proceedings 5th international workshop on C/H2O/energy balance and climate over boreal and arctic regions with special emphasis on eastern Eurasia, pp 39–43

Kotani A, Kononov AV, Ohta T, Maximov TC (2014) Temporal variations in the linkage between the net ecosystem exchange of water vapour and CO_2 over boreal forests in eastern Siberia. Ecohydrology 7:209–225. https://doi.org/10.1002/eco.1449

Kozlowski TT (1984) Flooding and plant growth. Academic, Orlando

Kozlowski TT (1997) Responses of woody plants to flooding and salinity. Tree Physiol 17:490. https://doi.org/10.1093/treephys/17.7.490

Kreuzwieser J, Gessler A (2010) Global climate change and tree nutrition: influence of water availability. Tree Physiol 30:1221–1234. https://doi.org/10.1093/treephys/tpq055

Kubota J, Suzuki K, Yamazaki Y, Ohata T, Vuglinsky V (2004) Water and energy budget in the Southern mountainous region of Eastern Siberia. In: Proceedings 6th international study conference on GEWEX in Asia and GAME (GAME CD-ROM Publ. 11), T1JK28Jul04102130

Kuwada T, Kotake T, Takeuchi S, Maximov TC, Yoshikawa K (2002) Relationships among water dynamics, soil moisture and vapor pressure deficit in a Larix gmelinii stand, eastern boreal Siberia. J Japn For Soc 84:246–254. in Japanese with English abstract

Lara MJ, Genet H, Mcguire AD, Euskirchen ES, Zhang Y, Brown DRN, Jorgenson MT, Romanovsky V, Breen A, Bolton WR (2016) Thermokarst rates intensify due to climate change and forest fragmentation in an Alaskan boreal forest lowland. Glob Chang Biol 22:816–829. https://doi.org/10.1111/gcb.13124

Lindroth A, Crill P (2011) Hydrology and biogeochemistry of Boreal forest. In: Forest hydrology and biogeochemistry: synthesis of pas research and future directions, Ecological studies 216. https://doi.org/10.1007/978-94-007-1363-5_14

Lopez CML, Saito H, Kobayashi K, Shirota T, Iwahana G, Maximov TC, Fukuda M (2007a) Interannual environmental-soil thawing rate variation and its control on transpiration from Larix cajanderi, Central Yakutia, Eastern Siberia. J Hydrol 338:251–260. https://doi.org/10.1016/j.jhydrol.2007.02.039

Lopez CML, Brouchkov A, Nakayama H, Takakai F, Fedorov AN, Fukuda M (2007b) Epigenetic salinization and water movement in the active layer of Central Yakutia, Eastern Siberia. Hydrol Process 21:103–109. https://doi.org/10.1002/hyp.6224

Lopez CML, Gerasimov E, Machimura T, Takakai F, Iwahana G, Fedorov AN, Fukuda M (2008) Comparison of carbon and water vapor exchange of forest and grassland in permafrost regions, Central Yakutia. Russia Agric For Meteorol 148:1968–1977. https://doi.org/10.1016/j.agrformet.2008.09.013

Lopez CML, Shirota T, Iwahana G, Koide T, Maximov TC, Fukuda M, Saito H (2010) Effect of increased rainfall on water dynamics of larch (Larix cajanderi) forest in permafrost regions, Russia: an irrigation experiment. J For Res 15:365–373. https://doi.org/10.1007/s10310-010-0196-7

Lopez CML, Takakai F, Iwahana G, Fedorov AN, Iijima Y, Hatano R, Fukuda M (2015) Snowmelt and the hydrological interaction of forest–grassland ecosystems in Central Yakutia, eastern Siberia. Hydrol Process 29:3074–3083. https://doi.org/10.1002/hyp.10424

Matsumoto K, Ohta T, Nakai T, Kuwada T, Daikoku K, Iida S, Yabuki H, Kononov AN, van der Molen MK, Kodama Y, Maximov TC, Dolman AJ, Hattori S (2008a) Energy consumption and evapotranspiration at several boreal and temperate forests in the Far East. Agric For Meteorol 148: 1978–1989. https://doi.org/10.1016/j.agrformet.2008.09.008

Matsumoto K, Ohta T, Nakai T, Kuwada T, Daikoku K, Iida S, Yabuki H, Kononov AN, van der Molen MK, Kodama Y, Maximov TC, Dolman AJ, Hattori S (2008b) Responses of surface conductance to forest environments in the Far East. Agric For Meteorol 148: 1926–1940. https://doi.org/10.1016/j.agrformet.2008.09.009

McNaughton KG, Jarvis PG (1983) Predicting effects of vegetation changes on transpiration and evaporation. In: Kozlowski TT (ed) Water deficits and plant growth, vol 7. Academic, New York, pp 1–47

Miyahara M, Takenaka C, Kuwada T, Ohta T, Maximov TC (2004) How much does cowberry transpiration contribute to evapotranspiration in larch forest? In: Proceedings international semi-open workshop "C/H2O/energy balance and climate over Boreal regions with special emphasis on Eastern Eurasia", pp 99–102

Miyazaki S, Ishikawa M, Baatarbileg N, Damdinsuren S, Ariuntuya A, Jambaljav Y (2014) Interannual and seasonal variations in energy and carbon exchanges over the larch forests on the permafrost in northeastern Mongolia. Pol Sci 8:166–182. https://doi.org/10.1016/j.polar.2013.12.004

Muskett RR, Romanovsky VE (2009) Groundwater storage changes in arctic permafrost watersheds from GRACE and in situ measurements. Environ Res Lett 4:045009. https://doi.org/10.1088/1748-9326/4/4/045009

Nakai T, Sumida A, Daikoku K, Matsumoto K, van der Molen MK, Kodama Y, Kononov AV, Maximov TC, Dolman AJ, Yabuki H, Hara T, Ohta T (2008) Parameterisation of aerodynamic roughness over boreal, cool- and warm-temperate forests. Agric For Meteorol 148:1916–1925. https://doi.org/10.1016/j.agrformet.2008.03.009

Ohta T, Hiyama T, Tanaka H, Kuwada T, Maximov TC, Ohata T, Fukushima Y (2001) Seasonal variation in the energy and water exchanges above and below a larch forest in eastern Siberia. Hydrol Process 15:1459–1476. https://doi.org/10.1002/hyp.219

Ohta T, Maximov TC, Dolman AJ, Nakai T, van der Molen MK, Kononov AV, Maximov AP, Hiyama T, Iijima Y, Moors EJ, Tanaka H, Toba T, Yabuki H (2008) Interannual variation of water balance and summer evapotranspiration in an eastern Siberian larch forest over a 7-year period (1998–2006). Agric For Meteorol 148:1941–1953. https://doi.org/10.1016/j.agrformet.2008.04.012

Ohta T, Kotani A, Iijima Y, Maximov TC, Ito S, Hanamura M, Kononov AV, Maximov AP (2014) Effects of waterlogging on water and carbon dioxide fluxes and environmental variables in a Siberian larch forest, 1998–2011. Agric For Meteorol 188:64–75. https://doi.org/10.1016/j.agrformet.2013.12.012

Pavlov IN (2015) Biotic and abiotic factors as caused of coniferous forests dieback in Siberia and Far East. Contemp Probl Ecol 8:440–456. https://doi.org/10.1134/S1995425515040125

Popova AS, Tokuchi N, Ohte N, Ueda MU, Osaka L, Maximov TC, Sugimoto A (2013) Nitrogen availability in the taiga forest ecosystem of northeastern Siberia. Soil Sci Plant Nutr 59:427–441. https://doi.org/10.1080/00380768.2013.772495

Price AG, Dunham K, Carleton T, Band L (1997) Variability of water fluxes through the black spruce (Picea mariana) canopy and feather moss (Pleurozium schreberi) carpet in the boreal forest of Northern Manitoba. J Hydrol 196:310–323. https://doi.org/10.1016/S0022-1694(96)03233-7

Sato H, Kobayashi H, Iwahana G, Ohta T (2016) Endurance of larch forest ecosystems in eastern Siberia under warming trends. Ecol Evol 6:5690–5704. https://doi.org/10.1002/ece3.2285

Sawada Y (2006) Preliminary results of the micro-topographical change and its effects on the active layer in boreal forest near Yakutsk, Eastern Siberia. In: Hatano R, Guggerberger G (eds) Symptom of environmental change in Siberian Permafrost region. Hokkaido University Press, Sapporo, pp 207–212

Schulz ED, Lloyd J, Kelliher FM, Wirth C, Rebmann C, Lühker B, Mund M, Knohl A, Milyukova IM, Schulze W, Ziegler W, Varlagin AB, Sogachev AF, Valentini R, Dore S, Grigoriev S, Kolle O, Panfyorov MI, Tchebakova N, Vygodskaya NN (1999) Productivity of forests in the Eurosiberian boreal region and their potential to act as a carbon sink –a synthesis. Glob Chang Biol 5:703–722. https://doi.org/10.1046/j.1365-2486.1999.00266.x

Schulze ED, Schulze W, Kelliher FM, Vygodskaya NN, Ziegler W, Kobak KI, Arneth A, Kustesova WA, Sogatchev A, Issajev A, Bauer G, Hollinger DY (1995) Above-ground biomass and nitrogen nutrition in a chronosequence of pristine Dahurian Larix stands in eastern Siberia. Can J For Res 25:943–960. https://doi.org/10.1139/x95-103

Schulze ED, Vygodskaya NN, Tchebakova NM, Czimszik CI, Kozlov DN, Lloyd J, Mollicone D, Parfenova E, Sidorov KN, Varlagin AV, Wirth C (2002) The Eurosiberian transect: an introduction to the experimental region. Tellus 54B:421–428. https://doi.org/10.1034/j.1600-0889.2002.01342.x

Shiklomanov AI, Lammers RB (2009) Record Russian river discharge in 2007 and the limits of analysis. Environ Res Lett 4:045015. https://doi.org/10.1088/1748-9326/4/4/045015

Sugimoto A, Yanagisawa N, Naito D, Fujita N, Maximov TC (2002) Importance of permafrost as a source of water for plants in east Siberian taiga. Ecol Res 17:493–503. https://doi.org/10.1046/j.1440-1703.2002.00506.x

Sugimoto A, Naito D, Yanagisawa N, Ichiyanagi K, Kurita N, Kubota J, Kotake T, Ohata T, Maximov TC, Fedorov AN (2003) Characteristics of soil moisture in permafrost observed in East Siberian taiga with stable isotopes of water. Hydrol Process 17:1073–1092. https://doi.org/10.1002/hyp.1180

Suzuki K, Kubota J, Yabuki H, Ohata T, Vuglinsky V (2007) Moss beneath a leafless larch canopy: influence on water and energy balances in the southern mountainous taiga of eastern Siberia. Hydrol Process 21:1982–1991. https://doi.org/10.1002/hyp.6709

Takenaka C, Miyahara M, Ohta T, Maximov TC (2016a) Effects of two-year variation in soil moisture condition on the development of Larch root system in Eastern Siberia. Am J Clim Chang 5:157–166. https://doi.org/10.4236/ajcc.2016.52015

Takenaka C, Miyahara M, Ohta T, Maximov TC (2016b) Response of larch root development to annual changes of water conditions in eastern Siberia. Pol Sci 10:160–166. https://doi.org/10.1016/j.polar.2016.04.012

Tanaka H, Ohta T, Hiyama T, Maximov TC (2000) Seasonal variation of photosynthesis and transpiration properties of a boreal deciduous forest: analysis using a single layer canopy model. J Japn For Soc 82:259–267. in Japanese with English abstract

Tanaka H, Hiyama T, Kobayashi N, Yabuki H, Ishii Y, Desyatkin RV, Maximov TC, Ohta T (2008) Energy balance and its closure over a young larch forest in eastern Siberia. Agric For Meteorol 148:1954–1967. https://doi.org/10.1016/j.agrformet.2008.05.006

Tchebakova NM, Kolle O, Zolotoukhine D, Arneth A, Styles JM, Vygodskaya NN, Schulze ED, Shibistva O, Lloyd J (2002) Inter-annual and seasonal variations of energy and water vapor fluxes above a Pinus sylvestris forest in the Siberian middle taiga. Tellus B 54:537–551. https://doi.org/10.1034/j.1600-0889.2002.01337.x

Tei S, Sugimoto A, Yonenobu H, Yamazaki T, Maximov TC (2013) Reconstruction of soil moisture for the past 100 years in eastern Siberia by using δ13C of larch tree rings. J Geophys Res G: Biogeosci 118:1256–1265. https://doi.org/10.1002/jgrg.20110

Toba T, Ohta T (2005) An observational study of the factors that influence interception loss in boreal and temperate forests. J Hydrol 313:208–220. https://doi.org/10.1016/j.jhydrol.2005.03.003

Troeva EI, Isaev AP, Cherosov MM, Karpov NS (2010) The far North: plant biodiversity and ecology of Yakutia. Springer, Dordrecht

Ueta A, Sugimoto A, Iijima Y, Yabuki H, Trofim TC (2014) Contribution of transpiration to the atmospheric moisture in eastern Siberia estimated with isotopic composition of water vapour. Ecohydrology 7:197–208. https://doi.org/10.1002/eco.1403

Velicogna I, Tong J, Zhang T, Kimball JS (2012) Increasing subsurface water storage in discontinuous permafrost areas of the Lena River basin, Eurasia, detected from GRACE. Geophys Res Lett 39:L09403. https://doi.org/10.1029/2012GL051623

Vygodskaya NN, Milyukova I, Varlagin A, Tatarinov F, Sogachev A, Kobak KI, Desyatkin R, Bauer G, Hollinger DY, Kelliher FM, Schulze ED (1997) Leaf conductance and CO_2 assimilation of Larix gmelinii growing in an eastern Siberian boreal forest. Tree Physiol 17:607–615. https://doi.org/10.1093/treephys/17.10.607

Wang AF, Roitto M, Lehto T, Zwiazek JJ, Calvo-Polanco M, Repo T (2013) Waterlogging under simulated late-winter conditions had little impact on the physiology and growth of Norway spruce seedlings. Ann For Sci 70:781–790. https://doi.org/10.1007/s13595-013-0325-5

Xue B, Komatsu H, Kumagai T, Kotani A, Otsuki K, Ohta T (2012) Interannual variation of evapotranspiration in an eastern Siberian larch forest. Hydrol Process. https://doi.org/10.1002/hyp.9195

Xue B, Li Z, Yin X, Zhang T, Iida S, Otsuki K, Ohta T, Guo Q (2014) Canopy conductance in a two-storey Siberian boreal larch forest, Russia. Hydrol Process 29:1017–1026. https://doi.org/10.1002/hyp.10213

Yabuki H, Ishii Y, Ohata T (2004) Comparison of water and heat balance on grassland and forest in Central Yakutia, East Siberia. In: Proceedings 6th international study Conference on GEWEX in Asia and GAME (GAME CD-ROM Publ. 11), T1HY30Jul04115511

Yoshida M, Ohta T, Kotani A, Maximov TC (2010) Environmental factors controlling forest evapotranspiration and surface conductance on a multi-temporal scale in growing seasons of a Siberian larch forest. J Hydrol 395:180–189. https://doi.org/10.1016/j.jhydrol.2010.10.023

Yoshida R, Sawada M, Yamazaki T (2012) Roles of Eastern Siberian mountain ranges in precipitation – Verkhoyansk, Dzhugdzhur and Stanovoy mountain ranges. SOLA 7:145–148. https://doi.org/10.2151/sola.2011–037

Yoshida R, Sawada M, Yamazaki T, Ohta T, Hiyama T (2013) Influence of land cover change on regional water cycles in eastern Siberia. J Appl Meteorol Climatol 52:484–497. https://doi.org/10.1175/JAMC-D-12-043.1

Zhang N, Yasunari T, Ohta T (2011) Dynamics of the larch taiga-permafrost coupled system in Siberia under climate change. Environ Res Lett 6:024003. https://doi.org/10.1088/1748-9326/6/2/024003

Zhang X, He J, Zhang J, Polyakov I, Gerdes R, Inoue J, Wu P (2012) Enhanced poleward moisture transport and amplified northern high-latitude wetting trend. Nat Clim Chang 3:47–51. https://doi.org/10.1038/NCLIMATE1631

Chapter 4
Carbon Cycles in Forests

Trofim C. Maximov, Ayaal P. Maksimov, Alexander V. Kononov, Ayumi Kotani, and A. Johannes Dolman

4.1 Introduction

The forests of eastern Siberia form one of the most natural borders in the cryolithozone and account for 45% of all Siberian forests. This forest ecosystem plays a significant role in terrestrial carbon cycles at the regional and global scale. Forest soils and plants act as a carbon pool, which is considered to be relatively stable because of the unfavourable conditions for decomposition. The vegetation and soil of the Siberian forest ecosystems retain 74 and 249 billion tons of carbon, respectively (Dixon et al. 1994). Almost 65% of the forest in eastern Siberia grows in the permafrost zone, and these forests have distinctive ecological characteristics enabling them to adapt to the physical environment in this region (e.g. Abaimov et al. 2002).

Studies of the carbon cycles in the eastern Siberian forest ecosystem (Central Yakutia) date back to the middle of the twentieth century (Chap. 1.3.2). The first multi-scale/multi-methodological carbon cycle study based on leaf- to canopy-scale observations in a *Larix gmelinii* forest in this region was conducted on the Aldan plateau (60°51′N, 128°16′E, 155 km south-west of the city of Yakutsk) under the guidance of Professor Ernst-Detlef Schulze (Germany). This comprehensive field campaign revealed the characteristics of the physiological and ecological responses of larch forest during the mid-growing season (Schulze et al. 1995; Hollinger et al. 1995; Arneth et al. 1996; Kelliher et al. 1997; Vygodskaya et al. 1997).

T. C. Maximov (✉) · A. P. Maksimov · A. V. Kononov
Institute for Biological Problems of Cryolithozone, RAS, Yakutsk, Russia
e-mail: t.c.maximov@ibpc.ysn.ru

A. Kotani
Graduate School of Bioagricultural Sciences, Nagoya University, Nagoya, Japan

A. J. Dolman
Vrije Universiteit Amsterdam, Amsterdam, The Netherlands

T. Ohta et al. (eds.), *Water-Carbon Dynamics in Eastern Siberia*,
Ecological Studies 236, https://doi.org/10.1007/978-981-13-6317-7_4

Since the 1990s, multi-seasonal and multi-year field studies of *Larix cajanderi* forest have been continuously conducted at Spasskaya Pad scientific station at the Institute for Biological Problems of the Cryolithozone, of the Siberian Branch of the Russian Academy of Sciences (IBPC SB RAS) (Maximov et al. 2010). This series of ongoing studies is updating our knowledge of seasonal and annual variation in the function of carbon cycles in larch forest. Spasskaya Pad is located on the left side of the valley in the middle basin of the Lena River in Central Yakutia, Russia (62°14′N, 129°37′ E; 213 m a.s.l.). The station is situated in a 200-year-old cowberry larch forest (*Laricetum vacciniosum*), which stands on permafrost pale-solodic soil based on a light old-alluvial sandy loam. Soils in Spasskaya Pad have a high sand content and low porosity. The water retention capacity of these soils is relatively low. The thickness of the humus horizon does not exceed 5 cm. The second field site of Elgeeii station is located in a highly productive forest in south-eastern Yakutia, on the third terrace of the left bank of the Aldan River in south-eastern Yakutia, Russia (60°00′N, 133°49′E; 220 m a.s.l.). The surrounding environment is a 180-year-old cowberry larch forest on permafrost dark-humus pale-slightly solodic soils based on a carbonated loam. Soils in Elgeeii are heavier than at Spasskaya Pad due to their granulometric composition; in addition, the content of the medium and thin particles and silt in the soil is 2–3 times more than at Spasskaya Pad. Porosity is high and water retention capacity is relatively high. The thickness of the humus horizon is 10–15 cm on average. An additional description of these study sites was provided in Chap. 3.

Carbon budget is expressed in net biome production (NBP) as balance of net ecosystem production (NEP), ecosystem heterotrophic respiration (HR) which includes microbe respiration and decomposition of standing dead trees and coarse woody debris, flux due to natural and human-induced disturbance and consumption (Dtc), and lateral flux to the lithosphere and hydrosphere (LEh) (e.g. Dolman et al. 2012):

$$\mathrm{NBP} = \mathrm{NEP} - \mathrm{HR} - \mathrm{Dtc} - \mathrm{LEh}. \tag{4.1}$$

Focus on forest ecosystem, NEP is given as follows.

$$\mathrm{NEP} = -\mathrm{NEE} = \mathrm{NPP} - \mathrm{HR} = \mathrm{GPP} - \mathrm{ER} \tag{4.2}$$

$$\mathrm{ER} = \mathrm{AR} + \mathrm{HR} \tag{4.3}$$

where NEE is net ecosystem exchange, NPP is net primary production, GPP is gross primary production, ER is ecosystem respiration, and AR is autotrophic (above-ground and root) respiration. These terms are built up from carbon circulation between land surface and atmosphere including assimilation and respiration processes.

This chapter reports the distinctive features of leaf-scale photosynthesis (Sect. 4.2), soil respiration (Sect. 4.3), and net ecosystem exchange (NEE) of CO_2 (Sect. 4.4), mainly based on long-term (1998–2014) observations in Spasskaya Pad larch forest, which were then compared to the results for other boreal forests.

4.2 Photosynthetic Activity of Larch Forests

Since the early 1990s, many studies have investigated the ecological and physiological features of the larch photosynthesis process in Siberia (Maximov et al. 1994, 1995, 2004, 2005a, b, 2010; Maximov 2007; Maximov and Ivanov 2003, 2005; Tabuchi et al. 1994; Hollinger et al. 1995; Schulze et al. 1995; Arneth et al. 1996; Koike et al. 1998, 1999; Vygodskaya et al. 1997; Fujita et al. 1998; Saito et al. 2003; Suzuki et al. 2003). In these studies, the questions of daytime and diurnal photosynthesis dynamics and the influence of environmental factors were considered in detail.

4.2.1 Diurnal Dynamics of Photosynthesis

Regardless of the annual variation in moisture conditions, the daily intensity of net photosynthesis (A_{net}) of *L. cajanderi* generally increases from early morning (4–6 a.m.) until noon and then gradually decreases (approximately from 9 p.m.) to negative values (Maximov et al. 2005b). The daytime depression of photosynthesis, which is typical of annual cultural plants, is not observed in larch trees. This indicates that larch is well adapted to the arid climate. Although the photoperiod, with a positive gas exchange, is 16–17 h during summertime (from 5–6 to 20–22), the peak A_{net} only occurs for approximately 2 h.

The average photosynthetic daily assimilation of *L. cajanderi* is 3.99 g C m^{-2} day^{-1} (332.6 mmol CO_2 m^{-2} day^{-1}) in wet years and 1.67 g C m^{-2} day^{-1} (139.5 mmol CO_2 m^{-2} day^{-1}) in extremely arid years. This variability is larger than the range reported in previous studies for other species of larch, i.e. from 2.04 to 2.64 g C m^{-2} day^{-1} (from 170 to 220 mmol CO_2 m^{-2} day^{-1}) (Benecke et al. 1981; Vygodskaya et al. 1997). Moreover, in late July of a wet year, a maximum of 5.95 g C m^{-2} day^{-1} (496 mmol CO_2 m^{-2} day^{-1}) is observed. This means that in wet years, *L. cajanderi* takes up 2.4 times more CO_2 than in arid and extremely dry years. The difference in the daily assimilation of CO_2 among the dry years is insignificant, e.g. 1.8 and 1.7 g C m^{-2} day^{-1} in 2001 and 2002, respectively (Maximov et al. 2005b; Maximov 2007).

The variability of the photosynthesis rate is dependent not only on environmental conditions but also on the structure and physiology of the plants. For *L. gmelinii* (*cajanderi*), this has been reported from field studies on the Aldan plateau (Vygodskaya et al. 1997), where A_{net} is suppressed by 40% as a result of structural and physiological variation, but mainly due to the nitrogen distribution in crown leaves. In addition, A_{net} is suppressed by 12% due to the low levels of illumination in the morning and evening.

4.2.2 Seasonal Dynamics of Photosynthesis

Larch exhibits a high A_{net} from the beginning of needle growth on the shoots of previous years (the third week of May to the first week of June). Under favourable hydrothermal conditions (an abundance of precipitation and high temperatures) during the initial stages of growth and development, high levels of photosynthesis in *L. cajanderi* can also be observed in July. During dry years, it is usually limited to the previous month (June). During wet years, the maximum A_{net} value in July is higher than in June. The direct dependence of the photosynthetic activity of this species on summer precipitation has been clearly identified. Maximov (2007) reported that during dry and extremely dry periods, the correlation coefficient (r^2) for the relationship between larch photosynthesis intensity and the amount of precipitation in June–August is 0.33, whereas during wet years it increases to 0.77.

Trees in Yakutia prefer to use rainwater in wet years and thawed groundwater in dry years, as shown by our studies using stable isotopes (Sugimoto et al. 2002). This shows that these tree species use atmospheric and soil moisture. This is advantageous under cold soil conditions, where there can be a deficiency of moisture and nutrients. In Yakutia, the relatively high level of photosynthesis in larch is maintained mainly by precipitation, but in dry seasons it is maintained by the soil moisture accumulated during the preceding autumn and spring (there is a marked increase in photosynthesis at the beginning of the vegetative period in the growing season). The capillary rise of meltwater from deeper layers of soil and its use to support growth processes and photosynthesis are also possible in further periods of plant growth and development (e.g. July and August); however, the effect of this is much weaker than the use of atmospheric moisture. The high and stable level of xylem water potential (up to 3–4 MPa) contributes significantly to the increased consumption and absorption of water by the root system from the lower horizons of the soil (Maximov et al. 1996). The increase in the transpiration surface and well-developed root system also favours the effective use of water by plants.

The results of a long-term observation at Spasskaya Pad have shown that a *L. cajanderi* forest absorbs up to 540 g CO_2 m^{-2} per growing season (May–August) in extremely dry years and up to 1440 gCO_2 m^{-1} $season^{-1}$ in humid years, which is 2.5 times more than in arid years. Recalculating these values as carbon gives 150 and 400 g C m^{-1} during the growing season in dry and humid years, respectively.

4.2.3 The Maximum Intensity of Photosynthesis (A_{max})

The maximum intensity of photosynthesis (A_{max}) of woody plants in eastern Siberia (Table 4.1) is well suited for both the theoretical (model) and experimental ranges of values in the boreal zone. Thus, according to the A_{max} allocation world biome map compiled by Woodward and Smith (1995), the theoretical values for our study area, predicted from the soil C and N content, are in the range of 12.6–15.1 μmol m^{-2} s^{-1}, while the experimental values are 7.6–10.1 μmol m^{-2} s^{-1}.

Table 4.1 Ecophysiological characteristics of larch (*Larix cajanderi* and *gmelinii*) in eastern Siberia (Yakutia)

Place, time, and tree age	Parameters							References
	A_{max} [μmol m^2 s^{-1}]	E [mmol m^2 s^{-1}]	I_C [μmol m^2 s^{-1}]	I_S [μmol m^2 s^{-1}]	N [mg g^{-1}]	NUE_I [μmol $mmol^{-1}$]	WUE_I [μmol mmol N^{-1} s^{-1}]	
Field observation								
62°15′N, 129°37′E					1.5%			Sassa (1993)
62°15′N, 129°37′E July	4.41* (~1.5)*	0.77* (~0.15)*		210 × 10^{-6} Em^{-2} s^{-1}*				Tabuchi et al. (1994)
60°51′N 128°16′E July, 125 ± 8 years	8.6–10.4*	22 mg m^{-2} s^{-1} (CL)		>300				Hollinger et al. (1995)
	5–6 (CL)							
60°51′N 128°16′ E July, 125 ± 8 years	10.1	3.9 (1 ± 0.8)		~500	15.6 ± 0.1			Vygodskaya et al. (1997)
	6.1 (CL) (2.7 ± 2.2)							
60°51′N 128°16′E July, 125 ± 8 years					16–22			Schulze et al. (1995)
62°18′N, 129°30′E; 62°13′N, 129°11′ E July, 23–171 years					16–20			Shibuya et al. (2001)
62°18′N, 129°30′E July, 200 years	13.6 ± 1.3[a]**		29 ± 6[a]	785 ± 166[a]				Saito et al. (2003)
	9.6 ± 0.5[b]**		18 ± 4[b]	387 ± 47[b]				

(continued)

Table 4.1 (continued)

Place, time, and tree age	Parameters							References
	A_{max} [μmol m^2 s^{-1}]	E [mmol m^2 s^{-1}]	I_C [μmol m^2 s^{-1}]	I_S [μmol m^2 s^{-1}]	N [mg g^{-1}]	NUE_I [μmol $mmol^{-1}$]	WUE_I [μmol mmol N^{-1} s^{-1}]	
62°15′N, 129°37′ E; 62°18′N, 129°30′ E	~7.5*			~700*				Suzuki et al. (2003)
Phytotron experiment	25–32.2*					0.014	1.1	Koike et al. (2000)

Modified by Maximov et al. (2010)

A_{max} maximum net assimilation (A_{net}), E transpiration rate, Ic light compensation point, Is light saturation point, N leaf nitrogen content, NUE_I instantaneous nitrogen use efficiency, WUE_I instantaneous water use efficiency

[a]light needle; [b]shade needle

*read from graphs or recalculation of data; **light saturated; ? mentioned but no data provided, *in brackets* average values, *CL* data scaled to canopy level

The values of the main photosynthetic parameters of larch at Spasskaya Pad that were investigated at the initial stage of the research period (from the 1990s to the early 2000s) are summarised in Table 4.1. Sometimes it is not easy, and often it is impossible, to compare the published data on a unified basis, because of the different methodological and temporal scales of measurements. Therefore, data were considered according to the authors' computations, with approximations from the graphs and recalculations, where possible. It should also be noted that during this period, overseas researchers did not distinguish between *L. gmelinii* and *L. cajanderi* but rather considered them to be one species: *Gmelin* or *L. gmelinii* (Abaimov et al. 2002).

In the artificial climate conditions of a growth chamber in a previous study, young larch had a very high A_{net} at 30 μmol m^2 s^{-1}, with a gradual increase in the concentration of CO_2 to 1500 ppm. When the CO_2 concentration was doubled and the air temperature was increased by 4 °C, all of the main tree species of Yakutia (*L. cajanderi*, *Pinus sylvestris*, and *Betula platyphylla*) had similar values and trends of A_{net} regardless of the growing conditions (Koike et al. 2000). There is a reason to believe that such a high A_{net} value is a common adaptive physiological feature of the Yakutian tree species that grow in arid climate conditions with a short vegetative period. The index of photosynthesis depends not only on environmental conditions but also on the structure and physiology of plants themselves and their organs (Mokronosov 1983; Tselniker et al. 1990). This has previously been reported for *L. gmelinii* (Vygodskaya et al. 1997); in that study, A_{net} was suppressed by 40% as a result of structural and physiological variation but mainly by the distribution of nitrogen in the leaves of the crown. In addition, A_{net} was reduced due to low lighting in the morning and in evening (by 12%) and low humidity (by 75%).

According to our measurements at Spasskaya Pad, the maximum A_{net} of maturated larch trees varies greatly during the growing season depending on the weather conditions. In our studies, during dry and extremely dry years (1998, 2001, and 2002), the maximum A_{net} was 6.3–7.5 μmol m^{-2} s^{-1}, while in wet years (1999, 2003, 2005, and 2006), it was 7.5–13.5 μmol m^{-2} s^{-1}. There was a clear difference in A_{net} (an average of 1.6 times) between wet and dry years. In very humid years, the highest A_{net} of *L. cajanderi* (13.5 μmol m^{-2} s^{-1}) was 1.3 times higher than that of larch forests in South Yakutia (Vygodskaya et al. 1997) and Central Siberia (Koike et al. 1998) and four times higher than that of European, Japanese, and American species (Maximov et al. 2010; Table 4.2). Vygodskaya et al. (1997) suggested that the high A_{net} values of the Yakut larch species are associated with high stomatal conductance and high transpiration intensity. The latter condition is necessary for the normal life of Yakut plants under drought conditions, because it prevents overheating and leaf heat stress (e.g. Stepanov 1976, Maximov 1989).

Geographical location within the bounds of Siberia makes no significant difference in the net photosynthesis of larch (Table 4.2). Vygodskaya et al. (1997) undertook a general comparison at the species level for *L. gmelinii* (*cajanderi*) in eastern Siberia and European *Larix decidua* (Table 4.3). In general, the needles of *L. cajanderi* and *L. decidua* share a similar anatomy, although the characteristics of the European species are more closely associated with those of the shade needles of Yakutian larch (Vygodskaya et al. 1997). *L. cajanderi* also shows wide intra-tree variation in the size and thickness of pine knot needles.

Table 4.2 CO_2 assimilation of *Larix* spp. in different regions (Maximov et al. 2010)

Region	Species	A_{net} [μmol CO_2 m^{-2} s^{-1}]	References
Europe	*Larix decidua*	3.0	Benecke et al. (1981)
Japan	*Larix leptolepis*	3.0	Matyssek and Schulze (1987) and Dang et al. (1991)
North America	*Larix laricina*	3.0	Matyssek and Schulze (1987) and Dang et al. (1991)
Moscow region	*Larix decidua*	25.0 ± 3.1[a]	Malkina (1995)
Central Siberia	*Larix gmelinii*	7.8–11.5	Koike et al. (1998)
Eastern Siberia (Irkutsk region)	*Larix sibirica*	22.0[a]	Shcherbatyuk et al. (1991)
Eastern Siberia (Central Yakutia)	*Larix gmelinii*	8.6–10.4	Hollinger et al. (1995), Schulze et al. (1995) and Vygodskaya et al. (1997)
Eastern Siberia (Central Yakutia)	*Larix cajanderi*	4.4–13.5	Data by the authors (SPA)

[a]A_{net} is calculated based on dry weight, mg CO_2 g^{-1} h^{-1}

Table 4.3 Physiological parameters of two larch species

	Larix decidua	*Larix gmelinii*	References
Stomatal density [mm^{-2}]	20	20–30	Meidner and Mansfield (1968) and Vygodskaya et al. (1997)
Stomatal aperture [μm]	20	20	Meidner and Mansfield (1968) and Vygodskaya et al. (1997)
Nitrogen content in leaves [mg g^{-1}]	24.7	15.6	Matyssek and Schulze (1987) and Vygodskaya et al. (1997)
Maximum net assimilation, A_{max} [μmol m^{-2} s^{-1}]	About 3	10.1	Benecke et al. (1981) and Vygodskaya et al. (1997)
Transpiration at VPD 1.5 KPa, E [mmol m^{-2} s^{-1}]	0.75	3.7	Benecke et al. (1981) and Vygodskaya et al. (1997)
Leaf conductance, g_s [mmol m^{-2} s^{-1}]	–	56 ± 60 (max 365)	Vygodskaya et al. (1997)
Light saturation, I_s [μmol m^{-2} s^{-1}]	About 500	About 500	Vygodskaya et al. (1997)
Average weight of needles [g m^{-2}]	–	138 ± 6	Vygodskaya et al. (1997)

4.2.4 *Ratio of Photosynthesis to Dark Respiration (R_{dark}) of Plants*

Larch species use about 60% of the carbon they absorb to breathe. About a quarter of this is via respiration in needles, with 13–16% in branches, and there are approximately equal proportions of overall respiration in the stem and roots. Thus, about

40% of the carbon goes to the formation of biomass (Scherbatyuk et al. 1991). To understand carbon allocation in plants, and its role in growth and maintenance processes, the relationship between assimilation and respiration, specifically A_{net} and R_{dark}, needs to be determined. This can be characterised by the annual hydrothermal regime, which is critical for plants. Usually the ratio of R_{dark} to A_{net} reaches a maximum at the beginning of the growing season. At this time, plants need large amounts of energy to grow new shoots and needles (Zabuga and Scherbatyuk 1982; Sherbatyuk, 1976). We found that while the shoots grew and A_{net} increased, the R_{dark} of larch decreased slightly in July and stabilised in August (Maximov et al. 2005b). During the growing season, the R_{dark} costs of the larch needles varied from 22 to 57% of the maximum A_{net} (A_{max}), depending on the ambient temperature and moisture deficit. During this period, the average value of the respiratory costs was 36.4% of the A_{max}. Such a value for the ratio between A_{max} and R_{dark} of larch indicates a strong adaptation of *L. cajanderi* to extremely arid conditions.

We analysed the specific features of the R_{dark} of the leaves of the dominant tree species in Yakutia, i.e. *L. cajanderi*, *P. sylvestris*, and *Betula platyphylla* (Atkin et al. 2015). The leaf respiration rate of all tree species (measured in the dark) fell in response to the prolonged drought in June–July (Fig. 4.1). It is important to note that respiration rates significantly increased in August and September as a result of the frequent precipitation. The analysis showed that the decline of R_{dark} on a dry plot was not a thermal adaptation but rather was induced by water stress. During this dry spell, light respiration was about 30% lower than R_{dark}. These results show that precipitation plays an important role in regulating the scale and magnitude of the CO_2 released (in both light and dark) by the larch forest ecosystem, in which CO_2 released as a result of leaf respiration can account for 1/3 of the entire ecosystem respiration.

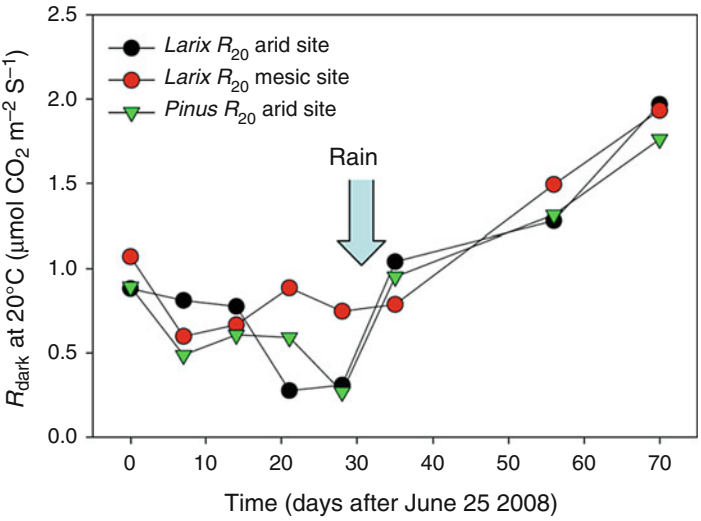

Fig. 4.1 Dark respiration of the larch (*L. cajanderi*) and pine (*P. sylvestris*) needles in different hydroclimatic plots of Spasskaya Pad station, June–September 2008

In other regions of Siberia where coniferous trees grow, R_{dark} amounts to 60% of A_{max} (Malkina 1995; Scherbatyuk et al. 1991). Compared to other conifers, such as spruce and pine, larch is distinguished by a high level of both photosynthetic activity and respiration in the light (Scherbatyuk et al. 1991). For pine and spruce, R_{dark} during the growing season is greater than light respiration, whereas in larch, light respiration dominates at this time. Photosynthesis and the release of CO_2 in the light are closely interrelated, and plants with a high intensity of photosynthesis are also characterised by high levels of light respiration (Laisk 1977; Bykov 1983, Atkin et al. 2015). Hence, with a high intensity of photosynthesis, the species of larch we studied may have low R_{dark} and high intensity of light respiration (Maximov 2007). As a result, Siberian larch is characterised by high daily photosynthesis productivity, e.g. 2.7 times higher than pine and 3.9 times higher than spruce (Ivanov and Kossovich 1932; Scherbatyuk et al. 1991).

The R_{dark} of Yakutian trees has been included as an integral part of a new global R_{dark} database based on leaf features (GlobResp), created from an assessment of 899 plant species in 100 sites from the Arctic to the tropics (Atkin et al. 2015). GlobResp data indicate that at ambient temperatures, R_{dark} increases only twofold from the Arctic to the tropics, although the temperature rises by 20 °C. At the same time, at a standard temperature of 25 °C, R_{dark} is three times higher in the Arctic than in the tropics and twice as high in dry plots compared to wet habitats. One of the interesting results of GlobResp is the high level of variation in R_{dark} among plant species and sites and along global gradients of temperature and aridity.

4.2.5 *Light Dependence of Photosynthesis*

The intensity of photosynthesis in larches in eastern Siberia indicates light saturation at a photosynthetic photon flux density (PPFD) of 300–500 μmol photons m^{-2} s^{-1}, which is about 20–25% of the maximum lighting (1500–2000 μmol photons m^{-2} s^{-1}) (Saito et al. 2003; Vygodskaya et al. 1997). A very high light saturation point (*I*s) of 1300 μmol photons m^{-2} s^{-1} for larch was recorded at the river side of a branch stream of the Yenisei River in central Siberia (Koike et al. 1998), while the A_{max}, light compensation point (I_C), and nitrogen content of the leaves were similar to those of Yakutian larch. The environmental conditions of the area require plant species growing there to be extremely light demanding, even for sciophilous species such as spruce, which has an I_S of about 500 μmol photons m^{-2} s^{-1} (Koike et al. 1998).

The effects of sunflecks on photosynthesis inside a forest are important but are usually not taken into account when evaluating the carbon balance. Flecks penetrating the canopy may contribute 10–80% of the PPFD, despite being present for less than 10% of the time (Chazdon 1998). In a larch forest near Yakutsk, the daily sum of the PPFD penetrating the stand canopy was equivalent to 18–23% of the crown incident irradiance (Saito et al. 2003). The portion of the PPFD exceeding the I_S was 20% for a shaded canopy and 10% for the forest floor, with almost all sunflecks occurring in the second half of the day.

The sum of the sunfleck PPFD was at the lower limit of the range reported by Chazdon (1998). Because we were not aware of any data for the boreal zone, available values for tropical and temperate regions were used for comparison. According to some investigations, sunflecks in tropical forests could account for 30–65% of the daily carbon sequestration (Pearcy and Calkin 1983; Pearcy 1987), which is much higher than in temperate zones, where the figure may be as little as 6–19% in deciduous forests (Schulze 1972; Weber et al. 1985). There are two likely reasons for this difference (Pearcy and Pfitsch 1995): (1) the predominance of diffusive light in deciduous forests, which reduces the relative importance of assimilation due to sunflecks, and (2) the low leaf photosynthetic capacity of deciduous plants compared to tropical species.

4.2.6 Nitrogen and Nutrients in a Larch Forest

Sassa (1993) was the first investigator to measure the mineral elements in larch needles in eastern Siberia (as well as in birch and pine). The data for individual nutrients were reported as percentages, approximately 1.5, 0.35, 0.5, 0.20, and 1.3% for N, P_2O_5, CaO, MgO, and K_2O, respectively. A nitrogen content of 1.5% in needles is considered normal for conifers and deciduous trees (Larcher 1995).

Various studies have obtained similar values for the carbon content in aboveground biomass and the nitrogen content in leaves of larch (Shibuya et al. 2001; Koike et al. 1998; Schulze et al. 1995; Vygodskaya et al. 1997; Table 4.1). It can be concluded from these studies that the nitrogen available for growth is rapidly fixed in non-photosynthesising organs and appears to be the main limiting factor of aboveground biomass development, stand dynamics, and the carbon stock of larch. Great variation in leaf nitrogen content has also been observed, with up to a 40% difference reported (Vygodskaya et al. 1997). This has been explained by the high variability of gas-exchange rates, both within the crown and between separate trees. Under the natural conditions of larch forest in eastern Siberia (Central Yakutia), growth/respiratory processes are limited by nitrogen availability rather than CO_2 assimilation.

4.2.7 Assessment of the Biochemical Parameters that Limit Photosynthesis

Alongside investigations of gas exchange to and from needles, the primary biochemical parameters that limit photosynthesis have been estimated from the relationship between the intercellular CO_2 concentration and A_{net} (e.g. Farquhar et al. 1980). The maximum PPFD values were determined for activating the main enzyme involved in carboxylation of the Calvin cycle in photosynthesis, i.e. ribulose-1,5-

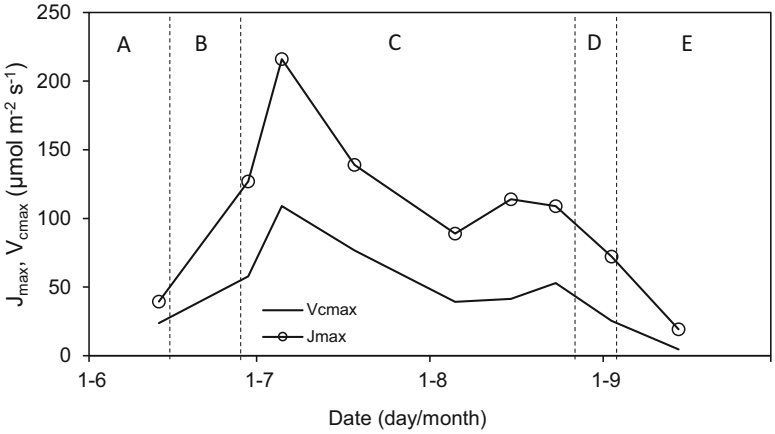

Fig. 4.2 Seasonal course of biochemical parameters (V_{cmax} and J_{max}) of *L. cajanderi* at Spasskaya Pad station. Data of 2008–2012 years are averaged. A. the beginning of active vegetation and buds' growth of the next year (needles have already completed their growth in early June); B, blooming of cones; C, the final phase of vegetation; D, the yellowing beginning of the needles and the buds formation of the next year; E, fallen needles

bisphosphate carboxylase/oxygenase (V_{cmax}), the electronic transport of regenerated ribulose-1,5-bisphosphate (J_{max}), and other related processes (the use of triose phosphate (TPU), light saturation (I_S), and so forth).

Long-term estimates (2000–2014) of V_{cmax} and J_{max} for *L. cajanderi* at Spasskaya Pad have shown that the seasonal variation in typical larch forests in central Yakutia is generally associated with the phases of needle and bud development, but in some years the seasonal trend may not be apparent. An example of the most complete and indicative seasonal course of the biochemical parameters of photosynthesis is shown in Fig. 4.2. These values (average of 40 and 94, maximum of 109 and 216 μmol m^{-2} s^{-1} for V_{cmax} and J_{max}, respectively) were within the range of theoretically expected and average values for similar plants and ecosystems (Wullschleger 1993).

4.3 Soil Respiration in a Larch Forest

Soil respiration result in the release of CO_2 produced by the living inhabitants of soil, i.e. microorganisms, other soil fauna, and plant organs (roots and rhizomes), from the soil surface to the atmosphere. Soil respiration reflects the respiratory activity of the soil biomass, during which soil organisms receive energy to sustain their life from the catabolism of dead organic matter.

Soil respiration is sometimes called underground or belowground respiration, as opposed to aboveground respiration, which refers to the production of CO_2 by plant organs that are located above the soil surface, i.e. stems, trunks, branches, and

leaves. The generally accepted definition of soil does not include dead undecomposed plant residues located on the soil surface in the litter layer, but CO_2 produced as a result of litter decomposition is usually included in soil respiration.

In some circumstances, these patterns may be disrupted. For example, during heavy showers, the air spaces in the soil can be physically degassed by the incoming water, which leads to considerable CO_2 emission from soil surface. At the same time, soil moisture, which increases during rain, may directly affect soil respiration through the activation of soil biomatter. It should also be noted that the chemical reactions of carbonic acid or the activity of methanogenic microorganisms can also lead to changes in the equilibrium of CO_2 in the soil. Nevertheless, these processes do not have a significant influence on CO_2 emissions in the long term, but can affect the rate of CO_2 efflux from soils over shorter time intervals.

It has been widely reported that the recent changes in the average annual ground temperature in the northern hemisphere have begun to rise, particularly in north-eastern Russia (Fedorov et al. 2006; Oberman and Shesler 2009; Romanovsky et al. 2010). An increase in summer precipitation is also expected, together with other environmental and social changes (IPCC 2013). The observed changes in air temperature and precipitation are likely to substantially affect the intensity of soil respiration, which is a key component of the global carbon balance. Thus, with current climate trends, stimulation of soil respiration is expected, which could reduce the carbon uptake capacity of terrestrial ecosystems.

Soil CO_2 efflux (almost equal to soil respiration or soil CO_2 emission) is one of the most intense carbon flux components in the global carbon cycle. Even very small variation in soil respiration due to climate change will cause considerable changes in annual carbon emissions into the atmosphere. The strong sensitivity of soil respiration to variation in soil temperature and moisture is also an interesting and very important issue to study.

The intensity of the CO_2 release from soils depends on climatic variation and the hydrothermal conditions of soils and their properties. It can also be influenced by the physiological state of plants and microbial communities, species composition, and vegetation density. Thus, soil respiration, to a certain extent, characterises the functional state of the ecosystem during the growing season. An analysis of the daily, seasonal, and interannual dynamics of soil respiration in different forests, growing on distinctly different soils, and a subsequent comparison of soil respiration values with certain standard values could explain the mechanisms of ecosystem functioning and reveal their regional components (e.g. Prokushkin et al. 2000a, b; Maximov et al. 2005a).

To more clearly understand the carbon balance characteristics of permafrost larch forest ecosystems, we investigated the long-term response of permafrost soil CO_2-efflux processes in larch forests to changing climatic conditions, at two sites with different ambient and edaphic environments: Spasskaya Pad (medium-productivity larch forest) and Elgeeii (highly productive larch forest) in eastern Siberia.

4.3.1 Daily Dynamics of Soil Respiration

The diurnal variations in soil respiration at Spasskaya Pad and Elgeeii sites fit a bell-shaped curve (Fig. 4.3) and were strongly correlated with temperatures at a depth of 10–40 cm, which means that most soil biological activity originated at those depths. This has been proven by root density and microbial activity studies (Spasskaya Pad; Ivanova et al. 2006). Under relatively moist conditions (soil moisture content, SMC > 14%), the strong correlation between the respiration flux and the soil temperature resulted in the highest soil respiration during the daytime. During relatively dry periods, SMC < 10%, respiration was strongly linked to the SMC, and even small increases in the soil moisture of the upper soil horizons during the night, due to condensation effects, caused an increase in the CO_2 flux. During these conditions, the highest levels of soil respiration occurred at the beginning of the night when the rising soil moisture coincided with the still relatively high soil temperature.

Precipitation events rapidly increased the moisture content in the upper soil layers, which led in turn to a rapid short-term increase in the soil respiration rate, through the enhancement of soil biota activity (Kononov 2006). However, soon after rain, when soil was drying, the pattern of soil respiration again followed the seasonal trend of soil temperature. These CO_2 peaks had virtually no effect on the total CO_2 emission in the short term, with the total seasonal amount of precipitation being the main factor affecting the annual soil CO_2 flux. In both dry and wet years, rainfall after drought in midsummer caused a strong response in soil biological activity (expressed as soil CO_2 emissions). Very small amounts of precipitation

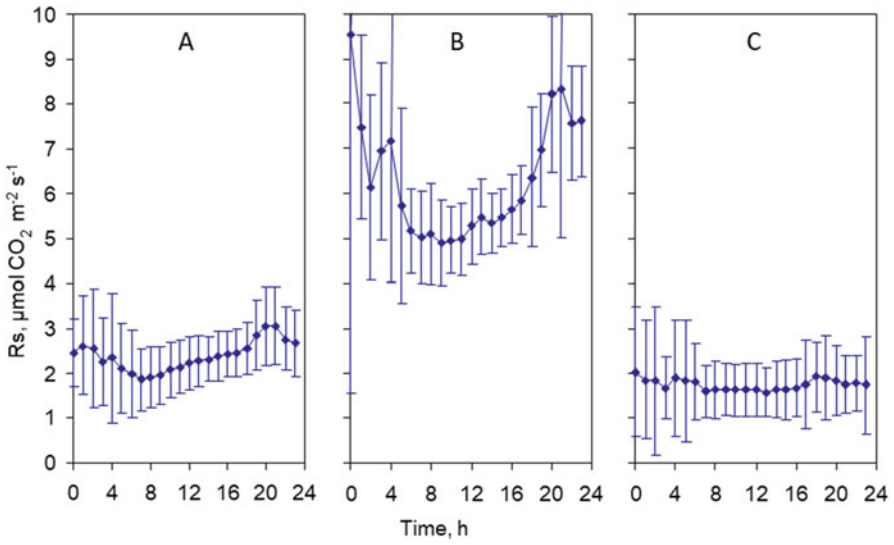

Fig. 4.3 Typical daily curves of soil respiration in Spasskaya Pad (SPA) station, 2006. (**a**) Early June, (**b**) mid-July, (**c**) late August (the error bars are standard deviations)

(2–3 mm day^{-1}) could cause an increase in the soil respiration rate (rise by 24–30%), whereas with much stronger rains (15–20 mm day^{-1}) during wet periods, the rise in the soil respiration rate was only 10–15%. Considerable amounts of precipitation during the cold period of late summer and early autumn did not have much effect on soil respiration, because the low soil temperatures would inhibit the respiratory metabolism of roots and soil organisms despite the abundance of soil moisture.

A high amplitude of daily soil respiration was observed in the mid-growing, with an increase in soil CO_2 emissions at day- or night-time during wet and dry years, respectively. At the beginning and end of the season, the daily curve was smoothed and almost flat, which could be explained by the stable soil temperature regime during these periods.

4.3.2 Seasonal Dynamics of Soil Respiration

There are not many soil respiration data under larch forests worldwide, and almost all the studies were carried out in boreal conifer forests, such as pine, fir, or spruce, mainly in Canada, Alaska, and Scandinavian Peninsula. For instance, in black spruce forests of Manitoba and Saskatchewan (Canada, latitude 54–55°N, sporadic permafrost), soil respiration rates vary from 0.60 to 3.20 μmol m^{-2} s^{-1} (Bond-Lamberty et al. 2004), while in Sweden (Scotch pine and Norway spruce forests, latitude 60–64°N, continuous permafrost), reported soil respiration rates are 1.45–-10.51 μmol m^{-2} s^{-1} (Bhupinderpal-Singh et al. 2003; Högberg et al. 2001; Eliasson et al. 2005; Moren and Lindroth 2000; Widen and Majdi 2001). In Russian climatic research station Zotino (ZOTTO) in the Krasnoyarsk Krai (Siberia, latitude 61°N, continuous permafrost), soil respiration rate was reported to be 1.90 μmol m^{-2} s^{-1} (Kelliher et al. 1999). Thus, estimation of soil respiration rates in boreal conifer forests varies widely, and the average value is around 2.7 μmol m^{-2} s^{-1}.

Data on eastern Siberian permafrost forests (Spasskaya and Elgeeii sites) show that the seasonal pattern of soil CO_2 efflux has a dome-like shape (Fig. 4.4). Minor detectable soil CO_2 releases began immediately after the snow cover started to melt

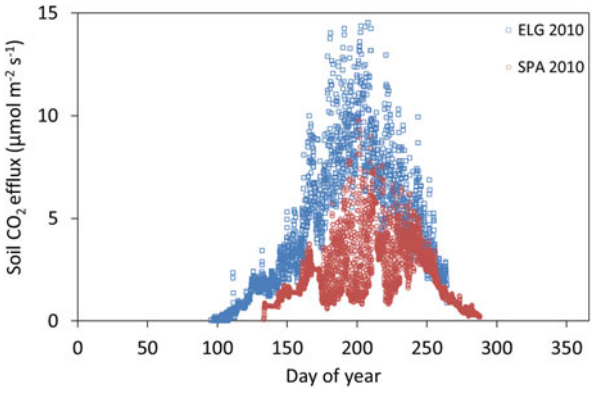

Fig. 4.4 Typical seasonal curves of soil respiration in Spasskaya Pad (SPA) and Elgeeii (ELG) stations, 2010

around the end of April–early May. Observable soil CO_2 emissions began at almost the same time at both sites, in the second week of May, but in Elgeeii they started a few days earlier (DOY 125–135). The maximum soil CO_2 emission in Spasskaya Pad was usually observed in late July–early August (DOY 199–232), with an average of 6.8 μmol CO_2 m^{-2} s^{-1}. In the highly productive Elgeeii site, the highest CO_2 emission (interannual mean: 12.5 μmol CO_2 m^{-2} s^{-1}) was recorded at the end of the second week in July (DOY 188 ± 3), which was 2–3 weeks earlier than at the medium-productivity Spasskaya site. This indicates the early occurrence of optimal conditions for the soil biota in the south-eastern site and can be explained by the physical properties of soils in south-eastern Yakutia (e.g. fast soil warming due to the higher thermal conductance and higher soil porosity of 48.8% versus 40.9% in central Yakutia).

The soil CO_2 efflux at SPA usually stopped in the middle of October (DOY 285–290). At Elgeeii, we measured soil respiration until early October, but based on an analysis of the timings, when the soil temperature reached freezing point, soil biological activity ended at a similar time, i.e. around the end of October.

The seasonal temporal trends of soil respiration mostly corresponded to the temporal variability of the CO_2 concentration along the soil profile. During late autumn and winter, bursts of CO_2 were observed aboveground, accompanied by a corresponding decrease in the CO_2 concentration in the deep soil layers. This could be explained by the release of CO_2 gas, which had previously become trapped under pressure between the upper soil layer and permafrost during the simultaneous freezing of soil horizons. Then the pressurised gas was released to the atmosphere through cracks in the soil that appeared during frost heave. The seasonal magnitude of soil respiration increased significantly with the rise of soil temperature and soil moisture. However, in waterlogged soil, soil respiration was reduced due to the inhibition of aerobic soil biota by over-wetting.

4.3.3 Interannual and Spatial Variation in Soil Respiration

Long-term observations of soil CO_2 emissions in larch forests during the warm period of the year (May–September) revealed significant interannual variation in CO_2 emissions from soils, which were mostly driven by weather conditions during the warm period (air and soil temperatures and precipitation). This was strongly correlated with the moisture reserve of soils, which in turn was highly dependent on the autumn precipitation of the previous year and the water reserves in the current year's snow cover. The long-term (2001–2014) trend of soil CO_2 emissions at Spasskaya Pad had a tendency to decrease slightly. The reasons for this were most likely connected to the general decrease in photosynthetic activity in larch forests that we had observed in the last 10 years, which were determined by plant physiology.

Substantial differences were identified in the magnitude of seasonal and annual CO_2 fluxes from soils in the medium-productivity larch forests at Spasskaya Pad

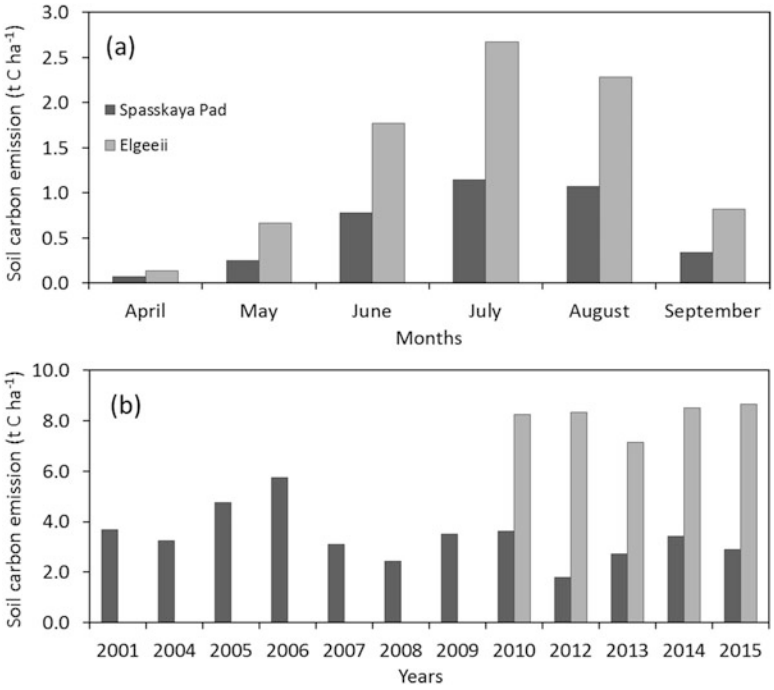

Fig. 4.5 Cumulative carbon fluxes at Spasskaya pad station (SPA, mid-productive forests), 2001–2015, and Elgeeii station (ELG, high-productive forest), south-eastern Yakutia, 2010–2015. (**a**) Long-term monthly averages of carbon emission from soils during the warm period of the year (April–September); (**b**) the interannual amounts of carbon emissions from soils

(central Yakutia) and highly productive larch forests at Elgeeii (south-eastern Yakutia) (Fig. 4.5). The mean annual cumulative carbon emissions from soils at Elgeeii were twice as high as those than at Spasskaya Pad (7.91 and 3.54 t C ha^{-1}, respectively, Fig. 4.6). The main reasons for this difference were as follows: (1) the soils at Elgeeii have a higher porosity and a greater water retention potential than soils at Spasskaya Pad; (2) the higher soil moisture was accompanied by a larger precipitation amount at Elgeeii than at Spasskaya Pad; (3) a longer frost-free period at Elgeeii, with a higher activity of soil biota (156 $\pm$ 14 days in Elgeeii vs. 145 $\pm$ 12 days in the Spasskaya Pad); and (4) a large biomass and high activity of soil biota (including roots, fungi, actinomycetes, and so forth) in the south-eastern region.

According to available data in Russian scientific literature, the cumulative soil carbon flux is 1.7–15.7 t C ha^{-1} per growing season in northern and southern Russian taiga, respectively (Kudeyarov et al. 1995).

As for eastern Siberian permafrost forests, the absolute value of soil CO_2 emissions significantly varies on a spatial basis, even within the central Yakutia region. Comparative studies there made in 2005–2006 (Kononov 2006) show that there are

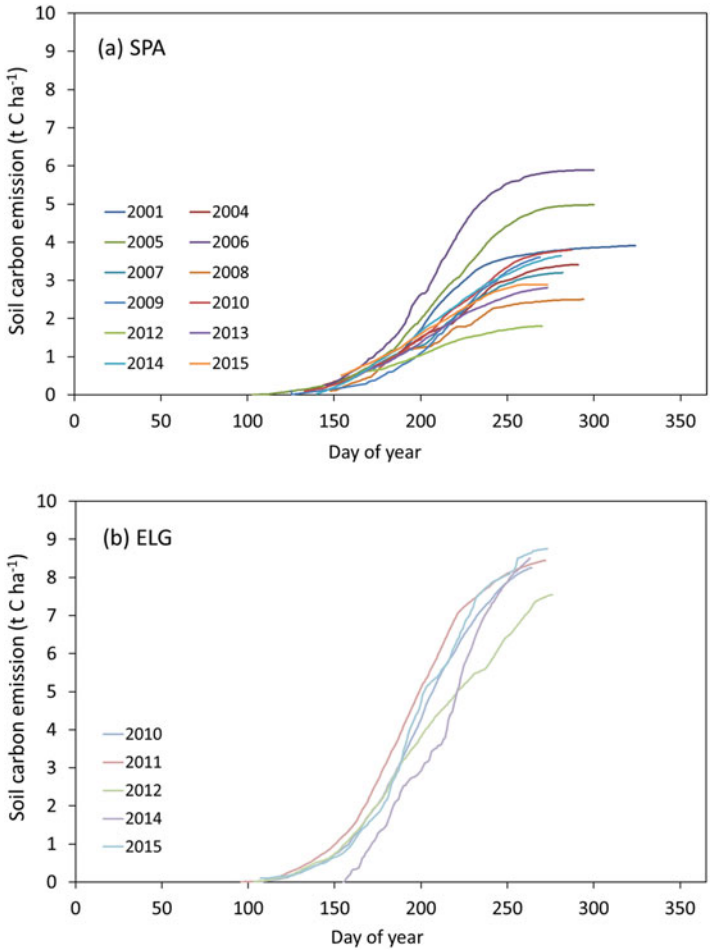

Fig. 4.6 Carbon fluxes from soils of larch forests at Spasskaya pad stations, Central Yakutia, 2001–2015, in (**a**) SPA site (mid-productive forest) and Elgeeii, south-eastern Yakutia, 2010–2015, in (**b**) ELG site (high-productive forest)

15–20% differences in soil respiration in the larch forests on the right and left banks of the Lena River central basin. At the same time, in the south-eastern part of the investigated region (Elgeeii), the cumulative emission of CO_2 reached 8.5 t C ha^{-1} during the growing season, which was more than twice as high as that recorded at sites along the Lena River in central Yakutia. These differences were largely due to hydrothermal conditions, but the pivotal factor was the soil type and its associated properties.

4.3.4 Environmental Dependencies of Soil Respiration

Several environmental dependencies of soil respiration were identified, which showed that the soil CO_2-efflux values during the growing season (F_s) had a strong positive correlation with the trend of soil temperature (T_s) at both sites ($r^2 = 0.74$ for Spasskaya Pad and $r^2 = 0.79$ for Elgeeii). The response of soil respiration to temperature (long-term average Q10 values) at Spasskaya Pad was 4.89 and was almost identical to that at Elgeeii (4.85), but base respiration (T_0) was 1.5 times higher at Elgeeii (1.53 vs. 0.99 at Spasskaya Pad). This indicates that the bigger CO_2 flux at the Elgeeii site could be explained not only by the relatively higher T_s but also by some endogenous factors, for example, a more massive microbial and fungal community. An analysis of other environmental dependencies showed that there were no soil CO_2-efflux correlations with net radiation, photosynthetically active radiation (PAR), or soil heat flux. A soil physics study indicated that the soils at Elgeeii had a higher porosity and water retention capacity compared to that of Spasskaya Pad soil. These soil qualities at Elgeeii led to a relatively stable soil moisture regime during the whole season. As a consequence, the soil conditions at Elgeeii were much more comfortable for soil biota, and therefore a higher annual soil carbon release (cumulative CO_2-flux) was observed at Elgeeii. It was also found that at the Spasskaya Pad site, the cumulative soil carbon efflux in early summer was strongly dependent on the precipitation levels in the autumn of the previous year. For example, if there was a large amount of precipitation registered in autumn, then in early summer of the following year, the soil CO_2 efflux would also be high. In late summer, the CO_2 efflux was mainly correlated with the current precipitation levels.

A comparative analysis of the properties and hydrothermal regime of soils of larch forests in different bioclimatic zones in Yakutia showed that the main factor limiting the seasonal biological activity of the ecosystem was the soil moisture in the upper soil horizons (0–20 cm), which corresponded to the specific properties of soils (porosity, texture, and composition) and the amount of precipitation. At the same time, precipitation (and accordingly soil moisture) also played an important role on a seasonal scale. The early summer soil CO_2 efflux had a strong correlation with the previous year's autumn precipitation. Soil respiration in the second half of summer was mainly correlated with the current year's late summer rains.

Based on an analysis of our data, obtained along the meridional transect, it was found that soil CO_2 emissions in the middle taiga of central Yakutia could be limited by the hydrothermal conditions of the season; however, the main factors were the types and properties of soils. The crucial endogenous factors that determined the soil respiration rate were the depth of the humus layer and accordingly the carbon content of the soil. The difference in soil respiration values of typical sod-pale-yellow solodic and pale-yellow solodic soils in larch forests of the middle Lena River Basin in central Yakutia was 15–20% (the humus reserves in the 0–50 cm layers of each soil type were 108.3 and 97.2 t C ha^{-1}, respectively). The soil respiration of

sod-pale-yellow typical soils along the middle Aldan River basin in the south-eastern part of central Yakutia (Elgeeii), with humus reserves of 137.0 t C ha^{-1}, was more than twice as high than the respiration of soils with a lower humus content. In the northern ecosystems, every change in the soil carbon stock (increase or decrease) may lead to rapid changes in the carbon balance of the whole ecosystem.

Thus, it must be concluded that the expected changes in precipitation and soil temperature in high latitudes are likely to cause an increase in soil biological activity, together with fluctuations in the levels of soil carbon. Therefore, an enhancement of the soil dead organic matter decomposition rates, accompanied by the intensification of CO_2 emissions from soils, could occur. Finally, we considered that these processes could lead to drastic changes in the carbon exchange in northern forest ecosystems.

4.4 NEE of CO_2 in Larch Forest

According to our calculations, in the Yakutian forest ecosystems, the total carbon reserves are 13.3–15.7 billion tons of carbon (Table 4.4). The carbon content in the vegetation and soil of forest ecosystems exceeds that of the tundra by an average of 63 and 2 times, respectively. Accumulated carbon stocks in the soils of forest and tundra ecosystems in eastern Siberia (Yakutia) are total 17.1 billion tons in a total area of 125.5 million hectares of forest and 37 million hectares of tundra. This is about 7 and 25% of the total carbon stock in the forest soils of Siberia and Russia, respectively (Maximov et al. 1996).

There has been an increase in the demand for wood that has coincided with changes in management practices to increase forest outcomes. Because the NEE in the forest is the balance of carbon uptake as the result of tree growth and carbon release as a result of soil respiration, management strategies oriented only to tree growth can have negative consequences for the capacity of the entire ecosystem to accumulate and emit carbon.

Table 4.4 Carbon pool of eastern Siberia, Republic of Sakha (Yakutia) (Maximov 2007)

	Carbon stocks [Gt C]
Forest ecosystem (126 million ha)	13.3–15.7
Vegetation	2.2–4.5
Soil	11.2
Tundra ecosystem (37 million ha)	5.9
Vegetation	0.053
Soil	5.9
Total	19.2–21.6

Table 4.5 Monthly average of net ecosystem exchange (NEE), as well as day- and night-time estimates, observed in larch forest of the scientific station "Spasskaya Pad". The duration of the daytime is from 5:00 a.m. to 21:00 p.m. of Yakutsk local time. Data of 2000–2014 years are averaged

	NEE [μmol m^{-2} s^{-1}]		
Month	All day	Daytime	Night-time
May	0.51	0.55	1.72
June	−3.20	−4.34	1.07
July	−2.01	−3.32	1.92
August	−1.24	−2.94	1.85
September	0.31	−0.49	1.12

4.4.1 The Daily and Seasonal Dynamics

According to eddy covariance flux observations in a larch forest in eastern Siberia, seasonal CO_2 uptake has a distinct pattern. In typical hydrothermal conditions, the Yakutian larch forest absorbs CO_2 mostly in June. Some decrease in the uptake is expected at the end of July and August (Table 4.5). When the needles fall in September, trees and soils continue to breathe and emit CO_2 before the soil freezes. When night and day conditions were reviewed separately, it was clear that the high uptake in June was mainly caused by a significant daytime uptake. June is the month with the highest physiological activity in this ecosystem (see Sect. 4.2). The largest positive values in night-time occurred in July and August.

During the growing period of 2001, the total NEE obtained by summing the daily values was estimated to be −206.4 g C m^{-2} (−17.2 mol C m^{-2}) in the larch forest at Spasskaya Pad (Dolman et al. 2004). By considering the CO_2 from soil respiration trapped in the unfrozen soil layer, which is created by the freezing of soils from both above and below in autumn (after September), a small emission of 1.6 mol C m^{-2} (19.2 g C m^{-2}) was estimated (Dolman et al. 2004). In a similar manner, we estimated the total NEE of the growing season in the larch forest to be −164 to −223 g C m^{-2} (−1.6 to −2.2 t C-CO_2 ha^{-1}) during 2001–2015. From these estimates, the annual uptake of CO_2 was determined to be 170 g C m^{-2} $year^{-1}$ (1.7 t C ha^{-1} $year^{-1}$) in an extremely dry year (2001) and 270 g C m^{-2} $year^{-1}$ (2.7 t C ha^{-1} $year^{-1}$) in a wet year (2006). It should be noted that this is not a long-term deposit of carbon into the ecosystem, but represents net biome production (NBP). The values of NEE that we calculated can be described optimally as net ecosystem production (NEP) (Körner 2003, Dolman et al. 2004). To assess the long-term NBP, the influence of disturbances such as fires should be taken into account. It has been established that forest fires, deforestation, and other disturbances significantly reduce NEP; about 10% of the NEP is locked into soil carbon in the form of NBP. According to Shvidenko and Nilsson (1994), the total area of larch forests in eastern Siberia is 168.8 × 10^3 km^2. We estimated the regional total of the annual carbon storage capacity to be 0.28 Gt C $year^{-1}$, which is probably not the upper limit and can vary significantly from year to year (Dolman et al. 2004).

These results obtained in a larch forest in eastern Siberia (central Yakutia) can be compared to other Siberian ecosystems. The overall NEE was comparable to values reported for birch and mixed forests in central Siberia (Röser et al. 2002), but they were slightly higher than our results for eastern Siberia. The most distinctive finding in eastern Siberia was a sharp increase in negative NEE (uptake) after the needles began to grow. The forest was completely dormant for 9 months, with photosynthesis suddenly beginning in June. June was definitely the month with the greatest absorption, whereas for the central Siberian forest, it is July (Röser et al. 2002).

The rate of CO_2 uptake in summer at Spasskaya Pad was quite high (18 μmol m^{-2} s^{-1}). The maximum negative NEE in a birch plot in central Siberia and at two plots in a mixed stand were −13, −10, and −8 μmol m^{-2} s^{-1}, respectively (Röser et al. 2002). For larch forest investigated in this study, Hiyama et al. (2001) reported a maximum rate of uptake in July of −15.9 μmol m^{-2} s^{-1}, which is comparable with the results of our measurements. High daily rates are supported by independent measurements of photosynthesis in 2003, which showed that at the leaf level, the maximum NEE was 12 μmol m^{-2} s^{-1} in July. With a leaf area index of about 2, a maximum rate of about 24 μmol m^{-2} s^{-1} was determined at the level of the canopy. Such a value lends credence to current estimates and suggests that the rate of CO_2 uptake by larch forests in eastern Siberia during the peak periods may be higher than those in pine forests growing in central Siberia (Dolman et al. 2004).

Then forests of the intracontinental areas in eastern Siberia have developed in severe conditions, with extremely low temperatures, low annual precipitation, and a strong nitrogen deficit. However, as our studies have shown, water stress was not observed, even in dry years, because soil water is accessible to trees and flows to the active root zone during thawing of the seasonally thawed layer (STL) that stabilises transpiration (Sugimoto et al. 2003). The maximum net carbon uptake occurs at the beginning of the summer (June) and then decreases in the hotter midsummer, while uptake rises on cool days at the end of summer.

4.4.2 Contribution of Permafrost Forest in the Terrestrial Carbon Cycle of Russia

Long-term studies of NEE in the larch forest and tundra zone in eastern Siberia are summarised in Fig. 4.7. There is significant interannual variation in cumulative NEE in the medium-productivity larch forest of central (Spasskaya Pad) and southern (Elgeeii) Yakutia (range from −170 to −270 g C m^{-1} $year^{-1}$). In the tundra ecosystem, the variation in NEE is small (range from −50 to −90 g C m^{-2} $year^{-1}$), due to the influence of the maritime climate in the tundra zone of Yakutia (Chokurdakh), where the climatic conditions are less variable than in the continental central Yakutia.

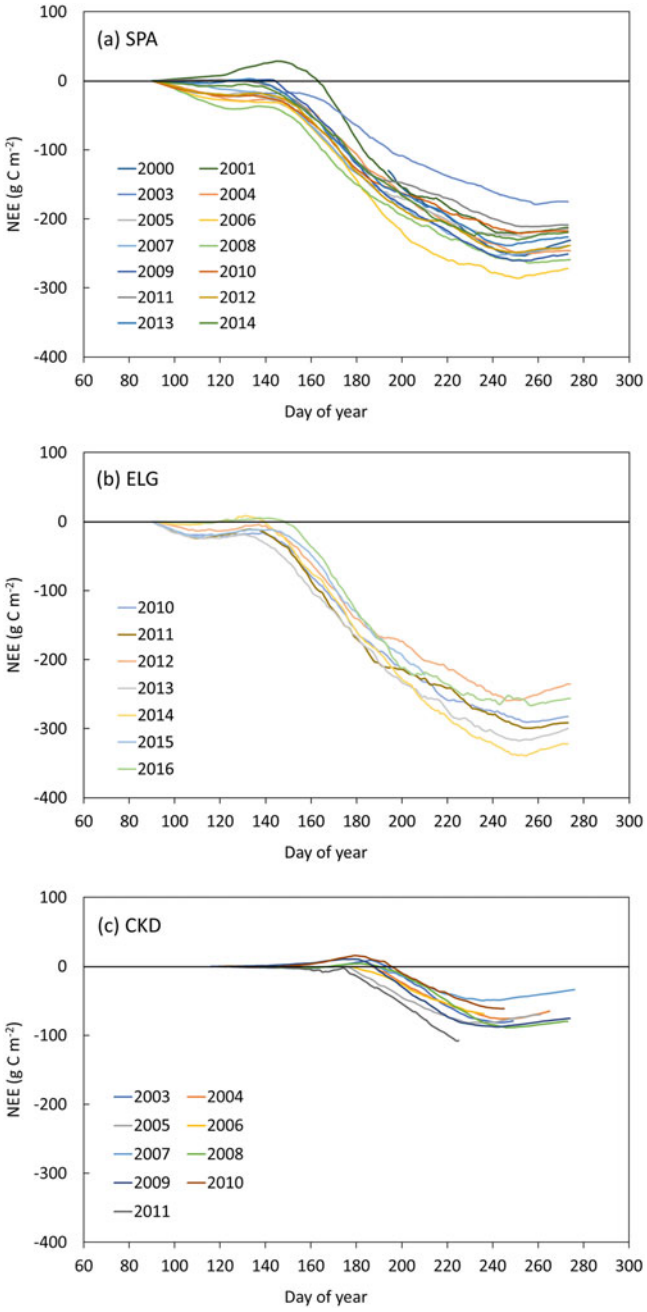

Fig. 4.7 Cumulative carbon accumulation in eastern Siberia, 2000−2014, by forest ecosystems in (**a**) SPA and (**b**) ELG sites and by tundra ecosystem in (**c**) CKD site

According to long-term eddy-correlation data, the annual NEE at Spasskaya Pad was 212 ± 34 g C m^{-2} $year^{-1}$, at Elgeeii was 243 ± 23 g C m^{-2} $year^{-1}$, and in Chokurdakh was 75 ± 14 g C m^{-2} $year^{-1}$.

Preliminary studies have estimated the drainage capacity of the Siberian forest to be between 50 and 250 g C m^{-2} $year^{-1}$, which is well within the limits indicated in the United Nations Framework Convention on Climate Change (UNFCC) proposal and the value obtained by an atmospheric inversion model (Schulze et al. 1999). Recent estimates using these atmospheric modelling methods assume a carbon flow capacity of 1.5 billion tons $year^{-1}$ for north Asia. This estimate includes all changes in land use over a 10-year period and is based on measurements of atmospheric CO_2 (Bousquet et al. 1999).

According to our data, the interannual variation in the NEE in the forest ecosystem of the permafrost zone is 1.7–2.7 t C ha^{-1} $year^{-1}$, which leads to an upper limit of annual deposition capacity of 0.45–0.71 Gt C $year^{-1}$ for 257.1 million ha area of these forests in Russia. In larch forests in eastern Siberia, there is an annual accumulation from 0.4 to 1.0 Gt C, which is comparable to the equivalent values for European and tropical forests. This calculation does not include the emissions from forest fires. According to Isaev et al. (1995), the carbon flux for the post-fire loss from Russian forests ranges from 0.053 to 0.058 Gt C $year^{-1}$. From satellite observations, CO_2 emissions after fires are estimated to be 0.14 Gt for area of Russia (Rödenbeck et al. 2003). The contribution of Siberian forests (located to the east of the Ural mountain) to this CO_2 budget excluding forest fire is estimated to be 55–62% of all Russian forests. The annual sink of the permafrost larch forests in Siberia is almost half that of all Russian forests (55%), and soil emissions are about 27% of all Russian forests (Table 4.6).

Comparing our experimental data with earlier studies using satellite data (Schimel et al. 2001; Goodale et al. 2002), it was clear that the earlier data were undervalued,

Table 4.6 Annual carbon budget of larch forests in Siberia and Yakutia (Maximov 2007)

Territory	CO_2 flux [Gt C $year^{-1}$]	Profit [%]
Assimilation		
Siberia[a]	1.3	100
Larch in Siberia	0.4–1.0	54
Larch in eastern Siberia (Yakutia)	0.2–0.4	23
Emission		
Russia's soil[b]	2.6–3.0	100
Larch in Siberia	0.8–0.9	27
Larch in eastern Siberia (Yakutia)	0.4	12
Net ecosystem gas exchange (NEE)		
Russia[b]	0.82	100
Larch in Siberia	0.45	55
Larch in eastern Siberia (Yakutia)	0.18	22

Without marks – our data
[a]Schimel et al. (2001), Goodale et al. (2002)
[b]Kudeyarov et al. (1995)

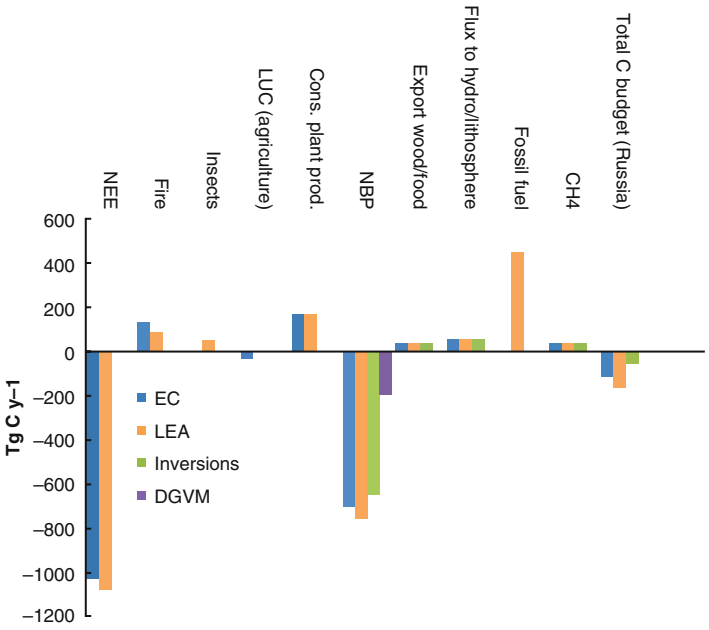

Fig. 4.8 Assessment of carbon budget of Russian 5 biome using three models, LEA (Land Ecosystem Assessment), Inversions and DGVM (Dynamic Global Vegetation Model), and tower experimental eddy covariance method (EC). (Dolman et al. 2012)

with a value of 0.7 Gt C year^{-1} (Dolman et al. 2012) against 1.3 Gt C year^{-1}. In recent years, an increase in the absorptive capacity of larch forests could be traced to climate warming, with an increase in the duration of the growing season, amendments in land use (afforestation or reforestation), and the nutrient fertilising effects of a CO_2 increase (Maximov 2007).

The net CO_2 flux from land to atmosphere in Russia, including Ukraine, Belarus, and Kazakhstan, was evaluated using inventory-based, eddy covariance, and inversion methods (Dolman et al. 2012). Our upper estimate (Dolman et al. 2012) was -0.342 G t C year^{-1} from the eddy covariance method, which is close to the upper bounds of the inventory-based Land Ecosystem Assessment (LEA) and inverse model estimates (Fig. 4.8). Our lower estimate was -1.3 Gt C year^{-1} from the inversion models. The average of the three methods was -0.6 Gt C year^{-1}. The methane emission was estimated separately, with a positive value of 0.041 Gt C year^{-1} derived. These three methods agreed well within their respective error bounds. There was thus good consistency between bottom-up and top-down methods. From the LEA, the forests of Russia had a net atmosphere to land flux of 0.7 Gt year^{-1}. It was remarkable that the three methods produced such close estimates (0.61, 0.66, and 0.55 Gt C year^{-1}) for the NBP, given the inherent uncertainties in all of the approaches.

The lack of recent forest inventories, the limited numbers of eddy covariance sites, and the associated uncertainty with upscaling and under-sampling of concentrations for the inversions were among the prime causes of the uncertainty. The dynamic global vegetation models suggested a much lower uptake of 0.091 Gt C $year^{-1}$, which we argue that it is caused by a high estimate of heterotrophic respiration compared to the other methods.

4.5 Concluding Remarks

During the short growing season in eastern Siberia, the growth and development of woody plants are provided by high levels of physiological processes (photosynthesis and transpiration) with relatively low R_{dark} and night respiration rates supporting growth and maintenance. The large interannual variability of the photosynthesis and R_{dark} for *L. cajanderi* plants indicates its excellent adaptability to the peculiar cryolithozone climatic conditions.

The seasonal maximum of photosynthetic activity of forest plants is observed in June in dry years and in July in wet years. It was found that in the eastern Siberia permafrost region, under natural conditions the A_{max} was substantially higher than the A_{max} of similar vegetation species in warmer regions, including Europe. The key morphophysiological adaptation to these conditions was a high stomatal conductance. The range of diurnal photosynthesis had a single peak, with no midday depression. Seasonal and annual fluctuations were reduced to a single pattern, clearly showing the difference in CO_2 assimilation dynamics over the year, with the most active month being July and the least active being May.

Long-term estimates of V_{cmax} and J_{max} have shown that in a larch forest in Yakutia, their seasonal character generally followed the phenological phases of needle, cone, and bud development. The variation in these parameters, which was not related to phenology, was caused by the nitrogen dynamics in the needles. The V_{cmax} and J_{max} values of *L. cajanderi* were within the theoretical ranges and were similar to the average values for the other plant species and ecosystems under similar environmental conditions. Both the initial and modelled relationships between V_{cmax} and J_{max} as well as their ratio with A_{max} had a strong correlation, providing a basis for the mutual analysis of the values.

Based on a study of 899 plant species from 100 sites (from the Arctic to the tropics), a new global database of the R_{dark} of plants (GlobResp) was created (Atkin et al. 2015), part of which includes the R_{dark} results for larch, pine, and birch in the taiga ecosystem of eastern Siberia.

With regard to the daily dynamics of the soil carbon emission, the main environmental factor affecting the soil respiration rate in the larch forests of eastern Siberia was the soil temperature, while the humidity of the upper soil horizons was only an additional factor contributing to the temperature sensitivity of soil respiration. A large amplitude in the daily soil respiration was observed in the mid-growing season, with an increase in the soil CO_2 emission during day and night in wet and dry years,

respectively. At the beginning and the end of the season, the curve showing the daily pattern of soil respiration was smooth and almost flat.

The maximum soil CO_2 emissions in permafrost soils during the growing season were observed from mid-July to mid-August, when the soil temperature reached a maximum and the soil moisture in upper soil horizons was minimal. At that time, the source of CO_2 was the deeper layers of soil. If the precipitation at that time was insufficient, the influence of the overnight soil moisture increase became stronger, but in years with a large rainfall during July and August, the soil moisture variation was not a factor limiting soil respiration. Early in the season, when the moisture content in the upper soil horizons was still high, the soil temperature played a dominant role. The heavy rains in the cold period of late summer and autumn were not able to affect the general seasonal course of soil respiration because the activity of soil biota at that time was suppressed by low soil temperatures despite the presence of sufficient soil moisture.

In future, the crucial endogenous factors that determine the soil respiration rate are the depth of the humus layer and, accordingly, the carbon content in the soil. In northern ecosystems, every change in the soil carbon stock (increase or decrease) may lead to rapid changes in the carbon balance of the whole ecosystem.

It must be concluded that the expected changes in precipitation and soil temperatures in high latitudes are likely to cause an increase in soil biological activity together with fluctuations in the soil carbon content. Therefore, soil organic matter decomposition rates could be enhanced, accompanied by the intensification of CO_2 emissions from soils. We considered that these processes could lead to drastic changes in the carbon exchange in northern forest ecosystems.

References

Abaimov AP, Zyryanova OA, Prokushkin SG (2002) Long-term investigations of larch forests in cryolithic zone of Siberia: brief history, recent results and possible changes under global warming. Eurasian J For Res 5(2):95–106

Arneth A, Kelliher FM, Bauer G, Hollinger DY, Byers JN, Hunt JE, McSeveny TM, Ziegler W, Vygodskaya NN, Milukova I, Sogachov A, Varlagin A, Schulze ED (1996) Environmental regulation of xylem sap flow and total conductance of Larix gmelinii trees in eastern Siberia. Tree Physiol 16:247–255. https://doi.org/10.1093/treephys/16.1-2.247

Atkin OK, Bloomfield KJ, Reich PB, Tjoelker MG, Asner GP, Bonal D, Bonisch G, Bradford MG, Cernusak LA, Cosio EG, Creek D, Crous KY, Domingues TF, Dukes JS, Egerton JJG, Evans JR, Farquhar GD, Fyllas NM, Gauthier PPG, Gloor E, Gimeno TE, Griffin KL, Guerrieri R, Heskel MA, Huntingford C, Ishida FY, Kattge J, Lambers H, Liddell MJ, Lloyd J, Lusk CH, Martin RE, Maksimov AP, Maximov TC, Malhi Y, Medlyn BE, Meir P, Mercado LM, Mirotchnick N, Niinemets DN, O'Sullivan OS, Phillips OL, Poorter L, Poot P, Prentice IC, Salinas N, Rowland LM, Ryan MG, Sitch S, Slot M, Smith NG, Turnbull MH, VanderWel MC, Valladares F, Veneklaas EJ, Weerasinghe LK, Wirth C, Wright IJ, Wythers KR, Xiang J, Xiang S, Zaragoza-Castells J (2015) Global variability in leaf respiration in relation to climate, plant functional types and leaf traits. New Phytol 206(2):614–637. https://doi.org/10.1111/nph.13253

Benecke U, Schulze ED, Matyssek R, Havnarek WM (1981) Environmental control of CO2-assimilation and leaf conductance in Larix decidua Mill. I. A comparison of contrasting natural environments. Oecologia 50:54–61. https://doi.org/10.1007/BF00378793

Bhupinderpal-Singh NA, Lofvenius MO, Högberg MN, Mellander PE, Högberg P (2003) Tree root and soil heterotrophic respiration as revealed by girdling of boreal Scots pine forest: extending observations beyond the first year. Plant Cell Environ 26:1287–1296

Bond-Lamberty B, Wang CK, Gower ST (2004) Contribution of root respiration to soil surface CO2 flux in a boreal black spruce chronosequence. Tree Physiol 24:1387–1395

Bousquet P, Ciais P, Peylin P, Ramonet M, Monfray P (1999) Inverse modelling of annual atmospheric CO_2 sources and sinks: 1 method and control inversion. J Geophys Res 104:26161–26178. https://doi.org/10.1029/1999JD900342

Bykov OD (1983) Sootnosheniye photosynteza I dykhaniya v CO_2-gazoobmene na svety u listyev C3-rasteniy v zavisimosti ot temperatury (Relationship between photosynthesis and respiration in light CO_2-exchange of C3-plants depending of temperature). Physiologiya rastenii 30:629–636

Chazdon RL (1998) Sunflecks and their importance to forest understory plants. Adv Ecol Res 18:1–63. https://doi.org/10.1016/S0065-2504(08)60179-8

Dang QL, Lieffers VJ, Rothwell RL (1991) A self-contained freezing chamber for tree ecophysiological studies in the field. For Sci 37:924–930

Dixon RK, Brown S, Houghton RA, Solomon AM, Trexler MC, Wisniewski J (1994) Carbon pools and flux of global forest ecosystems. Science 263:185–190. https://doi.org/10.1126/science.263.5144.185

Dolman AJ, Maximov TC, Moors EJ, Maximov AP, Elbers JA, Kononov AV, Waterloo MJ, van der Molen MK (2004) Net ecosystem exchange of carbon dioxide and water of far eastern Siberian Larch (Larix Dahurica) on permafrost. Biogeosciences 1:275–309. https://doi.org/10.5194/bg-1-133-2004

Dolman AJ, Shvidenko A, Schepaschenko D, Ciais P, Tchebakova N, Chen T, van der Molen MK, Belelli Marchesini L, Maksyutov S, Schulze ED (2012) An estimate of the terrestrial carbon budget of Russia: an estimate of the terrestrial carbon budget of Russia using inventory based, eddy covariance and inversion methods. Biogeosciences 9:5323–5340. https://doi.org/10.5194/bg-9-5323-2012

Eliasson PE, McMurtrie RE, Pepper DA, Stromgren M, Linder S, Agren GI (2005) The response of heterotrophic CO_2 flux to soil warming. Glob Chang Biol 11:167–181

Farquhar GD, von Caemmerer S, Berry JA (1980) A biochemical model of photosynthetic CO2 assimilation in leaves of C3 species. Plata 149:78–90. https://doi.org/10.1007/BF00386231

Fedorov AN, Maximov TC, Gavriliev PP (eds) (2006) Spasskaya Pad: kompleksniye issledovaniya landshaphtov (Spasskaya Pad: complex studies of landscapes). PI Publishing House, Yakutsk, p 210

Fujita N, Yanagisawa N, Sugimoto A (1998) Domination of an East-Siberian taiga around Yakutsk by Larix gmelinii, a deciduous conifer, supported by leafing phenology, photosynthetic characteristics and water use efficiency. Activity Rep GAME-Siberia 14:81–84

Goodale CL, Apps MJ, Birdsey RA, Field CB, Heath LS, Houghton RA, Jenkins JC, Kohlmaier GH, Kurz WA, Liu S, Nabuurs GJ, Nilsson S, Shvidenko AZ (2002) Forest carbon sinks in the Northern Hemisphere. Ecol Appl 12(3):891–899. https://doi.org/10.1890/1051-0761(2002)012[0891:FCSITN]2.0.CO;2

Hiyama T, Ohta T, Tanaka H, Fukushima Y (2001) Flux observations in eastern Siberia. In: Proceedings of International workshop for advanced flux network and flux evaluation Sapporo, 2000, p 43–51

Högberg P, Nordgren A, Buchmann N, Taylor AFS, Ekblad A, Högberg MN, Nyberg G, Ottosson-Lövenius M, Read DJ (2001) Large-scale forest girdling shows that current photosynthesis drives soil respiration. Nature 411:789–792

Hollinger DY, Kelliher FM, Schulze ED, Vygodskaya NN, Varlagin A, Milukova I, Byers JN, Sogatchov A, Hunt JE, McSeveny TM, Kobak KI, Bauer G, Arneth A (1995) Initial assessment

of multi-scale measures of CO2 and H2O flux in the Siberian taiga. J Biogeogr 22:425–431. https://doi.org/10.2307/2845939

IPCC (2013) Climate change 2013: the physical science basis. Contribution of working group I to the fifth assessment report of the intergovernmental panel on climate change. Cambridge University Press, Cambridge and New York, p 1535. https://doi.org/10.1017/CBO9781107415324

Isaev AS, Korovin GN, Suhikh VI, Titov SP, Utkin AI, Golub AA, Zamolodchikov DG, Pryazhnikov AA (1995) Ecologicheskiye problemy poglosheniya uglekislogo gaza posredstvom lesovosstanovleniya i lesorazvedeniya (Ecological problems of CO_2 uptake due to forest reforestation and regeneration). Center for ecological policy, Moscow, p 156

Ivanov LA, Kossovich NL (1932) O rabote assimilyatsionnogo apparata drevesnikh porod. (About activity of assimilation apparatus of woody species). Bot zhurnal 17(1):3–17

Ivanova TI, Kononova NP, Nikolaeva NV, Chevychelov AP (2006) Microjrganizmy v lesnukh pochvakh Cetralnoy Yakutii (Microorganisms in forest soils of Central Yakutia). Pochvovedenie 6:735–740

Kelliher FM, Hollinger DY, Schulze ED, Vygodskaya NN, Byers JN, Hunt JE, McSeveny TM, Milukova I, Sogatchev A, Varlargin A, Ziegler W, Arneth A, Bauer G (1997) Evaporation from an eastern Siberian larch forest. Agric For Meteorol 85:135–147. https://doi.org/10.1016/S0168-1923(96)02424-0

Kelliher FM, Lloyd J, Arneth A, Luhker B, Byers JN, McSeveny TM, Milukova I, Grigoriev S, Panfyorov M, Sogatchev A, Varlargin A, Ziegler W, Bauer G, Wong SC, Schulze ED (1999) Carbon dioxide efflux density from the floor of a central Siberian pine forest. Agric For Meteorol 94:217–232

Koike T, Mori S, Matsuura Y, Prokushkin SG, Zyranova OA, Kajimoto T, Abaimov AP (1998) Photosynthesis and foliar nutrient dynamics in larch and spruce grown on contrasting north- and south-facing slopes in the Tura Experiment Forest in Central Siberia. In: Mori S et al (eds) Proceedings of the 6th symposium on the joint Siberian permafrost studies between Japan and Russia in 1997, Sapporo, 1998, p 3–10

Koike T, Mori S, Matsuura Y, Prokushkin SG, Zyryanova OA, Kajimoto T, Sasa K, Abaimov AP (1999) Shoot growth and photosynthetic characteristics in larch and spruce affected by temperature of the contrasting north- and south-facing slopes in eastern Siberia. In: Shibuya M et al (eds) Proceedings of the 7th symposium on the joint Siberian permafrost studies between Japan and Russia in 1998, Sapporo, 1999, p 3–12

Koike T, Yazaki K, Funada R, Kitao M, Maruyama Y, Maximov TC, Takahashi K, Ivanov BI (2000) Photosynthetic characteristics of Dahurian larch, Scotch pine and white birch seedlings native to eastern Siberia raised under elevated CO_2. Eurasian J For Res 1:31–37

Kononov AV (2006) Emissiya uglekislogo gasa merzlontnymi pochvami listvennichnykh lesov tsentral'noy Yakutii v zavisimosti ot gidrotermicheskikh uslovyi (The carbon dioxide emissions from permafrost soils of larch forests in Central Yakutia depending on hydrothermal conditions). Abstract of Thesis for a Candidate Degree. Yakutsk

Körner C (2003) Slow in, rapid out–carbon flux studies and Kyoto targets. Science 300:1242–1243. https://doi.org/10.1126/science.1084460

Kudeyarov VN, Khakimova FI, Deyeva NF, Ilyina AA, Kuznetsova TV, Timchenko AV (1995) Otsenka dykhaniya pochv v Rossii (An estimation of Russia soil respirations). Pochvovedeniye 1:33–42

Laisk AK (1977) Kinetica photosynteza i photodykhaniya C3 rastenii (Kinetics of photosynthesis and photorespiration of C3-plants). Nauka, Moskva, p 193

Larcher W (1995) Physiological plant ecology: ecophysiology and stress physiology of functional groups, 3rd edn. Springer, Berlin, Heidelberg, p 506

Malkina IS (1995) CO_2 exchange of young larch trees. Lesovedenie 5:59–66 (in Russian)

Matyssek R, Schulze ED (1987) Heterosis in hybrid larch (Larix decidua x leptolepis). I. The role of leaf characteristics. Trees 1:219–224. https://doi.org/10.1007/BF01816819

Maximov TC (1989) Ekolo-fiziologicheskiye issledovaniya fotosinteza yachmenya v usloviyakh Yakutii (Ecological physiological studies of barley photosynthesis under conditions of Yakutia). Abstract of Thesis for a Candidate Degree. Yakutsk

Maximov TC (2007) Circulation of carbon in Larch forests of Yakutian sector of cryolithozone. YSC Publishing house, Yakutsk, p 46

Maximov TC, Ivanov BI (2003) The development of international studies of the regional and global carbon cycle in Yakutia permafrost ecosystems. In: The review of conditions and tendencies of climate changes in Yakutia, Yakutsk, p 34–43

Maximov TC, Ivanov BI (2005) Monitoring sostoyatiya merzlotnikh ecosystems: Spasskaya Pad, Yakutsk (The monitoring of permafrost ecosystems condition: Spasskaya Pad, Yakutsk). Sibirsky ecologichesky zhurnal 12(4):777–781

Maximov TC, Ivanov BI, Maximov AP, Kononov AV (1994) Interim report of joint research between FFPRI and YIB "carbon storage and carbon dioxide budget in Forest ecosystem", Sapporo, p 106

Maximov TC, Kononov AV, Koike T (1995) Photosynthetic activity of woody plants of Yakutia. In: Symposium on joint permafrost studies between Japan and Russia in 1992–1994, p 24–30

Maximov TC, Maximov AP, Kononov AV (1996) Balance of carbon dioxide and water in permafrost ecosystems of Yakutia. In: Proceedings of the third international study conference on GAWEX in Asia and GAME, Cheju, 1996, p 104–111

Maximov TC, Dolman AJ, van der Molen MK, Moors EJ, Ohta T, Sugimoto A, Maximov AP, Kononov AV, Ivanov BI (2004) The regional and global carbon scales of permafrost-dominated forest ecosystems. In: Proceeding of international semi-open work-shop "C/H2O/energy balance and climate over boreal regions with special emphasis on eastern Eurasia", Yakutsk, 2004, p 91–94

Maximov TC, Dolman AJ, Moors EJ, Ohta T, Sugimoto A, Ivanov BI (2005a) Parametry krugovorotov ugleroda i vody v lesnylh ecosystemakh cryolitozony (Circulation parameters of carbon and water in the forest ecosystems of cryolithozone). Doklady RAN 408(8):684–686

Maximov TC, Maksimov AP, Kononov AV, Dolman AJ, Sugimoto A, Moors EJ, van der Molen MK, Ivanov BI (2005b) Ecologo-physiologichesky osobennosti photosynteza listvenitsy Larix cajanderi v usloviyakh mnogoletney merzloty Yakutii (Ecophysiological paculiarities of Larix cajanderi photosynthesis in Yakutia permafrost condition). Lesovedeniye 6:3–10

Maximov TC, Kononov AV, Petrov KA, Ivanov BI (2010) Structural and functional peculiarities of the plants of Yakutia. In: Troyeva E, Isaev A, Cherosov M, Karpov N (eds) The far north: plant biodiversity and ecology of Yakutia. Springer, Dordrecht, pp 317–354

Meidner H, Mansfield TA (1968) In: Meidner H, Mansfield TA (eds) Physiology of stomata. McGraw-Hill Book Company, London, 179 p

Mokronosov AT (1983) Fotosinteticheskaya funktsiya i tselostnost rastitelnogo organizma (Photosynthetic function and integrity of the plant organism). 42d Timiryazev Readings. Nauka, Moscow

Moren AS, Lindroth A (2000) CO_2 exchange at the floor of a boreal forest. Agric For Meteorol 101:1–14

Oberman NG, Shesler IG (2009) Observed and projected changes in permafrost conditions within the European north-east of the Russian Federation. Problemy Severa I Arctiki Rossiiskoy Federacii (Problems and challenges of the North and the Arctic of the Russian Federation) 9:96–106

Pearcy RW (1987) Photosynthetic gas exchange responses of Australian tropical forest trees in canopy, gap and understory micro-environments. Funct Ecol 1:169–178. https://doi.org/10.2307/2389419

Pearcy RW, Calkin H (1983) Carbon dioxide exchange of C3 and C4 tree species in the understory of a Hawaiian forest. Oecologia 58:26–32. https://doi.org/10.1007/BF00384538

Pearcy RW, Pfitsch WA (1995) The consequences of sunflecks for photosynthesis and growth of forest understory plants. In: Schulze ED, Caldwell MM (eds) Ecophysiology of photosynthesis. Springer, Heidelberg, pp 343–359

Prokushkin SG, Masyagina OV, Mori S et al. (2000a). CO_2-emission of soil and vegetation cover in larch stands of continuous permafrost area of Central Siberia. In: Inoue G, Takenaka A (eds) Proceedings of the 8th symposium on the joint Siberian permafrost studies between Japan and Russia in 1999. Tsukuba, 2000, p 183–188

Prokushkin SG, Masyagina OV, Mori S et al. (2000b) Peculiarities of permafrost soil respiration in the Middle Siberia. In: Inoue G, Takenaka A (eds) Proceedings of the 8th symposium on the joint Siberian permafrost studies between Japan and Russia in 1999. Tsukuba, 2000, p 189–194

Rödenbeck C, Houweling S, Gloor M, Heimann M (2003) CO_2 flux history 1982–2001 inferred from atmospheric data using a global inversion of atmospheric transport. Atmos Chem Phys Discuss 3:2575–2659. https://doi.org/10.5194/acp-3-1919-2003

Romanovsky VE, Drozdov DS, Oberman NG, Malkova GV, Kholodov AL, Marchenko SS, Moskalenko NG, Sergeev DO, Ukraintseva NG, Abramov AA, Gilichinsky DA, Vasiliev AA (2010) Thermal state of permafrost in Russia. Permafr Periglac Process 21:136–155. https://doi.org/10.1002/ppp.683

Röser C, Montagnani L, Schulze ED, Mollicone D, Kolle O, Meroni D, Papale D, Marchesini LB, Frederici S, Valentini R (2002) Net CO_2 exchange rates in three different successional stages of the "Dark Taiga" of central Siberia. Tellus 54(5):642–654. https://doi.org/10.1034/j.1600-0889.2002.01351.x

Saito H, Yamamuro K, Tsuno Y, Iijima H, Shibuya M, Maximov TC, Takahashi K (2003) Spatial variations of light intensity and photosynthetic properties within a Larix gmelinii tree crown in eastern Siberia. In: Fukuda M, Saito H (eds) Proceedings of the 10th symposium on the joint Siberian permafrost studies between Japan and Russia in 2001, Tsukuba, 2001, p 7–14

Sassa T (1993) Nutrient analysis in tree leaves. In: Fukuda M (ed) Proceedings of first symposium on joint Siberian permafrost studies between Japan and Russia in 1992, Sapporo, 1992, p 66

Shcherbatyuk AS, Rusakova LV, Suvorova GG, Yankova LS (1991) Uglekislotny gazoobmen khvoinikh Predbaikalya (Carbon dioxide exchange of Predbaikalya conifers). Nauka, Novosibirsk, p 135

Schimel D, House J, Hibbard K, Bousquet P, Ciais P, Peylin P, Apps M, Baker D, Bondeau A, Brasswell R, Canadell J, Churkina G, Cramer W, Denning S, Field C, Friedlingstein P, Goodale C, Heimann M, Houghton RA, Melillo J, Moore B III, Murdiyarso D, Noble I, Pacala S, Prentice C, Raupach M, Rayner P, Scholes B, Steffen W, Wirth C (2001) Recent patterns and mechanisms of carbon exchange by terrestrial ecosystems. Nature 414:169–172. https://doi.org/10.1038/35102500

Schulze ED (1972) Die wirkung von licht und temperatur auf den CO_2-gaswechsel verschiedener lebensformen aus der krautschicht eines montanen buchenwaldes (The effect of light and temperature of the CO2 exchange of different life forms in the ground vegetation of a montane beech forest). Oecologia 9:223–234

Schulze ED, Schulze W, Kelliher FM, Vygodskaya NN, Ziegler W, Kobak KI, Koch H, Arneth A, Kusnetsova WA, Sogatchev A, Issajev A, Bauer G, Hollinger DY (1995) Aboveground biomass and nitrogen nutrition in a chronosequence of pristine Dahurian Larix stands in eastern Siberia. Can J For Res 25:943–960. https://doi.org/10.1139/x95-103

Schulze ED, Lloyd J, Kelliher FM, Wirth C, Rebmann C, Lühker B, Mund M, Knohl A, Milyukova I, Schulze W, Ziegler W, Varlagin A, Valentini R, Dore S, Grigoriev S, Kolle O, Vygodskaya NN (1999) Productivity of forests in the Eurosiberian boreal region and their potential to act as a carbon sink – a synthesis. Glob Chang Biol 5:703–722. https://doi.org/10.1046/j.1365-2486.1999.00266.x

Sherbatyuk AS (1976) Uglekislotnyi rezhim i photosynteticheskaya aktivnost sosnovykh molodnyakov (Carbon dioxide regime and photosynthetic activity of young Pine forests). In: Biophysicheskiye i systemnyie issledovaniya v lesnoy biogeotsenologii. Petrozavodsk, p 112–113

Shibuya M, Tsuno Y, Saito H, Takahashi K, Sawamoto T, Hatano R, Isaev AP, Maximov TC (2001) Chronosequental analysis of aboveground biomass and the carbon and nitrogen contents in natural Larix stands in eastern Siberia. In: Proceedings of the second international workshop

on global change: connection to the Arctic. Bulletin of research center for North Eurasia and North Pacific Regions, Hokkaido University 1:57–66
Shvidenko A, Nilsson S (1994) What do we know about the Siberian forests. Ambio 23:396–404
Stepanov GN (1976) Vodiy rezhim v usloviyakh Centralnoy Yakutii (Water exchange in Central Yakutia). PhD thesis (Biology), Leningrad, p 26
Sugimoto A, Yanagisawa N, Naito D, Fujita N, Maximov TC (2002) Importance of permafrost as a source of water for plants in east Siberian taiga. Ecol Res 17:493–503. https://doi.org/10.1046/j.1440-1703.2002.00506.x
Sugimoto A, Naito D, Yanagisawa N, Ichiyanagi K, Kurita N, Kubota J, Kotake T, Ohata T, Maximov TC, Fedorov AN (2003) Characteristics of soil moisture in permafrost observed in East Siberian taiga with stable isotopes of water. Hydrol Process 17:1073–1092. https://doi.org/10.1002/hyp.1180
Suzuki M, Saito H, Iijima H, Onoe T, Maximov TC, Takahashi K (2003) Photosynthetic and stomatal responses to air vapor deficit within a larch canopy in East Siberia. In: Fukuda M et al (eds) Proceedings of the 10th symposium on the joint Siberian permafrost studies between Japan and Russia in 2001, Tsukuba, 2001, p 15–19
Tabuchi R, Koike T, Maximov TC, Ivanov BI, Takahashi K (1994) Gas exchange measurements on some major tree species in Siberian permafrost region in summer. In: Takahashi K (ed) Carbon storage and carbon dioxide budget in forest ecosystems. Interim report on joint research project between Japan and Russia. Forestry and Forest Products Research Institute, Sapporo, p 47–51
Tselniker YL, Malkina IS, Yakshina AM (1990) Vertikalny gradient dykhaniya stvolv eli, duba I beryozy (Vergical gradient of stem respiration of spruce, oak and birch). Lesovedeniye 4:11–18
Vygodskaya NN, Milyukova I, Varlagin A, Tatarinov F, Sogachev A, Kobak KI, Desyatkin R, Bauer G, Hollinger DY, Kelliher FM, Schulze ED (1997) Leaf conductance and CO2 assimilation of Larix gmelinii growing in an eastern Siberian boreal forest. Tree Physiol 17:607–615. https://doi.org/10.1093/treephys/17.10.607
Weber JA, Jurik TW, Tenhunen JD, Gates DM (1985) Analysis of gas exchange in seedlings of Acer saccharum: integration of field and laboratory studies. Oecologia 65:338–347. https://doi.org/10.1007/BF00378907
Widen B, Majdi H (2001) Soil CO_2 efflux and root respiration at three sites in a mixed pine and spruce forest: seasonal and diurnal variation. Can J For Res 31:786–796
Woodward FI, Smith TM (1995) Predictions and measurements of the maximum photosynthetic rate, Amax, at the global scale. In: Schulze E-D, Caldwell MM (eds) Ecophysiology of photosynthesis. Springer, Berlin
Wullschleger SD (1993) Biochemical limitations to carbon assimilation in C3 plants – a retrospective analysis of the A/Ci curves from 109 species. J Exp Bot 44:907–920. https://doi.org/10.1093/jxb/44.5.907
Zabuga GA, Sherbatyuk AS (1982) Ecologiya photosynteza sosny obyknovennoi lesostepnogo Predbaikalya (Pine ecology of photosynthesis of forest-steppe Predbaikalya). Nauka, Novosibirsk, p 135

Chapter 5
Methane and Biogenic Volatile Organic Compound Emissions in Eastern Siberia

Jacobus van Huissteden

5.1 Introduction

Several landmark publications on CH_4 originate from data collected in Eastern Siberia (Walter et al. 2006, 2007a, b; Shakhova and Semiletov 2007; Rivkina et al. 2007; Zimov et al. 2006). These have put the spotlight on CH_4 emissions from thawing permafrost as a feedback that accelerates global warming (Schuur et al. 2008). Most of Eastern Siberia has not been glaciated during the Late Pleistocene (e.g. Zimov et al. 2006 and references therein), which allowed the accumulation of successions of ice-rich sediment under cold glacial conditions, known as 'Yedoma' (Schirrmeister et al. 2008, 2013). These deposits are highly vulnerable to thawing of permafrost, causing subsidence and ponding of water followed by increased CH_4 formation (Walter et al. 2006).

A recent review publication (Schuur et al. 2015) concluded that greenhouse gas (GHG) emissions from permafrost soils are unlikely to provoke abrupt climate change. They assume that release is gradual over decades and centuries, rather than showing large and rapid pulse emissions, and estimate these emissions are 13–17% of global fossil fuel emissions. Furthermore, it is uncertain how these greenhouse gas emissions are partitioned between CO_2 and CH_4. Incubation experiments suggest a more important role for CO_2 than for CH_4 because of the much more rapid aerobic decomposition versus anaerobic decomposition, although the ultimate effect depends on landscape changes (Schädel et al. 2016).

However, this does not dismiss the importance of CH_4. First, its radiative contribution to climate change has been upgraded. The 100 year global warming potential of CH_4 was revised upwards from 23 (Houghton et al. 2001) to 34 (Stocker et al. 2013) in the IPCC reports. Second, a renewed rise of atmospheric CH_4 concentration has started in 2007. The factors that contributed to this renewed rise

J. van Huissteden (✉)
Faculty of Sciences, Vrije Universiteit, Amsterdam, The Netherlands
e-mail: j.van.huissteden@vu.nl

T. Ohta et al. (eds.), *Water-Carbon Dynamics in Eastern Siberia*,
Ecological Studies 236, https://doi.org/10.1007/978-981-13-6317-7_5

remain unclear (Kirschke et al. 2013; Bergamaschi et al. 2013; Houweling et al. 2014). Worden et al. (2017) infer a net emission increase for both fossil fuel (±50–75% of total increase) and biogenic sources (including wetlands and agriculture) to reconcile isotope and atmospheric chemistry data with strength of sources. Model inversion by Bruhwiler et al. (2014) did not find an increase in CH_4 emission in the Arctic, but report large year-to-year variability. Third, there is high uncertainty in the emissions, and surprises cannot be ruled out (Schuur et al. 2015; Schädel et al. 2016).

Various CH_4 sources can be distinguished using isotopic signatures of the sources and atmospheric modelling (e.g. Worden et al. 2017; Thonat et al. 2017). Based on atmospheric modelling of CH_4 data collected at stations in Siberia and other Arctic sites, Thonat et al. (2017) conclude that CH_4 emissions from Eastern Siberia originate largely from terrestrial wetlands and freshwater sources in summer, while winter sources are dominated by marine, geologic, and anthropogenic (largely fossil fuel industry) emissions. At the East Siberian stations Tiksi and Cherskii, wetlands and freshwater sources dominate contributions to the concentration of CH_4 with resp. 68% and 82% from May to November; in winter these fall to 8% and 11%. The oceanic emissions from the East Siberian Arctic shelf at these stations are relatively high compared to other Arctic stations, with 17% and 11% in summer and 44% and 41% in winter. Anthropogenic emissions are modest and contribute resp. 25% and 23% in winter and 6% and 3% in summer, due to relatively minor East Siberian fossil fuel activities compared to West Siberia. Emissions from biomass burning are small, 1–2% in summer and 3–6% in winter. Geologic sources consisting of gas seepage at both sites contribute 24% in winter and 3–7% in summer (Thonat et al. 2017).

This chapter reviews these terrestrial sources and processes of CH_4 emission, with emphasis on research in Eastern Siberia (Yakutia and eastern provinces of Russia), but where necessary, reference to research in other parts of Siberia or other cold-climate areas will be made. The review will be process- and data-oriented and will focus on the CH_4 emissions from terrestrial environment in relation to the total greenhouse gas (GHG) budget of ecosystems; marine sources of CH_4 are not included; also CH_4 emission from wildfires or fossil fuel extraction is excluded. Three types of terrestrial biosphere CH_4 sources can be distinguished and will guide the discussion in this article (Fig. 5.1).

The ecosystem CH_4 source consists of wetlands, ponds, and lakes which are sources of CH_4, where the CH_4 carbon is largely derived from recent photosynthesis products of the ecosystem, although older soil carbon may be included. It is the balance of CO_2 uptake by vegetation and emission of CH_4 that matters whether ecosystems are net sources or sinks of greenhouse gases (Van der Molen et al. 2007; Walther-Anthony et al. 2014). Neither can ecosystem CH_4 be isolated from the nutrient cycle as discussed below.

The old-carbon CH_4 source in soil and sedimentary deposits may become available for methanogenesis by thaw of permafrost (e.g. Walter et al. 2006). Liberation of old carbon (fossil C of Holocene and Pleistocene age) contributes the strength of the permafrost carbon feedback, although part of its reworking may be the result of normal ecosystem processes.

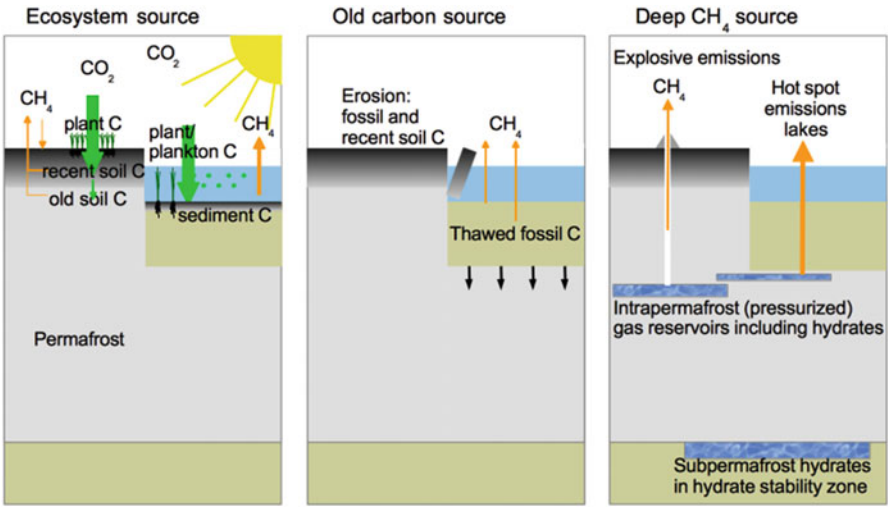

Fig. 5.1 Methane sources from permafrost: ecosystem source, old (fossil, Pleistocene) carbon source, and deep CH_4 sources from intra- and sub-permafrost gas and hydrate reservoirs

The deep CH_4 source is CH_4 stored in the deeper subsoil as gas hydrates or pressurized gas at tens to hundreds of metres depth is a third potential source (Rivkina et al. 2007; Kraev et al. 2012; Archer 2007). On the land surface, this may be liberated on deeper thaw of permafrost beneath lakes (e.g. Walter et al. 2007a, b) or, as recently observed in West Siberia, by eruptive emission (Leibman et al. 2016). These geological emissions may be triggered by climate change. Also in Eastern Siberia, this potential source is present (Rivkina et al. 2007; Kraev et al. 2012).

Besides CH_4, other volatile organic compounds originate from East Siberian ecosystems. Both forests and tundras are an important source of biogenic volatile organic compounds (BVOCs), emitted by plants during growth. BVOCs interact with CH_4: they compete with CH_4 for oxidation by the OH radical and therefore influence the lifetime of CH_4 (O'Connor et al. 2010, Thonat et al. 2017). Although the interactions of BVOC with CO_2, CH_4, and aerosols are complex (Arneth et al. 2016), emission of BVOCs may increase with climate warming (e.g. Kramshøj et al. 2016) and need to be considered in the interaction of ecosystems with climate.

5.2 The Ecosystem CH_4 Source

5.2.1 Data Uncertainty

Because of the challenging field research conditions, the spatial density of observations on terrestrial CH_4 fluxes is low in Eastern Siberia. Full winter season data – crucial for a full understanding of the CH_4 budget of permafrost ecosystems

(e.g. Mastepanov et al. 2008; Zona et al. 2016) – have been published only very recently for Eastern Siberia (Kittler et al. 2017). Sources of data uncertainty arise from differences of spatial scale of measurement methods (e.g. eddy covariance vs. chamber flux measurements), data gaps, and data processing. Eddy covariance data processing and gap filling for CH_4 is still a developing field (Wille et al. 2008; Parmentier et al. 2011b).

For assessing the spatial variability of fluxes from eddy covariance with a footprint typically in the order of tens to hundreds of metres across, a statistical footprint model is necessary to relate CH_4 sources to spatial variability of wetlands (Parmentier et al. 2011b; Budishchev et al. 2014). Chamber flux measurements can exactly pinpoint small-scale spatial variability but need many replicates for reliable flux estimation and are vulnerable to disturbance of the measurements (Sachs et al. 2008a, b; Kutzbach et al. 2004, 2007).

Data cited (e.g. in Table 5.1) are the data as presented by respective authors. Because data are reported in a wide range of units (fluxes in moles, units of mass, carbon mass flux, and with varying time scales), all fluxes have been converted to mg CH_4 m^{-2} h^{-1} for comparison purposes.

5.2.2 Processes

Water table and temperature, controlling the presence of anaerobic environments and reaction rate, are the most important drivers for CH_4 emission from wetlands (Turetsky et al. 2014). Permafrost impedes subsurface drainage by the presence of impervious frozen subsoils, while microrelief may impede surface runoff (Kutzbach et al. 2004). However, soil biogeochemistry and transport mechanisms of CH_4 from soil or water to atmosphere contribute to high spatial variability.

The ecosystem CH_4 source is CH_4 mostly driven by recently photosynthesized, labile organic material, released from the plant root system (Ström et al. 2003). Photosynthesis products can be transferred into CH_4 in a matter of hours as shown by ^{14}C-labelling experiments (King et al. 2002; Ström et al. 2003), and as a result a small percentage (2–3%) of the primary production of wetland ecosystems is returned to the atmosphere as CH_4 (King et al. 2002; Christensen et al. 2003; Wagner and Liebner 2009). The environment needs not be strictly anaerobic as shown by recent research; methanogens in anaerobic microsites in otherwise oxygenated soil may contribute to CH_4 production (Angle et al. 2017).

Methanogens prefer small and simple molecules which are usually end products of the metabolism of other microbes, e.g. iron reducers. The mineralization of organic matter under anaerobic conditions is performed by a chain of specialized microorganisms, with as intermediate products hydrogen, carbon dioxide, and acetate (Metje and Frenzel 2007; Wagner and Liebner 2009; Fig. 5.2). The two most well-known processes of bacterial methanogenesis are the acetoclastic pathway, using methyl groups of acetate and similar compounds, and CO_2 reduction (hydrogenotrophy), producing equal amounts of CO_2 and CH_4 (e.g. Sugimoto and

Table 5.1 Representative CH_4 emission and uptake in various terrestrial wetland environments in Siberia

References	Vegetation/microrelief	CH_4 flux mg m^{-2} h^{-1}
1	Dry floodplain levee, *Salix* brush	−0.04 ±0.04
1	Dry floodplain, grasses	1.3 ±1.8
1	Floodplain wetland, *Arctophila fulva* grass and mosses	37.0 ±5.3
1	Floodplain wetland, *Carex*, *Eriophorum*, grasses	12.6 ±10.1
1	Dry tundra, *Betula nana*, mosses, lichens	−0.22 ±0.34
1	Dry tundra, *Eriophorum* tussocks	−0.09 ±0.05
1	Dry tundra, grasses	0.71 ± 1.1
1	Tundra wetland, usually inundated, *Carex*, *Eriophorum*	8.0 ±3.0
1	Tundra wetland, *Sphagnum* hummocks	2.0 ±1.7
1	Tundra wetland, inundated polygon pond with *Sphagnum* or mosses	4.0 ±1.9
1	Ice wedge thaw pond	4.4 ±2.8
2	Polygon centres with mosses (*Scorpidium*, *Drepanocladus*, *Carex*)	±4.2*
2	Polygon rim	<0.42*
3	Polygon centre, mosses, *Carex aquatilis*, and other vascular plants	1.2 ±2*
3	Polygon rim, species-rich	0.18 ±0.03*
4	Floodplain with *Carex appendiculata* tussocks	8.2 ±3.4*
5	Floodplain with *Carex appendiculata* tussocks	13.8±7.0*
6	Mesotrophic fen in Larch forest, *Molinea* tussocks	1.3 ± 1.7
6	Eutrophic lake bank, grasses	11.9 ±15.5
6	Moist forest floor, water table 10–27 cm below surface, *Betula*	−0.26±0.45
6	Dry forest floor, *Larix* and *Pinus* with shrub and lichen understory	−0.37 ±0.47
7	Mineral forest soil, no permafrost, *Betula/Picea/Larix*, shrub understory	−0.06–0*
7	Mineral forest soil with permafrost	−0.04–0*
7	Peat plateau, permafrost, *Betula nana*, *Ledum palustre*, *Sphagnum*, mosses	−0.025–0*
7	Permafrost thaw pond	12 and larger

References: 1. Van Huissteden et al. (2009), 2. Sachs et al. (2008a, b), 3. Kutzbach et al. (2004), 4. Corradi et al. (2005), 5. Kwon et al. (2017), 6. Van Huissteden et al. (2008), Corradi et al. (2005) and 7. Flessa et al. (2008). Stars (*) mark values that have been recalculated to mg m^{-2} h^{-1}; negative values represent uptake from the atmosphere into the soils

Wada 1993; Corbett et al. 2015). Additionally, there is evidence that various other methylated substrates are being used for methanogenesis in wetland soils (Zalman et al. 2018). It has been assumed that CO_2 reduction is the main process in high-latitude wetlands (Hines et al. 2001) since acetate accumulates over the season in these soils. However, Ström et al. (2003, 2015) and Metje and Frenzel (2007) have

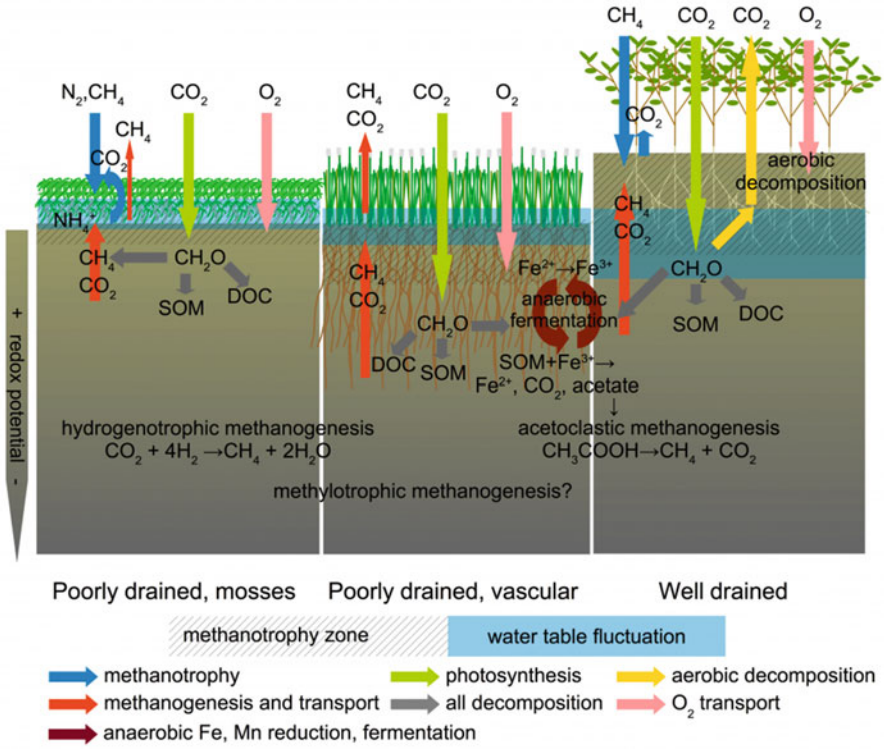

Fig. 5.2 Biochemical processes involved in CH_4 formation and oxidation in soil environments with varying water table and vegetation (non-vascular mosses without root system vs. vascular plants). Indicated processes are photosynthesis and transfer of organic compounds (CH_2O) to the soil, methanogenesis pathways, CH_4 oxidation by methanotrophy including N fixation (methanotrophy in mosses), transfer of O_2 to the soil, and anaerobic fermentation by Fe reduction producing substrate for methanogens, including recycling of Fe^{2+} to Fe^{3+} by oxidation (similar anaerobic reduction involves Mn, not shown here). *SOM* soil organic matter, *DOC* dissolved organic carbon

shown that acetate is a major substrate in high-latitude wetland soils, although CO_2 reduction remains locally important (Vaughn et al. 2016).

Despite the extreme climatic conditions in East Siberian permafrost soils, the abundance and composition of the methanogenic bacterial population is similar to that of temperate wetland soils (Wagner and Liebner 2009), although a distinct vertical zonation is found in permafrost, with more psychrophilic archaea at depth in the soil, close to the permafrost table. Activity of psychrophilic methanogenic archaea has been recorded at subzero temperatures (Rivkina et al. 2000).

The surface CH_4 flux from wetland soils is determined by the balance between CH_4 production by methanogens and its consumption by oxidation and bacterial methanotrophy (Wagner and Liebner 2009). In high Arctic areas with drier soils, the soil CH_4 sink dominates (Jørgenson et al. 2014). Also taiga forest soils in Siberia,

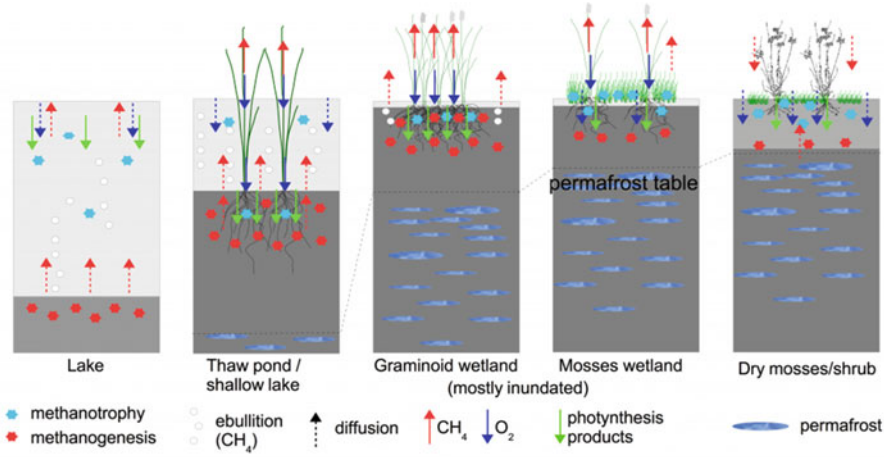

Fig. 5.3 Conceptual diagram of interactions between plants, substrate supply for methanogenesis, methanotrophy, and methane transport pathways in various lake and wetland environments in permafrost areas, from lake to dry soil. The main locations of methane formation and methanotrophy are indicated with stars

dry tundra soils and dry peat soils on peat plateaus are a significant sink of CH_4 (Morishita et al. 2003; Van Huissteden et al. 2005, 2008, 2009; Flessa et al. 2008).

In soils, several groups of prokaryotes oxidize CH_4 for carbon assimilation (e.g. Frenzel and Karofeld 2000; Wagner and Liebner 2009). Methanotrophic bacteria have a loose symbiosis with *Sphagnum* species (Raghoebarsing et al. 2006; Kip et al. 2010) and submerged brown mosses (Liebner et al. 2011). CO_2 from methanotrophy may account for up to 30% of carbon uptake of mosses (Larmola et al. 2010). Rates of this soil and moss-related methanotrophy have shown to be very high in East Siberian tundra environments (Knoblauch et al. 2008; Kip et al. 2010). Methanotrophy in brown mosses decreases the CH_4 emission from polygon ponds by at least 5% (Liebner et al. 2011); Knoblauch et al. (2015) found that 61–99% of produced CH_4 was consumed in submerged *Scorpidium scorpioides* moss. Symbiotic methanotrophs in *Sphagnum* contribute strongly to N_2 fixation in ombrotrophic peat bogs and are therefore related to the N cycle of peatlands (Vile et al. 2014; Larmola et al. 2014).

CH_4 is transported from soil and water bottom to the atmosphere by bubbles (ebullition), diffusion, and transport through plants (Fig. 5.3). The physical transport mechanisms of ebullition and diffusion depend on weather conditions. Ebullition fluxes can be triggered by air pressure variation (Sachs et al. 2008a, b; Kwon et al. 2017) and near-surface turbulence and atmospheric stability (Wille et al. 2008 and Parmentier et al. 2011b); higher turbulence and unstable conditions result in higher fluxes.

Vegetation has a strong and complicated effect on ecosystem CH_4 fluxes (Figs. 5.2 and 5.3). Aerenchyma in wetland plants transport CH_4 to the atmosphere;

the plant-mediated transport lies between 30% and 100% of the CH_4 flux and is species-dependent: graminoids transport more methane (±80%) than forbs (±60%) (Bhullar et al. 2013). In ponds in Northern Siberia, plant-mediated transport of CH_4 by emergent vegetation amounted between 70% and 90% of the total CH_4 flux (Kutzbach et al. 2004). However, the main function of aerenchyma is the transport of oxygen to the anoxic root zone. A part of this oxygen contributes to oxidation of CH_4 in the rhizosphere. On the other hand, this oxygen also regenerates alternative electron acceptors, such as Fe oxides, contributing to the anaerobic organic matter decomposition that produces the substrates for methanogens. The complex interplay between exudation of methanogenic substrate by roots, oxidation of CH_4 in the rhizosphere and transport of CH_4 is species-specific: *Carex rostrata* had higher CH_4 emissions due to lower CH_4 oxidation than *Eriophorum vaginatum* and *Juncus effusus* (Ström et al. 2005).

In lakes, a similar balance between CH_4 production and oxidation is found. In deeper lakes, bottom waters may be anoxic due to thermal stratification, which impedes the exchange of gases other than by slow diffusion. These deeper, anoxic bottom layers of the lakes (the hypolimnion) are the main CH_4 production zone. However, shallower, epilimnetic zones may emit more to the atmosphere. In these shallower zones, turbulence enhances CH_4 transport to the atmosphere, bypassing oxidation. In the littoral zone with emergent plants, plant transport in emergent water plants also contributes (Bastviken et al. 2008). The proportion of produced CH_4 that is oxidized in sediments and water column may amount 30–99% and includes anaerobic CH_4 oxidation (e.g. Deutzmann et al. 2014). The oxidation of CH_4 contributes carbon to the food web in lakes, influencing its carbon isotopic signature (Bastviken et al. 2003).

In deeper lakes CH_4 is stored in anoxic bottom water, which is released when the stratification is overturned seasonally. Turbulence also enhances the exchange of CH_4 from the bottom sediment to the water column (Bastviken et al. 2008). In many lakes the main transport pathway of CH_4 to the surface is ebullition (Bastviken et al. 2008). This is facilitated by energy input into the lake, as relations have been found with ice-free period, incoming shortwave radiation and water/sediment temperature (Wik et al. 2014).

5.2.3 Terrestrial Ecosystems: Spatial and Seasonal Variation

Table 5.1 shows studies of CH_4 fluxes in Eastern Siberia (Christensen et al. 1995; Nakano et al. 2000; Wagner et al. 2003; Kutzbach et al. 2004; Corradi et al. 2005; Van der Molen et al. 2007; Van Huissteden et al. 2005, 2008, 2009; Flessa et al. 2008; Sachs et al. 2008a, b; Takakai et al. 2008; Parmentier et al. 2011b; Budishchev et al. 2014). All these papers show significant variation of fluxes between vegetation types, including vegetation with similar water table (e.g. Van Huissteden et al. 2009). Large differences are shown between graminoid and moss-dominated

vegetations, where methanotrophy in mosses may play a role (e.g. Parmentier et al. 2011a).

Van Huissteden et al. (2005, 2008, 2009) found higher emissions in eutrophic environments compared to mesotrophic and oligotrophic environments: differences between a mesotrophic flooded fen and a nearby eutrophic lake and between mesotrophic sedge vegetations and sedge vegetations on a nutrient-rich river floodplain. Similar high fluxes on a floodplain were observed by Corradi et al. (2005). Floodplains, with a supply of additional nutrients by spring snowmelt flooding, are an overlooked strong source of ecosystem CH_4 (Table 5.1).

Microrelief (ice wedge polygons) created by the presence of permafrost also results in spatial variation of CH_4 fluxes (Fig. 5.4). This microrelief effect has been the subject of several studies in Eastern Siberia (Wagner et al. 2003; Kutzbach et al. 2004; Knoblauch et al. 2015). Ponded water is often present in the poorly drained centres of polygons (low-centred polygons) or troughs above (thawing) ice wedges. Other forms of microrelief have been described by Van Huissteden et al. (2005) and Berritella et al. (2017): a pattern of flat elongated ridges dominated by dwarf birch

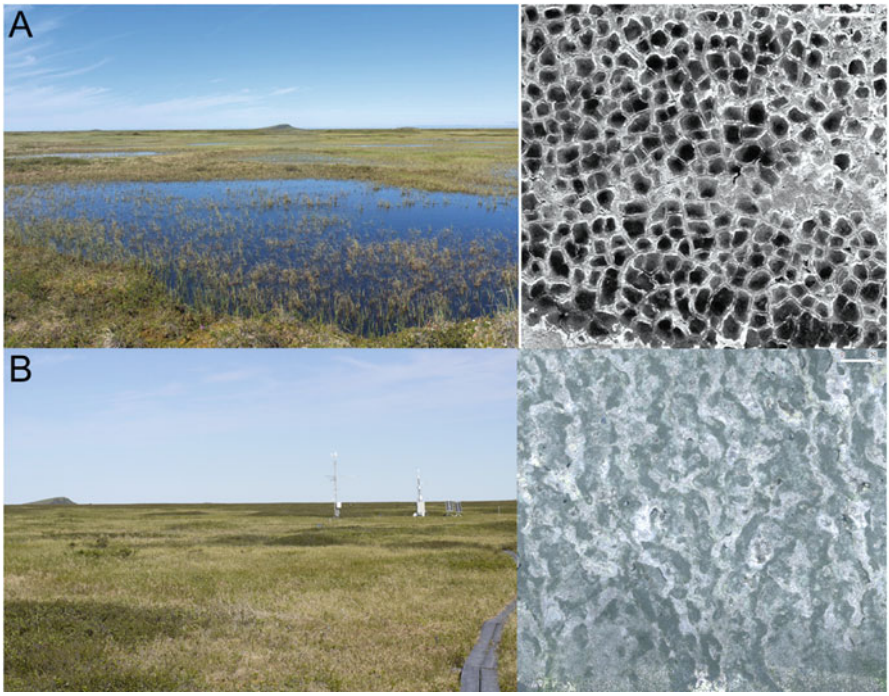

Fig. 5.4 Two types of microrelief that influence wetland characteristics in the Siberian north. A: polygonal ice wedge network, with low-centred polygons with central ponds. Left: view from the surface. Right: view from above at the same location (GeoEye panchromatic satellite image). B: peat mound – sedge meadow relief with *Betula nana*-covered peat mounds (dark patches.) Below right: view from above, air-photo, same location. The sedge meadows serve partly as drainage channels. Kytalyk tundra research station, near Chokurdagh, Indigirka lowlands, Northeast Siberia

(*Betula nana*) separated by shallow, densely vegetated (*Carex* and *Eriophorum* spp.) drainage channels. The ridges – resembling palsas – are a sink of CH_4.

At least three variables determine the spatial variability of CH_4 fluxes in East Siberian ecosystems: water table/microrelief, vegetation characteristics, and eutrophic-ombrotrophic gradients. Comparing summer fluxes in various ecosystem settings (Table 5.1), the following pattern with respect to vegetation emerges. Graminoid wetland vegetations with high water table, usually dominated by *Carex* and *Eriophorum* spp. and grasses like *Arctophila fulva*, show the highest fluxes. Eutrophic wetlands in floodplains and agriculturally used meadows are the strongest emitters of CH_4. Meso- and oligotrophic sites show lower fluxes with otherwise similar water table conditions. Thaw ponds formed by ground ice thaw show similar fluxes as the eutrophic graminoid vegetations. Stable ice wedge polygon centre ponds generally show lower fluxes than fresh thaw ponds. *Sphagnum*-rich and other mosses-rich ecosystems show the lowest fluxes. Dry environments, in particular on peat plateaus, palsas, and polygon rims, are a sink of CH_4. Also forests are sinks of CH_4, even when the water table is relatively high. However, forested wetlands are poorly represented in the data, and CH_4 fluxes through tree trunks (Gauci et al. 2010) never have been measured in Siberia.

Seasonal variation of emissions largely follows the growing season (Wille et al. 2008; Sachs et al. 2008b; Kwon et al. 2017). Also daily flux variation driven by soil temperature has been observed (Nakano et al. 2000). In permafrost environments high CH_4 emissions may occur in autumn and winter (Mastepanov et al. 2008, 2013) that even may surpass that of the growing season (Zona et al. 2016). Most of these emissions occur during soil freezing, when the soil remains for a long period at the freezing point ('zero curtain') due to the effect of latent heat of soil water. These fluxes are attributed to physical expulsion of stored soil CH_4 by freezing (Mastepanov et al. 2008, 2013) and ongoing bacterial activity at subzero temperatures (Zona et al. 2016).

The high autumn CH_4 fluxes are also observed in Eastern Siberia. Eddy covariance data by Wille et al. (2008) in the Lena Delta extending into October show erratic higher fluxes comparable to the highest summer emissions. Kwon et al. (2017) and Kittler et al. (2017) observed high fluxes in October–November in the Kolyma floodplain. These fluxes contribute 23% to the total annual flux and correlated with drops in air pressure. This is confirmed by the model inversions of Thonat et al. (2017). The high winter emissions show the urgency of all-season CH_4 flux observations in permafrost environments (Kittler et al. 2017).

Van der Molen et al. (2007) concluded that the tundra in the Indigirka lowlands is a net sink of greenhouse gases in summer. However, lack of autumn and winter data hampers construction of a year-round GHG budget including CH_4 at several sites. Wille et al. (2008) concluded that the tundra in the Lena Delta is a small source of greenhouse gases, because radiative forcing from CH_4 emission exceeds the effect of ecosystem CO_2 uptake over the year. A river floodplain near Cherskii was in summer a net source of greenhouse gases (CO_2 + CH_4) of 475±253 g C-CO_2-equivalent m^{-2} because of the high CH_4 flux (Merbold et al. 2009); also the more recent data from this site indicate a small net source (Kwon et al. 2017; Kittler et al. 2017).

5.2.4 The Ecosystem CH_4 Source in Ponds and Lakes

Alas lakes (thaw or thermokarst lakes) and ponds produced by thawing of ice-rich permafrost are of widespread occurrence in Siberia (Brouchkov et al. 2004; Grosse et al. 2013) and have attracted attention as CH_4 sources (Nakagawa et al. 2002; Walter et al. 2006, 2007a, b). The global northern latitude lake area is at least twice higher in permafrost regions than in non-permafrost regions (Grosse et al. 2013).

The lake sediment temperature beneath the maximum ice thickness remains above zero, permitting continuous methanogenesis. In high northern latitudes, lake ice thickness may reach over 2 m (Duguay et al. 2003). With ongoing ebullition of CH_4 from the sediment in winter, the lake ice becomes a large store of CH_4 frozen in bubbles in the ice (Zimov et al. 1997; Walter et al. 2006; Wik et al. 2011). Walter et al. (2006) make a distinction between low rate background ebullition, point sources, and hotspots with larger bubble plumes. Winter ebullition has been estimated by counting and sampling various type of bubble clusters (Walter et al. 2006), resulting in a 10–63% higher estimate of northern wetland CH_4 emission. However, quantification of ebullition emissions using bubble counting on ice has large uncertainties (Wik et al. 2011), and the CH_4 trapped in lake ice may be subject to microbial oxidation (Walter et al. 2008). Based on extrapolation from East Siberian and Alaskan lakes, Walter et al. (2007a, b) estimate the CH_4 emission of lakes in permafrost areas (total area 396.200 km^2) at 19.2±6.7 Tg CH_4 $year^{-1}$.

The background ebullition shows an isotopic signature ($\delta^{13}C$, δD, ^{14}C age of CH_4) that indicates approximately equal contributions from acetate and CO_2 reduction and a young age, representing decomposition of young organic material in surface sediments (Walter et al. 2008). CH_4 from point sources was much older than CH_4 derived from background ebullition, and the isotope fraction of C and H stable isotopes indicated CH_4 generated by the CO_2 reduction pathway (Walter et al. 2007a). The apparent ages of hotspot CH_4 in Siberian lakes ranged between 35.3 and 42.9 kyr BP, suggesting sources deep in the thawed Pleistocene deposits below the lakes. Point source CH_4 was younger but still ranging between 5.6 and 22.1 kyr BP, while surface sediment and background ebullition CH_4 had ages of Holocene to recent age.

Nakagawa et al. (2002) studied alases (thaw lake and wetland complexes) near Yakutsk. ^{14}C data of CH_4 from smaller alases indicated a modern origin, while that of larger alases was older, indicating a larger proportion of fresh organic matter supplied from the banks in smaller alases. The hotspot CH_4 of Walter et al. (2007a, b) is considerably older than the CH_4 from more southerly alases described by Nakagawa et al. (2002). Alas lakes in Central Yakutia behave differently compared to their northern counterparts. Water table and lake size vary stronger, shrinking during summer. Alases have a grass cover at low water table, often used as meadow or hay pasture. Morishita et al. (2003) and Takakai et al. (2008) report high CH_4 emissions from an alas pond and the frequently flooded grasslands surrounding the pond. Takakai et al. (2008) report fluxes from 5.7 to 54.6 mg m^{-2} h^{-1} from flooded grasslands, which considerably decreased after the sites dried out. In the pond the fluxes varied strongly with water temperature, ranging from 1.3 to 146.7 mg m^{-2} h^{-1}.

Thawing of lake ice in spring releases the stored CH_4 from the ice; however, data have not been published for Eastern Siberia. In a lake in Northern Sweden, 53% of the annual emission of CH_4 was released in spring (Jammet et al. 2015).

Small lakes and ponds dominate the lowlands of Siberia rather than large lakes (Grosse et al. 2008). Although small lakes and ponds may freeze to the bottom, the thermal effect of the presence of a water body results in prolonged above-zero temperatures. Langer et al. (2015) quantified CH_4 stored in pond ice in the Lena Delta. Winter emissions ranged between 0.01 and 5.8 mg m^{-2} day^{-1}. Sachs et al. (2010) measured summer fluxes in polygon ponds ranging on average between 78 and 100 mg m^{-2} day^{-1}.

Although thaw lakes are sources of CH_4, the net long-term effect may be still be a greenhouse gas sink due to carbon accumulation. Walter Anthony et al. (2014) assessed the carbon accumulation in 49 Holocene lake infill successions (including East Siberian lakes) in thaw lakes dating from the Last Glacial Termination and Early Holocene. The thaw lakes switched from a net radiative source from CH_4 emission to a sink by greenhouse gas uptake about 5000 years ago.

5.3 Old Soil Carbon as a Source of CH_4

Old soil carbon may become an increasing source of carbon for the ecosystem respiration upon warming of the permafrost in Eastern Siberia. Estimates of the soil carbon stocks in the Arctic are improving (Tarnocai et al. 2009; Strauss et al. 2013; Hugelius et al. 2014). Older, frozen soil carbon becomes available for decomposition by gradual increase of active layer thickness (ALT) or by rapid geomorphological processes such as erosion and pond formation (Van Huissteden and Dolman 2012).

To be available for methanogenesis, older soil carbon should contain labile organic compounds or needs to be converted into labile compounds. Zimov et al. (1997, 2006) were the first to draw attention to the labile nature of carbon in Pleistocene Yedoma (Ice Complex) deposits in Eastern Siberia. A survey of the carbon content of quaternary deposits in Northeast Siberia by Schirrmeister et al. (2011) shows that the superficial Pleistocene Yedoma deposits date mostly from the Last Glacial and consist of cold-climate fluvial and loessic sediments with large, syngenetic ice wedges. The ice content varies between 22 and 59 weight % (or roughly 50–80 volume %), and average total organic carbon (TOC) content varies between 1% and 5%. Holocene deposits (thaw lake infills and fluvial deposits) are equally ice-rich but have a somewhat higher TOC, ranging between 5% and 11% on average. Cold climatic conditions during deposition are assumed to have contributed to the preservation of labile compounds. C/N ratios (ranging between 0.03 and 38.4) and $\delta^{13}C$ values (−31.0–23.4‰) confirm the poorly decomposed and labile nature of the organic matter in the Yedoma deposits. It contains hardly *Sphagnum* peat and consists mostly of graminoid plant material which is more labile

(Schirrmeister et al. 2008, 2011). Recent incubation data of permafrost carbon from Yedoma deposits further confirms the very high lability of this organic matter store (Vonk et al. 2013).

However, Ganzert et al. (2007) and Hershey et al. (2013) showed that CH_4 production in sediment in East Siberian soils and in a small lake are substrate-limited. This suggests that despite the high lability of Arctic soil carbon, further biochemical transformations of the organic matter are needed and still limit methanogenesis (Metje and Frenzel 2007). Incubation experiments along a gradient of progressive thaw of permafrost in Swedish and Canadian bogs have shown that as thaw progresses, the lability of the thawed-out peat increases over the years, resulting in a larger CH_4 production and a shift from hydrogenotrophic to acetoclastic methanogenesis (Corbett et al. 2015; Hodgkins et al. 2014).

5.4 Deep Permafrost CH_4 Sources

Permafrost thaw may activate geologic seeps of CH_4 from ^{14}C-depleted deeper geologic reservoirs (Walter Anthony et al. 2012). Occurrences of deep gas seeps in Eastern Siberia are unknown, but there is abundant evidence for intra-permafrost gas, mainly of biogenic origin, that may be emitted to the atmosphere.

Brouchkov and Fukuda (2002) found values as high as 6000 ppmv CH_4 in frozen soil and ice wedges and low rate CH_4 production in deeper soil material at subzero temperatures. Thawing of permafrost may release this CH_4 if it does not pass through an aerobic soil zone where it is oxidized. Rivkina et al. (2001) measured CH_4 concentrations in drill cores up to 50 m depth in the East Siberian coastal plain west of the Kolyma River. These cores penetrated Holocene thaw lake and alluvial sediments, the Yedoma, and Plio-Pleistocene marine and terrestrial sands and silts. The CH_4 concentrations were highest in the Holocene (up to 20 ml/kg) and the Middle Pleistocene-Pliocene deposits (up to 50 ml/kg), but very low in the Yedoma. The dry, steppic environment under which the Ice Complex accumulated was assumed to be unfavourable for CH_4 accumulation. The CH_4 concentration did not show systematic trends with depth that would suggest seepage from a deep subsurface source.

Also evidence for the presence of CH_4 hydrates at shallow depths is found by Rivkina et al. (2001), well above the normal hydrate stability zone based on sediment column pressure and temperature (O'Connor et al. 2010). Rivkina et al. (2001) assume that within the pore spaces of the permafrost, high pressures may be created during freezing, allowing hydrate formation. $\delta^{13}C$ data of CH_4 from these cores demonstrate a biogenic origin of the CH_4, not thermogenic CH_4 from deeper gas sources. Active methanogenic cultures of both acetoclastic and hydrogenotrophic Archaea from Holocene and Pliocene samples were obtained (Rivkina et al. 2007). In West Siberia, hydrates and pressurized biogenic gas at shallow depths result in blowout risks for oil and gas drilling (Yakushev and Chuvilin 2000).

Gas seeps also have been observed in the Yana-Indigirka and Kolyma lowlands. Kraev et al. (2012) report a reservoir in coarse-grained fluvial deposits at 23 m depth in the Kolyma lowlands, which contained CH_4 with a considerable younger age (± 12 000 year) than the deposits in which it was found (±31 000 kyr). This gas should have been migrated into the reservoir from other (unfrozen) deposits. The proposed migration mechanism is expulsion of CH_4 by freezing of an unfrozen body of sediment. Epigenetic refreezing of taliks underneath former thaw lakes is common in the Northeast Siberian lowlands, as shown by the many closed system pingos which result from expulsion of pressurized water.

It is unlikely that deep gas hydrates in the gas hydrate stability zone are a source of CH_4 from permafrost in the near future (O'Connor et al. 2010), but shallower biogenic gas reservoirs may become a source upon warming of the permafrost. Part of the emission hotspots in thaw lakes could originate from this type of reservoir (Walter et al. 2008). The recent discovery of gas outburst craters in Yamal also originates from sources at depths of tens of metres. The first were discovered in 2014 and were up to then completely unknown to the permafrost research community (Leibman et al. 2014). The diameters of these craters are in the order of a few tens of metres; depths may be more than 50 m. Ejecta attest of a violent explosion. Inside the first crater, very high concentrations of CH_4 and H_2S were measured. Leibman et al. (2014) hypothesize that the crater may have originated from dissociation of a shallow hydrate reservoir following warming of the permafrost, which proceeds at a high pace in Yamal. It is expected that within a few years, it will look like a normal tundra lake (Babkina et al. 2017). On further climatic warming, it cannot be excluded that similar outbursts of CH_4 also appear in East Siberian Arctic lowlands.

5.5 Effects of Environmental Change

5.5.1 Climate Change

Warming in Eastern Siberia is strongest in winter (AMAP 2017). Decrease of sea ice cover is associated with higher temperatures over the nearby land areas, in particular in spring and late summer/autumn, and possibly also with precipitation increase (Bintanja and Selten 2014). Higher winter precipitation results in a thicker snow cover, warming the soil (Iijima et al. 2010; Johansson et al. 2013). Climate change also includes changes in the water balance (precipitation vs. evapotranspiration) of ecosystems. Model projections predict an increase in snow water equivalent of 15–30% over the Siberian sector. Snow cover duration decreases throughout the Arctic, but the least (10%) over Siberia (Callaghan et al. 2012).

From basic principles, higher soil and water temperatures should increase CH_4 emission, since the temperature sensitivity (Q10) of methanogenesis is higher than that of methanotrophy (Segers 1998). However, also wetter soil conditions will increase CH_4 emission. It is decisive to what extent climate change results in changes in temperature, water table, and other soil environmental conditions that enhance

methanogenic activity and exposure of additional SOM to methanogenesis. For the effects of climate change on permafrost, Grosse et al. (2011) make distinction between slow but gradual and widespread press disturbances, and rapid, generally local, and destructive pulse disturbances. To quantify the net effects of pulse disturbances, also ecosystem recovery needs to be taken into account (Van Huissteden and Dolman 2012).

5.5.2 *Direct Climate Warming Effects*

As yet, press disturbances for the CH_4 cycle in Eastern Siberia are difficult to distinguish from interannual variability because of the short and sparse observation time series (Parmentier et al. 2013). Evidence results from the analysis of the effects of short-term variability, space-for-time substitutions, and field and model experiments.

Land surface bottom-up models include soil and lake CH_4 emission models (e.g. McGuire et al. 2012). However, because of differences in model structure (Mi et al. 2014; Chadburn et al. 2017) and uncertainty in wetland and lake distribution (Petrescu et al. 2010), model results may deviate strongly from each other (Melton et al. 2013) and need model tuning on data (Petrescu et al. 2007; Budishchev et al. 2014).

Melton et al. (2013) evaluated the performance of ten CH_4 emission models with various resolution and model structure. Simulated wetland areas and CH_4 emissions over large subarctic wetland complexes (West Siberia, Hudson Bay lowlands) showed very large differences among models and deviations from data. The wetlands in the Yana-Indigirka-Kolyma lowlands were even missed by some of the models.

Parmentier et al. (2015) assessed the effect of decreasing sea ice cover on wetland CH_4 emission along the Circum-Arctic coast with three soil CH_4 models (LPJ-GUESS, TEM6, and PEATLAND-VU), driven by ERA-interim reanalysis data from 1981 to 2010 and a prescribed wetland distribution. Sea-ice cover area correlated negatively with nearby land surface temperatures, but no significant trend of precipitation was found. A clear negative correlation between modelled May–October CH_4 fluxes and sea ice extent was found for most of the Arctic including Northeast Siberia, with higher temperature-driven CH_4 emissions in years of lower sea ice extent. Compared to a baseline period of 1981–1990, the CH_4 emission between 2005 and 2010 increased on average by 1.7 (+0.4–4.1) Tg CH_4 $year^{-1}$. For Northeast Siberia, correlations of CH_4 emission with sea ice decline are strongest in June and September (Fig. 5.5).

Other evidence comes from the effects of short-term variability (yearly variations and shorter) of temperatures on CH_4 fluxes. Wille et al. (2008), Sachs et al. (2010), and Parmentier et al. (2011a, b) found a significant effect of soil surface temperature in chamber and eddy covariance CH_4 flux data. Radiocarbon datings on molecular soil organic markers (*n*-alkanes) exported by Siberian rivers (Ob, Yenisey, Lena,

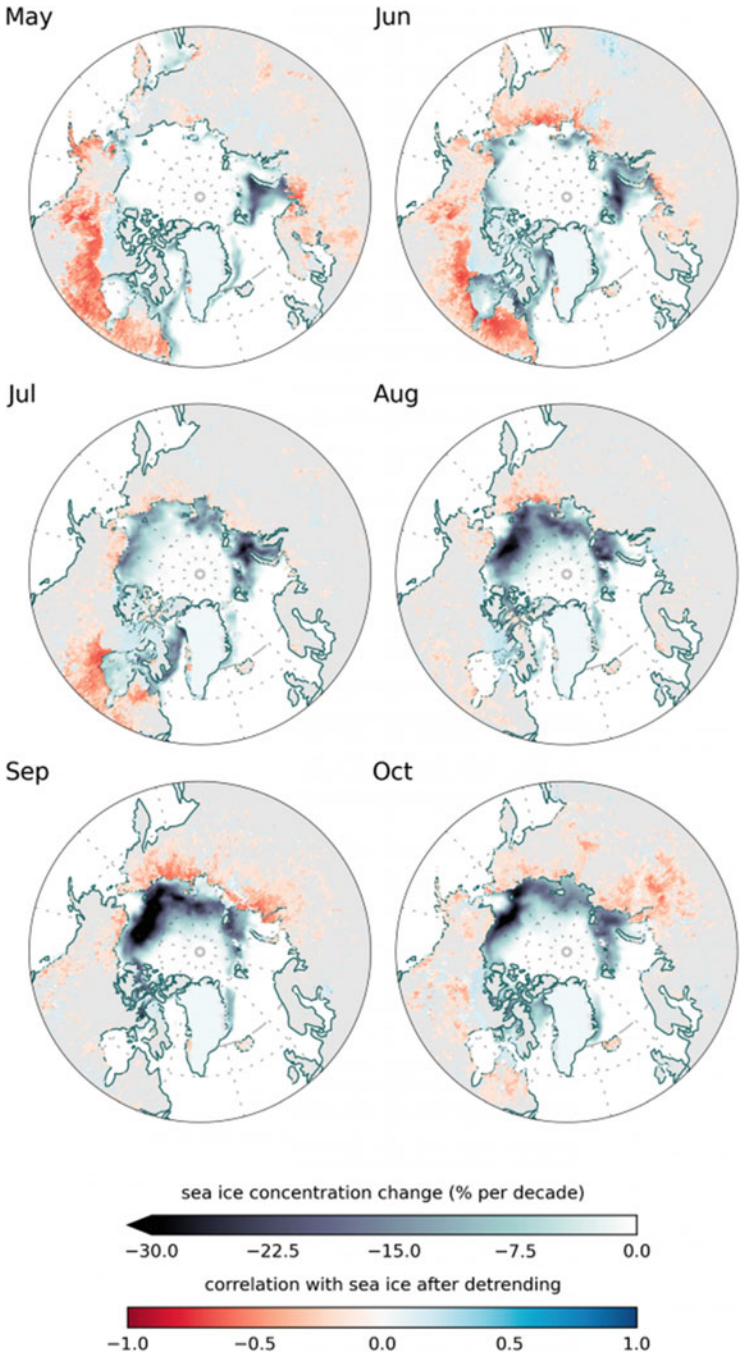

Fig. 5.5 Per month correlations between model-simulated 1981–2010 terrestrial methane emissions and sea ice concentration in a model study by Parmentier et al. (2015). Red to blue colours

Indigirka, and Kolyma) show an increasing age from east to west, which is also the gradient of increasing climate warming (Gustafsson et al. 2011). It is therefore likely that older soil carbon is contributing to CH_4 emitted from soils on a large scale.

Given the important role of vegetation in CH_4 emission, vegetation change is also a form of press disturbance on CH_4 emission. Extension of the growing season and higher growing season temperatures could enhance primary production, but since many ecosystems in Siberia are nutrient-limited (e.g. Beermann et al. 2015), the liberation of nutrients from thawing SOM may be a more important factor. Model simulations using a tundra vegetation model (Van der Kolk et al. 2016) suggest that warming favours shrub dominance, while graminoids (including wetland graminoids) profit from increased precipitation. Graminoids have better access to nutrients liberated in deeper soil layers compared to shrubs.

Warming soils may also result in bacterial community changes. Wagner and Liebner (2009) note a lack of experimental research on this subject. In a high Arctic peat from Spitsbergen, CH_4 production rates, the abundance of methanogenic archaea and their community structure changed with increasing temperature (Høj et al. 2008). On the other hand, little change was seen in the methanogenic archaea population in East Siberian peat soils (Metje and Frenzel 2007). Bacterial isolates from Siberian tundra soils still have their optimum in the temperature range between 25 and 35 °C. The bacterial diversity and quantity of active cells in a polygonal tundra soil in Northeast Siberia were found to be strongly related to the content of organic matter (Kobabe et al. 2004; Wagner and Liebner; 2009). Therefore, changes in the organic matter quality and quantity are likely to have a more important effect on bacterial communities than soil temperature itself.

The effect of warming on lake emissions has not been studied in Eastern Siberia. Data from the extreme warm summer of 2012 in West Siberia show an up to five times higher lake water CH_4 concentration compared to the previous summers (Pokrovsky et al. 2013). Hardenbroek et al. (2012) applied a paleoecological approach for lakes in the Indigirka lowlands, making use of the carbon isotopic effect of CH_4 on the lake food web (Bastviken et al. 2003). Low plankton $\delta^{13}C$ provides a proxy on the recycling of CH_4-derived carbon into a lake's food web. $\delta^{13}C$ in lake zooplankton was lowest in sediments deposited from ca AD 1250 to ca AD 1500 and after AD 1970. This coincided with warmer climate as indicated by tree rings (Sidorova et al. 2008).

Model-predicted summer precipitation trends for the end of the century indicate an increase of precipitation over Siberia by up to 10 mm per month (Overland et al. 2011), which could result in higher soil water tables in the summer, thicker active

Fig. 5.5 (continued) depict the correlation coefficient value of the correlation between modelled methane emissions and sea ice concentration within 2000 km distance, averaged for three ecosystem CH_4 emission models. The linear trend in sea ice concentration is shown to indicate areas of high sea ice retreat. Note that high correlations do not necessarily equal high emissions. (From Parmentier et al. 2015)

layer, and more widespread anaerobic soil conditions. Ohta et al. (2008) showed an increase of soil moisture and ALT between 1998 and 2006 in East Siberian larch (*Larix cajanderii*) forest, which could potentially increase CH_4 emission. Higher winter precipitation also produces higher and more prolonged flooding the next spring. Regional climate model simulations coupled to a hydrological model predict that flooded area increases by 2–5%; the highest increase is predicted in Northern Siberia (Shkolnik et al. 2017). Prolonged and more widespread flooding may result in higher CH_4 emissions from highly reactive floodplains (Van Huissteden et al. 2005, 2013).

5.5.3 Geomorphological Change

Pulse disturbances are largely the effect of geomorphological processes induced by thawing of ice-rich permafrost (Walvoord and Kurylyk 2016). The volume loss of Ice Complex deposits with volumetric ice content up to 90% (Schirrmeister et al. 2013) or of palsas and peat mounds in peatlands results in subsidence and formation of ponds (e.g. Kirpotin et al. 2011; Glagolev et al. 2011). Ponds may also form from coalescing low-centred polygon ponds as a result of general subsidence due to permafrost thaw or change of the water balance (Lara et al. 2015; Van Huissteden in prep). Pond formation alters the heat balance of the surface (Boike et al. 2015). In particular thawing ice wedges results in the formation of deeper ponds (Jorgenson et al. 2006; Liljedahl et al. 2016). If subsidence results in ponds that are deeper than the winter ice thickness, a perennial thaw bulb below the pond results. However, even shallow ponds prolong the period of time in which soil material is thawed (Langer et al. 2015).

The transition of ponds to larger thaw lakes is poorly documented. Fedorov and Konstaninov (2009) and Fedorov et al. (2014) describe the growth of an alas lake near Yakutsk, monitored since 1992. The average rate of subsidence of individual thaw depressions was 5–10 cm $year^{-1}$. Individual ice wedge thaw ponds coalesced into larger lakes and ponds. The lake expanded from an estimated volume of 195 m^2 in 1993 to 3135 m^2 in 2008. About one third of the water volume was derived from ground ice. When the lake expands, surface currents in summer cause erosion of banks, redistributing sediment and exposing more permafrost ice to the impact of solar radiation. Erosion rates are largest in deep and large lakes (Jorgenson and Shur 2007; Fig. 5.6). The thaw bulb below a lake can reach depths of tens of metres (Grosse et al. 2013).

Langer et al. (2015) quantified winter emissions in ponds based on CH_4 stored in ice. Stable ponds in stable polygonal tundra had emissions below 0.0058 mg m^{-2} h^{-1}, while ponds that showed clear signs of erosional expansion had emissions of two orders of magnitude higher. Goovaerts (2016) measured in the Indigirka lowlands an average CH_4 flux of 9.4 mg m^{-2} h^{-1} in shallow, active thaw ponds in summer. These ponds were also a large source of CO_2: 482.5 mg m^{-2} h^{-1}. Flessa

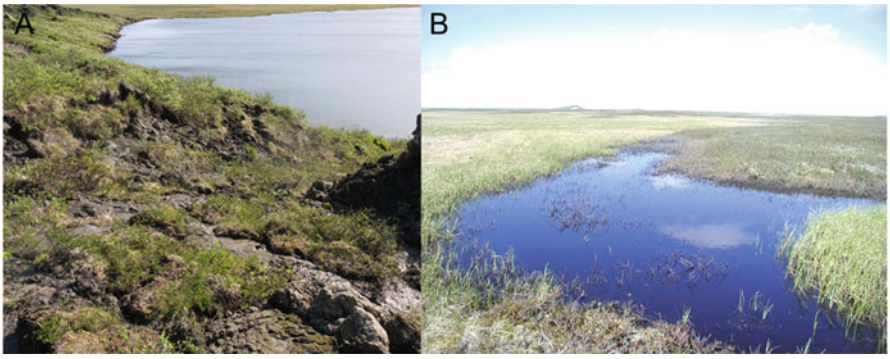

Fig. 5.6 Left: erosion of thaw lake bank in ice-rich Yedoma deposits, showing high transport of recent vegetation and topsoil along a thaw slump into the lake. Kytalyk tundra research station near Chokurdagh, Indigirka lowlands. Right: thaw pond at the transition of a sedge meadow to a *Betula nana*-covered peat mound (Fig. 5.2), with dead *Betula* branches protruding above the water

et al. (2008) report larger fluxes from thaw ponds in west Siberian mires, in the order of 5–12 mg m^{-} h^{-1} and higher.

Ponds develop easily in superficial ice bodies (Jorgenson et al. 2006; Nauta et al. 2014; Van Huissteden in prep). Given their high number, high rate of development, high CH_4 emission, and development in environments that were mostly CH_4 sinks, small thaw ponds are an important source of CH_4 emission resulting from permafrost thaw. Expansion of thaw ponds also results in drowning and erosion of vegetation at the edges of ponds (Fig. 5.6). This fresh organic matter contributes to high CH_4 production. The chain of bacterial organic matter decomposition that contributes to the substrate for methanogens should also be very active in these ponds, because much of the material is contributed from the biologically active topsoil. Therefore, in the early stages of permafrost collapse, CH_4 emission is very active, but not necessarily fed by old soil carbon. Since the CH_4 transport pathway to the atmosphere is short, the CH_4 production at the bottom of these ponds enters the atmosphere without much oxidation (Langer et al. 2015).

However, there are limits to pond expansion and associated CH_4 emission. Shallow ponds are in a few years colonized by wetland vegetation restoring at least the CO_2 sink (Li et al. 2017; Van der Kolk et al. 2016). Liljedahl et al. (2016) show that pond development on ice wedges can result in better drainage through ice wedge troughs. However, the net effect of drainage on GHG emissions is uncertain. The artificial drainage experiment by Kittler et al. (2017) shows a decrease of CH_4 emission, but the increase of aerobic CO_2 respiration and decline of CO_2 uptake resulted in a total net increase of the GHG source.

Compared to ponds, emissions from lakes are lower (Langer et al. 2015). In thaw lakes, ebullition is strongest in the nearshore zones where the contribution of soil carbon eroded from the banks is highest. Whole-year lake emissions in the Kolyma lowlands amounted to 24.9±2.3 g m^{-2} $year^{-1}$ (2.8 mg m^{-2} day^{-1}), but fluxes from the 15-m-wide band adjacent to actively eroded banks are considerably higher,

128±24 g m^{-2} $year^{-1}$(14 mg m^{-2} day^{-1}), representing 79% of the total lake flux (Walter et al. 2006). Isotopic analysis and radiocarbon dating of the emitted CH_4 from thaw lakes in Siberia and Alaska has shown that the CH_4 carbon is derived from old Pleistocene soil carbon and that methanogenesis shifts from the acetoclastic pathway towards CO_2 reduction if more old carbon is involved (Nakagawa et al. 2002; Walter et al. 2007).

Do thaw lakes and ponds expand in area, replacing terrestrial sink areas with large CH_4 sources, and can this be attributed to climate change? The areal changes of lakes and ponds are difficult to estimate; the area of ponds and lakes is influenced on year-to-year variability of the water balance (e.g. Plug et al. 2008; Fedorov et al. 2014). Smith et al. (2005) report an overall decrease of lake area by ±6% but in continuous permafrost an area increase of 12% with a 45% increase in the number of lakes, while in discontinuous permafrost areas, the lake area decreased. Kirpotin et al. (2009) observe a similar pattern in western Siberian peatlands. However, Karlsson et al. (2014) did not find a consistent trend in lake area in West Siberia based on a remote sensing study. Fedorov et al. (2014) report large expansion of a thaw lake from 195 m^2 in 1993 to 3135 m^2 in Central Yakutia.

Thawing permafrost can result in both decrease of lake area (if lakes drain through talik development or erosion of drainage thresholds) or increase (if lake recharge increases through thicker active layer and supra-permafrost taliks). Permafrost lake hydrology often lacks data on groundwater flow (Fedorov et al. 2014; Walvoord and Kurylyk 2016). Lakes and ponds disappear in various ways, in which catastrophic drainage by erosion is a frequent process (Kirpotin et al. 2008; Jones et al. 2011; Grosse et al. 2013). Other processes may be infilling by sedimentation, including peat formation (Walter Anthony et al. 2014). After drainage or infilling with sediments, ice-rich permafrost can be established again over time (Grosse et al. 2013). These lake basins may become carbon and greenhouse gas sinks by uptake of CO_2 in peat and vegetation (Walter Anthony et al. 2014; Van der Molen et al. 2007).

Large areas of Northern Siberia are covered with overlapping drained thaw lake basins, dating from the Last Glacial Termination to recent (Walter et al. 2007b). Assuming accelerated reworking of Yedoma deposits with labile carbon by thaw lake growth, Walter et al. (2007a) estimate that 50–100 Tg CH_4 $year-^{1}$) could be produced with future climate warming. However, many present lakes are secondary lakes, developing in older thaw lake basin sediments with less ice volume than Yedoma and probably less labile carbon because carbon in these sediments has undergone already a decomposition cycle from previous lake growth (Morgenstern et al. 2011, 2013). Also, present lakes expand in areas that already contain CH_4-emitting wetlands, of which the emission has to be taken into account. Future estimates of CH_4 emission from lake growth will strongly depend on rates of geomorphological processes of lake growth and drainage, lake hydrology, and carbon transformation. An approximation of landscape-scale lake development with a probabilistic cellular automata model of thaw lake expansion and erosional drainage shows that lake expansion has limits (Van Huissteden et al. 2011). For all future climate scenarios, the model shows a gradual expansion of lake area at first, followed by a decrease of lake area due to drainage. To reliably estimate future CH_4

emission from expanding thaw lakes, long-term geomorphological process and hydrological studies are necessary.

The net effect on carbon release from permafrost of push disturbances such as pond and lake development should include the life cycle and recovery rate of these features (Van Huissteden and Dolman 2012). Ponds revegetate over time, in the order of several years to decades, and may become sinks of CO_2 again; this CO_2 sink may even be stimulated by nutrient release from thawing SOM (Li et al. 2017). If recovery effects are not considered, an overestimate of the total emission results (Van Huissteden and Dolman 2012).

5.5.4 Other Anthropogenic Disturbances

Human activities increase in vulnerable permafrost ecosystems as a result of economic development. Permafrost ecosystems are fragile, and soils and vegetation are easily disturbed by frequent walking or motorized traffic. The vegetation shields permafrost soils from incoming solar radiation and high air temperatures. Blok et al. (2010, 2011) and Nauta et al. (2014) have demonstrated that the removal of a shrub cover on dry, ice-rich permafrost leads to an increased ALT and the development of thaw ponds, turning the shrub removal areas from a sink of CH_4 into a source in 5 years.

A drainage experiment on the Kolyma River floodplain near Cherskii started in 2004, resulting in an average water table drop of 20 cm (Merbold et al. 2009; Kwon et al. 2016, 2017). The main vegetation in the area consists of *Carex appendiculata* tussocks and *Eriophorum angustifolium* cotton grass. Drainage lowered the growing season of CH_4 flux by a factor of 20 as measured in 2013. The soil temperature profile changed as a result of changed thermal properties (dry organic soil has lower thermal conductivity). The deeper subsoil in the drained areas was colder, resulting in a decrease of thaw depth, while in the top layer temperature fluctuated more strongly. This water table and temperature profile change drives the differences in CH_4 flux, reducing methanogenesis at depth and promoting methanotrophy in the topsoil. Additionally, a decrease in abundance of *E. angustifolium* reduced aerenchymous transport of CH_4.

However, drainage of permafrost wetlands is probably not an option for mitigating CH_4 fluxes. Drainage enhanced aerobic decomposition in the organic-rich soil (Kwon et al. 2016; Kittler et al. 2017). Before drainage, the area was a summer greenhouse gas source of 475±253 g C-CO2-eq m^{-2}, which was reduced to 23±26 g C-CO_2-equivalent m^{-2} shortly after drainage (Merbold et al. 2009). After 10 years of drainage, CO_2 uptake decreased, and CO_2 emission increased, resulting in a larger net GHG source (Kwon et al. 2016, 2017). An important cause of decreased CO_2 uptake is vegetation change: the decline in abundance of *E. angustifolium*, which is a high CH_4-emitting species, also contributes strongly to CO_2 uptake.

These experiments on anthropogenic manipulation of permafrost ecosystems show that there are no simple answers on how to mitigate CH_4 emission from permafrost ecosystems. However, the experiment by Nauta et al. (2014) points convincingly to protection of the vulnerable vegetation cover of permafrost ecosystems; increasing human activities without this protection may result in increased GHG emission.

5.6 BVOC

Oxidation by OH radicals is the main atmospheric sink for CH_4, but also for many organic compounds of natural (vegetation, wildfires) and anthropogenic origin. Non-methane volatile organic compounds (NMVOC) therefore compete with CH_4 for this atmospheric sink and have significant impact on the lifetime of CH_4 and global or regional CH_4 budget (e.g. O'Connor et al. 2010, Thonat et al. 2017). A major component of NMVOC are the biogenic volatile organic compounds (BVOCs), emitted by vegetation. BVOCs consist of thousands of volatile organic chemical species, e.g. isoprenes, terpenoids, alkanes, alkenes, alcohols, esters, carbonyls, and acids. However, only a few of these are emitted at quantities that may impact the atmosphere. The most important of these compounds are terpenoids, including isoprene and monoterpene which are the most studied compounds (Guenther 2013). Taiga forests such as those in Eastern Siberia are an important source of BVOC (Arneth et al. 2007).

With climate change the emission of these compounds may increase by higher temperatures, plant stress, and increasing leaf area (e.g. Arneth et al. 2007; O'Connor et al. 2010; Kramshøj et al. 2016), causing the atmospheric lifetime of CH_4 to become longer, resulting in a further increase of atmospheric CH_4 concentration. However, the emission of the important BVOC component isoprene is reduced at higher atmospheric CO_2 concentrations (Arneth et al. 2007), and furthermore BVOCs also result in the production of secondary organic aerosols that scatter and absorb radiation and act as cloud condensation nuclei (Arneth et al. 2010, 2016 and references therein), reducing solar radiation at the Earth's surface, complicating the effect of BVOC on climate.

Emission factors (E_s) for BVOCs are influenced by environmental parameters, such as light, temperature, and intercellular CO_2 concentration in leaves. Other drivers that can influence E_s are environmental stress, past environmental conditions, leaf age, and seasonality. In particular drought and heat stress are important, but also include the effects of air pollution such as ozone. For some compounds, e.g. isoprene, formation and emission is directly related to current environmental conditions of the plants, but other compounds like monoterpene can be stored in plants which complicates the relation of E_s with the environment by emission from storage (Niinemets et al. 2010).

In assessments of global BVOC emission, the huge Siberian forests have been severely under-sampled. Emission rates for terpenoids at the level of shoots were measured first by Kajos et al. (2013) in *Larix cajanderi* forest near Yakutsk (SPA station). They identified seven different monoterpenes, six different sesquiterpenes, linalool isoprene, and 2-methyl-3-buten-2-ol (MBO). Monoterpenes were dominant and contributed between 61% and 92% of the total emissions; the second important component was linalool isoprene. The emissions varied between 0.5 and 18.5 μg g_{dw}^{-1} h^{-1} and followed the daily cycles of temperature and photosynthetically active radiation. However, the differences among the studied trees were large, possibly because of mechanical stress and herbivore attack in the tree with the highest emissions. The monoterpene emission rates were best described by a model that involves emissions from a both storage pool and emissions directly after synthesis.

Unfortunately not much is known about BVOC emissions in the northern tundras in Eastern Siberia. Emissions of isoprene, methanol, acetone, and acetaldehyde measured above a mire in Northern Sweden measured with disjunct eddy correlation showed a large contribution from this wetland environment: isoprene emission rates were 329 μgC m^{-2} (Holst et al. 2010). Kramshøj et al. (2016) measured BVOC emissions from tundra plants (*Salix glauca* and *Empetrum hermaphroditum*) in a warming experiment in Greenland tundra. Warming by on average 3.1 °C resulted in a 260% increase of BVOC emission. These data demonstrate the need for further study in the large tundra area in Eastern Siberia.

Formaldehyde (HCHO) is a product in the oxidation of VOC from various sources (vegetation, wildfires, anthropogenic sources) and are therefore a proxy for BVOC sources. Satellite observations of atmospheric column formaldehyde concentrations, in combination with inverse modelling of sources (fire and vegetation isoprene emissions), indicate a strong increasing trend (3.8% per year) of isoprene emissions over Siberia (Bauwens et al. 2016; Fig. 5.7). This is attributed to increasing temperature and leaf area index.

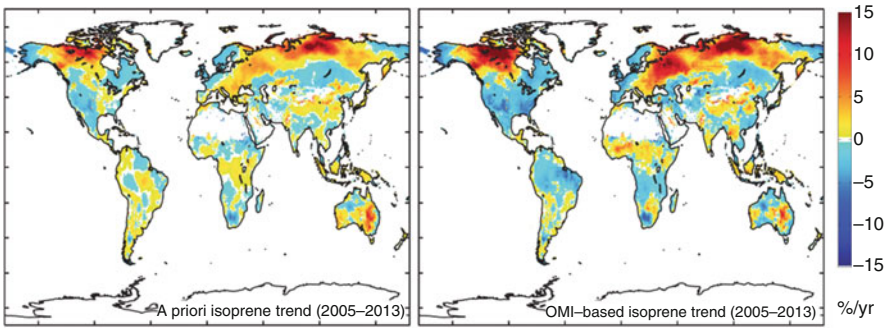

Fig. 5.7 Global distribution of annual isoprene emission trends over 2005–2013 according to an a priori model inversion of formaldehyde sources (left) and a top-down inventory from satellite formaldehyde data (right) expressed in percentage year. (From Bauwens et al. 2016)

Because of the complexity of interactions of BVOC emissions with greenhouse warming, Arneth et al. (2016) set up a modelling experiment for Eastern Siberia to assess these competing effects, including CO_2 emission from soil. The model experiment included the global vegetation model LPJ-GUESS and the ECHAM5.5-HAM2 climate model, with aerosol microphysics included. The emission factors for monoterpenes were taken from the minimum and maximum values measured in Siberia (Kajos et al. 2013), and CO_2 inhibition of BVOC formation was switched on and off in the models. Combined with CO_2 emission inhibition, BVOC emission decreased slightly by the end of this century. Without CO_2 inhibition, BVOC emissions almost tripled.

The model showed the importance of correctly predicting the effect of climate change on the leaf area index of tree species, since forest expansion would result in increasing BVOC emissions (although tundra emissions were not included). The effect on aerosol formation was considered small however, compared to the effects of aerosols from wildfires. The potential radiative effect of increasing BVOC emissions at the end of the century was a -0.2 W m^{-2} change on direct clear-sky radiation and an additional -0.5 W m^{-2} on the cloud radiative effect, but subject to large uncertainty. However, this modelling effort clearly shows the necessity of an integrative approach to the climate effect of BVOC emissions.

5.7 Conclusions

Field research based in Eastern Siberia has contributed significantly to process knowledge of the permafrost carbon feedback to climate change, in particular with respect to CH_4 emissions. However, more progress can be made. Winter emissions have shown to make up an important part of the yearly CH_4 budget of permafrost ecosystems; also spring thaw emissions from lake and pond ice can be substantial. Therefore, research efforts including the full winter season are urgently needed. Other CH_4 sources that need attention are:

- Spatial variabilities of ecosystem CH_4 emissions with attention to landscape-scale variation (lakes, drained thaw lake basins, floodplain wetlands).
- Transfer of old permafrost carbon to labile carbon compounds as substrate for methanogens.
- Potential emissions from deeper permafrost gas reservoirs in depth ranges that can be influenced by permafrost warming in the coming decades.
- Permafrost thaw and CH_4 emission resulting of human disturbance of ecosystems.
- Given the contribution of East Siberian ecosystems to global emission of BVOC and its effects on the oxidative OH sink of CH_4, also these emissions should be quantified better, in particular in the tundra regions of Eastern Siberia.

References

AMAP (2017) Snow, water, ice and permafrost in the Arctic (SWIPA) 2017. Arctic Monitoring and Assessment Programme (AMAP), Oslo

Angle JC, Morin TH, Solden LM, Narrowe AB, Smith GJ, Borton MA, Rey-Sanchez C, Daly RA, Mirfenderesgi G, Hoyt DW (2017) Methanogenesis in oxygenated soils is a substantial fraction of wetland methane emissions. Nat Commun 8(1):1567

Archer D (2007) Methane hydrate stability and anthropogenic climate change. Biogeosci Discuss 4 (2):993–1057

Arneth A, Niinemets Ü, Pressley S, Bäck J, Hari P, Karl T, Noe S, Prentice I, Serça D, Hickler T (2007) Process-based estimates of terrestrial ecosystem isoprene emissions: incorporating the effects of a direct CO_2-isoprene interaction. Atmos Chem Phys 7(1):31–53

Arneth A, Sitch S, Bondeau A, Butterbach-Bahl K, Foster P, Gedney N, de Noblet-Ducoudré N, Prentice IC, Sanderson M, Thonicke K, Wania R, Zaehle S (2010) From biota to chemistry and climate: towards a comprehensive description of trace gas exchange between the biosphere and atmosphere. Biogeosciences 7(1):121–149

Arneth A, Makkonen R, Olin S, Paasonen P, Holst T, Kajos MK, Kulmala M, Maximov T, Miller PA, Schurgers G (2016) Future vegetation–climate interactions in Eastern Siberia: an assessment of the competing effects of CO_2 and secondary organic aerosols. Atmos Chem Phys 16 (8):5243–5262. https://doi.org/10.5194/acp-16-5243-2016

Babkina E, Khomutov A, Leibman M, Dvornikov Y, Kizyakov A (2017) Babkin E Paragenesis of thermal denudation with gas-emission crater and lake formation, Yamal Peninsula, Russia. EGU General Assembly Conference Abstracts, In, p 6026

Bastviken D, Ejlertsson J, Sundh I, Tranvik L (2003) Methane as a source of carbon and energy for lake pelagic food webs. Ecology 84(4):969–981

Bastviken D, Cole JJ, Pace ML, Van de Bogert MC (2008) Fates of methane from different lake habitats: connecting whole-lake budgets and CH4 emissions. J Geophys Res Biogeosci 113(G2)

Bauwens M, Stavrakou T, Müller J-F, Smedt ID, Roozendael MV, Werf GR, Wiedinmyer C, Kaiser JW, Sindelarova K, Guenther A (2016) Nine years of global hydrocarbon emissions based on source inversion of OMI formaldehyde observations. Atmos Chem Phys 16(15):10133–10158

Beermann F, Teltewskoi A, Fiencke C, Pfeiffer E-M, Kutzbach L (2015) Stoichiometric analysis of nutrient availability (N, P, K) within soils of polygonal tundra. Biogeochemistry 122 (2-3):211–227

Bergamaschi P, Houweling S, Segers A, Krol M, Frankenberg C, Scheepmaker RA, Dlugokencky E, Wofsy SC, Kort EA, Sweeney C, Schuck T, Brenninkmeijer C, Chen H, Beck V, Gerbig C (2013) Atmospheric CH4in the first decade of the 21st century: inverse modeling analysis using SCIAMACHY satellite retrievals and NOAA surface measurements. J Geophys Res Atmos 118(13):7350–7369. https://doi.org/10.1002/jgrd.50480

Berrittella C, van Huissteden J, Warnsloh JM, Dolman AJ (2017) Permafrost ecosystem: wetlands characteristics and their influence on CH4 emissions in a drained thaw lake basin, Northeastern Siberia. In: Berrittella C (ed) Wetland methane emissions during Last Glacial climate warming. PhD thesis edn. VU University, Amsterdam

Bhullar GS, Edwards PJ, Olde Venterink H (2013) Variation in the plant-mediated methane transport and its importance for methane emission from intact wetland peat mesocosms. J Plant Ecol 6(4):298–304. https://doi.org/10.1093/jpe/rts045

Bintanja R, Selten F (2014) Future increases in Arctic precipitation linked to local evaporation and sea-ice retreat. Nature 509(7501):479

Blok D, Heijmans MM, Schaepman-Strub G, Kononov A, Maximov T, Berendse F (2010) Shrub expansion may reduce summer permafrost thaw in Siberian tundra. Glob Chang Biol 16 (4):1296–1305

Blok D, Heijmans MMPD, Schaepman-Strub G, van Ruijven J, Parmentier FJW, Maximov TC, Berendse F (2011) The cooling capacity of mosses: controls on water and energy fluxes in a Siberian Tundra site. Ecosystems 14(7):1055–1065. https://doi.org/10.1007/s10021-011-9463-5

Boike J, Georgi C, Kirilin G, Muster S, Abramova K, Fedorova I, Chetverova A, Grigoriev M, Bornemann N, Langer M (2015) Thermal processes of thermokarst lakes in the continuous permafrost zone of northern Siberia – observations and modeling (Lena River Delta, Siberia). Biogeosciences 12(20):5941–5965. https://doi.org/10.5194/bg-12-5941-2015

Brouchkov A, Fukuda M (2002) Preliminary measurements on methane content in permafrost, Central Yakutia, and some experimental data. Permafr Periglac Process 13(3):187–197. https://doi.org/10.1002/ppp.422

Brouchkov A, Fukuda M, Fedorov A, Konstantinov P, Iwahana G (2004) Thermokarst as a short-term permafrost disturbance, Central Yakutia. Permafr Periglac Process 15(1):81–87. https://doi.org/10.1002/ppp.473

Bruhwiler L, Dlugokencky E, Masarie K, Ishizawa M, Andrews A, Miller J, Sweeney C, Tans P, Worthy D (2014) CarbonTracker-CH_4: an assimilation system for estimating emissions of atmospheric methane. Atmos Chem Phys 14(16):8269–8293

Budishchev A, Mi Y, van Huissteden J, Belelli-Marchesini L, Schaepman-Strub G, Parmentier FJW, Fratini G, Gallagher A, Maximov TC, Dolman AJ (2014) Evaluation of a plot-scale methane emission model using eddy covariance observations and footprint modelling. Biogeosciences 11(17):4651–4664. https://doi.org/10.5194/bg-11-4651-2014

Callaghan TV, Johansson M, Brown RD, Groisman PY, Labba N, Radionov V, Barry RG, Bulygina ON, Essery RLH, Frolov DM, Golubev VN, Grenfell TC, Petrushina MN, Razuvaev VN, Robinson DA, Romanov P, Shindell D, Shmakin AB, Sokratov SA, Warren S, Yang D (2012) The changing face of Arctic snow cover: a synthesis of observed and projected changes. Ambio 40(S1):17–31. https://doi.org/10.1007/s13280-011-0212-y

Chadburn SE, Krinner G, Porada P, Bartsch A, Beer C, Belelli Marchesini L, Boike J, Ekici A, Elberling B, Friborg T, Hugelius G, Johansson M, Kuhry P, Kutzbach L, Langer M, Lund M, Parmentier FJW, Peng S, Van Huissteden K, Wang T, Westermann S, Zhu D, Burke EJ (2017) Carbon stocks and fluxes in the high latitudes: using site-level data to evaluate Earth system models. Biogeosciences 14(22):5143–5169. https://doi.org/10.5194/bg-14-5143-2017

Christensen TR, Jonasson S, Callaghan TV, Havström M (1995) Spatial variation in high latitude methane flux-a transect across tundra environments in Siberia and the European Arctic. J Geophys Res 100(D10):21035–21045

Christensen TR, Ekberg A, Ström L, Mastepanov M, Panikov N, Öquist M, Svensson BH, Nykänen H, Martikainen PJ, Oskarsson H (2003) Factors controlling large scale variations in methane emissions from wetlands. Geophys Res Lett 30(7). https://doi.org/10.1029/2002gl016848

Corbett JE, Tfaily MM, Burdige DJ, Glaser PH, Chanton JP (2015) The relative importance of methanogenesis in the decomposition of organic matter in northern peatlands. J Geophys Res Biogeosci 120(2):280–293

Corradi C, Kolle O, Walter K, Zimov SA, Schulze ED (2005) Carbon dioxide and methane exchange of a north-east Siberian tussock tundra. Glob Chang Biol 11:1910–1925. https://doi.org/10.1111/j.1365-2486.2005.01023.x

Deutzmann JS, Stief P, Brandes J, Schink B (2014) Anaerobic methane oxidation coupled to denitrification is the dominant methane sink in a deep lake. Proc Natl Acad Sci 111 (51):18273–18278

Duguay CR, Flato GM, Jeffries MO, Ménard P, Morris K, Rouse WR (2003) Ice-cover variability on shallow lakes at high latitudes: model simulations and observations. Hydrol Process 17 (17):3465–3483. https://doi.org/10.1002/hyp.1394

Fedorov AN, Konstantinov PY (2009) Response of permafrost landscapes of Central Yakutia to current changes of climate, and anthropogenic impacts. Geogr Nat Resour 30(2):146–150

Fedorov A, Gavriliev P, Konstantinov P, Hiyama T, Iijima Y, Iwahana G (2014) Estimating the water balance of a thermokarst lake in the middle of the Lena River basin, eastern Siberia. Ecohydrology 7(2):188–196

Flessa H, Rodionov A, Guggenberger G, Fuchs H, Magdon P, Shibistova O, Zrazhevskaya G, Mikheyeva N, Kasansky OA, Blodau C (2008) Landscape controls of CH4fluxes in a catchment of the forest tundra ecotone in northern Siberia. Glob Chang Biol 14(9):2040–2056. https://doi.org/10.1111/j.1365-2486.2008.01633.x

Frenzel P, Karofeld E (2000) CH_4 emission from a hollow-ridge complex in a raised bog: the role of CH_4 production and oxidation. Biogeochemistry 51(1):91–112

Ganzert L, Jurgens G, Munster U, Wagner D (2007) Methanogenic communities in permafrost-affected soils of the Laptev Sea coast, Siberian Arctic, characterized by 16S rRNA gene fingerprints. FEMS Microbiol Ecol 59(2):476–488. https://doi.org/10.1111/j.1574-6941.2006.00205.x

Gauci V, Gowing DJ, Hornibrook ER, Davis JM, Dise NB (2010) Woody stem methane emission in mature wetland alder trees. Atmos Environ 44(17):2157–2160

Glagolev M, Kleptsova I, Filippov I, Maksyutov S, Machida T (2011) Regional methane emission from West Siberia mire landscapes. Environ Res Lett 6(4):045214. https://doi.org/10.1088/1748-9326/6/4/045214

Goovaerts A (2016) An explorative study of carbon sources and greenhouse gas emissions in thermokarst lakes and rivers using stable isotopes (Chokurdakh, Yakutsk, Russia). Master Thesis, KU Leuven, Facultei Bio-Ingenieurswetenschappen:122

Grosse G, Romanovsky V, Walter K, Morgenstern A, Lantuit H, Zimov S (2008) Distribution of thermokarst lakes and ponds at three yedoma sites in Siberia. In: 9th International conference on Permafrost, Fairbanks, 2008. Proceedings 9th International conference on Permafrost. pp 551–556

Grosse G, Harden J, Turetsky M, McGuire AD, Camill P, Tarnocai C, Frolking S, Schuur EAG, Jorgenson T, Marchenko S, Romanovsky V, Wickland KP, French N, Waldrop M, Bourgeau-Chavez L, Striegl RG (2011) Vulnerability of high-latitude soil organic carbon in North America to disturbance. J Geophys Res 116. https://doi.org/10.1029/2010jg001507

Grosse G, Jones B, Arp C (2013) 8. 21 Thermokarst lakes, drainage, and drained basins. 325–353. https://doi.org/10.1016/b978-0-12-374739-6.00216-5

Guenther A (2013) Biological and chemical diversity of biogenic volatile organic emissions into the atmosphere. ISRN Atmos Sci 2013:1–27. https://doi.org/10.1155/2013/786290

Gustafsson Ö, van Dongen BE, Vonk JE, Dudarev OV, Semiletov IP (2011) Widespread release of old carbon across the Siberian Arctic echoed by its large rivers. Biogeosciences 8 (6):1737–1743. https://doi.org/10.5194/bg-8-1737-2011

Hershey AE, Northington RM, Whalen SC (2013) Substrate limitation of sediment methane flux, methane oxidation and use of stable isotopes for assessing methanogenesis pathways in a small arctic lake. Biogeochemistry 117(2-3):325–336. https://doi.org/10.1007/s10533-013-9864-y

Hines ME, Duddleston KN, Kiene RP (2001) Carbon flow to acetate and C1 compounds in northern wetlands. Geophys Res Lett 28(22):4251–4254

Hodgkins SB, Tfaily MM, McCalley CK, Logan TA, Crill PM, Saleska SR, Rich VI, Chanton JP (2014) Changes in peat chemistry associated with permafrost thaw increase greenhouse gas production. Proc Natl Acad Sci USA 111(16):5819–5824. https://doi.org/10.1073/pnas.1314641111

Hoj L, Olsen RA, Torsvik VL (2008) Effects of temperature on the diversity and community structure of known methanogenic groups and other archaea in high Arctic peat. ISME J 2 (1):37–48. https://doi.org/10.1038/ismej.2007.84

Holst T, Arneth A, Hayward S, Ekberg A, Mastepanov M, Jackowicz-Korczynski M, Friborg T, Crill PM, Bäckstrand K (2010a) BVOC ecosystem flux measurements at a high latitude wetland site. Atmos Chem Phys 10(4):1617–1634

Houghton JT, Ding Y, Griggs DJ, Noguer M, van der Linden PJ, Dai X, Maskell K, Johnson C (2001) Climate change 2001: the scientific basis. The Press Syndicate of the University of Cambridge, Cambridge

Houweling S, Krol M, Bergamaschi P, Frankenberg C, Dlugokencky EJ, Morino I, Notholt J, Sherlock V, Wunch D, Beck V, Gerbig C, Chen H, Kort EA, Röckmann T, Aben I (2014) A multi-year methane inversion using SCIAMACHY, accounting for systematic errors using TCCON measurements. Atmos Chem Phys 14(8):3991–4012. https://doi.org/10.5194/acp-14-3991-2014

Hugelius G, Strauss J, Zubrzycki S, Harden JW, Schuur EAG, Ping CL, Schirrmeister L, Grosse G, Michaelson GJ, Koven CD, O'Donnell JA, Elberling B, Mishra U, Camill P, Yu Z, Palmtag J, Kuhry P (2014) Improved estimates show large circumpolar stocks of permafrost carbon while

quantifying substantial uncertainty ranges and identifying remaining data gaps. Biogeosci Discuss 11(3):4771–4822. https://doi.org/10.5194/bgd-11-4771-2014

Iijima Y, Fedorov AN, Park H, Suzuki K, Yabuki H, Maximov TC, Ohata T (2010) Abrupt increases in soil temperatures following increased precipitation in a permafrost region, central Lena River basin, Russia. Permaf Periglac Process 21(1):30–41. https://doi.org/10.1002/ppp.662

Jammet M, Crill P, Dengel S, Friborg T (2015) Large methane emissions from a subarctic lake during spring thaw: mechanisms and landscape significance. J Geophys Res Biogeosci 120 (11):2289–2305. https://doi.org/10.1002/2015jg003137

Johansson M, Callaghan TV, Bosiö J, Åkerman HJ, Jackowicz-Korczynski M, Christensen TR (2013) Rapid responses of permafrost and vegetation to experimentally increased snow cover in sub-arctic Sweden. Environ Res Lett 8(3):035025. https://doi.org/10.1088/1748-9326/8/3/035025

Jones BM, Grosse G, Arp C, Jones M, Walter Anthony K, Romanovsky V (2011) Modern thermokarst lake dynamics in the continuous permafrost zone, northern Seward Peninsula, Alaska. J Geophys Res Biogeosci 116(G2):G00M03. https://doi.org/10.1029/2011JG001666

Jørgenson JC, Lund Johansen KM, Westergaard-Nielsen A, Elberling B (2014) Net regional methane sink in High Arctic soils of northeast Greenland. Nat Geosci 8(1):20–23. https://doi.org/10.1038/ngeo2305

Jorgenson MT, Shur Y (2007) Evolution of lakes and basins in northern Alaska and discussion of the thaw lake cycle. J Geophys Res Earth Surf 112(F2):F02S17. https://doi.org/10.1029/2006JF000531

Jorgenson MT, Shur YL, Pullman ER (2006) Abrupt increase in permafrost degradation in Arctic Alaska. Geophys Res Lett 33(2). https://doi.org/10.1029/2005gl024960

Kajos M, Hakola H, Holst T, Nieminen T, Tarvainen V, Maximov T, Petäjä T, Arneth A, Rinne J (2013) Terpenoid emissions from fully grown east Siberian Larix cajanderi trees. Biogeosciences 10(7):4705

Karlsson J, Lyon S, Destouni G (2014) Temporal behavior of lake size-distribution in a thawing permafrost landscape in Northwestern Siberia. Remote Sens 6(1):621–636. https://doi.org/10.3390/rs6010621

King J, Reeburgh W, Thieler K, Kling G, Loya W, Johnson L, Nadelhoffer K (2002) Pulse-labeling studies of carbon cycling in Arctic tundra ecosystems: the contribution of photosynthates to methane emission. Glob Biogeochem Cycles 16(4):1062. https://doi.org/10.1029/2001GB001456

Kip N, van Winden JF, Pan Y, Bodrossy L, Reichart G-J, Smolders AJP, Jetten MSM, Damsté JSS, Op den Camp HJM (2010) Global prevalence of methane oxidation by symbiotic bacteria in peat-moss ecosystems. Nat Geosci 3(9):617–621. https://doi.org/10.1038/ngeo939

Kirpotin S, Polishchuk Y, Zakharova E, Shirokova L, Pokrovsky O, Kolmakova M, Dupre B (2008) One of the possible mechanisms of thermokarst lakes drainage in West-Siberian North. Int J Environ Stud 65(5):631–635. https://doi.org/10.1080/00207230802525208

Kirpotin SN, Polishchuk Y, Bryksina N (2009) Abrupt changes of thermokarst lakes in Western Siberia: impacts of climatic warming on permafrost melting. Int J Environ Stud 66(4):423–431. https://doi.org/10.1080/00207230902758287

Kirpotin S, Polishchuk Y, Bryksina N, Sugaipova A, Kouraev A, Zakharova E, Pokrovsky OS, Shirokova L, Kolmakova M, Manassypov R, Dupre B (2011) West Siberian palsa peatlands: distribution, typology, cyclic development, present day climate-driven changes, seasonal hydrology and impact on CO_2 cycle. Int J Environ Stud 68(5):603–623. https://doi.org/10.1080/00207233.2011.593901

Kirschke S, Bousquet P, Ciais P, Saunois M, Canadell JG, Dlugokencky EJ, Bergamaschi P, Bergmann D, Blake DR, Bruhwiler L (2013) Three decades of global methane sources and sinks. Nat Geosci 6(10):813

Kittler F, Heimann M, Kolle O, Zimov N, Zimov S, Göckede M (2017) Long-term drainage reduces CO2 uptake and CH4 emissions in a Siberian permafrost ecosystem. Global Biogeochem Cycles 31 https://doi.org/10.1002/2017GB005774

Knoblauch C, Zimmermann U, Blumenberg M, Michaelis W, Pfeiffer E-M (2008) Methane turnover and temperature response of methane-oxidizing bacteria in permafrost-affected soils of northeast Siberia. Soil Biol Biochem 40(12):3004–3013

Knoblauch C, Spott O, Evgrafova S, Kutzbach L, Pfeiffer EM (2015) Regulation of methane production, oxidation, and emission by vascular plants and bryophytes in ponds of the northeast Siberian polygonal tundra. J Geophys Res Biogeosci 120(12):2525–2541

Kobabe S, Wagner D, Pfeiffer EM (2004) Characterisation of microbial community composition of a Siberian tundra soil by fluorescence in situ hybridisation. FEMS Microbiol Ecol 50(1):13–23. https://doi.org/10.1016/j.femsec.2004.05.003

Kraev GN, Schultze ED, Rivkina EM (2012) Cryogenesis as a factor of methane distribution in layers of permafrost. Dokl Earth Sci 451(2):882–885. https://doi.org/10.1134/s1028334x13080291

Kramshøj M, Vedel-Petersen I, Schollert M, Rinnan Å, Nymand J, Ro-Poulsen H, Rinnan R (2016) Large increases in Arctic biogenic volatile emissions are a direct effect of warming. Nat Geosci 9(5):349–352

Kutzbach L, Wagner D, Pfeiffer E-M (2004) Effect of microrelief and vegetation on methane emission from wet polygonal tundra, Lena Delta, Northern Siberia. Biogeochemistry 69 (3):341–362

Kutzbach L, Schneider J, Sachs T, Giebels M, Nykänen H, Shurpali N, Martikainen P, Alm J, Wilmking M (2007) CO_2 flux determination by closed-chamber methods can be seriously biased by inappropriate application of linear regression. Biogeosciences 4(6):1005–1025

Kwon MJ, Heimann M, Kolle O, Luus KA, Schuur EAG, Zimov N, Zimov SA, Göckede M (2016) Long-term drainage reduces CO_2 uptake and increases CO_2 emission on a Siberian floodplain due to shifts in vegetation community and soil thermal characteristics. Biogeosciences 13 (14):4219–4235. https://doi.org/10.5194/bg-13-4219-2016

Kwon MJ, Beulig F, Ilie I, Wildner M, Kusel K, Merbold L, Mahecha MD, Zimov N, Zimov SA, Heimann M, Schuur EAG, Kostka JE, Kolle O, Hilke I, Gockede M (2017) Plants, microorganisms, and soil temperatures contribute to a decrease in methane fluxes on a drained Arctic floodplain. Glob Chang Biol 23(6):2396–2412. https://doi.org/10.1111/gcb.13558

Langer M, Westermann S, Walter Anthony K, Wischnewski K, Boike J (2015) Frozen ponds: production and storage of methane during the Arctic winter in a lowland tundra landscape in northern Siberia, Lena River delta. Biogeosciences 12(4):977–990. https://doi.org/10.5194/bg-12-977-2015

Lara MJ, McGuire AD, Euskirchen ES, Tweedie CE, Hinkel KM, Skurikhin AN, Romanovsky VE, Grosse G, Bolton WR, Genet H (2015) Polygonal tundra geomorphological change in response to warming alters future CO_2 and CH_4 flux on the Barrow Peninsula. Glob Chang Biol 21 (4):1634–1651. https://doi.org/10.1111/gcb.12757

Larmola T, Tuittila E-S, Tiirola M, Nykänen H, Martikainen PJ, Yrjälä K, Tuomivirta T, Fritze H (2010) The role of Sphagnum mosses in the methane cycling of a boreal mire. Ecology 91 (8):2356–2365

Larmola T, Leppänen SM, Tuittila E-S, Aarva M, Merilä P, Fritze H, Tiirola M (2014) Methanotrophy induces nitrogen fixation during peatland development. Proc Natl Acad Sci 111(2):734–739

Leibman MO, Kizyakov AI, Plekhanov AV, Streletskaya ID (2014) New permafrost feature–deep crater in Central Yamal (West Siberia, Russia) as a response to local climate fluctuations. Environ Sustain 4:68–80

Li B, Heijmans MMPD, Blo D, Wang P, Karsanaev SV, Maximov TC, Van Huissteden J, Berendse F (2017) Thaw pond development and initial vegetation succession in experimental plots at a Siberian lowland tundra site. Pant Soil 420:147–162. https://doi.org/10.1007/s11104-017-3369-8

Liebner S, Zeyer J, Wagner D, Schubert C, Pfeiffer EM, Knoblauch C (2011) Methane oxidation associated with submerged brown mosses reduces methane emissions from Siberian polygonal tundra. J Ecol 99(4):914–922

Liljedahl AK, Boike J, Daanen RP, Fedorov AN, Frost GV, Grosse G, Hinzman LD, Iijma Y, Jorgenson JC, Matveyeva N, Necsoiu M, Raynolds MK, Romanovsky VE, Schulla J, Tape KD, Walker DA, Wilson CJ, Yabuki H, Zona D (2016) Pan-Arctic ice-wedge degradation in

warming permafrost and its influence on tundra hydrology. Nat Geosci 9(4):312–318. https://doi.org/10.1038/ngeo2674

Mastepanov M, Sigsgaard C, Dlugokencky EJ, Houweling S, Strom L, Tamstorf MP, Christensen TR (2008) Large tundra methane burst during onset of freezing. Nature 456(7222):628–630. https://doi.org/10.1038/nature07464

Mastepanov M, Sigsgaard C, Tagesson T, Ström L, Tamstorf MP, Lund M, Christensen T (2013) Revisiting factors controlling methane emissions from high-Arctic tundra. Biogeosciences 10 (7):5139

McGuire AD, Christensen TR, Hayes D, Heroult A, Euskirchen E, Kimball JS, Koven C, Lafleur P, Miller PA, Oechel W, Peylin P, Williams M, Yi Y (2012) An assessment of the carbon balance of Arctic tundra: comparisons among observations, process models, and atmospheric inversions. Biogeosciences 9(8):3185–3204. https://doi.org/10.5194/bg-9-3185-2012

Melton JR, Wania R, Hodson EL, Poulter B, Ringeval B, Spahni R, Bohn T, Avis CA, Beerling DJ, Chen G, Eliseev AV, Denisov SN, Hopcroft PO, Lettenmaier DP, Riley WJ, Singarayer JS, Subin ZM, Tian H, Zürcher S, Brovkin V, van Bodegom PM, Kleinen T, Yu ZC, Kaplan JO (2013) Present state of global wetland extent and wetland methane modelling: conclusions from a model inter-comparison project (WETCHIMP). Biogeosciences 10(2):753–788. https://doi.org/10.5194/bg-10-753-2013

Merbold L, Kutsch WL, Corradi C, Kolle O, Rebmann C, Stoy PC, Zimov SA, Schulze ED (2009) Artificial drainage and associated carbon fluxes (CO2/CH4) in a tundra ecosystem. Glob Chang Biol 15(11):2599–2614. https://doi.org/10.1111/j.1365-2486.2009.01962.x

Metje M, Frenzel P (2007) Methanogenesis and methanogenic pathways in a peat from subarctic permafrost. Environ Microbiol 9(4):954–964. https://doi.org/10.1111/j.1462-2920.2006.01217.x

Mi Y, van Huissteden J, Parmentier FJW, Gallagher A, Budishchev A, Berridge CT, Dolman AJ (2014) Improving a plot-scale methane emission model and its performance at a northeastern Siberian tundra site. Biogeosciences 11(14):3985–3999. https://doi.org/10.5194/bg-11-3985-2014

Morgenstern A, Grosse G, Günther F, Fedorova I, Schirrmeister L (2011) Spatial analyses of thermokarst lakes and basins in Yedoma landscapes of the Lena Delta. Cryosphere 5 (4):849–867. https://doi.org/10.5194/tc-5-849-2011

Morgenstern A, Ulrich M, Günther F, Roessler S, Fedorova IV, Rudaya NA, Wetterich S, Boike J, Schirrmeister L (2013) Evolution of thermokarst in East Siberian ice-rich permafrost: a case study. Geomorphology 201:363–379. https://doi.org/10.1016/j.geomorph.2013.07.011

Morishita T, Hatano R, Desyatkin RV (2003) CH4flux in an alas ecosystem formed by forest disturbance near Yakutsk, Eastern Siberia, Russia. Soil Sci Plant Nutr 49(3):369–377. https://doi.org/10.1080/00380768.2003.10410022

Nakagawa F, Yoshida N, Nojiri Y, Makarov V (2002) Production of methane from alasses in eastern Siberia: implications from its 14C and stable isotopic compositions. Glob Biogeochem Cycles 16(3)

Nakano T, Kuniyoshi S, Fukuda M (2000) Temporal variation in methane emission from tundra wetlands in a permafrost area, northeastern Siberia. Atmos Environ 34(8):1205–1213

Nauta AL, Heijmans MMPD, Blok D, Limpens J, Elberling B, Gallagher A, Li B, Petrov RE, Maximov TC, van Huissteden J, Berendse F (2014) Permafrost collapse after shrub removal shifts tundra ecosystem to a methane source. Nat Clim Chang 5(1):67–70. https://doi.org/10.1038/nclimate2446

Niinemets Ü, Arneth A, Kuhn U, Monson RK, Peñuelas J, Staudt M (2010) The emission factor of volatile isoprenoids: stress, acclimation, and developmental responses. Biogeosciences 7 (7):2203–2223. https://doi.org/10.5194/bg-7-2203-2010

O'Connor FM, Boucher O, Gedney N, Jones CD, Folberth GA, Coppell R, Friedlingstein P, Collins WJ, Chappellaz J, Ridley J, Johnson CE (2010) Possible role of wetlands, permafrost, and methane hydrates in the methane cycle under future climate change: a review. Rev Geophys 48 (4). https://doi.org/10.1029/2010rg000326

Ohta T, Maximov TC, Dolman AJ, Nakai T, van der Molen MK, Kononov AV, Maximov AP, Hiyama T, Iijima Y, Moors EJ, Tanaka H, Toba T, Yabuki H (2008) Interannual variation of water balance and summer evapotranspiration in an eastern Siberian larch forest over a 7-year period (1998–2006). Agric For Meteorol 148(12):1941–1953. https://doi.org/10.1016/j.agrformet.2008.04.012

Overland JE, Wang M, Walsh JE, Christensen JH, Kattsov VM, Chapman WL (2011) Climate model projections for the Arctic. In: Snow, water, ice and permafrost in the Arctic (SWIPA). Arctic Monitoring and Assessment Programme (AMAP), Oslo

Parmentier FJW, van Huissteden J, Kip N, Op den Camp HJM, Jetten MSM, Maximov TC, Dolman AJ (2011a) The role of endophytic methane-oxidizing bacteria in submerged *Sphagnum* in determining methane emissions of Northeastern Siberian tundra. Biogeosciences 8 (5):1267–1278. https://doi.org/10.5194/bg-8-1267-2011

Parmentier FJW, van Huissteden J, van der Molen MK, Schaepman-Strub G, Karsanaev SA, Maximov TC, Dolman AJ (2011b) Spatial and temporal dynamics in eddy covariance observations of methane fluxes at a tundra site in northeastern Siberia. J Geophys Res 116(G3). https://doi.org/10.1029/2010jg001637

Parmentier F-JW, Christensen TR, Sørensen LL, Rysgaard S, McGuire AD, Miller PA, Walker DA (2013) The impact of lower sea-ice extent on Arctic greenhouse-gas exchange. Nat Clim Chang 3(3):195–202. https://doi.org/10.1038/nclimate1784

Parmentier FW, Zhang W, Mi Y, Zhu X, van Huissteden J, Hayes DJ, Zhuang Q, Christensen TR, McGuire AD (2015) Rising methane emissions from northern wetlands associated with sea ice decline. Geophys Res Lett 42(17):7214–7222. https://doi.org/10.1002/2015GL065013

Petrescu A, Van Huissteden J, Jackowicz-Korczynski M, Yurova A, Christensen T, Crill PM, Maximov T (2007) Modelling CH_4 emissions from arctic wetlands: effects of hydrological parameterization. Biogeosci Discuss 4(5):3195–3227

Petrescu A, Van Beek L, Van Huissteden J, Prigent C, Sachs T, Corradi C, Parmentier F, Dolman A (2010) Modeling regional to global CH_4 emissions of boreal and arctic wetlands. Glob Biogeochem Cycles 24(4)

Plug LJ, Walls C, Scott B (2008) Tundra lake changes from 1978 to 2001 on the Tuktoyaktuk Peninsula, western Canadian Arctic. Geophys Res Lett 35:L03502. https://doi.org/10.1029/2007GL032303

Pokrovsky OS, Shirokova LS, Kirpotin SN, Kulizhsky SP, Vorobiev SN (2013) Impact of western Siberia heat wave 2012 on greenhouse gases and trace metal concentration in thaw lakes of discontinuous permafrost zone. Biogeosciences 10(8):5349–5365

Raghoebarsing AA, Pol A, van de Pas-Schoonen KT, Smolders AJ, Ettwig KF, Rijpstra WI, Schouten S, Damste JS, Op den Camp HJ, Jetten MS, Strous M (2006) A microbial consortium couples anaerobic methane oxidation to denitrification. Nature 440(7086):918–921. https://doi.org/10.1038/nature04617

Rivkina E, Friedmann E, McKay C, Gilichinsky D (2000) Metabolic activity of permafrost bacteria below the freezing point. Appl Environ Microbiol 66(8):3230–3233

Rivkina E, Gilichinsky DA, McKay C, Dallimore S (2001) Methane distribution in permafrost: evidence for an interpore pressure methane hydrate. In: Permafrost response on economic development, environmental security and natural resources. Springer, Dordrecht, pp 487–496

Rivkina E, Shcherbakova V, Laurinavichius K, Petrovskaya L, Krivushin K, Kraev G, Pecheritsina S, Gilichinsky D (2007) Biogeochemistry of methane and methanogenic archaea in permafrost. FEMS Microbiol Ecol 61(1):1–15. https://doi.org/10.1111/j.1574-6941.2007.00315.x

Sachs T, Giebels M, Wille C, Kutzbach L, Boike J (2008a) Methane emission from Siberian wet polygonal tundra on multiple spatial scales: vertical flux measurements by closed chambers and eddy covariance, Samoylov Island, Lena River Delta. In: 9th international conference on permafrost, Fairbanks, pp 1549–1554

Sachs T, Wille C, Boike J, Kutzbach L (2008b) Environmental controls on ecosystem-scale CH4emission from polygonal tundra in the Lena River Delta, Siberia. J Geophys Res 113. https://doi.org/10.1029/2007jg000505

Sachs T, Giebels M, Boike J, Kutzbach L (2010) Environmental controls on CH4 emission from polygonal tundra on the microsite scale in the Lena river delta, Siberia. Glob Chang Biol 16 (11):3096–3110

Schädel C, Bader MK-F, Schuur EA, Biasi C, Bracho R, Čapek P, De Baets S, Diáková K, Ernakovich J, Estop-Aragones C (2016) Potential carbon emissions dominated by carbon dioxide from thawed permafrost soils. Nat Clim Chang 6(10):950

Schirrmeister LHM, Wetterich S, Siegert C, Kunitsky VV, Grosse G, Kuznetsova TV, Derevyagin AY (2008) The Yedoma Suite of the Northeastern Siberian Shelf Region: characteristics and Concept of Formation. Proceedings Ninth International Conference On Permafrost 2:1595–1600

Schirrmeister L, Grosse G, Wetterich S, Overduin PP, Strauss J, Schuur EAG, Hubberten H-W (2011) Fossil organic matter characteristics in permafrost deposits of the northeast Siberian Arctic. J Geophys Res 116. https://doi.org/10.1029/2011jg001647

Schirrmeister L, Froese D, Tumskoy V, Grosse G, Wetterich S (2013) Yedoma: late Pleistocene ice-rich syngenetic permafrost of Beringia. In: Encyclopedia of quaternary science, 2nd edn. Elsevier, Amsterdam, pp 542–552. https://doi.org/10.1016/b978-0-444-53643-3.00106-0

Schuur EA, Bockheim J, Canadell JG, Euskirchen E, Field CB, Goryachkin SV, Hagemann S, Kuhry P, Lafleur PM, Lee H (2008) Vulnerability of permafrost carbon to climate change: implications for the global carbon cycle. Bioscience 58(8):701–714

Schuur EA, McGuire AD, Schadel C, Grosse G, Harden JW, Hayes DJ, Hugelius G, Koven CD, Kuhry P, Lawrence DM, Natali SM, Olefeldt D, Romanovsky VE, Schaefer K, Turetsky MR, Treat CC, Vonk JE (2015) Climate change and the permafrost carbon feedback. Nature 520 (7546):171–179. https://doi.org/10.1038/nature14338

Segers R (1998) Methane production and methane consumption: a review of processes underlying wetland methane fluxes. Biogeochemistry 41(1):23–51

Shakhova N, Semiletov I (2007) Methane release and coastal environment in the East Siberian Arctic shelf. J Mar Syst 66(1-4):227–243. https://doi.org/10.1016/j.jmarsys.2006.06.006

Shkolnik I, Pavlova T, Efimov S, Zhuravlev S (2017) Future changes in peak river flows across northern Eurasia as inferred from an ensemble of regional climate projections under the IPCC RCP8.5 scenario. Clim Dyn. https://doi.org/10.1007/s00382-017-3600-6

Sidorova OV, Siegwolf RT, Saurer M, Naurzbaev MM, Vaganov EA (2008) Isotopic composition ($\delta^{13}C$, $\delta^{18}O$) in wood and cellulose of Siberian larch trees for early Medieval and recent periods. J Geophys Res Biogeosci 113:G02019. https://doi.org/10.1029/2007JG000473

Smith LC, Sheng Y, MacDonald G, Hinzman L (2005) Disappearing arctic lakes. Science 308 (5727):1429–1429

Stocker TF, Qin D, Plattner G-K, Tignor M, Allen SK, Boschung J, Nauels A, Xia Y, Bex V, Midgley PM (eds) (2013) Climate change 2013: the physical science basis. Contribution of Working Group I to the Fifth Assessment Report of the Intergovernmental Panel on Climate Change. Cambridge University Press, Cambridge, United Kingdom and New York, NY, USA, 1535 pp.

Strauss J, Schirrmeister L, Grosse G, Wetterich S, Ulrich M, Herzschuh U, Hubberten HW (2013) The deep permafrost carbon pool of the Yedoma region in Siberia and Alaska. Geophys Res Lett 40(23):6165–6170. https://doi.org/10.1002/2013GL058088

Ström L, Ekberg A, Mastepanov M, Røjle Christensen T (2003) The effect of vascular plants on carbon turnover and methane emissions from a tundra wetland. Glob Chang Biol 9 (8):1185–1192

Ström L, Mastepanov M, Christensen TR (2005) Species-specific effects of vascular plants on carbon turnover and methane emissions from wetlands. Biogeochemistry 75(1):65–82

Ström L, Falk JM, Skov K, Jackowicz-Korczynski M, Mastepanov M, Christensen TR, Lund M, Schmidt NM (2015) Controls of spatial and temporal variability in CH_4 flux in a high arctic fen over three years. Biogeochemistry 125(1):21–35

Sugimoto A, Wada E (1993) Carbon isotopic composition of bacterial methane in a soil incubation experiment: contributions of acetate and CO_2H_2. Geochim Cosmochim Acta 57(16):4015–4027

Takakai F, Desyatkin AR, Lopez CML, Fedorov AN, Desyatkin RV, Hatano R (2008) CH_4 and N_2O emissions from a forest-alas ecosystem in the permafrost taiga forest region, eastern Siberia, Russia. J Geophys Res Biogeosci 113(G2). https://doi.org/10.1029/2007jg000521

Tarnocai C, Canadell JG, Schuur EAG, Kuhry P, Mazhitova G, Zimov S (2009) Soil organic carbon pools in the northern circumpolar permafrost region. Glob Biogeochem Cycles 23(2). https://doi.org/10.1029/2008gb003327

Thonat T, Saunois M, Bousquet P, Pison I, Tan Z, Zhuang Q, Crill PM, Thornton BF, Bastviken D, Dlugokencky EJ (2017) Detectability of Arctic methane sources at six sites performing continuous atmospheric measurements. Atmos Chem Phys 17(13):8371–8394

Turetsky MR, Kotowska A, Bubier J, Dise NB, Crill P, Hornibrook ER, Minkkinen K, Moore TR, Myers-Smith IH, Nykanen H, Olefeldt D, Rinne J, Saarnio S, Shurpali N, Tuittila ES, Waddington JM, White JR, Wickland KP, Wilmking M (2014) A synthesis of methane emissions from 71 northern, temperate, and subtropical wetlands. Glob Chang Biol 20 (7):2183–2197. https://doi.org/10.1111/gcb.12580

Van der Kolk H-J, Heijmans MMPD, van Huissteden J, Pullens JWM, Berendse F (2016) Potential Arctic tundra vegetation shifts in response to changing temperature, precipitation and permafrost thaw. Biogeosciences 13(22):6229–6245. https://doi.org/10.5194/bg-13-6229-2016

Van der Molen M, Van Huissteden J, Parmentier F, Petrescu A, Dolman A, Maximov T, Kononov A, Karsanaev S, Suzdalov D (2007) The growing season greenhouse gas balance of a continental tundra site in the Indigirka lowlands, NE Siberia. Biogeosciences 4(6):985–1003

Van Hardenbroek M, Lotter AF, Bastviken D, Duc N, Heiri O (2012) Relationship between δ13C of chironomid remains and methane flux in Swedish lakes. Freshw Biol 57(1):166–177

Van Huissteden J. The permafrost carbon cycle. Springer. (in preparation)

Van Huissteden J, Dolman AJ (2012) Soil carbon in the Arctic and the permafrost carbon feedback. Curr Opin Environ Sustain 4(5):545–551. https://doi.org/10.1016/j.cosust.2012.09.008

Van Huissteden J, Maximov TC, Dolman AJ (2005) High methane flux from an arctic floodplain (Indigirka lowlands, eastern Siberia). J Geophys Res Biogeosci 110(G2). https://doi.org/10.1029/2005jg000010

Van Huissteden J, Maximov TC, Kononov AV, Dolman AJ (2008) Summer soil CH4 emission and uptake in taiga forest near Yakutsk, Eastern Siberia. Agric For Meteorol 148(12):2006–2012. https://doi.org/10.1016/j.agrformet.2008.08.008

Van Huissteden J, Maximov TC, Dolman AJ (2009) Correction to "High methane flux from an arctic floodplain (Indigirka lowlands, eastern Siberia)". J Geophys Res Biogeosci 114(G2). https://doi.org/10.1029/2009jg001040

Van Huissteden J, Berrittella C, Parmentier F, Mi Y, Maximov T, Dolman A (2011) Methane emissions from permafrost thaw lakes limited by lake drainage. Nat Clim Chang 1(2):119

Van Huissteden J, Vandenberghe J, Gibbard PL, Lewin J (2013) Periglacial fluvial sediments and forms. In: Encyclopedia of quaternary science, 2nd edn. Elsevier, Amsterdam, pp 490–499. https://doi.org/10.1016/b978-0-444-53643-3.00108-4

Vaughn LJ, Conrad ME, Bill M, Torn MS (2016) Isotopic insights into methane production, oxidation, and emissions in Arctic polygon tundra. Glob Chang Biol 22(10):3487–3502. https://doi.org/10.1111/gcb.13281

Vile MA, Wieder RK, Živković T, Scott KD, Vitt DH, Hartsock JA, Iosue CL, Quinn JC, Petix M, Fillingim HM (2014) N2-fixation by methanotrophs sustains carbon and nitrogen accumulation in pristine peatlands. Biogeochemistry 121(2):317–328

Vonk JE, Mann PJ, Davydov S, Davydova A, Spencer RGM, Schade J, Sobczak WV, Zimov N, Zimov S, Bulygina E, Eglinton TI, Holmes RM (2013) High biolability of ancient permafrost carbon upon thaw. Geophys Res Lett 40(11):2689–2693. https://doi.org/10.1002/grl.50348

Wagner D, Liebner S (2009) Global warming and carbon dynamics in permafrost soils: methane production and oxidation. In: Permafrost soils. Springer, pp 219–236

Wagner D, Kobabe S, Pfeiffer EM, Hubberten HW (2003) Microbial controls on methane fluxes from a polygonal tundra of the Lena Delta, Siberia. Permafr Periglac Process 14(2):173–185

Walter Anthony KM, Anthony P, Grosse G, Chanton J (2012) Geologic methane seeps along boundaries of Arctic permafrost thaw and melting glaciers. Nat Geosci 5(6):419–426. https://doi.org/10.1038/ngeo1480

Walter Anthony KM, Zimov SA, Grosse G, Jones MC, Anthony PM, Chapin FS 3rd, Finlay JC, Mack MC, Davydov S, Frenzel P, Frolking S (2014) A shift of thermokarst lakes from carbon sources to sinks during the Holocene epoch. Nature 511(7510):452–456. https://doi.org/10.1038/nature13560

Walter KM, Zimov SA, Chanton JP, Verbyla D, Chapin FS, 3rd (2006) Methane bubbling from Siberian thaw lakes as a positive feedback to climate warming. Nature 443 (7107):71–75. https://doi.org/10.1038/nature05040

Walter KM, Edwards ME, Grosse G, Zimov SA, Chapin FS 3rd (2007a) Thermokarst lakes as a source of atmospheric CH4 during the last deglaciation. Science 318(5850):633–636. https://doi.org/10.1126/science.1142924

Walter KM, Smith LC, Chapin FS, 3rd (2007b) Methane bubbling from northern lakes: present and future contributions to the global methane budget. Philos Trans A Math Phys Eng Sci 365 (1856):1657–1676. https://doi.org/10.1098/rsta.2007.2036

Walter K, Chanton J, Chapin F, Schuur E, Zimov S (2008) Methane production and bubble emissions from arctic lakes: isotopic implications for source pathways and ages. J Geophys Res Biogeosci 113:G00A08. https://doi.org/10.1029/2007JG000569.

Walvoord MA, Kurylyk BL (2016) Hydrologic impacts of thawing permafrost—a review. Vadose Zone J 15 (6):0. https://doi.org/10.2136/vzj2016.01.0010

Wik M, Crill PM, Bastviken D, Danielsson Å, Norbäck E (2011) Bubbles trapped in arctic lake ice: potential implications for methane emissions. J Geophys Res Biogeosci 116(G3)

Wik M, Thornton BF, Bastviken D, MacIntyre S, Varner RK, Crill PM (2014) Energy input is primary controller of methane bubbling in subarctic lakes. Geophys Res Lett 41(2):555–560

Wille C, Kutzbach L, Sachs T, Wagner D, Pfeiffer E-M (2008) Methane emission from Siberian arctic polygonal tundra: eddy covariance measurements and modeling. Glob Chang Biol 14 (6):1395–1408. https://doi.org/10.1111/j.1365-2486.2008.01586.x

Worden JR, Bloom AA, Pandey S, Jiang Z, Worden HM, Walker TW, Houweling S, Röckmann T (2017) Reduced biomass burning emissions reconcile conflicting estimates of the post-2006 atmospheric methane budget. Nat Commun 8(1):2227

Yakushev V, Chuvilin E (2000) Natural gas and gas hydrate accumulations within permafrost in Russia. Cold Reg Sci Technol 31(3):189–197

Zalman C, Meade N, Chanton J, Kostka J, Bridgham S, Keller J (2018) Methylotrophic methanogenesis in Sphagnum-dominated peatland soils. Soil Biol Biochem 118:156–160

Zimov S, Voropaev YV, Semiletov I, Davidov S, Prosiannikov S, Chapin FS, Chapin M, Trumbore S, Tyler S (1997) North Siberian lakes: a methane source fueled by Pleistocene carbon. Science 277(5327):800–802

Zimov SA, Davydov SP, Zimova GM, Davydova AI, Schuur EAG, Dutta K, Chapin FS (2006) Permafrost carbon: stock and decomposability of a globally significant carbon pool. Geophys Res Lett 33(20). https://doi.org/10.1029/2006gl027484

Zona D, Gioli B, Commane R, Lindaas J, Wofsy SC, Miller CE, Dinardo SJ, Dengel S, Sweeney C, Karion A, Chang RY, Henderson JM, Murphy PC, Goodrich JP, Moreaux V, Liljedahl A, Watts JD, Kimball JS, Lipson DA, Oechel WC (2016) Cold season emissions dominate the Arctic tundra methane budget. Proc Natl Acad Sci USA 113(1):40–45. https://doi.org/10.1073/pnas.1516017113

Chapter 6
Stable Isotopes of Water in Permafrost Ecosystem

Atsuko Sugimoto

6.1 Introduction

6.1.1 Moisture in Permafrost Ecosystem

Climate in eastern Siberia is continental and severely dry with a mean annual precipitation of only about 230 mm. Besides, summer is not cool rather very hot, and monthly mean air temperature in July is more than 20 °C, while winter is extremely cold with a January mean air temperature of −40 °C, although winter air temperature increases recently. Under such severely dry climate, taiga that consists of deciduous conifer, larch, covers the area on permafrost (Archibold 1995).

Several species of larch are distributed in northern Eurasia, but *Larix gmelinii* and *L. cajandery* (Abaimov et al. 1998), known as Dahurian larch, form almost pure larch forest in northeastern Siberia. They are distributed not only in boreal zone but also in the Arctic zone, where soil is dry enough for them to survive (Liang et al. 2014), forming forest tundra. Southern boundary of taiga interestingly well agrees with southern boundary of permafrost distribution. This indicates that permafrost plays important role for larch forest distribution.

As explained later in this chapter, permafrost hydrology enable larch trees to survive by providing water under such dry climate as eastern Siberia. On the other hand, larch forests are essential source for atmospheric water vapor, as they transpire water. Returning of water, which fell as precipitation, from soil to the atmosphere is called “precipitation recycling” (e.g., Eltahir et al. 1998; Jasechko et al. 2013). It has been reported that atmospheric water vapor, particularly in summer in continental regions, is brought through evapotranspiration. In eastern Siberia, Numaguti (1999) showed that summer precipitation is formed by water vapor which is recycled at least twice in average by means of colored tracer technic with GCM. Hydrologic cycle in

A. Sugimoto (✉)
Arctic Research Center, Hokkaido University, Sapporo, Japan
e-mail: sugimoto@star.dti2.ne.jp

T. Ohta et al. (eds.), *Water-Carbon Dynamics in Eastern Siberia*,
Ecological Studies 236, https://doi.org/10.1007/978-981-13-6317-7_6

the permafrost ecosystem is figured out with the isotopic composition of water in the system.

6.1.2 Use of Stable Isotopes of Water

Stable isotopes of water have been widely used for researches on water cycle, particularly to investigate source of water, including water vapor, because water isotopes can be used as tracer of water (e.g., Gat 2000). Most of researches on precipitation recycling have applied stable isotopes of precipitation and water vapor to trace water (Jasechko et al. 2013; Kurita et al. 2003, 2004). In addition, stable isotopes of sap water in plants have been also used to know the source of water for plants in ecological studies (e.g., Dawson and Ehleringer 1991; Querejeta et al. 2007).

Applications of stable isotopes of water are generally made with isotope ratio of oxygen ($^{18}O/^{16}O$) and hydrogen (D/H) of water, and these isotope ratios are expressed with $\delta^{18}O$ and δD for oxygen and hydrogen, respectively, defined as a permil deviation from an international standard as below.

$$\delta^{18}O \text{ or } \delta D = [R_{SA}/R_{SMOW} - 1] \times 1000\ (‰),$$

where R_{SA} and R_{SMOW} are isotope ratios of oxygen or hydrogen for sample and international standard SMOW (standard mean ocean water). Adding to these δ values, another parameter d-excess (Dansgaard 1964) is used:

$$\text{d-excess} = \delta D - 8 \cdot \delta^{18}O\ (‰).$$

The d-excess has been widely used in many studies for mainly two different ways. One is to know a source of water vapor (e.g., Tian et al. 2001), because this value results from evaporation process of water vapor on sea surface and is conservative in condensation process. Other applications have been made for investigations on evaporation process from surface (e.g., Gibson et al. 2005; Gibson and Reid 2014).

It has been well known that isotopic composition of precipitation observed in most regions in the world is generally on a line, $\delta D = 8 \cdot \delta^{18}O + 10$, in $\delta D - \delta^{18}O$ plot, so-called meteoric water line. When liquid water is formed from water vapor, heavy isotopes (HDO and $H_2{}^{18}O$) condensate faster than light isotope ($H_2{}^{16}O$), because of a slightly different saturation vapor pressure among three isotopes. Therefore, as precipitation process proceeds, the δD and $\delta^{18}O$ values of water vapor gradually decrease, because heavy isotopes are removed from water vapor and enter into liquid phase, resulting in gradual decreases in δD and $\delta^{18}O$ of precipitation (liquid phase) which is formed from.

6.2 Water Budget of Taiga Forest Ecosystem

6.2.1 Changes in Soil Moisture and Its Water Isotopic Composition

6.2.1.1 Isotopic Composition of Precipitation in Eastern Siberia

Source of water in an ecosystem is basically precipitation. Interestingly, the isotopic composition of precipitation in this region shows outstanding seasonality like a seasonal variation in air temperature, with extremely low values during winter while high values in summer. Figure 6.1a shows the $\delta^{18}O$ of precipitation obtained daily sampling in 1998 and 1999. During summer (June, July, and August), precipitation shows high $\delta^{18}O$ values (mostly −15 to −10‰), which is not different from precipitation observed in mid-latitude region, whereas those in winter are extremely low (mostly lower than −30‰). This seasonality can be explained by the difference in precipitation recycling between summer and winter, as shown in Fig. 6.1b. In winter, evapotranspiration is negligible because of low temperature and no vegetation activity, resulting in continuous removal of heavy isotopes from water vapor through snowfall, leading to a remarkable decrease in $\delta^{18}O$ of snow inland, whereas

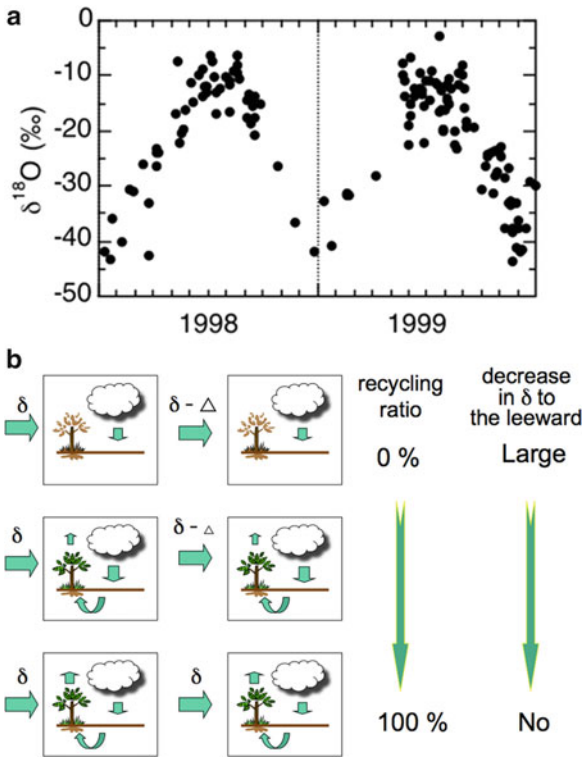

Fig. 6.1 The $\delta^{18}O$ values of precipitation sampled daily in 1998 and 1999 at Yakutsk (**a**) and schematic figure showing difference in recycling ratio between winter and summer (**b**). (The data shown in (**a**) is from Sugimoto and Maximov 2012)

in summer, high recycling ratio (large fraction of rainwater returning to the atmosphere) causes less decrease in $\delta^{18}O$ of water vapor and rainwater inland. If 100% of rainwater returned to the atmosphere through transpiration, no decrease in the $\delta^{18}O$ of water vapor would occur. As we usually observed seasonality for precipitation isotopes values, temperature difference in condensation process between summer and winter is also the secondary reason.

6.2.1.2 Soil Moisture Equivalent and the Water Isotopes

Water budget at a site can be written by a simple equation as below with a unit mm, when lateral flow is negligible:

$$P = ET + R + \Delta Qs,$$

where P, ET, and R are the amounts of precipitation, evapotranspiration, and runoff and the last term ΔQs is a change in the soil moisture equivalent. On an annual time scale, ΔQs is negligible in general. However, in a cold region especially in permafrost region, this ΔQs (annual change) is significantly large (e.g., Troy et al. 2011), and this is one of distinguishing features observed for soil moisture in this region and another cold region as well, although the long-term average of ΔQs is zero under stable climate. As seen in Fig. 6.2, soil moisture equivalent observed at Spasskaya Pad (see Sect. 3.2) shows large inter-annual variations.

In an observation of soil moisture, TDR (time-domain reflectance) sensor is frequently used. This sensor detects only liquid phase of water, and ice is not detected, since dielectric property of ice is not different from another materials in soil such as minerals. Therefore, soil moisture in a cold region, where the soil freezes in winter, can be observed only in summer, and inconveniently or conveniently TDR detects ice melt process in the soil. From a point of view of water budget, both amounts of ice and liquid water in the soil are necessary. Soil moisture equivalent shown in Fig. 6.2 includes both liquid water and ice in the soil, calculated by the same method by Sugimoto et al. (2003). They successfully calculated total soil moisture equivalent including ice, on the basis of the fact that soil moisture in the end of summer is kept as ice in the soil until the following summer. In this region, water is seldom to discharge from the site in fall and winter, because of impermeable property of frozen soil. Therefore, in most years, soil moisture equivalent in a soil layer before it freezes is almost equal to that after it thaws in the following summer, except for the surface soil layer in which snowmelt water infiltrates. Soil moisture equivalent including ice was thus estimated, assuming no change in it during freezing period if there is no difference in it between fall (before freeze) and following summer (after thaw).

Estimated soil moisture equivalent (Fig. 6.2) showed large intra- and inter-annual variations. In May in most years, surface soil layer (0–15 cm) showed clear increase in equivalent, indicating snowmelt water infiltrated into the layer. This was also supported by the observed decrease in $\delta^{18}O$ of soil water for that layer, resulted from infiltration of snowmelt water with very low $\delta^{18}O$ (Sugimoto et al. 2003). From an

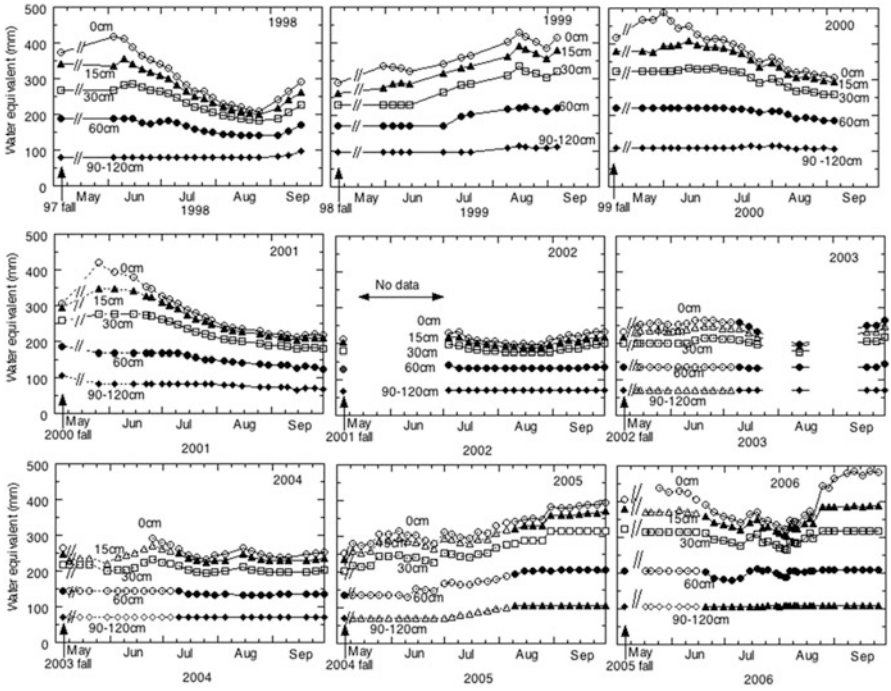

Fig. 6.2 Intra- and inter-annual variation of soil moisture water equivalent including ice from surface of mineral soil layer to 120 cm. Soil moisture water equivalent was estimated with the same method by Sugimoto et al. (2003). Data for 1998–2000 were obtained from their study

increase in the amount of snow equivalent and decrease in the $\delta^{18}O$ of soil moisture, fraction of snowmelt water which reaches to the mineral soil layer was estimated to be about 50%. The other half of snowmelt water is expected to be lost through evapotranspiration from surface organic layer and/or discharge from the site before reaching to the mineral soil layer.

After this increase in soil moisture equivalent by infiltration of snowmelt water, its variation clearly reflects summer rainfall (Fig. 6.2). In summer with large amount of rainfall (years 1999, 2005, and 2006), soil moisture increases, whereas in drought summer it decreases (years 1998, 2000, and 2001), depending on the balance between P and ET. Another important feature of soil moisture is the carry-over of soil moisture from fall to the following spring. By the end of warm season (September) in wet years, soil moisture increases, and in the following year, soil moisture variation starts from high level of soil moisture. This means that soil moisture available for vegetation depends on not only the amount of precipitation in the year but also on the amount of moisture carried over from the previous summer. As described below, the surface soil moisture equivalent differed from year to year, but in longer time scales, equivalent in the length of saw depth varied, and their isotopes also changed slightly.

As expected and also reported in many places, the $\delta^{18}O$ of soil water in shallow soil layer shows significant temporal variation depending on a fluctuation of isotopic composition of precipitation and subsequent evaporation from surface, while variability of isotopic composition of soil water decreases with depth and converges to a specific value (e.g., Hsieh et al. 1998). Figure 6.3a shows the $\delta^{18}O$ value of soil moisture including ice observed at Spasskaya Pad for the depth from 80 to 200 cm, which is the bottom part of active layer and upper part of permafrost. Obviously, the $\delta^{18}O$ of this depth of soil layer is almost constant (around −24‰). Active layer depth at this site is usually 1.2–1.4 m; therefore lower half of this figure is permafrost. The $\delta^{18}O$ values shown in this data figure (−24‰) are between summer rainfall and winter snowfall and are close to annual average value or slightly lower than the annual average, which is expected to be an average for water percolated into the deeper layer.

The $\delta^{18}O$ value of deeper soil layer converges to a specific value as seen in Fig. 6.3a, and variation of that value is not large, but may change slightly with a longer time scale. Figure 6.3c is an example of change in the $\delta^{18}O$ of soil water in deeper soil layer, showing that one of the vertical profiles of $\delta^{18}O$ observed in 2000 shifted to higher value. This is interpreted as percolation of summer rainwater fell in 1999 in sandy soil layer. The $\delta^{18}O$ of soil moisture (water and ice) in deeper layer is conservative but may slightly change depending on the water budget at the site with longer time scale. When summer precipitation exceeds evapotranspiration, it may shift to higher value, whereas it may shift to lower value when evapotranspiration exceeds precipitation.

6.2.2 Source of Water for Plants

Sap water that was absorbed from roots is transported to leaves in which transpiration occurs. During this transportation, no isotopic change occurs in general, though a transpiration enriches heavy isotopes in leaf water (Yakir and Sternberg 2000). This fact enables us to use sap water $\delta^{18}O$ to know source water for the plant. In addition in eastern Siberia, as described in Sect. 6.2.1, the $\delta^{18}O$ of precipitation shows extremely large seasonality with high $\delta^{18}O$ in summer rainfall and extremely low value in winter snowfall. This seasonality of $\delta^{18}O$ gives us advantages for applications with isotope ratios of water in ecosystem, by tagging water with different $\delta^{18}O$ values.

Sap water $\delta^{18}O$ of larch trees observed in June and August at Spasskaya Pad showed large intra- and inter-annual variations, ranging from about −23 to −12‰ (Fig. 6.4a). Observed $\delta^{18}O$ in June is low, and its variation is not so large compared to that in August, indicating that plant could use snow meltwater with low $\delta^{18}O$ every year (Sugimoto et al. 2002). On the other hand, large variation is found in August with very high $\delta^{18}O$ in wet summer and with low values in dry summer as described in Sect. 6.1, reflecting the $\delta^{18}O$ of soil moisture which was used by larch trees. In wet summer with enough amount of rainfall, surface soil is recharged with summer rainwater of which $\delta^{18}O$ is high, whereas in dry summer when the amount

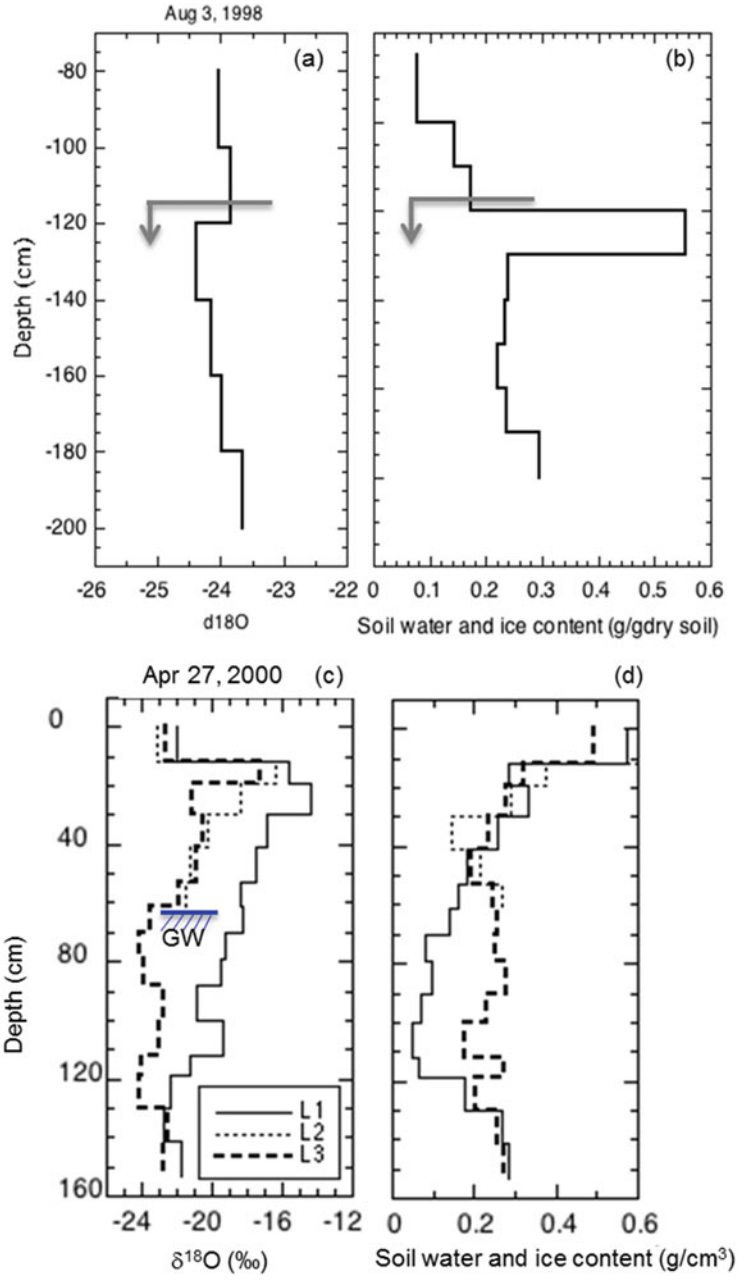

Fig. 6.3 The $\delta^{18}O$ value (**a**) and water content (**b**) of soil moisture (water and ice) in the layer from 80 to 200 cm observed on August 3 in 1998 and those from surface to 150 cm observed on April 27 in 2000 (**c** and **d**). Soil layer shown in (**a**) corresponds to lower half of active layer (80–140 cm) and upper part of permafrost (140–200 cm). GW in (**c**) is a water table of talik which was formed after heavy rainfall in 1999. (Data were modified from Sugimoto et al. 2003)

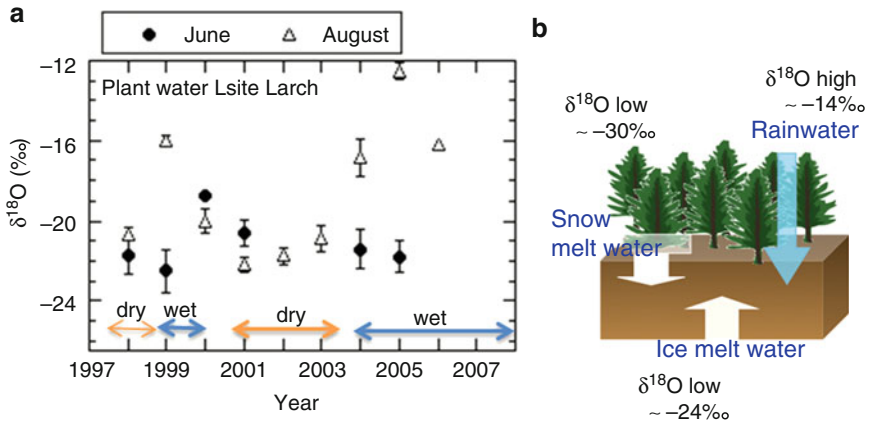

Fig. 6.4 Sap water $\delta^{18}O$ of larch trees (**a**) observed at Spasskaya Pad in June and August for years from 1998 to 2006 with description on the soil moisture condition (wet or dry) and schematic figure on source of water for larch trees (**b**), showing three sources of water for plants, snow meltwater, summer rainfall, and ice meltwater in the soil

of summer rainfall is not enough, soil water produced from ice meltwater in the soil of which $\delta^{18}O$ is low (around −24‰) is used by larch trees, resulting in the decrease in sap water $\delta^{18}O$.

This fact indicates that storage of water which was carried over from the previous fall is an important source of water for plants in drought summer, and in other words, soil moisture stored as ice during summer is an important source of water for plants during drought.

In summary, there are three sources of water for plants, snowmelt water, summer rainwater, and ice meltwater in the soil (Fig. 6.4b).

6.2.3 Role of Water and Ice in the Bottom Layer of Active Layer and Uppermost Layer of Permafrost

The $\delta^{18}O$ value of soil moisture (water and ice) shows large intra- and inter-annual variations in surface soil layer, while that in the deeper soil layer shows less variation, as already explained in Sect. 6.1. The same is true for the amount of soil moisture. Total amount of soil water and ice in the surface soil layer varies significantly seasonally and also inter-annually, while less variations are seen in deeper soil layer (60–120 cm) in Fig. 6.1. However, soil moisture in this layer also varies with longer time scale, depending on the water budget (Sugimoto et al. 2003), as described already.

Figure 6.5 shows the soil moisture equivalent (water and ice) and its $\delta^{18}O$ for every 30 cm depth of soil layer from surface to 150 cm depths observed in warm season, with the amount and the $\delta^{18}O$ of snowfall in previous winter and that in

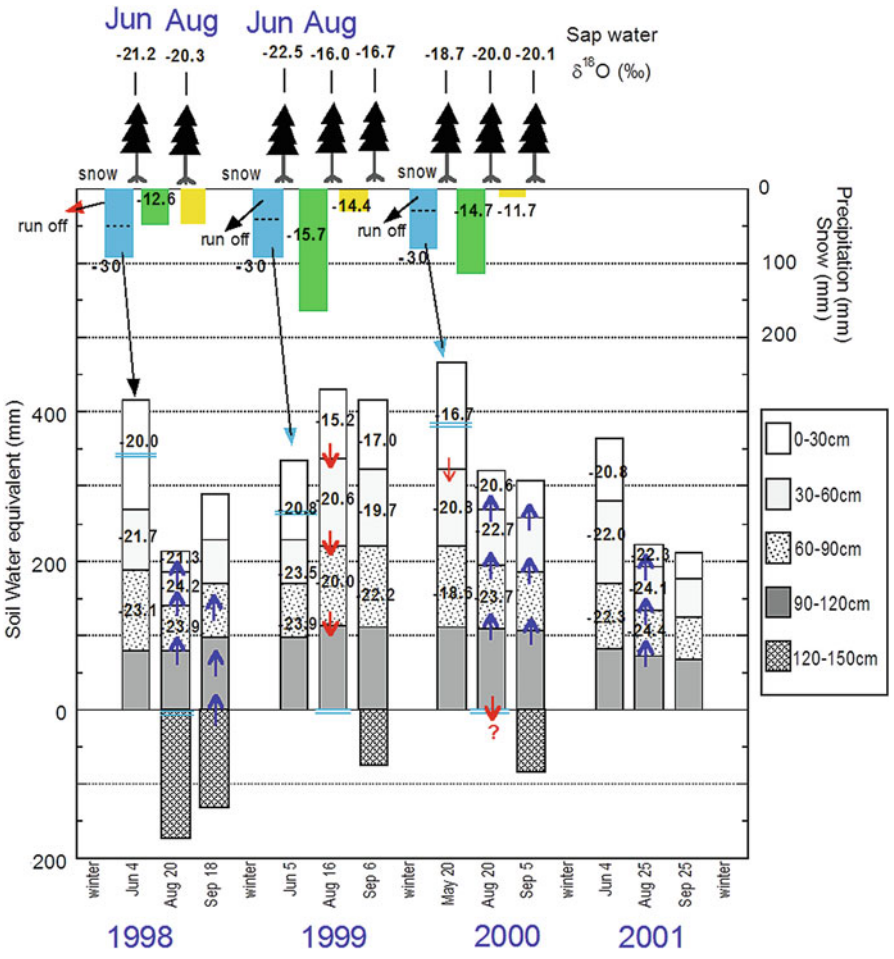

Fig. 6.5 Soil moisture water equivalent (water and ice) for every 30 cm of soil layer from surface to 150 cm with the $\delta^{18}O$ data. The amount of snowfall in previous winter and the amounts of rainfall in summer (June, July, and August) and September with their $\delta^{18}O$ are also shown. Schematic figure on the top of the figure shows the $\delta^{18}O$ of sap water of larch trees, that is, the $\delta^{18}O$ of water vapor transpired to the atmosphere. (Data for 1998–2000 were obtained from Sugimoto et al. 2003)

summer and fall. Change in the soil moisture equivalent and its $\delta^{18}O$ clearly depend on the summer precipitation. In wet summer with large amount of rainfall having high $\delta^{18}O$ in 1999, increase in the amount of soil moisture equivalent was observed in August with an increase in $\delta^{18}O$, indicating downward water transportation. On the other hand, in dry summer (1998, 2000, and 2001), decreases in soil moisture equivalent and $\delta^{18}O$ were seen, suggesting upward transportation of soil moisture.

As seen in Fig. 6.3b, soil moisture (water and ice) content in the bottom of active layer is high, and ice lenses are frequently observed. Thaw of this soil layer produces

liquid water, and it can be a source of plant during drought in the following year but not in the year, because soil thaw of this deep layer occurs in fall (September and the beginning of October), in other words after plant growing season was over. When liquid water is produced by soil thaw, and if upper soil layer is dry, it may be transported upward and carried over until next summer, which makes possibility to be used by plants in the following year.

The uppermost layer of permafrost, which has also high moisture (ice and water) content, plays the same role as that in the bottom of active layer as described above, because this layer and the bottom of active layer occasionally thaw (became active layer) and occasionally remain frozen for more than 2 years (permafrost). Therefore, from a point of view of water budget, these layers are considered as water storage with longer time scale.

These layers are conceptually the same as "transition zone" defined by Shur et al. (2005) which act as buffer between active layer and permafrost and protect permafrost by providing latent heat required for thaw. These layers also act as a moisture storage with longer time scale than that of upper part of active layer.

6.2.4 Discharge of Water from Land to River

Because of a dry climate, soil moisture decreases during summer season in many years at Spasskaya Pad (Fig. 6.2), indicating that evapotranspiration exceeds preparation in the site scale. In such case no discharge from land to river is expected. In addition, discharge through groundwater seldom occurs in this region because of impermeable property of permafrost. Discharge from land to river is produced through shallow soil layer, if it occurred, and it may happen only in very wet years when soil moisture is kept unfrozen in the soil as seen in Fig. 6.3c, d. Discharge from land to alas in wet year (1999–2000) was also pointed out from a calculation of isotope mass balance model on alas water (Ichiyanagi et al. 2003).

While the water budget on site scale indicates that precipitation exceeds evapotranspiration during summer, basin scale water budget shows discharge generation during summer (Serreze et al. 2002; Oshima et al. 2015), although there are still large uncertainties in baseline data set for estimation of water budget (e.g., Troy et al. 2011; Bring et al. 2016). Basin scale water budget reflects budget in each part of the river basin. Majority of discharge of the Lena river is generated in southern mountain taiga region (Ma et al. 2000).

The isotopic composition of the Lena river water exhibits a clear seasonal variation with a pulse of low $\delta^{18}O$ generated by snowmelt, followed by increases during summer and then decreases gradually in fall and winter, and shows relatively constant value around −20‰ (Fig. 6.6a). This seasonality of $\delta^{18}O$ allows us to figure out an outline of hydrological system of the Lena river basin. Obviously

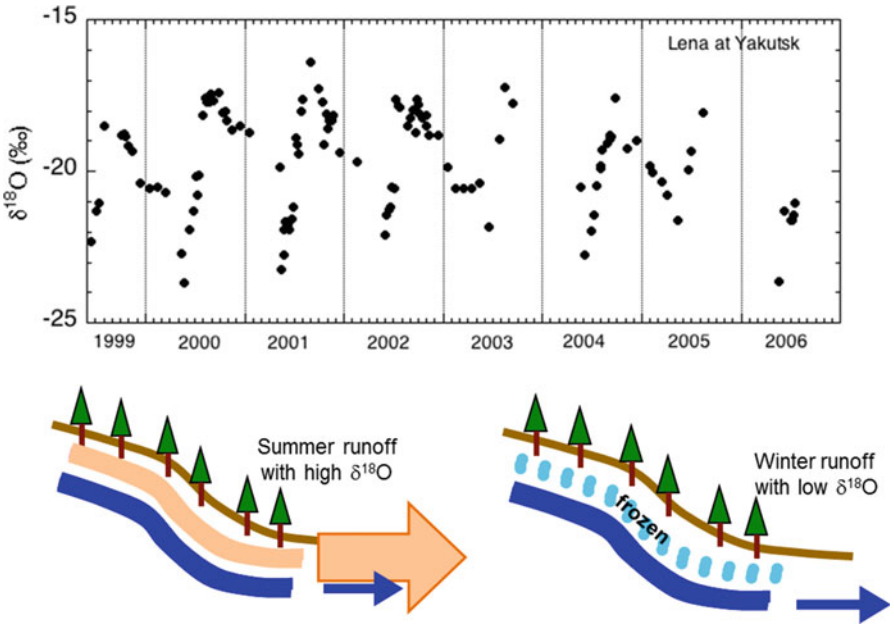

Fig. 6.6 Temporal variation of $\delta^{18}O$ of Lena river observed at Yakutsk (**a**) and schematic figures which explain runoff (**b**) in summer (left) and in winter (right). (Reproduced from Sugimoto and Maximov 2012)

summer runoff with high $\delta^{18}O$ water is generated in surface soil layer, having a large contribution of summer rainfall, whereas winter runoff with relatively low $\delta^{18}O$ seems to form unfrozen soil moisture in deeper soil layer below frozen surface soil, in southern mountain taiga region (Fig. 6.6b).

Welp et al. (2005) observed a similar seasonal variation in the isotopic composition of the Kolyma river water. They estimated fractions of snow origin and rain origin water in river water with the $\delta^{18}O$ values of those end members and revealed that substantial portion of snowmelt water remains in the basin and returns to the atmosphere through transpiration and also run off during summer. Their calculated results show that increase in the $\delta^{18}O$ of river water during summer after the pulse of snowmelt implies the decrease in fraction of snow origin water and increase in that of rain origin water.

Increase in Arctic river discharge especially in winter base flow has been reported, particularly in northeastern Eurasian rivers for which permafrost is observed in the basins (Peterson et al. 2002; McClelland et al. 2006). The isotopic composition of river water reflects of origin of runoff water as shown by Wepl et al. (2005). River isotope data may help us to figure out hydrological changes which may proceed invisibly.

6.3 Taiga as a Source of Atmospheric Water Vapor

As expected from the studies on precipitation recycling in eastern Siberia (Numaguti 1999; Kurita et al. 2003, 2004), water vapor transpired by plants contributes significantly to the atmosphere. Precipitation recycling is the good example to use water isotopes and is important terrestrial water fluxes not only for eastern Siberia but also the inland regions on the globes (Gat 2000; Jasechko et al. 2013; Wang et al. 2016; Winnick et al. 2014). Basically, there are two different usages of isotopes for the precipitation recycling. Using the d-excess and delta values of precipitation and/or atmospheric water vapor, transpiration and evaporation were separated (Jasechko et al. 2013; Wang et al. 2016), because transpiration does not change the isotope ratio for larger spatial and longer time scales, while evaporation makes water vapor with lower isotope ratios (Gat 2000). On the other hand, the isotopes of precipitation decrease inland, which is called continental effect. These continental effects showed different ways of decreasing, by adding the transpiration (Winnick et al. 2014).

Transpiration of vegetation is also important drivers of water cycle in such dry-climate region as eastern Siberia. Transpiration (precipitation recycling) has been also observed at Spasskaya Pad. Direct field observations of the isotopic composition of water vapor conducted in 2006, 2007, and 2008 at Spasskaya Pad revealed the importance of plant transpiration as a source of atmospheric water vapor (Ueta et al. 2013, 2014). Typical diurnal variation in the $\delta^{18}O$ of atmospheric water vapor on clear day observed at Spasskaya Pad was increased in the $\delta^{18}O$ in the morning with increasing mixing ratio and decreased in the afternoon (Fig. 6.7a, b). As shown in Fig. 6.7c, d, soil water with the $\delta^{18}O$ ranging from −18.8 to −11.2‰ was expected to be transpired by plants, and Ueta et al. (2013) report that the $\delta^{18}O$ of sap water of larch trees ranged from −17.9 to −13.3‰. The values for plants and soil $\delta^{18}O$ are considerably higher than those of the atmospheric water vapor that ranged from −29.7 to −18.4‰. Therefore, observed increase in the $\delta^{18}O$ values of water vapor with the increase of mixing ratio in the morning is explained by the addition of transpired water vapor with high $\delta^{18}O$ value. On the other hand, in the afternoon, decrease in $\delta^{18}O$ with decreasing mixing ratio is caused by entrainment of free atmosphere in which water vapor is expected to have a low $\delta^{18}O$.

Clear correlation between $\delta^{18}O$ of atmospheric water vapor and mixing ratio observed at midday has been found in midsummer (July) in 2006 and 2008 not only in diurnal time scale but also monthly time scale at Spasskaya Pad (Ueta et al. 2014), as an example for 2008 shown in Fig. 6.8. Clear correlation has been also observed between the $\delta^{18}O$ and d-excess. Simultaneous increases in the $\delta^{18}O$ and mixing ratio are observed when air temperature increases. This is also interpreted as a mixing of transpired vapor with high $\delta^{18}O$ and background water vapor with low $\delta^{18}O$. When air temperature increases, resulting in active transpiration, as a result, increase in contribution of transpired water vapor causes a high $\delta^{18}O$. Correlations of the $\delta^{18}O$ with mixing ratio and d-excess indicate a mixing of transpired water vapor with a background atmospheric water vapor, because the latter is expected to have a low $\delta^{18}O$ with a relatively high d-excess (Bariac et al. 1990). Assuming the $\delta^{18}O$ values

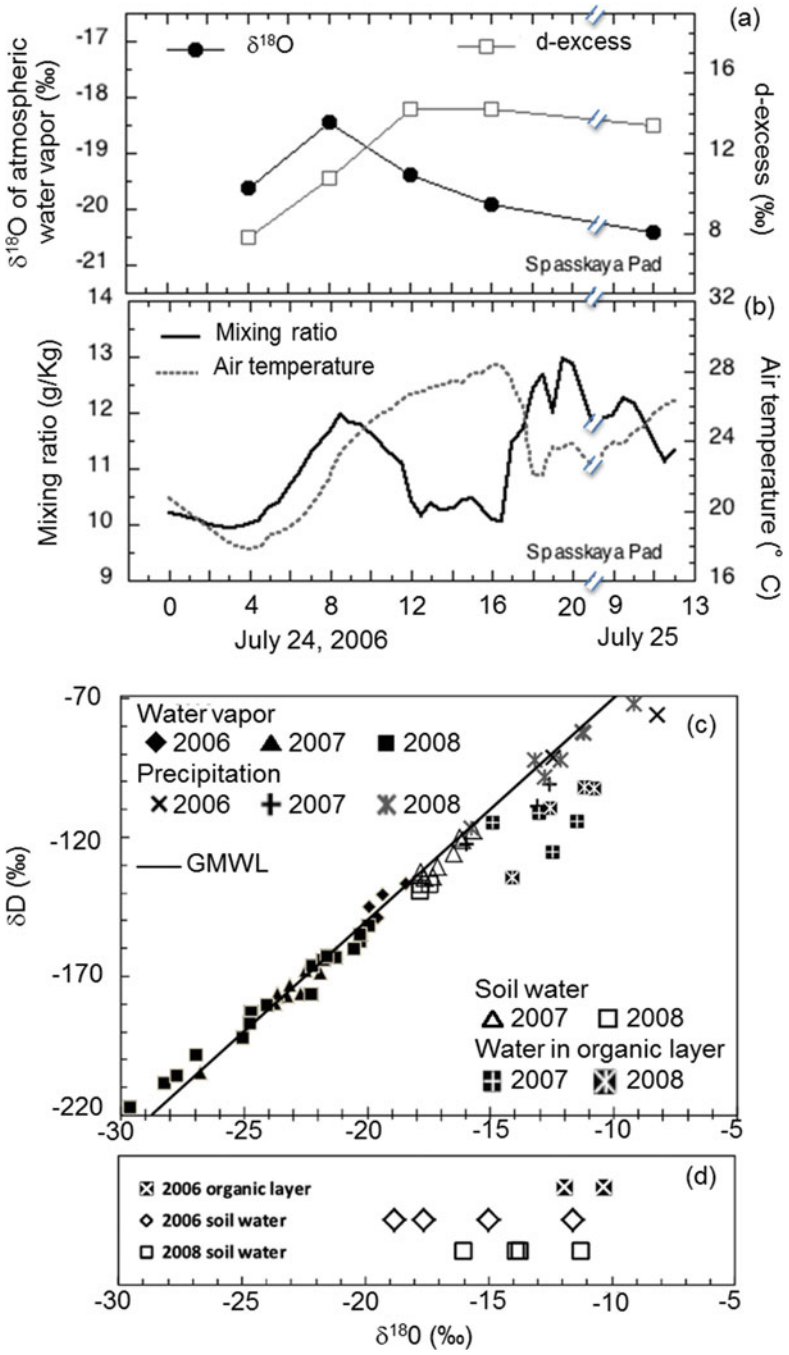

Fig. 6.7 Typical diurnal variations of $\delta^{18}O$ and d-excess (**a**) of atmospheric water vapor and air temperature and mixing ratio at 24 m (**b**) observed at Spasskaya Pad on fine day and δD- $\delta^{18}O$ plots for various water samples (**c**) and $\delta^{18}O$ of surface soil water (**d**). (Reproduced from Ueta et al. 2013)

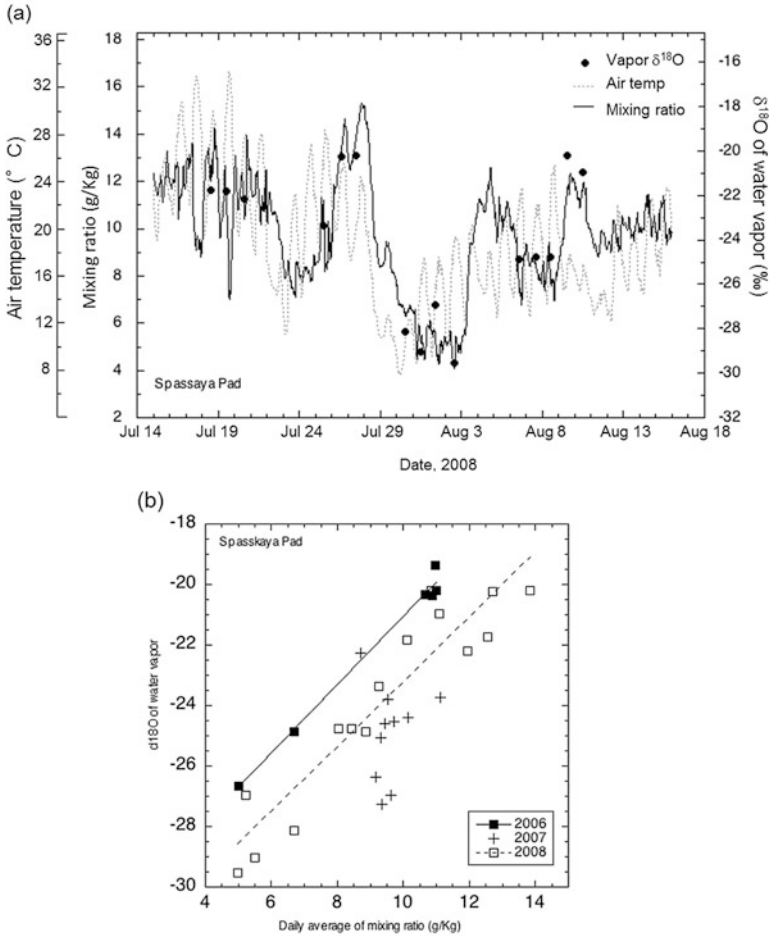

Fig. 6.8 The $\delta^{18}O$ values of atmospheric water vapor, mixing ratio, and temperature observed at canopy level in 2008 at Spasskaya Pad (**a**) and relationship between $\delta^{18}O$ and mixing ratio observed in 2006 (closed squares), 2007 (+), and 2008 (open squares). (Reproduced from Ueta et al. 2014)

of transpired vapor and background atmospheric water vapor, fraction of water vapor derived from transpiration is estimated to be up to 80%. Correlations of the $\delta^{18}O$ with mixing ratio usually occur during the summer, responding to the advection from any direction (Ueta et al. 2014). This suggests that water vapor from transpiration may be an important vapor source for precipitation.

Interestingly, correlation between $\delta^{18}O$ of atmospheric water vapor and mixing ratio was not observed in 2007 when extreme wet event occurred in this region, and waterlogging happened at depressions in the forest (Ueta et al. 2014). Sap flow rate observed in that year was very low and showed no response to precipitation. Many trees growing at depressions died in this extreme wet event, although the trees living

at ridges and well-drained sites grew well with plenty of water available in the soil. In this extreme wet condition, evaporation from the surface, not transpiration, may contribute to the atmospheric water vapor.

6.4 Concluding Remarks

Permafrost plays various important roles in water cycle in eastern Siberia. Water tagged with low $\delta^{18}O$ by snowmelt is useful tracer. Uppermost layer of permafrost is also tagged with this water, and soil moisture in the bottom of active layer has also the same $\delta^{18}O$. Continuity of this $\delta^{18}O$ of soil moisture (ice and water) indicates that "transition zone" consisting of bottom of active layer and uppermost layer of permafrost should also be considered from an isotopic point of view. This zone plays a role of water storage with a longer time scale (more than 5 years), because moisture in this layer seems to provide water to the middle active layer (about 60 cm depth at Spasskaya Pad), and to that depth larch tree roots may reach. During a long drought period (2001–2003), sap water $\delta^{18}O$ of larch trees became low, and soil moisture $\delta^{18}O$ in the bottom of active layer decreased, indicating that moisture in the transition zone provides water to larch trees.

Currently, transition zone plays a role of water storage with longer time scale and provides water to the depth reachable for larch roots. However, if active layer and transition zone deepen in the future, moisture in this zone may not be available for larch trees. On the other hand, extreme wet event also threatens the forest.

As will be described in Chap. 7, soil moisture reconstructed from carbon isotope ratio of larch tree ring shows that extreme wet event observed in 2007 was the wettest event in past 100 years in this forest (Tei et al. 2013). This extreme wet event made great impacts on water and carbon cycles in this forest, and frequency of such extreme wet event as observed in 2007 may increase under warming condition in the future (Hartmann et al. 2013; Collins et al. 2013).

Stable isotopes of water figured out the water cycle of permafrost ecosystem. Vegetation (larch trees) is one of the components of permafrost hydrologic system. It obviously plays an important role in precipitation recycling, and at the same time, it is also supported by the permafrost hydrologic system.

References

Abaimov AP, Lesinski JA, Martinsson O, Milyu-tin L (1998) Variability and ecology of Siberian larch species, p 123

Archibold OW (1995) Coniferous forests. In: Ecology of world vegetation. Chapman & Hall, London, pp 238–279

Bariac T, Jusserand C, Mariotti A (1990) Temporospatial development of the isotopic composition of water in the soilplant-atmosphere continuum. Geochim Cosmochim Acta 54(2):413–424. https://doi.org/10.1016/0016-7037(90)90330-n

Bring A, Fedorova I, Dibike Y, Hinzman L, Mard J, Mernild SH, Prowse T, Semenova O, Stuefer SL, Woo MK (2016) Arctic terrestrial hydrology: a synthesis of processes, regional effects, and research challenges. J Geophy Res Biogeosci 121(3):621–649. https://doi.org/10.1002/2015jg003131

Collins M et al (2013) Long-term climate change: projections, commitments and irreversibility. In: Stocker TF, Qin D, Plattner G-K, Tignor M, Allen SK, Boschung J, Nauels A, Xia Y, Bex V, Midgley PM (eds) Climate change 2013: the physical science basis. Contribution of working group I to the fifth assessment report of the intergovernmental panel on climate change. Cambridge University Press, Cambridge/New York, pp 1029–1136

Dansgaard W (1964) Stable isotopes in precipitation. Tellus 16:436–468

Dawson TE, Ehleringer JR (1991) Streamside trees that do not use stream water. Nature 350 (6316):335–337. https://doi.org/10.1038/350335a0

Eltahir EAB (1998) A soil moisture rainfall feedback mechanism 1. Theory and observations. Water Resources Research 34(4):765–776. https://doi.org/10.1029/97wr03499

Gat JR (2000) Atmospheric water balance - the isotopic perspective. Hydrol Process 14 (8):1357–1369. https://doi.org/10.1002/1099-1085(20000615)14:8<1357::aid-hyp986>3.0.co;2-7

Gibson JJ, Reid R (2014) Water balance along a chain of tundra lakes: A 20-year isotopic perspective. J Hydrol 519:2148–2164. https://doi.org/10.1016/j.jhydrol.2014.10.011

Gibson JJ, Edwards TWD, Birks SJ, Amour NAS, Buhay WM, McEachern P, Wolfe BB, Peters DL (2005) Progress in isotope tracer hydrology in Canada. Hydrol Process 19(1):303–327. https://doi.org/10.1002/hyp.5766

Hartmann DL et al (2013) Observations: atmosphere and surface. In: Stocker TF, Qin D, Plattner G-K, Tignor M, Allen SK, Boschung J, Nauels A, Xia Y, Bex V, Midgley PM (eds) Climate change 2013: the physical science basis. Contribution of working group I to the fifth assessment report of the intergovernmental panel on climate change. Cambridge University Press, Cambridge/New York, pp 159–254

Hsieh JCC, Chadwick OA, Kelly EF, Savin SM (1998) Oxygen isotopic composition of soil water: quantifying evaporation and transpiration. Geoderma 82(1–3):269–293. https://doi.org/10.1016/s0016-7061(97)00105-5

Ichiyanagi K, Sugimoto A, Numaguti A, Kurita N, Ishii Y, Ohata T (2003) Seasonal variation in stable isotopic composition of alas lake water near Yakutsk, Eastern Siberia. Geochem J 37 (4):519–530

Jasechko S, Sharp ZD, Gibson JJ, Birks SJ, Yi Y, Fawcett PJ (2013) Terrestrial water fluxes dominated by transpiration. *Nature 496*(7445):347. https://doi.org/10.1038/nature11983

Kurita N, Numaguti A, Sugimoto A, Ichiyanagi K, Yoshida N (2003) Relationship between the variation of isotopic ratios and the source of summer precipitation in eastern Siberia. J Geophys Res-Atmos 108(D11). https://doi.org/10.1029/2001jd001359

Kurita N, Yoshida N, Inoue G, Chayanova EA (2004) Modern isotope climatology of Russia: a first assessment. J Geophys Res-Atmos 109(D3). https://doi.org/10.1029/2003jd003404

Liang MC et al (2014) Importance of soil moisture and N availability to larch growth and distribution in the Arctic taiga-tundra boundary ecosystem, northeastern Siberia. Pol Sci 8 (4):327–341. https://doi.org/10.1016/j.polar.2014.07.008

Ma XY, Fukushima Y, Hiyama T, Hashimoto T, Ohata T (2000) A macro-scale hydrological analysis of the Lena River basin. Hydrol Process 14(3):639–651. https://doi.org/10.1002/(sici)1099-1085(20000228)14:3<639::aid-hyp959>3.0.co;2-0

McClelland JW, Dery SJ, Peterson BJ, Holmes RM, Wood EF (2006) A pan-arctic evaluation of changes in river discharge during the latter half of the 20th century. Geophys Res Lett 33(6). https://doi.org/10.1029/2006gl025753

Numaguti A (1999) Origin and recycling processes of precipitating water over the Eurasian continent: experiments using an atmospheric general circulation model. J Geophys Res-Atmos 104(D2):1957–1972. https://doi.org/10.1029/1998jd200026

Oshima K, Tachibana Y, Hiyama T (2015) Climate and year-to-year variability of atmospheric and terrestrial water cycles in the three great Siberian rivers. J Geophys Res-Atmos 120 (8):3043–3062. https://doi.org/10.1002/2014jd022489

Peterson BJ, Holmes RM, McClelland JW, Vorosmarty CJ, Lammers RB, Shiklomanov AI, Shiklomanov IA, Rahmstorf S (2002) Increasing river discharge to the Arctic Ocean. Science 298(5601):2171–2173. https://doi.org/10.1126/science.1077445

Querejeta JI, Estrada-Medina H, Allen MF, Jimenez-Osornio JJ (2007) Water source partitioning among trees growing on shallow karst soils in a seasonally dry tropical climate. Oecologia 152 (1):26–36. https://doi.org/10.1007/s00442-006-0629-3

Serreze MC, Bromwich DH, Clark MP, Etringer AJ, Zhang TJ, Lammers R (2002) Large-scale hydro-climatology of the terrestrial Arctic drainage system. J Geophys Res-Atmos 108(D2). https://doi.org/10.1029/2001jd000919

Shur Y, Hinkel KM, Nelson FE (2005) The transient layer: implications for geocryology and climate-change science. Permafr Periglac Process 16(1):5–17. https://doi.org/10.1002/ppp.518

Sugimoto, A. and T. C. Maximov (2012), Study on hydrological processes in Lena river basin using stable isotope ratios of river, in *Monitoring Isotopes in Rivers: Creation of the Global Network of Isotopes in Rivers (GNIR)*, IAEA-TECDOC-1673, IAEA, Vienna (2012) 41–49

Sugimoto A, Yanagisawa N, Naito D, Fujita N, Maximov TC (2002) Importance of permafrost as a source of water for plants in east Siberian taiga. Ecol Res 17(4):493–503. https://doi.org/10.1046/j.1440-1703.2002.00506.x

Sugimoto A, Naito D, Yanagisawa N, Ichiyanagi K, Kurita N, Kubota J, Kotake T, Ohata T, Maximov TC, Fedorov AN (2003) Characteristics of soil moisture in permafrost observed in east Siberian taiga with stable isotopes of water. Hydrol Process 17(6):1073–1092. https://doi.org/10.1002/hyp.1180

Tei S, Sugimoto A, Yonenobu H, Yamazaki T, Maximov TC (2013) Reconstruction of soil moisture for the past 100 years in eastern Siberia by using delta C-13 of larch tree rings. J Geophys Res Biogeosci 118(3):1256–1265. https://doi.org/10.1002/jgrg.20110

Tian L, Masson-Delmotte V, Stievenard M, Yao T, Jouzel J (2001) Tibetan Plateau summer monsoon northward extent revealed by measurements of water stable isotopes. J Geophys Res-Atmos 106(D22):28081–28088. https://doi.org/10.1029/2001jd900186

Troy TJ, Shedield J, Wood EF (2011) Estimation of the terrestrial water budget over northern Eurasia through the use of multiple data sources. J Clim 24:3272–3293. https://doi.org/10.1175/2011JCLI3936.1

Ueta A, Sugimoto A, Iijima Y, Yabuki H, Maximov TC, Velivetskaya TA, Ignatiev AV (2013) Factors controlling diurnal variation in the isotopic composition of atmospheric water vapour observed in the taiga, eastern Siberia. Hydrol Process 27(16):2295–2305. https://doi.org/10.1002/hyp.9361

Ueta A, Sugimoto A, Iijima Y, Yabuki H, Maximov TC (2014) Contribution of transpiration to the atmospheric moisture in eastern Siberia estimated with isotopic composition of water vapour. Ecohydrology 7(2):197–208. https://doi.org/10.1002/eco.1403

Wang SJ, Zhang MJ, Che YJ, Chen FL, Qiang F (2016) Contribution of recycled moisture to precipitation in oases of arid central Asia: a stable isotope approach. Water Resour Res 52 (4):3246–3257. https://doi.org/10.1002/2015wr018135

Welp LR, Randerson JT, Finlay JC, Davydov SP, Zimova GM, Davydova AI, Zimov S (2005) A high-resolution time series of oxygen isotopes from the Kolyma River: Implications for the seasonal dynamics of discharge and basinscale water use. Geophys Res Lett 32(14). https://doi.org/10.1029/2005gl022857

Winnick MJ, Chamberlain CP, Caves JK, Welker JM (2014) Quantifying the isotopic 'continental effect'. Earth Planet Sci Lett 406:123–133. https://doi.org/10.1016/j.epsl.2014.09.005

Yakir D, Sternberg LDL (2000) The use of stable isotopes to study ecosystem gas exchange. Oecologia 123:297–311. https://doi.org/10.1007/s004420051016

Chapter 7
Water-Carbon Cycle in Dendrochronology

Shunsuke Tei and Atsuko Sugimto

7.1 Introduction

Dendrochronology is the science of dating annual growth layers (rings) in woody plants to analyze temporal and spatial patterns of processes in the physical and cultural sciences. Scientists have long used dated tree rings to study issues of past and present climate and the local scale dynamics of forest stands and woodlands. The dated tree-ring records can provide valuable information to advance our understanding of terrestrial water and carbon cycling, because this is a powerful approach to extend the short-term record of the cycling in the decades preceding the monitoring data.

Tree-ring width and density proxies are traditionally used in both dendroclimatological and dendroecological studies. At present, however, the analysis of stable isotope ratios in tree rings is in development and is attracting attention because of its potential to provide additional plant physiological information regarding a tree's response to the changing environment (e.g., McCarroll and Loader 2004; Loader et al. 2007). Trees assimilate carbon from atmospheric carbon dioxide, and hydrogen and oxygen from soil water, as these elements are necessary for plants and trees to grow. The stable isotope ratios of these three elements are climatically/environmentally controlled by the tree's water and gas exchange budgets and therefore carry signals that can be interpreted in terms of past climate/local environments. These isotopes have the added advantage that they are reasonably well understood and relatively simple in comparison to the myriad of factors controlling annual growth increments. Because of this simplicity, fractionation of these isotopes is well modeled (e.g., Farquhar et al. 1982; Roden et al. 2000), and these models help to interpret the climate/local environment change signals.

S. Tei (✉) · A. Sugimto
Hokkaido University, Sapporo, Japan
e-mail: stei@arc.hokudai.ac.jp

T. Ohta et al. (eds.), *Water-Carbon Dynamics in Eastern Siberia*,
Ecological Studies 236, https://doi.org/10.1007/978-981-13-6317-7_7

Tree-ring parameters are widely regarded as useful long-term indicators of past and present climate and the local-scale dynamics of forest stands and woodlands (e.g., Tei et al. 2013a, b, 2017). However, it is worth noting that not only climate factors but also numerous unique or local factors at the scales of trees and forest stands could affect tree growth and physiologies and thereby present non-synchronous and/or non-climatic signals in time series of tree-ring proxies (e.g., Cook and Kairiukstis 1990; McCarroll and Loader 2004; Loader et al. 2007). For example, forest fires may destroy competition in a stand of trees, remove the shade, release minerals, and make more soil area available to the roots. Thus, after a forest fire, rings of some trees become wider, and the ring-width variations tend to be unrelated to climate. These phenomena result in very little year-to-year width variability common to all trees of a stand. Therefore, we should carefully select sites and trees to maximize climatic sensitivity and combine ring series from many locations. In addition, broadscale cross dating, i.e., synchrony, of patterns in tree-ring parameters across regions is important to obtain their time series related to climatic variations (e.g., Fritts 1976).

Trees growing in northern high-latitude regions are sensitive to global climate and regional environmental changes. There have been several reports of tree growth response to past climate changes using tree-ring parameters, i.e., ring width, density, and stable carbon and oxygen isotopes, in these regions (e.g., Briffa et al. 2001; Walker et al. 2015; Girardin et al. 2016). Using dendrochronological techniques allows researchers to obtain retrospective patterns of climate and forest dynamic changes. For example, summer temperature was successfully reconstructed in a subarctic forest in central Siberia by using tree-ring width and/or density (e.g., Yasue et al. 2000; Briffa et al. 2001; Vaganov et al. 2009) because of the trees' sensitivity to summer temperature. Similarly, hydroclimatic records, such as the Palmer Drought Severity Index (PDSI), were successfully reconstructed in southern boreal forests, in northern Mongolia (e.g., Davi et al. 2010) and eastern Siberia (e.g., Tei et al. 2013a, 2015). From a dendroecological point of view, Sidorova et al. (2009) observed a drastic change in the relationship between carbon and oxygen isotope ratios in tree rings from a negative to a positive correlation with a clear change in climate trends after the 1960s in a northern area of central Siberia, and they concluded that larch (*Larix gmelinii*) trees growing in the permafrost suffered from a water deficit over the last half century. Such investigations in the past preceding the use of monitoring data are extremely important in advancing our understanding of forest ecosystem response to climate change.

Eastern Siberia is located in a continental dry climate region characterized by a small amount of annual precipitation (200–300 mm) and continuous permafrost leading to the existence of characteristic water and carbon cycling. In this chapter, I will analyze the spatial and temporal variabilities in tree-ring parameters, i.e., ring width and stable carbon isotope, in the eastern Siberian forest in relation to climate change and consider the application of dendrochronological techniques to the investigation of characteristic water and carbon cycling in boreal forests and tundra ecosystems over the region.

7.2 Stable Carbon Isotope in Tree Rings

7.2.1 Analysis and Theory

Carbon has two stable isotopes, ^{12}C and ^{13}C. In nature, the ^{12}C isotope comprises 98.89% of all carbon, with ^{13}C comprising the remaining 1.11%. Both isotopes have six protons, with six and seven neutrons for ^{12}C and ^{13}C, respectively. These isotopes have almost identical chemical properties but often have different physical and biological processes, thereby imparting an environmental signal. By convention, the isotope ratio of ^{13}C to ^{12}C is expressed with the delta notation with reference to a standard material for which the isotopic ratio is known as follows:

$$\delta^{13}C_{sample} = \left(R_{sample}/R_{standard} - 1\right) \times 1000 \ (‰) \tag{7.1}$$

where R_{sample} and $R_{standard}$ are isotope ratios ($^{13}C/^{12}C$) of the sample and the Vienna Pee Dee Belemnite (VPDB) standard, respectively.

Analysis of stable carbon isotopes in extracted wood cellulose is conventionally recommended (e.g., Saurer et al. 1997; Anderson et al. 1998). However, there is a growing body of evidence that climatic information can be obtained satisfactorily using bulk wood (e.g. Loader et al. 2003; Cullen and Grierson 2006; Tei et al. 2013a). These studies show a highly linear relationship between the $\delta^{13}C$ values between of bulk wood and wood cellulose, which led us to use bulk wood for the production of the tree-ring $\delta^{13}C$ series. The use of bulk wood has merit both in avoiding possible secondary contamination during cellulose extraction and in rapid production of raw data. Recently, both methods have been widely used for tree-ring carbon isotope studies; therefore, researchers should pay attention to how data are analyzed, if there is an interest in the absolute values of tree-ring carbon isotope ratios.

Carbon isotope composition in C3 plants is generally expressed by the following equation (Farquhar et al. 1982):

$$\delta^{13}C_p = \delta^{13}C_a - a - (b - a)C_i/C_a, \tag{7.2}$$

where $\delta^{13}C_p$ and $\delta^{13}C_a$ are the carbon isotope compositions of photosynthetic products and atmospheric CO_2, respectively, and a and b are discrimination coefficients during diffusion (4.4‰) (Craig 1954) and CO_2 fixation by ribulose-1,5-bisphosphate carboxylase/oxygenase (RuBisCO) (29‰) (Farquhar and Richards 1984), including the effect of CO_2 dissolution in cell sap, respectively. The values of C_i and C_a are leaf intercellular and ambient atmospheric CO_2 concentrations, respectively. Under a steady state, photosynthetic rate (A_p) depends on the conductance at the boundary layer and stomatal pores (g_p) and the difference in the CO_2 concentrations ($C_a - C_i$) expressed as

$$A_p = g_p(C_a - C_i) \tag{7.3}$$

These two equations can be combined into one as follows:

$$\delta^{13}C_p = \delta^{13}C_a - a + (b-a)A_p/g_pC_a \tag{7.4}$$

According to this model, a positive deviation of $\delta^{13}C_p$ is caused by enhanced photosynthetic rate (A_p) or reduced conductance at the boundary layer and stomatal pores (g_p), when $\delta^{13}C_a$ and C_a are constant. A_p and g_p can be affected by environmental factors such as light intensity, relative humidity, temperature, and soil moisture. It is expected that dry conditions may cause a decrease in g_p, resulting in a decrease in C_i and an increase in plant $\delta^{13}C$, and dry conditions may limit tree growth as well. Therefore, ring width decreases with an increase in tree-ring $\delta^{13}C$, resulting in a negative correlation between ring width and $\delta^{13}C$ when drought is a limiting factor of tree growth (e.g., Kagawa et al. 2003).

7.2.2 Corrections

Tree-ring $\delta^{13}C$ values were corrected by taking into account both the changes in the isotope ratio of atmospheric CO_2 ($\delta^{13}C_a$) and the plant physiological response to changes in atmospheric CO_2 concentration (C_a). Since the 1800s, $\delta^{13}C_a$ decreased with an increase in the atmospheric CO_2 concentration because of the addition of CO_2 from fossil fuel burning. First, tree-ring $\delta^{13}C$ values are corrected for changes in $\delta^{13}C_a$ using available data for the $\delta^{13}C_a$ derived from ice cores (e.g., Francey et al. 1999) and direct measurements (e.g., Keeling et al. 1979).

Second, tree-ring $\delta^{13}C$ series generally are corrected for changes in plant physiological response to the increased concentration of CO_2. A nonlinear detrending method of the tree-ring $\delta^{13}C$ series "pin correction," which was developed by McCarroll et al. (2009), has been well applied. The pin correction method is based on two logical constraints delimited by the likely physiological response of trees: first, that a unit increase in atmospheric CO_2 concentration (C_a) does not result in more than the same unit increase in the internal concentration of CO_2 (C_i) (passive response), and second, that increases in water-use efficiency as a result of an increase in atmospheric CO_2 concentration (C_a) are limited to maintaining a constant C_i/C_a ratio (active response). The pin correction method was implemented with R statistical software (R Core Team 2017) using atmospheric CO_2 concentration-time series data.

7.2.3 *Intrinsic Water-Use Efficiency*

Farquhar et al. (1982) described the dependence of difference (Δ) between $\delta^{13}C_p$ and $\delta^{13}C_a$ on plant physiological properties, in particular on C_i/C_a, as shown in Eq. (7.2). This equation holds for any time in the past when the respective tree ring was formed. From Eq. (7.2), it follows that C_i/C_a is linearly related to Δ and can be calculated from

$$C_i/C_a = (\Delta - a)/(b - a) \tag{7.5}$$

using literature data for *a* (Craig 1954) and *b* (Farquhar and Richards 1984), $\delta^{13}C_a$ (Keeling et al. 1979; Friedli et al. 1986; Francey et al. 1999), and measured data $\delta^{13}C_p$. From Eq. (7.5), C_i/C_a as well as C_i can easily be estimated with literature data for C_a.

Further, the intrinsic water-use efficiency (iWUE), the ratio of photosynthetic rate (A_p) to conductance for water vapor (g_c), is given by Ehleringer and Cerling (1995)

$$\mathrm{iWUE} = A_p/g_c = (C_a - C_i)/1.6 \tag{7.6}$$

where the denominator of 1.6 is the ratio of gaseous diffusivities of CO_2 and water vapor in the air. The iWUE is a component of the long-term water-use efficiency (WUE), the ratio of carbon uptake to water loss at the plant level, and represents an integrated change in plant physiological leaf-level condition during plant carbon assimilation. Although actual WUE is also influenced in particular by respiratory loss, this influence cannot be assessed in iWUE. The iWUE may be regarded as the potential rather than the actual WUE. In principle, a decrease in C_i coupled with high values of plant $\delta^{13}C$ causes an increase in iWUE through a higher carbon assimilation rate (CO_2 fertilization effect) with relatively less water loss because of a reduction of stomatal conductance (g_{st}).

Tree-ring $\delta^{13}C$-based reconstruction of iWUE has been attempted for several regions and ecosystems in recent years (e.g., Saurer et al. 2004; Gagen et al. 2011; Nock et al. 2011), and the results mostly indicate an increase in iWUE over the twentieth century, resulting from recent elevated concentrations of atmospheric CO_2 (C_a). However, it is also known that not only atmospheric CO_2 concentration (C_a) but also local meteorological variables, such as summer temperature and precipitation, affect iWUE and C_i (e.g., Andreu-Hayles et al. 2011; Tei et al. 2014).

7.3 Analysis of Tree Physiological Response to Past Climate Change

7.3.1 Study Sites

Three study sites were established in Yakutia, Russian Federation (Fig. 7.1). One is located at the taiga-tundra boundary ecosystem near Chokurdakh (70°37′N, 147°54′E). The sampling site, Kodak site, is located on the Indigirka Lowland, along the tributaries of the Indigirka River. Several sphagnums (e.g., *Sphagnum balticum*) and other moss species (e.g., *Aulacomnium turgidum*) generally cover the ground surface of the Indigirka Lowland, while graminoids (especially cotton sedges) grow in waterlogged depressions. Several woody species are also present at the sites: larch trees (*Larix gmelinii*) grow at relatively higher topographical locations, while alders (*Alnus fruticosa*) and willows (*Salix boganidensis*) are located in depressions and more frequently disturbed areas. The site is a typical taiga-tundra boundary landscape with flat topography.

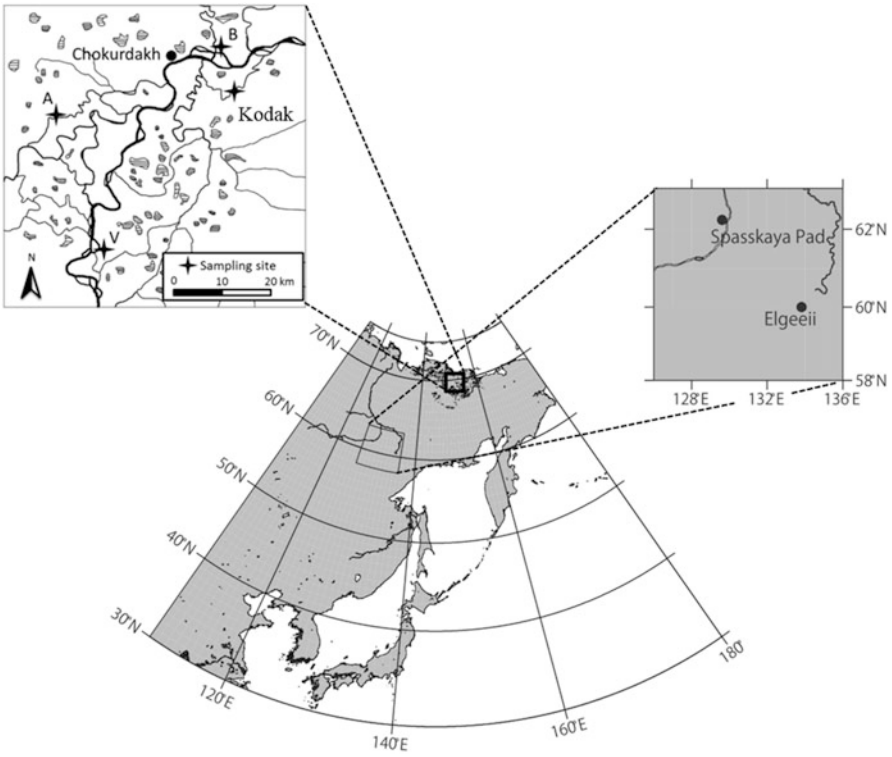

Fig. 7.1 Location of the study sites (Kodak [70°37′N, 147°54′E], Spasskaya Pad near Yakutsk [62°15′N, 129°14′E], and Elgeeii [60°00′N, 133°49′E]). (Modified from Tei et al. 2014 and Liang et al. 2014)

The other two sites are located in the southern parts of the Lena River basin in eastern Siberia: the Spasskaya Pad Scientific Forest Station (62°14′N, 129°37′E), near Yakutsk, and the Elgeeii station (60°00′N, 133°49′E), 300 km southeast of Yakutsk. These areas are dominated by larch (*Larix cajanderi*), with birch (*Betula platyphylla*) at Spasskaya Pad and birch (*Betula platyphylla*) and willow (*Salix* spp.) at Elgeeii. Both forest sites are located in continental dry climate regions, but the climate is relatively milder (wetter) in Elgeeii due to larger summer (June-July-August; JJA) precipitation (141.1 mm at Elgeeii and 112.1 mm at Spasskaya Pad from 1961 to 2008 from BMDS version 5.0; Yabuki et al. 2011), and the forest in Elgeeii, therefore, is more productive. According to Kotani et al. (2014), the stand density of larch (*Larix cajanderi*) trees (with a height > 1 m) is 1090 trees ha^{-1} at Elgeeii and 770 trees ha^{-1} at Spasskaya Pad, and the mean stand height of the upper canopy (larch trees) is approximately 25 m at Elgeeii and 20 m at Spasskaya Pad. The plant area index in the summer was 2.1 at Elgeeii and 1.4 at Spasskaya Pad, respectively. Both sites have similar understory vegetation comprised mainly of evergreen cowberry (*Vaccinium vitis-idaea*) mixed with several herbs (e.g., *Calamagrostis langsdorfii*).

7.3.2 Positive Tree Growth Response to Warming in a Subarctic Forest Ecosystem

Figure 7.2 shows results from correlation function (CF) and response function (RF) analyses in the Kodak site using DendroClim 2002 software (Biondi and Waikul 2004) to identify the relationships between the monthly records of temperature or precipitation obtained from CRU TS 3.22 (1901–2012, 0.5° longitude by 0.5° latitude degree) (Harris et al. 2014) and the tree-ring parameters, i.e., ring widths and $\delta^{13}C$. CF is a set of Pearson's correlation coefficients, whereas RF represents the result of principal component (PC) analysis in which climate variables are decorrelated (Fritts 1976; Cook and Kairiukstis 1990). In the RF analysis, we reduced the multicollinearity among monthly climatic variables by extracting their principal components (PCs). We then excluded the eigenvectors with relatively low values calculated from the monthly climate variables. The relationships between tree-ring parameters and the PCs of the monthly variables were back-transformed to relationships with the monthly climate variables, i.e., the coefficient of RF analyses.

The results show pronounced positive correlations of both CF and RF analyses for tree-ring width with June and July temperatures in the current year (Fig. 7.2). In addition, tree-ring $\delta^{13}C$ was also positively correlated with July temperatures in the current year for both CF and RF analyses. According to the Farquhar model (see Eq. (7.4)), positive correlation of $\delta^{13}C$ with summer temperatures suggests either stomatal closure (g_{st}) or an increase in photosynthetic rate (A_p) along with warming. If taken together with the observed positive correlation of ring width with summer temperatures, it could be considered that higher summer temperatures demonstrate a

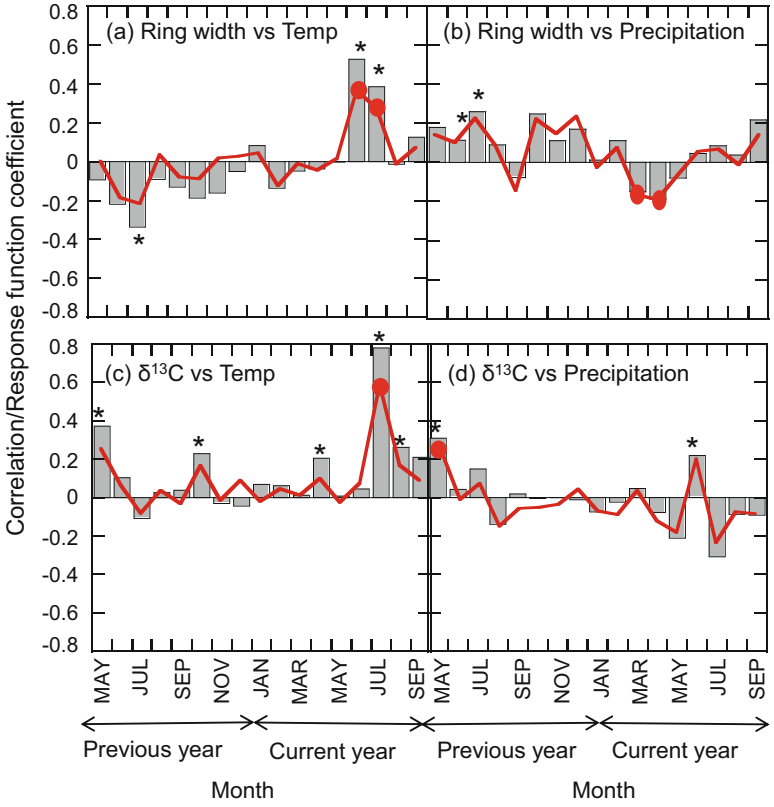

Fig. 7.2 Correlation coefficient (bars) and response function coefficient (lines) between tree-ring parameters (ring widths and $\delta^{13}C$) and climate data for the Kodak site: (**a**) ring width and monthly temperature, (**b**) ring width and monthly precipitation, (**c**) $\delta^{13}C$ and monthly temperature, and (**d**) $\delta^{13}C$ and monthly precipitation. Asterisks and circles indicate statistical significance at the 95% confidence level

higher photosynthetic rate (A_p) in larch (*Larix gmelinii*) trees, resulting in larger tree growth in this cold region. Tei et al. (2017) reported that the positive response of tree radial growth to summer temperature is often found over the subarctic region of eastern Siberia.

The positive response of tree growth to warmth in subarctic forests has been frequently reported not only in eastern Siberia (e.g., Kirdyanov et al. 2008; Blok et al. 2011) but also at various locations in the Siberian forest (e.g., Naurzbaev and Vaganov 2000; Kirdyanov et al. 2003, 2007) and Eurasian forest (e.g., Vaganov et al. 1999). These studies showed a pronounced positive relationship of tree growth with spring and/or summer temperatures. However, at the same time, some of those studies suggest that these temperatures are not only a limiting factor for tree growth. Vaganov et al. (1999) and Kirdyanov et al. (2003) reported that the date of snowmelt is highly correlated with tree growth in subarctic Eurasian forests, and a recent delay

in snowmelt caused by an increase trend in winter precipitation over the past century could have a significant effect on tree growth. The results of our RF analyses also show a significant negative correlation of ring width with April and May precipitation (Fig. 7.2), which may suggest some effects of snow conditions on larch (*Larix gmelinii*) tree radial growth in subarctic forests in eastern Siberia. In addition, Blok et al. (2011) reported moisture environments in the late summer season to have a considerable effect on shrub growth even in the subarctic environment of northern east Siberia. The results of our CF analysis also showed significant negative and positive correlations between tree radial growth and the previous late summer (July and/or August) temperatures and precipitation, respectively (Fig. 7.2). This result also suggests a considerable effect of water availability on larch (*Larix gmelinii*) physiology even in the subarctic environment of the northern part of eastern Siberia.

7.3.3 *Negative Tree Growth Response to Warming in Southern Boreal Forests*

Figure 7.3 shows the past 150 years of tree-ring width and $\delta^{13}C$ chronologies in the southern boreal forest at the Spasskaya Pad and Elgeeii. Larch (*Larix cajanderi*) tree physiological response to climate change was deduced from CF and RF analyses with the tree-ring width and $\delta^{13}C$ chronologies and the monthly records of temperature or precipitation obtained from CRU TS 3.22 (Fig. 7.4).

In general, at Spasskaya Pad, both ring widths and $\delta^{13}C$ show a pronounced response to climate conditions in the summer. Significant negative CF and RF in ring width in July and August of the previous summer are worthy of mention because it is a completely opposite tree growth response to summer temperatures from larch (*Larix gmelinii*) trees in the Kodak site of the subarctic forest (Fig. 7.2).

The negative relationship of tree radial growth with summer temperatures has also been reported in several dry areas of the northern high-latitude region. This may be explained as a temperature-induced drought stress: higher summer temperatures can cause higher evapotranspiration from surfaces, resulting in dryer conditions (e.g., Barber et al. 2000). In addition, positive correlations have been observed for $\delta^{13}C$ with June and July temperatures, and negative correlations have been observed with summer precipitation in the current year (Fig. 7.4). According to the Farquhar model (see Eq. (7.4)), a positive (negative) correlation of $\delta^{13}C$ with summer temperatures (precipitation) suggests either stomatal closure (g_{st}) or an increase in photosynthetic rate (A_p), along with warming (increased rain water). Taken together with the observed negative (positive) correlation of ring width with summer temperatures (summer precipitation), the relationship between tree-ring $\delta^{13}C$ and climate variables is well explained by the temperature-induced drought stress in which higher summer temperatures demonstrate stomatal closure (g_{st}) of larch (*Larix cajanderi*) trees, resulting in a reduction of tree growth in the southern boreal forests of Spasskaya Pad and Elgeeii. Although the statistical significance differed between

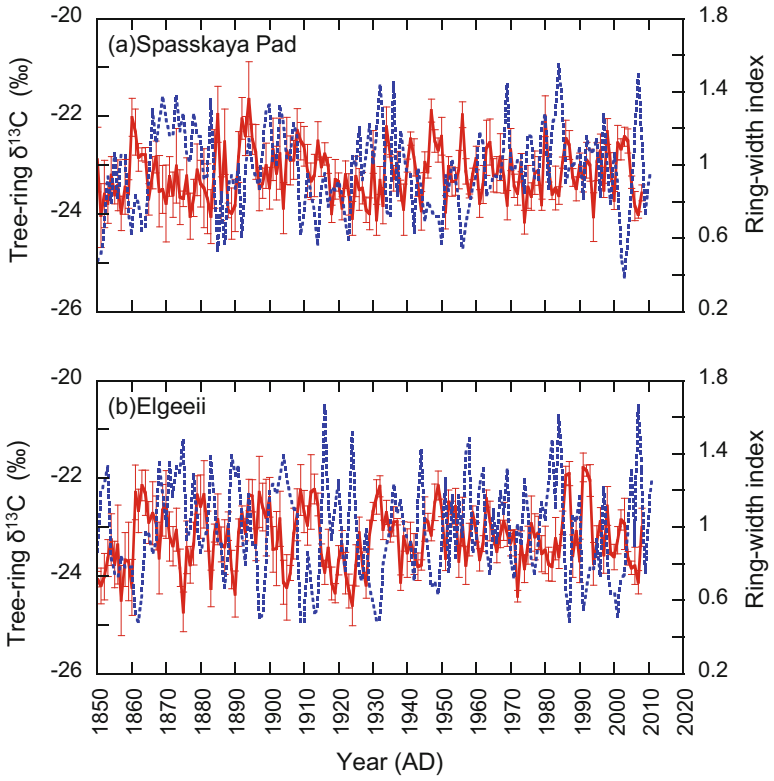

Fig. 7.3 Year-to-year variations in tree-ring $\delta^{13}C$ (solid line) and ring-width index (dotted line) for 1850 to 2011 at (**a**) Spasskaya Pad and (**b**) Elgeeii. Tree-ring $\delta^{13}C$ chronology shows average values for four trees with standard deviations (error bars). (Modified from Tei et al. 2014)

the two sites, CF and RF for Elgeeii generally showed similar patterns to those of Spasskaya Pad (Tei et al. 2014). These results indicate the importance of soil moisture conditions for the photosynthetic activity of larch (*Larix cajanderi*) trees in the southern boreal forest sites. This idea was supported by the observed negative correlation between tree-ring $\delta^{13}C$ and ring width for Spasskaya Pad ($r = 0.39$, $p < 0.01$) and Elgeeii ($r = 0.50$, $p < 0.01$). This negative relationship is generally expected when tree growth is limited by moisture conditions (e.g., Kagawa et al. 2003).

Figure 7.5 shows interdecadal variation in radial growth at Spasskaya Pad and Elgeeii. It shows significant reduction in tree radial growth in the recent warmest period (1991–2011) at both sites, suggesting the negative influence of summer temperatures for tree growth. Therefore, both interannual variations (Fig. 7.4) and interdecadal trends (Fig. 7.5) in growth are negatively influenced by summer temperatures at the boreal forest sites: Spasskaya Pad and Elgeeii. Interestingly, it also shows that high growing season temperatures affected tree growth due to the high temperature-induced water stress at Spasskaya Pad, where the climate is dryer,

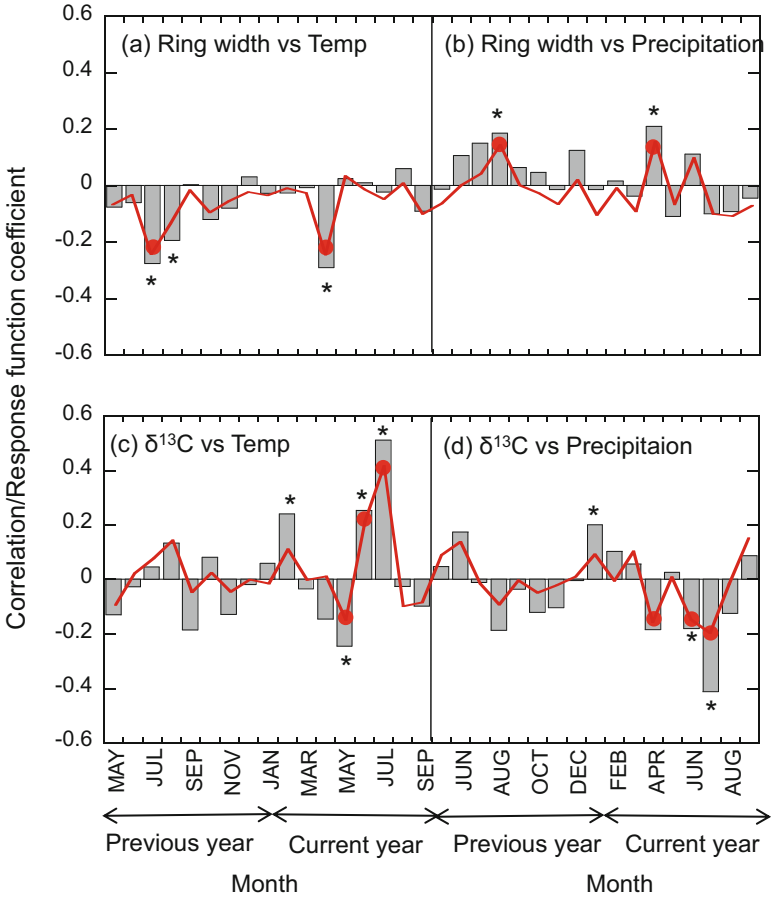

Fig. 7.4 Correlation coefficient (bars) and response function coefficient (lines) between tree-ring parameters (ring widths and $\delta^{13}C$) and climate data for Spasskaya Pad: (**a**) ring width and monthly temperature, (**b**) ring width and monthly precipitation, (**c**) $\delta^{13}C$ and monthly temperature, and (**d**) $\delta^{13}C$ and monthly precipitation. Asterisks and circles indicate statistical significance at the 95% confidence level. (Modified from Tei et al. 2014)

but, since the 1990s, the negative effect of high temperatures has become more significant at the Elgeeii, where climate is relatively milder (wetter) and the forest is more productive. A possible interpretation is that the larger the forest biomass the greater the demand for water, resulting in severe competition for water, as reported in a temperate forest ecosystem by McDowell et al. (2002).

The above results are also supported by a decadal trend in iWUE calculated from tree-ring $\delta^{13}C$ series at both Spasskaya Pad and Elgeeii, which showed a significant increasing trend (linear regression: $r^2 = 0.55$, $p < 0.001$) for both sites during the period from 1850 to 2008 (Table 7.1), which agrees with previous studies in northern

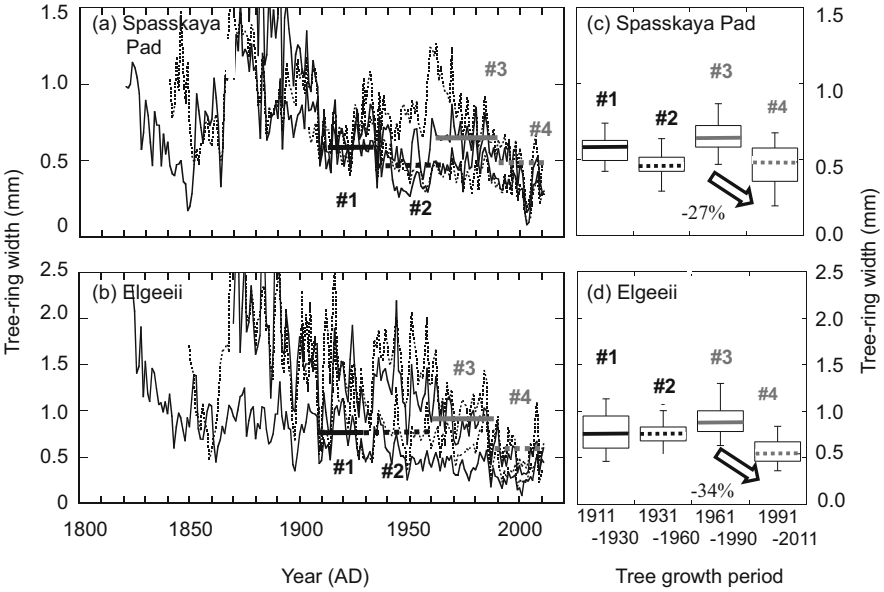

Fig. 7.5 Left panels (**a** and **b**): mean raw ring widths for four age classes (black solid line, 170–190 years; black dotted line, 140–170 years; gray solid line, 110−140 years; gray dotted line, 90–110 years) for (**a**) Spasskaya Pad and (**b**) Elgeeii. Horizontal lines (#1−4) show mean ring widths at the time of tree age range (90–110 years) for each age class. Right panels (**c** and **d**): box plots of these mean ring widths against tree growth periods for (**c**) Spasskaya Pad and (**d**) Elgeeii. (Modified from Tei et al. 2014)

Table 7.1 Summary of intrinsic water-use efficiency (iWUE) from tree-ring $\delta^{13}C$ at Spasskaya Pad and Elgeeii

	iWUE calculated from tree-ring $\delta^{13}C$					
	Spasskaya Pad			Elgeeii		
Period	iWUE	Rate[a]	R^{2} [b]	iWUE	Rate[a]	R^{2} [b]
1851–2008	**83.2 (7.5)**	**0.12**	**0.55**	**84.8 (9.1)**	**0.15**	**0.55**
1851–1970	80.4 (5.6)	0.10	0.39	81.3 (6.5)	0.10	0.30
1971–2008	90.8 (6.6)	0.32	0.27	95.5 (8.0)	0.44	0.37

Modified from Tei et al. (2014)
Values in parentheses are standard deviations of the means for each period. Bold characters indicate those variables for the whole period (1851–2008)
[a]The slope of the linear regressions is shown for rate
[b]R^2 is the coefficient of determination, and all R^2 values in the table are significant at the 99% confident level

Eurasia (Saurer et al. 2004), the Iberian Peninsula (Andreu-Hayles et al. 2011), and several other regions in the world (e.g., Gagen et al. 2011; Nock et al. 2011).

The increased rates of iWUE observed at the two forest sites are some of the highest values to have ever been observed. Although this trend was mainly caused

by the Ca rise, we detected a significant difference in the increasing rate of iWUE between these two sites from 1971 to 2008, with rapid warming (Table 7.1). At Elgeeii, the recent (1971–2008) increased rate of iWUE was greater than that at Spasskaya Pad, indicating more severe water stress for tree growth in Elgeeii, probably due to the larger forest biomass.

Carbon uptake by larch (*Larix cajanderi*) trees in eastern Siberian forests significantly decreased over the past two decades, presumably due to increase in summer temperatures (Fig. 7.5). Significant reductions in tree growth occurred alongside rapid increases in iWUE at both sites (Table 7.1), but these phenomena were more remarkable at Elgeeii, where the forest is more productive than Spasskaya Pad. Therefore, it was concluded that recent warming negatively affects the tree radial growth in the southern part of eastern Siberia, and the reduction in tree growth was more serious in a highly productive forest.

Tei et al. (2017) confirmed that the negative response of tree radial growth to warming is a widespread phenomenon in the circumpolar region, which has been observed not only in eastern Siberia but also in other continental dry climate regions, such as inner Alaska and Canada and the southern part of Europe. However, the authors also reported that the current version of the dynamic global vegetation model (SEIB-DGVM; Sato et al. 2016) could not reproduce the dominant negative response of tree growth to warming in those regions. The difficulty to reproduce the tree growth response to climate change when using the current model could be attributed to the lack of available data to perform a local calibration. Further efforts to synthesize multiple data streams, e.g., tree ring, model simulation, satellite images, and in situ eddy covariance CO_2 flux observation, would contribute to improving the empirical estimates, model structure, and calibrations and projections of the physiological responses of trees to climate changes.

7.3.4 *Challenges for the Future Development of Tree-Ring Carbon Cycling Research*

The use of tree rings in carbon cycling research has been increasing yearly due to increasing recognition of its reciprocal benefits among scientists. Yet, basic questions still persist with respect to what tree-ring parameters represent at the ecosystem level (e.g., Babst et al. 2014). For example, Girardin et al. (2016) compared tree-ring width chronologies and remotely sensed spectral vegetation indices, i.e., normalized difference vegetation index (NDVI), over Canada, and found disagreement in their trends over extensive areas; the accelerated trend of tree-ring width chronologies over some regions was not necessarily correlated with greening and, inversely, with browning, where trees experienced a slower growth.

Such uncertainties in growth trends deduced from tree-ring width chronologies provide justification for more direct monitoring of carbon cycling, such as in situ

eddy covariance CO_2 flux observation. Tree-ring research for carbon cycling should be performed cooperatively with more direct observations in the future. Such efforts are expected to improve our understanding of forest carbon cycling and place current developments into a long-term perspective of tree-ring research. It could also help to evaluate the performance of earth system models regarding the simulated magnitudes and dynamics of carbon cycling. Past long-term reconstructions of tree physiological responses to climate change inform these models about their growth responses to climatic drivers, which could significantly contribute to our understanding of future terrestrial carbon cycling, as well as the global climate.

7.4 Reconstruction of Past Climate and Environmental Changes

7.4.1 Hydroclimatic Reconstruction Based on Larch Tree-Ring $\delta^{13}C$

A highly significant correlation between tree-ring parameters and various climatic and environmental variables (e.g., temperature, precipitation, humidity, and soil moisture) allows us to reconstruct the variables in the decades preceding monitoring data. As an example, larch (*Larix cajanderi*) tree-ring $\delta^{13}C$-based reconstruction of summer PDSI in the boreal forests of the southern part of eastern Siberia, Spasskaya Pad and Elgeeii, is described below.

The multi-regression model, which is an analysis focused on the relationship between a dependent variable (here, summer PDSI) and several independent variables (here, tree-ring width and $\delta^{13}C$ of previous and current years), was built for the period of 1908–2005 (calibration period) and was checked for 1908–1956 and 1957–2005 (verification period) for Spasskaya Pad, and for the period 1920–2005 (calibration period), and was checked for 1920–1963 and 1964–2005 (verification period) for Elgeeii, respectively. Statistical parameters of the final calibration model accounted for 21.3% of the total variance ($p < 0.01$) for Spasskaya Pad and 28.9% of the total variance ($p < 0.01$) for Elgeeii, respectively, and passed all calibration and verification statistical requirements. The split-period calibration and verification showed satisfactory results, demonstrating the high reliability of those models.

Severe drought periods at the Spasskaya Pad were observed for 1891–1896 and 1947–1950 with progressed aridification at least after the late Little Ice Age to the modern period of global warming (Fig. 7.6a). The latter is a well-known severe drought event described in local documents, and a growth decrement of larch (*Larix cajanderi*) and pine (*Pinus sylvestris*) trees was also reported by a previous study in this region (Nikolaev et al. 2009). On the other hand, severe drought periods at the Elgeeii were detected for 1908–1914 and 1991–1993 (Fig. 7.6b). The latter was the most severe drought in the past 160 years in the region and was also detected in the Kolyma River basin in northeastern Siberia from tree-ring analysis (Berner et al.

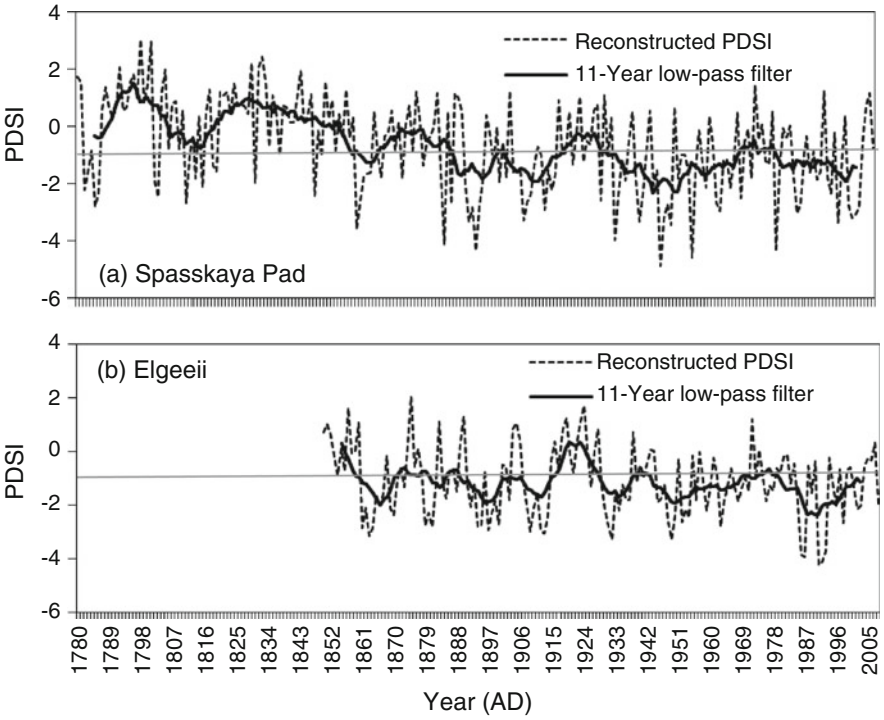

Fig. 7.6 (**a**) Reconstructed summer PDSI (dotted line) and its interdecadal variations obtained by an 11-year low-pass filter (solid line) for Spasskaya Pad (**a**) and Elgeeii (**b**). Horizontal gray lines show average value of −1.10 for Spasskaya Pad and −1.11 for Elgeeii, respectively (from 1850 to 2008). (Modified from Tei et al. 2013a, 2015)

2013). Although both reconstructions have significantly correlated for interannual variation from 1850 to 2008 ($r = 0.44$, $p < 0.01$), at a decadal range, there are differences in the persistency of the dry and wet periods.

Soil properties are different between Spasskaya Pad and Elgeeii. Kotani et al. (2014) reported that there is difference of soil carbon accumulation between those sites, showing a higher accumulation rate for Elgeeii than for Spasskaya Pad. The larger amount of organic carbon in the surface soil with the larger amount of summer (JJA) precipitation (141.1 mm at Elgeeii and 112.1 mm at Spasskaya Pad from BMDS version 5.0, Yabuki et al. 2011) could provide a longer retention time of soil water, which results in specific long-term variations of soil moisture in Elgeeii. This suggests that the local hydrological conditions are largely affected not only by precipitation but also by local soil moisture conditions. Regional studies are therefore essential to precisely depict the spatiotemporal variability of hydrological changes in eastern Siberia. Although a model study, such an effect of local soil properties on long-term patterns in soil moisture has been reported in North America (Salley et al. 2016).

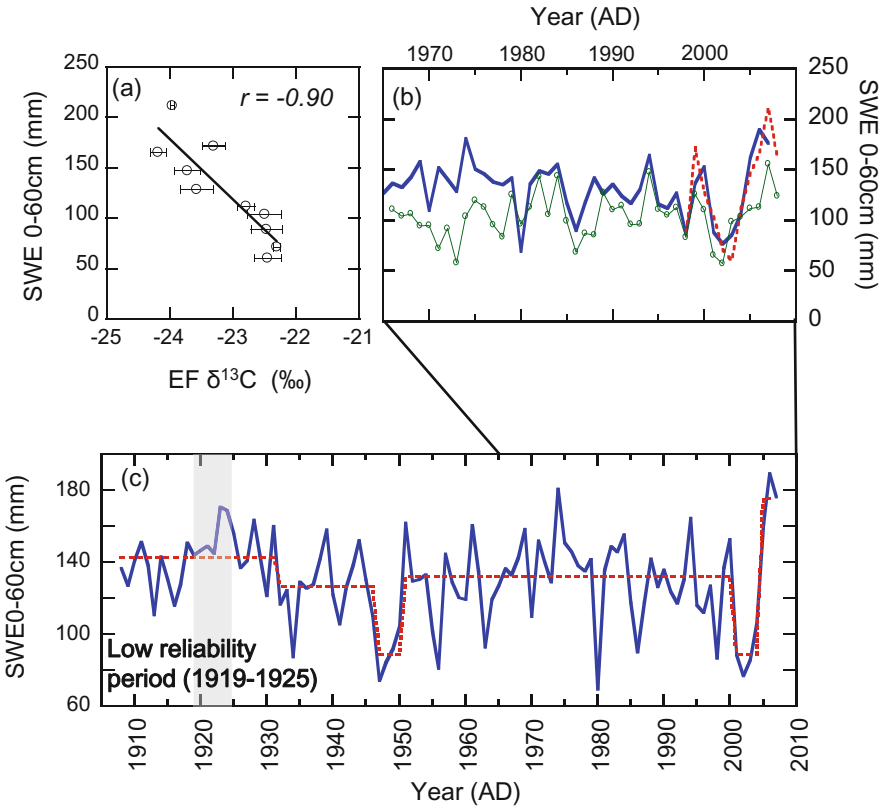

Fig. 7.7 (**a**) Relationship between EF $\delta^{13}C$ (combination of latewood in the current year and earlywood in the following year) and soil moisture water equivalent (SWE) (0–60 cm) in the late growing period (LGP: 15 July–31 August); (**b**) SWE estimated from EF $\delta^{13}C$ (solid line), observed SWE (dotted line), and SWE estimates with a one-dimensional land surface model 2LM (thin line with circle) (Yamazaki et al. 2007); (**c**) reconstructed SWE (solid line) and the changes in mean state estimated by STARS method (Rodionov 2004) (dotted line). (Modified from Tei et al. 2013b)

7.4.2 *Reconstruction of In Situ Soil Moisture Observational Record Based on Larch Tree-Ring $\delta^{13}C$*

Figure 7.7 shows soil moisture at Spasskaya Pad, reconstructed over the past 100 years, at the southern part of eastern Siberia using larch (*Larix cajanderi*) tree-ring $\delta^{13}C$ chronologies. As seen in Sect. 7.4.1, PDSI has been successfully reconstructed in Spasskaya Pad using tree-ring parameters with a statistical approach due to a property of PDSI, that is, a relatively long-term data period available. On the other hand, the available period for in situ observational soil moisture data is too short to reconstruct with the conventional statistical approach. Such a short observation period makes it difficult to reconstruct the in situ observational soil moisture

record by using tree-ring parameters. However, long-term reconstruction of in situ observational soil moisture is unquestionably useful. Such long records from the past, for example, could be directly used as validation data for land surface model simulations.

To extend such in situ soil moisture records with short observation periods, four sets of tree-ring width and $\delta^{13}C$ chronologies were generated, earlywood (EW), latewood (LW), total wood (TW), and wood calculated from a combination of LW of the current year and EW of the following year (EF), and were directly compared with the seasonal observed soil water equivalent (SWE) from 1998 to 2008, that is, June, July, August, JJA, and the late growing season (LGS; 15 July to 31 August), to find the most robust calibration model for past SWE reconstruction. Based on the correlation analyses between the above in situ observational SWE and tree-ring parameters, it was found that the highest correlation was between SWE in LGS and EF $\delta^{13}C$. The explained variance accounts for 81% of the total variance (Fig. 7.7a).

This region is located on continuous permafrost and therefore has characteristic water cycling. Sugimoto et al. (2003) reported that there is a carryover effect of late summer soil moisture maintained in the active layer above the permafrost to the next growing season. Therefore, soil moisture in late summer could affect plant photosynthetic activity in the next growing season. It is also known that carbohydrates accumulated in previous summers are utilized to produce EW cells, as demonstrated by tracer experiment using larch trees in this region (Kagawa et al. 2006). These carryovers of soil moisture and/or carbohydrates photosynthesized in previous summers to the next growing season contribute this highest correlation between SWE in LGS and EF $\delta^{13}C$; EW $\delta^{13}C$ shows higher correlation with SWE in the previous year than in the current year (Tei et al. 2013b).

The reconstructed SWE from EF $\delta^{13}C$ was supported by a physical model output using a one-dimensional land surface model (Fig. 7.7b). The reconstructed SWE shows large variations and a repeated occurrence of severe drought over the past 100 years, including the documented record of a severe drought in the 1940s (Fig. 7.7c). The reconstruction revealed that the soil moisture observed from 2006 to 2007 was the highest, and it was an extreme event in the past 100 years.

Although the reconstruction exhibited a generally good performance, it is also important to show reliability; it is necessary to prove whether tree-ring $\delta^{13}C$ values reflect soil moisture conditions at any periods. The reconstruction of soil moisture is based on a theory assuming that tree-ring $\delta^{13}C$ is exclusively controlled by stomatal conductance (g_{st}). In that case, the $\delta^{13}C$ negatively correlates with tree-ring width. To evaluate reliability, the temporal stability of the relationship between the $\delta^{13}C$ and ring width was investigated. This relationship was negative, as we expected, in most periods (Tei et al. 2013b). However, during a period of relatively low air temperature from 1919 to 1925, the negative relationship was weaker, and the reconstructed SWE was larger than expected from the amount of annual precipitation. Low-temperature conditions associated with low radiation possibly affected the photosynthetic rate (A_p) and as a result caused a decrease in $\delta^{13}C$ in addition to the effect of stomata opening (g_{st}) controlled by soil moisture (see Eq. (7.4)). Evaluation

of the reliability of the reconstruction is important because the accuracy of the reconstructed soil moisture is not equal for the whole period (Fig. 7.7c).

Soil moisture is obviously one of the most important factors controlling the water and energy balance between the land and atmosphere. Climate change in high-latitude regions could greatly affect the water cycle in boreal forests and cause significant changes of the cycle. Because this reconstruction is made independently from the precipitation records that include large uncertainties, the results are expected to greatly contribute to a future analysis of the water and carbon cycle in eastern Siberia, especially as validation data for a land surface model.

It should be noted that the relationship between tree-ring parameters and soil moisture conditions as observed here is expected only under a dry climate. For example, similar results have been reported in northern Mongolia (e.g., Davi et al. 2010) and forest steppe zone in the north (Sidorova et al. 2009) and south (Knorre et al. 2010) of central Siberia, where water availability for plants is low because trees are growing on a plateau. On the other hand, tree-ring parameters in a subarctic forest in central Siberia significantly related with summer temperature, and it was successfully reconstructed (e.g., Yasue et al. 2000; Briffa et al. 2001; Vaganov et al. 2009). From a plant physiological point of view, both soil moisture condition and temperature can greatly affect tree growth, and which climatic factors greatly affect the growth depends on the climatic zone of target region.

7.5 Conclusion Remarks

The tree-ring record is quite a useful tool for investigating past forest dynamics and climate/environmental changes in the decades preceding monitoring data. Analysis of tree-ring parameters, i.e., ring width and $\delta^{13}C$, indicated that tree growth in a subarctic forest (Kodak site) of eastern Siberian has been strongly regulated by summer temperatures but by summer soil moisture conditions in the southern boreal forests of Spasskaya Pad and Elgeeii. Using this sensitivity of tree-ring parameters to soil moisture conditions, the summer PDSI and in situ observational soil moisture record were successfully reconstructed in two southern boreal forests of eastern Siberia: Spasskaya Pad and Elgeeii. Tree-ring-based analyses for past tree growth response to climate change and for past climate/environment variability are expected to greatly contribute to future methods of analyzing the water and carbon cycle in eastern Siberia. They could also help to evaluate the performance of earth system models regarding the simulated magnitude and dynamics of water and carbon cycling, which could contribute to our understanding of these processes, as well as the global climate.

Reference

Anderson WT, Bernasconi SM, McKenzie JA, Saurer M (1998) Oxygen and carbon isotopic record of climatic variability in tree ring cellulose (Picea abies): an example from central Switzerland (1913–1995). J Geophys Res 103:31625–31636

Andreu-Hayles L, Planells O, Gutierrez E, Muntan E, Helle G, Anchukaitis KJ, Schleser GH (2011) Long tree-ring chronologies reveal 20th century increases in water-use efficiency but no enhancement of tree growth at five Iberian pine forests. Glob Chang Biol 17:2095–2112

Babst F, Alexander MR, Szejner P, Bouriaud O, Klesse S, Roden J, Ciais P, Poulter B, Frank D, Moore DJP, Trouet V (2014) A tree-ring perspective on the terrestrial carbon cycle. Oecologia 176:307–322

Barber VA, Juday GP, Finney BP (2000) Reduced growth of Alaskan white spruce in the twentieth century from temperature-induced drought stress. Nature 405:668–673

Berner LT, Beck SA, Bunn AG, Goetz SJ (2013) Plant response to climate change along the forest-tundra ecotone in northeastern Siberia. Glob Chang Biol 19:3449–3462

Blok D, Sass-Klaassen U, Schaepman-Strub G, Heijmans M, Sauren P, Berendse F (2011) What are the main climate drivers for shrub growth in Northeastern Siberian tundra? Biogeosciences 8:1169–1179

Biondi F, Waikul K (2004) DENDROCLIM2002: A C++ program for statistical calibration of climate signals in tree-ring chronologies. Comput Geosci 30:303–311

Briffa KR, Osborn TJ, Schweingruber FH, Harris IC, Jones PD, Shiyatov SG, Vaganov EA (2001) Low-frequency temperature variations from a northern tree ring density network. J Geophys Res 106:2929–2941

Cook ER, Kairiukstis A (1990) Methods of dendrochronology: applications in the environmental sciences. Kluwer Academic Press, Dordrecht

Craig H (1954) Carbon-13 in plants and the relationship between carbon-13 and carbon-14 variations in nature. J Geol 62:115–149

Cullen LE, Grierson PF (2006) Is cellulose extraction necessary for developing stable carbon and oxygen isotopes chronologies from Callitris glaucophylla? Palaeogeogr Palaeoclimatol 236:206–216

Davi N, Jacoby G, Fang K, Li J, D'Arrigo R, Baatarbileg N, Robinson D (2010) Reconstructing drought variability for Mongolia based on a large-scale tree ring Network. J Geophys Res 115:1520–1993

Ehleringer JR, Cerling TE (1995) Atmospheric CO_2 and the ratio of intercellular to ambient CO_2 concentrations in plants. Tree Physiol 15:105–111

Farquhar GD, Oleary MH, Berry JA (1982) On the relationship between carbon isotope discrimination and the inter-cellular carbon-dioxide concentration in leaves. Aust J Plant Physiol 9:121–137

Farquhar GD, Richards RA (1984) Isotope composition of plant carbon correlates with water-use efficiency of wheat genotypes. Aust J Plant Physiol 11:539–552

Francey RJ, Allison CE, Etheridge DM, Trudinger CM, Enting IG, Leuenberger M, Langenfelds RL, Michel E, Steele LP (1999) A 1000-year high precision record of $\delta^{13}C$ in atmospheric CO_2. Tellus 51:170–193

Friedli H, Lotscher H, Oeschger H, Siegenthaler U, Stauffer B (1986) Ice core record of the 13C/12C ratio of atmospheric CO2 in the past 2 centuries. Nature 324:237–238

Fritts HC (1976) Tree-rings and climate. Academic, New York/London/San Francisco. 236pp

Gagen M, Finsinger W, Wagner-Cremer W (2011) Evidence of changing intrinsic water-use efficiency under rising atmospheric CO_2 concentrations in Boreal Fennoscandia from subfossil leaves and tree ring $\delta^{13}C$ ratios. Glob Chang Biol 17:1064–1072

Girardin MP, Bouriaud O, Hogg EH, Kurz W, Zimmermann NE, Metsaranta JM, Jong R, Frank DC, Esper J, Büntgen U, Guo XJ, Bhatti J (2016) No growth stimulation of Canada's boreal forest under half-century of combined warming and CO_2 fertilization. Proc Natl Acad Sci USA 113:8406–8414

Harris I, Jones PD, Osborn TJ, Lister DH (2014) Updated high-resolution grids of monthly climatic observations – the CRU TS3.10 Dataset. Int J Climatol 34:623–642

Kagawa A, Naito D, Sugimoto A, Maximov TC (2003) Effects of spatial and temporal variability in soil moisture on widths and $\delta^{13}C$ values of eastern Siberian tree rings. J Geophys Res 108. https://doi.org/10.1029/2002JD003019

Kagawa A, Sugimoto A, Maximov TC (2006) Seasonal course of translocation, storage and remobilization of C-13 pulse-labeled photoassimilate in naturally growing Larix gmelinii saplings. New Phytol 171:793–804

Keeling CD, Mook WG, Tans PP (1979) Recent trends in the $^{13}C/^{12}C$ ratio of atmospheric carbon-dioxode. Nature 277:121–123

Knorre AA, Siegwolf RTW, Saurer M, Sidorova OV, Vaganov EA, Kirdyanov AV (2010) Twentieth century trends in tree ring stable isotope ($\delta^{13}C$ and $\delta^{18}O$) of Larix sibirica under dry conditions in the forest steppe in Siberia. J Geophys Res 115. https://doi.org/10.1029/2009JG000930

Kotani A, Kononov AV, Ohta T, Maximov TC (2014) Temporal variation in the linkage between net ecosystem exchange of water vapor and CO_2 over boreal forests in eastern Siberia. Ecohydrology 7:209–225. https://doi.org/10.1002/eco.1449

Kirdyanov A, Hughes MK, Vaganov EA, Schweingruber F, Silkin P (2003) The importance of early summer temperatures and date of snow melt for tree growth in Siberian subarctic. Trees 17:61–69

Kirdyanov AV, Vaganov EA, Hughes MK (2007) Separating the climatic signal from tree-ring width and maximum latewood density records. Trees 21:37–44

Kirdyanov AV, Treydte KS, Nikolaev A, Helle G, Schleser GH (2008) Climate signals in tree-ring width, density and delta C-13 from larches in Eastern Siberia (Russia). Chem Geol 252:31–41

Liang M, Sugimoto A, Tei S, Bragin IV, Takano S, Morozumi T, Shingubara R, Maximov TC, Kiyashko SI, Velivetskaya TA, Ignatiev AV (2014) Importance of soil moisture and N availability to larch growth and distribution in the Arctic taiga-tundra boundary ecosystem, northeastern Siberia. Polar Science 8:327–341

Loader NJ, Robertson I, McCarroll D (2003) Comparison of stable carbon isotope ratios in the whole wood, cellulose and lignin of oak tree-rings. Palaeogeogr Palaeoclimatol 196:395–407

Loader NJ, McCarroll D, Gagen MH, Robertson I, Jalkanen R (2007) Extracting climate information from stable isotopes in tree rings. In: Dawson T, Siegwolf R (eds) Isotopes as indicators of ecological change. Elsevier, The Netherlands, pp 23–44

McCarroll D, Loader NJ (2004) Stable isotopes in tree rings. Quat Sci Rev 23:771–801

McCarroll D, Gagen MH, Loader NJ, Robertson I, Anchukaitis KJ, Los S, Young GHF, Jalkanen R, Kirchhefer A, Waterhouse JS (2009) Correction of tree ring stable carbon isotope chronologies for changes in the carbon dioxide content of the atmosphere. Geochim Cosmochim Acta 73:1539–1547

McDowell NG, Phillips N, Lunch C, Bond BJ, Ryan MG (2002) Aninvestigation of hydraulic limitation and compensation in large, old Douglas-fir trees. Tree Physiol 22:763–774

Naurzbaev MM, Vaganov EA (2000) Variation of early summer and annual temperature in east Taymir and Putoran (Siberia) over the last two millennia inferred from tree rings. J Geophys Res 105:7317–7326

Nikolaev AN, Fedorov PP, Desyatkin AR (2009) Influence of climate and soil hydrothermal regime on radial growth of Larix cajanderi and Pinus sylvestris in Central Yakutia, Russia. Scand J Forest Res 24:217–226

Nock CA, Baker PJ, Wanek W, Leis A, Grabner M, Bunyavejchewin S, Hietz P (2011) Long-term increases in intrinsic water-use efficiency do not lead to increased stem growth in a tropical monsoon forest in western Thailand. Glob Chang Biol 17:1049–1063

R Core Team (2017) R: a language and environment for statistical computing. R Foundation for Statistical Computing, Vienna. https://www.R-project.org/

Roden JS, Lin GG, Ehleringer JR (2000) A mechanistic model for interpretation of hydrogen and oxygen isotope ratios in treering cellulose. Geochim Cosmochim Acta 64:21–35

Rodionov SN (2004) A sequential algorithm for testing climate regime shifts. Geophysi Res Lett 31. https://doi.org/10.1029/2004GL019448

Salley SW, Sleezer RO, Bergstrom RM, Martin PH, Kelly EF (2016) A long-term analysis of the historical dry boundary for the Great Plains of North America: implications of climatic variability and climatic change on temporal and spatial patterns in soil moisture. Geoderma 274:104–113

Sato H, Kobayashi H, Iwahana G, Ohta T (2016) Endurance of larch forest ecosystems in eastern Siberia under warming trends. Ecol Evol 6:5690–5704

Saurer M, Borella S, Schweingruber F, Siegwolf R (1997) Stable carbon isotopes in tree rings of beech: climatic versus site-related influences. Trees-Struct Funct 11:291–297

Saurer M, Siegwolf RTW, Schweingruber FH (2004) Carbon isotope discrimination indicates improving water-use efficiency of trees in northern Eurasia over the last 100 years. Glob Chang Biol 10:2109–2120

Sidorova OV, Siegwolf RTW, Saurer M, Shashkin AV, Knorre AA, Prokushkin AS, Vaganov EA, Kirdyanov AV (2009) Do centennial tree-ring and stable isotope trends of Larix gmelinii (Rupr.) Rupr. indicate increasing water shortage in the Siberian north? Oecologia 161:825–835

Sugimoto A, Naito D, Yanagisawa N, Ichiyanagi K, Kurita N, Kubota J, Kotake T, Ohata T, Maximov TC, Fedorov AN (2003) Characteristics of soil moisture in permafrost observed in East Siberian taiga with stable isotopes of water. Hydrol Process 17:1073–1092

Tei S, Sugimoto A, Yonenobu H, Hoshino Y, Maximov TC (2013a) Reconstruction of summer Palmer Drought Severity Index from $\delta^{13}C$ of larch tree rings in East Siberia. Quat Int 290-291:275–281

Tei S, Sugimoto A, Yonenobu H, Yamazaki T, Maximov TC (2013b) Reconstruction of soil moisture for the past 100 years in eastern Siberia by using $\delta^{13}C$ of larch tree rings. J Geophys Res 118. https://doi.org/10.1002/jgrg.20110

Tei S, Sugimoto A, Yonenobu H, Ohta T, Maximov TC (2014) Growth and physiological responses of larch trees to climate changes deduced from tree ring widths and d13C at two forest sites in eastern Siberia. Polar Science 8:183–195

Tei S, Yonenobu H, Sugimoto A, Ohta T, Maximov TC (2015) Reconstructed summer Palmer Drought Severity Index since 1850 AD based on δ13C of larch tree rings in eastern. J Hydrol 529(Part2):442–448

Tei S, Sugimoto A, Yonenobu H, Matsuura Y, Osawa A, Sato H, Fujinuma J, Maximov TC (2017) Tree-ring analysis and modeling approaches yield contrary response of circumboreal forest productivity to climate change. Glob Chang Biol 23:5179–5188

Vaganov EA, Hughes MK, Kirdyanov AV, Schweingruber FH, Silkin PP (1999) Influence of snowfall and melt timing on tree growth in subarctic Eurasia. Nature 400:149–151

Vaganov EA, Schulze ED, Skomarkova MV, Knohl A, Brand WA, Roscher C (2009) Intra-annual variability of anatomical structure and $\delta^{13}C$ values within tree rings of spruce and pine in alpine, temperate and boreal Europe. Oecologia 161:729–745

Walker X, Michelle CM, Johnstone JF (2015) Stable carbon isotope analysis reveals widespread drought stress in boreal black spruce forests. Glob Chang Biol 21:3102–3113

Yabuki H, Park H, Kawamoto H, Suzuki R, Razuvaev VN, Bulygina ON, Ohata T (2011) Baseline Meteorological Datain Siberia (BMDS) Version 5.0, RIGC, JAMSTEC, Yokosuka, Japan, distributed by CrDAP, Digital media

Yamazaki T, Ohta T, Suzuki R, Ohata T (2007) Flux variation in a Siberian Taiga fores near Yakutsk estimated by a one-dimensional model with routine data, 1986–2000. Hydrol Process 21:2009–2015

Yasue K, Funada R, Kobayashi O, Ohtani J (2000) The effects of tracheid dimensions on variations in maximum density of Picea glehnii and relationships to climate factors. Trees 14:223–229

Chapter 8
Permafrost-Forest Dynamics

Yoshihiro Iijima and Alexander N. Fedorov

8.1 Introduction

Permafrost is defined as perennially cryotic earth materials, and its location and extent are therefore linked to the climate. Consequently, recent observations of warming and thawing permafrost have been interpreted as evidence of global warming (Walsh et al. 2005; Lemke et al. 2007). Most studies have focused on the concurrent relationship between permafrost degradation and climatic change on decadal and longer time scales in conjunction with warming trends in air temperatures over the last century (Pavlov 2003; Chudinova et al. 2006; Romanovsky et al. 2007). Changes in other climatic and environmental factors, such as snow cover conditions, soil properties, vegetation types, and geological/geomorphological conditions, have been shown to affect both the active-layer thickness and soil temperatures over shorter time scales (interannual) and smaller spatial scales (Varlamov et al. 2002; Frauenfeld et al. 2004; Zhang 2005) when the observed air temperature alone cannot account for variations in the thermal state of permafrost (Zhang et al. 2001; Osterkamp 2007). Furthermore, anthropogenic disturbances, such as forest fires, extensive agricultural land use, and construction of infrastructure, have also enhanced permafrost degradation.

The interactions between highly variable climatic variables, such as rainfall, snow amounts and duration, air temperature, and the thermal state of permafrost, can be modelled as a complicated, dynamic, and self-regulating system which manifests itself in processes related to soil moisture migration, evaporation, sublimation, and freezing or thawing of the active layer (Hinzman et al. 1991; Kane et al. 2001). In addition, soil moisture variations within the active layer, potentially regulated by the

Y. Iijima (✉)
Graduate School of Bioresources, Mie University, Tsu, Mie, Japan
e-mail: yiijima@bio.mie-u.ac.jp

A. N. Fedorov
Melnikov Permafrost Institute, RAS, Yakutsk, Russia

T. Ohta et al. (eds.), *Water-Carbon Dynamics in Eastern Siberia*,
Ecological Studies 236, https://doi.org/10.1007/978-981-13-6317-7_8

precipitation regime, drive unique interactions with the underlying frozen ground through subsidence processes to form thermokarst and alas landscapes (Fedorov and Konstantinov 2003). They also interact with the atmosphere through energy balance and evapotranspiration processes (Ohta et al. 2001, 2008).

Eastern Siberia is at the centre of a continuous permafrost zone in the Eurasian continent. The most prominent feature of this permafrost zone is its deciduous coniferous boreal forest (called the "taiga" and consisting of larch trees). In addition, an extensive and massive ice layer within the permafrost (called the "Yedoma") underlies the boreal ecosystem, in particular, in the central Yakutian region bounded by the large Lena and Aldan rivers (Fig. 8.1). Major parts of this interfluve region are covered by ice-rich silty loam containing up to 80% of the volumetric ice content that mainly exists as huge syngenetic ice wedges. These ice complex deposits form the Yedoma uplands that surround alas basins (Soloviev 1973).

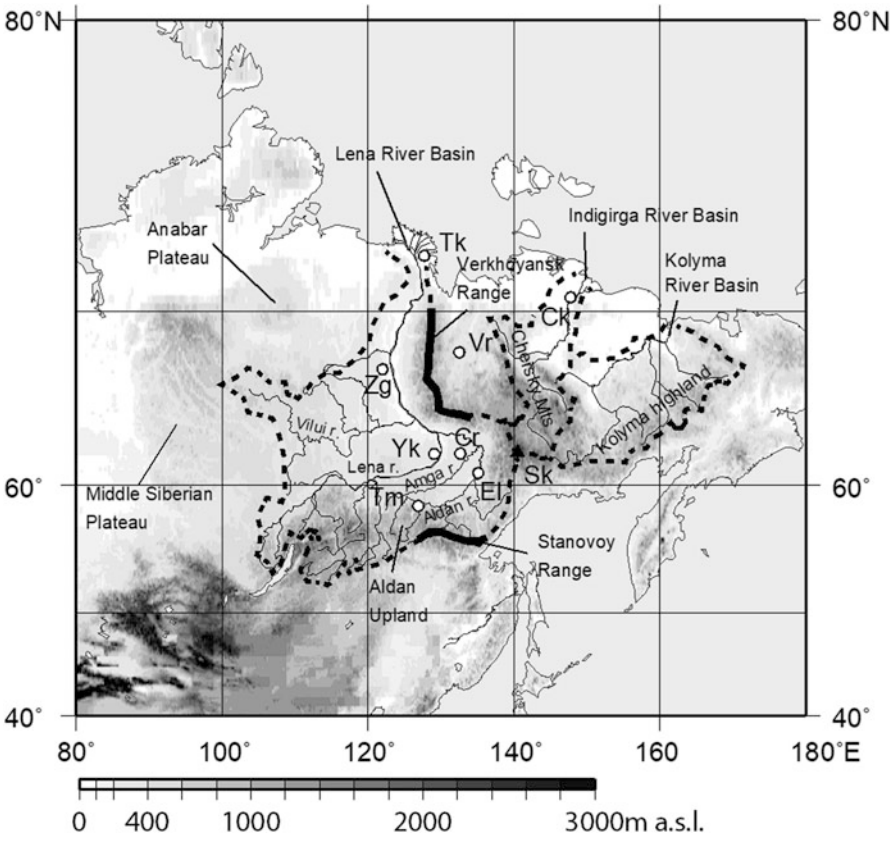

Fig. 8.1 Topographical map in eastern Siberia with major river basins and main observational points
Tk Tiksi, *Ck* Chokurdakh, *Vr* Verkhoyansk, *Zg* Zhigansk, *Yk* Yakutsk, *Cr* Churapcha, *El* Elgeeii, *Tm* Tommot, *Sk* Suntar-Khayata. (Mt. Mus-Khaya: 2959 m)

In this chapter, a holistic overview of the landscape, structure, and thermal regime of permafrost in eastern Siberia is provided based on research conducted in Russian and international collaborative studies. The review of the permafrost literature is then extended to consider the effect of concurrent changes in temperature and the active layer and actualized degradation processes on the land surface underlying permafrost in boreal forests and grasslands. The geographical territory covering topic in this chapter is shown in Fig. 8.1.

8.2 Permafrost-Related Landscape

The central Yakutian lowlands, at the centre of a boreal forest with underlying permafrost, are one of the most extensive permafrost regions in the world. Their most notable feature is the depth of permafrost, which extends to 300–500 m in most areas and over 1000 m in some locations along the upper Viliui River (Czudek and Demek 1970). The central part of the Lena basin is characterized by landscapes of vast boreal (taiga) forest, large grassland depressions (alas), and transitional topography under permafrost degradation (thermokarst). The eastern Sakha Republic is rather mountainous, consisting of the Verkhoyansk, Chersky, and Suntar-Khayata ranges. The Suntar-Khayata Range (Russian: Сунтар-Хаята) is a granite mountain range rising along the border of the Sakha Republic in the north with Amur Oblast and Khabarovsk Krai in the south. The highest point of the range is Mus-Khaya Mountain in the Sakha Republic, at a height of 2959 m. The Suntar-Khayata Range is a watershed divide between the Aldan River, which eventually flows into the Lena River and the Arctic Ocean, and the Sea of Okhotsk. It contains the southernmost glaciers in the Russian Far East with a periglacial permafrost landscape.

8.2.1 Geological History of Permafrost Evolution

Permafrost evolution in eastern Siberia, particularly the Sakha Republic (Yakutia), was initiated in the Early Pleistocene. During the Holocene, glacial-interglacial cycles formed a deepening permafrost layer in central Yakutia and the river terrace of the Lena River basin.

At the end of the Early Pleistocene (350–300 thousand years ago), repeated continental glaciations occurred at the middle and high latitudes (Groswald 1998). This led to the freezing of grounds to a depth of hundreds or even more than 1000 m, thereby forming the initial permafrost zone (Balobaev 1991).

In the Pleistocene, the northern part of the Yakutian covered icecap had a thickness of 1.5–2 km, with shallower glaciers in the north-east of Yakutia. A glacier from the Verkhoyansk Mountains blocked the valley of the Lena River in the region of the Orulgan ridge (near Zhigansk), and in the central Yakutian lowlands, a large glacial lake formed.

During the glaciation period 60–37 thousand years ago (the Ziryanovsk glaciation), swampy landscapes similar to modern tundra existed on the Abalakh plain of central Yakutia (absolute height 165–230 m) around the glacial lake on the modern Lena and Aldan river valleys. Wet soils here experienced frost cracking, formation of polygonal relief, and active accumulation of ice wedges, leading to the formation of the ice complex (ice-rich, fine-grained permafrost sequence) of the Abalakh plain.

The ice complex of the Abalakh plain has a depth of up to 60 m, and the ground is composed of loam. The width of the large ice wedges reaches more than 10 m in some regions. Ice volume accounts for around 55–60% of the ice complex, and a syngenetic freezing occurred due to waterlogging along the active layer 45–56 thousand years ago (Katasonov et al. 1979).

During the Sartan glaciation (26–14 thousand years ago), the volume of the glacial lake area along the modern Lena and Aldan river valleys decreased. Swampy landscapes also existed at the level of the Tyungyulyu (Töngülü) plain of central Yakutia (absolute height 140–165 m). Here, the same cryogenic processes occurred along with the formation of ice wedges, which led to the formation of the Tyungulu plain ice complex.

Similar to the Abalakh plain, the ice complex of the Tyungulu plain has a depth of up to 40 m, and the grounds are composed of loam. The width of the ice wedges reaches 6–8 m. Ice volume accounts for around 40–50% of the ice complex, and the deposits are alluvial swamp (Katasonov and Ivanov 1973). The age of the Tyungulu level deposits was estimated from radiocarbon dating to be from 14 to 22 thousand years (Katasonov et al. 1979).

8.2.2 Yedoma and Alas Formation

During the Late Pleistocene (< 126 thousand years ago), glaciation occurred repeatedly, with ice shields covering large parts of northern and central Eurasia. The regions of central Yakutia and large parts of the eastern Siberian lowlands did not undergo glaciation, although the soil surface was exposed to very low air temperatures over a long period. Freezing of the ground and permafrost build-up extended to depths of several hundred metres (e.g. Hubberten et al. 2004).

In the later period of the Late Pleistocene, a protrusion of the icecap from the Verkhoyansk Mountains blocked the valley of the northern part of the Lena River near the present-day town of Zhigansk. In the territory of central Yakutia, a large glacial lake was formed. Among other territories, large parts of the Lena-Aldan interfluve were occupied by the glacial lake and adjacent wetlands (Desyatkin et al. 2014). Wet soils here experienced frost cracking, formation of polygonal relief, and active development of ice wedges. Repeated changes in climatic conditions, water levels, erosion, and sedimentation led to the formation of terraces, notably the Abalaakh terrace (~56–45 thousand years ago) and the Tyungyulyu terrace (~22–14 thousand

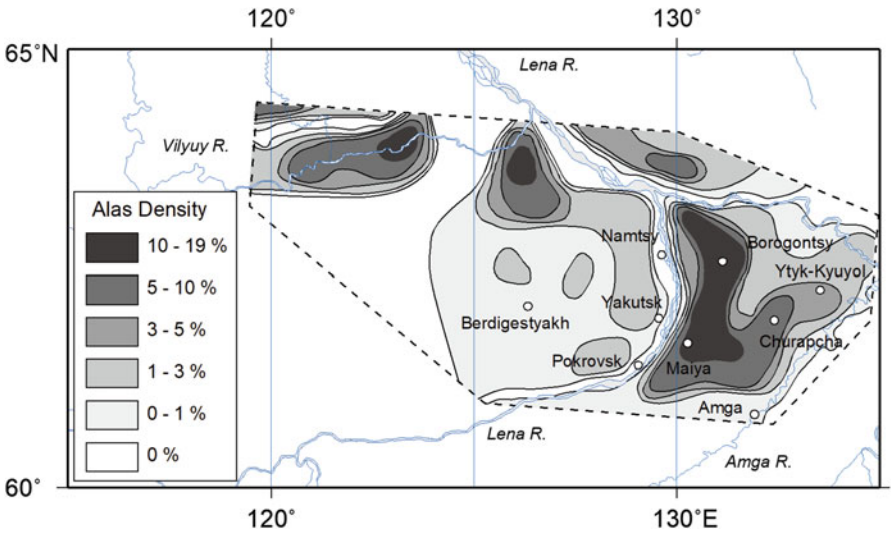

Fig. 8.2 Density of alas lake in CY. (Modified after Bosikov 1991)

years ago) (Katasonov et al. 1979). Annual cycles of thaw and freeze together with a syngenetic accumulation of sediments led to the gradual development of ice wedges, reaching 60 m depth and 10 m width on the Abalaakh terrace and 40 m depth and 8 m width on the Tyungyulyu terrace.

These ice complex deposits (i.e. Yedoma deposits) are thus characterized by very high ground-ice contents of more than 60% by volume (Soloviev 1959; Katasonov et al. 1979). The ice-wedge volume alone is estimated to account for about 50% of the total upper permafrost volume (Ivanov 1984). This is crucial for the development of large alas because surface subsidence is related to ice-volume loss (e.g. Romanovskii et al. 2000; Ulrich et al. 2014). Warming during the Pleistocene-Holocene transition caused a reduction of glaciers and the disappearance of the glacial lake in central Yakutia. It also initiated the thawing of the ice complex and thermokarst development over a vast area. Fluctuations in climate conditions during the Early Holocene led to extensive thermokarst formation caused by the degradation (i.e. thawing) of the ice-rich permafrost deposits and subsequent surface subsidence (Bosikov 1991; Katamura et al. 2006; Grosse et al. 2013).

There are approximately 16,000 alases in the central Yakutian lowlands, covering a total area of ~4400 km^2 or ~17% of the total land area of this region. In some of its subregions, notably between the lower reaches of the Aldan and the Lena rivers, alas covers up to 30% of the territory's surface (Fig. 8.2; Bosikov 1991). Alas also constitutes typical landscape features further west in the Republic of Sakha, to the north and south of the Viliui River.

8.2.3 *Recent Thermokarst Depression*

The thermokarst formation process, in general, is initiated by an active-layer (i.e. seasonal thaw layer) deepening and the subsequent thawing of the ice complex because of soil heating after periods of climate change, but it also can result from temporally and spatially limited non-climatic factors, such as the destruction of the vegetation cover, local erosion, forest fire, or land use change. Thermokarst evolution takes place in four main stages resulting in successive thermokarst landforms identified by Sakha language (Fig. 8.3; Crate et al. 2017) – *byllar*, *dyede* (*düöd'e*), and *tuumpu* – and, finally, over several thousand years, in a stable thermokarst basin (i.e. *alas*; Bosikov 1991; Soloviev 1973). The initiation and the subsequent enlargement of thermokarst lakes in the byllar and dyede stages, however, may occur over decades or within a few hundred years (Fedorov et al. 2014b; Soloviev 1973; Katamura et al. 2006). Long-term surface subsidence below thermokarst lakes results in large steep-sided and flat-floored thermokarst basins. The lower mean annual air temperatures and low precipitation since the Late Holocene are probably caused by the decrease in the lake volume in central Yakutia. Grasslands have begun spreading within the drained alas systems from 2000 years BP (Katamura et al. 2006).

Important with regard to climate change and ecosystem resilience is the spatio-temporal character of alas development: is it unidirectional or cyclical? The model of unidirectional thermokarst evolution includes initiation, expansion, drainage, and cessation (e.g. Morgenstern et al. 2013). However, this model contradicts that of thaw-lake cycles, which postulate repeated thermokarst events during the Holocene (e.g. Brouchkov et al. 2004; Hinkel et al. 2003; Grosse et al. 2013). According to the latter model, secondary thermokarst activity in drained basins could occur after

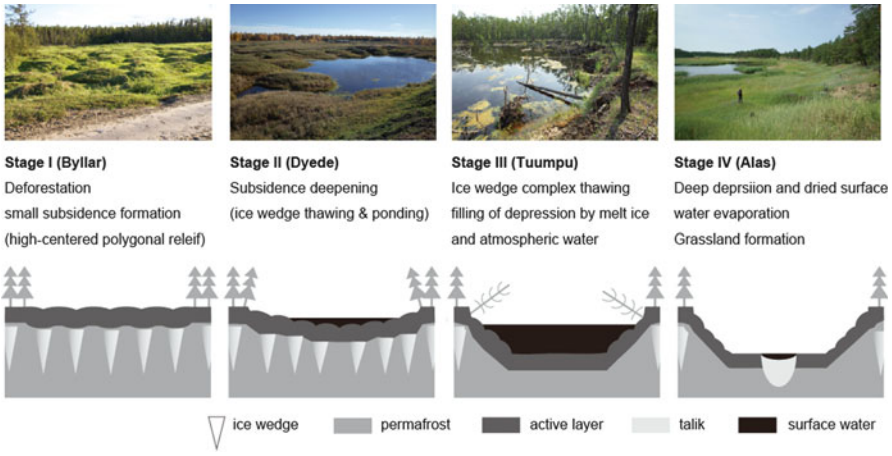

Fig. 8.3 Thermokarst stages in ice-rich permafrost in the boreal zone of central Yakutia. (Based on Crate et al. 2017)

sufficient sediment infilling, ice aggradation, and frost heaving (Soloviev 1973). However, evidence of several complete thaw-lake cycles, especially in the central Yakutian permafrost lowlands during the Holocene, is lacking (e.g. Pestryakova et al. 2012).

Today, all stages of thermokarst evolution exist in the central Yakutian lowlands. However, the highly spatially heterogeneous processes of thermokarst dynamics and their driving factors are not yet clearly understood, due to the complex interaction of geological, climatic, geomorphological, cryological, hydrological, ecological, and sociocultural interrelations.

Located within the boreal coniferous forest (taiga) zone, the central Yakutian lowlands are dominated by larch forest. However, alas is generally bare of forest vegetation. Three different vegetation zones – wetland, moist grassland, and dry grassland – extend concentrically around the lakes that are typically located in the centre of each alas, in line with edaphic and hydrological conditions (Desyatkin 2008).

8.2.4 Mountain Permafrost

The mountain permafrost in eastern Siberia is typical for the Byrranga and the Putoran mountains, the Anabar Plateau and the Aldan Upland, the Verkhoyansk and the Chersky mountain ranges, the Kolyma highland, and the Stanovoi mountain range system. The main common features between these heterogeneous geological formations are the mountain relief and the presence of a high-altitude belt distribution of permafrost landscapes.

The maximum permafrost thickness in the highest mountain ranges and highlands with a wide development of mountain deserts and tundra reaches 1000–1300 m, and the most typical permafrost thickness varied from 150 to 700 m (Kondratieva et al. 1989; Romanovskii et al. 1989). In the mountainous areas of eastern Siberia, a continuous distribution of permafrost is generally found, with the exception of certain areas of the Aldan Upland (the Chulman and Elgin plateaus), where discontinuous and sporadic permafrost is predominant. The valleys of mountain rivers are characterized by taliks (layers with unfrozen ground), with which numerous icings (*taryns*; frozen spring water formed in cold season and the groundwater is originally from inter-permafrost layer) are associated.

The ice content of permafrost in mountain landscapes does not differ greatly. The most ice-covered areas are regions with peat in boggy mountain tundra and *taiga mari* (swampy grass marsh and sphagnum larch forests that meet in eastern Siberia and the Far East; Milkov 1970), on the foothills of mountain ranges and uplands, and valleys of mountain rivers. The volumetric ice content is mainly around 0.4–0.6 and sometimes more than 0.6. Often, they contain Holocene polygonal ice wedges with a thickness of 2–5 m. Eluvial, eluvial-deluvial, deluvial-colluvial and colluvial deposits are found on the plateaus and mountain ranges, mostly slightly ice-free with a volumetric ice content of 0.2, and in some areas the ice content reaches 0.2–0.4.

The temperature of permafrost and the active-layer thickness depend on the landscape. In mountainous areas with continuous permafrost, the distribution of these characteristics of permafrost occurs according to the altitudinal zonation: in the mountain desert, the permafrost temperature and active-layer thickness vary from −9 to −14 °C and 0.3–0.8 m, respectively; for mountain tundra from −7 to −11 °C and 0.5–1.4 m, respectively; for subalpine shrub thickets from −3 to −9 °C and 1.3–1.8 m, respectively; and for mountain woodlands from −3 to −7 °C and 0.8–1.8 m, respectively. In discontinuous and sporadic permafrost in mountain taiga, the ground temperature is from 0 to −2 °C when frozen and up to 2 °C in unfrozen zones, and the active-layer and seasonally frozen-layer thickness reach 3–4 m (Fedorov et al. 1989).

Cryogenic processes and phenomena are also diverse in the mountainous regions of eastern Siberia. The thermokarst associated with the thawing of underground ice develops on the valleys of mountain rivers. Solifluction, the flow of soil down the slope along ice-rich permafrost, is typical for deluvial-solifluction slopes, in mountain woodlands with solifluction, and connected by "drunken" forests with curved tree trunks. Thermoerosion is found on virtually all slopes, which takes the form of dales, ravines, and small valleys. Wet and dispersed deposits are dominated by frost cracking, and low centred polygons are formed on wetland tundra areas. On the waterlogged foothills of the mountain ranges and upland slopes, seasonal frost heaving is typical, and these areas are characterized by medallion spots, formed during the extrusion of clay soils in the active layer.

In the mountains, the frosty sorting of rocky material, which forms stone polygons, occurs on gentle slopes. These slopes also have kurums, peculiar stone streams, moving under gravity when thawing underground ice is present. In the river valleys, icings (*taryns*) often occur, which are formed by freezing of the outflowing groundwater. Over the winter, icings accumulate tens and hundreds of thousands of cubic metres of ice. The largest icing, the Ulakhan-Taryn, forms annually on the Moma River (uppermost stream in Indigirka River Basin) and covers an area of about 110 million m^2, and the thickness of the ice can reach 7 m.

8.3 Permafrost Structure (Profile, Ice)

8.3.1 Ice Complex (Yedoma) Distribution in Lena-Aldan Interfluve

Considering the extent of fossil ice, we should stress once more that, firstly, it is a specific genesis of ice type, namely, ice wedges; secondly, based on drilling data and on the geomorphological method of fossil ice charting for the extent of alases by Grave (1944; Grave and Zaklinskaya 1951), we can chart an ice complex, but not individual ice massifs.

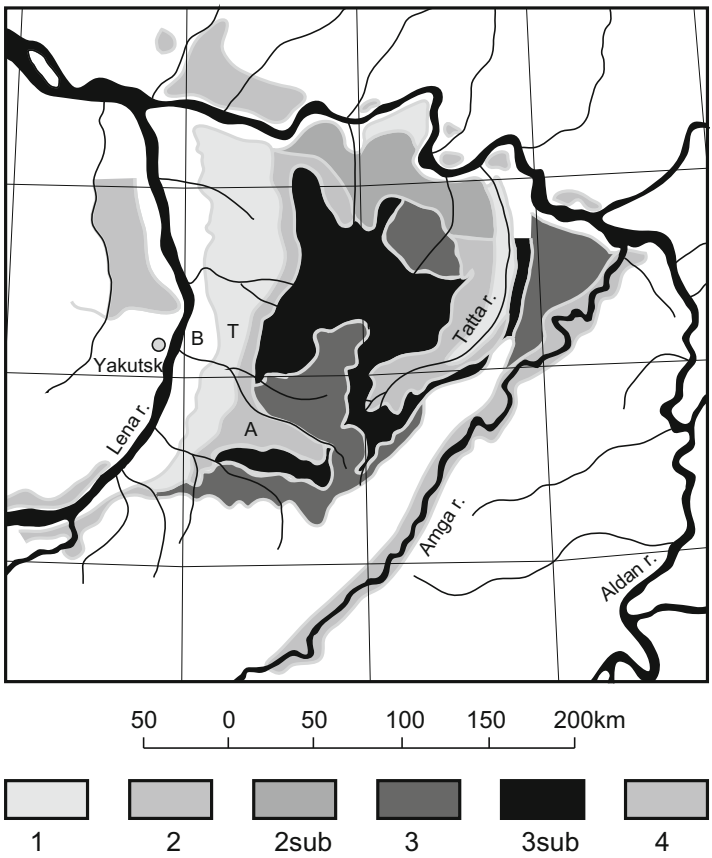

Fig. 8.4 Type of distribution in ice complex in Lena-Aldan interfluvial area. (Modified after Soloviev 1959)
1:Ice complex is confined to extensive flat watersheds in between recent river valleys. 2: Ice complex spreads both at watersheds and on the slopes and on some terraces in river valleys. 2 sub: Subregion of type 2 with erosion-alas relief. 3: Ice complex spreads mostly along old terraces in river valleys and is poorly developed within watersheds and slopes of valleys. 3 sub: Subregion of type 3 with extensive fossil ice at watersheds. 4: Types of sites listed above interlace depending on the type of terrace
B Bestyakh terrace, *T* Tyungyulyu terrace, *A* Abalaakh terrace

The ice complex in Yakutia from the remains of the Pleistocene glaciations occupies up to 1 million km^2, or 1/3 of the total area of permafrost. Ice content in the ice complex is different in various natural zones. The depth of the ice upper boundary in the tundra zone is 0.5–1.0 m and 1.9–2.3 m in the taiga zones.

The ice complex spreads within the limits of medium-altitude terraces, respective alluvial plains, and earlier relief elements; however, it does not cover them completely (Fig. 8.4). As a rule, ice veins are underdeveloped or do not exist on

flat tops of the most elevated relief elements in this region, especially if their area is small. However, on the lower parts of slopes of such elevations, the ice complex reaches its highest thickness due to ice growth from deluvium and syngenetic ice veins. The bottoms of alases, alas plains, and river valleys that developed due to later erosion are invariably ice-free (a certain degree of common sense is required for estimates of the possibility of plains being ice-free at the Magan terrace and older elements. Here, in the higher parts of the plains, we can find sites where the ice complex constituting the old plain bottom is not cut by the later erosion, and inter-alas areas of
relief are almost indistinguishable compared to a modern flood-plain). Generally, the ice complex can be found at almost all other elements of macrorelief in the area. In some regions, the ice complex is mostly connected with relief elements.

At Tyungyulyu terrace, the ice complex forms vast, flat watersheds with relatively low desiccation between the valleys of recent small rivers that are embedded in older rock formations. In the strip of land adjacent to the valleys (about 0.1–1.0 km wide) and on the slopes of the valleys, the ice complex usually does not exist, and within interfluves it covers both elevated and depressed sites of the inter-alas area. Within the region of oriented-alas relief, the ice complex, as a rule, occurs at old degradations and lies in strips between sand ridges.

At the Abalakh terrace (discussion of medium-altitude terraces also include their respective alluvial plains), the ice complex composes interfluve areas, as well as the terraces that correspond to the Tyungyulyu terrace in valleys and, as a rule, their slopes. In this area, elevations without an ice complex at the highest points are more frequent, but in general, like at the Tyungyulyu terrace, the ice complex forms an almost continuous field interrupted only by alas bottoms, river valleys, and individual ice-free elevations. We can often observe how the ice complex failed to develop in the medium part of the slopes of the Abalakh terrace.

The degree of dissection of the ice complex with ice-free sites of the types listed above varies quite a lot. In extreme cases, the ice complex is dissected into individual massifs – remnants of inter-alas areas – due to thermokarst processes or recent erosion at some sites; at other sites, it forms a solid massif torn by individual alases.

At the Magan terrace, the ice complex is connected with the Tyungyulyu and Abalakh terraces in the valleys of the rivers compartmentalizing it. On the slopes and watersheds between valleys, the ice complex is rarely found; it enters only along drainage cloughs in the upper parts of some valleys. In the northern parts of the interfluve, where the Magan terrace is highly dissected and quite low, an ice complex with a lower thickness covers large areas of the watersheds; in some locations, thick segregation ice can cover extensive areas, for instance, in the northern parts of the Tatta and Amga rivers' watershed.

It would be more feasible and practical to map fossil ice with a medium-scale topographic basis, if the connection between the occurrence of the ice complex and certain relief elements is taken as a basis for geographical demarcation. Judging from the thickness, depth, and frequency of the occurrence of fossil ice (Grave 1944;

Soloviev 1947), geographical demarcation should be considered not quite successful due to intra-region variations of the listed characteristics.

8.3.2 Shielding Layer

In areas of ice complex distributions, or Yedoma, the shielding layer (Efimov and Grave 1940), located between the boundary of the active layer and the upper part of the ice wedges, is important. In the literature, the shielding layer is also called the transition layer (Yanovsky 1933) and the transient layer (Shur 1988; Shur et al. 2005). The main function of this layer is to protect the ice complex from thawing under climate warming and anthropogenic disturbances, so we will adhere to the concept of "shielding layer".

The shielding layer contains a sufficient amount of ice and thereby increases the latent heat required for thaw, which gives stability to the permafrost from various influences (Shur et al. 2005). The thickness of the shielding layer varies depending on the environmental conditions and disturbance of the landscape. In eastern Siberia in the tundra zone, the thickness of the shielding layer under undisturbed conditions in the tundra is 0.4–0.6 m, 0.6–0.8 m in northern light forests, and 0.8–1.0 m in the middle taiga, although in damaged and recovering landscapes, the thickness of the shielding layer is usually less. The volumetric water content of the shielding layer is usually very different to the active layer and ground parts of the ice complex. Thus, in central Yakutia, the volumetric water content of the shielding layer (40–45%) is much higher than in the active layer (25–30%) and less than in the ice complex (55–60%).

The shielding layer, depending on climatic conditions and surface disturbances, is quite variable. According to our observations, in central Yakutia, on the disturbed sections of the ice complex (due to deforestation and burning of grassland, glades, and arable land, the shielding layer is only 0.3–0.1 m), the geocryological situation is critical. In warm and snowy years, the shielding layer completely disappears, since the active-layer thickness reaches the upper parts of the ice wedges. With the restoration of forest vegetation and the stabilization of the temperature regime of permafrost, the shielding layer self-regenerates.

The variability of the climate also affects the thickness of the shielding layer by increasing or decreasing the active-layer thickness. For example, the coefficient of variation in the active-layer thickness in the eastern part of central Yakutian ranges from 2.5 to 18.8% (Vasiliev 1982) and in the western part of central Yakutia from 4.5 to 24.9% (Vasiliev 2005). Based on the CALM (Circumpolar Active Layer Monitoring) data for Russia, the coefficient of variation is from 5 to 26%, with most values ranging from 5 to 15%. Analysis of the soil temperature data at the meteorological stations of central Yakutia shows that the most significant reductions in the protective layer occurred in the late 1970s to early 1980s, in early 1990s, and in the second half of the 2000s.

In opened grassland areas, there is a significant reduction in the shielding layer with its disappearance. In forest areas, the reduction of the shielding layer is insignificant, which is most likely due to the increase in above-ground biomass. Calculations using the method presented in Feldman et al. (1988) show that an increase in the above-ground biomass by 30% in the landscapes of the ice complex in central Yakutia causes a decrease in soil temperature by 0.3 °C and a decrease in the active-layer thickness by 0.08 m. This is confirmed by the fact that in the mature larch forests in central Yakutia we observed insignificant changes in the temperature of the soils and the active-layer thickness during the period of maximum warming, 1980–2010 (Varlamov et al. 2014), whereas in the open grassland areas of the ice complex, there is an active development of thermokarst with the degradation of permafrost.

New growth of the shielding layer is also possible under recent climatic fluctuations. We observed this phenomenon in studies of surface subsidence after clear-cutting in the Kys-Alas site on the left bank of the Lena River near Yakutsk in the period in early winter with less snow in 2002–2004. The early formation of thermokarst with a total surface subsidence of 10–15 cm for 1997–2001 was stopped with complete freezing of the formed talik zone and heaving of the ground. At the same time, the volumetric ice content in the interval of the thawed layer of 1.2–2 m was around 50–55% versus 30–35% before the subsidence. Soil heaving improved the drainage conditions, and regeneration of the birch forest began, and after 2004 the surface subsidence stopped due to the cessation of thawing of icy grounds. Here we see a combination of two stabilizing factors to the restoration of permafrost landscapes: the effect of short-term frost and the growth of vegetation. In contrast, if landscape is changed from boreal forest in ice complex to grassland in the thermokarst depression (alas), absolute height of landscape level changed till 4–10 m in average. Base line reaches the level of the ice complex surface.

Here we concur with the statement of Shur et al. (2005) on the essential role of the shielding (transient) layer in determining the dynamics of permafrost landscapes on the ice complex.

8.4 Permafrost Temperature Change

8.4.1 Long-Term Changes in Northern Eurasia

Russia has long records of ground temperature observations at a number of meteorological stations, with some records beginning in the 1890s and many others beginning in the 1930s or 1950s (Frauenfeld et al. 2004). Analyses of these observations have provided useful information about changes in thermal state of permafrost, such as the long-term deepening of the active layer (Frauenfeld et al. 2004) and increased permafrost temperatures (Romanovsky et al., 2007). More than half of Russia is composed of seasonally frozen non-permafrost zones, in which the maximum annual depth of soil freezing tended to be shallow from 1930 to 2000

(Frauenfeld and Zhang 2011). This geographical variation in Russia can result in regional differences in the response of ground temperature to changes in climate. These regional differences could explain the possible causes of the recent permafrost warming.

Composite time series of the surface air temperature (SAT), snow depth (SND), and ground temperature (T_{SOIL}: at the depth of 1.6 m) or all of west and east Russia were considered in Jones et al. (1999), who noted two distinct warming periods in the Arctic SAT time series, 1920–1945 and from 1975 to present. Similarly, the SAT warming since 1980 was the most significant in the Russian time series, where the maximum annual SAT anomaly reached 2 °C in 2007, coincident with the recorded minimum in Arctic sea ice cover. Warming over the last decade has been faster than during the 1930s and 1940s. Polyakov et al. (2003) reported that, over a large area north of 62°N, the 1938 maximum in the annual Arctic SAT anomaly was 1.69 °C, compared with the 2000 maximum of 1.49 °C. However, the earlier warming was not as fast as previously reported, with only slightly positive anomalies in the 1920s and 1930s. The earlier positive anomaly was more apparent in western than in eastern Siberia. Polyakov et al. (2003) reported that the SATs in western Siberia were strongly correlated with the North Atlantic Oscillation (NAO) index, whereas the Pacific influenced eastern Siberia.

The Russian SAT time series exhibited multidecadal variability with two distinct positive phases (1930–1950 and from 1980 to present) and two negative phases (before 1930 and 1950–1980), as reported by Polyakov et al. (2003). However, the negative phase from 1950 to 1980 was less prominent than in the pan-Arctic SAT time series considered by Serreze and Francis (2010) and AMAP (2011, pp. 2–4). The T_{SOIL} time series from 1950 to present also exhibited multidecadal variability, which is superimposed on the background warming trend of the SAT. Soil temperature is strongly dependent on SAT, and therefore T_{SOIL} trends generally follow SAT trends. The Russian T_{SOIL} anomalies changed from negative values to positive values by 1980, closely following the SAT phase change.

An interesting finding is that the multidecadal variability, found in the SAT and T_{SOIL} data, was also replicated in the composite time series of the SND anomalies. The SND exhibited negative values until 1980 and then changed to positive values. These positive SND anomalies since 1980 may have further amplified T_{SOIL} warming, in combination with higher SATs. In contrast, the decrease in SND in previous years could have enhanced the cooling of T_{SOIL}, in combination with cold winter SATs. The sharp decrease in SND in western Siberia during the last decade is associated with a pause in T_{SOIL} warming. This result suggests that the SND may be a factor that affects the trends in T_{SOIL} variability.

8.4.2 Long-Term Changes in Eastern Siberia

Permafrost area in Russian territory shows heterogeneous long-term trends in ground temperature (Pavlov and Malkova 2009): larger warming trends in ground

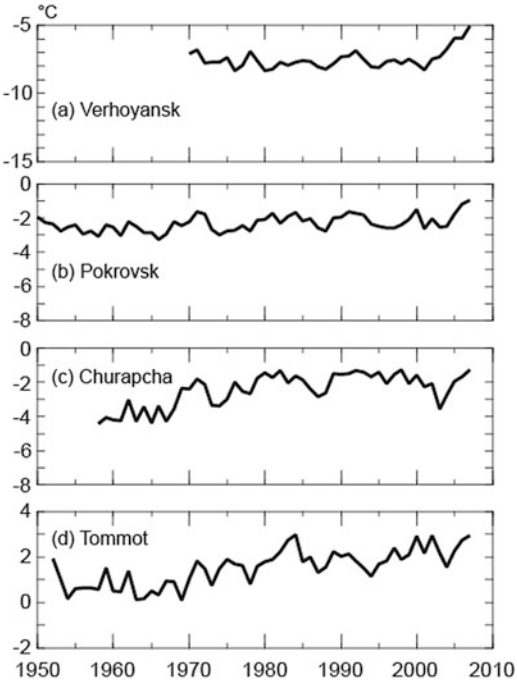

Fig. 8.5 Long-term variations in mean annual soil temperature at 3.2-m depth at (**a**) Verkhoyansk, (**b**) Pokrovsk, (**c**) Churapcha, and (**d**) Tommot

temperature with more than 0.03 °C year^{-1} in southern and western Siberia near the boundary of permafrost distribution, corresponding with warming trends in air temperature with more than 0.05 °C year^{-1}. There is also a large warming trend in central Yakutia with warming trends of ground temperature of 0.03 °C year^{-1}. In contrast, there are small or no significant trends (stable) in the tundra area along the coastal area in Lena and Kolyma river basins.

The long-term variations in the mean annual and annual minimum soil temperature at a depth of 3.2 m show regional characteristics at four stations in eastern Siberia since 1950 (Fig. 8.5). Until 2000, there are few coincident variations between stations: a strong warming trend was observed at Tommot in southern Lena (+0.024 °C year^{-1} during 1970–2000; $p < 0.01$), but no significant warming or cooling trends were observed at Pokrovsk and Churapcha (both in central Yakutia) or Verkhoyansk (in the Verkhoyansk mountain ranges). Romanovsky et al. (2007) reported a statistically significant positive trend in air temperature at most stations in the Lena River basin for the period 1956–1990. In addition, trends in ground temperature generally follow those of air temperature, with more pronounced warming occurring at lower latitudes. Fedorov and Konstantinov (2003) examined air temperature data at Yakutsk from 1931 to 2001 and found that a large positive anomaly was present after 1992. As suggested in previous studies, the long-term trend in ground temperatures, particularly in the continuous permafrost region, is less apparent than the trend in air temperature until 2004. Conversely, soil temperatures increased markedly at all stations after 2004. The mean annual temperature

anomalies in 2007 relative to the climatological mean (1970–2000) were + 2.6 °C at Verkhoyansk, +1.2 °C at Pokrovsk, +0.7 °C at Churapcha, and + 1.1 °C at Tommot, and the highest mean annual temperatures were recorded in 2007 at three continuous permafrost stations (Verkhoyansk, Pokrovsk, and Churapcha). The soil warming occurred abruptly at these stations and was particularly apparent for minimum temperatures. These observations imply a reduction in freezing due to changes in hydrothermal properties within the active layer as observed at the Spasskaya Pad site (Iijima et al. 2010). The soil warming that has occurred at these stations, which is consistent with the distribution of positive rainfall and snow depth anomalies, indicates that precipitation changes in both summer and winter have had a marked effect on hydrothermal conditions within the active layer and upper part of the permafrost in the continuous permafrost zone in eastern Siberia.

8.5 Active-Layer Thickness Change

The active-layer thickness (ALT) is one of the most important properties of permafrost environments. Many factors influence its variability. Spatial variability in the active-layer thickness primarily depends on landscape conditions, particularly lithological and geobotanical conditions. Its temporary variability depends on climatic conditions and anthropogenic influences. In this section, we consider only the spatiotemporal variability of the active-layer thickness.

8.5.1 Russia

Pavlov et al. (2004) analysed data from three geocryological stations – Vorkutinsky (1980–2003), Marre-Sale (1978–2002), and Chabyda (1986–2002) – and concluded that the trends in modern changes of the ALT vary with location: no trend at Vorkuta, positive at Marre-Sale, and negative at Chabyda. This demonstrates that the ALT is not a suitable indicator of global climate change.

An analysis of the temporal variability of the ALT was conducted by Frauenfeld et al. (2004), across the depths of the 0 °C isotherm using data from 31 weather stations on permafrost in central and eastern Siberia and the Far East. They found a statistically significant increase in the ALT of 20 cm for 1954–1990.

Zhang et al. (2005) estimated the variability of the ALT in Russia, in the basin of the Ob, Yenisei, and Lena rivers. The ALT was calculated and modelled using the thawing index, in the basin of the Lena River from the temperature data of 17 weather stations for 1956–1990. It was revealed that during this period the mean ALT increased by 32 cm, with a trend of 0.9 cm year^{-1}. However, they noted the difficulty in assessing the ALT response to predicted climate warming, especially due to the uncertainty in the influence of major natural factors such as seasonality of increasing trends of air temperature and spatial heterogeneity of snow cover.

Park et al. (2013) compared the variability of the ALT in Eurasia and North America in 1948–2006 based on the simulation results, depending on the thawing index, snow cover height, and soil moisture. For Russia, the simulation results were compared with field observations, which produced a relatively good correlation. According to the trends that they calculated, it can be estimated that the ALTs in the basins of the Ob, Yenisei, and Lena rivers were increased by 27, 11, and 12 cm, respectively. At the same time, it should be noted that there has been a general increase in the ALT since the 1990s.

Trends in the soil temperature and ALT in the Russian permafrost zone were studied using the daily soil temperature at weather stations in Russia at various depths (Sherstyukov and Sherstyukov 2015). For 2001–2011, the positive trend of the ALT was from 1 to 3 cm year^{-1}, and for many regions of permafrost, these trends were greater than those for the whole period of 1963–2011 (about 1 cm year^{-1}). However, during this period, areas with negative trends of ALT were also noted, for example, in south-west of Yakutia and the southern Baikal region. Analysis of the CALM data for Russia shows that almost all sites show an increase in the ALT from 1993 to 2016. In most areas, the linear trends in the increase of the ALT range from 0 to 0.5 cm year^{-1} (42% of the total number of sites). Significant trends from 0.5 to 1 cm year^{-1} were noted at 36% of the sites, and trends of 1 to 3.5 cm year^{-1} were found at 19% of sites, and only 2.8% of sites have a negative trend. Some of the differences in trends from previous results using daily temperature data for the determination of ALT are most likely due to the fact that the CALM sites are exposed to natural conditions and many weather stations (e.g. Yakutsk, Berdigestyah, Suntar, and Nyurba) are experiencing anthropogenic influence, primarily the waterlogging of the soils of the surrounding landscapes.

8.5.2 Central Yakutia

In central Yakutia, the variability of the ALT is well understood. Vasiliev and Torgovkin (1996) estimated the variability of the ALT across a 0 °C isotherm from the meteorological stations at Yakutsk, Pokrovsk, and Churapcha for 1967–1992. They noted large variations in the ALT with 9–11-year periodicity in its temporal dynamics. For this period, they note an increase in the ALT of 5–10%. Interannual variation in ALT shows synthesized temporal changes regardless of landscape types including boreal forest, grassland, and meadow in central Yakutia (Fig. 8.6). Deepening active-layer events had taken place from 2005 to 2008 due to continuous warm and wet climate years (Iijima et al. 2010).

Varlamov et al. (2014) published the results of long-term observations of the soil temperature and ALT in central Yakutia for different landscapes. The ALT was measured at the end of the thawing season by probing with a steel rod and by hand boring. The changes in the ALT from 1982 to 2013 indicated a positive trend in the bushy small valley and larch woodlands on peaty soils, up to 0.4 cm year^{-1}, and a negative trend on the slopes and watershed areas of plateaus of −0.15 to −1.9 cm year^{-1}.

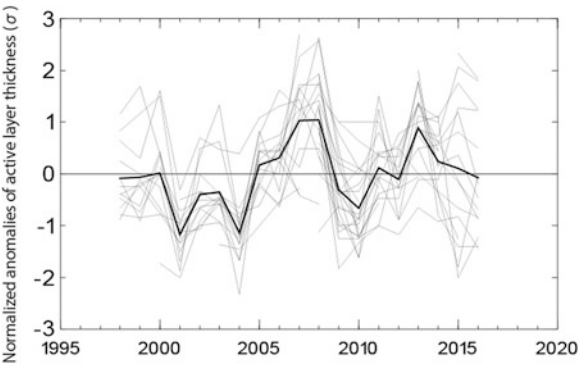

Fig. 8.6 Normalized anomalies of active-layer thickness monitored at various ladscape sites (27 sites) in central Yakutia A bold line denotes averge of all the data

Dynamics of the ALT have been performed at two CALM (Circumpolar Active Layer Monitoring) sites at Tuymada and Neleger in Yakutsk (R42 and R43 in CALM site code, respectively) using frost tubes from 2008 to present. Tuymada site is located on a sandy ridge of the second terrace of the Lena River with dry grassland, and Neleger site is located on the ice complex of the VII (Maganskaya) terrace of the Lena River with a typical larch forest. The trend of increasing ALT is not significant for the period 2008–2016 and is 0.17 and 0.15 cm year^{-1}.

Since 1998, at several sites with different landscapes near Yakutsk, at the Spasskaya Pad and Neleger stations, the ALTs were monitored by single frost tube on the ice complex at the Neleger station and on the slope of the Prilensky plateau at the Spasskaya Pad station for the period 1998–2016. Positive trends of 0.85 and 0.70 cm year^{-1} were observed, respectively. Both stations are characterized by typical larch forest on permafrost pale soils on sandy-loamy superficial deposits. On sandy ridges with pine forest at the Spasskaya Pad station, the ALT trend is 1.61 cm year^{-1} for the same period. In contrast, negative trends of the ALT has been observed with trends of -0.02 to -0.53 cm year^{-1} at serial landscape (birch-larch and birch forests regenerating after clear-cutting and fires with herbage-grass cover) at the same stations. Accumulating biomass in regenerative successions not only reduces the ALT but also lowers the permafrost temperature. Therefore, the study of the dynamics of the ALT should take into account the stages of successions in boreal ecosystem. Our landscape observations show that in central Yakutia, only 30% of the forest territory is occupied by invariant mature forests, and the rest are serial regenerative forests (Fedorov et al. 2006).

8.6 Permafrost Degradation in Forests (Forest Fires, Wetting)

The distribution of larch forest (taiga) over the extremely dry continental region in eastern Siberia can be explained by the existence of continuous, ice-rich permafrost which prevents deeper infiltration of the limited rainwater. The soil moisture is

stored within the active layer and consequently effectively used for vegetation. Conversely, forest vegetation acts as a thermal insulation buffer against heat and water exchange between the ground and the atmosphere, with the coexistence of permafrost and forest sustaining the taiga ecosystem. Increasing forest disturbances, such as forest fires, clear-cutting, and waterlogging during wet years, destroy much of the permafrost-surface vegetation symbiotic relationship by altering ground and surface conditions and ecohydrological aspects. To assess the atmosphere-vegetation-soil interaction in permafrost ecosystems, it is first necessary to understand the thermal and hydrological dynamics in the active layer after these disturbances.

8.6.1 Forest Fire

Forest fires are a recurrent disturbance in eastern Siberia among other disturbances (clear-cutting, agriculture, and construction). In particular, forest fires cause the largest disturbance in space in a short period. The resilience of the permafrost after the fire is the key factor in closely conjunction with forest regeneration. The fire disturbance in this region goes on different consequences due to its intensity and frequency; that is, the land surface recovers as previous state in case of shallower permafrost thawing, while it becomes irreversible with the formation of thermokarst depressions due to deeper permafrost thawing, namely, disappearance of shielding layer, and salinization originating from salt release from the melting ice within permafrost.

Extreme fire seasons now occur with more frequency and are characterized by dry periods during the warm season with high air temperatures and low relative humidity. Recent studies show that the period of increased risk of fire under current climate conditions in the central and western lowlands of the Sakha Republic is as long as 50–60 days (Dalbinov and Isaev 2006; Hayasaka et al. 2003). According to future climate scenarios, this will increase on average by 20–30 days by the end of the twenty-first century (Tchebakova et al. 2009). The overall trend of increasing forest fire occurrence further exacerbates the unprecedented thermal and hydrological conditions of the active layer described above and the related changes in vegetation.

For successful regeneration, the patterns of forest stand development after a fire are closely related to the recovery of the permafrost (Timofeev 2003; Gabysheva and Isaev 2015). The active-layer thickness becomes deeper (120–140 cm or more) shortly after a fire due to decreased albedo on the burnt surface and increased absorption of solar radiation on the forest floor. The increasing in ALT persists for several decades. Seedlings of larch rapidly grow, and self-thinning by intraspecific competition occurs during this period. Soil near the surface is warmer with high nutrient availability at this stage. By ca. 30 years after a fire, a ground cover of mosses and other plants regenerates on the forest floor and starts to act as an effective thermal insulator. This helps reduce the soil temperature during the summer and allows the aggregation of the permafrost table to rise towards the ground surface. The recovery of the permafrost table to pre-fire levels takes around 30 years.

8.6.2 Clear-Cutting

Iwahana et al. (2005) performed a field experiment on the effects of clear-cutting in larch forest on perennial changes in the hydrothermal regime of the active layer and the upper part of the permafrost near Yakutsk. Thermal and hydrological conditions in the active layer were investigated for a mature larch forest and cutover site during the thawing season in 2001 and 2002. Clear-cutting enhanced ground thawing, and the difference in the active-layer thickness between the forest and the cutover after 1 year was 14 cm. The soil water content drastically decreased in the forest, while that at the cutover was retained during the first thaw season after clear-cutting. Although the ground heat flux continued to increase at the cutover (the difference in the total amounts between sites from May to August was 44 and 69 MJ m^{-2} during 1 and 2 years after the clear-cutting, respectively), marked changes in the active-layer conditions were limited only to the first thaw season. The corresponding differences in the active-layer thickness between the sites were 16 and 14 cm after 2 and 3 years, respectively. Further increases in the maximum thaw depth at the cutover site were inhibited by the thermal inertial effect of the larger amount of ice in the second spring after the disturbance.

The overall impacts of forest clearing on the active layer were as follows (Fedorov et al. 2017): (1) There was a significant increase in soil temperature and the maximum thaw depth at the 1-year cutover site due to a larger ground heat flux. (2) There was a marked increase in soil water storage caused by reduced evapotranspiration at the 1-year cutover site. This suggests a self-retention mechanism for the active-layer thickness after a forest disturbance in this continuous permafrost zone.

8.6.3 Wet Climate

Iijima et al. (2010) observed unusual increases in the ground temperature and active-layer thickness within the central Lena River basin in eastern Siberia that had occurred in response to increases in both rainfall during pre-winter periods and snow accumulation observed between 2005 and 2008. Anomalous increases in snow depth and rainfall, which occurred throughout the central and southern parts of the Lena River basin during this 3-year period, resulted in increased levels of soil moisture and appear to have altered the thermal properties of the active layer. It was suggested that during previous years in which a prevailing dry climate was observed, permafrost thaw caused by increased ALT could have supplied water to trees, allowing the forest to function as normal (Sugimoto et al. 2003). Surpluses of surface water in recent years have provided positive feedbacks that have enhanced not only the degradation of permafrost but also the degradation of vegetation due to water being impounded in subsiding depressions. Iwasaki et al. (2010) observed yellowing and browning of larch tree (*Larix cajanderi* Mayr.) leaves resulting from

an abnormally high soil water content within the same undisturbed forest observed by Iijima et al. (2010). The potential impact of increased soil moisture on boreal ecosystems is great and must be considered when examining environmental perturbations induced by Arctic climatic change.

The changes in temperature and hydrology are evidenced by direct and cascading ecosystem change. With the large increase in precipitation in the research region since 2004/2005 winter in combination with near-surface permafrost thawing, soil moisture has increased substantially (Iijima et al. 2010; Hiyama et al. 2013). These perennially waterlogged conditions increase soil subsidence and affect the boreal forest habitat, specifically by changing soil conditions that no longer support the historical floral species. Increasingly, boreal forest trees are withering and dying throughout the region. According to multi-year sap flow measurements from 2006 to 2009, transpiration from larch trees was significantly reduced in conjunction with the deepening and moistening of the active layer (Fig. 8.7; Iijima et al. 2014). At the same research site, the number of living larch decreased by 15% from 1998 to 2011

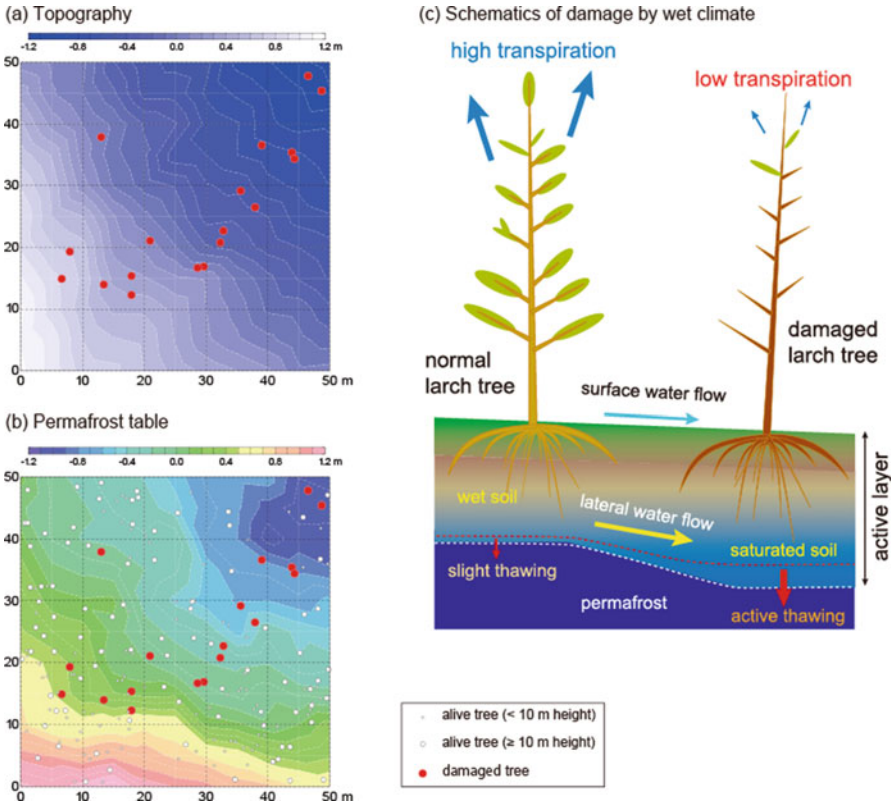

Fig. 8.7 (**a**) Microtopography and (**b**) permafrost table within a 50 × 50 m quadrate plot located within a larch forest in Spasskaya Pad, Yakutsk, with (**c**) schematic diagram of damage by wet climatic conditions

due to unusual waterlogged conditions, and the composition of floor vegetation changed from dense cowberry to grasses and shrubs with high water tolerance (Ohta et al. 2014). These same processes are evident at the aforementioned Yukechi site (Iijima et al. 2010; Fedorov et al. 2014a, b), with the increased moisture and deepening of the active layer in side slopes of thermokarst lakes resulting in lake expansion, topographic instability, and adjacent forest erosion.

8.7 Permafrost Degradation in Grassland (Thermokarst, Alas)

8.7.1 Evolution of Yedoma and Thermokarst Lakes

Field observations clearly indicate that thermokarst-lake basins have been expanding and the permafrost underneath has been thawing, due to both the warming climate and shifting hydrological processes. The exact extent of change is highly dependent on the specific context of each alas's physical characteristics. Data from Yukechi, a field site of central Yakutia located ca. 55 km ENE of Yakutsk, on the Abalaakh terrace illustrates the scope and speed of change.

The role of permafrost thawing in the water balance of a growing thermokarst lake was evaluated by long-term observations during the last two decades (1992–2008) at a thermokarst monitoring site in Yukechi. During the observation period, enhanced thermokarst activities have been observed since the early 1990s, and thus the water surface area increased steadily from 195 m^2 in 1993 to 3135 m^2 in 2008, and the lake water volume increased from 33.7 m^3 in 1993 to 3503 m^3 in 2008 (Fig. 8.8; Fedorov et al. 2014a). Melting ground ice has significantly contributed to the lake growth. Water balance estimates have shown that ground ice melt accounted for up to one third of the total water inflow into the lake. The total inflow of water

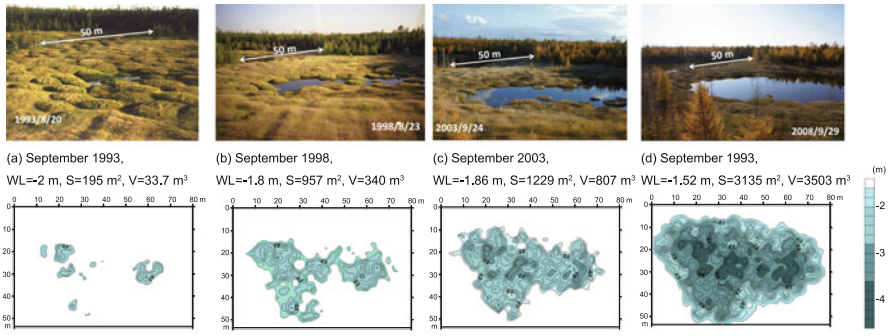

Fig. 8.8 Changes in the water body in the thermokarst lake in 1993 (**a**), 1998 (**b**), 2003 (**c**), and 2008 (**d**), at the Yukechi site. *WL* water level (m), *S* water body's area (m^2), *V* water body's volume (m^3). (Modified after Fedorov et al. 2014a)

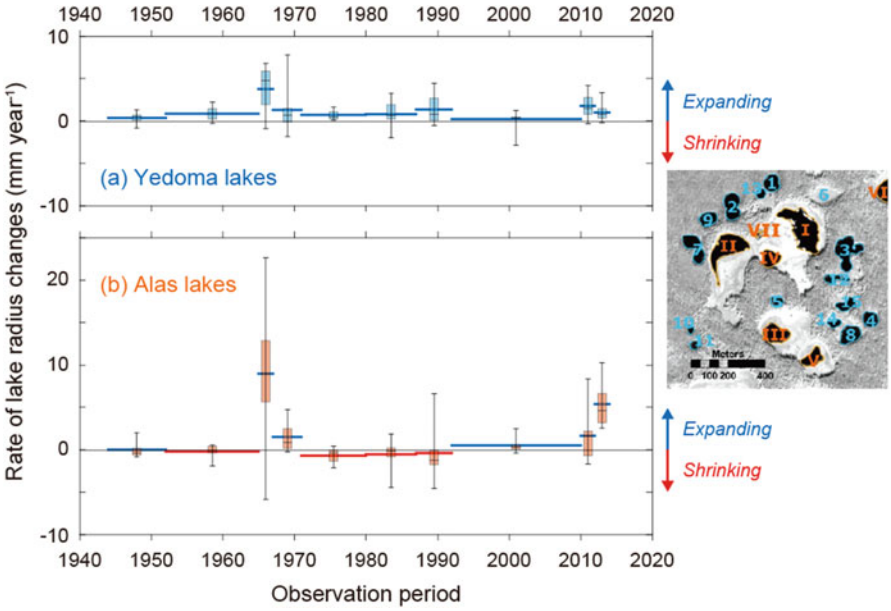

Fig. 8.9 The rates of Yedoma- and alas-lake radius changes (RLRC) for different time periods at Yukechi observation site in central Yakutia
The mean RLRCs during the individual time periods are plotted additionally as the arithmetric average values (blue, expanding; red, shrinking). The boxes are defined by the lower and upper quartiles. The line in the centre represents the median, and the whiskers at the end of each box indicate minimum and maximum outliers

from melting ground ice increased 2.4- and 5-fold in 1999–2003 and 2004–2008, respectively, compared with 1994–1998. The rapid development of growing thermokarst lakes indicates an ecological risk on the edges of cryogenic landscapes.

These young thermokarst lakes show different hydrological time series from old alas lakes (Fig. 8.9). Satellite and historical airborne imagery as well as high-resolution topographical data in Yukechi could exhibit the differences in thermokarst-lake sizes and evolution (Ulrich et al. 2017). Young thermokarst lakes have been rapidly evolving on Yedoma uplands during the last 70 years (since the 1950s). The thermokarst activity was mainly initiated by the anthropogenic destruction of forest cover and notably increased during the last two decades due to changing climatic and permafrost conditions. The area of residual lakes within alas basins oscillates with changing climatic conditions, but comparatively large catchment areas and subsurface hydrological conditions could also have played an important role. Statistical analyses of long-term climatic data show that winter precipitation and winter temperatures as well as active-layer properties are the main significant factors controlling the water balance of both kinds of lakes, but summer weather and permafrost conditions also influence significantly the Yedoma-lake growth.

8.7.2 *Emerging Degradation in Dry Grassland (Churapcha)*

Churapcha is one of the largest rural settlements in the middle reaches of the Lena River in the central Yakutian region of eastern Siberia. The landscape of this area is dominated by boreal forest (larch) with numerous thermokarst depressions (alas) and dry grassland (mixtoherboso-graminesum with steppe flora; Karavaev 1955; Andreev et al. 1987) that have been preserved from the end of the Pleistocene through the Holocene (Soloviev 1959); both the forest and grassland overlay an extensive ice complex (10–15 m depth; Gorokhov et al. 2011). One of the largest dry grasslands was initially developed as an airport runway, but the runway was closed at the end of the 1980s. In addition to the grassland, agricultural fields developed in the 1970s, and a construction site in the settlement has also experienced considerable subsidence in recent decades. Since 2010, thermokarst subsidence and ponding along with polygonal trough formation have occurred extensively in the dry grassland (Gorokhov et al. 2011).

At a high-centred polygon with a diameter of ca. 5 m near the abandoned runway (61°59 N, 132°27E), a clear difference in active-layer conditions was detected between the troughs and top of the polygon. Based on a detailed description of soil profiles, the distribution of silty loam soils (bulk density of 2.7 g cm^{-3}) was homogeneous, regardless of the presence or absence of underlying ice wedges in these grasslands. The top of the ice wedges appeared at depths of around 2.2 m at most measurement points in the dry grassland. Troughs, therefore, developed on melted syngenetic ice wedges (Soloviev 1959; Czudek and Demek 1970) and exhibited 50–70 cm of thermokarst subsidence during recent decades.

An additional notable feature of the active-layer structure was the presence of a very soft layer detected by measurements using a handheld penetrometer (Iijima et al. 2017). Small Nc values (1–3), which are a function of the number of impacts required for every 10 cm of penetration, were observed at the deeper part of the active layer below troughs. This soft layer was associated with a high soil moisture content that reached the liquid limit (Fig. 8.10). It is considered that the wet layer might be caused by a combination of melted ice wedge and the penetration of precipitated water and snow melt water along polygonal troughs. The combined anomalous effect of precipitation in summer and snow in winter on soil wetting has been commonly observed in central Yakutia as shown in Sect. 8.6.3. The increased precipitation observed prior to the winter of 2004 resulted in a high soil moisture content, which led to both increased thermal conductivity during summer and a deeper active layer in subsequent years. The soft layer was still present in 2014 at the Spasskaya Pad and Yukechi research sites near Yakutsk. The existence of a wet (soft) layer in the deeper parts of the active layer is very important for increasing heat conductivity and capacity. Consequently, the perennially wet active layer will be a good measure for permafrost degradation under wet climatic conditions.

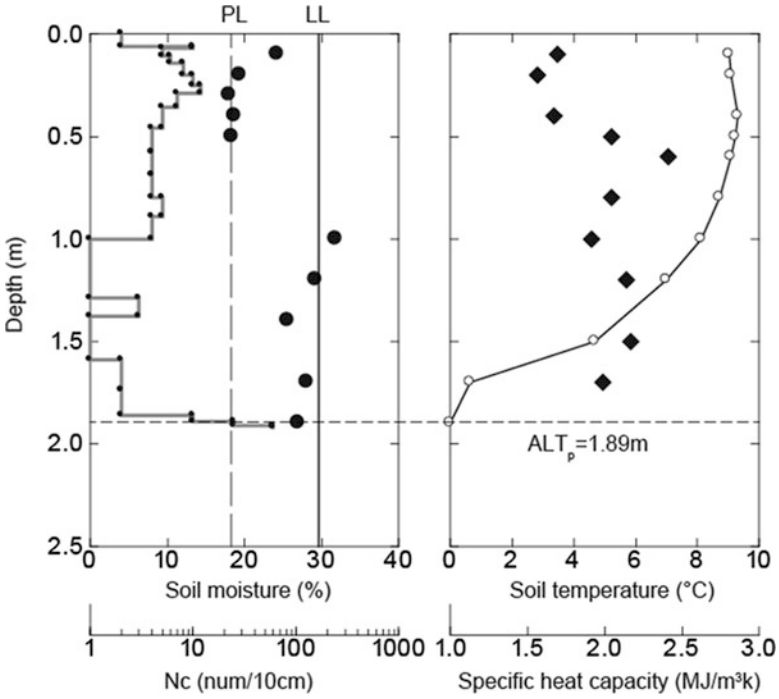

Fig. 8.10 Vertical profiles of Nc values and soil properties at a grassland site at Churapcha (September 2014). (Modified after Iijima et al. 2017)
(**a**) Nc values and soil moisture: Grey line = Nc values; solid circles = volumetric soil moisture content (VSM). PL and LL of soil samples are based on laboratory measurements at the Melnikov Permafrost Institute, Yakutsk
(**b**) Soil temperature and specific heat capacity: Diamonds = specific heat capacity; thin line with open circles = soil temperature. *Nc* Number of impacts required for every 10 cm of penetration, *ALTp* active-layer thickness indicated by the penetrometer, *PL* plastic limit, *LL* liquid limit

8.8 Future Climate Projection

The Intergovernmental Panel on Climate Change's (IPCC) fifth assessment clearly links increasing air temperatures with permafrost decrease (IPCC 2013). It also predicts that by the end of the twenty-first century, the near-surface permafrost area will shrink by 37%, even in the lowest emissions scenario (RCP2.6). Scientists also predict a significant thawing of the near-surface permafrost by the end of the twenty-first century for large parts of Russia, Alaska, and Canada (Romanovsky et al. 2008; Zhang et al. 2008; Jafarov et al. 2012). This thawing will increase the active layer and expand taliks (i.e. bodies of unfrozen ground within the permafrost) and thermokarst processes. Assuming an increase of the mean active-layer depth of only 10 cm under the soil conditions of central Yakutia, one can estimate that this will release on average about 30 mm of water, or 30,000 tons of water per km^2 (Desyatkin unpublished data). Such amounts of water will expand lakes and adjacent

waterlogged territories and, with enhancing precipitation, cause catastrophic flooding of small rivers in summer. Increasing the depth of seasonal thaw transforms the water balance of permafrost areas which will greatly affect biodiversity, ecosystem productivity, and human use of large areas.

Prediction of permafrost landscape change is not straightforward but still hindered with much uncertainty, considering the cascading ecosystem effects, the sociocultural interactions, and the current incomplete understanding of hydrothermal processes. The IPCC estimate for the mean global temperature increase using its conservative RCP2.6 emissions scenario is around +1 °C by the end of this century (IPCC 2013), which is close to the level of warming during the Holocene climate optimum, when most of the alas in central Yakutia formed. The alas density map (Fig. 8.2) suggests that the consequences of such temperature change today may be less drastic that expected, as it shows that with a + 1 °C temperature change during the Holocene climate optimum only 10–20% of the ice complex of central Yakutia had experienced degradation. This strongly indicates that the resilience of alas permafrost landscapes might be sufficient for 80–90% of the permafrost areas of the ice complex type to remain, i.e. areas with underlying large ice wedges and high ground-ice contents.

To illustrate the dynamism of this system further, this resilience can be offset by vulnerability specific to local/regional conditions, including vegetative land-cover conditions and geomorphology (Jorgenson et al. 2010). In forested areas, permafrost stability is usually buffered by the shielding layer, which prevents the underlying icy deposits from thawing even under severe climate change (Shur et al. 2005). Research suggests that in the Late Pleistocene and Early Holocene, the shielding layer below forested permafrost landscapes prevented the ice complex from thawing (Konishev 2011). The presence of a sufficiently strong shielding ground layer (up to 1 m thick) in the contemporary boreal forests of the Sakha Republic testifies to the stability of permafrost in forest landscapes. Katamura et al. (2009), however, show that forest fires were only one of multiple causes that induced the formation of alas, as evidenced by the remains of charcoal in alas sediments. The risk of permafrost degradation is thus generally higher in disturbed landscapes (e.g. those affected by forest fires) and open, treeless areas in which the shielding layer is shallower or even absent. If in such areas the depth of seasonal thawing reaches the horizon of the ice complex, rapid permafrost degradation is very likely to ensue.

Geomorphological characteristics also factor into vulnerability. According to Bosikov and Ivanov (1978), in previous warming climate events, the better-drained surface of the Abalaakh ice complex in the Lena-Amga interfluve region was less affected by degradation than the less drained surface of the Tyungulu terrace, which accumulated considerable amounts of surface and supra-permafrost water.

Moreover, future predictions must accommodate a multitude of nascent factors relevant to our contemporary world, with perhaps the most important being the alteration of carbon fluxes and greenhouse gas (GHG) emissions. Three aspects relevant to alas ecosystems are as follows: (1) the reduction of the soil carbon stock from utilization of thermokarst basins as pastures and haymaking areas (Desyatkin et al. 2009); (2) the increased emission of GHGs from medium moist and wet

grasslands in hot summers (Takakai et al. 2008); and (3) the increased emission of methane due to decomposition of carbon stored in flooded grasslands and during thaw processes below thermokarst lakes (Walter et al. 2006; Desyatkin et al. 2009; Schuur et al. 2015).

8.9 Concluding Remarks

Understanding thermal and hydrological changes in permafrost near the surface in eastern Siberia in terms of the initiation of the melting Yedoma ice complex and geographical distribution of already degraded and/or potentially destabilized landscape is essential. Permafrost landscape changes will impact indigenous livelihood and economies, as has already been witnessed at the local and regional levels, and regional, continental, and global influences will amplify feedback mechanisms between the climate and water and carbon cycling through permafrost degradation accompanying with boreal ecosystem changes.

Investigating the spatial and temporal distribution of permafrost and the impact of changes in permafrost-related processes from ecological, hydrological, and sociological perspectives will thus help to understand the factors influencing the warming and thawing of the permafrost, estimate the future landscape evolution, and evaluate the local and global impacts on land surface interactions in a changing climate.

References

AMAP (2011) Snow, Water, Ice and Permafrost in the Arctic (SWIPA): climate change and the cryosphere

Andreev VN, Galaktionova TF, Perfilieva VI, Sherbakov IP (1987) Main specialty of vegetation cover of Yakutskaya ASSR. Yakutsk, 157 p. (in Russian)

Balobaev VT (1991) Geothermy of the frozen zone of the lithosphere of the north of Asia. Nauka, Novosibirsk, 194 p. (in Russian)

Bosikov NP (1991) Evolution of Alases in Central Yakutia. Permafrost Institute, Siberian Division of Russian Academy of Science, Yakutsk, Russia, 127 p. (in Russian)

Bosikov NP, Ivanov MS (1978) in Geokriologicheskie usloviia v gorakh i na ravninakh Azii [Geocryological conditions in the mountain ranges and plains of Asia] (eds: Nekrasov IA, Klimovskii IV). Institut merzolotovedeniia SO AN SSSR, Yakutsk, pp 113–118 (in Russian)

Brouchkov A, Fukuda, M, Fedorov A, Konstantinov P, Iwahana G (2004) Thermokarst as a short-term permafrost disturbance. Central Yakutia, Permafrost Periglac., Proc, 15, pp 81–87

Chudinova SM, Frauenfeld OW, Barry RG, Zhang T, Sorokovikov VA (2006) Relationship between air and soil temperature trends and periodicities in the permafrost regions of Russia. J Geophys Res 111:F02008. https://doi.org/10.1029/2005JF000342

Crate S, Ulrich M, Habeck JO, Desyatkin AR, Desyatkin RV, Fedorov AN, Hiyama T, Iijima Y, Ksenofontov S, Mészáros C, Takakura H (2017) Permafrost livelihoods: a transdisciplinary review and analysis of thermokarst-based systems of indigenous land use. Anthropocene 18:89–104. https://doi.org/10.1016/j.ancene.2017.06.001

Czudek T, Demek J (1970) Thermokarst in Siberia and its influence on the development of lowland relief. Quat Res 1:103–120

Dalbinov AA, Isaev AP (2006) Reconstruction of forest fires in the 20th century (on the example of Namsky, Khangalassky and Yakut leskhozes). Forest research in Yakutia: results, status and prospects. Vol. 1: Permafrost silvics and forestry. Forest ecology. Zkutsk University Press, Yakutsk, pp 100–103

Desyatkin RV (2008) Soil formation in thermokarst depressions – Alases of cryolithozone, Novosibirsk "Nauka" (in Russian)

Desyatkin AR, Takakai F, Fedorov PP, Nikolaeva MC, Desyatkin RV, Hatano R (2009) CH4 emission from different stages of thermokarst formation in Central Yakutia. Soil Sci Plant Nutr 55:558–570

Desyatkin AR, Takakai F, Hatano R (2014) Flood effect on CH4 emission from the alas in Central Yakutia, East Siberia. Soil Sci Plant Nutr 60:242–253

Efimov AI, Grave NA (1940) Buried ice of the region of Abalakh lake, socialist construction. Yakutsk 10–11:65–78 (in Russian)

Fedorov AN, Konstantinov P (2003) Observations of surface dynamics with thermokarst initiation, Yukechi site, central Yakutia. In: Proceedings of the 8th International conference on Permafrost, Zurich, Switzerland, pp 239–243

Fedorov AN, Botulu TA, Varlamov SP, Vasiliev IS, Gribanova SP, Dorofeev IV, Klimovsky IV, Samsonova VV, Soloviev PA et al (1989) Permafrost landscapes of Yakutia. Explanatory note to the permafrost landscape Yakutskaya ASSR map scale of 1: 2 500 000. GUGK, Novosibirsk, 170 p. (in Russian)

Fedorov AN, Maximov TC, Gavriliev PP, Skachkov YB, Desyatkin RV, Isaev AP, Konstantinov PY, Vasiliev IS, Ugarov IS, Efremov PV, Argunov RN, Nikolaev AN (2006) Spasskaya Pad: complex studies of permafrost landscapes. Permafrost Institute, Yakutsk, 210 p. (in Russian)

Fedorov AN, Gavriliev PP, Konstantinov PY, Hiyama T, Iijima Y, Iwahana G (2014a) Estimating the water balance of a thermokarst lake in the middle of the Lena River basin, eastern Siberia. Ecohydrology 7(2):188–196. https://doi.org/10.1002/eco.1378

Fedorov AN, Ivanova RN, Park H, Hiyama T, Iijima Y (2014b) Recent air temperature changes in the permafrost landscapes of northeastern Eurasia. Polar Sci 8(2):114–128. https://doi.org/10.1016/J.POLAR.2014.02.001

Fedorov AN, Iwahana G, Konstantinov PY, Machimura T, Argunov RN, Efremov PV, Lopez LMC, Takakai F (2017) Variability of permafrost and landscape conditions following clear cutting of larch forest in Central Yakutia. Permafr Periglac Process 28(1):331–338. https://doi.org/10.1002/ppp.1897

Feldman GM, Tetelbaum AS, Shender NI, Gavriliev RI (1988) Handbook of temperature forecast of the soils in Yakutia. Permafrost Institute, Yakutsk, 240 p. (in Russian)

Frauenfeld and Zhang (2011) An observational 71-year history of seasonally frozen ground changes in the Eurasian high latitudes. Environ Res Lett 6:044024

Frauenfeld OW, Zhang T, Barry RG, Gilichinsky D (2004) Interdecadal changes in seasonal freeze and thaw depths in Russia. J Geophys Res 109:D05101. https://doi.org/10.1029/2003JD004245

Gabysheva LP, Isaev AP (2015) Forest fires impact on microclimatic and soil conditions in the forests of cryolithic zone (Yakutia, North-Eastern Russia). Sibirskij Lesnoj Zhurnal (Siberian J For Sci) 6:96–111 (in English with Russian abstract)

Gorokhov AN, Fedorov AN, Skorve J, Makarov VS (2011) Assessment of anthropogenic variability of landscapes surrounding area with Churapcha (Central Yakutia) on the basis of remote sensing data. Probl Reg Ecol 4: 7–13 (in Russian with English abstract)

Grave NA (1944) Fossil ices of Lena and Aldan watersheds. In: Trudy of V.A. Obruchev permafrost institute, vol 4. Publishing House of the Academy of Sciences of the USSR, Leningrad, pp 10–32. (in Russian)

Grave NA, Zaklinskaya ED (1951) About buried ice at the mouth of the Anadyr River and some moments of the quaternary history of this area. In: Proceedings of the meeting on the study of ice

and snow. Publishing House of the Academy of Sciences of the USSR, Moscow, pp 230–245. (in Russian)
Grosse G, Jones B, Arp C (2013) Thermokarst lakes, drainage, and drained basins. In: Shroder JF (ed) Treatise on geomorphology. Academic, San Diego, pp 325–353
Groswald MG (1998) Paleohydrology of Eurasia in the era of the last glaciation. Materials of glaciological studies, vol 84, pp 121–129. (in Russian)
Hayasaka H, Fukuda M, Kushida K, Jandt R, Fedorov AN (2003) Forest fires and climate in Alaska and Sakha: forest fires near Yakutsk. In: Second International wildland fire ecology and fire management Congress and fifth symposium on fire and forest meteorology, 16–20 November 2003, Orlando, FL [program volume and electronic resource]. American Meteorological Society, Boston, MA, p 164
Hinkel KM, Eisner WR, Bockheim JG, Nelson FE, Peterson KM, Dai X (2003) Spatial extent, age, and carbon stocks in drained thaw lake basins on the Barrow Peninsula, Alaska. Arct Antarct Alp Res 35:291–300
Hinzman LD, Kane DL, Gieck RE, Everett KR (1991) Hydrologic and thermal properties of the active layer in the Alaskan Arctic. Cold Reg Sci Technol 19:95–110
Hiyama T, Asai K, Kolesnikov AB, Gagarin LA, Shepelev VV (2013) Estimation of the residence time of permafrost groundwater in the middle of the Lena River basin, eastern Siberia. Environ Res Lett 8:035040. https://doi.org/10.1088/1748-9326/8/3/035040
Hubberten HW, Andreev A, Astakhov VI et al (2004) The periglacial climate and environment in northern Eurasia during the last glaciation. Quat Sci Rev 23:133–1357
Iijima Y, Fedorov AN, Park H, Suzuki K, Yabuki H, Maximov TC, Ohata T (2010) Abrupt increases in soil temperatures following increased precipitation in a permafrost region, central Lena River basin, Russia. Permafr Periglac Process 21:30–41. https://doi.org/10.1002/ppp.662
Iijima Y, Ohta T, Kotani A, Fedrov AN, Kodama Y, Maximov TC (2014) Sap flow changes in relation to permafrost degradation under increasing precipitation in an Eastern Siberian larch forest. Ecohydrology 7:177–187. https://doi.org/10.1002/eco.1366
Iijima Y, Park H, Konstantinov PY, Pudov GG, Fedorov AN (2017) Active layer thickness measurements using a handheld penetrometer at boreal and tundra sites in eastern Siberia. Permafr Periglac Process 28:306–313. https://doi.org/10.1002/ppp.1908
IPCC (Intergovernmental Panel on Climate Change) (2013) Climate change 2013: the physical science basis. Contribution working group I to the fifth assessment report of the intergovernmental panel on climate change (eds: Stocker TF, Qin D, Plattner G-K, Tignor M, Allen SK, Boschung J, Nauels A, Xia J, et al) Cambridge University Press, Cambridge, pp 3–29
Ivanov MS (1984) The cryogenic structure of quaternary deposits of Lena-Aldan depression. Nauka, Novosibirsk (in Russian)
Iwahana G, Machimura T, Kobayashi Y, Fedorov AN, Konstantinov PY, Fukuda M (2005) Influence of forest clear-cutting on the thermal and hydrological regime of the active layer near Yakutsk, eastern Siberia. J Geophys Res 110:G02004. https://doi.org/10.1029/2005JG000039
Iwasaki H, Saito H, Kuwao K, Maximov TC, Hasegawa S (2010) Forest decline caused by high soil water conditions in a permafrost region. Hydrol Earth Syst Sci 14:301–307
Jafarov EE, Marchenko SS, Romanovsky VE (2012) Numerical modeling of permafrost dynamics in Alaska using a high spatial resolution dataset. Cryosphere 6:613–624
Jones PD, New M, Parker DE, Martin S, Rigor IG (1999) Surface air temperature and its changes over the past 150 years. Rev Geophys 37:173–199
Jorgenson MT, Romanovsky V, Harden J, Shur Y, O'Donnell J, Schuur EAG, Kanevskiy M, Marchenko S (2010) Resilience and vulnerability of permafrost to climate change. Can J For Res 40:1219–1236. https://doi.org/10.1139/X10-060
Kane DL, Hinkel KM, Goering DJ, Hinzman LD, Outcalt SI (2001) Non-conductive heat transfer associated with frozen soils. Glob Planet Chang 29:275–292
Karavaev MN (1955) Paleogeographycal reconstruction of landscapes of Central Yakutian plain in Cainozoe. Doklady Academii nauk USSR 102(4):797–799

Katamura F, Fukuda M, Bosikov NP, Desyatkin RV, Nakamura T, Moriizumi J (2006) Thermokarst formation and vegetation dynamics inferred from a palynological study in central Yakutia, eastern Siberia, Russia. Arct Antarct Alp Res 38:561–570

Katamura F, Fukuda M, Bosikov NP, Desaytkin RV (2009) Charcoal records from thermokarst deposits in central Yakutia, eastern Siberia: Implications for forest fire history and thermokarst development. Quat Res 71:36–40

Katasonov EM, Ivanov MS (1973) Cryolitology of Central Yakutia. Guide to tours of Lena and Aldan. Rotaprint of the OUPES Siberian Branch of Academy of Sciences of the USSR, Yakutsk, p 37. (in Russian)

Katasonov EM, Ivanov MS, Pudov GG, Katasonova EG, Siegert C (1979) The structure and absolute geochronology of alas deposits in Central Yakutia. Edited by Katasonov. Nauka, Novosibirsk, p 95. (in Russian)

Kondratieva KA, Fotiev SM, Danilova NS (1989) Geocryology USSR. Middle Siberia. Edited by Ershov. Nedra, Moscow. 413 p. (in Russian)

Konishev VN (2011) Permafrost reaction on Global Warming. The Earth Cryosphere XV(4):15–18

Lemke P, Ren J, Alley RB, Allison I, Carrasco J, Flato G, Fujii Y, Kaser G, Mote P, Thomas RH, Zhang T (2007) Observations: changes in snow, ice and frozen ground. In: Solomon S, Qin D, Manning M, Chen Z, Marquis M, Averyt KB, Tignor M, Miller HL (eds) Climate Change 2007: The physical science basis. Contribution of working group I to the Fourth assessment report of the Intergovernmental Panel on Climate Change. Cambridge University Press, Cambridge, pp 337–383

Milkov FN (1970) Dictionary-handbook of physical Geography. Mysl, Moscow, 235 p. (in Russian)

Morgenstern A, Ulrich M, Günther F, Roessler S, Fedorova IV, Rudaya NA, Wetterich S, Boike J, Schirrmeister L (2013) Evolution of thermokarst in East Siberian ice-rich permafrost – a case study. Geomorphology 201:363–379

Ohta T, Hiyama T, Tanaka H, Kuwada T, Maximov TC, Ohata T, Fukushima Y (2001) Seasonal variation in the energy and water exchanges above and below a larch forest in eastern Siberia. Hydrol Process 15:1459–1476. https://doi.org/10.1002/hyp.219

Ohta T, Maximov TC, Dolman AJ, Nakai T, van der Molen MK, Kononov AV, Maximov AP, Hiyama T, Iijima Y, Moors EJ, Tanaka H, Toba T, Yabuki H (2008) Interannual variation of water balance and summer evapotranspiration in an eastern Siberian larch forest over a 7-year period (1998-2006). Agric For Meteorol 148:1941–1953. https://doi.org/10.1016/j.agrformet.2008.04.012

Ohta T, Kotani A, Iijima Y, Maximov TC, Ito S, Hanamura M, Kononov AV, Maximov AP (2014) Effects of waterlogging on water and carbon dioxide fluxes and environmental variables in a Siberian larch forest, 1988–2011. Agric For Meteorol 188:64–75. https://doi.org/10.1016/j.agrformet.2013.12.012

Osterkamp TE (2007) Causes of warming and thawing permafrost in Alaska. Eos Trans AGU 88 (48):522. https://doi.org/10.1029/2007EO480002

Park H, Walsh J, Fedorov AN, Sherstiukov AB, Iijima Y, Ohata T (2013) The influence of climate and hydrological variables on opposite anomaly in active-layer thickness between Eurasian and North American watersheds. Cryosphere 7:631–645

Pavlov AV (2003) Permafrost-climatic changes in northern Russia: observations, forecast. Izvestiya RAS Seriya geograficheskaya 6:39–50. (in Russian)

Pavlov AV, Malkova GB (2009) Small-scale cartography of trends modern changes of temperature of soils. Kriosfera Zemli 13(4):32–39 (in Russian)

Pavlov AV, Skachkov YB, Kakunov NB (2004) The correlation between perennial changes of soil seasonal thawing depth and meteorological factors. Kriosfera Zemli 8(4):3–11 (in Russian)

Pestryakova LA, Herzschuh U, Wetterich S, Ulrich M (2012) Present-day variability and Holocene dynamics of permafrost-affected lakes in central Yakutia (Eastern Siberia) inferred from diatom records. Quat Sci Rev 51:50–70

Polyakov IV, Bekryaev RV, Alekseev GV, Bhatt US, Colony RL, Johnson MA, Maskshtas AP, Walsh D (2003) Variability and trends of air temperature and pressure in the maritime Arctic, 1875–2000. J Clim 15:2067–2077

Romanovskii NN, Gavrilov AV, Zaitsev VN (1989) Geocryology USSR. Eastern Siberia and the far east. Edited by Ershov. Nedra, Moscow, 516 p. (in Russian)

Romanovskii NN, Hubberten H-W, Gavrilov AV, Tumskoy VE, Tipenko GS, Grigoriev MN, Siegert C (2000) Thermokarst and land-ocean interactions, Laptev Sea Region, Russia. Permafr Periglac Process 11:137–152

Romanovsky VE, Sazonova TS, Balobaev VT, Shender NI, Sergueev DO (2007) Past and recent changes in air and permafrost temperatures in eastern Siberia. Glob Planet Chang 56:399–413

Romanovsky VE, Kholodov AL, Marchenko SS, Oberman NG, Drozdov DS, Malkova GV, Moskalenko NG, Vasiliev AA, Sergeev DO, Zheleznyak MN (2008) Thermal state and fate of permafrost in Russia: first results of IPY. In: Kane DL, Hinkel KM (eds) Proceedings of the ninth International conference on Permafrost, University of Alaska, Fairbanks, June 29–July 3, 2008, pp 1511–1518

Serreze MC, Francis JA (2010) The Arctic amplification debate. Clim Chang 76:241–264

Sherstyukov AB, Sherstyukov BG (2015) Spatial features and new trends in the thermal state of soils changes and the depth of seasonal thawing in the permafrost zone. Meteorol Hydrol 2:5–12 (in Russian)

Shur YL (1988) The upper horizon of permafrost and thermokarst. Nauka, Novosibirsk. 213 p. (in Russian)

Shur YL, Hinkel KM, Nelson FE (2005) The transient layer: implication for geocryology and climate-change science. Permafr Periglac Process 16:5–17

Soloviev PA (1947) Distribution of fossil firn ice distribution in the Lena-Amga interfluve. Permafrost 2(2). (in Russian)

Soloviev PA (1959) Cryolithozone of the northern part of Lena-Amga interfluve. Academy of Science of the USSR Press, Moscow, p 144

Soloviev PA (1973) Thermokarst phenomena and landforms due to frost heaving in central Yakutia. Biul Peryglac 23:135–155

Sugimoto A, Naito D, Yanagisawa N, Ichiyanagi K, Kurita N, Kubota J, Kotake T, Ohata T, Maximov TC, Fedorov AN (2003) Characteristics of soil moisture in permafrost observed in East Siberian taiga with stable isotopes of water. Hydrol Process 17:1073–1092. https://doi.org/10.1002/hyp.1180

Takakai F, Desyatkin AR, Lopez CML, Fedorov AN, Desyatkin RV, Hatano R (2008) CH4 and N2O emissions from a forest-alas ecosystem in the permafrost taiga forest region, eastern Siberia, Russia. J Geophys Res 113:G02002. https://doi.org/10.1029/2007JG000521

Tchebakova NM, Parfenova E, Soja AJ (2009) The effects of climate, permafrost and fire on vegetation change in Siberia in a changing climate. Environ Res Lett 4(4). https://doi.org/10.1088/1748-9326/4/4/045013

Timofeev PA (2003) Forests of Yakutia. Composition, resources, use and protection. Nauka, Novosibirsk, 193 p

Ulrich M, Grosse G, Strauss J, Schirrmeister L (2014) Quantifying wedge-ice volumes in Yedoma and thermokarst-basin deposits. Permafr Periglac Proc 25(3):151–161

Ulrich M, Matthes H, Schirrmeister L, Schütze J, Park H, Iijima Y, Fedorov AN (2017) Differences in behavior and distribution of permafrost-related lakes in Central Yakutia and their response to climatic drivers. Water Resour Res 53:1167–1188. https://doi.org/10.1002/2016WR019267

Varlamov SP, Skachkov YB, Skryabin PN (2002) Thermal regime of Permafrost landscapes in Central Yakutia (Temperaturnyi rezhim merzlotnykh landshaftov Centralnoi Yakutii). Permafrost Institute Press, Yakutsk, 218pp (In Russian)

Varlamov S, Skachkov Y, Skryabin P (2014) Current climate change effects on the ground thermal regime in Central Yakutia. Sci Cold Arid Regions 6(4):282–292

Vasiliev IS (1982) The regularities seasonal thawing in Eastern Yakutia. Nauka, Novosibirsk, 133 p. (in Russian)

Vasiliev IS (2005) Spatio-temporal patterns of formation of the active layer in the landscapes of Western Yakutia. GEO, Novosibirsk, 228 p. (in Russian)

Vasiliev IS, Torgovkin YI (1996) Impact of climate on soil temperature and seasonal thawing depth. In: Impact of climate on permafrost landscapes of Central Yakutia. Permafrost Institute, Yakutsk, 152 p. (in Russian)

Walsh JE et al (2005) Cryosphere and hydrology. In: Arctic climate impact assessment. Cambridge University Press, Cambridge/New York, pp 183–242

Walter KM, Zimov S, Chanton JP, Verbyla D, Chapin FS III (2006) Methane bubbling from Siberian thaw lakes as a positive feedback to climate warming. Nature 443:71–75

Yanovsky VK (1933) Expedition to the Pechora River on the definition of the southern boundary of permafrost. In: Proceedings of Commission for the study of permafrost. Academy of Science of USSR, Leningrad, pp 65–149 (in Russian)

Zhang T (2005) Influence of the seasonal snow cover on the ground thermal regime: an overview. Rev Geophys 43:RG4002. https://doi.org/10.1029/2004RG000157

Zhang T, Barry RG, Gilichinsky D, Bykhovets SS, Sorokovikov VA, Ye J (2001) An amplified signal of climatic change in soil temperatures during the last century at Irkutsk. Russ Clim Chang 49:41–76

Zhang T, Frauenfeld OW, Serreze MC, Etringer A, Oelke C, McCreight J, Barry RG, Gilichinsky D, Yang D, Ye H, Ling F, Chudinova S (2005) Spatial and temporal variability in active layer thickness over the Russian Arctic drainage basin. J Geophys Res 109:D16101. https://doi.org/10.1029/2004JD005642

Zhang Y, Chen W, Riseborough DW (2008) Transient projections of permafrost distribution in Canada during the21st century under scenarios of climate change. Glob Planet Chang 60:443–456

Chapter 9
River Discharge

Tetsuya Hiyama, Shigemi Hatta, and Hotaek Park

9.1 Introduction

The Arctic Ocean is an important water body that is affected by and has an effect on global climate via changes in its energy and water cycles. It is surrounded by the continents of North America and Eurasia that provide a supply of fluvial freshwater. The pan-Arctic river discharge, which is main topic of this chapter, annually contributes about twice the amount of freshwater as net precipitation (precipitation minus evaporation) over the ocean (Haine et al. 2015), and it acts as a conveyor of substantial quantities of nutrients, carbon, and other elements from its diverse watersheds (Bring et al. 2016). River discharge from the pan-Arctic watershed (or pan-Arctic drainage basin) also influences the salinity and water temperature of the Arctic Ocean, the effects of which can extend to the mid-latitudes constituting a feedback system of the global climate (Prowse et al. 2015a, b). Peterson et al. (2006) reported that changes in freshwater inputs and ocean storage occur in conjunction with amplification of the North Atlantic Oscillation (NAO) and rising air temperatures. Indeed, the long-term effects on the climate system from changing pan-Arctic river discharge are substantial (Rawlins et al. 2010; Haine et al. 2015). Thus, pan-Arctic watershed discharge is considered one of the clearest indicators of the effects of climate change and current global warming.

Recently, Bring et al. (2016) reviewed the principal freshwater processes of terrestrial Arctic drainage with consideration of their function and variation across seven hydrophysiographical regions (i.e., Arctic tundra, boreal plains, shield,

T. Hiyama (✉)
Institute for Space-Earth Environmental Research (ISEE), Nagoya University, Nagoya, Japan
e-mail: hiyama@nagoya-u.jp

S. Hatta
National Institute of Technology, Tomakomai College, Tomakomai, Japan

H. Park
Japan Agency for Marine-Earth Science and Technology (JAMSTEC), Yokosuka, Japan

T. Ohta et al. (eds.), *Water-Carbon Dynamics in Eastern Siberia*,
Ecological Studies 236, https://doi.org/10.1007/978-981-13-6317-7_9

Fig. 9.1 Map of the pan-Arctic river basins showing catchments and the annual discharge of the six major Eurasian rivers that contribute water to the Arctic Ocean. (Modified from Peterson et al. 2002)

mountains, grasslands, glaciers/ice caps, and wetlands). Their research emphasized the need for coordinated monitoring, modeling, and processing studies at various scales to improve the understanding of change, particularly at the interfaces between hydrology, the atmosphere, ecology, resources, and oceans. Previously, Peterson et al. (2002) reported that average annual discharge of freshwater from the six largest Eurasian rivers (i.e., the Kolyma, Lena, Yenisei (or Yenisey), Ob (or Ob'), Pechora, and Severnaya Dvina rivers; Fig. 9.1 and Table 9.1) to the Arctic Ocean increased by 7% from 1936 to 1999. Shiklomanov and Lammers (2009) showed that annual discharge from the Eurasian pan-Arctic watershed during 1980–2007 demonstrated an unprecedented increase at a rate of 10 km^3 $year^{-1}$, i.e., almost five times higher than that documented by Peterson et al. (2002) during the period 1936–1999. They also suggested that significant acceleration of the hydrological cycle in the Eurasian pan-Arctic has occurred over the last three decades.

Of all the rivers that flow into the Arctic Ocean, three Siberian rivers (i.e., the Lena, Yenisei, and Ob rivers) are the largest in terms of freshwater discharge (R) (Oshima et al. 2015). Studies on the atmospheric and terrestrial water cycles of these major Siberian rivers have been conducted previously (e.g., Fukutomi et al. 2003; Serreze et al. 2003). Based on a decomposition analysis of atmospheric

Table 9.1 Drainage area and annual discharge data of the six Eurasian rivers indicated in Fig. 9.1 and those of the Mackenzie River in North America

River	Station	Drainage area (km^2)	Discharge (km^3 $year^{-1}$)
Kolyma	Kolymskoye	526,000	102.6
Lena	Kusur	2,430,000	528.5
Yenisei (Yenisey)	Igarka	2,440,000	580.1
Ob (Ob')	Salekhard	2,950,000	394.0
Pechora	Oksino	312,000	138.1
Severnaya Dvina	Ust'Pinega	348,000	105.0
Mackenzie	Norman Wells	1,570,000	266.3

Note that values of annual discharge are slightly different from those indicated in Fig. 9.1 because of the different averaging years (durations)

moisture flux, Oshima et al. (2015) revealed that moisture transport associated with cyclone activity dominates the climatological features of precipitation minus evapotranspiration (P − ET) over the Lena River, whereas moisture transport associated with seasonal mean winds dominates the P − ET features over the Ob River. Conversely, both transport processes have an effect over the Yenisei River (see also Chap. 2). Oshima et al. (2015) also analyzed the R and the P − ET estimated from six atmospheric reanalysis data sets. Although previous studies (e.g., Serreze et al. 2003, 2006) have shown considerable deviations in the variations of P − ET and R, Oshima et al. (2015) found that interannual variations agreed very well with each other when appropriate seasonal time lags were taken into account. Suzuki et al. (2016) found that soil water conditions during the previous fall and winter affect the Lena River runoff and that the time lag between P − ET and R could be attributed partly to snowmelt infiltration into the frozen ground. This means that the terrestrial water storage (TWS) of the Lena River basin in fall is important regarding its discharge the following year.

The Lena River basin in eastern Siberia is one of the largest pan-Arctic river basins of the Eurasian continent (Fig. 9.1 and Table 9.1), contributing about 15% of the total freshwater inflow into the Arctic Ocean (Aagaard and Carmack 1989; Bamber et al. 2012). Yang et al. (2002) used hydrometeorological data (i.e., air temperature, precipitation, flow rate, river ice thickness, and active layer thickness) from the Lena River basin, acquired during 1935–1999, to address the trends of increasing wintertime runoff and increasing early snowmelt. They also claimed that changes in the hydrological processes of the Lena River basin are closely associated with the state of frozen ground (i.e., permafrost), which is affected considerably by climate warming in eastern Siberia. In this context, Brutsaert and Hiyama (2012) proposed methods to relate low river flows (or base flows) of the Lena River during the open water season to the rate of change of the active groundwater layer thickness resulting from permafrost thawing at the scale of the upstream river basin. They suggested that during 1950–2008, the active layer thickness increased at average rates of approximately 0.3–1.0 cm $year^{-1}$ in areas with discontinuous permafrost and at average rates about half as large in colder eastern areas with continuous permafrost.

Warming permafrost changes the hydrological regime, particularly through altered surface and subsurface interactions (Bring et al. 2016). Changes in temperature and precipitation also interact to produce variations in evapotranspiration, runoff, seasonal snow accumulation, and snow season length in permafrost basins. Short-term changes in air temperature, ice cover, and soil moisture do not trigger systematic hydrological shifts in permafrost, although they do provide a "memory" that is manifest during the following warm season, as shown in a recent model–observation study (Park et al. 2013a). Therefore, new research field studies are required to evaluate fully the changing sources, quantity, quality, seasonality, and fate/effect of freshwater in the Arctic regime (Prowse et al. 2015b) and the pan-Arctic watershed, including the Lena River basin.

9.2 Lena River Basin

9.2.1 Geographical Scope

Because the precise geographical features of the Lena River basin have been described in Chap. 1, only those characteristics with importance regarding the drainage basin and the terrestrial water budget are discussed in what follows.

The drainage area of the Lena River basin is 2,430,000 km^2 (Table 9.1), approximately 79% of which is underlain by continuous permafrost (Ye et al., 2009). The Lena River basin consists of three major subbasins: the "Upper Lena" (UL), "Aldan" (AL), and "Vilui" (VI) (Fig. 9.2 and Table 9.2). The Lena River channel is completely covered by snow and ice from November to April; then, spring flooding occurs in May and June (Bennett and Prowse 2010). Because the Lena River basin is underlain by permafrost and because the water storage capacity is low, base flow (low flow) during the winter season (from late November to early May) is the lowest, and peak flow during spring flooding (from late May to early June) is the highest.

As mentioned in the previous section, the large-scale hydroclimatology of the terrestrial drainage system in the pan-Arctic watershed has been examined previously (e.g., Serreze et al. 2003; Oshima et al. 2015). Water-year time series of river discharge (R) and net precipitation (P − ET) in the Lena River basin are correlated strongly (Oshima et al. 2015), reflecting the importance of the extensive permafrost in the basin.

9.2.2 Seasonal Changes in Lena River Discharge

Seasonal changes in Lena River discharge can be divided into the low-flow period (from November to April) and the high-flow period (from May to October). The lowest flow appears in April, and the highest discharge (spring flooding) is in May and June, resulting from the combination of snowmelt water accumulation and ice

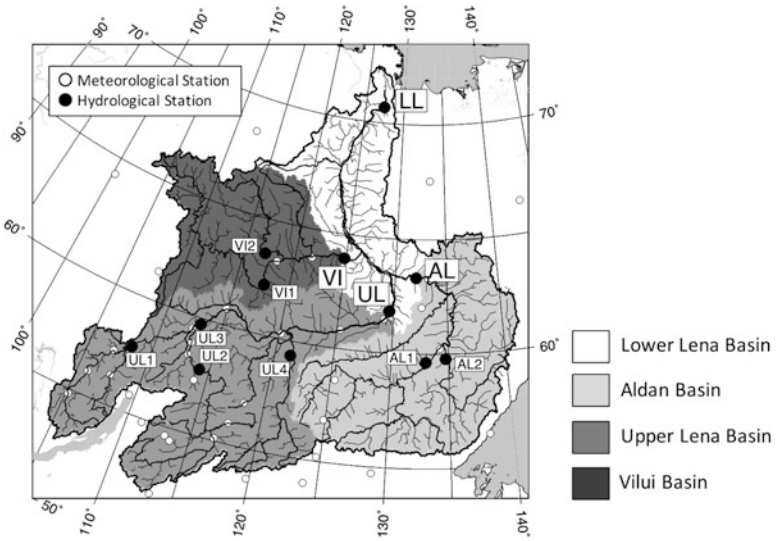

Fig. 9.2 Divisions of the four subbasins of the Lena River, together with locations of hydrological and meteorological stations. Hydrological stations LL, UL, AL, and VI refer to "Lower Lena," "Upper Lena," "Aldan," and "Vilui," respectively

Table 9.2 Station names, drainage areas, and mean annual discharges of the four major subbasins of the Lena River

Station code	Station name	Drainage area ($\times 10^3 km^2$)	Annual discharge ($km^3\ year^{-1}$)
LL	Kusur	2430	529
UL	Tabaga	897	221
UL1	Zmeinovo	140	35.4
UL2	Bodaibo	186	49.2
UL3	Krestovski	440	131
UL4	Kudu-Kel	115	32.2
AL	Verhoyanski' Perevoz	696	165
AL1	Ust-Mil	269	86.3
AL2	Chabda	165	36.6
VI	Hatyrik-Homo	452	46.7
VI1	Suntar	202	24.8
VI2	Malyukai	89.6	12.3

Abbreviations are the same as in Fig. 9.2

jam flooding. Figure 9.3 shows the seasonal change in river discharge (i.e., a hydrograph) observed in 1987 at site AL2 (see Fig. 9.2). After the onset of the snowmelt event in the basin, river discharge at site AL2 rose drastically during the middle of May. The highest (annual maximum) flow occurred at the beginning of

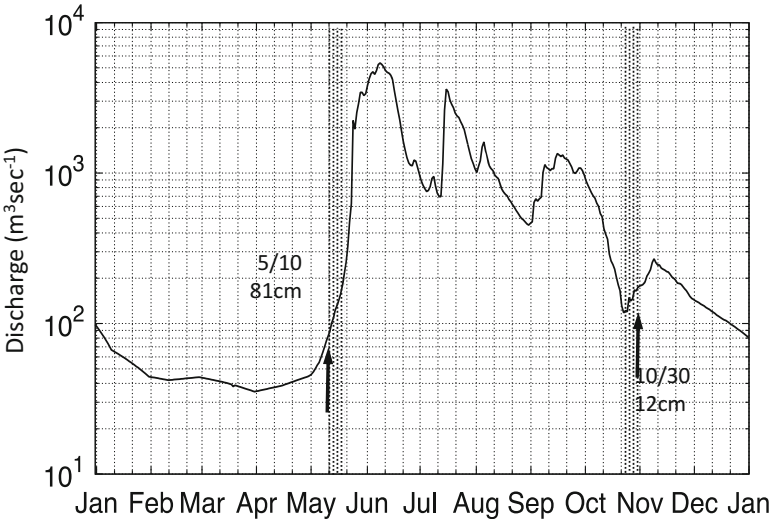

Fig. 9.3 Typical seasonal change in daily river discharge (i.e., hydrograph) observed at site AL2 (Fig. 9.2) in 1987. This hydrograph was reconstructed from the relationship between river discharge and river water level measured at site UL (Fig. 9.2) during 2000–2008. The two arrows in the figure indicate the dates of final (10 May) and first (30 October) appearance of river ice in 1987. River ice thickness on the two dates is also indicated in the figure. Shaded durations are the 10 days after the dates of final disappearance (10 May) and before first appearance (30 October) of river ice

June. Thereafter, several peaks in river flow corresponded to precipitation events. A large drop in river discharge occurred at the end of October. This drop was related to the formation of river ice in the late fall following a period without precipitation (rainfall). The two arrows in the figure indicate the dates of final (10 May) and first (30 October) appearance of river ice in 1987. The ice thickness for both dates is also indicated in the figure. It should be noted that river ice observations were available every 10 days. A sudden increase of river discharge (i.e., a steep slope of the hydrograph) can be seen following the date of ice disappearance. Conversely, a dramatic drop of river discharge can be observed just before the date of the first observation of river ice.

Figure 9.4 shows the seasonal changes of daily river discharge in 2000 observed at stations LL, UL, AL, and VI (see Fig. 9.2). In the three subbasins (UL, AL, and VI), intermittent peaks can be seen following the spring high discharge peaks. These were caused by summer precipitation events in the subbasins. Thus, on the subbasin scale, summer river flooding is not negligible (Gautier et al. 2018). However, at site LL (i.e., the lowest measurement station on the Lena River; Fig. 9.2), the spring discharge had a significantly high peak, and there were no further clear peaks during the summer season. This might be related to the relatively small effects of summertime precipitation events on the river discharge of the entire Lena River basin. Additionally, there are inundation effects in summer in the riverine lowlands between the middle (Hiyama and Takakura 2018) and the

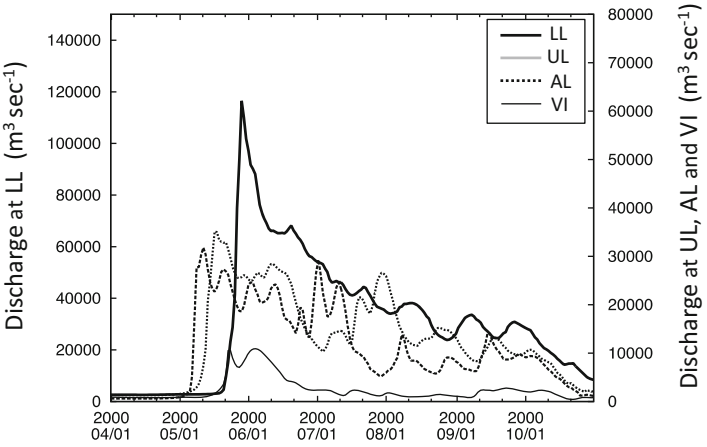

Fig. 9.4 Daily river discharge in 2000 observed at the four hydrological stations (i.e., LL, UL, AL, and VI)

lower reaches of the Lena River. The secondary flood peaks in summer and the inundations of riverine lowlands and/or islands in summer have been increasing in recent years because of the effects of ongoing climate change (Hiyama and Takakura 2018; Gautier et al. 2018).

9.2.3 Long-Term Trend of Lena River Discharge

Long-term records of meteorological–hydrological variables such as air temperature, precipitation, river discharge, river ice thickness, and active layer thickness in Siberian river basins have been previously analyzed intensively (e.g., Yang et al. 2002; Ye et al. 2004; Berezovskaya et al. 2005). Berezovskaya et al. (2004) reported inconsistency in the long-term (1936–1998) changes of basin precipitation and river discharge. For example, they found that Yenisei River runoff increased significantly, while precipitation showed mostly negative trends; the Ob River did not show any significant trend in either precipitation or runoff, and a positive trend in Lena River runoff was accompanied by a weak increase in precipitation. However, it was determined that the precipitation increase in the Lena River basin was not sufficient to support the observed change in runoff. Ye et al. (2003) analyzed long-term (1936–1999) monthly discharge records for the major subbasins within the Lena River basin in order to document significant streamflow hydrology changes induced both by human activities (particularly reservoirs) and by natural variations/changes. They showed that the upper streams of the Lena River basin, relatively free from human impact, experience an increase of runoff in winter, spring, and particularly summer, and a discharge decrease in fall. They also found that reservoir regulation has substantially altered the monthly discharge regimes over the lower reaches of the

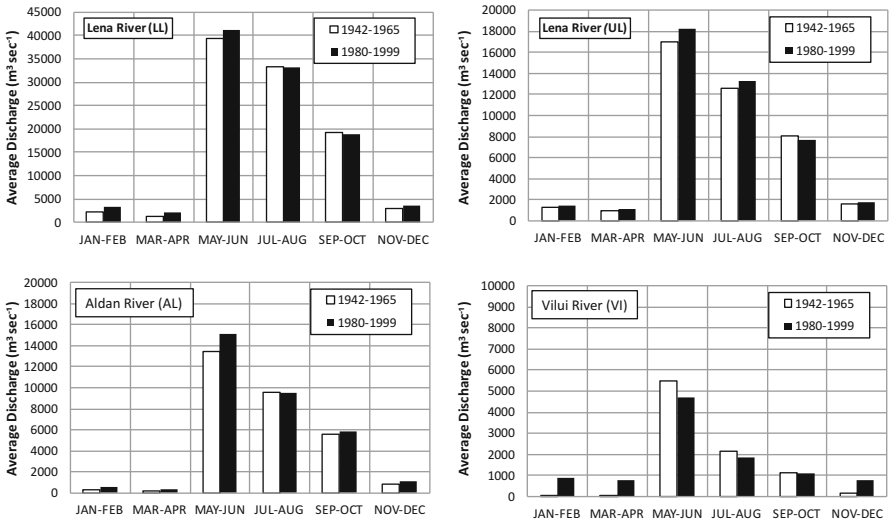

Fig. 9.5 Two-month mean river discharge during 1942–1965 and 1980–1999, as observed at the four hydrological stations (i.e., LL, UL, AL, and VI)

Lena River. Because of a large dam in the west of the Lena River basin (the Vilui subbasin), monthly summertime flows at the Vilui valley outlet (almost 1000 km downstream of the dam) have been reduced by up to 55%, whereas wintertime low flows have increased. Because of the combination and integration of streamflow hydrology changes over the upper and western Lena River basin regions, strong trends of increase (up to 90%) have been observed at the basin outlet during the low-flow (winter) months, and weak trends of increase (<10%) have been found in the high-flow (summer) season. This reservoir regulation affects not only the basin-scale river discharge but also the temperature of the river water (Liu et al. 2005).

Figure 9.5 compares the average discharge every 2 months (January–February, March–April, May–June, July–August, September–October, November–December) observed at LL, UL, AL, and VI (Fig. 9.2) for 1942–1965 and 1980–1999. In order to discard reservoir construction effect on the Vilui discharge, period for 1966–1979 was omitted in the figure. As mentioned above, at the Vilui (VI) River subbasin, discharge in the winter season has increased drastically, while summer discharge has decreased because of the reservoir effect. In contrast, discharge in the Upper Lena (UL) and Aldan (AL) subbasins has increased in both winter and summer. These discharges, which all contribute to the annual flow of the Lena River, as observed at LL, show that the reservoir regulation effect from the Vilui River is relatively small.

Smith et al. (2007) reported rising minimum daily flows in northern Eurasian rivers, and they speculated on the growing influence of groundwater on the high-latitude hydrological cycle. Spring water discharge of mixed water from supra-permafrost and intra-permafrost groundwater (e.g., Hiyama et al. 2013) from taliks (more specifically, perennially unfrozen zones) might contribute to the increase of low river flow.

9.3 Hydrological Modeling for Arctic River Discharge

Observations of meteorological and hydrological variables are less dense in the northern high latitudes, in comparison with lower latitudes, making it difficult to obtain reliable estimates of the water budget components and other surface variables used to assess hydroclimatological variability. Numerical models offer considerable benefits for enlightenment regarding large-scale hydrology in data-sparse regions such as the pan-Arctic watershed. A number of land surface models capable of representing the dynamics of land–atmosphere water and energy exchanges have been developed, and these have been used to evaluate the effects of climate change on hydrological processes at regional to global scales (Slater et al. 2007; Park et al. 2016). The combination of observations and numerical models can capture various aspects of Arctic hydrology and identify those features that contain uncertainties. The Arctic hydrology differs from that of temperate regions in several important ways, primarily related to the unique conditions associated with cold temperatures, which include the dominance of snow cover and spring snowmelt flow, presence of permafrost, and prevalence of lakes and wetlands. In other words, these unique conditions comprise the major elements or characteristics of the Arctic hydrological cycle. Thus, modeling studies have paid attention to parameterization for a wide range of geophysics, particularly with respect to cold processes. Certain models have also been combined with river routing and discharge models in both off-line and coupled modes to simulate channel flows of pan-Arctic rivers (Park et al. 2016).

Coupled hydrological models have been used to explore the spatial and temporal variabilities of pan-Arctic freshwater components. As part of this process, experiments incorporating model comparisons have been conducted to evaluate the capabilities of models to simulate the hydrological processes across the pan-Arctic drainage basin over long time scales. One such representative experiment was the Project for Intercomparison of Land Surface Parameterization Schemes (PILPS) that tested 21 land surface models with respect to their capabilities of representing snow processes, soil freeze/thaw and permafrost, and runoff generation (Bowling et al. 2003). The PILPS intercomparison obtained valuable knowledge regarding the identification of problems in the representations of snow cover, surface runoff, and other physical processes in cold region (Essery and Clark 2003; van den Hurk and Viterbo 2003). Slater et al. (2007) compared the performance of five land surface models with regard to the simulation of pan-Arctic hydrological processes. They found that the models generally simulated the seasonal discharge of large rivers well; however, in comparison with observations, the modeling hydrographs were often out of phase with peak flows that were too high, especially in relation to the Ob and Mackenzie rivers. The overestimations for the Ob and Mackenzie basins have been attributed to the relatively higher snowmelt and runoff inputs in these basins in comparison with other basins (Park et al. 2016). Substantial portions of the Ob (11% of basin area) and Mackenzie (49%) basins are covered by wetlands and lakes that reduce runoff and peak river discharge rates. Therefore, model deficiencies in representing wetland and lake processes could be another possible reason for the

overestimation of peak discharges. The Variable Infiltration Capacity (VIC) macroscale hydrology model, using observed streamflow, snow cover extent, and the dates of lake freeze-up and breakup, has been shown capable of simulating the observed spring peak discharge of the two basins (Su et al. 2005).

Generally, a hydrological model consists of three submodels: a one-dimensional land surface model (LSM), river routing (runoff) model, and river ice model. Several LSMs are reviewed in Chap. 12. Thus, this section focuses only on the modeling of river runoff and river ice processes.

9.3.1 River Runoff Modeling

Ma et al. (2000) developed a distributed hydrological model for application to the river runoff of the Lena River basin. Subsequently, Ma and Fukushima (2002) combined a land surface model with a hydrological model that included river ice processes, demonstrating that it is possible to reproduce daily hydrographs. This pioneering study was important because their modeling showed that the incorporation of the effects of river ice processes enables reconstruction of daily hydrographs for rivers of the pan-Arctic drainage basin, even when observational data are insufficient. Hatta et al. (2009) developed another distributed hydrological model (see Fig. 9.6) for the Lena River basin, capable of estimating daily runoff over long periods (from 1987 to 2003). They showed that daily minimum flows (low flows or base flows) and river ice during winter have considerable effects on the hydrograph.

If contribution of permafrost thaw could be negligible, approximately 60% of the Arctic annual river discharge is attributable to snow-induced water, and the remainder is derived from summer precipitation. Examples of the distributions of net precipitation (P − ET) and thus river discharge (R) during the snowmelt season (end of April to end of May), calculated using the land surface model of Hatta et al. (2009), are shown in Fig. 9.7. Because most of the summer precipitation is accounted for in evapotranspiration (Park et al. 2008), the contribution of summer precipitation to river discharge is relatively low. A considerable proportion of summer discharge is generated from southern mountainous regions (Hatta et al. 2009) where the amount of precipitation is comparatively large. However, the existent meteorological data sets indicate low bias in relation to mountainous precipitation, resulting in underestimation of model-derived summer discharge, which is particularly significant for the rivers of Siberia (Slater et al. 2007; Park et al. 2016). Adam and Lettenmaier (2003) produced a bias-corrected global precipitation data set, which was based on separate average calendar monthly catch ratios for rainfall and snowfall rates for each half-degree grid cell, with adjustment of precipitation rates to allow for the effects of orography. Simulations with the VIC model using forcing data of bias-corrected precipitation were found capable of reproducing the seasonal and interannual variations of discharge of the pan-Arctic rivers (Su et al. 2005), highlighting the large precipitation-related uncertainties in simulations of pan-Arctic river discharge. The increase of satellite monitoring has

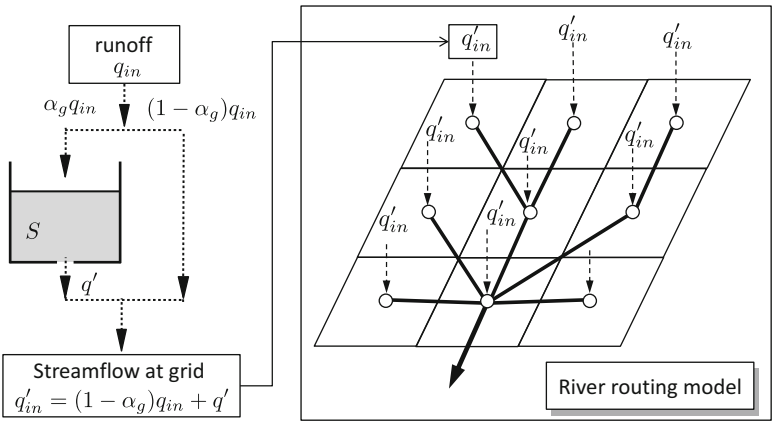

Fig. 9.6 Schematics of tank model (left) and river routing model (right). In the left figure, calculated value of q_{in} (namely, P − ET) from the land surface model is divided into slow groundwater flow component (q') through storage (S) and fast infiltration water component $(1 - \alpha_g)\, q_{in}$ in a grid. A parameter α_g is the ratio of the slow groundwater flow component in the target grid. The calculated streamflow q'_{in} in each grid is used in the river routing model of the right figure

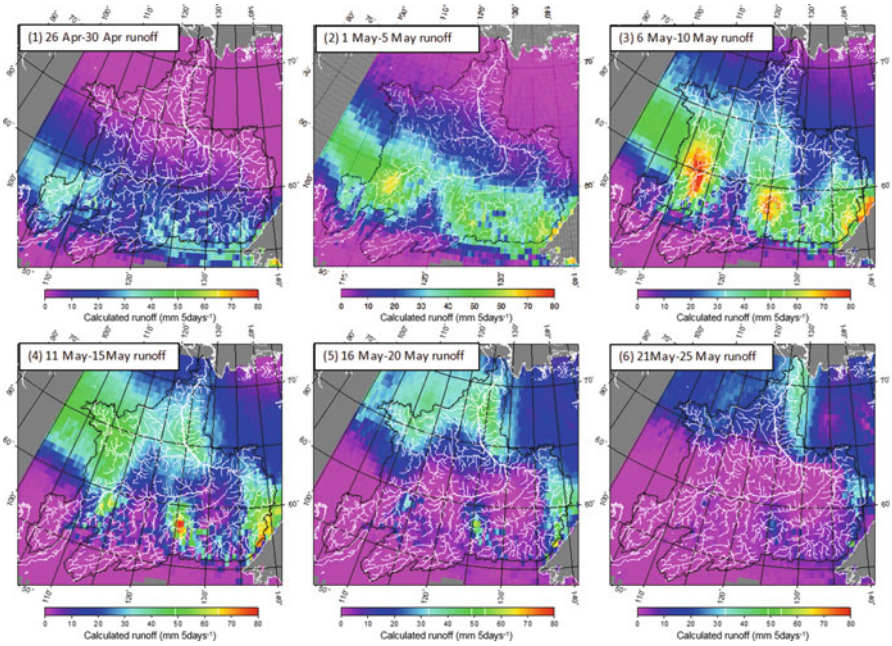

Fig. 9.7 Distributions of river discharge (R) calculated from the land surface model (as mean values of P − ET for the period 1986–2003)

contributed partly to the reduction of such uncertainties; however, satellite observations of the Arctic region have inherent uncertainties related to cloud, snow cover, ice, and permafrost.

In the pan-Arctic watershed, hydrological processes are controlled primarily by the presence or absence of permafrost. Such processes are particularly influenced by both the thickness of the active layer and the total thickness of the underlying permafrost. As permafrost becomes thinner or decreases in areal extent, the interaction between surface runoff and intra-permafrost groundwater becomes more important. The inability of soil moisture to infiltrate to deeper groundwater zones because of ice-rich permafrost could result in very wet surficial soils (White et al. 2007), likely to enhance subsurface runoff and increase discharge. The hydraulic properties of frozen soil have been parameterized as an ice impedance function with a power-law form. A parameter-coupled model simulated significantly higher moisture contents in near-surface soils in permafrost regions, particularly during spring, which brought considerable improvements in comparison with observed hydrographs of large Siberian rivers (Swenson et al. 2012). However, Brutsaert and Hiyama (2012) found that a warming temperature-induced deeper active layer was related positively to increased base flows in areas with discontinuous permafrost in the upper reaches of the Lena River. Similarly, based on observational data from the Lena River basin during 1925–2013, Tananaev et al. (2016) identified that increases in daily minimum flows in the headwaters of the basin were underlain by discontinuous permafrost. An evident fact supported by these results is that warming permafrost contributes to the increase of pan-Arctic river discharge. However, existent models have a consistent problem in representing the presence and physical properties of ground ice within permafrost. Consequently, models cannot account for the mechanism by which warming permafrost-induced water contributes to increasing discharge. One possible way to reduce this deficiency might be to incorporate an isotope process into the model, because it offers the potential for both quantitative assessment and source analysis of the discharge water.

9.3.2 River Ice Modeling

River ice is a major component of the terrestrial cryosphere, and it plays an important role in affecting a range of geophysical systems, e.g., extreme events (or floods) induced by river ice breakup (Bennett and Prowse 2010; Beltaos 2008). However, its entire geographic coverage has not been documented fully. On the continental scale, Bennett and Prowse (2010) analyzed the spatial extent of river networks relative to the location of three 0 °C isotherm periods, recognizing that both the freeze-up and the breakup of river ice are associated closely with the timing of 0 °C air temperatures. On the local scale, Sakai et al. (2015) examined the use of Landsat Thematic Mapper/Enhanced Thematic Mapper Plus (TM/ETM+) imagery to monitor the spatial and temporal extents of spring breakup floods on the Lena River. They suggested that images from Landsat TM/ETM+ sensors could be regarded as data

suitable for operational use in flood monitoring of the pan-Arctic rivers, because of their wide geographic coverage, high temporal resolution, and adequate spatial resolution.

As mentioned above, pan-Arctic rivers have distinctive seasonal phenology (freezing in fall and breaking in spring). This seasonality affects seasonal river discharge, with several small rises of water level in the fall and the large spring flood pulse. Runoff induced by river ice breakup has an effect on the timing of peak discharge at a river outlet in spring. Most models that do not include the ice effect tend to produce peaks in simulated hydrographs that are too early relative to observations (Slater et al. 2007). However, some models that do incorporate a river ice scheme can generate adequate simulations for spring peak discharges in various rivers (Ma and Fukushima 2002; Hatta et al. 2009; Park et al. 2016).

The accumulation and melting of river ice can be estimated based on the use of freezing and thawing indices with units of degree days. In order to determine river ice thickness, we can use Stefan's equation, as follows:

$$I_c = \kappa\sqrt{D_f}, \tag{9.1}$$

where I_c is the river ice thickness (cm), D_f is the freezing index (°C day) since the formation of the river ice cover, and κ is a coefficient (cm (°C day)$^{-1/2}$). Theoretically, coefficient κ is 3.48, but it is known that for river ice covered by snow, the appropriate range of values of κ is 1.4–1.7 (Beltaos 1995).

The melting of river ice involves complexities such as thermal and mechanical factors, and it is difficult to account for all these factors in runoff modeling. Using meteorological data, Hatta et al. (2009) set a statistical threshold value for the thawing index based on the maximum river ice thickness. The threshold value for the ice breakup date is given by the following equation:

$$I_{\mathrm{cmax}} = \frac{\sqrt{D_{\mathrm{m0}}}}{\gamma}, \tag{9.2}$$

where I_{cmax} is the maximum ice thickness (cm), D_{m0} is the thawing index on the ice breakup date (°C day), and γ is a coefficient. Hatta et al. (2009) used the mean observed value as $\gamma = 0.037$. Because the ice breakup date calculated using Eq. (9.2) does not mean the date when river ice has completely disappeared from the river's surface, Hatta et al. (2009) expressed the gradual decrease of the thickness of river ice (I_c) from the ice breakup date using the following equation:

$$I_c = I_0 e^{-\zeta t_{\mathrm{day}}} \tag{9.3}$$

where I_0 is the ice thickness on the ice breakup date (cm), t_{day} is the number of days after ice breakup (day), and ζ is a coefficient. Because of the lack of a physical method to determine the value of coefficient ζ, it can only be estimated by trial and error based on observed river discharge data.

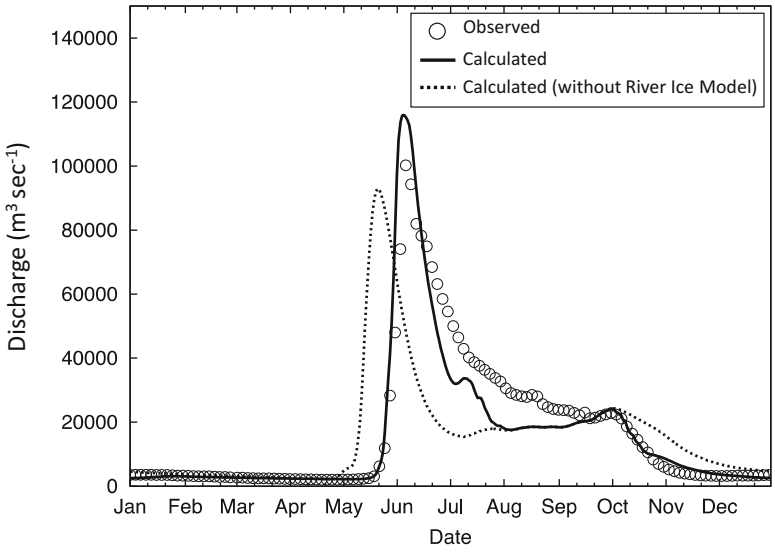

Fig. 9.8 Observed and calculated river discharges of the Lena River (as mean values during 1986–2003). Calculated discharge values were based on simulations with and without river ice modeling

Based on the above methodology, a model experiment (Hatta et al. 2009) was performed that assessed quantitatively that the peak spring discharge simulated by a model that could account for river ice was about 10 days later than a baseline simulation using a model that excluded the impact of river ice (see Fig. 9.8). Similar results were reproduced by a hydrological model for the larger rivers of the pan-Arctic watershed (Park et al. 2016). Frozen river ice grows during winter depending on atmospheric heat fluxes. The winter ice growth reduces river water storage, resulting in reduced low flows in winter. Capturing the correct low flow for pan-Arctic rivers is an ongoing problem for discharge models (Slater et al. 2007). Hatta et al. (2009) emphasized that a greater contribution of permafrost-induced slow groundwater to the winter low flow could account for 30% of the annual discharge.

9.3.3 Future Projections

Historically, observations have generally indicated that the discharge of many pan-Arctic rivers has increased (Peterson et al. 2006). However, a trend of decrease has been observed in some North American rivers during the previous few decades, partly due to flow regulation and storage for enhanced hydropower production (Déry et al. 2005, 2016). Thus, the overall increase during the most recent decade has been significant although it may be associated with climate variability (such as the Arctic

Oscillation). For example, the increase in discharge from all observed rivers draining into the Arctic Ocean during 2000–2010 was 300 km^3 greater than during 1980–2000 (Haine et al. 2015). Global climate models have projected that discharges will generally continue to increase over much of the pan-Arctic watershed (Holland et al. 2007). Simulations with hydrological models that adopt inputs from climate models have also shown increased discharges of the order of 10%–50% for most pan-Arctic rivers (Walsh et al. 2005; van Vliet et al. 2013), although regional decreases have been identified in southern interior regions of the pan-Arctic watershed (van Vliet et al. 2013).

Model projections considered atmospheric and oceanic dynamics have provided quantitative values of the changes in discharge of pan-Arctic rivers under future climatic conditions. To understand these changes, address them adequately, and plan for adaptation; however, there is need for more detailed projections and better information regarding uncertainties. In response to these needs, Bring et al. (2017) estimated projected multimodel and multiscenario changes in annual river discharge for 2061–2090 and compared them with model-simulated historical values during 1961–1990. The analyzed results are displayed in Fig. 9.9. It can be seen that significant increases in the projected discharges are concentrated in Siberia, Alaska, and Northern Canada. For regions across Central Canada and both western and central Siberia, the projections indicate significant change, but they disagree on the sign of that change (Fig. 9.9). This finding suggests that existing stations across these regions could form a prioritized set in the monitoring network. Interestingly, the regions where projected changes are significant are consistent with the areas of highest projected increase in snow (Brown and Mote 2009). This highlights the impact of snow associated with increasing precipitation on river discharge in the future. For example, northern Siberia is predicted to experience increasing snow depth under current projections of a warming climate. Park et al. (2013b) reported high statistical correlation between increased terrestrial snow and reduced Arctic sea ice. The decline of Arctic sea ice will become increasingly accelerated under future climatic changes. Global climate models have projected increases in Arctic precipitation during the twenty-first century, which peak in late fall and winter, primarily because of intensified local surface evaporation resulting from retreating winter sea ice (Bintanja and Selten 2014). The increase of the winter precipitation signals the future amplified Arctic hydrological cycle as enhancing permafrost and snow implicated fluxes (Rawlins et al. 2010; Bintanja and Selten 2014).

9.4 River Water Chemistry in the Arctic

9.4.1 Importance of River Water Chemistry in the Arctic

River discharge and the water chemistry (geochemical qualities, geochemical fingerprints) of freshwater influence the physical, chemical, and biological processes of the Arctic Ocean, including stratification and vertical mixing, ocean heat flux,

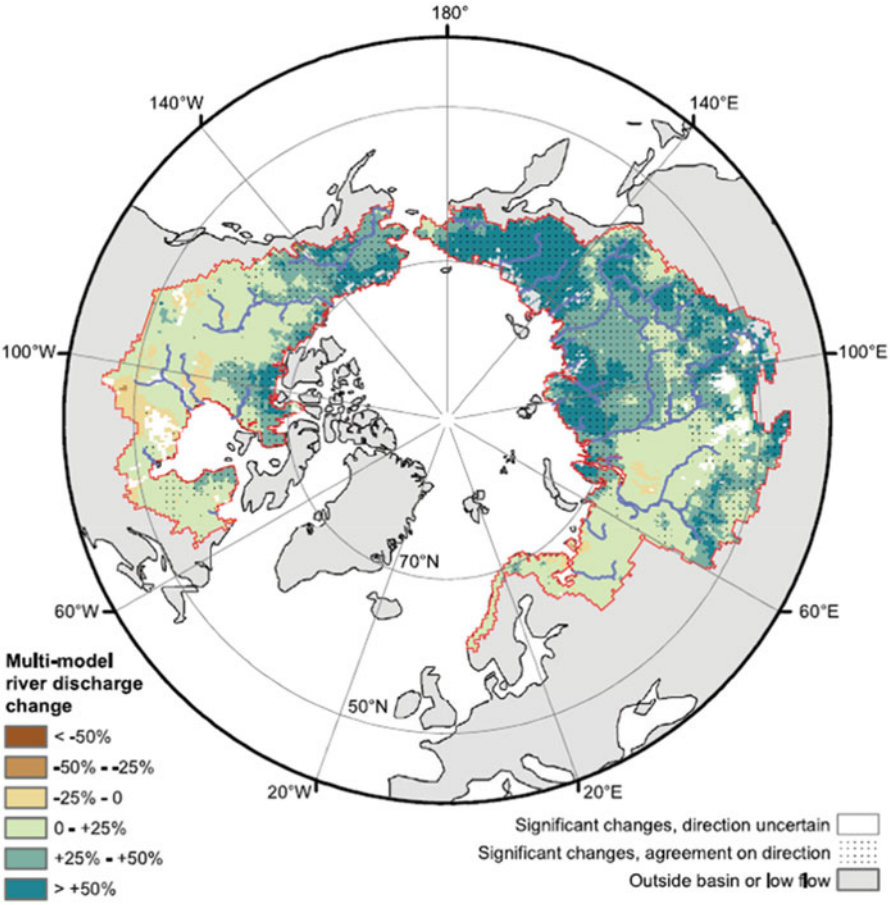

Fig. 9.9 Changes to Arctic river flows. The map shows projected changes in average discharge across the pan-Arctic watershed from 1961–1990 to 2061–2090. White areas, indicating agreement on significant changes but disagreement on sign, show where model agreement (i.e., at least half of the models indicate significant changes ($p < 0.05$) using a two-tailed t-test) is fulfilled. Stippled areas show where model agreement (i.e., as above, and where 80% of the models that show significant change also agree on the sign of change) is fulfilled. Areas that are neither white nor stippled indicate changes with nonsignificant changes. Areas inside the red border on the map but shown in gray are masked because of low average flows (<1 $m^3 s^{-1}$). (Bring et al. 2017)

nutrient supply, primary production, ocean acidification, and biogeochemical cycling. Long-term monitoring of both water discharge and water chemistry in rivers is thus essential for identifying and understanding changes in the Arctic. Important geochemical fingerprints of the Arctic Ocean are dissolved organic carbon (DOC), dissolved inorganic carbon (DIC), dissolved organic nitrogen (DON), dissolved inorganic nitrogen (DIN), and total dissolved phosphorus (TDP), which are known collectively as dissolved organic matter (DOM). Particulate matter such as

particulate organic carbon (POC) and particulate nitrogen (PN) are also valuable for investigating the physical, chemical, and biological processes within the Arctic Ocean. It is also interesting to monitor the concentrations and source/composition indicators such as alkalinity, stable water isotopes (HDO and $H_2{}^{18}O$ concentrations, or δD and $\delta^{18}O$ values), nitrate ($NO_3{}^-$), silica (Si), C/N ratio, $\delta^{13}C$, $\Delta^{14}C$, and $\delta^{15}N$ for detecting the permafrost condition and degradation in pan-Arctic river basins.

Frey and McClelland (2009) highlighted linkages between permafrost dynamics and river biogeochemistry in the Arctic, including consideration of the likely impacts that warming-induced changes in permafrost could have on the delivery of organic matter, inorganic nutrients, and major ions to the Arctic Ocean. This is because the Arctic terrestrial freshwater system is likely to undergo transition from a surface water-dominated system to a groundwater-dominated system as the result of permafrost thaw (e.g., Brutsaert and Hiyama 2012). Frey and McClelland (2009) also speculated that there could be important shifts in fluvial transport of organic matter, inorganic nutrients, and major ions, which might in turn have critical implications regarding primary production and carbon cycling in the interior of the Arctic Ocean basin as well as on the shelves. In this context, Carmack et al. (2016) also overviewed the importance of geochemical fingerprints of the Arctic Ocean acquired under the scientific assessment of the Arctic Freshwater Synthesis (AFS) (Prowse et al. 2015a).

9.4.2 Monitoring of River Water Chemistry in the Arctic

In contrast to river discharge data, long-term data sets on river water chemistry in the Arctic are relatively rare, and we do not yet have sufficient information to assess change on a pan-Arctic scale (McClelland et al. 2015). However, the two types of data are not always collected at the same locations, and decisions regarding whether to continue monitoring river discharge and water chemistry are often made independently (McClelland et al. 2015). Thus, parallel sampling programs on the six largest Arctic rivers (i.e., the Ob, Yenisei, Lena, Kolyma, Yukon, and Mackenzie rivers), which began as the Pan-Arctic River Transport of Nutrients, Organic matter, and Suspended Sediments (PARTNERS) project in 2003 and continued as the Arctic Great Rivers Observatory (Arctic-GRO) in 2008, have been established to improve understanding of the biogeochemical fluxes from the pan-Arctic watershed to the Arctic Ocean (McClelland et al. 2015). Scientists from the United States, Canada, and Russia have participated in both the implementation and the management of this program. The PARTNERS/Arctic-GRO effort has captured wide seasonal and geographical variations in water chemistry that relate to watershed characteristics such as geology, vegetation, permafrost coverage, and active layer thickness. These relationships have provided a framework for tracking future changes in watershed characteristics through river water chemistry (McClelland et al. 2008). Key characteristics of the watersheds drained by the PARTNERS/Arctic-GRO rivers, including catchment area, permafrost coverage, and human population density, have been

provided in Holmes et al. (2012). The river chemistry data set includes approximately 50 parameters, and 24 of these parameters were shown in Fig. 1 of McClelland et al. (2008).

The study by Holmes et al. (2012) was the first attempt to focus on the seasonal and annual fluxes of total dissolved nitrogen (TDN), DON, DIN, NO_3^-, TDP, Si, and DOC of the six largest Arctic rivers mentioned above. Tank et al. (2012) examined the magnitudes of riverine DIC fluxes of these same Arctic rivers, and they showed that DIC concentration had considerable and synchronous seasonal variation across the six largest Arctic rivers, estimating the annual DIC flux to be 30 Tg C $year^{-1}$. They also showed that chemical weathering was dominated by inputs from carbonate rocks in the North American (Yukon and Mackenzie) watersheds, but silicate rocks had a more important role in Siberian (Yenisei and Kolyma) watersheds. Very interestingly, in the coastal ocean, river water-induced decreases in aragonite saturation (i.e., an ocean acidification effect) appeared much more pronounced in the Siberian Arctic than in the North American Arctic and stronger in winter and spring than in the late summer.

Concentrations of uranium, barium, calcium, sulfate, and total alkalinity were much higher in the North American rivers compared with the Eurasian rivers (McClelland et al. 2008). In contrast, the seasonal patterns in chemistry were remarkably similar among the rivers. This seasonality is linked closely to hydrographic variations in all of the rivers. For example, DOC, POC, and PN showed positive correlations with discharge (McClelland et al. 2016), whereas major cations, anions, and DIC had negative correlations (Tank et al. 2012). Interestingly, annual POC yields and exports were consistently smaller than annual DOC yields and exports for the major rivers (see McClelland et al. 2016); however, PN export was found roughly equal to dissolved nitrogen (DN) export. They also found that the seasonal patterns in concentrations and source/composition indicators (C/N ratio, $\delta^{13}C$, $\Delta^{14}C$, and $\delta^{15}N$) were broadly similar among the rivers but with distinct regional differences.

In conjunction with the $\Delta^{14}C$-age of C ($\Delta^{14}C$-DOC and $\Delta^{14}C$-POC), Raymond et al. (2007) first determined the export and $\Delta^{14}C$-age of DOC for the Ob, Yenisei, Lena, Mackenzie, and Yukon rivers for 2004–2005. The total annual DOC flux from these five large rivers was estimated to be around 16 Tg C $year^{-1}$, and the total annual input of DOC from the pan-Arctic watershed to the Arctic Ocean was estimated as 25–36 Tg C $year^{-1}$. These fluxes were 2.5 times greater than temperate rivers with similar watershed sizes and water discharges. Based on $\Delta^{14}C$-age estimations, they also predicted that around 50% of DOC exported during the spring thaw was 1–5 years old, 25% was 6–10 years in age, and 15% was 11–20 years old. This implies that a small pool of DOC slightly depleted in $\Delta^{14}C$ is exported with the base flow but the large pool exported with the spring thaw is enriched in $\Delta^{14}C$ (Fig. 9.10). It is interesting to see in Fig. 9.10 that depleted (older) $\Delta^{14}C$-DOC is exported with the base flow in the Ob and Yukon rivers. Conversely, the younger bulk $\Delta^{14}C$-POC ages (non-depleted $\Delta^{14}C$-POC) in the Ob, Yenisei, and Lena rivers suggest that either the organic matter contributions from surface soil layers are proportionally greater or the older organic matter sources such as Yedoma are less influential in the case of particulate matter (McClelland et al. 2016).

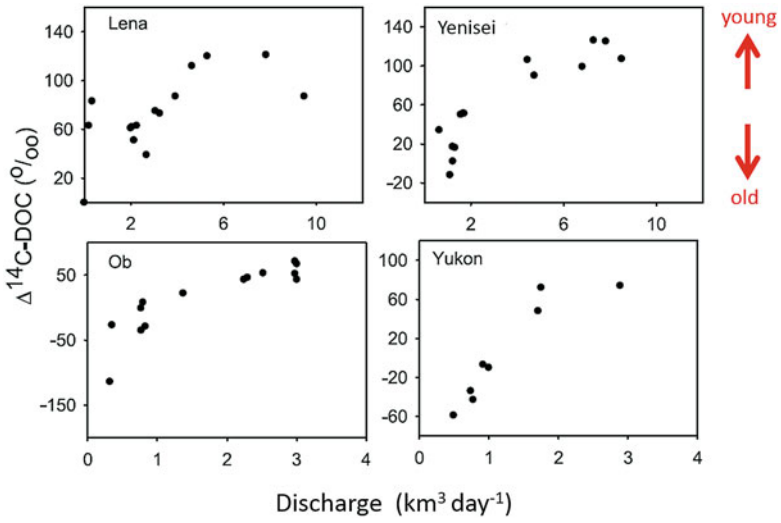

Fig. 9.10 Discharge versus Δ^{14}-DOC plots for all rivers except the Mackenzie River (Modified from Raymond et al. 2007)

9.5 Concluding Remarks

This chapter first provided an overview of the geographical scope of the Lena River basin and the seasonal changes and long-term trends of the Lena River discharge. Then, recent progress in hydrological modeling (i.e., river runoff and river ice modeling) targeting the discharge of the Lena River and other pan-Arctic rivers was described. Additionally, future projections regarding pan-Arctic river discharges were also mentioned. Because underdeveloped infrastructure within the pan-Arctic watershed is susceptible to damage during breakup floods in spring, projections of future discharge and the development of adaptation strategies for mitigating the effects of river floods and/or climate change-induced river disasters will be important regional considerations (e.g., Hiyama and Takakura 2018). In the latter half of this chapter, the importance of both river water chemistry (geochemical fingerprints) and past and ongoing activities regarding the monitoring of river water chemistry in the pan-Arctic rivers was overviewed.

Reductions of ice and snow coverages not only in the Arctic Ocean but also over the pan-Arctic watershed will enhance the regional hydrological cycle. As reviewed by Prowse et al. (2015a, b), there have been and there are projected to be major reductions in the durations of lake and river ice coverage. Such large reductions in ice coverage and the associated enhancement of heating of the water bodies have potential to create a major new flux of moisture to the atmosphere (Vihma et al. 2016). Quantifying the magnitude of moisture loss from freshwater bodies is important, because changes in water budgets/levels and associated alterations in the physical, chemical, and biological conditions contribute to the carbon and/or

methane fluxes in the pan-Arctic watershed (Wrona et al. 2016). These changes in hydrological and biogeochemical cycles could also be related to the enhancement of permafrost thaw. Therefore, new field studies are required to evaluate fully the changing sources, quantity, quality, seasonality, and effects of freshwater in the pan-Arctic watershed. To address these issues, continuous measurements of daily river runoff data are essential for producing a data set that can be employed in the future as an input to hydrological models.

References

Aagaard K, Carmack EC (1989) The role of sea ice and other fresh-water in the Arctic circulation. J Geophys Res 94(C10):14485–14498. https://doi.org/10.1029/JC094iC10p14485

Adam JC, Lettenmaier DP (2003) Adjustment of global gridded precipitation for systematic bias. J Geophys Res 108(D9):4257. https://doi.org/10.1029/2002JD002499

Bamber J, van den Broeke M, Ettema J, Lenaerts J, Rignot E (2012) Recent large increases in freshwater fluxes from Greenland into the North Atlantic. Geophys Res Lett 39:L19501. https://doi.org/10.1029/2012GL052552

Beltaos S (ed) (1995) River ice jams. Water Resources Publications, LLC, Colorado, 372p. isbn:978-091833487-9

Beltaos S (ed) (2008) River ice breakup. Water Resources Publications, LLC, Colorado, 462p. isbn:978-188720150-6

Bennett KE, Prowse TD (2010) Northern hemisphere geography of ice-covered rivers. Hydrol Process 24:235–240. https://doi.org/10.1002/hyp.7561

Berezovskaya S, Yang D, Kane DL (2004) Compatibility analysis of precipitation and runoff trends over the large Siberian watersheds. Geophys Res Lett 31:L21502. https://doi.org/10.1029/2004GL021277

Berezovskaya S, Yang D, Hinzman L (2005) Long-term annual water balance analysis of the Lena River. Glob Planet Chang 48:84–95. https://doi.org/10.1016/j.gloplacha.2004.12.006

Bintanja R, Selten FM (2014) Future increases in Arctic precipitation linked to local evaporation and sea-ice retreat. Nature 509:479–482. https://doi.org/10.1038/nature13259

Bowling LC, Lettenmaier DP, Nijssen B, Graham LP, Clark DB, Maayar ME, Essery R, Goers S, Gusev YM, Habets F, van den Hurk B, Jin J, Kahan D, Lohmann D, Ma X, Mahanama S, Mocko D, Nasonova O, Niu G-Y, Samuelsson P, Shmakin AB, Takata K, Verseghy D, Viterbo P, Xia Y, Xue Y, Yang Z-L (2003) Simulation of high-latitude hydrological processes in the Torne-Kalix basin: PILPS phase 2(e) 1: experiment description and summary intercomparisons. Glob Planet Chang 38:1–30. https://doi.org/10.1016/S0921-8181(03)00003-1

Bring A, Fedorova I, Dibike Y, Hinzman L, Mård J, Mernild SH, Prowse T, Semenova O, Stuefer SL, Woo M-K (2016) Arctic terrestrial hydrology: a synthesis of processes, regional effects, and research challenges. J Geophys Res Biogeosci 121:621–649. https://doi.org/10.1002/2015JG003131

Bring A, Shiklomanov A, Lammers RB (2017) Pan-Arctic river discharge: prioritizing monitoring of future climate change hot spots. Earth's Future 5:72–92. https://doi.org/10.1002/2016EF000434

Brown RD, Mote PW (2009) The response of northern hemisphere snow cover to a changing climate. J Clim 22:2124–2145. https://doi.org/10.1175/2008JCLI2665.1

Brutsaert W, Hiyama T (2012) The determination of permafrost thawing trends from long-term streamflow measurements with an application in eastern Siberia. J Geophys Res 117:D22110. https://doi.org/10.1029/2012JD018344

Carmack EC, Yamamoto-Kawai M, Haine TWN, Bacon S, Bluhm BA, Lique C, Melling H, Polyakov IV, Straneo F, Timmermans M-L, Williams WJ (2016) Freshwater and its role in the Arctic marine system: sources, disposition, storage, export, and physical and biogeochemical consequences in the Arctic and global oceans. J Geophys Res Biogeosci 121:675–717. https://doi.org/10.1002/2015JG003140

Déry SJ, Stieglitz M, McKenna EC, Wood EF (2005) Characteristics and trends of river discharge into Hudson, James, and Ungava bays, 1964-2000. J Clim 18:2540–2557. https://doi.org/10.1175/JCLI3440.1

Déry SJ, Stadnyk TA, MacDonald MK, Gauli-Sharma B (2016) Recent trends and variability in river discharge across northern Canada. Hydrol Earth Syst Sci 20:4801–4818. https://doi.org/10.5194/hess-20-4801-2016

Essery R, Clark DB (2003) Developments in the MOSES 2 land-surface model for PILPS 2e. Glob Planet Chang 38:161–164. https://doi.org/10.1016/S0921-8181(03)00026-2

Frey KE, McClelland JW (2009) Impacts of permafrost degradation on arctic river biogeochemistry. Hydrol Process 23:169–182. https://doi.org/10.1002/hyp.7196

Fukutomi Y, Igarashi H, Masuda K, Yasunari T (2003) Interannual variability of summer water balance components in three major river basins of northern Eurasia. J Hydrometeorol 4:283–296. https://doi.org/10.1175/1525-7541(2003)4<283:IVOSWB>2.0.CO;2

Gautier E, Dépret T, Costard F, Virmoux C, Fedorov A, Grancher D, Konstantinov P, Brunstein D (2018) *Going with the flow*: hydrologic response of middle Lena River (Siberia) to the climate variability and change. J Hydrol 557:475–488. https://doi.org/10.1016/j.jhydrol.2017.12.034

Haine TWN, Curry B, Gerdes R, Hansen E, Karcher M, Lee C, Rudels B, Spreen G, de Steur L, Stewart KD, Woodgate R (2015) Arctic freshwater export: status, mechanisms, and prospects. Glob Planet Chang 125:13–35. https://doi.org/10.1016/j.gloplacha.2014.11.013

Hatta S, Hayakawa H, Park H, Yamazaki T, Yamamoto K, Ohta T (2009) Long term runoff analysis of the Lena river basin using a distributed hydrological model. J Jpn Soc Hydrol Water Resour 22:177–187. https://doi.org/10.3178/jjshwr.22.177 (in Japanese with English abstract)

Hiyama T, Takakura H (2018) Global warming and human-nature dimension in Northern Eurasia. Global Environmental Studies (GES)/Springer, Singapore, 224p. isbn:978-981-10-4647-6. https://doi.org/10.1007/978-981-10-4648-3

Hiyama T, Asai K, Kolesnikov AB, Gagarin LA, Shepelev VV (2013) Estimation of the residence time of permafrost groundwater in the middle of the Lena River basin, eastern Siberia. Environ Res Lett 8:035040. https://doi.org/10.1088/1748-9326/8/3/035040

Holland MM, Finnis J, Barret AP, Serreze MC (2007) Projected changes in Arctic Ocean freshwater budgets. J Geophys Res 112(G4):G04S55. https://doi.org/10.1029/2006JG000354

Holmes RM, McClelland JW, Peterson BJ, Tank SE, Bulygina E, Eglinton TI, Gordeev VV, Gurtovaya TY, Raymond PA, Repeta DJ, Staples R, Striegl RG, Zhulidov AV, Zimov SA (2012) Seasonal and annual fluxes of nutrients and organic matter from large rivers to the Arctic Ocean and surrounding seas. Estuar Coasts 35:369–382. https://doi.org/10.1007/s12237-011-9386-6

Liu B, Yang D, Ye B, Berezovskaya S (2005) Long-term open-water season stream temperature variations and changes over Lena River basin in Siberia. Glob Planet Chang 48:96–111. https://doi.org/10.1016/j.gloplacha.2004.12.007

Ma X, Fukushima Y (2002) A numerical model of the river freezing process and its application to the Lena River. Hydrol Process 16:2131–2140. https://doi.org/10.1002/hyp.1146

Ma X, Fukushima Y, Hiyama T, Hashimoto T, Ohata T (2000) A macro-scale hydrological analysis of the Lena River basin. Hydrol Process 14:639–651. https://doi.org/10.1002/(SICI)1099-1085(20000228)14:3<639::AID-HYP959>3.0.CO;2-0

McClelland JW, Holmes RM, Peterson BJ, Amon R, Brabets T, Cooper L, Gibson J, Gordeev VV, Guay C, Milburn D, Staples R, Raymond PA, Shiklomanov I, Striegl R, Zhulidov A, Gurtovaya T, Zimov S (2008) Development of a pan-Arctic database for river chemistry. EOS Trans Am Geophys Union 89(24):217–218. https://doi.org/10.1029/2008EO240001

McClelland JW, Tank SE, Spencer RGM, Shiklomanov AI (2015) Coordination and sustainability of river observing activities in the Arctic. Arctic 68. https://doi.org/10.14430/arctic4448

McClelland JW, Holmes RM, Peterson BJ, Raymond PA, Striegl RG, Zhulidov AV, Zimov SA, Zimov N, Tank SE, Spencer RGM, Staples R, Gurtovaya TY, Griffin CG (2016) Particulate organic carbon and nitrogen export from major Arctic rivers. Glob Biogeochem Cycles 30:629–643. https://doi.org/10.1002/2015GB005351

Oshima K, Tachibana Y, Hiyama T (2015) Climate and year-to-year variability of atmospheric and terrestrial water cycles in the three great Siberian rivers. J Geophys Res Atmos 120:3043–3062. https://doi.org/10.1002/2014JD022489

Park H, Yamazaki T, Yamamoto K, Ohta T (2008) Tempo-spatial characteristics of energy budget and evapotranspiration in the eastern Siberia. Agric For Meteorol 148:1990–2005. https://doi.org/10.1016/j.agrformet.2008.06.018

Park H, Walsh J, Fedorov AN, Sherstiukov AB, Iijima Y, Ohata T (2013a) The influence of climate and hydrological variables on opposite anomaly in active-layer thickness between Eurasian and North American watersheds. Cryosphere 7:631–645. https://doi.org/10.5194/tc-7-631-2013

Park H, Walsh JE, Kim Y, Nakai T, Ohata T (2013b) The role of declining Arctic Sea ice in recent decreasing terrestrial Arctic snow depths. Pol Sci 7:174–187. https://doi.org/10.1016/j.polar.2012.10.002

Park H, Yoshikawa Y, Oshima K, Kim Y, Ngo-Duc T, Kimball JS, Yang D (2016) Quantification of warming climate-induced changes in terrestrial Arctic River ice thickness and phenology. J Clim 29:1733–1754. https://doi.org/10.1175/JCLI-D-15-0569.1

Peterson BJ, Holmes RM, McClelland JW, Vorosmarty CJ, Lammers RB, Shiklomanov AI, Shiklomanov IA, Rahmstorf S (2002) Increasing river discharge to the Arctic Ocean. Science 298:2171–2173. https://doi.org/10.1126/science.1077445

Peterson BJ, McClelland J, Curry R, Holmes RM, Walsh JE, Aagaard K (2006) Trajectory shifts in the Arctic and subarctic freshwater cycle. Science 313:1061–1066. https://doi.org/10.1126/science.1122593

Prowse T, Bring A, Mård J, Carmack E (2015a) Arctic freshwater synthesis: introduction. J Geophys Res Biogeosci 120:2121–2131. https://doi.org/10.1002/2015JG003127

Prowse T, Bring A, Mård J, Carmack E, Holland M, Instanes A, Vihma T, Wrona FJ (2015b) Arctic freshwater synthesis: summary of key emerging issues. J Geophys Res Biogeosci 120:1887–1893. https://doi.org/10.1002/2015JG003128

Rawlins MA, Steele M, Holland MM, Adam JC, Cherry JE, Francis JA, Groisman PY, Hinzman LD, Huntington TG, Kane DL, Kimball JS, Kwok R, Lammers RB, Lee CM, Lettenmaier DP, McDonald KC, Podest E, Pundsack JW, Rudels B, Serreze MC, Shiklomanov A, Skagseth Ø, Troy TJ, Vörösmarty CJ, Wensnahan M, Wood EF, Woodgate R, Yang D, Zhang K, Zhang T (2010) Analysis of the Arctic system for freshwater cycle intensification: observations and expectations. J Clim 23:5715–5737. https://doi.org/10.1175/2010JCLI3421.1

Raymond PA, McClelland JW, Holmes RM, Zhulidov AV, Mull K, Peterson BJ, Striegl RG, Aiken GR, Gurtovaya TY (2007) Flux and age of dissolved organic carbon exported to the Arctic Ocean: a carbon isotopic study of the five largest arctic rivers. Glob Biogeochem Cycle 21:GB4011. https://doi.org/10.1029/2007GB002934

Sakai T, Hatta S, Okumura M, Hiyama T, Yamaguchi Y, Inoue G (2015) Use of Landsat TM/ETM+ to monitor the spatial and temporal extent of spring breakup floods in the Lena River, Siberia. Int J Remote Sens 36:719–733. https://doi.org/10.1080/01431161.2014.995271

Serreze MC, Bromwich DH, Clark MP, Ertringer AJ, Zhang T, Lammers R (2003) Large-scale hydro-climatology of the terrestrial Arctic drainage system. J Geophys Res 108(D2):8160. https://doi.org/10.1029/2001JD000919

Serreze MC, Barrett AP, Slater AG, Woodgate RA, Aagaard K, Lammers RB, Steele M, Moritz R, Meredith M, Lee CM (2006) The large-scale freshwater cycle of the Arctic. J Geophys Res 111:C11010. https://doi.org/10.1029/2005JC003424

Shiklomanov AI, Lammers RB (2009) Record Russian river discharge in 2007 and the limits of analysis. Environ Res Lett 4:045015. https://doi.org/10.1088/1748-9326/4/4/045015

Slater AG, Bohn TJ, McCreight JL, Serreze MC, Lettenmaier DP (2007) A multimodel simulation of pan-Arctic hydrology. J Geophys Res 112(G4):G04S45. https://doi.org/10.1029/2006JG000303

Smith LC, Pavelsky TM, MacDonald GM, Shiklomanov AI, Lammers RB (2007) Rising minimum daily flows in northern Eurasian rivers: a growing influence of groundwater in the high-latitude hydrologic cycle. J Geophys Res 112:G04S47. https://doi.org/10.1029/2006JG000327

Su F, Adam JC, Bowling LC, Lettenmaier DP (2005) Streamflow simulations of the terrestrial Arctic domain. J Geophys Res 110(D8):D08112. https://doi.org/10.1029/2004JD005518

Suzuki K, Matsuo K, Hiyama T (2016) Satellite gravimetry-based analysis of terrestrial water storage and its relationship with run-off from the Lena River in eastern Siberia. Int J Remote Sens 37:2198–2210. https://doi.org/10.1080/01431161.2016.1165890

Swenson SC, Lawrence DM, Lee H (2012) Improved simulation of the terrestrial hydrological cycle in permafrost regions by the community land model. J Adv Model Earth Syst 4:M08002. https://doi.org/10.1029/2012MS000165

Tananaev NI, Makarieva OM, Lebedeva LS (2016) Trends in annual and extreme flows in the Lena River basin, northern Eurasia. Geophys Res Lett 43:10764–10772. https://doi.org/10.1002/2016GL070796

Tank SE, Raymond PA, Striegl RG, McClelland JW, Holmes RM, Fiske GJ, Peterson BJ (2012) A land-to-ocean perspective on the magnitude, source and implication of DIC flux from major Arctic rivers to the Arctic Ocean. Glob Biogeochem Cycle 26:GB4018. https://doi.org/10.1029/2011GB004192

van den Hurk B, Viterbo P (2003) The Torne-Kalix PILPS 2(e) experiment as a test bed for modifications to the ECMWF land surface scheme. Glob Planet Chang 38:165–173. https://doi.org/10.1016/S0921-8181(03)00027-4

van Vliet MTH, Franssen WHP, Yearsley JR, Ludwig F, Haddeland I, Lettenmaier DP, Kabat P (2013) Global river discharge and water temperature under climate change. Glob Environ Chang 23:450–464. https://doi.org/10.1016/j.gloenvcha.2012.11.002

Vihma T, Screen J, Tjernström M, Newton B, Zhang X, Popova V, Deser C, Holland M, Prowse T (2016) The atmospheric role in the Arctic water cycle: a review on processes, past and future changes, and their impacts. J Geophys Res Biogeosci 121:586–620. https://doi.org/10.1002/2015JG003132

Walsh J et al (2005) Cryosphere and hydrology. In: Arctic climate impact assessment. Cambridge University Press, Cambridge, pp 183–242

White D, Hinzman L, Alessa L, Cassano J, Chambers M, Falkner K, Francis J, Gutowski WJ Jr, Holland M, Holmes RM, Huntington H, Kane D, Kliskey A, Lee C, McClelland J, Peterson B, Rupp TS, Straneo F, Steele M, Woodgate R, Yang D, Yoshikawa K, Zhang T (2007) The arctic freshwater system: changes and impacts. J Geophys Res 112(G4):G04S54. https://doi.org/10.1029/2006JG000353

Wrona FJ, Johansson M, Culp JM, Jenkins A, Mård J, Myers-Smith IH, Prowse TD, Vincent WF, Wookey PA (2016) Transitions in Arctic ecosystems: ecological implications of a changing hydrological regime. J Geophys Res Biogeosci 121:650–674. https://doi.org/10.1002/2015JG003133

Yang D, Kane DL, Hinzman L, Zhang X, Zhang T, Ye H (2002) Siberian Lena River hydrologic regime and recent change. J Geophys Res 107(D23):4694. https://doi.org/10.1029/2002JD002542

Ye B, Yang D, Kane DL (2003) Changes in Lena River streamflow hydrology: human impacts versus natural variations. Water Resour Res 39:1200. https://doi.org/10.1029/2003WR001991

Ye H, Yang D, Zhang T, Zhang X, Ladochy S, Ellison M (2004) The impact of climatic conditions on seasonal river discharges in Siberia. J Hydrometeorol 5:286–295. https://doi.org/10.1175/1525-7541(2004)005<0286:TIOCCO>2.0.CO;2

Ye B, Yang D, Zhang Z, Kane DL (2009) Variation of hydrological regime with permafrost coverage over Lena Basin in Siberia. J Geophys Res 114(D17):D07102. https://doi.org/10.1029/2008JD010537

Chapter 10
Remote Sensing of Vegetation

Shin Nagai, Hideki Kobayashi, and Rikie Suzuki

10.1 Introduction

In eastern Siberia, interactions between terrestrial ecosystems above permafrost and the atmosphere affect global warming through their effects on carbon, water, and energy cycles. For instance, thawing permafrost produces continuous humid conditions, leading to forest degradation (Iijima et al. 2014), which reduces photosynthetic activity and thus the magnitude of the carbon sink, changes available water by decreasing evapotranspiration, and increases albedo, causing long-wave emissions to increase. The resulting increase in the thermokarst area may cause methane emission to increase (Flessa et al. 2008). Such increases in greenhouse gas emissions and albedo accelerate global warming. For an in-depth understanding of global climate change, it is essential to evaluate the spatiotemporal variability of ecosystem functions such as photosynthesis and evapotranspiration and ecosystem services (especially climate control) in eastern Siberia.

To evaluate the spatiotemporal variability of ecosystem functions and services, accurate observations of (1) aboveground biomass (stems, branches, and leaves), (2) plant functional type (PFT; e.g., deciduous coniferous or deciduous broad-leaved forest), and (3) growing season duration (i.e., the period from leaf-flush to leaf-fall) must be made over wide areas. These three parameters affect the carbon cycle through their effects on annual photosynthetic capacity and the carbon stock. Changes in PFT caused by climate change and human activities lead to changes in photosynthetic capacity, which in turn lead to changes in annual photosynthetic activity. Here, photosynthetic capacity refers to the maximum potential annual rate of photosynthesis and depends on leaf traits as well as the growing season duration (Wright et al. 2004; Richardson et al. 2013). In contrast, the annual gross primary production (GPP) reflects the actual rate of photosynthesis or photosynthetic activity

S. Nagai (✉) · H. Kobayashi · R. Suzuki
Japan Agency for Marine-Earth Science and Technology, Yokohama, Japan
e-mail: nagais@jamstec.go.jp

T. Ohta et al. (eds.), *Water-Carbon Dynamics in Eastern Siberia*,
Ecological Studies 236, https://doi.org/10.1007/978-981-13-6317-7_10

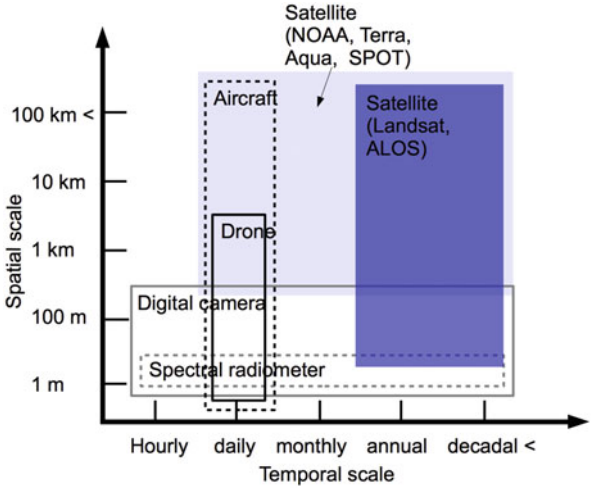

Fig. 10.1 Spatial and temporal scales of remote-sensing observations according to platform and sensor type

under daily weather conditions and is affected by long-term meteorological changes. Changes in photosynthetic activity cause changes in size of the annual carbon sink, which is determined by subtracting heterotrophic and autotrophic respiration from GPP, and in the amount of carbon (carbon stock) stored in stems and branches. Thus, mutual relationships among aboveground biomass, PFT, and growing season duration affect carbon flows and the carbon stock through their effects on photosynthesis.

Remote-sensing techniques, which use sensors such as digital cameras, spectral radiometers, and lasers mounted on platforms, including towers, drones, aircraft, and satellites, to observe targeted parameters from a distance, are useful means of obtaining data to evaluate spatiotemporal variabilities of aboveground biomass, PFT, and growing season duration (Fig. 10.1). The great advantage of remote-sensing techniques is that they make it possible to observe remote, mostly inaccessible areas, which are extensive in eastern Siberia. In this chapter, we review recent studies and discuss the use of remote-sensing techniques to observe terrestrial ecosystems in eastern Siberia. We focus on aboveground biomass, PFT, and growing season duration and how they affect interactions between terrestrial ecosystems and the atmosphere in the region.

10.2 Observation of Aboveground Biomass

Forest ecosystems in eastern Siberia play an important role in stabilizing the local and regional climate system through the surface energy transfer as evapotranspiration. Further, carbon assimilation by woody and soil ecosystem components helps to mitigate climate change through its effect on the global carbon cycle. Assimilated carbon in wood (i.e., forest biomass) generally represents the available biological resources. Remote-sensing techniques specifically detect the dry weight of the forest

biomass that is visible from satellites, that is, the aboveground biomass. The proportions of stems, branches, and leaves composing the aboveground biomass depend on the tree species. The allometric relationships between these components in Siberian larch (*Larix gmelinii*, *L. cajanderi*, and *L. sibirica*), a dominant tree species in eastern Siberia, and the total aboveground biomass have been studied by ground-based surveys (Kajimoto et al. 1999, 2006) at a limited number of field sites. Remote-sensing observations together with these allometric relationships can potentially be used to determine the spatial distributions over all of eastern Siberia of not only total aboveground biomass but also leaf biomass, the distribution of which must be known to estimate photosynthesis by the forest canopy.

10.2.1 Vegetation Indices

In satellite remote-sensing applications, vegetation indices have been widely used as proxies for aboveground biomass since the 1970s. One commonly used vegetation index is the normalized difference vegetation index (NDVI), which is derived from red and near-infrared (NIR) surface reflectances observed from satellites, where NDVI = (NIR − red)/(NIR + red) (Tucker 1979). NDVI, which typically takes a value between 0 (bare soil) and 1 (fully vegetated surfaces), is an indicator of the "amount of vegetation" and thus is closely related to biomass. High NDVI values imply large amounts of vegetation and abundant aboveground biomass (Fig. 10.2).

The effects of Arctic warming on the dynamics of boreal forests, including the forests of eastern Siberia, have been investigated by using NDVI data obtained by satellite-borne sensors. The Advanced Very High Resolution Radiometer (AVHRR) onboard National Oceanic Atmospheric Administration (NOAA) earth-observing satellites (hereafter NOAA-AVHRR) observed global vegetation dynamics from the 1980s to the 2000s (e.g., James and Kalluri 1994; Pinzon and Tucker 2014). Global analyses of NOAA-AVHRR data ($NDVI_{AVHRR}$) have detected decadal-scale NDVI changes (Myneni et al. 1997a; Zhou et al. 2001). These remote-sensing studies have revealed lengthening growing seasons and increases in maximum summertime NDVI values across the northern high latitudes, including in the larch forests of eastern Siberia. These results suggest that the amount of vegetation in the northern high latitudes was increased by the warming trend during the last 20 years of the twentieth century. However, the trend toward increasing the amount of vegetation in response to Arctic warming may not be monotonic. Studies in Eurasia covering an analysis period extending to 2006 have reported that NDVI showed a consistent increasing trend only until 1997 (1.8×10^{-3} year^{-1}), after which it started to decrease (-1.3×10^{-3} year^{-1}, Piao et al. 2011). In eastern Siberia, in particular, although the precipitation has a long-term increasing trend between 1982 and 2006 (0.39 mm yr.$^{-1}$, Piao et al. 2011), the growing season precipitation was decreased by -3.19 mm yr^{-1} in the time period between 1997 and 2006. This decreasing trend after 1997 potentially caused the decrease in summer NDVI trend (Piao et al. 2011).

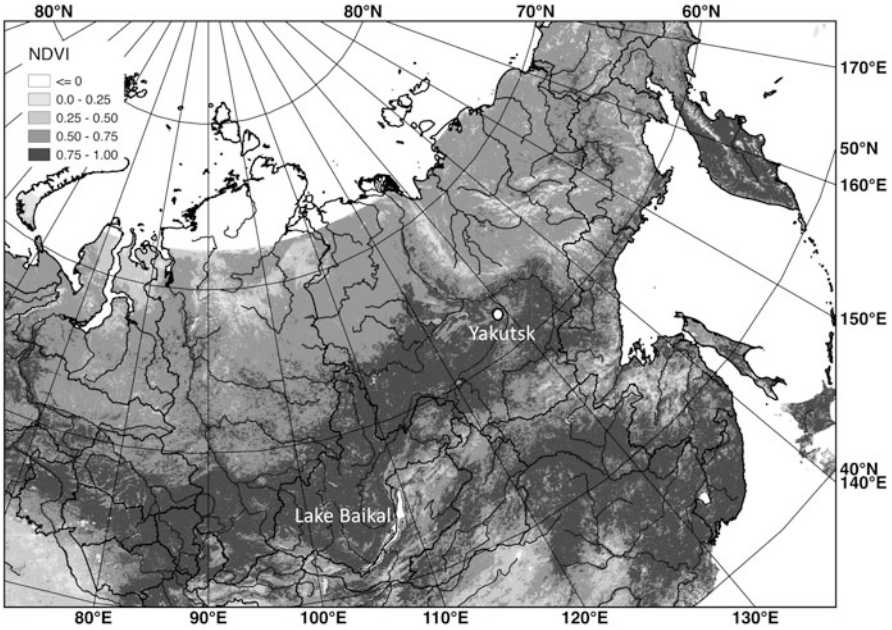

Fig. 10.2 NDVI distribution in eastern Siberia observed by SPOT-VGT in July 2010. The Russian political boarders are shown in bold lines. Rivers are shown in gray lines. White area shows higher NDVI values. Yakutsk is located in the middle of Lena River, and the NDVI values around the city of Yakutsk are higher than other regions

Although satellite-based NDVI is an effective way to investigate at large scale the duration of the forest growing season and the magnitude of vegetation changes, its interpretation is limited in several ways, particularly because changes in atmospheric conditions affect the monitoring results. For example, large-scale forest fires, which occur frequently in eastern Siberia, enhance aerosol loading in the atmosphere, and the presence of more aerosols in the atmosphere may cause the NDVI to decrease, even though no actual change in the vegetation status has occurred. In addition, cloud cover above eastern Siberia often prevents detection of vegetation signals. Most satellite NDVI data are processed by applying a maximum-value compositing procedure to extract the best NDVI values obtained during a specified time period and using those values to create the NDVI product. $NDVI_{AVHRR}$ products often use time periods of 10 days. If no days during a 10-day period are clear, then the highest NDVI value is selected regardless of cloudiness. Because the sky in many parts of eastern Siberia is likely to be cloud covered for periods exceeding 10 days, some NDVI values are affected by clouds.

Furthermore, NDVI values can depend on the data processing procedures that have been applied, such as sensor-related geometric and radiometric corrections, atmospheric correction schemes, and post-processing schemes (gap filling, compositing). Thus, to interpret the NDVI trends accurately, multiple data sets

should be compared to better understand the nature of the vegetation signal. These limitations are further described in Sect. 10.4.2.

NDVI is often used as an indicator of "vegetation greenness" or the "amount of vegetation," but these parameters do not directly correspond to any forest structure parameters. However, to the extent that aboveground biomass is related to leaf biomass, NDVI also correlates with leaf biomass. The aggregate $NDVI_{AVHRR}$ throughout the growing season is significantly correlated with ground-based measurements of the aboveground biomass of diverse tree species across boreal and temperate forests, and the relationship obtained by regression analysis between NDVI and aboveground biomass can be used to quantify the large-scale geographical distribution of aboveground biomass (Myneni et al. 2001). It must be noted that, unlike synthetic aperture radar (SAR), which can be used to estimate aboveground biomass more directly (see Sect. 10.2.3), NDVI-based biomass estimation is an indirect approach, because NDVI is sensitive mainly to leaf biomass rather than to total woody biomass. Thus, the interpretation of biomass data derived from NDVI data has inherent uncertainty.

10.2.2 Leaf Area Index

Among the three major aboveground biomass elements, leaf biomass, trunk biomass, and branch biomass, leaf biomass is the one important for characterizing forest canopy photosynthesis and thus productivity. In terrestrial biogeochemical models, leaf biomass is often represented by the leaf area index (LAI), which is defined as the one-sided leaf area per unit of ground area ($m^2\ m^{-2}$). LAI is derived by dividing the leaf biomass (g m^{-2}) by the leaf mass per unit of leaf area (leaf mass area, LMA; g m^{-2}). When the forest LAI is larger, the amount of sunlight intercepted by leaves increases, thus enhancing canopy-scale photosynthesis. The typical LAI of a forest ecosystem varies greatly, depending on the tree species, climate, topography, and soil water and nutrient conditions. In eastern Siberia, most forests are sparse, and the maximum LAI in summer is less than 4 (Kobayashi et al. 2010). The actual LAI varies spatially over eastern Siberia; however, so to evaluate forest ecosystem carbon dynamics, the regional LAI distribution must first be determined. Because the ground-based measurements cannot cover the whole area, remote-sensing observations are essential for producing regional distribution maps of LAI in eastern Siberia.

Two remote-sensing methods are used to produce regional- to global-scale LAI distribution maps. The first method, the so-called vegetation index-based method, is based on the biome-specific regression relationships between NDVI and LAI. Once the NDVI–LAI regression relationship is determined, it can be applied to satellite NDVI data sets to map LAI across eastern Siberia. NDVI is computed from the red and NIR spectral reflectances (e.g., red, 0.58–0.68 μm, and NIR, 0.725–1.00 μm for NOAA-AVHRR; see Sect. 10.2.1). Red reflectance is sensitive to the total chlorophyll content of the canopy, and NIR, which results from multiple scatterings within the canopy, is sensitive to the quantity of leaves. The chlorophyll content of the

forest canopy increases as LAI increases. As a result, more red sunlight is absorbed by the leaves, and the red reflectance decreases. Because no pigments absorb sunlight in the NIR spectral domain, when LAI increases, sunlight is reflected by or transmitted through the leaf surfaces many times, enhancing the NIR reflectivity of the forest canopy surface. These distinct features of the red and NIR spectral domains explain why NDVI increases when LAI increases (e.g., Myneni et al. 1997b). Once the NDVI and LAI relationship is determined from field measurements of LAI and red and NIR spectral reflectances, the relationship can be applied to large-scale mapping of LAI. The vegetation index method (NDVI–LAI relationship) is easy to apply to various forests once the NDVI–LAI relationship for the specific forest types such as an open needleleaf forest is determined. However, because of differences in forest structure, spatial leaf distribution (clumping), and leaf-angle distribution, a single LAI value may be associated with several NDVI values, which is a limitation on the accuracy of the LAI values retrieved by using this simple empirical approach.

The second method uses a sophisticated forest canopy radiative transfer model for inverse estimation of LAI from satellite-observed spectral reflectances. The improved accuracy of the surface spectral reflectances retrieved by the VEGETATION sensor onboard the French satellite SPOT (hereafter SPOT-VGT), which was launched in 1998, and the Moderate Resolution Imaging Spectroradiometer (MODIS) sensor onboard the US National Aeronautics and Space Administration (NASA) satellite Terra (hereafter Terra-MODIS), compared with NOAA-AVHRR data, allows LAI to be estimated by using a physically based radiative transfer model inversion approach (Knyazikhin et al. 1998). For example, canopy total LAI for application to climatic and vegetation dynamics studies has been operationally mapped, including in eastern Siberia, with spatial resolutions of 500 m to 1 km by using Terra-MODIS data acquired every 4–8 days since 2000 by the NASA MODIS science team (Myneni et al. 2002, Fig. 10.3). Canopy LAI maps from Terra-MODIS and SPOT-VGT are useful for studying eastern Siberia as a whole, though a regional-scale study might need a higher-resolution data set. In this regard, the Landsat series satellites provide reflectance images with a spatial resolution of 30 m. By using Landsat data, a detailed map of LAI in a specific area of eastern Siberia can be produced. For example, a LAI distribution map of the forest around the Lena River near the city of Yakutsk produced by radiative transfer model inversion (Kushida et al. 2007) shows that in larch forests on the left bank of the Lena River, LAI varies from 1 to 3 in the summer.

The dominant genus of trees in eastern Siberia is larch (*Larix gmelinii*, *L. cajanderi*, and *L. sibirica*), where it forms large forests, either as pure stands or in association with pine (*Pinus sylvestris*), spruce (*Picea obovata*), and other species. More than 50% of the total forested area in eastern Siberia (2.5×10^6 km^2) consists of larch forest. Most larch forests are sparse with a typical LAI of no more than 4. Therefore, a large amount of sunlight penetrates the larch canopy and reaches understory and forest floor plants. This light environment provides favorable conditions for forest floor species such as cowberry (*Vaccinium vitis-idaea*, a small shrub), mosses, and lichens. Because the floor of a larch forest is mostly covered by such

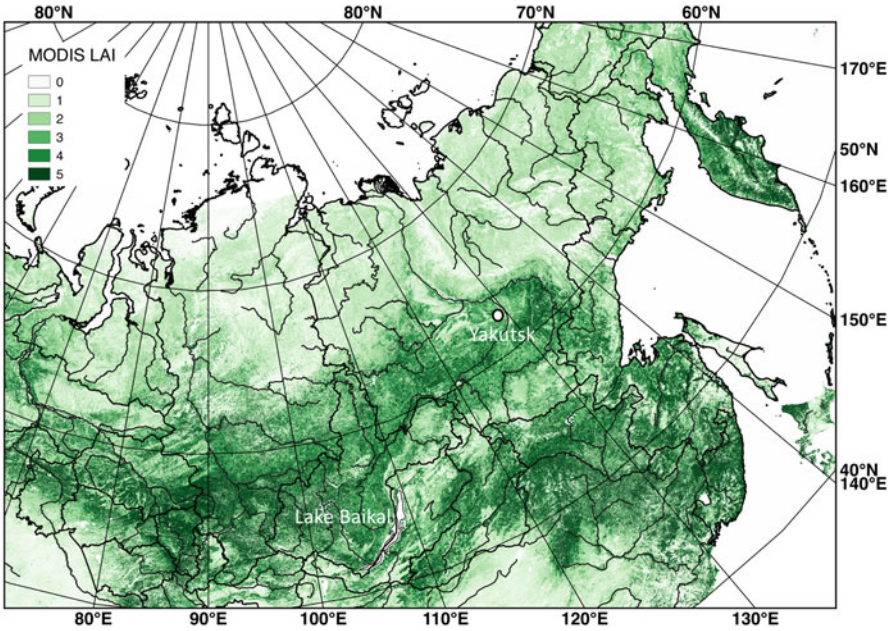

Fig. 10.3 LAI distribution in eastern Siberia estimated from Terra-MODIS data sets

plants, their contributions to photosynthesis and evapotranspiration of the forest as a whole are not negligible. Although the size of their contributions depends on the age of the forest stand, Iida et al. (2009) reported that more than 50% of total evapotranspiration from a larch forest near Yakutsk was attributable to the forest floor layer.

The contribution of the forest floor vegetation to photosynthesis and evapotranspiration can be evaluated by estimating the LAI of the larch overstory and the forest floor plants separately. Even though larch forests are sparse, satellites can rarely observe the forest floor vegetation in summer owing to the greenness of the larch canopy (Kobayashi et al. 2007). However, because larch is a deciduous needle-leaved tree, during early spring (after snow melt and before larch foliation), it is possible to monitor the forest floor vegetation by satellite (e.g., Kobayashi et al. 2010; Liu et al. 2017). Most forest floor plants such as cowberry are evergreen, so the seasonal changes in their LAI are small. Once the forest floor plants' signature which is related to the forest floor LAI is determined from springtime satellite data, then the LAI of the larch overstory can be estimated by using the forest floor information as background data. Under the assumption that the forest floor LAI is constant throughout the growing season, seasonal changes in satellite reflectance signals can be attributed to seasonal changes in the larch canopy. For example, Kobayashi et al. (2010) estimated the larch overstory LAI in Siberian larch forests from the seasonal increase in the normalized difference water index (NDWI) after snow melt, where NDWI = (NIR − shortwave infrared)/(NIR + shortwave infrared). The relationship

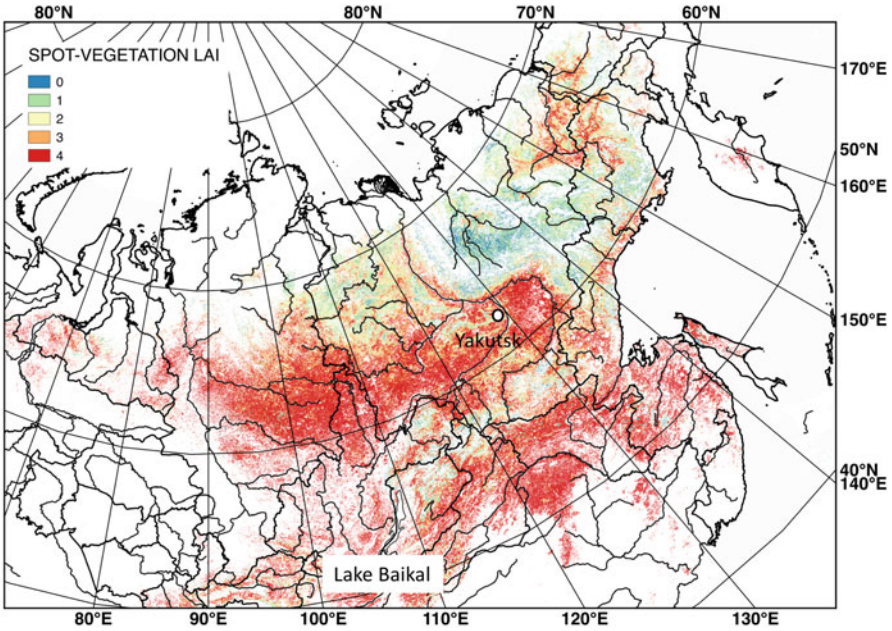

Fig. 10.4 Larch overstory LAI in eastern Siberia estimated from SPOT-VGT data sets

between increases in NDWI and LAI has been calibrated for various forest floor LAI data sets by using a radiative transfer model. The spatial distribution of the larch overstory LAI in eastern Siberia shows a distinct north–south gradient in summer (Fig. 10.4). In addition, LAI can vary along elevation; LAI is lower in the Stanovoy Mountains than in surrounding regions. The estimated LAI distribution is useful for validating the LAI distribution simulated by ecosystem models. For example, Sato et al. (2016) used satellite-based summer maximum (July) overstory LAI data averaged over 1998 to 2013 in order to validate the latitudinal gradient of simulated LAI at the present time (the year of 2005). The present study also estimated the geographical distribution of forest floor information that is related to the forest floor LAI (it was called as apparent forest floor LAI). However, the accurate quantification of understory LAI is one of the challenging parts because there are few field observations that are used for validation and calibration of the remote-sensing measurements.

10.2.3 Radar and LiDAR Remote Sensing

Microwave satellite remote-sensing techniques provide a different view of forest ecosystems. SAR is an active microwave radar technology commonly used in satellite remote sensing. SAR observations, for example, those of the Phased

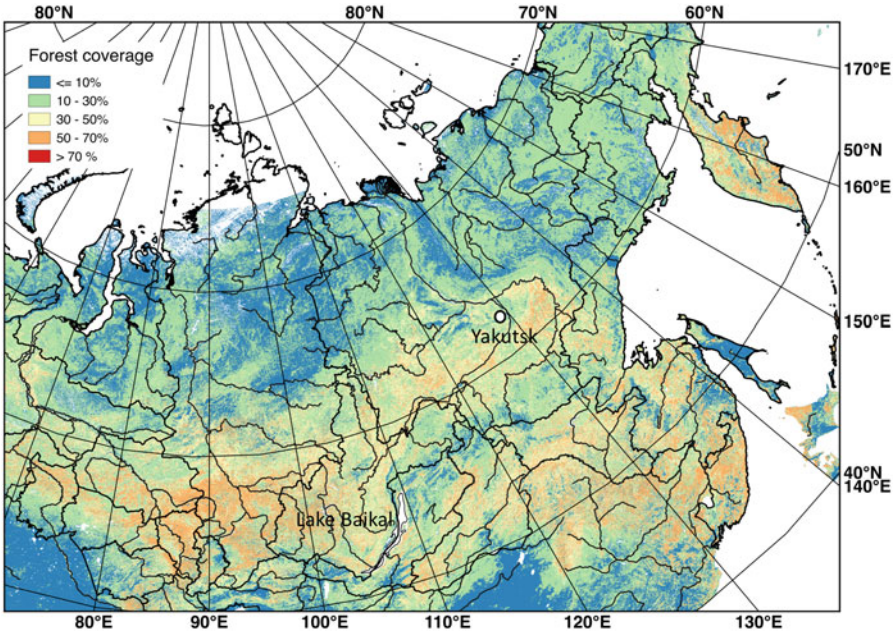

Fig. 10.5 Map of forested (black) and non-forested areas of eastern Siberia determined by using ALOS-2-PALSAR data sets

Array type L-band Synthetic Aperture Radar (PALSAR) onboard the Advanced Land Observing Satellite (ALOS), are particularly useful for distinguishing aboveground biomass between forested and other regions (Fig. 10.5). L-band microwaves with a wavelength of 23 cm, which penetrate the forest canopy and are scattered by tree trunks, a phenomenon called volume scattering, are particularly useful for estimating the aboveground biomass of the forest, because the returning backscattered L-band SAR signal is an indicator of the trunk biomass. When the aboveground biomass is relatively small, it can be estimated from SAR data merely by removing the micro-topographical effect. However, the backscattered SAR signal saturates as the aboveground biomass becomes higher.

The aboveground biomass can also be estimated by using canopy height information obtained by the satellite-based laser altimetry measurements. The Geoscience Laser Altimeter System (GLAS) onboard NASA's Ice, Cloud, and land Elevation Satellite (ICEsat), which was operational during 2003–2009, provided a global canopy height map with a spatial resolution of 1 km (Simard et al. 2011). In eastern Siberia, the forest canopy height in the middle basin of Lena River near Yakutsk reaches up to 30 m and higher than downstream regions in the high latitudes (Fig. 10.6), where LAI in the same region is also higher than other regions (LAI = 3–4; see Figs. 10.3 and 10.4).

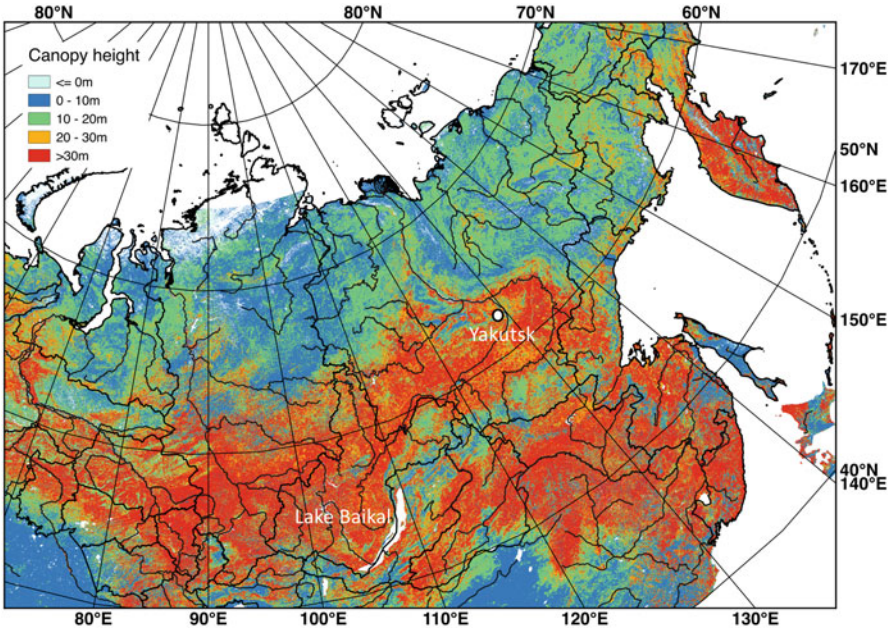

Fig. 10.6 Forest canopy height (m) distribution in eastern Siberia estimated from ICEsat-GLAS data sets

10.3 Observation of Plant Functional Type

Plant functional type (PFT) is a classification system for plant species and simplification of floristic complexity in global vegetation models (Prentice et al. 1992). Species-specific mapping of plants at a continental scale is not feasible, so PFT is mapped by first classifying the plant species in various regions according to plant traits. PFT maps compiled in this way are used as fundamental information on the ecosystem model simulation. PFT maps of eastern Siberia have been produced by Terra/Aqua-MODIS (MCD12Q; resolution 500 m) and the Medium Resolution Imaging Spectrometer (MERIS) onboard European Space Agency Envisat satellites (GlobCover2009; resolution 300 m). Suzuki et al. (2004) produced a detailed regional-scale PFT map from airborne observations of the area around the Lena River from April 24 to June 19, 2000. These regional maps show spatial patterns of larch on permafrost, evergreen needle-leaved species, and birch, as well as the spatial pattern of thermokarst features such as alases.

During long-term environmental monitoring, the temporal variability of PFT distributions must be taken into account. In eastern Siberia, large forest fires that burn canopy trees, forest floor vegetation, and soil organic matter occur on a decadal scale. Spatial and temporal variations of burned areas can be estimated by comparing satellite images acquired before and after fires. For example, in eastern Siberia, the burned area fraction in 0.25° latitude × 0.25° longitude grids was mapped by using

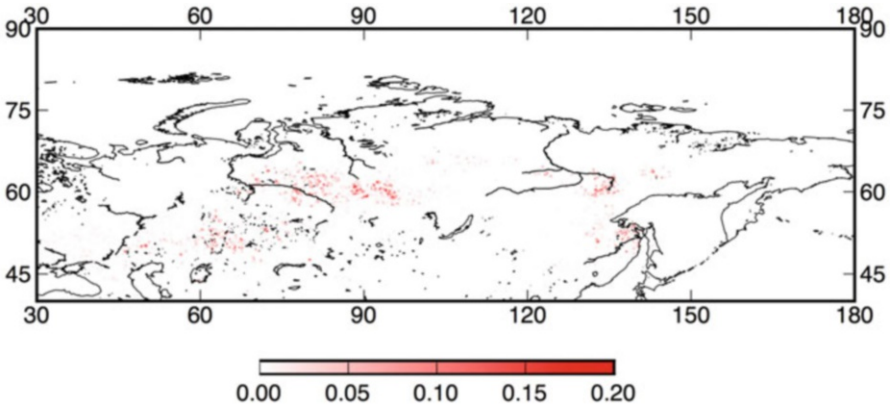

Fig. 10.7 Burned area fraction in eastern Siberia in July 2010 mapped by using data from the GFED

data from the Global Fire Emissions Database (GFED version 4.0; Giglio et al. 2013; Fig. 10.7). Such burned area maps are useful for monitoring not only forested area changes but also greenhouse gas and aerosol emissions (CO_2, CO, black carbon) from fires.

10.4 Observations of Growing Season Duration

10.4.1 Satellite Observation

AVHRR-NOAA, SPOT-VGT, and the MODIS sensors onboard Terra and Aqua (hereafter Terra/Aqua-MODIS), which observe the whole world at a daily time step, allow spatiotemporal variability in the timing of the start (SGS) and end (EGS) of the growing season to be detected. The $NDVI_{AVHRR}$ time series, which covers more than 30 years, is remarkable for its length, although there are some serious issues to be considered (see Sect. 10.4.2) (Buitenwerf et al. 2015). Buitenwerf et al. (2015) showed that the average of growing season duration from 2003 to 2012 became longer in boreal regions than that from 1981 to 1990. The average of timing of SGS from 2003 to 2012 became earlier than that from 1981 to 1990. In contrast, the difference between the average of timing of EGS from 2003 to 2012 and that from 1981 to 1990 showed spatial characteristics. In the northern areas, the average of timing of EGS became earlier. In the further south areas, the average of timing of EGS did not change. In the still further south areas, the average of timing of EGS became later. Delbart et al. (2006), who analyzed time series of $NDVI_{AVHRR}$ and SPOT-VGT-based normalized difference water index (NDWI) from 1982 to 2004, reported year-to-year variability in the spatial distribution of the timing of SGS in Siberia. The NDWI data have the advantage that they allow the timing of snow melt

to be distinguished from that of SGS. Their analysis also showed that from 1982 to 2004, the timing of SGS tended to occur earlier each year in Northeast Siberian taiga and areas from Lake Baikal toward Ob River's mouth, but they observed delayed trend in eastern Siberia (Yakutsk region).

Suzuki et al. (2001) examined the spatial characteristics of the relationships among $NDVI_{AVHRR}$, PFT, temperature, and precipitation. These relationships explain the spatial differences in the growing season duration in boreal ecosystems. Suzuki et al. (2007) showed that $NDVI_{AVHRR}$ was positively correlated with temperature and negatively correlated with precipitation in eastern Siberia. These relationships indicate that interannual changes in vegetation and the resultant interannual changes in evapotranspiration are controlled by temperature in the northern low-temperature region of eastern Siberia (Suzuki et al. 2007).

10.4.2 Satellite Observation Issues

Despite the usability of satellite remote-sensing observations, five issues remain that can cause uncertainty in the detection of the growing season in eastern Siberia as well as misleading results.

10.4.2.1 Issue 1: Systematic Noise

NOAA-AVHRR satellite data include systematic noise caused by satellite drift and large volcanic eruptions (Jin and Treadon 2003). The SPOT-VGT and Terra/Aqua-MODIS products have reduced systematic noise due to satellite drift, but no satellite sensors can eliminate systematic noise due to large volcanic eruptions.

10.4.2.2 Issue 2: Atmospheric Noise and Cloud Contamination

Satellite observations are affected by atmospheric noise (e.g., smoke and chemical emissions, yellow sand dust storms) and cloud cover. Motohka et al. (2011) showed that about 40% of satellite data observed by Terra-MODIS with cloud screening by the state flag of satellite product still included cloud contamination. In eastern Siberia, satellite observations are often affected by atmospheric noise due to haze and smoke from forest fires.

10.4.2.3 Issue 3: Heterogeneity of Plant Functional Type

PFT heterogeneity within single pixels of satellite data causes uncertainty in phenological observations. This uncertainty is larger in data from SPOT-VGT and Terra/

Aqua-MODIS, which have spatial resolutions of 1.1 km and 250 m, than in data from Landsat series satellites, with a spatial resolution of 30 m.

10.4.2.4 Issue 4: Effect of Solar Zenith and View Angles

In the high latitudes, the effect of solar zenith and view angles on satellite data also causes uncertainty in phenological observations (Kobayashi et al. 2016). Particularly in autumn (late August and September), the solar zenith angle becomes very high (over 60°), and in boreal forests, sunlight coming from an oblique direction is mainly reflected from the top of the canopy; the forest floor is rarely illuminated. As a result, even in a sparse forest, phenological information about forest floor plants from satellite observations is limited (Kobayashi et al. 2016).

10.4.2.5 Issue 5: Insufficient Ground-Truthing

Ecological interpretation of satellite data is difficult because the data are not yet sufficiently constrained by ground-truthing (Nasahara and Nagai 2015). In areas receiving heavy snowfall, in situ observations have shown that vegetation indices in spring reflect both melting snow and leaf-flush, and in autumn they reflect both leaf-fall and snowfall (Nagai et al. 2010). Confusion between phenological phenomena, leaf-flush and leaf-fall, and melting and falling snow in time series of satellite-observed vegetation indices produces misleading analysis results regarding the timing of SGS and EGS.

10.4.3 In Situ Observations

To resolve these problems, satellite remote-sensing observations must be validated by performing field studies with, for example, time-lapse digital cameras and spectral radiometers (Nasahara and Nagai 2015). Continuous observations of phenological phenomena such as leaf-flush, leaf-coloring, and leaf-fall by time-lapse digital cameras, along with measurements of CO_2 and H_2O fluxes and micrometeorological observations, have been carried out since June 2013 in a deciduous coniferous (larch) forest at the Spasskaya Pad Scientific Forest Station near Yakutsk in eastern Siberia (62°15′18”N, 129°37′08″E) (see Chap. 3). Time-lapse digital cameras (Coolpix-4300/4500, Nikon, Tokyo, Japan) were installed at heights of 32 m on a CO_2 flux tower and 3 m on the forest floor. The cameras acquire plant phenology images of the overstory (forest canopy) and understory vegetation (forest floor) every hour during the daytime (Nagai et al. 2018). This larch forest site is part of the Phenological Eyes Network (http://www.pheno-eye.org; Nasahara and Nagai 2015).

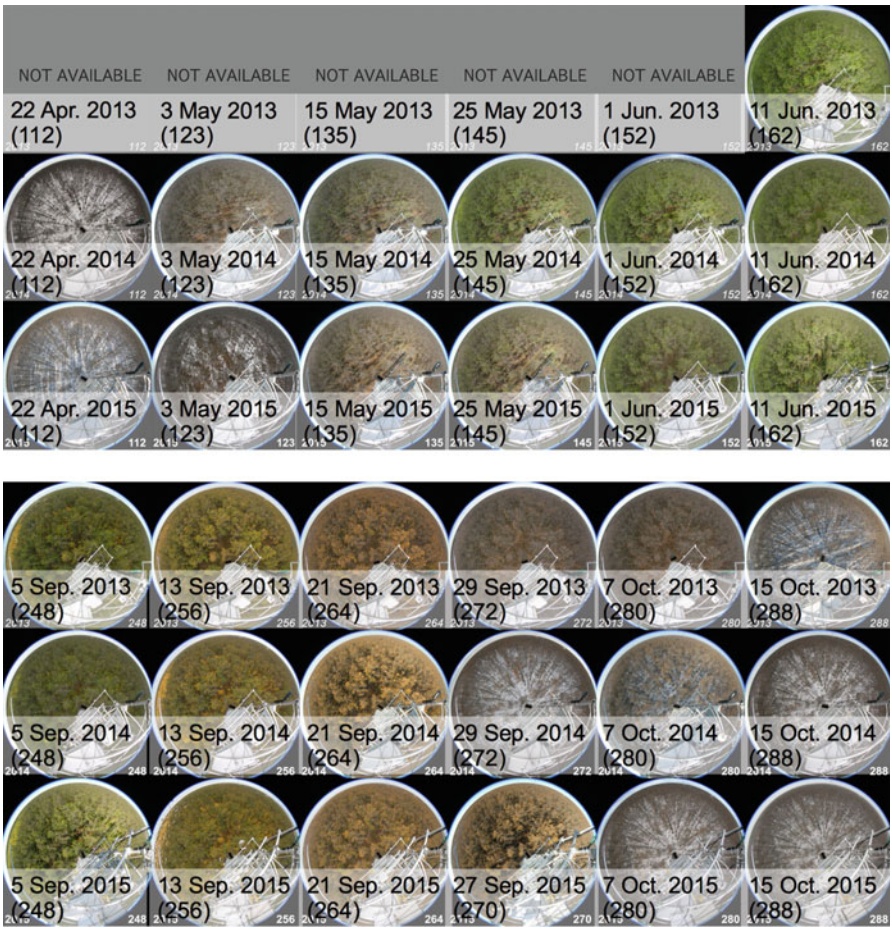

Fig. 10.8 Typical phenological images in spring (top) and autumn (bottom) of the Spasskaya Pad larch forest from June 2013 to June 2016. Date and day of year (in parenthesis) are shown on each phenological image

Typical phenological images of the Spasskaya Pad larch forest (Fig. 10.8) obtained over a 3-year period show the timing of phenological events: leaf-flush in larch during mid- to late May, leaf-coloring in birch from early to mid-September, and leaf-fall in larch from late September to mid-October. In addition, snow melt was imaged between late April and early May, and the first snowfall was observed between late September and early October. In birch, an understory component, leaf-flush occurred about a week later than it did in larch, which composes the overstory. In contrast, leaf-coloring was about a week earlier in birch than in larch. In larch, leaf-flush occurred 13 days earlier in 2014 than in 2015, and leaf-fall occurred about 10 days earlier in 2013 than in 2014 and 2015. Examination of the seasonal

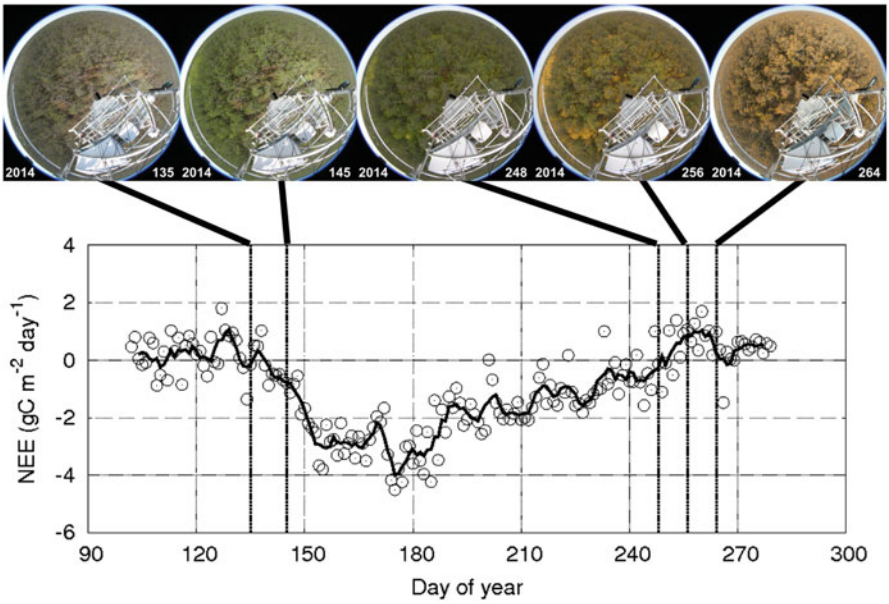

Fig. 10.9 Seasonal changes in flux-based NEE in 2014 (from Kotani et al. unpublished) in relation to typical phenological images of the Spasskaya Pad larch forest. The solid line shows the 5-day moving average

relationships between CO_2 flux-based net ecosystem exchange {NEE, where NEE = − [GPP – autotrophic (AR) and heterotrophic respiration (HR)]; see Chap. 4} and typical phenology (Fig. 10.9) showed that the first date on which NEE was less than zero in spring (i.e., the first date on which carbon absorption was greater than carbon emission) occurred just after leaf-flush in larch, whereas the first date on which NEE was more than zero in autumn occurred before both leaf-coloring in birch and leaf-fall in larch.

Long-term continuous phenological images are useful for detecting year-to-year variations in the timing of leaf-flush, leaf-coloring, and leaf-fall in each tree species as well as in the snow-covered period. However, visual inspection of phenological images is qualitative. Depending on the individual conducting the inspection, the timing of each phenological phenomenon can differ by as much as a few days. Phenological images consist of red (DN_R), green (DN_G), and blue digital numbers (DN_B), each of which can range from 0 to 255. Therefore, the timing of leaf-flush, leaf-coloring, and leaf-fall can be determined quantitatively by examining time series of proportions of DN_R, DN_G, and DN_B values as percentages of total DN (denoted as %R, %G, %B, respectively) and a vegetation index based on average DN_R, DN_G, and DN_B values, such as the green excess index (denoted as GEI; Richardson et al. 2007) in the region of interest.

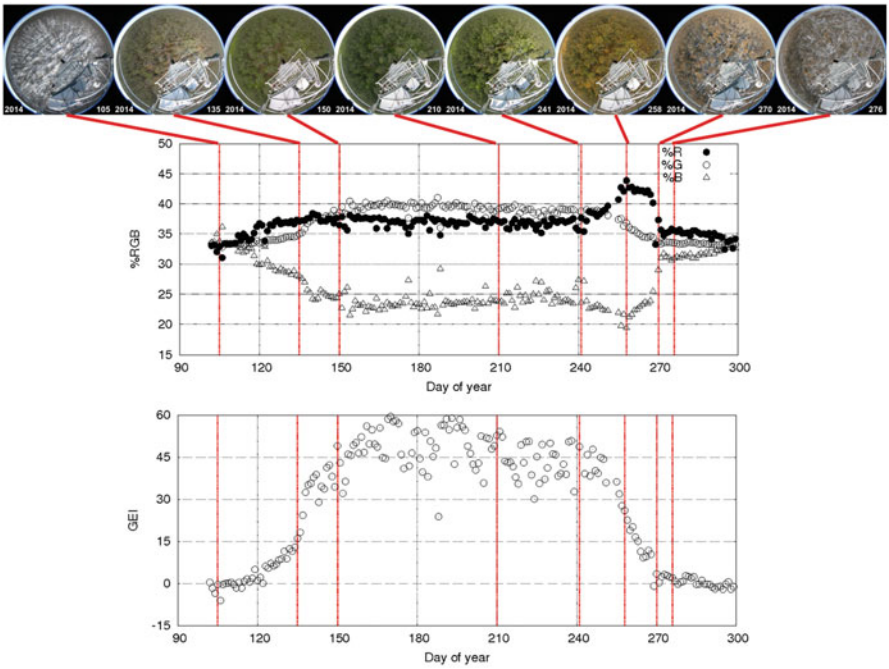

Fig. 10.10 Seasonal changes in %R, %G, %B (upper graph), and GEI (lower graph) from April to October 2014 along with typical phenological images of the Spasskaya Pad larch forest (SSP). Date and day of year (in parenthesis) are shown on each phenological image

$$\%\mathrm{R} = \mathrm{DN_R}/(\mathrm{DN_R} + \mathrm{DN_G} + \mathrm{DN_B}) \tag{10.1}$$

$$\%\mathrm{G} = \mathrm{DN_G}/(\mathrm{DN_R} + \mathrm{DN_G} + \mathrm{DN_B}) \tag{10.2}$$

$$\%\mathrm{B} = \mathrm{DN_B}/(\mathrm{DN_R} + \mathrm{DN_G} + \mathrm{DN_B}) \tag{10.3}$$

$$\mathrm{GEI} = (\mathrm{DN_G} - \mathrm{DN_R}) + (\mathrm{DN_G} - \mathrm{DN_B}) \tag{10.4}$$

Among ecosystems and tree species, %R, %G, %B, and GEI show characteristic seasonal patterns (Nagai et al. 2011; Wingate et al. 2015). At the Spasskaya Pad site in 2014 (Fig. 10.10), %G increased during leaf-flush (DOY 135–150), but %B decreased rapidly. During leaf-coloring and leaf-fall (DOY 240–270), %G decreased. In contrast, %R first increased just before the leaf-coloring peak (DOY 258), after which %R fell steeply, while %B increased rapidly. The GEI time series was characterized by a rapid increase during leaf-flush and a rapid decrease during leaf-coloring and leaf-fall.

By selecting suitable threshold values of %R, %G, %B, and GEI, it is possible to detect year-to-year variations in the timing of leaf-flush, leaf-coloring, and leaf-fall. For example, Nagai et al. (2013) developed a statistical phenological model for estimating the timing of leaf-flush and leaf-fall in a deciduous broad-leaved forest in Japan by examining the relationship between leaf-flush and leaf-fall dates

determined from daily phenological images and daily mean air temperature. The development of a statistical phenological model, based on observations obtained with time-lapse digital cameras at multiple field sites, would be useful for estimating leaf-flush and leaf-fall dates in eastern Siberia and for characterizing their spatial distribution along a latitudinal gradient. Toward this aim, inexpensive, battery-driven time-lapse digital cameras (e.g., Garden Watch Cam, Brinno, Taiwan) have been installed at multiple field sites in Alaska (Kobayashi et al. 2016).

10.4.4 Integrating In Situ and Satellite Observations

Long-term continuous phenological images allow testing and validation of the timing of SGS and EGS values determined by using satellite-observed vegetation indices. In NDVI and enhanced vegetation index (EVI), where $EVI = G \times \{(NIR - red)/[NIR + (C1 \times red) - (C2 \times blue) + L]\}$ ($G = 2.5$, $C1 = 6$, $C2 = 7.5$, and $L = 1$ are constants; Huete et al. 2002), analyses, it is more difficult to determine the timing of EGS than of SGS, because the timing and spatial patterns of leaf-coloring and leaf-fall vary among tree species (Nagai et al. 2010, 2014).

The green–red vegetation index (GRVI), where GRVI = (green – red)/(green + red) (Tucker 1979; Motohka et al. 2010), which is based only on seasonal changes in the color of the canopy, is more suitable for determining the timing of EGS in deciduous broad-leaved forests than either NDVI or EVI (Nagai et al. 2014). Before leaf-flush begins in spring, GRVI shows negative values, and it again becomes negative values after the peak of leaf-coloring and leaf-fall in autumn (Motohka et al. 2010; Nagai et al. 2014).

At the Spasskaya Pad site (Fig. 10.11), the first date in each year from 2003 to 2015 on which $GRVI_{MODIS}$ was more than or equal to zero in spring corresponded to the beginning of leaf-flush in larch, whereas the first date on which $GRVI_{MODIS}$ was less than zero in autumn corresponded to the peak of leaf-coloring in birch, which was earlier than the leaf-coloring peak in larch. These results indicate that $GRVI_{MODIS} = 0$ is a useful criterion for detecting both the start and end of the functional growing season (i.e., duration of photosynthetic capacity) in larch forests in eastern Siberia.

Using these ground-truthing data, we analyzed the spatial distribution of the first dates on which $GRVI_{MODIS}$ was more than or equal to zero in spring and the first dates on which it was less than zero in autumn in 2015 for the whole of eastern Siberia (Fig. 10.12). The timing of SGS was earlier at low latitudes and elevations than at high latitudes and elevations. In contrast, the timing of EGS was later at low latitudes and elevations than at high latitudes and elevations. A similar analysis for the period from 2003 to 2015 revealed the spatial characteristics of the year-to-year variability in the timing of SGS and EGS (not shown). Analyses of the relationships among year-to-year variability in the timing of SGS and EGS, PFT, aboveground biomass, topography, and latitudinal gradients in eastern Siberia might allow the sensitivity and vulnerability of plant phenology to climate change to be evaluated.

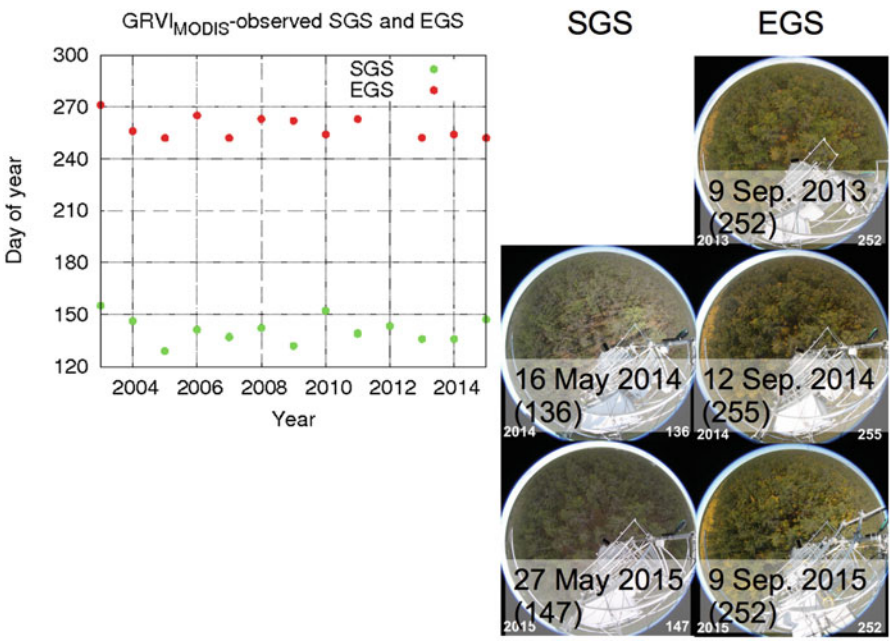

Fig. 10.11 Year-to-year variability in SGS and EGS (day of year, DOY), based on GRVI observed by Terra/Aqua-MODIS (GRVI$_{MODIS}$), in the Spasskaya Pad larch forest, along with phenological images obtained on the first date on which GRVI$_{MODIS}$ was more than or equal to zero in spring (SGS) and the first date on which it less than zero in autumn (EGS). We substituted the canopy surface image on 12 September 2014 for the missing image on 11 September 2014. EGS in 2012 was missing

10.5 Concluding Remarks

In this chapter, we summarized the usefulness and uncertainties of remote-sensing techniques to monitor the spatiotemporal variability of aboveground biomass, PFT, and growing season duration in eastern Siberia by refereeing previous studies and introducing our own developed studies. To increase our understanding of interactions between terrestrial ecosystems and the atmosphere in eastern Siberia, the following three challenging tasks should be undertaken.

The spatiotemporal variability of the aboveground biomass and growing season duration detected by remote-sensing observations are important for evaluating photosynthetic capacity. However, this information cannot be used to evaluate photosynthetic activity directly. One remote-sensing technique that allows their activities to be directly evaluated is the measurement of the fluorescent intensity of chlorophyll. Solar-induced chlorophyll fluorescence is being observed by the thermal and NIR sensor for carbon observation–Fourier transform spectrometer sensor onboard Japan's Greenhouse Gases Observing Satellite (GOSAT) (Frankenberg et al. 2011).

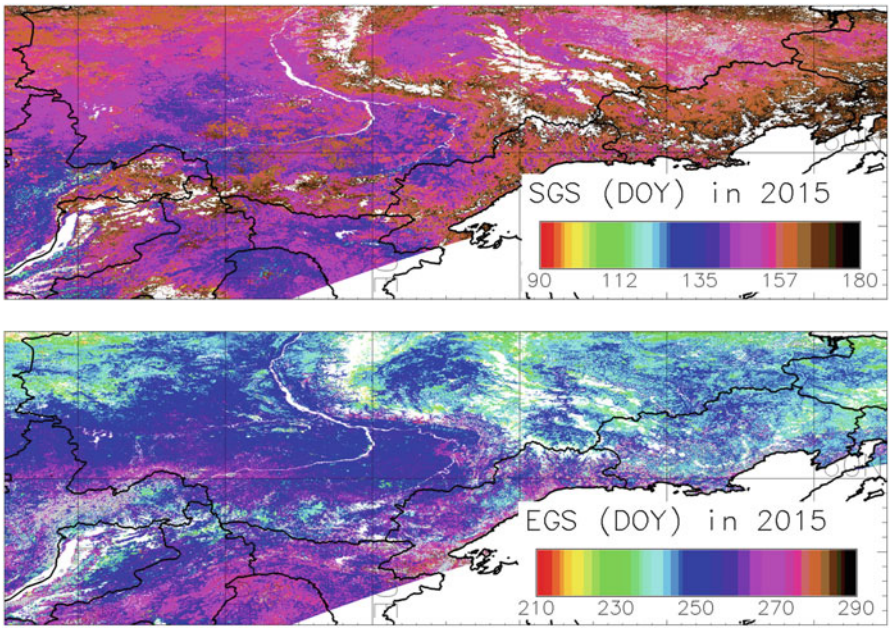

Fig. 10.12 Spatial distribution of the first date on which $GRVI_{MODIS}$ was more than zero in spring (i.e., SGS; top) and the first date on which $GRVI_{MODIS}$ was less than zero in autumn (i.e., EGS; bottom) in 2015 in eastern Siberia between 70°N and 50°N and 105°E and 165°E. The color scales show day of year (DOY)

To accurately detect the degradation of forests, the transition of forested areas to bogs, and the expansion of alases in eastern Siberia, analyses of satellite data with a high spatial resolution, such as data acquired by the AVNIR-2 (Advances Visible and Near Infrared Radiometer type 2) sensor onboard ALOS (spatial resolution, 10 m) or the WorldView-3 satellite (spatial resolution, 1.24 m), are required. Satellite observations by SAR, such as PALSAR-2 onboard ALOS-2, which are not affected by atmospheric noise or cloud contamination and have a spatial resolution of 3–10 m, are also useful for this purpose.

Ecosystem ecotones such as that between forest and tundra are considered to be highly sensitive and vulnerable to climate change, but ground-truthing of high-latitude ecotones is still insufficient. At the Kodac site near Chokurdakh in the northern part of eastern Siberia (70°33′47”N, 148°15′49″E), CO_2 fluxes have been measured, and phenological observations have been made by using inexpensive battery-powered time-lapse cameras since 2013. Further field studies at additional ecosystem ecotone sites are needed for the validation and testing of satellite remote-sensing observations.

References

Buitenwerf R, Rose L, Higgins SI (2015) Three decades of multi-dimensional change in global leaf phenology. Nat Clim Chang 5:364–368

Delbart N, Le Toan T, Kergoat L, Fedotova V (2006) Remote sensing of spring phenology in boreal regions: a free of snow-effect method using NOAA–AVHRR and SPOT–VGT data (1982–2004). Remote Sens Environ 101:52–62

Flessa H, Rodionov A, Guggenberger G, Fuchs H, Magdon P, Shibistova O, Zrazhevskaya G, Mikheyeva N, Kasansky OA, Blodau C (2008) Landscape controls of CH_4 fluxes in a catchment of the forest tundra ecotone in northern Siberia. Glob Chang Biol 14:2040–2056

Frankenberg C, Butz A, Toon GC (2011) Disentangling chlorophyll fluorescence from atmospheric scattering effects in O-2 A-band spectra of reflected sun-light. Geophys Res Lett 38:L03801. https://doi.org/10.1029/2010GL045896

Giglio L, Randerson JT, Werf GR (2013) Analysis of daily, monthly, and annual burned area using the fourth-generation global fire emissions database (GFED4). J Geophys Res Biogeo 118 (1):317–328

Huete A, Didan K, Miura T, Rodriguez EP, Gao X, Ferreira LG (2002) Overview of the radiometric and biophysical performance of the MODIS vegetation indices. Remote Sens Environ 83:195–213

Iida SI, Ohta T, Matsumoto K, Nakai T, Kuwada T, Kononov AV et al (2009) Evapotranspiration from understory vegetation in an eastern Siberian boreal larch forest. Agric For Meteorol 149 (6):1129–1139

Iijima Y, Ohta T, Kotani A, Fedorov AN, Kodama Y, Maximov TC (2014) Sap flow changes in relation to permafrost degradation under increasing precipitation in an eastern Siberian larch forest. Ecohydrology 7:177–187

James ME, Kalluri SN (1994) The Pathfinder AVHRR land data set: an improved coarse resolution data set for terrestrial monitoring. Int J Remote Sens 15(17):3347–3363

Jin M, Treadon RE (2003) Correcting the orbit drift effect on AVHRR land surface skin temperature measurements. Int J Remote Sens 20:4543–4558

Kajimoto T, Matsuura Y, Sofronov MA, Volokitina AV, Mori S, Osawa A, Abaimov AP (1999) Above- and belowground biomass and net primary productivity of a *Larix gmelinii* stand near Tura, Central Siberia. Tree Physiol 19:815–822

Kajimoto T, Matsuura Y, Osawa A, Abaimov AP, Zyryanova OA, Isaev AP, Yefremov DP, Mori S, Koike T (2006) Size-mass allometry and biomass allocation of two larch species growing on the continuous permafrost region in Siberia. For Ecol Manag 222:314–325

Knyazikhin Y, Martonchik JV, Myneni RB, Diner DJ, Running SW (1998) Synergistic algorithm for estimating vegetation canopy leaf area index and fraction of absorbed photosynthetically active radiation from MODIS and MISR data. J Geophys Res 103(D24):32257

Kobayashi H, Suzuki R, Kobayashi S (2007) Reflectance seasonality and its relation to the canopy leaf area index in an eastern Siberian larch forest: multi-satellite data and radiative transfer analyses. Remote Sens Environ 106(2):238–252

Kobayashi H, Delbart N, Suzuki R, Kushida K (2010) A satellite-based method for monitoring seasonality in the overstory leaf area index of Siberian larch forest. J Geophys Res Biogeo 115: G01002. https://doi.org/10.1029/2009JG000939

Kobayashi H, Yunus AP, Nagai S, Sugiura K, Kim Y, Van Dam B, Nagano H, Zona D, Harazono Y, Bret-Harte MS, Ichii K, Ikawa H, Iwata H, Oechel WC, Ueyama M, Suzuki R (2016) Latitudinal gradient of spruce forest understory and tundra phenology in Alaska as observed from satellite and ground-based data. Remote Sens Environ 177:160–170

Kushida K, Isaev AP, Maximov TC, Takao G, Fukuda M (2007) Remote sensing of upper canopy leaf area index and forest floor vegetation cover as indicators of net primary productivity in a Siberian larch forest. J Geophys Res Biogeo 112(112):G02003. https://doi.org/10.1029/2006JG000269

Liu Y, Liu R, Pisek J, Chen JM (2017) Separating overstory and understory leaf area indices for global needleleaf and deciduous broadleaf forests by fusion of MODIS and MISR data. Biogeosciences 14(5):1093

Motohka T, Nasahara KN, Oguma H, Tsuchida S (2010) Applicability of green–red vegetation index for remote sensing of vegetation phenology. Remote Sens 2:2369–2387

Motohka T, Nasahara KN, Murakami K, Nagai S (2011) Evaluation of sub-pixel cloud noises on MODIS daily spectral indices based on in situ measurements. Remote Sens 3:1644–1662

Myneni RB, Keeling CD, Tucker CJ, Asrar G, Nemani RR (1997a) Increased plant growth in the northern high latitudes from 1981 to 1991. Nature 386(6626):698

Myneni RB, Nemani RR, Running SW (1997b) Estimation of global leaf area index and absorbed PAR using radiative transfer models. IEEE Trans Geosci Remote Sens 35(6):1380–1393

Myneni RB, Dong J, Tucker CJ, Kaufmann RK, Kauppi PE, Liski J, Zhou L, Alexeyev V, Hughes MK (2001) A large carbon sink in the woody biomass of northern forests. Proc Nat Acad Sci USA 98(26):14784–14789

Myneni RB, Hoffman S, Knyazikhin Y, Privette JL, Glassy J, Tian Y, Wang Y, Song X, Zhang Y, Smith GR, Lotsch A (2002) Global products of vegetation leaf area and fraction absorbed PAR from year one of MODIS data. Remote Sens Environ 83(1):214–231

Nagai S, Nasahara KN, Muraoka H, Akiyama T, Tsuchida S (2010) Field experiments to test the use of the normalized difference vegetation index for phenology detection. Agric For Meteorol 150:152–160

Nagai S, Maeda T, Gamo M, Muraoka H, Suzuki R, Nasahara KN (2011) Using digital camera images to detect canopy condition of deciduous broad-leaved trees. Plant Ecol Diver 4:78–88

Nagai S, Saitoh TM, Kurumado K, Tamagawa I, Kobayashi K, Inoue T, Suzuki R, Gamo M, Muraoka H, Nasahara KN (2013) Detection of bio-meteorological year-to-year variation by using digital canopy surface images of a deciduous broad-leaved forest. SOLA 9:106–110

Nagai S, Inoue T, Ohtsuka T, Kobayashi H, Kurumado K, Muraoka H, Nasahara KN (2014) Relationship between spatio-temporal characteristics of leaf-fall phenology and seasonal variations in near surface- and satellite-observed vegetation indices in a cool-temperate deciduous broad-leaved forest in Japan. Int J Remote Sens 35:3520–3536

Nagai S, Akitsu T et al (2018) 8 million phenological and sky images from 29 ecosystems from the Arctic to the tropics: the Phenological eyes network. Ecol Res 33(6):1091. https://doi.org/10.1007/s11284-018-1633-x

Nasahara KN, Nagai S (2015) Review: development of an in-situ observation network for terrestrial ecological remote sensing—the Phenological eyes network (PEN). Ecol Res 30:211–223

Piao S, Wang X, Ciais P, Zhu B, Wang TAO, Liu JIE (2011) Changes in satellite-derived vegetation growth trend in temperate and boreal Eurasia from 1982 to 2006. Glob Chang Biol 17 (10):3228–3239

Pinzon JE, Tucker CJ (2014) A non-stationary 1981-2012 AVHRR NDVI3g time series. Remote Sens 6(8):6929–6960

Prentice IC, Cramer W, Harrison SP, Leemans R, Monserud RA, Solomon AM (1992) A global biome model based on plant physiology and dominance, soil properties and climate. J Biogeogr 19:117–134

Richardson AD, Jenkins JP, Braswell BH, Hollinger DY, Ollinger SV, Smith M-L (2007) Use of digital webcam images to track spring green-up in a deciduous broadleaf forest. Oecologia 152:323–334

Richardson AD, Keenan TF, Migliavacca M, Ryu Y, Sonnentag O, Toomey M (2013) Climate change, phenology, and phenological control of vegetation feedbacks to the climate system. Agri Forest Meteorol 169:156–173

Sato H, Kobayashi H, Iwahana G, Ohta T (2016) Endurance of larch forest ecosystems in eastern Siberia under warming trends. Ecol Evol 6(16):5690–5704

Simard M, Pinto N, Fisher JB, Baccini A (2011) Mapping forest canopy height globally with spaceborne lidar. J Geophys Res 116:G04021. https://doi.org/10.1029/2011JG001708

Suzuki R, Nomaki T, Yasunari T (2001) Spatial distribution and its seasonality of satellite-derived vegetation index (NDVI) and climate in Siberia. Int J Climatol 21:1321–1335

Suzuki R, Hiyama T, Asanuma J, Ohata T (2004) Land surface identification near Yakutsk in eastern Siberia using video images taken from a hedgehopping aircraft. Int J Remote Sens 25 (19):4015–4028

Suzuki R, Masuda K, Dye DG (2007) Interannual covariability between actual evapotranspiration and PAL and GIMMS NDVIs of northern Asia. Remote Sens Environ 106:387–398

Tucker CJ (1979) Red and photographic infrared linear combinations for monitoring vegetation. Remote Sens Environ 8:127–150

Wingate L, Ogée J, Cremonese E, Filippa G, Mizunuma T, Migliavacca M et al (2015) Interpreting canopy development and physiology using a European phenology camera network at flux sites. Biogeosciences 12:5995–6015

Wright IJ, Reich PB, Westoby M, Ackerly DD, Baruch Z, Bongers F et al (2004) The worldwide leaf economics spectrum. Nature 428:821–827

Zhou L, Tucker CJ, Kaufmann RK, Slayback D, Shabanov NV, Myneni RB (2001) Variations in northern vegetation activity inferred from satellite data of vegetation index during 1981 to 1999. J Geophys Res Atmos 106(D17):20069–20083

Chapter 11
Remote Sensing of Terrestrial Water

Kazuyoshi Suzuki and Koji Matsuo

11.1 Introduction

Terrestrial water (TW) is a critical component of ecosystems and is important for hydroclimatology and human usage. As described by Suzuki (2011), the considerable snow and ice coverage in eastern Siberia are essential components in estimating the amount of terrestrial water in the region (both in liquid and frozen state). With regard to the role of terrestrial water in ecosystems in eastern Siberia, Sugimoto et al. (2003) showed that soil moisture (SM) acts as a reservoir for plant growth when summer precipitation is insufficient. In addition, Suzuki et al. (2006) demonstrated that SM and snow water equivalent in the fall affect runoff from snowmelt in the following year. Having said this, terrestrial water is an important resource for people living in eastern Siberia, and thus, the security of terrestrial water is crucial (Dudarev et al. 2013). According to Suzuki (2011), the depth of permafrost is more than 100 m. Thus, locals in eastern Siberia find the groundwater located at greater depths difficult to use. In this chapter, we explain the manner in which recently developed remote sensing techniques are used to quantify terrestrial water and review the available datasets and previously obtained research results in eastern Siberia. The region is predominantly covered by the taiga forest, which is dominated by species such as larch. The forest cover hinders the detection of TW from space; the effects of the forest and other vegetation cover on remote sensing-based retrievals of terrestrial water must be considered. Terrestrial water is equivalent to terrestrial water storage (TWS), which includes all of water stored on land, such as SM, snow, surface water (SW), and ice in the permafrost. However, we have ignored the glaciers in eastern Siberia because they are relatively smaller in size (Earl and Gardner 2016). We have also ignored the water

K. Suzuki (✉)
Japan Agency for Marine-Earth Science and Technology, Yokohama, Japan
e-mail: skazu@jamstec.go.jp

K. Matsuo
The Geospatial Information Authority of Japan, Tsukuba, Japan

T. Ohta et al. (eds.), *Water-Carbon Dynamics in Eastern Siberia*,
Ecological Studies 236, https://doi.org/10.1007/978-981-13-6317-7_11

present below the permafrost because the depth of permafrost is too deep, and the water can be isolated from the terrestrial water cycle system. Therefore, the current chapter will focus on SM, snow, and SW. Ice in permafrost are included in the TWS anomaly estimates covering eastern Siberia. We have addressed those changes using TWS anomalies assessed using satellite remote sensing.

In Sect. 11.2 of this chapter, we describe remote sensing-based techniques for assessing TWS. In Sects. 11.3, 11.4, and 11.5, we then describe remote sensing-based techniques for assessing different components of TWS, specifically SM, snow, and SW, respectively, in eastern Siberia. Section 11.6 discusses recent advancements in data assimilation techniques using remote sensing data. Since remote sensing data are only available over limited geographic and temporal ranges, they must be merged with other sources of information to generate spatially and temporally consistent datasets. Each section contains several subsections, including an outline, a description of the available datasets, results of previous studies, and a perspective. Finally, in Sect. 11.7, we provide concluding remarks and research perspectives for the near future.

11.2 Terrestrial Water Storage (TWS)

This section describes remote sensing methods for estimating TWS and their scientific applications in eastern Siberia. It is difficult to directly assess the actual TWS from space, but it has recently become possible to measure TWS anomalies from space using satellite gravimetric observations.

11.2.1 Remote Sensing of TWS

Masuda et al. (2001) assessed the seasonal characteristics of TWS in large rivers worldwide using river runoff and reanalysis datasets. However, the interannual variations in TWS cannot be estimated by this method because the climatological TWS was derived only as the residual term of the atmospheric water balance. To determine monthly changes in TWS, alternative methods are required.

The measurements of TWS anomalies from space have been available since 2002 and are based on data obtained from gravity observation satellite missions, such as the Gravity Recovery And Climate Experiment (GRACE) (Wahr et al. 1998). GRACE uses twin satellites that are separated by approximately 220 km and follow the same orbital path and altitude in a near-polar orbit at approximately 500 km above the Earth. A precise microwave distance-measuring device (K-band ranging, KBR) with two frequencies (24-GHz K-band and 32 GHz Ka-band) is on board both satellites and is used to measure changes in the distance between the twin satellites. This instrument is extremely sensitive, enabling the measurement of changes in the inter-satellite distance to an accuracy of 1 μm.

One of the major goals of the GRACE mission is to perform high-precision measurements of the Earth's static gravity field. In the same way, the mission is also intended to observe the dynamics of the Earth's gravity field (i.e., the time-variable gravity field). GRACE can measure the Earth's gravity field to an accuracy of several μGal (i.e., hundreds of millionths of Earth standard gravity) with spatial and temporal resolutions of a few hundred kilometers and a month, respectively. By observing gravity, we can directly estimate mass changes, such as those associated with precipitation, evaporation, and river runoff. In this article, we describe the observations of mass changes related to climate change.

Seasonal gravity changes over continental areas mainly reflect changes in the soil water content caused primarily due to rainfall and snowfall (Tapley et al. 2004). Conspicuous gravity changes are observed in low-latitude areas (from 30°N to 30°S), particularly in South America, Africa, northern Australia, and southeastern Asia. The gravity force in these areas increases in summer through autumn and decreases in winter through spring; this closely corresponds to the temporal rainfall pattern of the tropical monsoon climate. Conspicuous gravity changes are also seen in the high-latitude regions of the Northern Hemisphere (from 45°N to 75°N). The gravity force there increases in winter through spring and decreases in summer through autumn; it parallels the temporal patterns of rainfall and snowfall seen in the damp climate of the subarctic zone.

11.2.2 TWS Datasets

GRACE data processing is conducted at various analysis centers, and changes in the inter-satellite distance are converted to gravity data. There are three main analysis centers: the Center for Space Research (CSR) at the University of Texas, the Jet Propulsion Laboratory (JPL) of the National Aeronautics and Space Administration (NASA), and the GeoForschungsZentrum (GFZ) in Potsdam, Germany. In addition, the Center National d'Etudes Spatiales (CNES) and the Delft University of Technology (DMT), as well as other centers, have also developed original analytic solutions. The products of the first processing step that is applied to the measured inter-satellite distance changes are called the Level-1B data. A second treatment is then performed to convert the data to spherical harmonic coefficients (also called Stokes coefficients) of the change in the gravitational potential over the entire Earth, which are called the Level-2 data. In this step, various geophysical corrections, such as corrections for tidal effects, atmospheric and oceanic effects, and non-gravitational accelerations, are applied (e.g., Bettadpur 2012). Using the Level-2 data, we can estimate TWS anomalies using the following steps: (1) corrections for postglacial rebound (PGR) or glacial isostatic adjustment (GIA) are made using geophysical models (e.g., Geruo et al. 2013); (2) a filter (specifically a Gaussian or stochastic filter) is applied to remove north-south striping noises and high-frequency noises (Kusche 2007); (3) the changes in the degree-1 components of the Earth's gravity field (the center of mass of the Earth) are accounted for via

reanalysis output, using the methods described by Swenson and Wahr (2006); (4) the change in equivalent water thickness (EWT) is estimated using the methods described by Wahr et al. (1998); and (5) the uncertainties in EWT are estimated using error variance matrices of GRACE observations (Wahr et al. 2004).

The GRACE EWT products, after the abovementioned data processing, are termed Level-3 data. These data are available for download from the Internet [e.g., from NASA JPL (ftp://podaac-ftp.jpl.nasa.gov/allData/grace)]. The Level-3 data are represented on a grid that expands up to a degree and order 60 in terms of spherical harmonics. The Level-2 data are also available in the form of the spherical harmonic coefficients up to degree and order 96, but the effective spatial resolution is approximately 300 km. Data covering the period from April 2002 to June 2017 are available from the following three websites:

The GRACE Tellus website (http://grace.jpl.nasa.gov/) provides maps of surface mass anomalies. This site also provides products created synergistically with GRACE and TOPEX (TOPography EXperiment) /Jason-1 missions (a joint satellite mission between NASA, the US space agency, and CNES, the French space agency, to map ocean surface topography). The CU GRACE website (http://geoid.colorado.edu/) provides mass anomalies in regional or global time series. The NASA GRACE website (https://podaac.jpl.nasa.gov/) provides the GRACE Level-1B and Level-2 products. The GFZ GRACE website (http://isdc.gfz-potsdam.de/grace-isdc/) provides the GRACE Level-1B and Level-2 products. The ICGEM website (http://icgem.gfz-potsdam.de/ICGEM/ICGEM.html) distributes a full range of current and historical static Earth gravity field models.

11.2.3 Scientific Applications of TWS

We will first explain the manner in which GRACE-based TWS has been used in estimating the wetting and drying of terrestrial land in recent years and the linkage between TWS and river runoff in eastern Siberia.

The Lena River basin is the second-largest source of freshwater inflow into the Arctic Ocean. Hydrological studies conducted in cold regions have shown that TWS strongly affects the amount of river flow from basins (Quinton et al. 2003; Papa et al. 2008; Hood and Hayashi 2015). Therefore, it is important to evaluate the variability of TWS. Muskett and Romanovsky (2009) and Velicogna et al. (2012) reported that GRACE data showed increased TWS throughout the Lena River basin from 2002 to 2010 primarily because of rising groundwater levels in the discontinuous permafrost zone. In contrast, Vey et al. (2013) noted that such an increasing trend in TWS was cancelled by a decreasing trend in TWS, after 2009, in the Lena River basin. Suzuki et al. (2016) used 146 months of data from GRACE spanning April 2002 to August 2015 to analyze TWS in the Lena River basin. A negative trend in TWS in the downstream reaches of the Lena River basin was primarily due to evapotranspiration. The coefficient of determination indicates that 37% of the variance in regional TWS can be explained by a linear function of evapotranspiration. In turn, summer air

temperatures control evapotranspiration, which mostly occurs from June to August. Further warming during summer at high latitudes in the Lena River basin might enhance the already-substantial reduction in TWS in the area.

Next, we will present basin-scale TWS changes in the Lena River basin. Figure 11.1(a) shows the temporal variations in the basin-averaged monthly TWS anomalies determined by GRACE and GLDAS (Global Land Data Assimilation System). The GRACE- and GLDAS-based TWS (TWS_{GRACE} and TWS_{GLDAS}) results are highly correlated ($r = 0.71$, $p < 0.0001$). The correlation coefficient "r" indicates the strength of the linear relationship between TWS_{GRACE} and TWS_{GLDAS}; the coefficient of determination R^2 indicates the degree to which the variance can be explained by a linear model. Based on the high degree of correlation between the two TWS datasets, we were able to calculate a basin-scale TWS change of approximately 50% using GLDAS, thus allowing us to determine the primary factor controlling the changes in TWS_{GRACE}. The similarity between the two datasets implied that both TWS_{GLDAS} and TWS_{GRACE} depend largely on snow water equivalent (SWE) and SM.

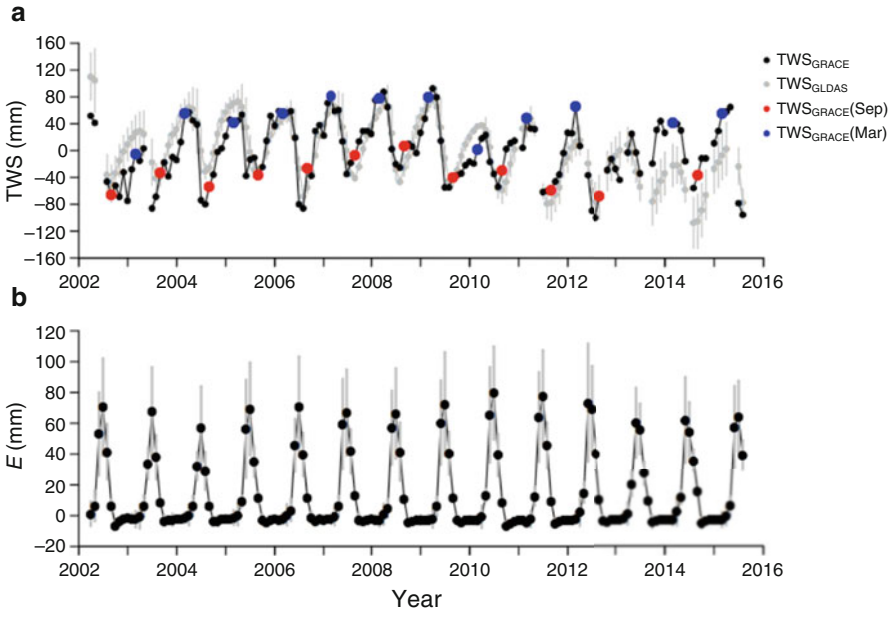

Fig. 11.1 (**a**) Temporal variations in TWS in the Lena River basin. Black and gray circles indicate TWS_{GRACE} and TWS_{GLDAS} data, respectively, and red and blue circles indicate GRACE-based TWS estimates in September (TWS_{GRACE}(Sep)) and March (TWS_{GRACE}(Mar)), respectively. Vertical gray bars indicate the standard deviation of the multi-model GLDAS ensemble. (**b**) Temporal variations in the monthly evapotranspiration (E), shown with the standard deviation of the multi-model GLDAS ensemble. Reproduced from Fig. 2 in (Suzuki et al. 2016)

As reported previously (Vey et al. 2013), the basin-averaged TWS_{GRACE} shown in Fig. 11.1(a) does not exhibit any clear trend because of the decrease in TWS after 2009. To explain this apparent lack of trend in TWS_{GRACE}, we examined monthly basin-averaged evapotranspiration [Fig. 11.1(b)]. Evapotranspiration from June to August 2009 was more than 12 mm greater than the 14-year average and more than 20 mm greater during the following 3 years. Consistent with these higher evapotranspiration levels, TWS_{GRACE} in September decreased steadily from 2010 to 2012. This finding suggests that the increased summer evapotranspiration from 2009 to 2012 caused a decrease in TWS in the Lena River basin beginning in 2010. The TWS did not exhibit an overall trend from 2002 to 2015, as shown in Fig. 11.1(a).

Next, we will demonstrate another example of research using GRACE-based TWS because these data are useful for understanding SW storage and river runoff as well as vegetation and solid precipitation in eastern Siberia.

The GRACE-based TWS data were used to understand changes in air temperature and the normalized difference vegetation index (NDVI). NDVI is commonly used as an index of vegetation activity. The relationship between NDVI and the 2-m air temperature (Ta) due to changes in TWS was investigated (Geruo et al. 2015). A strong correlation between NDVI and Ta was found for the Viluy River basin, which lies within the Lena River basin, but the NDVI values over the remainder of the Lena River basin were controlled by water availability (i.e., the NDVI–TWS relationship). During 2002 to 2011, wetter conditions in the Lena River basin were associated with increased NDVI. In these studies, the water from snowmelt was also an important controlling factor for early spring NDVI.

Solid precipitation is a dominant component of the hydrological cycle during winter. However, weather stations and observation networks are sparse in eastern Siberia. Therefore, space-based remote sensing techniques are useful for measuring solid precipitation in this region. Seo et al. (2010) estimated winter precipitation using GRACE-based TWS and snow data obtained using the Advanced Microwave Scanning Radiometer-Earth Observing System (AMSR-E). The authors found that the pattern of solid precipitation during winter derived from GRACE-based TWS is better than that derived from the AMSR-E snow product, when both datasets were compared with independent precipitation products. Specifically, the following products were used for comparison: the Global Precipitation Climatology Project (GPCP), the Climate Prediction Center's Merged Analysis of Precipitation (CMAP), and three reanalysis data products, namely, the National Centers for Environmental Prediction/National Center for Atmospheric Research (NCEP/NCAR) reanalysis, the European Center for Medium-Range Weather Forecasts' ERA-Interim reanalysis, and the Japan Meteorological Agency's Climate Data Assimilation System (JCDAS) reanalysis. Among these estimates, the AMSR-E estimates differ the most from the other estimates; this indicates a possible large uncertainty in the AMSR-E-based estimates that might be caused by the physical properties of snowpack and the underlying surface and forest parameterization assumed in the current AMSR-E SWE algorithm. Therefore, using GRACE-based TWS is reliable for estimating winter

precipitation in eastern Siberia. However, the spatial and temporal resolutions of such winter precipitation estimates are very low.

The Arctic freshwater budget is critical for understanding the climate in the northern regions. However, the hydrology of the Arctic circumpolar tundra region and the largest pan-Arctic rivers are still not well understood. Suzuki et al. (2018) analyzed the spatiotemporal variations in the TWS of the Arctic circumpolar tundra region, including three of its largest pan-Arctic river basins (Lena, Mackenzie, and Yukon), using monthly GRACE data from 2002 to 2016. Together with global land reanalysis, and river runoff, they identified declining TWS trends throughout the Arctic circumpolar tundra region that we attributed largely to increasing evapotranspiration driven by increasing summer air temperatures. At the basin scale, Suzuki et al. (2018) showed that, in the Lena River basin, the autumnal TWS signal persisted until the winter of the following year, while in the Mackenzie River basin, TWS levels during autumn and winter showed no significant impact in the following year. This disparity may be due to differences in the continuous permafrost distribution between the two river basins. Since global warming is expected to be particularly significant in the northern regions, these results are important for understanding future TWS trends, as further declines are possible given the fact that Arctic temperatures continue to rise.

11.2.4 Perspectives on TWS Remote Sensing

Information on TWS is critical because it is both a component of the hydrological cycle and climate system and a key resource. GRACE has provided considerable advances in scientific knowledge in those areas. The power supply of the measuring instrument had been ensured by suspending measurements for approximately 1 month in every 6 months, beginning in 2011, to extend the practical use of the satellites; the useful lifetime of GRACE satellites ended in November 2017.

Therefore, a follow-on satellite mission is clearly needed and was planned by NASA and German Research Centre for Geosciences. The NASA/German Research Centre for Geosciences' Gravity Recovery and Climate Experiment Follow-On (GRACE-FO) spacecraft was successfully launched in May 2018; GRACE-FO plans to extend and improve its first GRACE mission. Though the resolution will be the same as GRACE (approximately 300 km), the accuracy could be improved by inter-satellite laser ranging system. The resulting data will foster major breakthroughs in several branches of the Earth sciences. For instance, GRACE-FO will offer details on the movement of water on the planet. In addition, GRACE-FO will provide more detailed TWS data in eastern Siberia, which will improve the understanding of regional water movement under climate change.

Given the availability of TWS data, the analysis of the relationship between river runoff and TWS anomalies was limited. Further improvements in our understanding of the Arctic freshwater cycle will require additional GRACE-based TWS estimates.

11.3 Soil Moisture (SM)

TWS includes deeper groundwater and snow, as well as SM; however, vegetation is largely dependent on surface SM. To assess soil evaporation and transpiration from vegetation in eastern Siberia, SM must be estimated. Estimating SM near the surface is important for understanding the partitioning of energy and water between the land and atmosphere as well as the cycling of carbon and other materials through life cycles of vegetation or the wetness of the surface soil layer. Therefore, many efforts have been made to retrieve SM from space. In this section, we review recently developed remote sensing techniques for performing SM retrievals.

11.3.1 Remote Sensing of SM

Optical remote sensing techniques have been used to measure proxies for SM, such as surface albedo and surface temperature, from space. However, these sensors cannot detect areas with cloud or vegetation cover.

Microwave remote sensing techniques are not obstructed by clouds. Moreover, these sensors can measure the dielectric constant of soil, which is related to water content. In addition, microwave sensors are useful even at night, when solar radiation is not available. Microwave remote sensing techniques are widely used to retrieve SM from space. The Institute of Electrical and Electronics Engineers (IEEE) has defined an IEEE Standard 521–1984, a system of electromagnetic frequency bands used for radio and radar. Microwaves comprise the L-band, which has a frequency range from 1 to 2 GHz, which corresponds to wavelengths of 30 cm to 15 cm; S-band, which has a frequency range of 2–4 GHz (wavelengths 15–5 cm); C-band with a frequency range of 4–8 GHz (wavelengths 5–3.75 cm); X-band, ranging from 8 to 12 GHz (wavelengths 3.75–2.5 cm); Ku-band, ranging from 12 to 18 GHz (wavelengths 2.5–1.6 cm); K-band, ranging from 18 to 26 GHz (wavelengths 1.6–1.2 cm); Ka-band, ranging from 26 to 40 GHz (wavelengths 1.2 cm to 750 mm); V-band, ranging from 40 to 75 GHz (wavelengths 750–40 mm); and W-band, ranging from 75 to 111 GHz (wavelengths 40 mm to 28 mm). Estimates of SM from microwave information commonly use the L and C bands, which are unaffected by atmospheric conditions.

There are two types of microwave techniques involving either active or passive microwave sensors. Active microwave techniques provide fine spatial resolution but coarse temporal resolution; for example, scatterometers typically have a temporal resolution of 30 days but a spatial resolution of $0.1^\circ \times 0.1^\circ$. In contrast, passive microwave techniques offer coarse spatial resolution but high temporal resolution; for example, radiometers typically have a temporal resolution of 1–3 days but a spatial resolution of 38 km $\times$ 38 km.

In this section, we will describe the recently developed microwave remote sensing products and some research results obtained using those products in eastern Siberia.

11.3.2 SM Datasets

Table 11.1 shows the list of available SM datasets presented by Petropoulos et al. (2015). Researchers who require high-resolution data for specific purposes may wish to consider using the PALSAR (Phased Array type L-band Synthetic Aperture Radar) and ERS (Earth Resources Satellite) data, but the SM index must be retrieved from the original data provided by such sensors. The spatial resolution of these data is very fine (approximately 10 m), whereas their measurement interval is comparatively long at 10 days or much longer.

Here, we discuss the properties of each dataset presented in Table 11.1. The microwave frequencies that can be used to measure microwaves from the Earth's surface through the atmosphere include the L-band and C-band.

We introduce the operational SM analyses that are listed in Table 11.1.

Table 11.1 Operational soil moisture products produced using remote sensing techniques

	ASCAT	AMSR2	SMOS	SMAP
Instrument type	C-band (5.255 GHz) (Advanced Scatterometer)	Eight channels from 6.93 to 89.0 GHz (Advanced Microwave Scanning Radiometer-2)	L-band (1.4 GHz) (L-band radiometer)	L-band (1.2–1.4 GHz) (an L-band radar and an L-band radiometer) Note: The L-band radar stopped working on July 7, 2015
Temporal coverage	Since 2007	Since 2012	Since 2010	Since 2015
Spatial resolution	25 km	25 km, 50 km	35 km	40 km
Temporal resolution	3 days	0.5 days	1–3 days	3 days
References	Figa-Saldaña et al. (2002), Wagner et al. (2013)	Kachi et al. (2015)	Kerr et al. (2010)	Entekhabi et al. (2010)
Distributed by	European Organization for the Exploitation of Meteorological Satellites (EUMETSAT)	Japan Aerospace Exploration Agency (JAXA)	European Space Agency (ESA)	National Aeronautics and Space Administration (NASA)
Download portal	http://www.remss.com/missions/ascat	https://gcom-w1.jaxa.jp/auth.html	https://smos-ds-02.eo.esa.int/oads/access/	https://smap.jpl.nasa.gov/data/

11.3.2.1 ASCAT

This SM dataset is based on radar backscatter measurements within the C-band recorded by the Advanced Scatterometer (ASCAT) instrument aboard the EUMETSAT MetOp satellite. These data are first normalized to a common incidence angle (40°) using a radar backscatter model. The physical basis for the capability of ASCAT to measure SM is the strong dependence of C-band backscatter on the SM content in the topsoil layer (usually held to be 1–2 cm thick). The algorithm for the ASCAT SM product was developed by the Vienna University of Technology (TU Wien) and was designed to be a change detection method. The obtained radar backscatter coefficient is a function of the SM: low values correspond to a low SM, whereas high values are associated with a high SM. Radar backscatter values are scaled between 0% (dry soil) and 100% (wet soil that is saturated with water). The backscatter values are affected by soil texture and roughness. Thus, it is important to minimize those effects on SM estimation.

The surface SM content m_s is estimated in one of the last processing steps using:

$$m_s = \frac{\sigma^{\mathrm{o}} - \sigma^{\mathrm{o}}_{\mathrm{dry}}}{\sigma^{\mathrm{o}}_{\mathrm{wet}} - \sigma^{\mathrm{o}}_{\mathrm{dry}}} \tag{11.1}$$

where σ^{o} is the backscatter measurement to be inverted and $\sigma^{\mathrm{o}}_{\mathrm{dry}}$ and $\sigma^{\mathrm{o}}_{\mathrm{wet}}$ are the backscattering measurements representing dry and wet earth, respectively. For cold regions, the validation for ASCAT SM products was carried out at the Naqu site on the Tibetan Plateau.

11.3.2.2 AMSR2

The AMSR2 instrument, which is onboard the first-generation Global Change Observation Mission-Water (GCOM-W1) satellite, is a multifrequency, total-power microwave radiometer system with dual polarization channels for all frequency bands (Imaoka et al. 2010; Kachi et al. 2015). This sensor is a successor to the AMSR sensor that is on board the Advanced Earth Observing Satellite-II (ADEOS-II) and AMSR-E onboard NASA's Aqua satellite. The GCOM-W1 satellite was launched from the Japan Aerospace Exploration Agency (JAXA) on May 18, 2012 (JST), and was placed in orbit in front of the Aqua satellite. This was done to provide continuity with the AMSR-E observations (from June 2002 to October 2011) and provide synergy with the other instruments on A-Train (a satellite constellation, a string of meteorological and environmental Earth observation) satellites. JAXA releases AMSR2 geophysical parameters to the public through the GCOM-W1 data providing service system (https://gcom-w1.jaxa.jp). The validation for AMSR2 SM products was carried out in Mongolia.

11.3.2.3 SMOS

Another SM operational product that has become available more recently is based on data from the Soil Moisture and Ocean Salinity (SMOS) mission. SMOS was designed to measure SM over continental surfaces as well as ocean salinity using the low-microwave frequency (1.4 GHz) Microwave Imaging Radiometer with Aperture Synthesis (MIRAS) instrument. As of the beginning of October 2010, SMOS SM products were distributed to all relevant researchers. The SM products provide not only SM retrievals but also a series of ancillary data derived from the processing, namely, nadir optical thickness, surface temperature, and roughness parameter (namely, dielectric constant and brightness temperature retrieved at top of atmosphere and on the surface) with their corresponding uncertainties. For cold regions, the validation for SMOS SM products was carried out at the Naqu site on the Tibetan Plateau, China.

11.3.2.4 SMAP

The SMAP measurement approach is to integrate an L-band radar and an L-band radiometer as a single observation system, thereby combining the relative strengths of active and passive remote sensing for enhanced SM mapping. It was intended that the radar and radiometer measurements could be effectively combined to derive SM maps that approach the accuracy of radiometer-only retrievals. However, the radar measurements ceased 3 months after the launch (July 7, 2015), and, as of today, only the L-band radiometer remains functional. Since the effects of vegetation and surface roughness are dependent on incidence angle, the SMAP mission adopted a conical scan, constant incidence angle approach. This approach reduces the retrieval complexity and facilitates the use of time series retrieval algorithms. A 40° incidence angle was adopted for SMAP as a suitable angle for both radiometer and radar designs. The wide swath that results from this approach enables SMAP observations to provide global coverage in 2–3 days. For cold regions, the validation for the SMAP SM product was carried out in Manitoba and Winnipeg, Canada.

11.3.2.5 Land Parameter Retrieval Model (LPRM)

In addition to the datasets listed in Table 11.1, a useful historical climatology of continuous satellite-derived global land surface SM has been developed using the LPRM (Owe et al. 2008). The data consist of surface SM retrievals derived from all available historical and active satellite microwave sensors, including the Nimbus-7 Scanning Multichannel Microwave Radiometer, Defense Meteorological Satellites Program Special Sensor Microwave Imager, Tropical Rainfall Measuring Mission Microwave Imager, and Aqua Advanced Microwave Scanning Radiometer for Earth

Observing System, and span the period from November 1978 to the end of 2007. The validation for the LPRM SM product was carried out against other SM retrievals, such as ASCAT and SMOS.

11.3.3 Scientific Applications of SM

Eastern Siberia is mainly covered by forest, and thus, retrieving SM from satellite-based remote sensing measurements is challenging in this region as the forest canopy obscures the signal from water within the soil. Consequently, few studies have examined the application of SM retrieval data for this area.

Bartsch et al. (2009) showed that SM anomalies obtained using active microwave data are related to forest fire occurrence in Central Siberia. The authors showed an analysis of satellite-derived SM anomaly data from ERS-1/2 (ERS: Earth Resources Satellite) scatterometer data and burned area maps from MODIS/AVHRR/ATSR (Moderate Resolution Imaging Spectroradiometer/Advanced Very High-Resolution Radiometer/Along-Track Scanning Radiometer) over Central Siberia for the years 1992–2000. The results showed that wet surface SM conditions limit the extent of burned area and can prevent the outbreak of fires. Approximately 80% of all events occurred under drier conditions in July; the fire area was below 50 km^2 under moist conditions. Larger burned areas have not generally been detected when the surface wetness deviation exceeded +5%. Monitoring surface SM in Siberia will contribute to predicting forest fires in the region in the near future.

Current satellite remote sensing data products that include estimates of SM are limited to the surface soil layer extending to a depth of 5 cm. Estimating SM at greater depths is also important for understanding vegetation growth and water and carbon absorption in eastern Siberia. Van der Molen et al. (2016) evaluated whether the assimilation improved SiBCASA's SM and its effect on simulated carbon fluxes. The SiBCASA model was developed by Schaefer et al. (2008). Through a comparison with unique in situ SM observations, van der Molen et al. (2016) showed that the passive microwave SM product (AMSR-E) did not improve the SM simulated by SiBCASA, but the active microwave data, such as those from ASCAT, seem promising in some aspects. Thus, SM data obtained using ASCAT can improve the assessed spatial variation of net carbon. Hence, active microwave measurements can be useful for detecting SM beneath the forest canopy.

To overcome the shortcomings of satellite-retrieved surface SM data, Ford et al. (2014) used cross-correlation analysis to quantify the association between near-surface and root zone SM using in situ data from the United States Great Plains. The authors demonstrated that there was generally a strong relationship between near-surface and root zone SM. An exponential decay filter was used to estimate root zone soil moisture using near-surface soil moisture derived from the SMOS satellite. Root zone soil moisture derived from SMOS surface retrievals was compared to in situ soil moisture observations in the United States. Overall, the authors showed a useful approach for estimating root zone soil moisture from SMOS surface retrievals.

11.3.4 Perspectives on SM Remote Sensing

Operational SM data obtained using radiometers and scatterometers cover the past several years. However, these SM data have relatively low spatial resolutions of 25–50 km. Therefore, subpixel variations in SM can be affected by the SW fraction in the northern regions (Hogstrom and Bartsch 2016) because the pixel-wise microwave data for SM can be contaminated with SW coverage. Thus, such sub-grid scale distribution of SW causes uncertainty in SM products.

To obtain more reliable SM retrievals, fusion techniques that use data from multiple satellites are becoming important (Petropoulos et al. 2015). In the near future, this family of techniques will overcome the problems (such as low spatial resolution) associated with presently available datasets. To improve the spatial resolution of the ~40-km resolution passive microwave-derived SM, Merlin et al. (2010) used a methodology based on 1-km resolution MODIS red, near-infrared, and thermal-infrared data. The three components of this method were (1) fractional vegetation cover, (2) soil evaporative efficiency, and (3) a downscaling relationship. Airborne L-band data collected over an Australian agricultural area were used to both generate ~40-km resolution microwave pixels and verify the disaggregation results at a 4-km resolution. Among 36 different disaggregation algorithms, one was identified as being more robust. Further advancement of multi-satellite fusion and downscaling methods will improve SM estimates within eastern Siberia.

11.4 Snow

11.4.1 Remote Sensing of Snow

Snow is one of the dominant forms of water in Siberia during winter (Suzuki 2011); water from snowmelt is important for vegetation growth and water resources in eastern Siberia. Therefore, it is important to estimate the mass of snow in this region. To carry out this task, remote sensing techniques are very useful in capturing the large-scale distribution of snow, which can be detected by both optical and microwave sensor onboard satellites.

Optical sensors, such as MODIS and the National Oceanic and Atmospheric Administration (NOAA) Advanced Very High-Resolution Radiometer (AVHRR), were used to estimate fractional snow coverage at fine spatial scales; however, this method is not available when the sky is cloudy, at night, or during the polar night. Passive microwave sensors such as radiometers (SSM/I and AMSR2) are useful under cloudy conditions or in the absence of solar radiation. Although the spatial resolution of these sensors is low, their observation frequency is high (typically 1–3 days).

In this section, we describe the available snow retrieval datasets as well as the scientific results obtained using remote sensing-retrieved snow data in eastern Siberia.

11.4.2 Snow Datasets

The available snow datasets and the methods used to produce them were reviewed by Dietz et al. (2012). Consulting the study by Dietz et al. (2012), we will compile the snow datasets for eastern Siberia. In this section, we first focus on snow coverage datasets obtained using visible wavelength data, such as those obtained from MODIS and the Interactive Multisensor Snow and Ice Mapping System (IMS) instruments. Moreover, we introduce the SWE datasets obtained using the Special Sensor Microwave/Imager (SSM/I) and AMSR2 microwave sensors.

11.4.2.1 Snow Coverage Area

11.4.2.1.1 MODIS

MODIS snow products can be obtained from NASA. MODIS uses a sensor that detects in the visible wavelengths to estimate snow coverage area. MODIS snow products include two types of snow coverage area products, namely, binary snow coverage and fractional snow coverage.

Binary Snow Coverage Method (Hall and Riggs 2007; Hall et al. 2002)
The normalized difference snow index (NDSI) is used to divide regions into snow-covered and non-snow-covered areas and can be written as:

$$\left.\begin{array}{l} \mathrm{NDSI} = \dfrac{\rho_4 - \rho_6}{\rho_4 - \rho_6} \\ \text{Threshold value when exists NDSI} \geq 0.4, \\ \text{and} \quad \begin{array}{l} \rho_2 > 0.11 \\ \rho_4 < 0.10 \end{array} \end{array}\right\} \tag{11.2}$$

where ρ is the surface reflectance in each band and the subscripts denote MODIS band numbers. MODIS instruments acquire data at three spatial resolutions, depending on the band. Bands 1–2 have a spatial resolution of 250 m, bands 3–7 are 500 m, and bands 8–36 are 1000 m. The wavelength ranges of band 2, band 4, and band 6 are 841–876 nm, 545–565 nm, and 1628–1652 nm, respectively.

The MODIS snow product was adjusted based on coverage by dense vegetation such as forests. If the NDVI ≅0.1, the pixel may be mapped as snow even if the NDSI <0.40. MODIS binary snow cover products typically underestimate low-elevation snow cover by ~12% and typically overestimate high-elevation snow cover by ~15% (Klein and Barnett 2003; Parajka and Bloschl 2008).

Fractional Snow Coverage Method (Painter et al. 2003, 2009)
Fractional snow coverage is estimated using the multiple-end-member method for determining fractional snow cover and grain size.

11.4.2.1.2 IMS (Interactive Multisensor Snow and Ice Mapping System)

In addition to the MODIS snow coverage area data, a daily visual analysis of satellite data is carried out by analysts who are experienced in interpreting IMS data (Ramsay 1998). This dataset is coarser than the MODIS snow coverage area dataset. By primarily using satellite data covering the visible portion of the electromagnetic spectrum, maps of snow cover (for land areas) and sea ice cover (for ocean surface areas) are generated on a grid with a 4-km resolution. The satellite data used originate from polar orbiting satellites, e.g., AVHRR and MODIS, as well as geostationary satellites, e.g., GOES and European Union meteorological satellite (METEOSAT). Gaps due to cloud coverage and/or the absence of daylight are filled by including assessments of snow cover using passive microwave satellite data; in addition, the persistence of the snow cover is considered.

11.4.2.1.3 NOAA Weekly Data

The weekly Northern Hemisphere SCE (snow cover extent) Climate Data Record (Brown and Robinson 2011) spans the period from late 1966 to the present, comprising the longest satellite-based climate data record of any environmental variable. This CDR combines the NOAA visible satellite-based SCE analyses generated weekly through May 1999 and daily since June 1999 to form a continuous Northern Hemisphere record. The resulting continental SCE product informs climate studies, climate change monitoring, and climate model validation. The data are available from https://www.ncdc.noaa.gov/cdr/terrestrial/snow-cover-extent-northern-hemisphere.

11.4.2.2 Snow Water Equivalent (SWE)

11.4.2.2.1 Passive Microwave Instruments (SSM/I and AMSR2) (Foster et al. 2005; Tedesco and Jeyaratnam 2016)

This method uses a linear relationship between the differences between the 19 and 37 GHz brightness temperatures and SWE. Forest canopies disturb this relationship, and their effect on SWE estimates must be taken into account. Derksen (2008) showed that AMSR-E brightness temperature has highlighted the problematic dependence of 36.5 GHz measurements on vegetation, which can render relationships with SWE as spurious, and the differences between the 18.7 and 10.7 GHz brightness temperatures displayed a stronger correlation with SWE in boreal forest regions of Canada than the differences between the 19 and 37 GHz brightness temperatures. AMSR2 SWE datasets are available as the New LANCE NRT AMSR2 Daily L3 Global Snow Water Equivalent EASE-Grids dataset, which can be found online at https://ghrc.nsstc.nasa.gov/home/content/new-lance-nrt-amsr2-daily l3-global-snow-water-equivalent-ease-grids-data set-available.

11.4.2.2.2 GlobSnow, European Space Agency (ESA)

This dataset includes SWE and snow coverage area data (Takala et al. 2011). To estimate SWE, an emission model is used to obtain snow depth from brightness temperatures for grid cells co-located with weather stations. The observed snow density values are finally used to convert snow depths into SWE. Access to this dataset is restricted, and the data provider must be contacted for their usage.

11.4.3 Scientific Applications of Snow

Here, we introduce studies using each of the different snow products. Initially, Yang et al. (2007) used snow coverage area and SWE datasets to understand the hydrological cycle in large Siberian river basins. The SWE data aid in developing an understanding of runoff generation from snowmelt in these large river basins.

Next, in terms of SCE products, using the weekly Northern Hemisphere SCE Climate Data Record, as shown in Fig. 11.2., Iijima et al. (2007) showed that the increase in air temperature and water vapor that accompanies the melting of snow was due to the advection of wet, warm air, and enhanced water vapor convergence over the central Lena River basin during the 30-day period prior to snow disappearance.

Finally, snow coverage area products can be used for model validation because of their high reliability. For instance, Suzuki et al. (2015) simulated the fine-scale distribution of snow in the Lena River basin and verified this distribution using snow coverage area data. Other climate models have used snow coverage area datasets for validation purposes (Nitta et al. 2014),

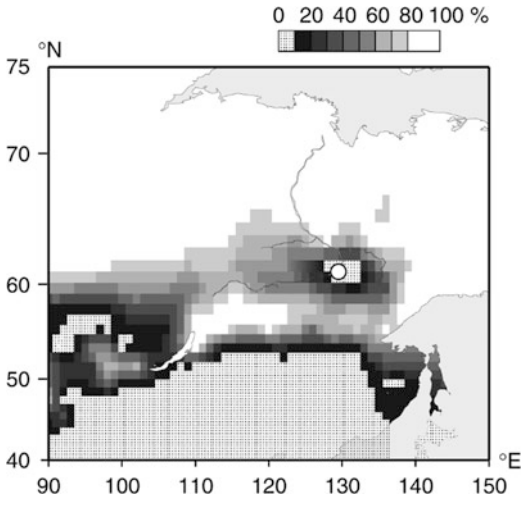

Fig. 11.2 Fifteen-year (1986–2000) composite of the ratio of snow cover existing during the week of snow disappearance in the central Lena River basin (60°N, 130°E) using NESDIS data. Reproduced from Figure 3 in (Iijima et al. 2007)

particularly the ESA GlobSnow dataset. Thus, snow retrievals by remote sensing techniques are important in the development and validation of large- or global-scale models.

11.4.4 Perspectives on Snow Remote Sensing

Snow coverage area products, especially fractional snow coverage datasets, are highly reliable and are used for model validation and many other types of studies. However, cloud and forest coverage still present many problems for performing snow retrievals. Further development of sensors for remote sensing and of more reliable retrieval algorithms is required. For instance, SWE products are less reliable in boreal forests and tundra regions. Thus, SWE products must be further developed before they can be used for research in eastern Siberia. Additionally, snow coverage area products are not reliable in areas with dense forest cover. Thus, caution is advised when applying snow coverage area products to the dense forest areas of eastern Siberia.

11.5 Surface Water (SW)

11.5.1 Remote Sensing of SW

SW is an important water resource because it can be easily used for multiple purposes, for example, as drinking water and in industrial processes. Therefore, determining the distribution of SW in eastern Siberia is critical. In addition, Huntington (2006) demonstrated that the Earth's hydrological cycle has intensified in several ways. SW is a key indicator of local and global hydrological cycles. In this section, we will describe several remote sensing techniques for assessing SW and their applications in scientific research. SW is composed of inundated areas such as lakes, ponds, and wetlands. We also introduce the major techniques for performing SW retrievals using optical sensors, passive microwave sensors, and multiple sensors and their application to scientific research in eastern Siberia.

11.5.2 SW Datasets

Here, we describe the SW retrievals performed using different sensors.

11.5.2.1 Landsat-TM

Two major products based on Landsat-TM data have been released recently. A high-resolution dataset describing lake density (the proportion of land covered by lakes) was established by Paltan et al. (2015), who used a density-slicing technique to define lake density using the shortwave infrared band 5 (1.55–1.75 μm). An SW fraction dataset with a spatial resolution of 30–90 m was constructed by Yamazaki et al. (2015) and Pekel et al. (2016), who used the normalized difference water index (NDWI: Xu 2006) and incorporated vegetation effects using NDVI data. The major difference in the products obtained by Yamazaki et al. (2015) and Pekel et al. (2016) resulted from the number of Landsat-TM images used: Yamazaki et al. (2015) used 30,000 images, whereas Pekel et al. (2016) used more than 3,000,000 images. Thus, the temporally resolved fractional SW dataset produced by Pekel et al. (2016) is more reliable than that of Yamazaki et al. (2015). The SW data (the Global 3 arc-second Water Body Map) by Yamazaki et al. (2015) can be found at http://hydro.iis.u-tokyo.ac.jp/~yamadai/G3 WBM/index.html. The dataset produced by Pekel et al. (2016) is located at https://global-surface-water.appspot.com/.

11.5.2.2 AMSR-E/AMSR2

Passive microwave sensors were used to derive the fractional open water cover (Fw) (Watts et al. 2012) using brightness temperatures measured at 18.7 and 23.8 GHz. The data required to produce this product are more frequently available because they are collected twice daily, but the spatial resolution is 0.25°. These data can be found at https://daac.ornl.gov/cgi-bin/dsviewer.pl?ds_id=1362.

11.5.2.3 Multiple Sensors

Prigent et al. (2007) developed the first global SW dataset that reported monthly mean inundation extent using passive microwave emissivity (as measured by the SSM/I), active microwave backscattering coefficients (as determined from ERS observations), and NDVI (as determined from AVHRR observations). The spatial resolution of this dataset is 0.25°, but its temporal resolution is only monthly. The fraction of SW coverage was also reported in the dataset. The benefit of using these data is that they represent a long-term SW record for use in climate studies. This dataset is located at https://lerma.obspm.fr/spip.php?article91&lang=en.

11.5.3 Scientific Applications of SW

Understanding the carbon balance in the Arctic is important because the Arctic permafrost represents a large carbon pool. Warming and thawing of this permafrost

will cause the carbon within the permafrost to be released as carbon dioxide or methane. SW area is very important in determining methane fluxes from the Arctic. Thus, Watts et al. (2014) estimated methane fluxes using the Fw data.

The hydrological cycle in large Arctic rivers in eastern Siberia is related to SW extent. Papa et al. (2008) showed the relationships between inundation area and runoff in the three largest Siberian rivers. In the case of the Lena River, there is a clear linear relationship between SW area and runoff. However, two distinct cases exist, namely, the spring runoff and summer-to-autumn phases.

Next, we show the SW distribution around Yakutsk region in the Lena River watershed. Figure 11.3 shows the spatial distribution of water body fraction over 30 years as determined by Pekel et al. (2016). The percentage of water bodies in this area is 5.7%, and there are clearly many temporary water bodies around Yakutsk in eastern Siberia. When the SW data of Yamazaki et al. (2015) is used, the percentage of water bodies is approximately 4.0% in the area. This discrepancy occurs because Pekel et al. (2016) used 100 times more Landsat-TM data than Yamazaki et al. (2015) and estimated temporary water bodies more accurately. Therefore, the dataset provided by Pekel et al. (2016) is suitable for analyzing temporal changes in SW in eastern Siberia.

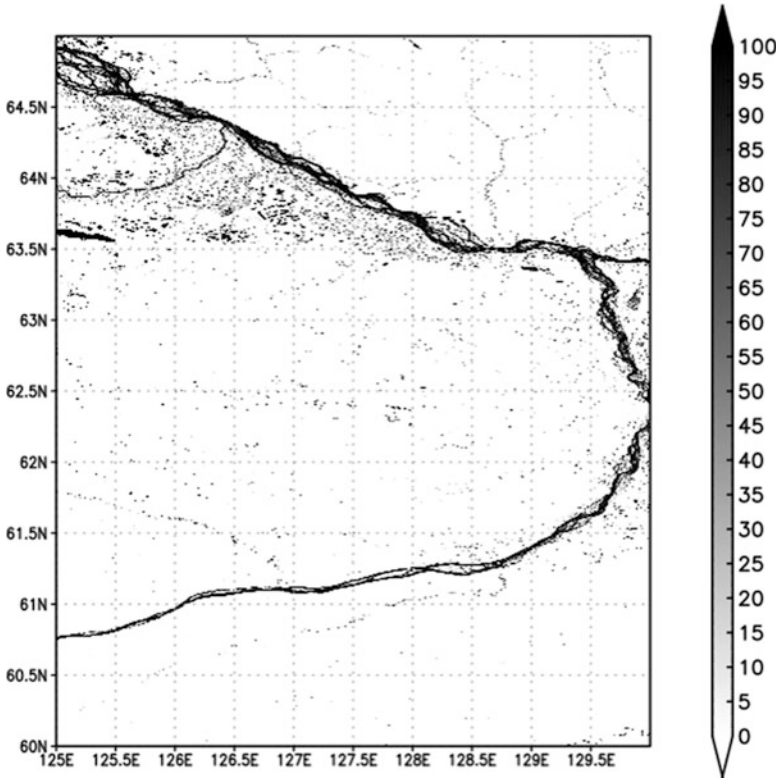

Fig. 11.3 Spatial distribution of water body fraction averaged over 30 years, estimated using the data of (Pekel et al. 2016) around Yakutsk in eastern Siberia

11.5.4 Perspectives on SW Remote Sensing

SW is a very important component of terrestrial water, both for the climate system and because its accessibility makes it convenient for usage for humans. Fine-scale spatially resolved SW data are now available, and long-term SW datasets have been developed using remote sensing techniques. To characterize the water and carbon cycles in eastern Siberia, SW retrievals can be used in many ways. Further development of SW retrieval methods will contribute to an improved understanding of the water and carbon dynamics in eastern Siberia.

11.6 Emerging Research: Data Assimilation

In this chapter, recently developed remote sensing techniques, which are used to derive TW components such as TWS, SM, snow, and SW, are reviewed. Ground-based observations neglect vast areas within eastern Siberia as accessibility is limited, and ground-based observations are too expensive. By contrast, satellite data are useful for observing TW over this large area. However, many issues must be resolved in order to enhance the accuracy of satellite retrievals.

Land surface data assimilation uses land surface models and satellite measurements. Thus, it is becoming popular because this method can fill the gaps in current satellite-based datasets. For example, each component of TW has been studied—specifically, TWS (Kumar et al. 2016), SM (Reichle et al. 2007), snow (Che et al. 2014), and SW (Revilla-Romero et al. 2016). These types of land surface data assimilation products are increasing in number, with rising applications.

The next step will involve coupled atmosphere and land surface data assimilation. This method will yield various benefits, including improved estimation of both the state of the atmosphere and TW at ground level. Such coupled atmosphere-land surface data assimilation studies are emerging in the field (Rasmy et al. 2012; Suzuki et al. 2017).

11.7 Concluding Remarks

Figure 11.4 shows a schematic of remote sensing techniques for performing TW retrievals. Only gravimetric observations can provide estimates of TWS. Optical sensors primarily detect snow and SW; passive microwave sensors primarily detect SM, snow, and SW; and active microwave sensors are mainly used to estimate SM. Passive microwave sensors provide the finest temporal resolution, followed by active microwave sensors, with optical sensors exhibiting the coarsest temporal resolution. However, in terms of spatial resolution, the ordering of the sensor

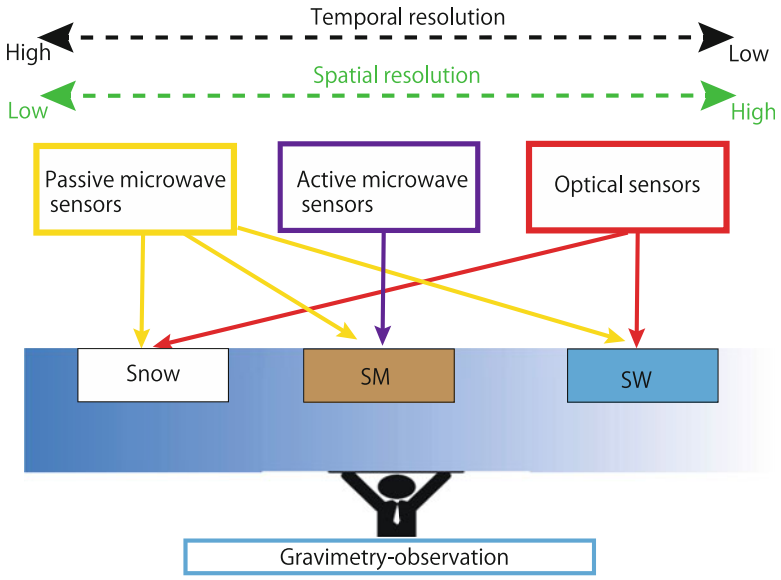

Fig. 11.4 Schematic diagram of remote sensing sensors in relation to each TW component. Solid lines (yellow, purple, red and light blue lines) indicate direct and indirect methods for estimating each TW component, respectively

types is reversed. The fusion of data from multiple satellites will produce better results than single sensors because each sensor has comparative advantages and disadvantages, and therefore, the use of fusion techniques can compensate for the drawbacks of each.

TW data can be used for a wide variety of studies, including those that address hydrology and the carbon cycle. Techniques for the remote sensing of TW are still advancing, and the development of data products depends on international satellite missions. To validate the accuracy of remote sensing retrievals, producing ground-based in situ validation data is necessary. Emerging data assimilation methods will fill the gaps between the demands of users and the shortage of remote sensing retrievals.

References

Bartsch A, Balzter H, George C (2009) The influence of regional surface soil moisture anomalies on forest fires in Siberia observed from satellites. Environ Res Lett 4(4). https://doi.org/10.1088/1748-9326/4/4/045021

Bettadpur S (2012) Gravity recovery and climate experiment UTCSR Level-2 Processing Standards Document (Rev 4.0 May 29, 2012) (For Level-2 Product Release 0005). ftp://podaac.jpl.nasa.gov/allData/grace/docs/L2-CSR0005_ProcStd_v4.0.pdf

Brown RD, Robinson DA (2011) Northern hemisphere spring snow cover variability and change over 1922–2010 including an assessment of uncertainty. Cryosphere 5(1):219–229. https://doi.org/10.5194/tc-5-219-2011

Che T, Li X, Jin R, Huang C (2014) Assimilating passive microwave remote sensing data into a land surface model to improve the estimation of snow depth. Remote Sens Environ 143 (C):54–63. https://doi.org/10.1016/j.rse.2013.12.009

Derksen C (2008) The contribution of AMSR-E 18.7 and 10.7 GHz measurements to improved boreal forest snow water equivalent retrievals. Remote Sens Environ 112(5):2701–2710. https://doi.org/10.1016/j.rse.2008.01.001

Dietz AJ, Kuenzer C, Gessner U, Dech S (2012) Remote sensing of snow – a review of available methods. Int J Remote Sens 33(13):4094–4134. https://doi.org/10.1080/01431161.2011.640964

Dudarev AA, Dushkina EV, Sladkova YN, Alloyarov PR, Chupakhin VS, Dorofeyev VM et al (2013) Food and water security issues in Russia II: water security in general population of Russian Arctic, Siberia and Far East, 2000–2011. Int J Circumpolar Health 72(0):1–11. https://doi.org/10.3402/ijch.v72i0.22646

Earl L, Gardner A (2016) A satellite-derived glacier inventory for North Asia. Ann Glaciol 57 (71):50–60. https://doi.org/10.3189/2016AoG71A008

Entekhabi D, Njoku EG, O'Neill PE, Kellogg KH, Crow WT, Edelstein WN et al (2010) The soil moisture active passive (SMAP) mission. Proc IEEE 98(5):704–716. https://doi.org/10.1109/JPROC.2010.2043918

Figa-Saldaña J, Wilson JJW, Attema E, Gelsthorpe R, Drinkwater MR, Stoffelen A (2002) The advanced scatterometer (ASCAT) on the meteorological operational (MetOp) platform: a follow on for European wind scatterometers. Can J Remote Sens 28(3):404–412. https://doi.org/10.5589/m02-035

Ford TW, Harris E, Quiring SM (2014) Estimating root zone soil moisture using near-surface observations from SMOS. Hydrol Earth Syst Sci 18(1):139–154. https://doi.org/10.5194/hess-18-139-2014

Foster JL, Sun C, Walker JP, Kelly R, Chang A, Dong J et al (2005) Quantifying the uncertainty in passive microwave snow water equivalent observations. Remote Sens Environ 94(2):17–17. https://doi.org/10.1016/j.rse.2004.09.012

Geruo A, Wahr J, Zhong S (2013) Computations of the viscoelastic response of a 3-D compressible earth to surface loading: an application to glacial isostatic adjustment in Antarctica and Canada. Geophys J Int 192(2):557–572. https://doi.org/10.1093/gji/ggs030

Geruo A, Velicogna I, Kimball JS, Kim Y (2015) Impact of changes in GRACE derived terrestrial water storage on vegetation growth in Eurasia. Environ Res Lett 10(12):1–10. https://doi.org/10.1088/1748-9326/10/12/124024

Hall DK, Riggs GA (2007) Accuracy assessment of the MODIS snow products. Hydrol Process 21 (12):1534–1547. https://doi.org/10.1002/hyp.6715

Hall DK, Kelly R, Riggs GA, Chang A, Foster JL (2002) Assessment of the relative accuracy of hemispheric-scale snow-cover maps. Ann Glaciol 34(1):24–30. https://doi.org/10.3189/172756402781817770

Hogstrom E, Bartsch A (2016) Impact of backscatter variations over water bodies on coarse-scale radar retrieved soil moisture and the potential of correcting with meteorological data. IEEE Trans Geosci Remote Sens 55(1):3–13. https://doi.org/10.1109/TGRS.2016.2530845

Hood JL, Hayashi M (2015) Characterization of snowmelt flux and groundwater storage in an alpine headwater basin. J Hydrol 521:482–497

Huntington TG (2006) Evidence for intensification of the global water cycle: review and synthesis. J Hydrol 319(1–4):83–95

Iijima Y, Masuda K, Ohata T (2007) Snow disappearance in eastern Siberia and its relationship to atmospheric influences. Int J Climatol 27(2):169–177. https://doi.org/10.1002/joc.1382

Imaoka K, Kachi M, Fujii H, Murakami H, Hori M, Ono A, Igarashi T, Nakagawa K, Oki T, Honda Y, Shimoda H (2010) Global Change Observation Mission (GCOM) for monitoring carbon, water cycles, and climate change. Proc IEEE 98(5):717–734

Kachi M, Maeda T, Tsutsui H, Imaoka K (2015) The water-related parameters and datasets derived from GCOM-W/AMSR2. IGARSS. https://doi.org/10.1109/IGARSS.2015.7326979

Keiji Imaoka, Misako Kachi, Hideyuki Fujii, Hiroshi Murakami, Masahiro Hori, Akiko Ono, Tamotsu Igarashi, Keizo Nakagawa, Taikan Oki, Yoshiaki Honda, Haruhisa Shimoda, Global Change Observation Mission (GCOM) for Monitoring Carbon, Water Cycles, and Climate Change. Proceedings of the IEEE 98 (5):717-734

Kerr YH, Waldteufel P, Wigneron J-P, Delwart S, Cabot F, Boutin J et al (2010) The SMOS mission – new tool for monitoring key elements of the global water cycle. Proc IEEE 98 (5):666–687. https://doi.org/10.1109/JPROC.2010.2043032

Klein AG, Barnett AC (2003) Validation of daily MODIS snow cover maps of the upper Rio Grande River basin for the 2000-2001 snow year. Remote Sens Environ 86(2):162–176. https://doi.org/10.1016/S0034-4257(03)00097-X

Kumar SV, Zaitchik BF, Peters-Lidard CD, Rodell M, Reichle R, Li B et al (2016) Assimilation of gridded GRACE terrestrial water storage estimates in the north American land data assimilation system. J Hydrometeorol 17(7):1951–1972. https://doi.org/10.1175/JHM-D-15-0157.1

Kusche J (2007) Approximate decorrelation and non-isotropic smoothing of time-variable GRACE-type gravity field models. J Geod 81(11):733–749. https://doi.org/10.1007/s00190-007-0143-3

Masuda K, Hashimoto Y, Matsuyama H, Oki T (2001) Seasonal cycle of water storage in major river basins of the world. Geophys Res Lett 28(16):3215–3218. https://doi.org/10.1029/2000GL012444

Merlin O, Bitar Al A, Walker JP, Kerr Y (2010) An improved algorithm for disaggregating microwave-derived soil moisture based on red, near-infrared and thermal-infrared data. Remote Sens Environ 114(10):2305–2316. https://doi.org/10.1016/j.rse.2010.05.007

Muskett RR, Romanovsky VE (2009) Groundwater storage changes in arctic permafrost watersheds from GRACE and in situ measurements. Environ Res Lett 4(4):045009. https://doi.org/10.1088/1748-9326/4/4/045009

Nitta T, Yoshimura K, Takata K, O'ishi R, Sueyoshi T, Kanae S et al (2014) Representing variability in subgrid snow cover and snow depth in a global land model: offline validation. J Clim 27:3318–3330. https://doi.org/10.1175/JCLI-D-13-00310.1

Owe M, de Jeu R, Holmes T (2008) Multisensor historical climatology of satellite-derived global land surface moisture. J Geophysical Res 113(F1):687–617. https://doi.org/10.1029/2007JF000769

Painter TH, Dozier J, Roberts DA, Davis RE, Green RO (2003) Retrieval of subpixel snow-covered area and grain size from imaging spectrometer data. Remote Sens Environ 85(1):64–77. https://doi.org/10.1016/S0034-4257(02)00187-6

Painter TH, Rittger K, McKenzie C, Slaughter P, Davis RE, Dozier J (2009) Retrieval of subpixel snow covered area, grain size, and albedo from MODIS. Remote Sens Environ 113(4):868–879. https://doi.org/10.1016/j.rse.2009.01.001

Paltan H, Dash J, Edwards M (2015) A refined mapping of Arctic lakes using Landsat imagery. Int J Remote Sens 36(23):5970–5982. https://doi.org/10.1080/01431161.2015.1110263

Papa F, Prigent C, Rossow WB (2008) Monitoring flood and discharge variations in the large Siberian rivers from a multi-satellite technique. Surv Geophysi 29(4–5):297–317. https://doi.org/10.1007/s10712-008-9036-0

Parajka J, Bloschl G (2008) Spatio-temporal combination of MODIS images – potential for snow cover mapping. Water Resour Res 44(3). https://doi.org/10.1029/2007WR006204

Pekel J-F, Cottam A, Gorelick N, Belward AS (2016) High-resolution mapping of global surface water and its long-term changes. Nature 540(7633):418–422. https://doi.org/10.1038/nature20584

Petropoulos GP, Ireland G, Barrett B (2015) Surface soil moisture retrievals from remote sensing: current status, products & future trends. Phys Chem Earth 83–84:36–56. https://doi.org/10.1016/j.pce.2015.02.009

Prigent C, Papa F, Aires F, Rossow WB, Matthews E (2007) Global inundation dynamics inferred from multiple satellite observations, 1993–2000. J Geophys Res 112(D12):D12107–D12113. https://doi.org/10.1029/2006JD007847

Quinton WL, Hayashi M, Pietroniro A (2003) Connectivity and storage functions of channel fens and flat bogs in northern basins. Hydrol Process 17(18):3665–3684

Ramsay BH (1998) The interactive multisensor snow and ice mapping system. Hydrol Process 12 (1):1537–1546. https://doi.org/10.1002/(SICI)1099-1085(199808/09)12:10/11<1537::AID-HYP679>3.3.CO;2-1

Rasmy M, Koike T, Kuria D, Mirza CR, Li X, Yang K (2012) Development of the coupled atmosphere and land data assimilation system (CALDAS) and its application over the Tibetan plateau. IEEE Trans Geosci Remote Sens 50(11):4227–4242. https://doi.org/10.1109/TGRS.2012.2190517

Reichle RH, Koster RD, Liu P, Mahanama SPP, Njoku EG, Owe M (2007) Comparison and assimilation of global soil moisture retrievals from The Advanced Microwave Scanning Radiometer For the Earth Observing System (AMSR-E) and the Scanning Multichannel Microwave Radiometer (SMMR). J Geophys Res Atmos 112(D):D09108. https://doi.org/10.1029/2006JD008033

Revilla-Romero B, Wanders N, Burek P, Salamon P, de Roo A (2016) Integrating remotely sensed surface water extent into continental scale hydrology. J Hydrol 543(Part B):659–670. https://doi.org/10.1016/j.jhydrol.2016.10.041

Schaefer K, Collatz GJ, Tans P, Denning AS, Baker I, Berry J, Prihodko L, Suits N, Philpott A (2008) Combined simple biosphere/carnegie-Ames-Stanford approach terrestrial carbon cycle model. J Geophys Res Biogeo 113:G03034. https://doi.org/10.1029/2007jg000603

Seo K-W, Ryu D, Kim B-M, Waliser DE, Tian B, Eom J (2010) GRACE and AMSR-E-based estimates of winter season solid precipitation accumulation in the Arctic drainage region. J Geophys Res 115(D20):D20117–D20118. https://doi.org/10.1029/2009JD013504

Sugimoto A, Naito D, Yanagisawa N, Ichiyanagi K, Kurita N, Kubota J et al (2003) Characteristics of soil moisture in permafrost observed in east Siberian taiga with stable isotopes of water. Hydrol Process 17(6):1073–1092. https://doi.org/10.1002/hyp.1180

Suzuki K (2011) Siberia. In: Encyclopedia of snow, ice and glaciers. Springer Netherlands, Dordrecht, pp 1028–1031. https://doi.org/10.1007/978-90-481-2642-2_486

Suzuki K, Kubota J, Ohata T, Vuglinsky V (2006) Influence of snow ablation and frozen ground on spring runoff generation in the Mogot experimental watershed, southern mountainous taiga of eastern Siberia. Hydrol Res 37(1):21–29. https://doi.org/10.2166/nh.2005.027

Suzuki K, Liston GE, Matsuo K (2015) Estimation of continental-basin-scale sublimation in the Lena River Basin, Siberia. Adv Meteorol 2015(22):1–14. https://doi.org/10.1155/2015/286206

Suzuki K, Matsuo K, Hiyama T (2016) Satellite gravimetry-based analysis of terrestrial water storage and its relationship with run-off from the Lena River in eastern Siberia. In J Remote Sen 37(10):2198–2210. https://doi.org/10.1080/01431161.2016.1165890

Suzuki K, Zupanski M, Zupanski D (2017) A case study involving single observation experiments performed over snowy Siberia using a coupled atmosphere-land modelling system. Atmos Sci Lett 18(3):106–111. https://doi.org/10.1002/asl.730

Suzuki K, Matsuo K, Yamazaki D, Ichii K, Iijima Y, Yanagi Y et al (2018) Hydrological variability and changes in the Arctic circumpolar tundra and the three largest pan-Arctic river basins from 2002 to 2016. Remote Sens 2018(10):402. https://doi.org/10.3390/rs10030402

Swenson S, Wahr J (2006) Post-processing removal of correlated errors in GRACE data. Geophys Res Lett 33(8):L08402–4. https://doi.org/10.1029/2005GL025285

Takala M, Luojus K, Pulliainen J, Derksen C, Lemmetyinen J, Kärnä J-P et al (2011) Estimating northern hemisphere snow water equivalent for climate research through assimilation of space-

borne radiometer data and ground-based measurements. Remote Sens Environ 115 (12):3517–3529. https://doi.org/10.1016/j.rse.2011.08.014

Tapley BD, Bettadpur S, Ries JC, Thompson PF, Watkins MM (2004) GRACE measurements of mass variability in the Earth system. Science 305(5683):503–505. https://doi.org/10.1126/science.1099192

Tedesco M, Jeyaratnam J (2016) A new operational snow retrieval algorithm applied to historical AMSR-E brightness temperatures. Remote Sens 8(12):1037. https://doi.org/10.3390/rs8121037

van der Molen MK, de Jeu RAM, Wagner W, van der Velde IR, Kolari P, Kurbatova J et al (2016) The effect of assimilating satellite-derived soil moisture data in SiBCASA on simulated carbon fluxes in Boreal Eurasia. Hydrol Earth Syst Sci 20(2):605–624. https://doi.org/10.5194/hess-20-605-2016

Velicogna I, Tong J, Zhang T, Kimball JS (2012) Increasing subsurface water storage in discontinuous permafrost areas of the Lena River basin, Eurasia, detected from GRACE. Geophy Res Lett 39(9):L09403. https://doi.org/10.1029/2012GL051623

Vey S, Steffen H, Müller J, Boike J (2013) Inter-annual water mass variations from GRACE in Central Siberia. J Geod 87(3):287–299. https://doi.org/10.1007/s00190-012-0597-9

Wagner W, Hahn S, Kidd R, Melzer T, Bartalis Z, Hasenauer S et al (2013) The ASCAT soil moisture product: a review of its specifications, validation results, and emerging applications. Meteorol Z 22(1):5–33. https://doi.org/10.1127/0941-2948/2013/0399

Wahr J, Molenaar M, Bryan F (1998) Time variability of the Earth's gravity field: hydrological and oceanic effects and their possible detection using GRACE. J Geophys Res 103 (B12):30205–30229. https://doi.org/10.1029/98JB02844

Wahr J, Swenson S, Zlotnicki V, Velicogna I (2004) Time-variable gravity from GRACE: first results. Geophys Res Lett 31(11). https://doi.org/10.1029/2004GL019779

Watts JD, Kimball JS, Jones LA, Schroeder R, McDonald KC (2012) Satellite microwave remote sensing of contrasting surface water inundation changes within the Arctic–Boreal region. Remote Sens Environ 127:223–236. https://doi.org/10.1016/j.rse.2012.09.003

Watts JD, Kimball JS, Bartsch A, McDonald KC (2014) Surface water inundation in the boreal-Arctic: potential impacts on regional methane emissions. Environ Res Lett 9(7):075001. https://doi.org/10.1088/1748-9326/9/7/075001

Xu H (2006) Modification of normalised difference water index (NDWI) to enhance open water features in remotely sensed imagery. Int J Remote Sens 27(14):3025–3033. https://doi.org/10.1080/01431160600589179

Yamazaki D, Trigg MA, Ikeshima D (2015) Development of a global ~90 m water body map using multi-temporal Landsat images. Remote Sens Environ 171(C):337–351. https://doi.org/10.1016/j.rse.2015.10.014

Yang D, Zhao Y, Armstrong R, Robinson D, Brodzik M-J (2007) Streamflow response to seasonal snow cover mass changes over large Siberian watersheds. J Geophys Res Earth Surf 112(F): F02S22. https://doi.org/10.1029/2006JF000518

Chapter 12
Carbon-Water Cycle Modeling

Hotaek Park and Takeshi Yamazaki

12.1 Introduction

In the past few decades, considerable progress has been made in improving land surface models based on biogeochemical and physical principles. Pitman (2003) reviewed the history of the development of land surface models designed for climate models. The "Manabe bucket model" (Manabe 1969) is considered the first generation of land surface models. In this model, evaporation was limited by soil water content, and additional precipitation generated runoff as soil moisture exceeded the holding capacity. Deardorff (1978) introduced a method called the "force-restore method" to simulate soil temperature (T_{SOIL}) and moisture in two layers, in which vegetation was introduced as a single bulk layer shielding the ground. More realistic vegetation–soil systems that included biophysical control of evapotranspiration (*ET*) were proposed in two land surface models: the Biosphere–Atmosphere Transfer Scheme (Dickinson 1984) and the Simple Biosphere Model (Sellers et al. 1986). In the latter, a deliberate effort was made to base radiative, momentum, and heat/mass transfer properties of vegetated surfaces on a set of directly measurable surface parameters. The Canadian Land Surface Scheme for general circulation models highlighted boreal processes in a global climate simulation (Verseghy 1991; Verseghy et al. 1993). During the last few decades, various dynamic global vegetation models have been developed to simulate potential shifts in vegetation and associated biogeochemical and hydrological cycles in response to climate change (Foley et al. 1996; Cox et al. 1998; Levis et al. 2004).

H. Park (✉)
Japan Agency for Marine-Earth Science and Technology (JAMSTEC), Yokosuka, Japan
e-mail: park@jamstec.go.jp

T. Yamazaki
Tohoku University, Sendai, Japan

T. Ohta et al. (eds.), *Water-Carbon Dynamics in Eastern Siberia*,
Ecological Studies 236, https://doi.org/10.1007/978-981-13-6317-7_12

The Boreal Ecosystem-Atmosphere Study (BOREAS) was conducted as a large-scale international field experiment in a region in Canada from 1993 to 1997 (Sellers et al. 1997). BOREAS focused on improving our understanding of the exchanges of radiative energy, heat, water, carbon dioxide, and trace gases between the boreal forest and atmosphere. Betts et al. (2001) documented the impact of BOREAS on the development of a new land surface parameterization in the European Centre for Medium-Range Weather Forecasts global forecast system. In particular, the parameterization of snow albedo has reduced systematic cold temperature biases in models both at the surface and in the lower troposphere at high northern latitudes, especially in spring (Viterbo and Betts 1999).

The developed models capable of representing feedback, interaction, and linkage interconnections have been offered various insights into changes in the Arctic system over a broad spectrum of temporal and spatial scales. Such models have simulated increases in snow depth (SND) in Arctic terrestrial regions, showing subsequent effects on permafrost degradation (Park et al. 2015) and increases in the decomposition rate of soil organic matter within the permafrost (Gouttevin et al. 2012). Furthermore, model simulations have been showed increased Arctic river discharge in response to increased precipitation, particularly snowmelt water (Rawlins et al. 2010). Sensitivity analyses offer a general approach to quantify changes in land processes by altering the states of objective variables. Such experiments have addressed the significant impacts of soil organic carbon (SOC) on soil thermal and hydraulic properties (Lawrence and Slater 2008), permafrost impedance on river discharge via soil moisture (Swenson et al. 2012), and changes in vegetation structure on surface energy budget (Yamazaki et al. 2004). The synthetic integration and coordination of these partial studies can improve our understanding of the reality of the changes occurring in the Arctic, including river systems, and determine the causes of the variability in the processes.

The Japanese research community has made various efforts to identify changes at watershed and pan-Arctic scales through observational and modeling studies. Since the mid-1990s, observations of water and carbon exchanges have been undertaken, with a focus on larch and pine forests in eastern Siberia (Ohta et al. 2001, 2014). In addition, a model that numerically simulates the exchanges in the atmosphere–vegetation–soil system has been developed (Yamazaki et al. 2004; Park et al. 2011). Model intercomparison projects have been performed since the 1990s. Recently, 22 domestic and international models participated in the GRENE-TEA model intercomparison project (Miyazaki et al. 2015), which was designed to enhance communication and understanding between modeling and field scientists and to assess the uncertainty and variations stemming from variability in model implementation and design. Improved models have been extended to the Lena River watershed (Park et al. 2008, 2013a) and then to a pan-Arctic scale (Park et al. 2015, 2016b) with heterogeneous landscapes and climates over longer time scales.

This chapter offers a synthetic overview of the changes in the Arctic ecohydrological cycles in the context of climate change from the perspective of a key hypothesis that high levels of winter snow under declining sea ice fuels change in the Arctic terrestrial processes through feedback loops and interactions between

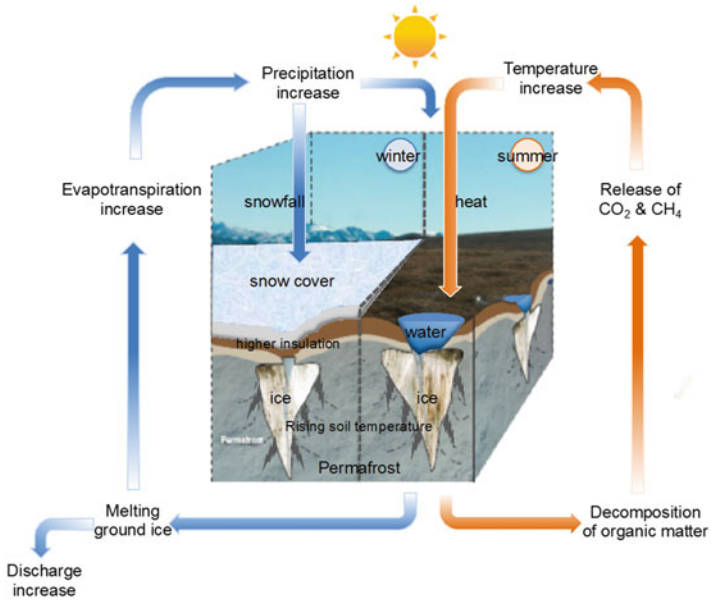

Fig. 12.1 The Arctic is a highly coupled system with clear linkages and strong interdependence among system processes and components

heat and water cycles (Fig. 12.1). This hypothesis is demonstrated following a simple approach whereby one-dimensional land surface models are expanded from specific site scales to the Lena River of eastern Siberia and pan-Arctic scales.

12.2 Model Assessment at Site-Specific Scales

A one-dimensional land surface model was developed to simulate processes in intensely cold regions and assess changes in water and energy exchanges in boreal forests. The model was applied to old larch (Spasskaya Pad, see Chap. 3), young larch, pine, and grassland sites near Yakutsk, and the simulations were compared to observations.

12.2.1 Model Description

The one-dimensional land surface model is composed of three submodels (of vegetation, snow cover, and soil) to calculate water and energy fluxes above and within the forest when meteorological data over the forest are given as inputs (Yamazaki et al. 2004).

In the vegetation submodel, canopy is divided into a crown space and a trunk space (without leaves), and the crown space is subdivided into two layers (2LM). The heat balance is resolved with respect to radiative, sensible, and latent heat fluxes among the atmosphere and two crown layers. Sensible and latent heat fluxes are described as proportional to temperature and specific humidity differences, respectively. Stomatal conductance is the proportional coefficient used to calculate transpiration generated in the canopy layer. The 2LM employs a Jarvis-type stomatal conductance model (Jarvis 1976). The Jarvis model is simple; it does not express photosynthesis processes and has the limitation that environmental variables do not provide feedback to each other (Yamazaki et al. 2013). However, this model has the benefit of enabling the analysis of environmental elements (i.e., light, vapor pressure deficit, leaf temperature, and volumetric soil water content) that restrict transpiration. Parameter values are fitted simultaneously using a nonlinear least-square technique to minimize the root–mean–square error between the measured and estimated values of stomatal conductance. First, the within-site parameters for each site are determined using only the data measured at each site and for each species. In principle, the model is expected to reasonably simulate energy and water balance for certain sites and species based on the site parameters. However, these within-site parameters do not apply to other sites and species. Therefore, a set of pooled common parameters is determined using pooled measurement data of all sites.

The snow cover submodel (Yamazaki 2001) utilizes simple assumptions regarding both the structure and physical process of snow. The number of snow layers depends on SND, and the thickness of each layer is 0.02 m. To apply this model to intensely cold regions, the snow cover submodel can incorporate depth hoar using an effective temperature gradient and calculate snow temperature, density, and water content profiles.

In the soil submodel, a heat conduction equation is used to calculate T_{SOIL}. The heat of fusion in frozen soil is considered using a method in which the heat capacity is regarded as larger within a smaller temperature range near the melting point. Liquid water movement is also considered in this submodel. The equation is characterized by ground surface resistance, which includes the effects of understory vegetation.

12.2.2 Water and Energy Balance

The model reasonably simulated diurnal and seasonal changes in heat fluxes for forest (larch on the right bank of Lena River (RLena), larch and pine on the left bank (LLar, LPin)), and grassland (right bank of Lena River (RGrass)) near Yakutsk (Yamazaki et al. 2004). At the grassland site, the Bowen ratio (sensible heat/latent heat) was 0.2 in midsummer, lower than that at the forest sites (~1). Sensitivity experiments have indicated that leaf area should be given accurately along with the total plant area index, including stem and branch areas. Using both plant and leaf areas, an outline of the seasonal heat balance could be simulated using the same

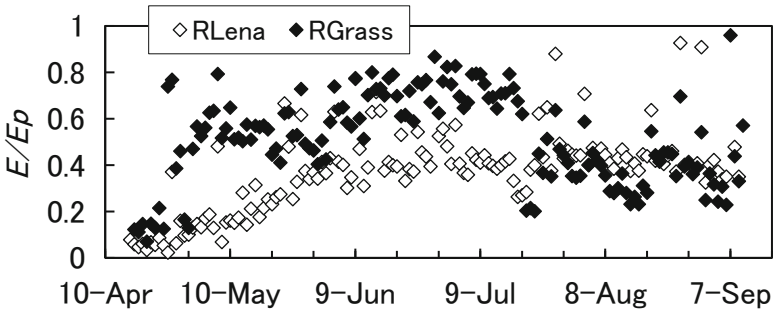

Fig. 12.2 Daily evapotranspiration normalized by potential evaporation in larch forest (RLena) and grassland (RGrass) in 2000 (Yamazaki et al. 2004)

stomatal parameters for forests and grassland sites. Moreover, seasonal changes in energy and water fluxes at three Japanese sites in temperate forests were reproduced well with the 2LM using both within-site and pooled common parameters. The results suggest that energy and water fluxes can be simulated using one common parameter set with no parameter tuning, at least for forests in a wide region of East Asia (Yamazaki et al. 2013).

Figure 12.2 shows the seasonal change in daily *ET* normalized to potential evaporation (*Ep*; *ET/Ep*) at RLena and RGrass. At RLena, *ET/Ep* was 0.1 in the leafless season, which increased rapidly to 0.4 after leaf out. *ET/Ep* occasionally spiked irregularly above 0.6 due to higher canopy interception caused by rainfall events. At RGrass, this feature differed from the forest sites; *ET/Ep* reached 0.7 before grass cutting (21 July) and decreased to around 0.4 after cutting. Because the dependence of evaporation on meteorological conditions was removed by normalization to *Ep*, the gap around 20 July was caused solely by grass cutting. *ET/Ep* reached as high as 0.5 or 0.6 between snow disappearance (26 April) and grass growth at RGrass, and it was low (~0.1) until snow disappearance. This is because ground is treated as pure snow cover before snow disappearance and as a wet soil surface thereafter.

Figure 12.3 shows the water budget from 21 April to 31 August at each site and year (1998, 1999, and 2000). The two bars for each site and year indicate the input containing precipitation in this period and snow at the beginning of the period on the left and *ET* containing three components: interception (E_{int}), transpiration (T), and understory *ET* (E_{und}), on the right.

At LLar, input water showed high interannual variation, with less precipitation (82 mm) in 1998, more (236 mm) in 1999, and a relatively normal amount (143 mm) in 2000. For comparison, the average precipitation from April to August in Yakutsk was 139 mm. However, total *ET* (E_{tot}) showed a smaller range of <50 mm (maximum: 265 mm in 1988, minimum: 211 mm in 2000) at LLar. This is consistent with the suggestion that ice meltwater from deeper soil is transported upward and used for transpiration when it is dry in summer according to a stable isotope analysis (Sugimoto et al. 2003;see Chap. 6).

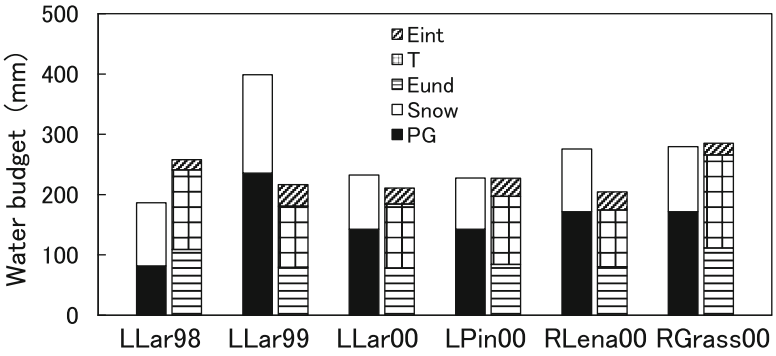

Fig. 12.3 Water budget from 21 April to 31 August for each site and year. The left bar in each site is input containing precipitation in this period and snow at 21 April. The right bar is evapotranspiration containing interception, transpiration, and understory evapotranspiration (Yamazaki et al. 2004)

The ratio of E_{und}/E_{tot} ranged from 0.37 (LLar2000 and LPin) to 0.44 (RGrass). Additional observations revealed a ratio of 0.35 at LLar in 1998 (Ohta et al. 2001) and 0.4–0.5 at LPin (Hamada et al. 2004). Although E_{und}/E_{tot} was larger in pine forests according to these observations, the model yielded similar results among each site and year.

The ratio of E_{int} to precipitation (P_G) (E_{int}/P_G) was 0.15–0.21 at the forest sites, where the minimum was observed at LLar1999 and the maximum at LLar1998 and LPin. In LLar1999, the absolute value of E_{int} was large (36 mm), but P_G was larger, resulting in a small ratio. According to observations, the ratio was 0.15 at LLar1998 (Ohta et al. 2001) and approximately 0.3 at LPin (Toba and Ohta 2005). Conversely, from this study, the ratio was 0.11 at RGrass. By comparison, a model simulation yielded a fractional range of 10–20% for E_{int}/ET in a larch forest of eastern Siberia, where T comprised 67% of ET and was dependent on summer P_G; evaporation from soil surface (E_{soil}) accounted for about 20% of ET (Park et al. 2011), much lower than previous results of about 50% (Iida et al. 2009).

The simulation showed solid water storage in the canopy, mainly intercepted snow, from October to March (Yamazaki et al. 2007), in agreement with photographs of the site. Intercepted snow and ice decreased rapidly in March due to sublimation. Evaporation was low (0.01–0.05 mm day^{-1}) in midwinter due to the low air temperature. The average ratios of E_{int}/P_G were 0.16 in winter (October–March), 0.03–0.09 in midwinter (November–February), and 0.57 in March. Net radiation roughly balanced sensible heat flux in midwinter, during which albedo was almost constant at 0.35. Frost on the canopy was negligible in these simulations. Temperature warming reduces the winter freezing period, while it likely increases the rate of E_{int}. However, long-term variability in the E_{int} rate is rarely observed due to the difficulty of direct measurements. Moreover, few simulations have quantitatively assessed the E_{int} rate at site and pan-Arctic scales.

12.2.3 Rapid Increases in Soil Temperature and Moisture

Snow cover forms depth hoar in intensely cold regions because it is exposed to a large vertical temperature gradient. For example, air temperature reaches −50 °C in winter in Siberia, but T_{SOIL} is warmer, typically −10 °C. Hoar forms in snow cover due to the upward transport of water vapor due to the large water vapor gradient caused by the dependence of saturation water vapor pressure on temperature. Depth hoar has a low density and low thermal conductivity, and it influences not only energy and water exchange but also soil freezing conditions. Due to its low thermal conductivity, depth hoar acts as thermal insulation, protecting the soil layer from rapid cooling. Therefore, 2LM included depth hoar processes and realistically simulated T_{SOIL} profiles in February 1988 in Yakutsk (Yamazaki 2001). Meanwhile, the comparison between the simulation and observation indicated that the simulated T_{SOIL} was unrealistically low when depth hoar was not considered.

Since 2004, soil moisture and temperature have increased rapidly, and the active layer has become deep since 2004 (Ohta et al. 2008; Iijima et al. 2010). Iijima et al. (2010) noted that soil warming is caused by abnormally high pre-winter rainfall, which results in a high soil water content in fall and snowfall in early winter. The recent rapid change in soil conditions was reproduced by 2LM, which clarified the influences of pre-winter rainfall and snowfall on the increases in soil moisture and temperature.

Summer (May–September) and fall (October–November) P_G were analyzed from 1966 to 2008. The mean and standard deviation of P_G were 181 mm and 50 mm in summer and 40 mm and 16 mm in fall, respectively. From 2003 to 2007, P_G ranged from 143 to 286 in summer and 19 to 75 in fall and was greater on average in most years during this period. The model-calculated annual maximum soil thaw depth revealed a higher sensitivity to summer/fall P_G. The effect of the change in P_G on soil conditions was tested with model sensitivity experiments. Figure 12.4 shows the

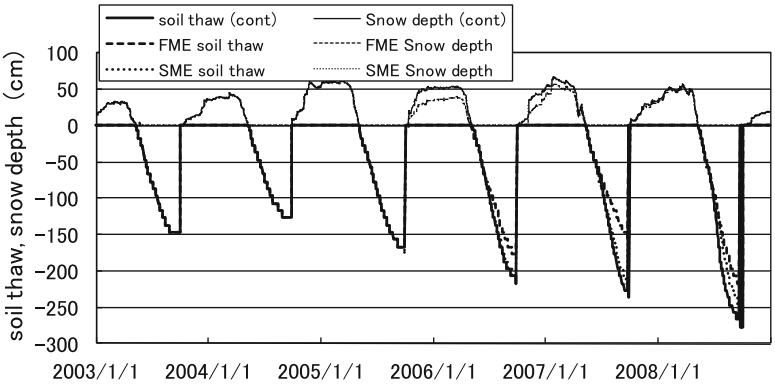

Fig. 12.4 Effect of precipitation change on soil thaw and snow depth. FME: precipitation is replaced by mean in fall (October and November) from 2005 to 2007. SME: precipitation is reduced by mean in summer (from May to September) from 2005 to 2007

results of two cases of P_G changes. P_G was replaced by the mean value in fall or early winter (October–November) from 2005 to 2007 (FME in Fig. 12.4) and replaced by the mean value in summer (May–September) from 2005 to 2007 (SME in Fig. 12.4). These simulations indicate that deepening soil thaw is more sensitive to changes in fall P_G than that in summer and that deeper snow caused by fall P_G offers higher insulation, maintaining a higher T_{SOIL} that rises rapidly after spring.

12.3 Pan-Arctic Model Simulation

12.3.1 Model Description

The coupled hydrological and biogeochemical model (CHANGE; Park et al. 2011) is a process-based model combined with submodels of soil thermal and hydrologic states, snow hydrology, and plant stomatal physiology and photosynthesis. The model represents permafrost dynamics, including an explicit treatment of soil freezing/thawing phase changes in a 50 m soil column. The effects of soil organic carbon on the soil thermal and hydraulic processes are represented by parameterizations that considered the vertical distribution estimated inherently by the model. The calculated soil water and temperature are fed back to photosynthesis and stomatal conductance, which in turn are coupled to the behavior of plant phenology. The snow submodel includes energy and mass balance budgets to express changes in heat and water contents in the snowpack to simulate snow accumulation and snowmelt at the land surface. The calculated snow density and snow water equivalent determine the thickness of the snowpack. The vertical water flux between soil column layers is solved with Darcy's law. The blocking effect of permafrost on the water infiltration is represented by a parameterization for soil ice impedance.

12.3.2 Increasing Snow in Siberia

Both observations and simulations have identified increases in snow depth (SND) in northeastern Siberia (Bulygina et al. 2009; Park et al. 2015) and decreases in North America (Park et al. 2013a). The increase in SND in northeastern Siberia was associated with an increase in winter P_G, especially in early winter (Iijima et al. 2010; Park et al. 2013b). Some studies have suggested a potential influence of the declining Arctic sea ice on the increased snow in Siberia (Ghatak et al. 2010; Cohen et al. 2012). A composite differential method has been used to examine the relationship between sea ice loss and terrestrial snow. Years when the anomalous sea ice extent (SIE) in September was either less or larger than one standard deviation of the mean of the 1979–2006 period were selected for the composite analysis. Figure 12.5 represents the composite differences in fall mean P_G (a) and SND (b). The composite differences based on the actual reversed SIE exhibited increases in fall P_G across

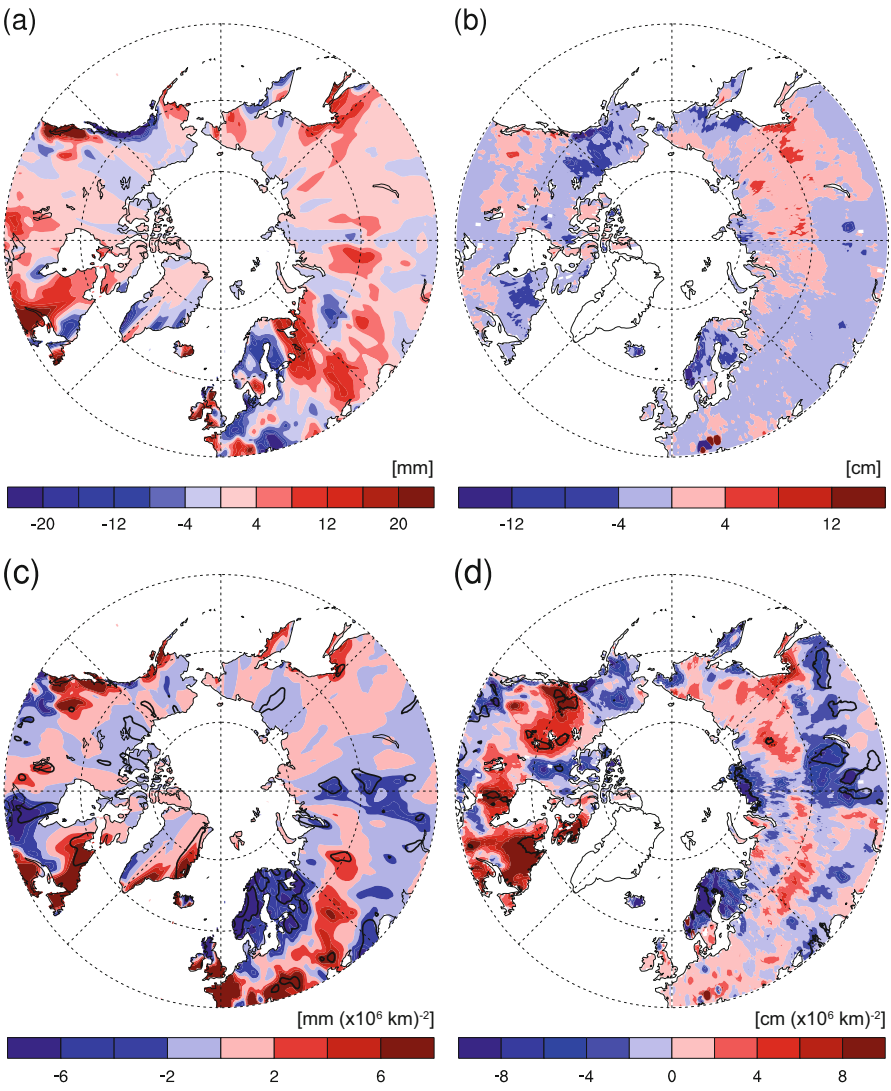

Fig. 12.5 The difference between composites of autumnal (September–November) precipitation (**a**) and mean snow depth (**b**) with September sea ice extents that were less and greater than one standard deviation from the 1979 to 2006 period. Linear regressions of winter (Dec–Feb) precipitation (**c**) and mean snow depth (**d**) on the detrended September sea ice extent (Park et al. 2013b)

wide areas of the terrestrial Arctic. Significant increases in P_G were found in ambient regions of Hudson Bay, central Siberia, and western Eurasia (Fig. 12.5a). The increased P_G was linked to an increase in SND in fall. In the composite analysis, fall SND over northern Siberia showed positive anomalies with the decrease in SIE (Fig. 12.5b). Routine meteorology measurements have identified recent increases in

surface humidity in northern regions of Siberia (Cohen et al. 2012). Increased atmosphere moisture may result in higher P_G efficiency. Observations have shown that an anomalously low ice extent in fall contributes to increases in humidity in far eastern Siberia, leading to higher SND (Liu et al. 2012).

Influences of detrended SIE on winter weather were found in the linear regressions of the reversed SIE with P_G (Fig. 12.5c) and SND (Fig. 12.5d) in winter (December–February), where detrended SIEs in September were used. The P_G regression showed higher regional heterogeneity in its distribution. Higher P_G was found over the Canadian region and western Eurasia. The regression of SIE with winter SND was similar to the P_G regression, and increases in P_G tended to be linked to higher SND. Decreased SIE resulted in increased SND in northeastern Siberia and the Canadian region. The regression suggested that decreased sea ice coverage was correlated to increases in SND. In the regression, the increased SND resulted in the coldest SAT in central Siberia, where SAT anomalies were 2–3 °C below normal (Park et al. 2013b).

12.3.3 Warming and Permafrost Degradation

As described in the previous section, SND has shown increased anomalies in recent decades. Such increases are significant in the northernmost regions of Siberia (Park et al. 2015), adjacent to the shelf ocean and underlain by continuous permafrost. Water evaporated from the open sea surface could be transported to the neighboring terrestrial regions through atmospheric recycling. Cohen et al. (2012) observed increases in surface air humidity over 1979–2010 at the northernmost regions. Interestingly, observed T_{SOIL} values have shown larger warming amplitudes in the northern tundra regions of Siberia (Fedorov et al. 2014), suggestive of the influence of SND on T_{SOIL} warming associated with warming surface air temperature (SAT). There is substantial interest in determining the magnitude of the relative influences of SND and SAT on T_{SOIL} warming. Figure 12.6 shows the proportion of T_{SOIL} variance explained by SAT and SND at stations across Russia, which was estimated with a multilinear regression method. There were regionally apparent differences in the main contributors correlated with T_{SOIL}. SND was strongly correlated with T_{SOIL} at most stations in eastern Siberia underlain by permafrost, which was larger than the contribution of SAT (Fig. 12.6). In the Arctic, winter SAT has increased in the last few decades (Bekryaev et al. 2010). However, eastern Siberia is still characterized by severe freezing winter. Therefore, increased SND readily contributes to T_{SOIL} warming because of its lower thermal conductivity. Conversely, the impact of SAT on T_{SOIL} was significant in western Siberia where soil freezes seasonally. Model experiments based on seasonally altered snow amounts have also shown the highest sensitivities of T_{SOIL} to changes in snow cover in Siberian permafrost regions (Park et al. 2015).

Figure 12.7 compares annual active layer thickness (ALT) anomalies derived from the CHANGE model, ERA-Interim reanalysis data, satellite (MODIS), and field observations in Siberia. Satellite-estimated ALT did not include the insulating

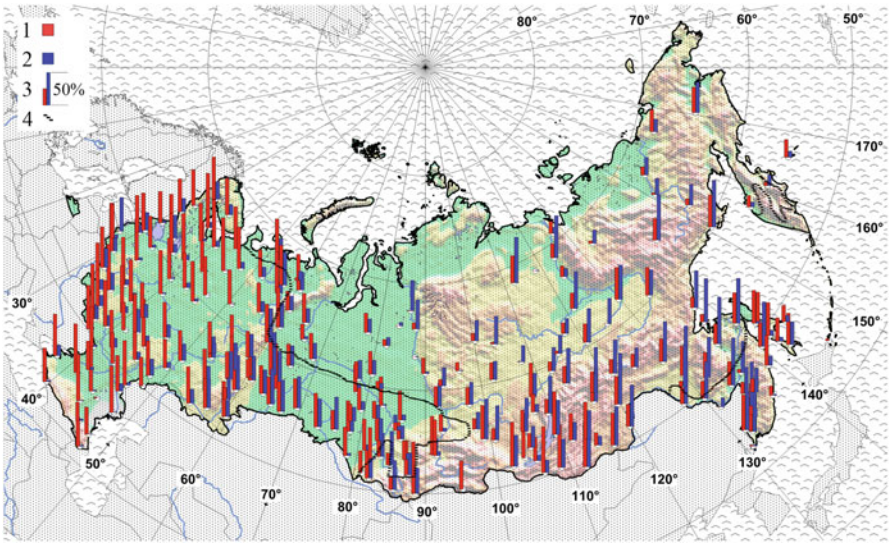

Fig. 12.6 Proportional contributions of SAT (red) and SND (blue) to T_s at each station computed for 1963–2011 based on multilinear regression analysis. Number 3 in the map legend represents the percent contribution of the variables. The boundary of the permafrost area is indicated by a black dashed line (Park et al. 2014)

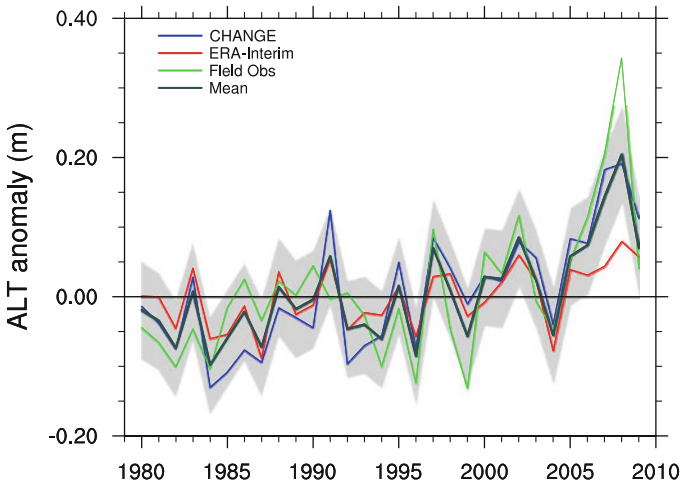

Fig. 12.7 Interannual anomaly variation (relative to long-term mean) and estimated regional trends of permafrost active layer thickness (ALT) derived from CHANGE, ERA-Interim SAT, and sparse network station observations within a Siberia subregion (60–70N, 115–165 E) from 1979 to 2009 (Park et al. 2016a). Mean represents the averaged value of three ALTs, and gray shadow is the range of standard deviation of the mean

effects of SND and SOC. However, observed and estimated ALT records showed similar interannual variability and increasing regional trends over the past 30 years. Relatively stronger increases in ALT were apparent after 2004 (Ohta et al. 2014; Park et al. 2016a), coincident with reported increases in regional SAT and SND (Bulygina et al. 2009; Park et al. 2014). In the same region, increases in winter SND (Bulygina et al. 2009; Park et al. 2014) and summer soil moisture (Ohta et al. 2014) in recent years have resulted in T_{SOIL} warming (Iijima et al. 2010; Fedorov et al. 2014; Park et al. 2014) and, by consequence, deeper ALT (Park et al. 2013a). Conversely, a process-based model simulated a negative ALT anomaly in the Mackenzie and Yukon watersheds after 1990, highlighting the effects of both decreased SND and soil moisture (Park et al. 2013a).

Climate warming results in a deeper ALT with melt of ground ice in surface permafrost. The ice melt leads to subsidence of the ground surface and expansion of thermokarst lakes, observed in the central Lena watershed (Ulrich et al. 2017). The expanded lake increases water storage capacity and thus temporarily decreases the contribution of snowmelt water to river discharge, although some portion of the stored water is likely to release to river network. Channeling between lakes likely contributes more water to river discharge; such channel flows had been observed in the Arctic coastal areas (Liu et al. 2014). Lakes in the inner terrestrial regions have larger influence on evaporation than on discharge (Ulrich et al. 2017), that is, lakes increase the recycling rate of the evaporated water (Serreze et al. 2006). The recycling precipitation is likely to derive deeper ALT (Iijima et al. 2010), consequently larger thermokarst lakes, hence, accelerating the speed of water cycle. A modeling study addressed the contribution due to warming climate through methane release from the thermokarst tundra lake in northeastern Siberia (Huissteden et al. 2011). However, very few model experiments examined the correlation between thermokarst lake expansion and Arctic terrestrial water cycle.

12.3.4 Changes in Hydrologic Processes in Eastern Siberia

Precipitation over terrestrial regions is primarily divided into *ET* and river discharge, while the remainder is stored in soil. Because storage is near zero in the water budget over longer periods, it tends to be neglected. Although P_G over land area peaks in summer, *ET* of the terrestrial Arctic tends to exceed P_G such that net P_G (i.e., $P_G - ET$) is smaller or negative (Park et al. 2008). Over terrestrial regions, a considerable fraction of summer P_G is caused by regional recycling of water vapor from *ET*, pointing to the strong influence of land surface (Serreze et al. 2006). From fall through spring, most P_G exists as snow over the land surface. However, uncertainty remains regarding mean total annual P_G in the Arctic, due to gauge undercatch and sparse station networks (Yang 1999). Although existing datasets of P_G include large uncertainties, they show increasing trends in Arctic regions in recent decades (data not shown). In addition, snow water has increased in recent decades (Park et al. 2015).

Changes in discharge from Siberian rivers, particularly Lena River, are reviewed in detail in Chap. 9, including the long-term dynamics analyzed with tree-ring data (see Chap. 2). Therefore, only a brief description of the changes in river discharge at a pan-Arctic scale is given here. Arctic river discharge is characterized by distinct seasonality, with prominent spring freshet and extreme low flow in winter together with river ice formation. In spring, the snowmelt-induced peak discharge accounts for about two-thirds of the annual discharge. Moreover, changes in snow processes can alter the seasonality of discharge. For example, the daily discharge of Russian rivers in 2015 showed an earlier and higher peak spring discharge relative to the 1980–1989 average (Holmes et al. 2015), which was consistent with the earlier melt of deeper snow (Park et al. 2016a). The CHANGE model showed a significant increasing trend (6.8 km^3 $year^{-1}$) in pan-Arctic discharge in May from 1979 to 2013 (Park et al. 2017). These increases led to an increase of 300 km^3 in annual Arctic discharge during 2000–2010 relative to that during 1980–2000 (Haine et al. 2015). The recent shift toward an earlier peak discharge has resulted in decreased summer discharge, with a negative trend in June and July (Park et al. 2017). Meanwhile, discharge in cold months has apparently increased (Park et al. 2017). Studies have suggested the influence of warming permafrost on increased winter low flows (Tananaev et al. 2016).

In cold regions, *ET* is most active in early summer and is dependent on SAT. An SAT warming-derived longer growing season likely results in more carbon uptake by vegetation via photosynthesis under the increased atmospheric carbon amount. The resultant higher leaf area index contributes to greater transpiration and canopy interception. The earlier snowmelt supports greater soil evaporation in early spring when radiation is highest over the soil surface. Models have simulated increases in the Siberian (Park et al. 2008) and pan-Arctic (Zhang et al. 2009) *ET* in the last few decades. Satellite-derived estimations showed an increase in 3.8 mm $decade^{-1}$ in the pan-Arctic *ET* from 1983 to 2005 (Zhang et al. 2009). The cumulative *ET* in summer accounts for about 50–60% of the water budget. Summer *ET* tends to exceed summer P_G (Park et al. 2008), which decreases the contribution rate of P_G to river discharge. Therefore, the decreases in pan-Arctic discharge in June and July (Park et al. 2017) could be partly explained by the increased *ET*. The influences of higher soil moisture produced by permafrost warming on *ET* have been highlighted; however, they have not been quantitatively examined. Sublimation from snow cover in winter accounts for a portion of *ET*, and winter SAT warming can affect sublimation (Nakai et al. 2013). However, few studies have estimated sublimation at a pan-Arctic scale.

12.3.5 Changes in Carbon Fluxes in Eastern Siberia

In cold regions, SAT is a primary factor driving ecohydrological processes. SAT warming enhances the biogeochemical activity of vegetation. For example, when there is low soil moisture stress, plants can use more water for transpiration and

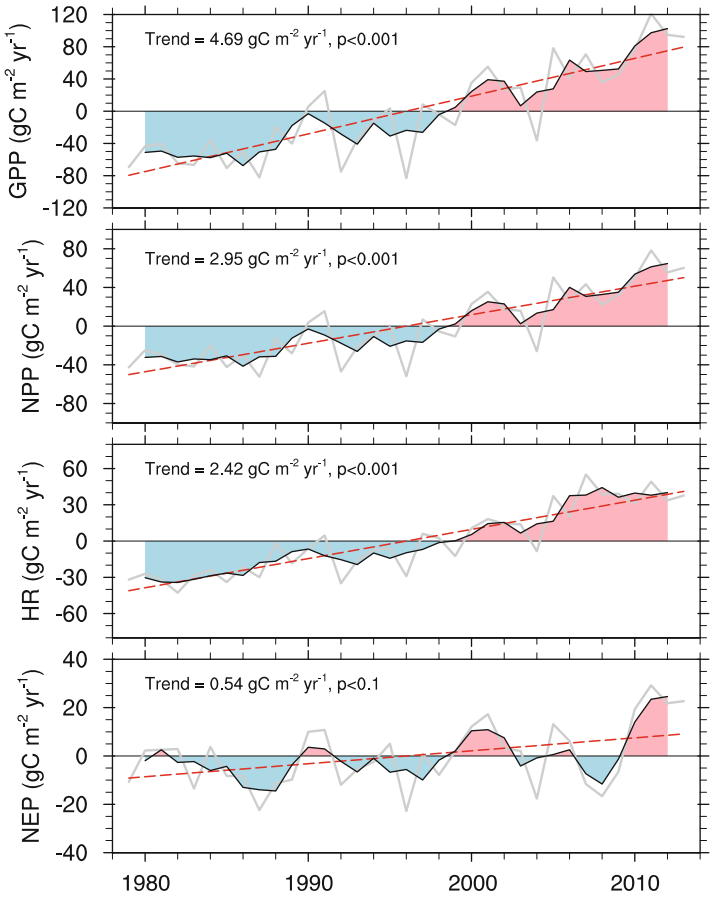

Fig. 12.8 Interannual variability and trend (red dashed lines) of components in the carbon budget at pan-Arctic terrestrial regions for the 1979–2013 simulation period. In the figures, the gray and black lines denote annual value and 3-year average, respectively

absorb more carbon from the atmosphere via photosynthesis. Increased snow water (Park et al. 2015) can contribute to the soil water content in the spring and early summer. Under these wet conditions, the CHANGE model simulated an increase in gross primary productivity (GPP) from photosynthesis and net primary productivity (NPP) over the terrestrial Arctic from 1979 to 2013 (Fig. 12.8). These increases were significant after 2000, when SAT warming was greater. The trend of simulated pan-Arctic GPP (4.69 g C m^{-2} $year^{-1}$) was substantially larger than values (1.8 g C m^{-2} $year^{-1}$) in Eurasia averaged from simulations of nine land surface models from 1960 to 2009 (Rawlins et al. 2015). A positive linear trend in NPP has been consistently identified from satellite-based model estimations, with an increase in pan-Arctic NPP of 0.34% per year across a period of 1983–2005 (Zhang et al. 2008). The earlier onset and lengthening of the growing season under SAT warming are potential drivers of these positive trends in GPP and NPP.

The permafrost stores a large amount (~1000 Pg) of SOC in the upper 3 m (Hugelius et al. 2014), which is similar in magnitude to atmospheric carbon storage. Permafrost warming as a result of climate change can enhance the decomposition of SOC, releasing more carbon into the atmosphere. Simulated heterotrophic respiration (HR) exhibited an increasing trend, showing temporal variations consistent with GPP and NPP (Fig. 12.8). The increase in HR is attributable to permafrost warming and deepened ALT. Satellite observations have captured earlier land surface thawing in spring (Park et al. 2016a), which can effectively increase soil respiration. Model simulations have indicated that carbon emissions from thawing permafrost soil are potentially in the same order of magnitude as carbon emissions by global deforestation (Schuur et al. 2015). The magnitude of the trend in ecosystem respiration has not exceeded that of GPP, resulting in increased net ecosystem productivity over time. Models have simulated a positive trend in net ecosystem productivity over Eurasia (Rawlins et al. 2015). Although the temporal variability in net ecosystem productivity is larger than other carbon flux variables, these results show that the Arctic terrestrial ecosystem is trending toward a state of carbon uptake.

Arctic ecosystems are characterized by heterogeneous surfaces, such as the boreal–tundra transition zone in the north and boreal forest in the south. Models have simulated a poleward shift in boreal forest as a result of climate warming (Starfield and Chapins 1996), and observations have found an increase in the number of shrubs in northern Alaska in the 1980s and 1990s (Chapin et al. 1995). Moreover, satellite observations have identified increased and earlier greening of arctic ecosystems (Buermann et al. 2003), together with an increase in the normalized difference vegetation index in high-latitude areas in recent decades (Tucker et al. 2001). These results indicate that Arctic ecosystems are sequestering large amounts of carbon at increased rates (Rawlins et al. 2015).

12.4 Concluding Remarks

This chapter reviews changes in the processes and components of the terrestrial Arctic under climate change. These changes have been examined on the basis of observational records and one-dimensional model simulations at point and watershed scales. The model simulations were made through two parallel applications; the first included the diagnosis of impactors on the warming permafrost temperature through sensitivity experiments at specific sites, and the other included model simulations at watershed and pan-Arctic scales. The simulations indicated that the changes in the terrestrial processes were significant during the recent decade when SAT was significantly warm. Among them, one remarkable change was the increase in SND over eastern Siberia. Studies have implicated the decreased extent of sea ice on the increase in SND. Moreover, higher levels of snow contribute to higher peak discharges in spring. Meanwhile, the warming SAT causes earlier snowmelt resulting in an earlier shift in peak discharge. Snow cover offers increased soil insulation in winter, resulting in T_{SOIL} warming, thereby contributing to deeper

ALT, which is particularly significant in Siberian permafrost. These changes in turn affect SOC decomposition in permafrost. Models have simulated an increase in soil respiration along with higher SOC decomposition. Previous studies have examined the relationship between permafrost warming and an increase in winter low flow. However, because existing models are not highly representative of permafrost-related processes, more studies are required to understand this relationship.

It is evident that the Arctic is changing, and these changes are both greater and occurring more rapidly than those seen in historic times. Both observations and model simulations have been used to identify and quantify these changes. However, observations in the Arctic tend to be limited, and models show deficiencies in their representation of some processes, likely increasing the uncertainty of modeled projections. Most climate models have projected further Arctic warming in the future, but improvements are required to decrease the uncertainties associated with these projections.

References

Bekryaev RV, Polyakov IV, Alexeev VA (2010) Role of polar amplification in long-term surface air temperature variations and modern Arctic warming. J Clim 23:3888–3906. https://doi.org/10.1175/2010JCLI3297.1

Betts AK, Viterbo P, ACM B, van den Hurk BIJM (2001) Impact of BOREAS on the ECMWF forecast model. J Geophys Res 106:33593–33604

Buermann W, Anderson B, Tucker CJ, Dickinson RE, Lucht W, Potter CS, Myneni RB (2003) Interannual covariability in Northern Hemisphere air temperature and greenness associated with El Nino-Southern oscillation and the Arctic oscillation. J Geophys Res 108:4396. https://doi.org/10.1029/2002JD002630

Bulygina ON, Razuvaev V, Korshunova N (2009) Change in snow cover northern Eurasia in the last decades. Environ Res Lett 4:045026. https://doi.org/10.1088/17489326/14/4/045026

Chapin FS, Shaver GR, Giblin AE, Nadelhoffer KG, Laundre JA (1995) Response of arctic tundra to experimental and observed changes in climate. Ecology 76:694–711

Cohen J, Furtado J, Barlow M, Alexeev V, Cherry J (2012) Arctic warming, increasing snow cover and widespread boreal winter cooling. Environ Res Lett 7:014007. https://doi.org/10.1088/1748-9326/1/1/014007

Cox PM, Huntingford C, Harding RJ (1998) A canopy conductance and photosynthesis model for use in a GCM land surface scheme. J Hydrol 212–213:79–94

Deardorff JW (1978) Effective prediction of ground surface temperature and moisture with inclusion of a layer of vegetation. J Geophys Res 83:1889–1903

Dickinson RE (1984) Modeling evapotranspiration for three-dimensional global climate models. In: Hansen JE, Takahashi T (eds) Climate processes and climate sensitivity, Geophysical monograph, 29. American Geophysical Union, Washington, DC, pp 58–72

Fedorov AN, Ivanova RN, Park H, Hiyama T, Iijima Y (2014) Recent air temperature changes in the permafrost landscapes of northeastern Eurasia. Pol Sci 8:114–128. https://doi.org/10.1016/j.polar.2014.02.001

Foley JA, Prentice IC, Ramankutty N, Levis S, Pollard D, Sitch S, Haxeltine A (1996) An integrated biosphere model of land surface processes, terrestrial carbon balance, and vegetation dynamics. Global Biogeochem Cycles 10(4):603–628

Ghatak D, Frei A, Gong G, Stroeve J, Robinson D (2010) On the emergence of an Arctic amplification signal in terrestrial Arctic snow extent. J Geophys Res 11:D24105. https://doi.org/10.1029/2010JD014007

Gouttevin I, Menegoz M, Domine F, Krinner G, Koven C, Ciais P, Tarnocai C, Boike J (2012) How the insulating properties of snow affect soil carbon distribution in the continental pan-Arctic area. J Geophys Res 117:G02020. https://doi.org/10.1029/2011JG001916

Haine TWN et al (2015) Arctic freshwater export: status, mechanisms, and prospects. Glob Planet Chang 124:13–35. https://doi.org/10.1016/j.gloplacha.2014.11.013

Hamada S, Ohta T, Hiyama T, Kuwada T, Takahashi A, Maximov TC (2004) Hydrometeorological behaviour of pine and larch forests in eastern Siberia. Hydrol Process 18:23–39

Holmes RM, Shiklomanov AI, Tank SE, McClelland JW, Tretiakov M (2015) River discharge. Arctic Report Card. http://www.arctic.noaa.gov/Report-Card/Report-Card-2015/ArtMID/5037/ArticleID/227/River-Discharge

Hugelius G et al (2014) Estimated stocks of circumpolar permafrost carbon with quantified uncertainty ranges and identified data gaps. Biogeosciences 11:6573–6593

Iida S et al (2009) Evapotranspiration from understory vegetation in an eastern Siberian boreal larch forest. Agric For Meteorol 149:1129–1139. https://doi.org/10.1016/j.agrformet.2009.02.003

Iijima Y, Fedorov AN, Park H, Suzuki K, Yabuki H, Maximov TC, Ohata T (2010) Abrupt increases in soil temperatures following increased precipitation in a permafrost region, Central Lena River basin, Russia. Permafr Periglac Process 21:30–41

Jarvis PG (1976) The interpretation of the variations in leaf water potential and stomatal conductance found in canopies in the field. Philos Trans R Soc Lond B Biol Sci 273:593–610

Lawrence DM, Slater AG (2008) Incorporating organic soil into a global climate model. Clim Dyn 30:145–160. https://doi.org/10.1007/s00382-007-0278-1

Levis, SG, Bonan B, Vertenstein M, Oleson KW (2004) The Community Land Model's Dynamic Global Vegetation Model (CLM-DGVM): Technical Description and User's Guide, NCAR Tech. Note TN-459+lA, 50 pp, National Center for Atmospheric Research, Boulder, Colorado

Liu J, Curry J, Wang H, Song M, Horton R (2012) Impact of declining Arctic Sea ice on winter snowfall. Proc Natl Acad Sci. https://doi.org/10.1073/pnas.1114910109

Liu L, Schaefer K, Grosse G, Jones BM, Zhang T, Parsekian AD, Zebker HA (2014) Seasonal thaw settlement at drained thermokarst lake basins. Arctic Alaska Cryosphere 8:815–826. https://doi.org/10.5194/tc-8-815-2014

Manabe S (1969) Climate and the ocean circulation: 1, the atmospheric circulation and the hydrology of the Earth's surface. Mon Weather Rev 97:739–805

Miyazaki S et al (2015) The GRENE-TEA Model Intercomparison Project (GTMIP): overview and experiment protocol for Stage 1. Geosci Model Dev 8:2841–2856

Nakai T et al (2013) Characteristics of evapotranspiration from a permafrost black spruce forest in interior Alaska. Pol Sci 7:136–148. https://doi.org/10.1016/j.polar.2013.03.003

Ohta T, Hiyama T, Tanaka H, Kuwada T, Maximov TC, Ohata T, Fukushima Y (2001) Seasonal variation in the energy and water exchanges above and below a larch forest in eastern Siberia. Hydrol Process 15:1459–1476

Ohta T, Maximov TC, Dolman AJ, Nakai T, van der Molen MK, Kononov AV, Maximov AP, Hiyama T, Iijima Y, Moors EJ, Tanaka H, Toba T, Yabuki H (2008) Interannual variation of water balance and summer evapotranspiration in an eastern Siberian larch forest over a 7-year period (1998–2006). Agric For Meteorol 148:1941–1953

Ohta T, Kotani A, Iijima Y, Maximov TC, Ito S, Hanamura M, Kononov AV, Maximov AP (2014) Effects of waterlogging on water and carbon dioxide fluxes and environmental variables in a Siberian larch forest, 1998–2011. Agric For Meteorol 188:64–75

Park H, Yamazaki T, Yamamoto K, Ohta T (2008) Tempo-spatial characteristics of energy budget and evapotranspiration in the eastern Siberia. Agric For Meteorol 148:1990–2005. https://doi.org/10.1016/j.agrformet.2008.06.018

Park H, Iijima Y, Yabuki H, Ohta T, Walsh J, Kodama Y, Ohata T (2011) The application of a coupled hydrological and biogeochemical model (CHANGE) for modeling of energy, water, and CO_2 exchanges over a larch forest in eastern Siberia. J Geophys Res 116:D15102. https://doi.org/10.1029/2010JD01586

Park H, Walsh J, Fedorov AN, Sherstiukov AB, Iijima Y, Ohata T (2013a) The influence of climate and hydrological variables on opposite anomaly in active-layer thickness between Eurasian and North American watersheds. Cryosphere 7:631–645. https://doi.org/10.5194/tc-7-631-2013

Park H, Walsh JE, Kim Y, Nakai T, Ohata T (2013b) The role of declining Arctic sea ice in recent decreasing terrestrial Arctic snow depths. Pol Sci 7:174–187. https://doi.org/10.1016/j.polar.2012.10.002

Park H, Sherstiukov AB, Fedorov AN, Polyakov IV, Walsh JE (2014) An observation-based assessment of the influence of air temperature and snow depth on soil temperature in Russia. Environ Res Lett 9:064026. https://doi.org/10.1088/1748-9326/9/6/064026

Park H, Fedorov AN, Zheleznyak MN, Konstantinov PY, Walsh JE (2015) Effect of snow cover on pan-Arctic permafrost thermal regimes. Clim Dyn 44:2873–2895. https://doi.org/10.1007/s00382-014-2356-5

Park H, Kim Y, Kimball JS (2016a) Widespread permafrost vulnerability and soil active layer increases over the high northern latitudes inferred from satellite remote sensing and process model assessments. Remote Sens Environ 175:349–358. https://doi.org/10.1016/j.rse.2015.12.046

Park H, Yoshikawa Y, Oshima K, Kim Y, Ngo-Duc T, Kimball JS, Yang D (2016b) Quantification of warming climate-induced changes in terrestrial Arctic river ice thickness and phenology. J Clim 29:1733–1754. https://doi.org/10.1175/JCLI-D-15-0569-1

Park H, Yoshikawa Y, Yang D, Oshima K (2017) Warming water in Arctic terrestrial rivers under climate change. J Hydrometeorol. https://doi.org/10.1175/JHM-D-16-0260.1

Pitman AJ (2003) The evolution of, and revolution in, land surface schemes designed for climate models. Int J Climatol 23:479–510

Rawlins MA et al (2010) Analysis of the Arctic system for freshwater cycle intensification: observations and expectations. J Clim 23:5715–5737. https://doi.org/10.1175/2010JCLI3421.1

Rawlins MA et al (2015) Assessment of model estimates of land-atmosphere CO_2 exchange across Northern Eurasia. Biogeosciences 12:4385–4405. https://doi.org/10.5194/bg-12-4385-2015

Schuur EAG et al (2015) Climate change and the permafrost carbon feedback. Nature 520:171–179

Sellers PJ, Mintz Y, Sud YC, Dalcher A (1986) A simple biosphere model (SiB) for use within general circulation models. J Atmos Sci 43:505–531

Sellers PJ et al (1997) BOREAS in 1997: experiment overview, scientific results, and future directions. J Geophys Res 102:28731–28769

Serreze MC et al (2006) The large-scale freshwater cycle of the Arctic. J Geophys Res 111:C11010. https://doi.org/10.1029/2005JC003424

Starfield A, Chapins FS (1996) Model of transient changes in arctic and boreal vegetation in response to climate and land use change. Ecol Model 6:842–864

Sugimoto A, Naito D, Yanagisawa N, Ichiyanagi K, Kurita N, Kubota J, Kotake T, Ohata T, Maximov TC, Fedorov AN (2003) Characteristics of soil moisture in permafrost observed in east Siberian taiga with stable isotopes of water. Hydrol Process 17:1073–1092

Swenson SC, Lawrence DM, Lee H (2012) Improved simulation of the terrestrial hydrological cycle in permafrost regions by the Community Land Model. J Adv Model Earth Syst 4:M08002. https://doi.org/10.1029/2012MS000165

Tananaev NI, Makarieva OM, Lebedeva LS (2016) Trends in annual and extreme flows in the Lena River basin, Northern Eurasia. Geophys Res Lett 43:10764–10772. https://doi.org/10.1002/2016GL070796

Toba T, Ohta T (2005) An observational study of the factors that influence interception loss in boreal and temperate forests. J Hydrol 313:208–220

Tucker CJ, Slayback DA, Pinzon JE, Los SO, Myneni RB, Taylor MG (2001) Higher northern latitude normalized difference vegetation index and growing season trends from 1982 to 1999. Int J Biometeorol 45:184–190

Ulrich M, Matthes H, Schirrmeister L, Schütze J, Park H, Iijima Y, Fedorov AN (2017) Differences in behavior and distribution of permafrost-related lakes in Central Yakutia and their response to climatic drivers. Water Resour Res 53. https://doi.org/10.1002/2016WR019267

Van Huissteden J, Berrittella C, Parmentier FJW, Mi Y, Maximov TC, Dolman AJ (2011) Methane emissions from permafrost thaw lakes limited by lake drainage. Nat Clim Chang 1:119–123. https://doi.org/10.1038/NCLIMATE1101

Verseghy DL (1991) CLASS -A Canadian land surface scheme for GCMs, Part I: Soil model. Int J Climatol 11:111–133

Verseghy DL, McFarland NA, Lazare M (1993) CLASS -A Canadian land surface scheme for GCMs, Part II: Vegetation model and coupled runs. Int J Climatol 13:347–370

Viterbo P, Betts AK (1999) Impact on ECMWF forecasts of changes to the albedo of the boreal forests in the presence of snow. J Geophys Res Atmos 104(D22):27803–27810

Yamazaki T (2001) A one-dimensional land surface model adaptable to intensely cold regions and its applications in Eastern Siberia. J Meteorol Soc Jpn 79:1107–1118

Yamazaki T, Yabuki H, Ishii Y, Ohta T, Ohata T (2004) Water and energy exchanges at forests and a grassland in eastern Siberia evaluated using a one-dimensional land surface model. J Hydrometeorol 5:504–515

Yamazaki T, Yabuki H, Ohata T (2007) Hydrometeorological effects of intercepted snow in an eastern Siberian taiga forest using a land surface model. Hydrol Process 21:1148–1156. https://doi.org/10.1002/hyp.6675

Yamazaki T, Kato K, Ito T, Nakai T, Matsumoto K, Miki N, Park H, Ohta T (2013) A common stomatal parameter set to simulate the energy and water balance over boreal and temperate forests. J Meteorol Soc Jpn 91:273–285. https://doi.org/10.2151/jmsj.2013-303

Yang D (1999) An improved precipitation climatology for the Arctic Ocean. Geophys Res Lett 26:1525–1528

Zhang K, Kimball JS, Hogg EH, Zhao M, Oechel WC, Cassano JJ, Running SW (2008) Satellite-based model detection of recent climate-driven changes in northern high-latitude vegetation productivity. J Geophys Res 113:G03033. https://doi.org/10.1029/2007JG000621

Zhang K, Kimball JS, Mu Q, Jones LA, Goetz SJ, Running SW (2009) Satellite based analysis of northern ET trends and associated changes in the regional water balance from 1983 to 2005. J Hydrol 379:92–110. https://doi.org/10.1016/j.jhydrol.2009.09.047

Chapter 13
Water and Carbon Dynamics in Eastern Siberia: Concluding Remarks

Takeshi Ohta and Tetsuya Hiyama

13.1 Introduction

Numerous interesting research topics are being explored in ongoing studies of the dynamics of water and carbon cycles in high-latitude regions of the Northern Hemisphere, particularly in eastern Siberia. These include one-dimensional observations and watershed-scale analyses of water, energy, and carbon fluxes under different permafrost conditions; analyses of satellite remote sensing data; and water and carbon flux modelling. Eastern Siberia is characterised as a "vegetation–permafrost symbiotic system" owing to the presence of permafrost and vegetation cover, which is dominated by larch (*Larix cajanderi*) forest ("light taiga") and tundra. Current climate warming in this region is causing large environmental variability and wetting–drying conditions. The eastern Siberian environment is also being affected by global climatic and abrupt socio-economic changes. Thus, the research findings and educational issues introduced in this book are of great importance.

13.2 Main Results in the Water and Carbon Dynamics in Eastern Siberia

Under global warming, atmospheric water vapour pressure trends to increase as air temperature increases, particularly in eastern Siberia, where the regional climate has been shaped by topography, distance from the ocean, vegetation types, and

T. Ohta (✉)
Graduate School of Bioagricultural Sciences, Nagoya University, Nagoya, Japan
e-mail: takeshi_1956@grace.ocn.ne.jp

T. Hiyama
Institute for Space-Earth Environmental Research (ISEE), Nagoya University, Nagoya, Japan
e-mail: hiyama@nagoya-u.jp

T. Ohta et al. (eds.), *Water-Carbon Dynamics in Eastern Siberia*,
Ecological Studies 236, https://doi.org/10.1007/978-981-13-6317-7_13

permafrost. These phenomena have been identified using upper- and lower-atmospheric analyses (Chap. 2) and modelling studies (Chap. 12). At smaller scales, one-dimensional fluxes of energy, water, and carbon have been estimated using land surface models, and these have been compared to data observed in situ in both wet and dry conditions in a larch forest stand (Chap. 12).

Due to current global warming, the water cycle has been enhancing through a reduction in Arctic sea ice extent. These changes to the water cycle have induced large amounts of rain and snow, surface runoff, and river discharge during the snowmelt season throughout the region. Accelerating soil water infiltration, evapotranspiration, and river discharge in summer have also been detected in the region. Rainfall and snowfall were higher in 2005–2008 than in the past century, with significant discharge events in the Lena River basin and other Eurasian pan-Arctic watersheds (Chap. 9). Soil water infiltrated from rain water and snowmelt water is transported from hillslopes to the Lena River. Permafrost plays a critical role in infiltration processes at high latitudes due to seasonal changes in air temperature. As amounts of rainfall and snowmelt water have increased, the active layers thickness of surface permafrost zones have gradually increased, and the effects of deepening these active layers have prolonged over the seasonal scales of water–carbon cycles (Chaps. 3, 4, and 8). The lengthening of the growing season affects ecological feedback not only in larch forests but also in grassland and bare lands (Chap. 8), and vegetation changes steadily (Chap. 7). Vertical and horizontal soil water content profiles have changed dramatically in larch forests, and soil water movement differs dramatically between wetting and drying periods. In the Spasskaya Pad experimental forest, differences in soil water uptake (extraction) by larch tree roots in wet and dry years were detected using stable water isotopes (Chap. 6). Studies of spatial variation in ecosystem CH_4 emissions with attention to landscape-scale variation are very important in tundra regions such as the Chokurdakh site (Chap. 5). At longer time scales, ecosystem H_2O, CO_2, and CH_4 emissions will change drastically as a result of different environmental factors, because precipitation, soil water content, permafrost conditions, and vegetation activities will change over time (Chap. 1).

Water and carbon cycles in eastern Siberia differ spatiotemporally, and there are vast regions of less-populated localities. The spatiotemporal variation in above-ground biomass and the growing season in eastern Siberia are monitored by several remote sensing techniques, which are useful for deciduous forests and other poorly accessible places not only in eastern Siberia but also throughout the Northern Hemisphere (Chap. 10). To determine terrestrial water storage, optical sensors are available primarily for detecting snow cover, whereas passive microwave sensors can detect surface water conditions. By contrast, active microwave sensors can detect surface soil moisture. Remote sensing sensors onboard several satellites can be used to detect terrestrial water, and their development is continuing to advance (Chap. 11). Although remote sensing techniques are extensively used (Chaps. 10 and 11), some types of data collection via remote sensing, such as data on leaf area and soil water content, still require development.

The effects of global warming have advanced greatly in eastern Siberia, where hydrological and meteorological measurements have demonstrated intensive wetting phenomena from 2005 to 2008; however, strong drought has not been detected

within the past two decades. From 2001 to 2004, a weak drought period occurred in central Yakutia, with an annual minimum precipitation of 111 mm in 2001 (Chap. 3). Tree-ring analyses were used to detect this drought; however, dendrochronological measurements showed that vegetation has not been drastically altered (Chap. 7). These trends in meteorological conditions during drying events are not yet clearly understood from ecological, physiological, and hydrological perspectives.

13.3 Future Works in Eastern Siberia

The environmental factors related to wetting and drying conditions in eastern Siberia should be studied in hydrological and meteorological systems from the one-dimensional scale to the watershed scale. Continuous wetting years were detected during the two decades in which we observed hydro-meteorological variables, and the hydrological and meteorological data related to wetting phenomena in the region have helped to clarify regional water and carbon dynamics. In the near future, drying conditions and their hydrological ecosystem feedbacks should be studied intensively.

Such research projects have revealed much new information on ecological feedbacks to the global climate from a hydro-meteorological perspective, clarifying water and carbon cycles in forests and grasslands worldwide (Malhi et al. 1999; Ciais et al. 2005). In eastern Asia (including eastern Siberia), a large forest belt extends broadly from tropical forests to boreal forests (Yasunari 2007). Therefore, similar studies have been conducted or planned in boreal, temperate, and tropical regions from northern Eurasia to south-eastern Asia. These continuously vegetated areas, which include boreal, temperate, and tropical forests, are defined as a green belt; eastern Siberia is located at its northern edge. Future research in this region should regularly be conducted on topics including water, energy, and carbon dynamics and their feedback systems in conjunction with climate change.

References

Ciais P, Reichstein M, Viovy N, Granier A, Ogee J, Allard V, Aubinet M, Buchmann N, Bernhofer C, Carrara A, Chevallier F, De Noblet N, Friend AD, Friedlingstein P, Grunwald T, Heinesch B, Keronen P, Knohl A, Krinner G, Loustau D, Manca G, Matteucci G, Miglietta F, Ourcival JM, Papale D, Pilegaard K, Rambal S, Seufert G, Soussana JF, Sanz MJ, Schulze ED, Vesala T, Valentini R (2005) Europe-wide reduction in primary productivity caused by the heat and drought in 2003. Nature 437:529–533. https://doi.org/10.1038/nature03972

Malhi Y, Baldocchi DD, Jarvis PG (1999) The carbon balance of tropical, temperate and boreal forests. Plant Cell Environ 22:715–740. https://doi.org/10.1046/j.1365–3040.1999.00453.x

Yasunari T (2007) Role of land–atmosphere interaction on Asian monsoon climate. J Meteorol Soc Jpn 85B:55–75. https://doi.org/10.2151/jmsj.85B.55

Index

T. Ohta et al. (eds.), *Water-Carbon Dynamics in Eastern Siberia*,
Ecological Studies 236, https://doi.org/10.1007/978-981-13-6317-7